SOLID STATE SPECTROSCOPY : LASER SELECTIVE EXCITATION OF HOLMIUM IONS IN CRYSTALLINE SOLIDS

A thesis
submitted in partial fulfilment
of the requirements of the Degree
of
Doctor of Philosophy in Physics
in the
University of Canterbury
by
MARJORIE MUJAJI

University of Canterbury
1992

To my parents

ABSTRACT

The technique of laser selective excitation has been used to study the spectra of 23 Ho^{3+} centres present in CaF_2 and SrF_2 crystals, in mixed $Ca_{0.99}Sr_{0.01}F_2$ and $Ca_{0.99}Ba_{0.01}F_2$ crystals and in $CsCdBr_3$ crystals.

The polarisation of the fluorescence from <100> and <111> oriented crystals has been used to assign specific Ho^{3+} site symmetries to the various centres and to label the crystal-field energy levels of each centre by their group irreps.

The two principal Ho^{3+} centres (A and B) observed in both $CaF_2:Ho^{3+}$ and $SrF_2:Ho^{3+}$ crystals have been shown to be of C_{4v} and C_{3v} symmetry respectively. The four new centres identified in $Ca_{0.99}Sr_{0.01}F_2:Ho^{3+}$ and $Ca_{0.99}Ba_{0.01}F_2:Ho^{3+}$ crystals, are derived from the parent CaF_2 C_{4v} symmetry (A) centre by an on-axis and an off-axis placement of a dopant cation, Sr^{2+} or Ba^{2+}, in the vicinity of the Ho^{3+} - F^- pair. The three additional centres found in $SrF_2:Ho^{3+}$ crystals are from similar Ca^{2+} and Ba^{2+} substitutions in the SrF_2 lattice.

Seven centres associated with D^- charge compensation were observed in deuterated $CaF_2:Ho^{3+}$ and $SrF_2:Ho^{3+}$ crystals, with no C_{4v} symmetry centre being apparent.

For the $CsCdBr_3:Ho^{3+}$ system, spectra of the principal dimer centre and three other minority centres are reported. Strong upconversion fluorescence was observed for the principal dimer centre, enabling crystal-field energy levels for 18 Ho^{3+} multiplets to be determined. Low symmetry crystal-field splittings and pair splittings were observed on some of the sharper transitions.

Crystal-field analyses performed for all the C_{4v} and C_{3v} symmetry centres in $CaF_2:Ho^{3+}$, $SrF_2:Ho^{3+}$ and $CsCdBr_3:Ho^{3+}$ crystals are reported and the resulting crystal-field parameters discussed. Fluorescence lifetimes determined for the major Ho^{3+} centres are also presented.

The high resolution and ODNMR results for the C_{4v} symmetry A and SB1 centres in SrF_2:Ho^{3+} crystals confirm the centre symmetry assignments and the model configurations proposed on the basis of the polarisation ratio measurements. The superhyperfine ODNMR frequencies correlate well with the changes in the crystal-field parameters between the two centres.

ACKNOWLEDGEMENTS

I dedicate this thesis to my parents, whose faith in me, understanding and constant encouragement made the four years away from home bearable - only just!

I would especially like to thank my supervisors, Dr. G.D. Jones and Dr. R.W.G. Syme, for their guidance and the time they put into the discussions at various stages of this project.

I would also like to express my thanks to :

- Wayne Smith, Ron Culley, Ross Ritchie, Tom Walker and other workshop staff, for invaluable technical assistance;
- Robert McGregor and Dave Macdonald of the Chemistry Department, for invaluable advice on glass blowing;
- Dr. Y.L. Khong, for assistance with equipment in the early stages of this project and Keith Murdoch, for helpful discussions;
- Nick Sheen and John Laban, for assistance with adapting the Mössbauer least squares fitting program for lifetime transients;
- Dr. M.F. Reid, for assistance with the crystal-field fitting program;
- Dr. N.B. Manson of the Australian National University, Canberra, for providing the opportunity and financial support for a three week visit to the A.N.U. for high resolution and ODNMR measurements;
- Dr. J.P.D. Martin and Tosporn Boonyarith of the A.N.U., for assisting with the high resolution and ODNMR measurements;
- Steven Hemmingsen, for tracing out the absorption and high resolution spectra;
- Mary Kinnaird, Gill Evans and Beverley Bristowe for skillfully typing this thesis and for being tolerant with the alterations.

I am indebted to the late Dr. P.C. Makado for my interest in the subject.

Finally, I would like to thank the Campbell family and Mrs G. Andrews, for making me feel at home, so far away from home.

Financial support was provided by a Postgraduate Scholarship from the New Zealand Ministry of External Relations and Trade - External Aid Division and a Staff Development Fellowship from the University of Zimbabwe.

CONTENTS

Page

LIST OF FIGURES

Figure **Page**

Figure **Page**

Figure **Page**

LIST OF TABLES

CHAPTER 1

INTRODUCTION

The results presented in this thesis are from a spectroscopic study of trivalent holmium ions in CaF_2, SrF_2 and $CsCdBr_3$ crystals. These crystals are ideal as hosts for optical studies as they are transparent over a wide spectral range. However, a disadvantage of the CaF_2 and SrF_2 crystals is that the axial symmetry centres formed have orientational degeneracy as a result of the equivalence of the symmetry axes, such that centres along the <100>, <010> and <001> directions for example, are indistinguishable. Two disadvantages of the $CsCdBr_3$ crystals are that they are (i) soluble in water and (ii) brittle.

The primary objectives of any spectroscopic investigation viz, (i) establishing energy level schemes and the point group symmetries of the various centres present and (ii) establishing the symmetry properties of the wavefunctions of the crystal-field levels, have been achieved in this study.

This chapter presents a summary of the properties of rare-earth ions, Ho^{3+} in particular, and of the crystal structures of the CaF_2, SrF_2 and $CsCdBr_3$ hosts. As a brief review of previous work relevant to each chapter is presented at the beginning of the appropriate chapter, only other studies of Ho^{3+} ions, not directly related to the results presented here, are outlined in Section 1.4 below. An outline of the thesis is presented in Section 1.5.

1.1 The Rare-Earth Ions

The rare-earth ions comprise two groups of fourteen elements each, known as the lanthanide and the actinide series. The lanthanide series, which ranges from cerium (with atomic number $Z = 58$) to lutecium ($Z = 71$), is characterised by the progressive filling of the 4f shell of the electronic configuration, as one goes along the series, while the actinide series, which ranges from thorium ($Z = 90$) to lawrencium ($Z = 103$) is characterised by the progressive filling of the 5f shell.

The electronic configuration of the neutral lanthanide atoms consists of a Xenon structure core of 54 electrons ((Xe) = $1s^2\ 2s^2\ 2p^6\ 3s^2\ 3p^6\ 3d^{10}\ 4s^2\ 4p^6\ 4d^{10}\ 5s^2\ 5p^6$), the partially filled 4f shell and two to three electrons in the outer 6s and 5d shells ($6s^2$ or $5d\ 6s^2$). As the charge Z increases along the lanthanide series, the potential seen by the 4f electrons deepens as a result of the increased effective nuclear charge caused by the imperfect shielding of the 4f electrons and their orbitals show a systematic decrease in radius. This regular decrease in the size of the lanthanide with increasing atomic number is known as the lanthanide contraction [132].

The lanthanides can be ionised by removal of the outer electrons, and the most common ionic state is the trivalent in which all the electrons, except for those in the 4f shell, are in closed shells and therefore spectroscopically inactive in the visible region. The electronic configuration of the trivalent ions is given by $(Xe)4f^N$, for N increasing from 1 for Ce^{3+} to 14 for Lu^{3+}. Interactions between the 4f electrons and the nucleus and between the 4f electrons themselves, give rise to the energy level structure. Transitions within the $4f^N$ configuration result in the sharp lines observed in optical spectra of rare-earth ions in crystalline hosts because of the lanthanide contraction and resultant effective shielding of the 4f electrons from the crystal environment by the $5s^2\ 5p^6$ closed shells. The transition groups are basically those of the free RE^{3+} ions and their energies are found to be largely independent of the crystal host.

1.1.1 Properties of the Ho^{3+} ion

As the results reported in this thesis are for the Ho^{3+} ion, the properties of the lanthanide Ho are now specifically discussed.

Holmium, with atomic number 67, appears towards the end of the lanthanide series. Apart from the Xenon structure core as described above, the electronic configurations of the holmium atom and ions are as follows (with the ground multiplet in brackets) :

Ho	Ho^+	Ho^{2+}	Ho^{3+}
$4f^{11}6s^2(^4I_{15/2})$	$4f^{11}6s(^5I_8)$	$4f^{11}(^4I_{15/2})$	$4f^{10}(^5I_8)$.

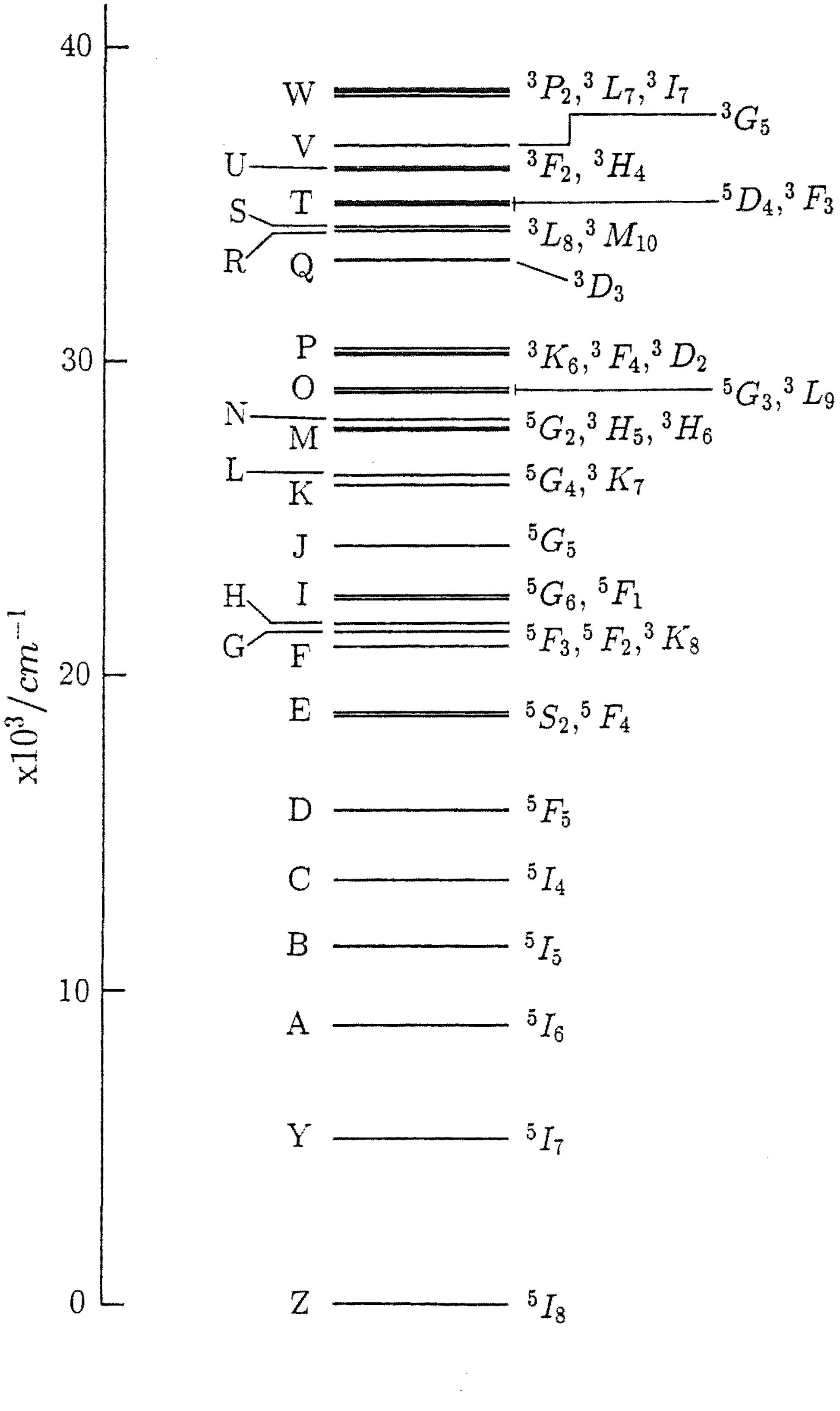

Figure 1.1: Free ion energy level structure of the $4f^{10}$ configuration of Ho^{3+}.

Table 1.1: Some ionic data

Ion	Ca^{2+}	Sr^{2+}	Ba^{2+}	F^-	Ho^{3+}	Cs^+	Cd^{2+}	Br^-	Na^+
Radius (Å)	0.99	1.12	1.34	1.33	0.89	1.67	0.97	1.96	0.97
Atomic Weight	40.08	87.62	137.34	19.00	164.93	132.91	112.40	79.90	22.99

Trivalent holmium has an even number of 4f electrons and hence is a non-Kramer's ion. It has an ionic radius of 0.89Å. Its $4f^{10}$ configuration comprises 107 LSJ multiplets. The free ion energy level structure is presented in Figure 1.1, with multiplets labelled by the $^{2S+1}L_J$ and the letter notations. Both notations are used in this text, with the M_J levels resulting from the crystal-field interaction for a particular LSJ multiplet identified by the letter (identifying the multiplet) and a numerical subscript. The ground multiplet $^5I_8$ is also referred to as the Z multiplet, with the ground state labelled by Z_1, and subsequent levels Z_2, Z_3 etc.

The holmium nucleus ^{165}Ho is 100% abundant with nuclear spin I of $^7/_2$.

1.2 The Fluorite Lattice Structure

The CaF_2 and SrF_2 crystal structure, commonly known as the fluorite structure, comprises a cubic lattice arrangement of F^- ions with a Me^{2+} (Ca^{2+} or Sr^{2+}) ion occupying every other cube centre, as shown in Figure 1.2. The separations between the Ca^{2+} or Sr^{2+} ions are 5.45 Å or 5.75 Å respectively. Ionic radii are presented in Table 1.1. The crystal has O_h^5 space group symmetry while the F^- ion sites have T_d point group symmetry and both the Me^{2+} ions and the vacant interstitial sites, O_h symmetry.

When a rare-earth ion is introduced into the MeF_2 lattice, it occupies the position which is normally occupied by the alkaline-earth Me^{2+} ion. For trivalent rare-earth doping therefore, some form of charge compensation is required to maintain the overall neutrality of the system. This is usually in the form of additional interstitial F^- ions, and the various positions of these charge compensating interstitial F^- ions give rise to different crystal-field symmetries (sites) for the rare-earth ion. The different types of centres arising are discussed in Sections 1.2.1 and 1.2.2 below.

The distribution of the positions of the charge compensating F^- ions depends on the concentration of the dopant rare-earth ion as well as the thermal

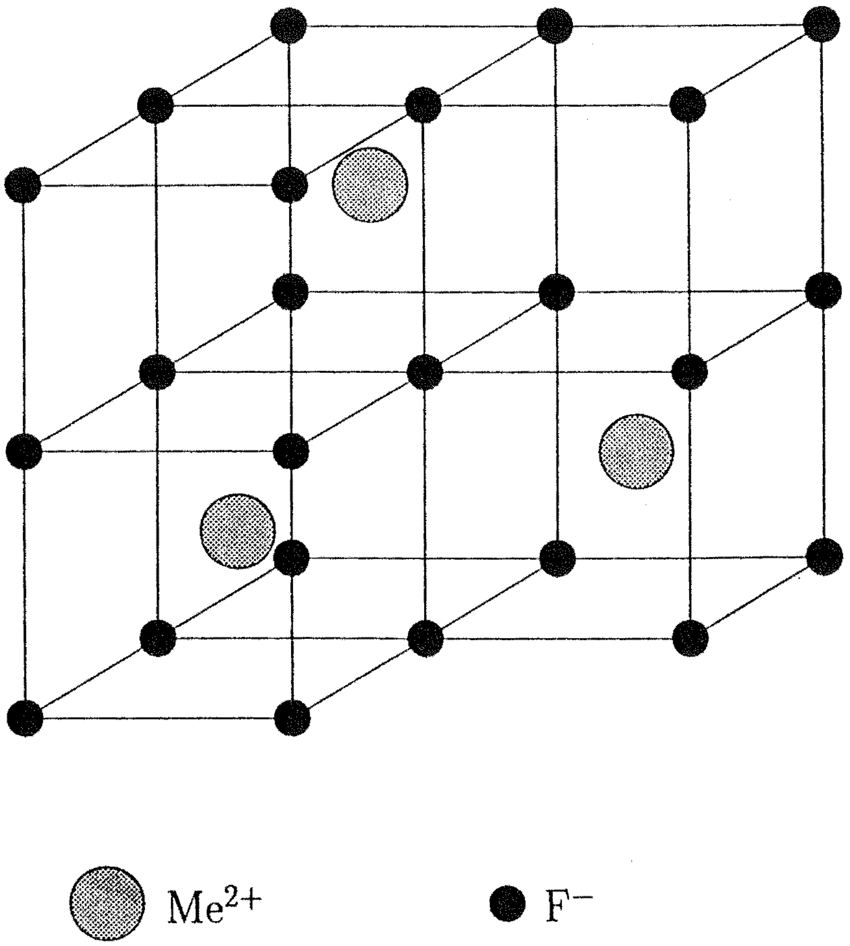

Figure 1.2: Structure of the alkaline-earth fluoride (MeF_2) crystal lattice.

history of the crystal and on the particular alkaline-earth ion host lattice.

1.2.1 The C_{4v} and C_{3v} symmetry centre configurations

The two simplest and most common forms of charge compensation in the fluorite lattice crystals, for rare-earth ion concentrations of 0.05% or less, are shown in Figure 1.3. In Figure 1.3(a), the charge compensating interstitial F^- ion occupies the cube next to the rare-earth ion in a <100> direction, the so-called nearest neighbour (NN) interstitial position. The rare-earth ion resides in a site of C_{4v} point group symmetry, with the RE^{3+} - F^- pair forming a C_{4v} (tetragonal) symmetry centre. In Figure 1.3(b), the charge compensating interstitial F^- ion occupies the next nearest neighbour (NNN) interstitial position, which gives the rare-earth ion site C_{3v} point group symmetry and the resulting RE^{3+} - F^- centre, C_{3v} (trigonal) symmetry.

The C_{4v} symmetry centre is the most common centre present in all CaF_2:RE^{3+} crystals and in SrF_2:RE^{3+} crystals for rare-earth dopants from the first part of the series while the C_{3v} symmetry centre is prevalent in SrF_2:RE^{3+} crystals for rare-earth ions in the latter part of the series [18]. Both types of centres have been identified for Ho^{3+} ions in CaF_2 and SrF_2 crystals here and will be discussed in Chapters 4 and 5.

The crystal field at the rare-earth ion site splits the energy levels of the rare-earth ion to a different pattern and extent for different symmetries, giving a pattern of crystal-field levels characteristic of a given centre.

The different centres can be studied by the laser selective excitation technique developed by Tallant and Wright [122]. In this technique, if the laser is tuned to a well isolated absorption transition of a given centre, the resulting fluorescence belongs just to this single distinct centre and, monitoring a particular intense fluorescence transition gives the excitation spectrum of only the given centre. The absorption transitions can all be identified as to centre in this manner and the spectrum of each centre studied separately.

For higher rare-earth dopant concentrations, cluster centres, formed by

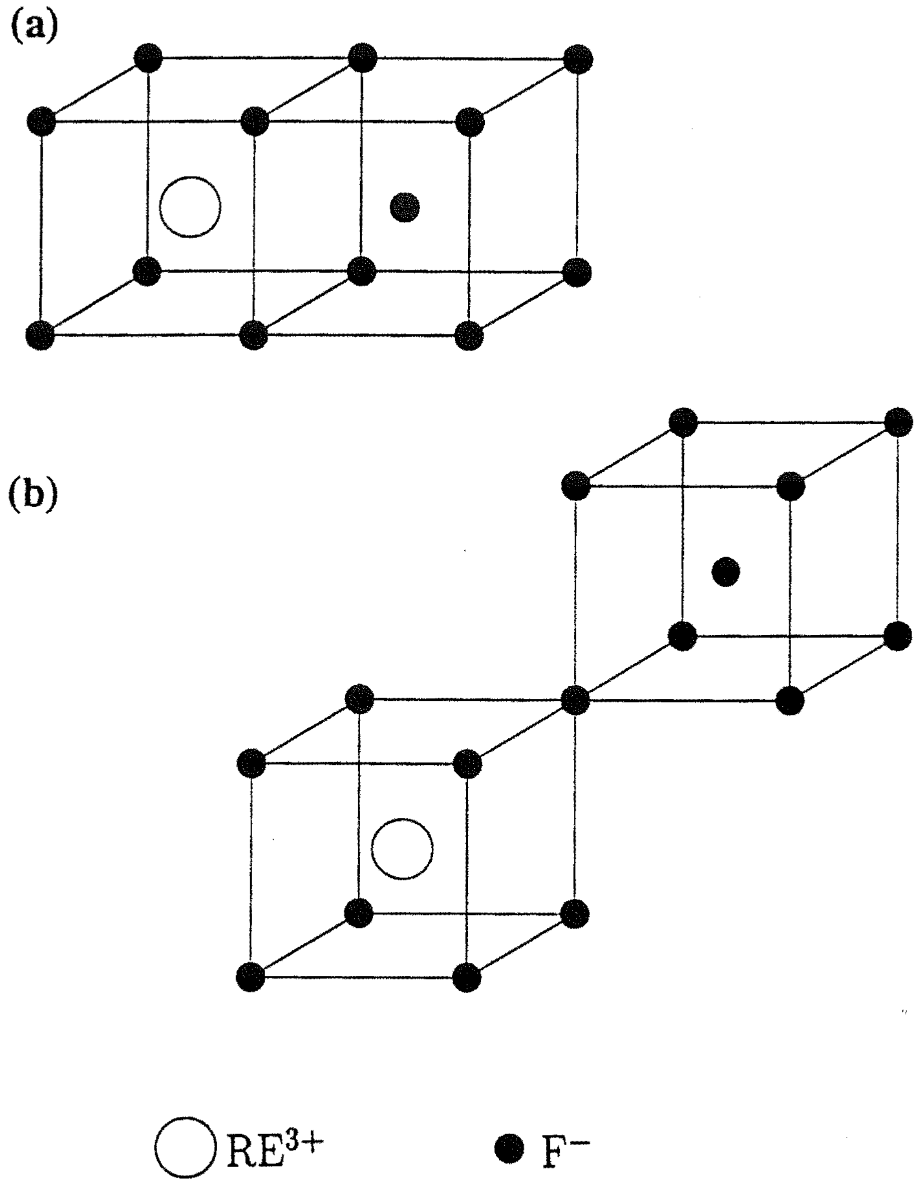

Figure 1.3: Model configurations of the two main centres formed by RE^{3+} ions in the MeF_2 lattice :
(a) the C_{4v} (tetragonal) symmetry centre;
(b) the C_{3v} (trigonal) symmetry centre.

aggregation of two or more RE^{3+} ions may result [68, 117, 120, 121, 122]. Such centres were not observed here at the low Ho^{3+} concentrations of 0.02% or less chosen.

By deuterating $CaF_2:RE^{3+}$ and $SrF_2:RE^{3+}$ crystals, using the method described in Chapter 3, some new centres arise from the charge compensation by D^- rather than F^- ions, as well as from D^- substitutions of one or more lattice F^- ions. These new centres can either have the same symmetry as the corresponding F^- centres, differing only in transition energies and hence energy levels or have lower symmetry because of the lattice substitutions of F^- ions. Comparison of these deuterated crystals with hydrogenated and tritiated crystals gives information about the D^- and T^- isotope shifts.

1.2.2 The modified C_{4v} symmetry centre configurations

CaF_2 crystals containing up to 1% of either Sr^{2+} or Ba^{2+} ions and SrF_2 crystals containing up to 1% of Ca^{2+} or Ba^{2+} ions, contain a further two new centres, both of which are derived from the C_{4v} symmetry centre discussed in Section 1.2.1 above. One of these new centres retains the C_{4v} symmetry of the parent centre, while the second is a C_s symmetry centre as shown in Figure 1.4. The introduced Sr^{2+}, Ba^{2+} or Ca^{2+} cation will be referred to as the dopant alkaline-earth or dopant Me^{2+} ion, while the new crystal is referred to as "mixed", to distinguish it from the parent crystal.

As shown in Figure 1.4(a), the dopant alkaline-earth ion substituting for the host alkaline-earth ion next to the interstitial F^- ion, on the RE^{3+} - F^- axis opposite to the RE^{3+} ion gives a centre which preserves the C_{4v} point group symmetry. The dopant alkaline-earth ion substituting for the host alkaline-earth ion off the RE^{3+} - F^- axis as in Figure 1.4 (b) and (c) gives rise to a C_s symmetry centre. The (100) plane C_s symmetry centre (Figure 1.4(b)) and the (110) plane C_s symmetry centre (Figure 1.4(c)) are spectroscopically distinguished by their polarisation behaviour, as discussed by Khong [63] for the case of Pr^{3+} and discussed here in Chapter 4 for Ho^{3+}. Modified C_{4v} symmetry centres with the

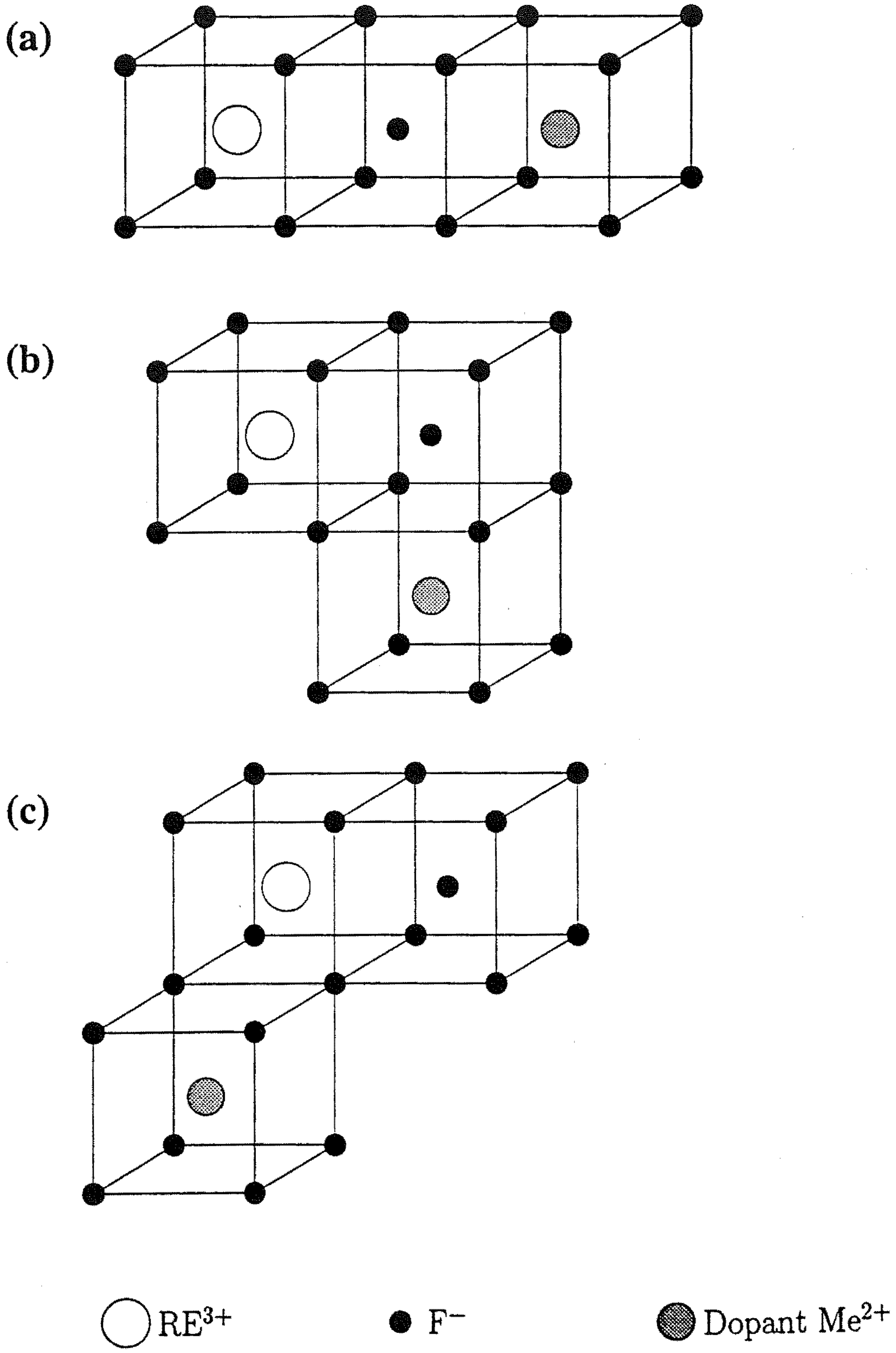

Figure 1.4: Model configurations of the centres arising from the introduction of a different alkaline-earth cation into the regular MeF_2 lattice :
(a) the on-axis modified C_{4v} symmetry centre;
(b) the off-axis (100) plane C_s symmetry centre - the C_s(b) configuration;
(c) the off-axis (110) plane C_s symmetry centre - the C_s(a) configuration.

configurations in Figure 1.4 (a) and (b) have been identified in both CaF_2:Ho^{3+} and SrF_2:Ho^{3+} type crystals and are discussed in Chapters 4 and 5 respectively.

Further more remote replacements of the host cation by the dopant cation are still possible, but these will occur at least two lattice spacings away from the rare-earth ion and do not have a large effect on its immediate surroundings and hence its crystal-field levels. Centres comprising more than one dopant alkaline-earth are statistically not expected for the 1% or less dopant alkaline-earth concentrations used in this study and were not apparent in any of the spectra studied.

1.3 The $CsCdBr_3$ Structure

The compound $CsCdBr_3$ belongs to a large group of halide salts which adopt the hexagonal crystal structure of $CsNiCl_3$ [84]. These halide salts, commonly referred to as ABX_3 compounds, have infinite linear chains of $[BX_6]^{4-}$ octahedra lying parallel to the crystallographic **c** axis as shown in Figure 1.5, with the monovalent A ions located between the chains maintaining the overall neutrality of the system.

As the separation between adjacent divalent (B^{2+}) ions is much smaller within the chains than between the chains, the intra-chain ion-ion interaction is much stronger than any inter-chain interaction, giving the compounds a pseudo one-dimensional character (Figure 1.6(a)). For the $CsCdBr_3$ case, the Cd^{2+} ions have separations of 3.35 Å along a given chain and 7.68 Å between neighbouring chains [69].

For most of the ABX_3 compounds, the $[BX_6]^{4-}$ octahedra have a slight departure from exact octahedral geometry [84], being elongated along the **c** axis, resulting in a overall trigonal distortion along that axis. This elongation was attributed to intra-chain electrostatic repulsion between neighbouring B^{2+} ions by McPherson et al. [84].

When trivalent rare-earth ions are introduced into the $CsCdBr_3$ crystals, the

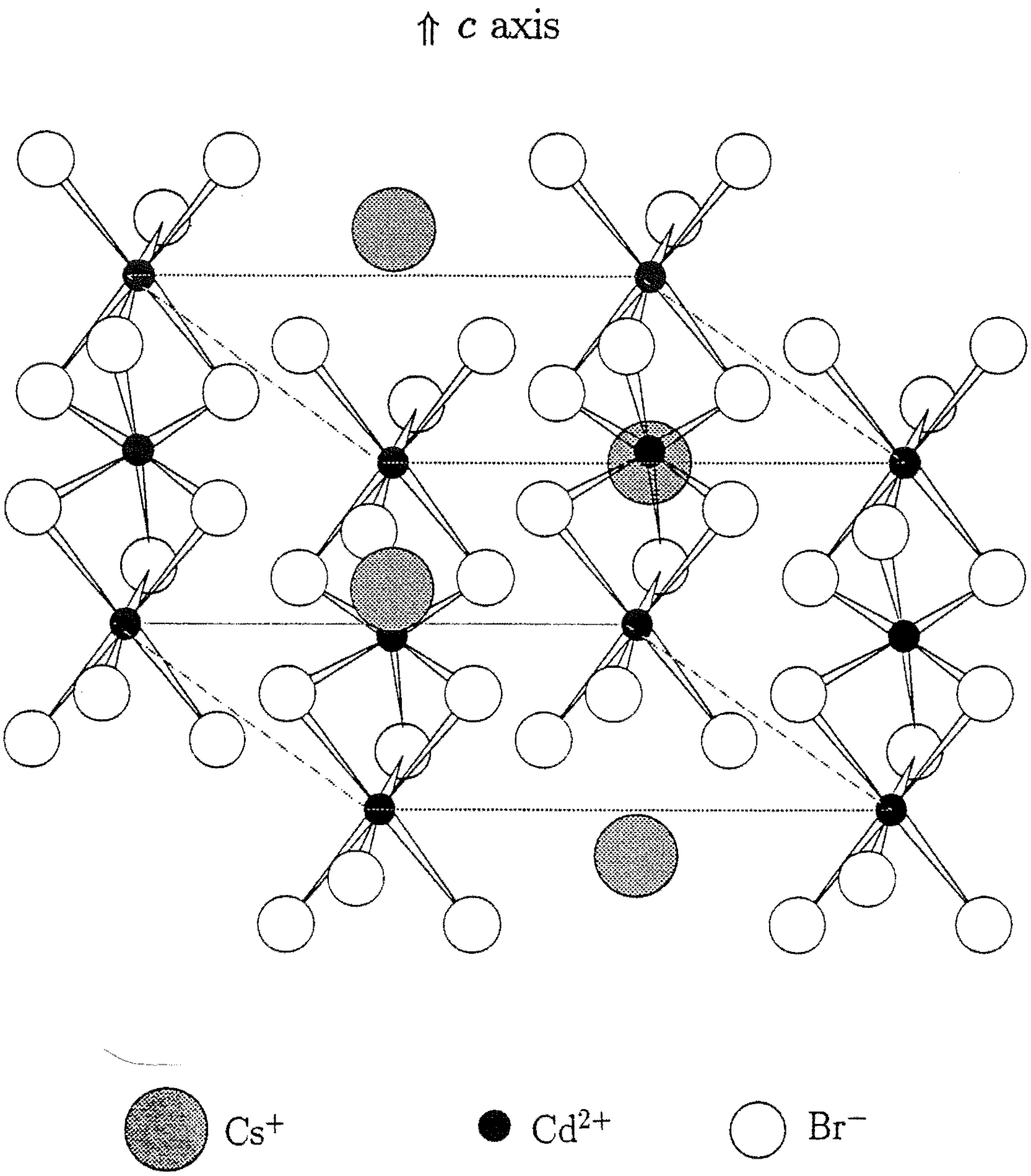

Figure 1.5: Structure of the $CsCdBr_3$ crystal lattice.

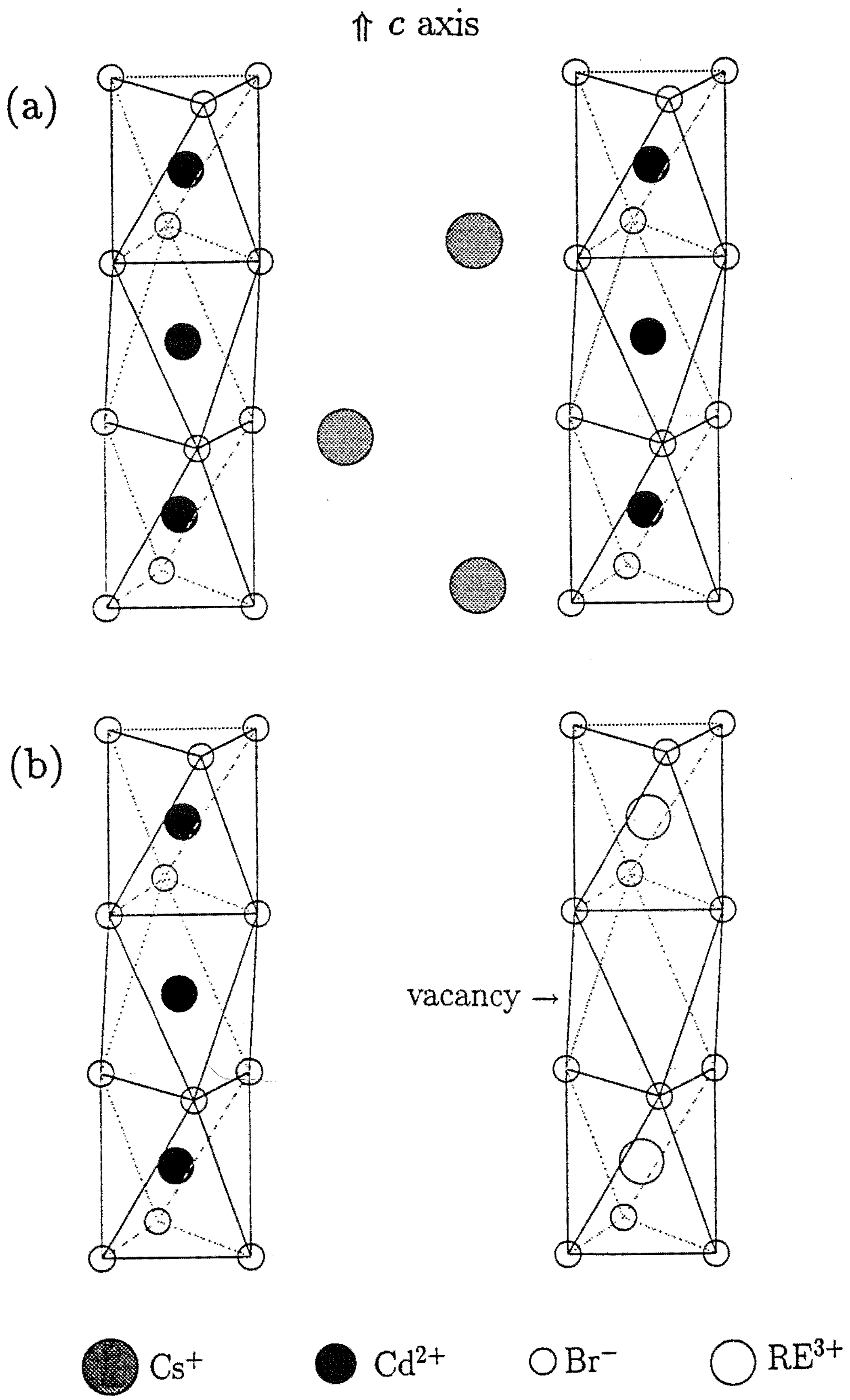

Figure 1.6: Cross-section of the $CsCdBr_3$ lattice showing :
(a) the linear chain structure;
(b) the model configuration of the principal centre formed by RE^{3+} ions.

most prevalent centre formed is of the RE^{3+} - vacancy - RE^{3+} arrangement, as shown in Figure 1.6(b). As three Cd^{2+} ions are replaced by two trivalent (RE^{3+}) ions, overall charge neutrality is realised. EPR measurements on Gd^{3+} [52] and optical measurements on both Nd^{3+} [11] and Tb^{3+} [13] have shown that at least 90% of the RE^{3+} ions introduced into the $CsCdBr_3$ crystals exist in such pair arrangements.

Formation of the dimer centre at low dopant concentrations to 0.01% readily occurs, in contrast to other crystalline hosts such as CaF_2 and $LiYF_4$ which require dopant concentrations of at least 1%. This is the main justification for the study of the ABX_3 compounds. Further, all RE^{3+} ion pairs along the chains have a common well defined separation and the same crystalline environment. Because of the interaction between the two ions, the dimer centre exhibits unusually strong upconversion, whereby fluorescence is observed from higher energy multiplets than excited. The upconversion mechanisms may be studied through spectral and temporal measurements.

The $CsCdBr_3$ crystal has the D_{6h}^4 space group symmetry and the Cd^{2+} ions are at sites of D_{3d} point group symmetry. Because of the presence of the other RE^{3+} ion, the RE^{3+} ion of a given pair resides in a site of C_{3v} point group symmetry.

Other minority centres of either the form RE^{3+} - RE^{3+} - vacancy or single RE^{3+} with remote RE^{3+} charge compensation or nearby impurity charge compensation are also observed to form, as discussed by Barthou and Barthem [12] for the Nd^{3+} case and discussed here in Chapter 6 for the Ho^{3+} case. Further varieties of the RE^{3+} - vacancy - RE^{3+} dimer centre may be achieved through heterogeneous RE^{3+} co-doping as shown by McPherson and McPherson [82] for the Ce^{3+} - Tm^{3+} pair. Furthermore, co-doping the RE^{3+} ion with a monovalent (M^+) ion such as Li^+, Ag^+ or Na^+ gives a new single RE^{3+} centre of the form RE^{3+} - M^+, as discussed by Barthem et al. [11] for Nd^{3+}.

1.4 Some Aspects of Other Spectroscopic Studies of Ho^{3+} Ions

Ho^{3+} ions are also studied in various other host crystals through energy transfer, two photon absorption and upconversion phenomena. Such studies are prompted by the fact that holmium is the second most extensively used rare-earth activator in laser crystals, after neodymium [61]. For the Ho^{3+} ion, $^5I_7 \rightarrow {}^5I_8$ is the principal transition for stimulated emission and the host crystals include $YAlO_3$, $YLiF_4$, BaY_2F_4, HoF_3, YAG and $CaWO_4$ among many other materials discussed by Kaminskii [61].

The high level of interest in the Ho^{3+} ion, both spectroscopically and for possible technological applications, is highlighted by the diversity of these studies.

Watts [126] reported on fluorescence from the $^5F_3$, $^5F_4$ and $^5S_2$ multiplets of Ho^{3+} for excitation of the $^2F_{7/2} \rightarrow {}^2F_{5/2}$ transition of Yb^{3+} in $LiYF_4$ crystals doubly doped with Ho^{3+} and Yb^{3+} ions. Absorption by the Yb^{3+} ion and subsequent transfer of the energy to the Ho^{3+} $^5I_6$ multiplet was the energy transfer mechanism proposed for the visible fluorescence observed with infrared excitation. The energy mismatch of about 1000 cm^{-1} between the $^5I_6$ - $^5I_8$ multiplets of Ho^{3+} and the $^2F_{5/2}$ - $^2F_{7/2}$ multiplets of Yb^{3+} could be accounted for by emission of two phonons as $LiYF_4$ has phonon energies of up to 500 cm^{-1}.

Results from two photon absorption studies have been reported for $CaF_2:Ho^{3+}$ at 300 K for excitation by neodymium glass and ruby lasers [40]. The resulting $^5S_2,{}^5F_4 \rightarrow {}^5I_8$ fluorescence was found to be strongly dependent on temperature and this temperature dependence was attributed to electron - phonon interaction effects. Upconversion fluorescence was also observed for two photon excitation of Ho^{3+} ions in CaF_2, SrF_2 and CdF_2 crystals [91]. Sequential two photon absorption $^5I_8 \rightarrow {}^5F_5 \rightarrow {}^3D_2$, and direct two photon absorption $^5I_8 \rightarrow {}^3L_8$, were proposed as the mechanisms resulting in the observation of fluorescence from the higher energy $^3D_2$ and $^3L_8$ multiplets, respectively.

More recently, room temperature laser emission has been obtained in Ho^{3+} doped YAG [65] and fibres [5, 17, 46]. In $YAG:Ho^{3+}:Tm^{3+}$[65], laser emission was observed at 2.1 μm from the $^5I_7 \rightarrow {}^5I_8$ transition of Ho^{3+} with excitation of the $^3H_4$ multiplet of Tm^{3+}. Laser emission at 2.08 μm and 1.38 μm was observed in Ho^{3+} doped fluorozirconate fibres [17], arising from the $^5I_7 \rightarrow {}^5I_8$ and $^5S_2 \rightarrow {}^5I_5$ transitions respectively, for excitation with the 488 nm argon ion laser line. The $^5I_7 \rightarrow {}^5I_8$ emission was also observed at 2.04 μm [46] in Ho^{3+} doped silica fibres for excitation with the 457.9 nm argon ion laser line. In the fluorozirconate fibre [5], laser emission has been reported at 0.55 μm ($^5S_2 \rightarrow {}^5I_8$) and 0.75 μm ($^5S_2 \rightarrow {}^5I_7$) for a Krypton ion laser excitation of the $^5F_5$ multiplet. The two upconversion pathways proposed involve initial excitation to the $^5F_5$ multiplet, followed by non-radiative relaxation to either the $^5I_6$ or the $^5I_7$ multiplets. A second excitation populates either the $^5G_5$ or the $^5F_3$ multiplets respectively, and non-radiative relaxation from either multiplet populates the $^5S_2$ multiplet, from whose fluorescence transitions lasing occurs.

1.5 Outline of the Thesis

The objectives of this study were :

(i) to determine the Ho^{3+} centres present in each of the CaF_2, SrF_2 and $CsCdBr_3$ crystal systems and derive the energy level schemes for the various centres from their excitation and fluorescence spectra. Although the excitation and fluorescence spectra for the two centres of C_{4v} and C_{3v} symmetry, present in the parent CaF_2:Ho^{3+} crystals have been reported [117], the corresponding energy level schemes have not been derived;

(ii) to determine the point group symmetry of each identified Ho^{3+} centre through polarisation ratio measurements of the transitions in (i);

(iii) to assign irreducible representation (irrep) labels to the various crystal-field levels of each centre, based on the polarisation ratio measurements of (ii);

(iv) to compare the various centres, both within the same host and between different hosts;

(v) to carry out crystal-field fits and obtain energy level irrep labels to compare with and supplement those determined from polarisation measurements;

(vi) to obtain fluorescence lifetimes for the centres;

(vii) to independently determine the centre symmetry and ground state Z_1 irrep label assignments for the particular centres in SrF_2 and $CsCdBr_3$ crystals through high resolution and ODNMR measurements.

In Chapters 2 and 3, the theoretical and experimental aspects respectively, relevant to the results presented here, are discussed. The theoretical aspects include crystal-field theory, electric dipole and polarisation selection rules, electron - phonon interaction effects and electric dipole transition probabilities. Crystal growth and preparation, cryogenic systems, laser selective excitation and fluorescence lifetime measurement techniques are discussed in Chapter 3.

The laser selective excitation and transition polarisation results obtained for the Ho^{3+} centres in CaF_2, SrF_2 and $CsCdBr_3$ crystals are presented in Chapters 4, 5 and 6 respectively. Energy level schemes are derived for each centre, irrep label assignments made for the crystal-field levels and model configurations proposed for the different centres. The discussion section at the end of each chapter compares the results for the various centres. For SrF_2:Ho^{3+} whose laser selective excitation has not been reported before, it is shown that the dominant centre is of C_{4v} symmetry, in contrast to the EPR measurements of Ranon and Lee [103], where resonances for the C_{3v} symmetry centre only were observed. An explanation of this paradox is given. For the $CsCdBr_3$:Ho^{3+} system which has not been studied at all before, upconversion mechanisms are proposed for the principal dimer centre and the several small splittings observed on some of the sharper transitions interpreted.

Chapter 7 summarises results from the crystal-field fits for the C_{4v} and C_{3v} symmetry centres in the three crystal systems, CaF_2, SrF_2 and $CsCdBr_3$. Crystal-field parameters are compared with those for Er^{3+}, for the parent C_{4v} and C_{3v} symmetry Ho^{3+} centres in both CaF_2 and SrF_2 crystals. For the dimer centre in $CsCdBr_3$:Ho^{3+}, the crystal-field parameters are compared with those of the Nd^{3+} and Er^{3+} dimer centres in the same host.

In Chapter 8, the temporal results for the various centres are presented and qualitatively interpreted in terms of the changes in the crystal-field parameters, for centres in CaF_2 and SrF_2 type crystals. For the dimer centre in $CsCdBr_3$:Ho^{3+}, the upconversion mechanisms are further discussed in relation to the fluorescence lifetimes of the various multiplets and energy transfer rates compared to those for the dimer centre in $CsCdBr_3$:Er^{3+}.

In Chapter 9, the hyperfine and superhyperfine lines of two of the three C_{4v} symmetry centres observed in SrF_2:Ho^{3+} are presented and compared with those for the previously studied CaF_2 C_{4v} symmetry centre. These confirm the C_{4v} symmetry centre assignments made for the centres in SrF_2:Ho^{3+}. For the dimer centre in $CsCdBr_3$:Ho^{3+}, results from a preliminary high resolution study are also presented.

Lastly, in Chapter 10, the main results and conclusions from this study of Ho^{3+} ions in the CaF_2, SrF_2 and $CsCdBr_3$ hosts are summarised and suggestions for further work given.

CHAPTER 2

THEORETICAL ASPECTS

This chapter presents an overview of the theoretical aspects relevant to the work done here. These aspects include crystal-field theory, electric dipole selection rules and polarisation selection rules. Electron-phonon coupling effects and electric dipole transition probabilities are also briefly discussed.

Crystal-field theory is extensively discussed in the work of Wybourne [132], Judd [57], Hüfner [53] and Dieke [35] among others. Transition probabilities are discussed by Riseberg and Weber [114] while local mode vibrations are discussed by Newman [92].

2.1 Crystal-Field Theory

For trivalent rare-earth ions, transitions within the $4f^N$ configuration give rise to the optical line spectra observed. Such transitions usually arise from an electric dipole transition process, made possible by the mixing-in of opposite parity states from the $4f^{N-1}$ 5d configuration, which occurs for rare-earth ions residing in sites without inversion symmetry.

The three main interactions responsible for the energy level structure of rare-earth ions are

(i) the Coulomb interaction between the electrons, H_c ;

(ii) the spin-orbit coupling, H_{so} ;

and (iii) the crystalline electric field, V_{cf}.

For a rare-earth ion in a crystalline environment, the total Hamiltonian can be written as

$$H = H_{fi} + V_{cf} \tag{2.1}$$

where H_{fi} and V_{cf} are the free ion and crystal-field Hamiltonians respectively.

2.1.1 The free ion Hamiltonian

For a free ion with charge Ze and N electrons, H_{fi} is given by

$$H_{fi} = \frac{-\hbar^2}{2m}\sum_{i=1}^{N} \nabla_i^2 - \sum_{i=1}^{N} \frac{Ze^2}{r_i} + \sum_{i<j}^{N} \frac{e^2}{r_{ij}} + \sum_{i=1}^{N} \zeta(r_i)(s_i \cdot \ell_i) , \qquad 2.2$$

where the first two terms represent the total kinetic energy of the electrons and the potential energy of the electrons in the Coulomb field of the nucleus respectively. The third term is the Coulomb potential energy (H_c) arising from repulsion between pairs of electrons while the last term is the spin-orbit interaction energy (H_{so}).

As the exact solution of this Hamiltonian cannot be obtained for systems of more than one electron, the central field approximation is evoked to solve equation 2.2 [132]. In this approximation, each electron is assumed to be moving in a spherically symmetric potential $-U(r_i)/e$, independent of the other electrons. The potential $-U(r_i)/e$ arises from the field of the nucleus and the spherically averaged potential fields of each of the other electrons.

The Hamiltonian for the central field approximation, H_{cf}, is then given by

$$H_{cf} = \sum_{i=1}^{N} [\frac{-\hbar^2}{2m}\nabla_i^2 + U(r_i)] .$$

This Hamiltonian is a sum of single electron Hamiltonians and the Schrodinger's equation can be solved by a product of single electron wavefunctions. The state of each electron is denoted by the quantum numbers n, ℓ, m_ℓ, and m_s, while the configuration of N electrons is labelled by n and ℓ only. In the central field approximation, all the states of a particular configuration have the same energy.

The combined perturbation potential V, from the residual electrostatic potential and the spin-orbit interaction, given by

$$V = \sum_{i=1}^{N} [-\frac{Ze^2}{r_i} - U(r_i)] + \sum_{i<j}^{N} \frac{e^2}{r_{ij}} + \sum_{i=1}^{N} \zeta(r_i)(s_i \cdot \ell_i) ,$$

gives the free ion energy level structure.

As the first term of the residual electrostatic potential, $\sum_{i=1}^{N} [-\frac{Ze^2}{r_i} - U(r_i)]$, is spherically symmetric, it shifts the whole energy level structure without removing any degeneracies. The repulsive Coulomb (for electrons in incomplete shells) and spin-orbit terms lift the degeneracy of the $4f^N$ configuration to give free ion $|LSJ>$ energy levels.

There are three appropriate approaches to calculating the free ion energy levels of the $4f^N$ configuration :

(i) the Russell-Saunders (LS) coupling scheme where the Coulomb interaction is much larger than the spin-orbit interaction. The energy level structure is obtained from diagonalising the Coulomb interaction with the spin-orbit interaction added as a small perturbation. This is applicable for the lighter elements;

(ii) the j-j coupling scheme, for which the spin-orbit interaction term is much larger than the Coulomb term and the latter is treated as a small perturbation. This is applicable for the heavier elements;

(iii) the intermediate coupling scheme, for which the Coulomb and spin-orbit interactions are comparable in magnitude. The LS and j-j coupling limits are not adequate representations and matrix elements for the combined interaction have to be diagonalised. This is the scheme best adopted for the rare-earth ions.

Using the tensor operator methods of Racah, energies for the Coulomb and spin-orbit interactions are derived [132] to be

$$E_c = \sum_{k=0,2,4,6} f_k F^k \qquad 2.3(a)$$

for the Coulomb interaction where the F^k are the Slater radial integrals and the f_k represent the angular part of the interaction;

and

$$E_{so} = A_{so} \zeta \qquad 2.3(b)$$

for the spin-orbit interaction where ζ as in equation 2.3(b) is the spin-orbit integral and A_{so} represents the angular part of the spin-orbit interaction.

Derivation of these Coulomb and spin-orbit interaction energy expressions are discussed in Wybourne [132], Judd [57] and Hüfner [53] among others.

Configuration interaction effects, both Coulombic and magnetic, are sometimes added to the free ion Hamiltonian of equation 2.2, to improve the correlation between the observed and the calculated free ion energies [100]. These effects are included in second-order perturbation, through the two-body and three-body effective operators.

The Coulombic part of the configuration interaction [58], H_{c-ci} is given by

$$H_{c-ci} = \alpha L(L+1) + \beta G(G_2) + \gamma G(R_7) + \sum_{i=2,3,4,6,7,8} t_i T^i \ , \qquad 2.4(a)$$

where α, β and γ are the parameters associated with the two-body Coulombic correction terms; $G(G_2)$ and $G(R_7)$ are Casimir's operators for the G_2 and R_7 groups respectively and L is the total orbital angular momentum. The parameters α, β and γ represent those Coulombic correction terms which, because they do not transform as the f_k operators, cannot be absorbed into the F^k parameters. The three-body Coulombic effects which are relevant for configurations with three of more f electrons, are expressed through the T^i parameters and the corresponding t_i operators.

The magnetic-correlated part of the configuration interaction [60], H_{m-ci} is given by

$$H_{m-ci} = \sum_{f=2,4,6} p_f P^f + \sum_{h=0,2,4} m_h M^h , \qquad 2.4(b)$$

where the P^f are the electrostatically correlated parameters with the corresponding operators, p_f. The Marvin integrals M^h represent the spin-spin and spin-other-orbit relativistic corrections and the m_h are the corresponding operators. The first term is the more significant of the two two-body magnetic correction terms.

Inclusion of these Coulombic and magnetic correction terms to give the total free ion Hamiltonian H'_{fi} as

$$H'_{fi} = H_{fi} + H_{c-ci} + H_{m-ci} \qquad 2.5$$

significantly reduces the discrepancies between the experimental and the calculated free ion energy levels.

2.1.2 The crystal-field Hamiltonian

In order to be able to solve the Hamiltonian

$$H = H_{fi} + V_{cf}$$

by perturbation theory, it is necessary to compare the relative magnitudes of the crystal-field interaction and the free ion interactions of Section 2.1.1 above. Three cases arise :-

(i) $V_{cf} > H_c > H_{so}$

(ii) $H_c > V_{cf} > H_{so}$

and (iii) $H_c > H_{so} > V_{cf}$.

Case (i) is applicable for paramagnetic ions with incomplete 4d and 5d shells. Case (ii) is common for elements of the 3d group and case (iii) is applicable for rare-earth ions. The crystal-field interaction is small in this case because the incompletely filled $4f^N$ shell is shielded from the influence of its environment by the outer completely filled $5s^2$ and $5p^6$ shells.

Because the interaction of the rare-earth ion with the crystalline environment is relatively weak, sharp lines are observed in the spectra of rare-earth ions in solids and this coupled with the multitude of energy levels possible for a given f^N configuration, gives a large amount of spectral information about the ions.

The relative magnitudes of the energy splittings resulting from the three interaction terms applicable to rare-earth ions are shown in Figure 2.1. The electrostatic Coulomb interaction gives rise to Russell-Saunders LS terms with separations of about 10000 cm^{-1} and the spin-orbit interaction splits each of these terms into several J multiplets with typical separations of 1000 cm^{-1}. Finally, the crystal field either partially or fully removes the J degeneracy of each multiplet. The resulting Stark energy levels extend over several 100 cm^{-1}.

The crystal-field Hamiltonian is treated as a perturbation to the free ion Hamiltonian. Since the free ion eigenfunctions have spherical symmetry and transform as the spherical harmonics $Y_{kq}(\theta,\phi)$, the crystal-field Hamiltonian is also conveniently expressed in terms of operators $C_q^{(k)}$ that transform as spherical harmonics :

$$V_{cf} = \sum_{k,q,i} B_q^k (C_q^{(k)})_i \,, \qquad 2.6$$

where the summation in i is over all the electrons of the $4f^N$ configuration. The B_q^k are the crystal-field parameters representing the radial part of the crystal-field Hamiltonian and the $C_q^{(k)}$ are the Racah spherical tensors of rank k representing the angular part of the interaction. The Racah spherical tensor operators are related to the spherical harmonics Y_{kq} by

$$C_q^{(k)} = \sqrt{\frac{4\pi}{2k+1}}\, Y_{kq} \,.$$

The possible (k,q) values allowed are governed by the following conditions :-

(i) the triangular rule, that for angular momenta ℓ_1 and ℓ_2, $\ell_1+\ell_2 \leqslant k$. For f electrons $\ell = 3$, therefore $k \leqslant 6$.

(ii) for interaction within a configuration of equivalent electrons, the odd k terms vanish as only the even parity terms are allowed.

Therefore the even k values 0, 2, 4 and 6 only need be considered.

As the first term in the crystal-field expansion, $k = q = 0$, is spherically symmetric and therefore shifts all the energy levels by the same amount, it does not contribute to energy level splittings. This leaves only the $k = 2, 4, 6$ terms to be considered.

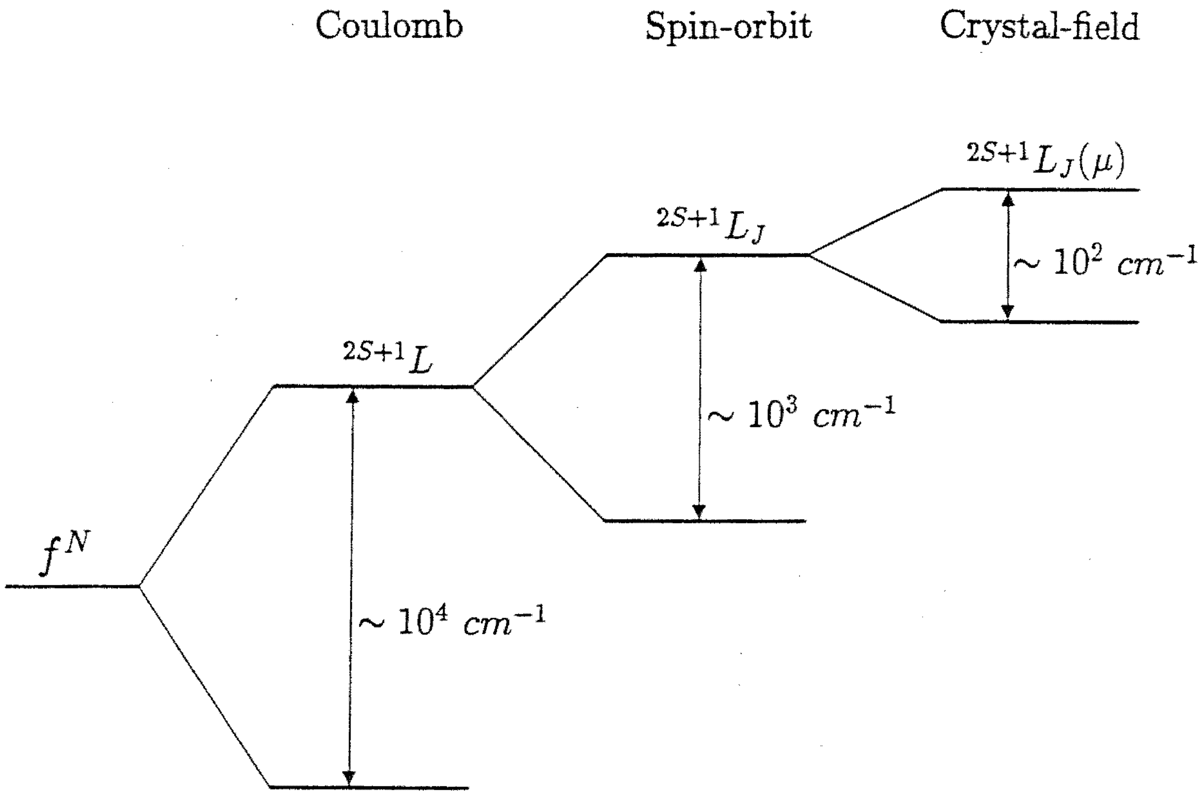

Figure 2.1: Schematic diagram of the splittings of the energy levels of the RE^{3+} ion as a result of the Coulomb, spin-orbit and crystal-field interactions.

Further, the possible $B^k_q\, C^{(k)}_q$ terms are restricted by the site symmetry of the rare-earth ion to those satisfying the n-fold rotational symmetry of the RE^{3+} ion site. In the JM basis representation, the non-zero $B^k_q\, C^{(k)}_q$ terms are :

(a) for a C_{4v} symmetry centre, V_{cf} is given by

$$\begin{aligned} V_{C_{4v}} = {} & B^2_A\, C^{(2)}_0 \\ & + B^4_A\, [C^{(4)}_0 - \sqrt{\tfrac{7}{10}}\,(C^{(4)}_4 + C^{(4)}_{-4})] \\ & + B^6_A\, [C^{(6)}_0 + \sqrt{\tfrac{1}{14}}\,(C^{(6)}_4 + C^{(6)}_{-4})] \\ & + B^4_C\, [C^{(4)}_0 + \sqrt{\tfrac{5}{14}}\,(C^{(4)}_4 + C^{(4)}_{-4})] \\ & + B^6_C\, [C^{(6)}_0 - \sqrt{\tfrac{7}{2}}\,(C^{(6)}_4 + C^{(6)}_{-4})]\,, \end{aligned} \qquad 2.7(a)$$

where B^4_C and B^6_C are the parameters of the cubic crystal-field terms and the B^k_A are the crystal-field parameters of the axial crystal-field terms which are chosen as orthogonal combinations of the cubic crystal-field terms.

This Hamiltonian is related to the

$$\begin{aligned} V'_{C_{4v}} = {} & B^2_0\, C^{(2)}_0 + B^4_0\, C^{(4)}_0 + B^6_0\, C^{(6)}_0 \\ & + B^4\, [C^{(4)}_0 + \sqrt{\tfrac{5}{14}}\,(C^{(4)}_4 + C^{(4)}_{-4})] \\ & + B^6\, [C^{(6)}_0 - \sqrt{\tfrac{7}{2}}\,(C^{(6)}_4 + C^{(6)}_{-4})] \end{aligned} \qquad 2.7(b)$$

used by Freeth et al. [42, 43] through the following relations of the crystal-field parameters :

$$\begin{aligned} B^2_A &= B^2_0 \\ B^4_A &= \tfrac{5}{12} B^4_0 \\ B^6_A &= \tfrac{7}{8} B^6_0 \\ B^4_C &= B^4 + \tfrac{7}{12} B^4_0 \\ B^6_C &= B^6 + \tfrac{1}{8} B^6_0\,. \end{aligned} \qquad 2.7(c)$$

(b) for a C_{3v} symmetry centre, V_{cf} is given by

$$
\begin{aligned}
V_{C_{3v}} &= B^2_A\, C^{(2)}_0 \\
&+ B^4_A\, [C^{(4)}_0 - \tfrac{1}{2}\sqrt{\tfrac{7}{10}}\,(C^{(4)}_3 - C^{(4)}_{-3})] \\
&+ B^6_A\, [\sqrt{\tfrac{11}{42}}\,(C^{(6)}_3 - C^{(6)}_{-3}) + \sqrt{\tfrac{5}{21}}\,(C^{(6)}_6 + C^{(6)}_{-6})] \\
&+ \hat{B}^6_A\, [C^{(6)}_0 + \tfrac{4}{7}\sqrt{\tfrac{10}{21}}\,(C^{(6)}_3 - C^{(6)}_{-3}) - \tfrac{4}{7}\sqrt{\tfrac{11}{21}}\,(C^{(6)}_6 + C^{(6)}_{-6})] \\
&+ B^4_C\, [C^{(4)}_0 + \sqrt{\tfrac{10}{7}}\,(C^{(4)}_3 - C^{(4)}_{-3})] \\
&+ B^6_C\, [C^{(6)}_0 - \sqrt{\tfrac{35}{96}}\,(C^{(6)}_3 - C^{(6)}_{-3}) + \tfrac{1}{8}\sqrt{\tfrac{77}{3}}\,(C^{(6)}_6 + C^{(6)}_{-6})],
\end{aligned}
\tag{2.8(a)}
$$

where B^4_C and B^6_C are the crystal-field parameters of the cubic crystal-field terms referred to the <111> axis as the z axis. The B^k_A are the trigonal crystal-field parameters of the axial crystal-field terms, which are combinations of the $C^{(k)}_q$ chosen to be orthogonal to the cubic crystal-field terms. These parameters are related to the those of the Hamiltonian

$$
\begin{aligned}
V'_{C_{3v}} &= B^2_0\, C^{(2)}_0 + B^4_0\, C^{(4)}_0 + B^6_0\, C^{(6)}_0 \\
&+ B^4_3\, (C^{(4)}_3 - C^{(4)}_{-3}) \\
&- B^6_3\, (C^{(6)}_3 - C^{(6)}_{-3}) \\
&+ B^6_6\, (C^{(6)}_6 + C^{(6)}_{-6})
\end{aligned}
\tag{2.8(b)}
$$

of Hutchings [54] by the relations :

$$
\begin{aligned}
B^2_A &= B^2_0 \\
B^4_A &= \frac{2\sqrt{70}}{27}\left(\sqrt{\frac{10}{7}}\,B^4_0 - B^4_3\right) \\
B^6_A &= \frac{\sqrt{42}}{21}\left(\sqrt{10}\,B^6_6 - \sqrt{11}\,B^6_3\right) \\
\hat{B}^6_A &= \frac{56}{81}\left(\frac{7}{8}\,B^6_0 - \sqrt{\frac{10}{21}}\,B^6_3 - \sqrt{\frac{11}{21}}\,B^6_6\right) \\
B^4_C &= \frac{2\sqrt{70}}{27}\left(\frac{1}{2}\sqrt{\frac{7}{10}}\,B^4_0 + B^4_3\right) \\
B^6_C &= \frac{56}{81}\left(\frac{4}{7}\,B^6_0 + \sqrt{\frac{10}{21}}\,B^6_3 + \sqrt{\frac{11}{21}}\,B^6_6\right).
\end{aligned}
\tag{2.8(c)}
$$

The crystal field either partially or fully removes the J degeneracy of the multiplet to give a set of crystal-field energy levels. The wavefunctions of these resulting crystal-field levels can be expressed as linear combinations of the basis functions, $|\gamma SLJJ_z>$, characterised by the L, S, J and J_z quantum numbers. The matrix elements for the crystal-field interaction between these JJ_z basis states are then given by

$$<\gamma SLJJ_z|V_{cf}|\gamma' SL'J'J'_z> \; = \sum_{k,q} B^k_q < \gamma SLJJ_z|U^{(k)}_q|\gamma' SL'J'J'_z> <\ell\|C^{(k)}\|\ell> \tag{2.9}$$

where

$$<\ell\|C^{(k)}\|\ell> \; = (-1)^{\ell}(2\ell+1)\begin{pmatrix} \ell & k & \ell \\ 0 & 0 & 0 \end{pmatrix} .$$

The $<\gamma SLJJ_z|U^{(k)}_q|\gamma' SL'J'J'_z>$ are diagonal in S and, by application of the Wigner-Erckart theorem, can be reduced to

$$< \gamma SLJJ_z|U^{(k)}_q|\gamma' SL'J'J'_z> = (-1)^{J-J_z}\begin{pmatrix} J & k & J' \\ -J_z & q & J'_z \end{pmatrix} <\gamma SLJ\|U^{(k)}\|\gamma' SL'J'>, \tag{2.10}$$

where

$$<\gamma SLJ\|U^{(k)}\|\gamma' SL'J'> = (-1)^{S+L'+J+k}\sqrt{(2J+1)(2J'+1)}\begin{Bmatrix} J & J' & k \\ L' & L & S \end{Bmatrix}$$
$$\times <\gamma SL\|U^{(k)}\|\gamma' SL'>.$$

The 3j and 6j symbols introduced here are tabulated by Rotenberg et al. [115] and the doubly reduced matrix elements of the tensor operator $U^{(k)}$ are tabulated by Nielson and Koster [93].

Diagonalising the energy matrix generated from equation 2.9 yields eigenvalues and corresponding eigenfunctions for the particular point group symmetry crystal field. The resulting eigenvalues correspond to the crystal-field energy levels observed experimentally while the eigenfunctions are the corresponding $|JJ_z>$ label combination wavefunctions.

It is also possible to include correlation effect terms to the crystal-field Hamiltonian but, as these additional effects are not included in any of the crystal-field fittings done here, they will not be discussed further.

2.2 Electric Dipole Selection Rules for the C_{4v}, C_{3v} and C_s Symmetry Groups

The crystal-field wavefunctions for a centre having a RE^{3+} ion in a cubic symmetry site are labelled by the irreducible representations (irreps) Γ_i of the O_h group. For axial symmetry centres such as C_{4v} and C_{3v} symmetry centres, the wavefunctions can be labelled by irreps Γ_i and γ_i where Γ_i is the irrep label of the parent cubic wavefunction and γ_i is the point group irrep label. For an even electron system like Ho^{3+}, the energy levels can have one of the irreps Γ_1 to Γ_5 of the O_h group, and in the C_{4v} symmetry case, these energy levels also belong to one of the irreps γ_1 to γ_5 of the C_{4v} group. For C_{3v} symmetry, the energy levels can have one of the C_{3v} point group irreps γ_1, γ_2 and γ_3 in addition to the Γ_i irrep of the O_h group, and, for C_s symmetry, the applicable point group irrep labels are γ_1 and γ_2 of the C_s group.

The decomposition from O_h to one of the lower symmetry groups C_{4v}, C_{3v} or C_s, is given by the compatibility tables such as listed by Koster et al. [67]. The number of crystal-field energy levels of a particular irrep symmetry can therefore be derived for each multiplet. For the $Z(^5I_8)$, $Y(^5I_7)$, $D(^5F_5)$, $E(^5S_2,^5F_4)$ and $F(^5F_3)$ multiplets of Ho^{3+}, these are summarised in Table 2.1 (a), (b) and (c), for the C_{4v}, C_{3v} and C_s symmetry centres respectively.

In addition to the crystal-field selection rules outlined below, electric dipole transitions are also governed by the selection rules applicable for strict Russell-Saunders L S J states [132]:

$$\Delta \ell = \pm 1$$

$$\Delta S = 0$$

$$|\Delta L|, |\Delta J| \leqslant 2\ell$$

Table 2.1: Symmetries of the crystal-field energy levels for the $^5I_8$, $^5I_7$, $^5F_5$, $^5S_2$, $^5F_4$ and $^5F_3$ multiplets of the Ho^{3+} ions in sites of
(a) C_{4v} point group symmetry;
(b) C_{3v} point group symmetry;
(c) C_s point group symmetry.

(a)

	Symmetry					
C_{4v}	γ_1	γ_2	γ_3	γ_4	γ_5	**Multiplet**
No. of levels	3	2	2	2	4	$^5I_8$
	1	2	2	2	4	$^5I_7$
	1	2	1	1	3	$^5F_5$
	1	-	1	1	1	$^5S_2$
	2	1	1	1	2	$^5F_4$
	-	1	1	1	2	$^5F_3$

(b)

	Symmetry			
C_{3v}	γ_1	γ_2	γ_3	**Multiplet**
No. of levels	3	2	6	$^5I_8$
	2	3	5	$^5I_7$
	1	2	4	$^5F_5$
	1	-	2	$^5S_2$
	2	1	3	$^5F_4$
	1	2	2	$^5F_3$

(c)

	Symmetry		
C_s	γ_1	γ_2	**Multiplet**
No. of levels	9	8	$^5I_8$
	7	8	$^5I_7$
	5	6	$^5F_5$
	3	2	$^5S_2$
	5	4	$^5F_4$
	3	4	$^5F_3$

(a) C_{4v} symmetry centres:

For the C_{4v} symmetry group, the electric dipole operator γ_{ed} transforms as either the γ_1 (z) or the γ_5 (x,y) irreps. An electric dipole transition $\gamma_a \rightarrow \gamma_b$ is therefore allowed (i.e. can have a non-vanishing transition probability) if

$$\gamma_a \times \gamma_{ed} \supset \gamma_b \; .$$

Using the C_{4v} group multiplication table on page 45 of Koster et al. [67], the electric dipole selection rules governing transitions between levels of different irrep symmetries can be derived. The selection rules applicable for an even-electron system such as Ho^{3+} are presented in Table 2.2(a), where π and σ polarisations are defined as the E vector of the incident radiation parallel and perpendicular respectively, to the C_{4v} symmetry z axis.

(b) C_{3v} symmetry centres:

For the C_{3v} symmetry group, the electric dipole operator γ_{ed} transforms as either the γ_1 (z′) or the γ_3 (x′,y′) irreps. Transitions $\gamma_a \rightarrow \gamma_b$ are allowed if

$$\gamma_a \times \gamma_{ed} \supset \gamma_b \, .$$

For the γ_1, γ_2 and γ_3 irreps in C_{3v} symmetry, the selection rules obtained from the C_{3v} group multiplication table on page 55 of Koster et al. [67], are presented in Table 2.2(b). Here π and σ polarisations are defined by the E vector of the incident radiation parallel and perpendicular to the three-fold C_3 principal axis z′.

(c) C_s symmetry centres:

For the C_s symmetry group, the electric dipole operator transforms as either the γ_1 (x″,z″) or the γ_2 (y″) of the C_s group.

For the C_s symmetry γ_1 and γ_2 irreps, the C_s group multiplication table on page 33 of Koster et al. [67], gives the selection rules presented in Table 2.2(c). Here π and σ polarisations are defined by the E vector of the incident radiation parallel and perpendicular to the y″ axis of the C_s group. The y″ axis is perpendicular to the x″z″ reflection plane.

Table 2.2: Electric dipole selection rules for even electron systems for:
(a) the C_{4v} group;
(b) the C_{3v} group;
(c) the C_s group.

(a)

C_{4v}	γ_1	γ_2	γ_3	γ_4	γ_5
γ_1	π				σ
γ_2		π			σ
γ_3			π		σ
γ_4				π	σ
γ_5	σ	σ	σ	σ	π

(b)

C_{3v}	γ_1	γ_2	γ_3
γ_1	π		σ
γ_2		π	σ
γ_3	σ	σ	$\pi\sigma$

(c)

C_s	γ_1	γ_2
γ_1	σ_{xz}	π
γ_2	π	σ_{xz}

2.3 Polarisation Behaviour of Electric Dipole Transitions

The electric dipole selection rules, as given in Section 2.2 above, are for an individual centre located at a particular orientation. To obtain the overall polarisation effect for a particular centre having several equivalent orientations, one needs to sum over all the possible orientations of that particular centre with respect to some specified polarisation geometry. It is assumed that there are equal populations of all the possible orientations.

The polarisation geometry shown in Figure 2.2, was used for the measurements here. The nomenclature x(ab)z is adopted where :

x is the direction of the incident laser radiation;

a (= y or z) is the polarisation of the E vector of the incident laser radiation ;

b (= y or x) is the polarisation of the emitted fluorescence radiation;

and z is the direction of propagation of the fluorescence radiation.

The crystals used for polarisation studies are oriented in either the <100> or the <111> geometries as described in Chapter 3. The polarisation ratios predicted for the C_{4v}, C_{3v} and C_s symmetry centres in CaF_2 and SrF_2 type crystals, for even electron systems, are presented in Tables 2.3, 2.4 and 2.5 respectively. The derivations of these polarisation ratios are documented by Reeves et al.[106] for the C_{4v} and C_{3v} symmetry centres and by Khong [63] for the C_s symmetry centres.

Transitions of C_{4v} symmetry centres have well defined polarisation ratios for either <100> or <111> orientations. In contrast, C_{3v} symmetry centres do not have any net polarisation effects in <100> oriented crystals [32]. C_{3v} symmetry centres are therefore studied through the polarisation behaviour of their fluorescence transitions in the <111> orientation in which well defined polarisation ratios are expected (Table 2.4). These predicted polarisation ratios are independent of the direction of the laser beam within the selected <111> plane [32].

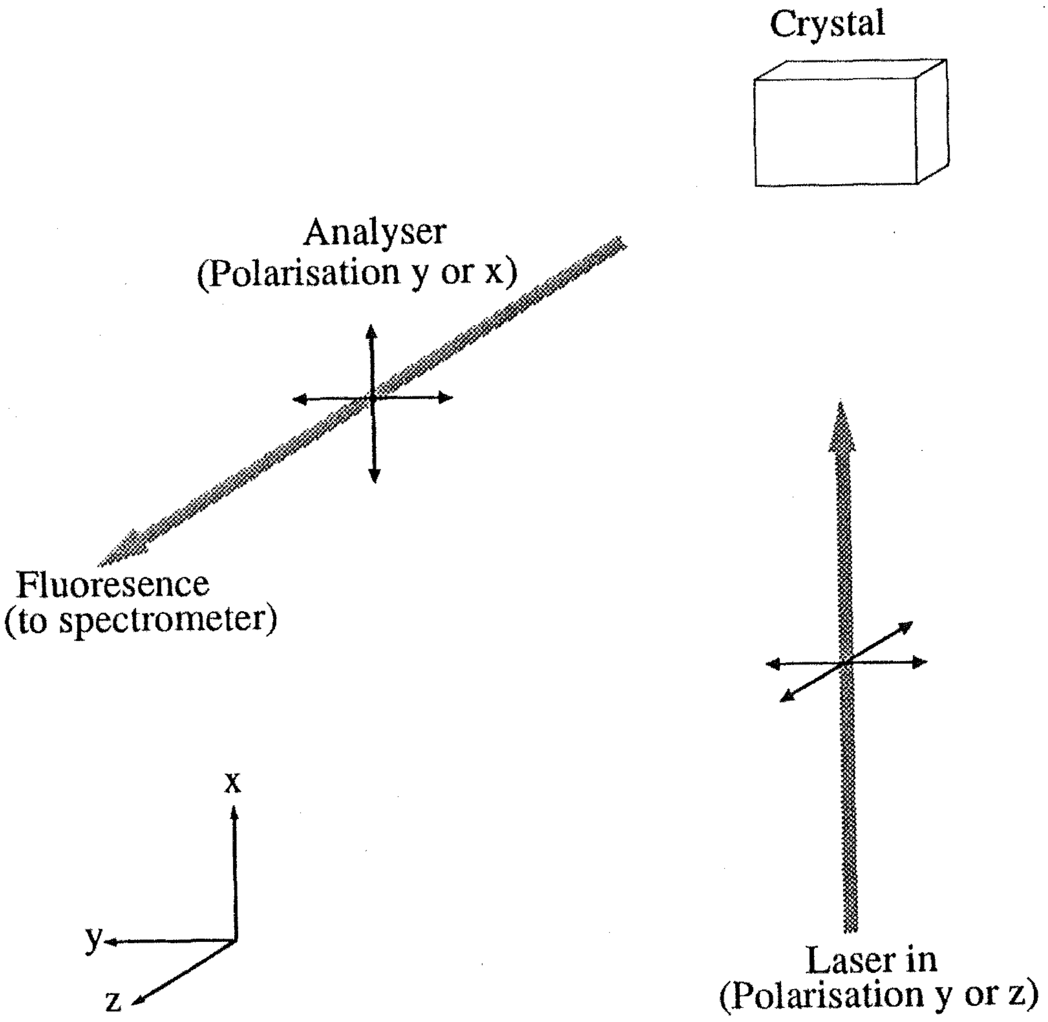

Figure 2.2: Schematic diagram of the experimental geometry adopted for polarisation studies.

Table 2.3: Polarisation intensity ratios predicted for electric dipole transitions for the C_{4v} symmetry centre in <100> and <111> oriented crystals.

		<100> orientation			**<111> orientation**	
Pump transition	**Decay transition**	**x(yy)z**	**x(yx)z**	$\mathbf{x(z\overset{x}{y})z}$	$\mathbf{\frac{x'(y'y')z'}{x'(y'x')z'}}$	$\mathbf{\frac{x'(y'x')z'}{x'(z'x')z'}}$
$\gamma_a \rightarrow \gamma_a$	$\gamma_a \rightarrow \gamma_a$	1	0	0	3	$^1/_2$
	$\gamma_{a'} \rightarrow \gamma_5$	0	1	1	$^3/_5$	$^5/_4$
$\gamma_{a'} \leftrightarrow \gamma_5$	$\gamma_a \rightarrow \gamma_a$	0	1	1	$^3/_5$	$^5/_4$
	$\gamma_{a'} \rightarrow \gamma_5$	2	1	1	$^9/_7$	$^7/_8$

a = 1, 2, 3, 4 or 5

a′ = 1, 2, 3 or 4

Table 2.4: Polarisation intensity ratios predicted for electric dipole transitions for the C_{3v} symmetry centre in <111> oriented crystals.

Pump transition	**Decay transition**	$\frac{x'(y'y')z'}{x'(y'x')z'}$	$\frac{x'(y'x')z'}{x'(z'x')z'}$
$\gamma_a \to \gamma_a$	$\gamma_a \to \gamma_a$	3	2
	$\gamma_a \leftrightarrow \gamma_3$	$^3/_7$	$^7/_8$
	$\gamma_3 \to \gamma_3$	$^3/_7 \to 3$	$^7/_8 \to 2$
$\gamma_a \leftrightarrow \gamma_3$	$\gamma_a \to \gamma_a$	$^3/_7$	$^7/_8$
	$\gamma_a \leftrightarrow \gamma_3$	$^{15}/_{11}$	$^{11}/_{10}$
	$\gamma_3 \to \gamma_3$	$^3/_7 \to {}^{15}/_{11}$	$^7/_8 \to {}^{11}/_{10}$
$\gamma_3 \to \gamma_3$	$\gamma_a \to \gamma_a$	$^3/_7 \to 3$	$^7/_8 \to 2$
	$\gamma_a \leftrightarrow \gamma_3$	$^3/_7 \to {}^{15}/_{11}$	$^7/_8 \to {}^{11}/_{10}$
	$\gamma_3 \to \gamma_3$	arbitrary	arbitrary

a = 1 or 2

Table 2.5: Polarization intensity ratios predicted for electric dipole transitions for the C_s symmetry centres in <100> oriented crystals.

		$C_s(a)$			$C_s(b)$		
Pump transition	**Decay transition**	**$x(yy)z$**	**$x(yx)z$**	**$x(z\overset{x}{y})z$**	**$x(yy)z$**	**$x(yx)z$**	**$x(z\overset{x}{y})z$**
$\gamma_a \rightarrow \gamma_a$	$\gamma_a \rightarrow \gamma_a$	$0 \leqslant \frac{yx}{yy} \leqslant 1$		$0 \leqslant \frac{z\overset{x}{y}}{yy} \leqslant 1$	$0 \leqslant \frac{yx}{yy} \leqslant \frac{1}{2}$		$0 \leqslant \frac{z\overset{x}{y}}{yy} \leqslant \frac{1}{2}$
	$\gamma_a \rightarrow \gamma_b$	$\frac{yx}{yy} \geqslant \frac{1}{2}$		$\frac{z\overset{x}{y}}{yy} \geqslant \frac{1}{2}$	0	1	1
$\gamma_a \rightarrow \gamma_b$	$\gamma_b \rightarrow \gamma_b$	$\frac{yx}{yy} \geqslant \frac{1}{2}$		$\frac{z\overset{x}{y}}{yy} \geqslant \frac{1}{2}$	0	1	1
	$\gamma_b \rightarrow \gamma_a$	2	1	1	1	0	0

a = 1 or 2

b = 2 or 1

From polarisation ratio measurements on suitably oriented crystals, the following deductions can be made about a particular rare-earth ion centre :-

(i) the symmetry of the centre can be established;

(ii) the numbers of transitions observed in both the excitation and fluorescence spectra can be accounted for;

and (iii) irrep labels for the individual energy levels can be determined.

2.4 Electron - Phonon Interaction Effects

Electron - phonon interactions effects are important in rare-earth doped crystal systems in which light ions, hydrogen (H^-) or deuterium (D^-) for example, replace the fluorine (F^-) ions as charge compensators. This interaction then arises from the modulation of the crystal field at the rare-earth ion site by the vibration of the light ions (H^- or D^-).

The coupling between the electronic levels of the rare-earth ion and the local mode vibrational levels of the H^- or D^- ion are revealed in the fluorescence spectra through the presence of local mode vibronic transitions. Local mode vibronic fluorescence transitions occur at energies of the transitions between the electronic levels of the rare-earth ion less the appropriate local mode vibrational energies of the H^- and D^- ion respectively. These usually occur at about 1% of the intensity of the usual electronic transitions. Local mode vibrational energies of H^- ions adjacent to the rare-earth ions are reviewed by Newman [92].

The centre of gravity of the electronic energy levels of the rare-earth ion is lower for the H^- and D^- charge compensated centres compared to the F^- compensated centres. This arises from the change in the covalent bonding between the rare-earth ion and its ligand ions, especially the H^- and D^- ions and also from the changes in the crystal field at the rare-earth ion site for H^- and D^- charge compensation compared to F^- charge compensation. Covalency effects have been shown to give the major contribution to this decrease [56].

2.5 Transition Probabilities and Fluorescence Lifetimes

As discussed earlier in Section 2.1, electric dipole transitions are allowed within the $4f^N$ configuration as a result of the opposite parity admixtures from excited configurations of appropriate parity like $4f^{N-1}$ 5d and $4f^{N-1}$ 5g. The odd - k spherical harmonics $C_q^{(k)}$ in the static or dynamic crystal field are responsible for these admixtures. For ions in non-centrosymmetric sites, these admixtures are contained in the odd - k (odd parity) terms of the crystal-field expansion V_{cf}.

Considering states ϕ_β from opposite parity configurations which have been admixed into the states of the $4f^N$ configuration, the eigenfunctions of the a^{th} level in the $4f^N$ configuration is, to first order, given by

$$|\psi_a> = |\phi_a> - \sum_\beta \frac{<\phi_\beta|V_{cf}^{odd}|\phi_a>|\phi_\beta>}{E_a - E_\beta} \qquad 2.11$$

where $|\phi_a> = |f^N \gamma SLJJ_z>$.

The electric dipole operator P given by

$$\mathbf{P} = -e \sum_{q,i} r_i (C_q^{(1)})_i , \qquad 2.12$$

with components $P_\varrho = -e \sum_i r_i(C_\varrho^{(1)})_i$ for $\varrho = 0, \pm 1$, has matrix elements between the states $|\psi_a>$ and $|\psi_b>$ of the form :

$$<\psi_a|\mathbf{P}|\psi_b> = \sum_\beta \left[\frac{<\phi_a|\mathbf{P}|\phi_\beta><\phi_\beta|V_{cf}^{odd}|\phi_b>}{E_b - E_\beta} + \frac{<\phi_a|V_{cf}^{odd}|\phi_\beta><\phi_\beta|\mathbf{P}|\phi_b>}{E_a - E_\beta} \right] . \qquad 2.13$$

The evaluation of these matrix elements is hindered by lack of knowledge of the odd-k terms of the crystal field and the energy levels of the excited configuration. However, by adopting the Judd [59] and Ofelt [94] approach which is based on the assumptions that

(i) all excited configuration levels are degenerate with respect to all the quantum numbers except n and ℓ so that summation over β can be carried out (closure of equation 2.13);

(ii) both the energy denominators $E_b - E_\beta$ and $E_a - E_\beta$ can be approximated by a common average energy denominator ΔE_{av}.

The matrix elements can then be written as

$$< \psi_a | \mathbf{P}_\varrho | \psi_b > = \sum_{q,\lambda \text{ even}} Y(\lambda,q,\varrho) < f^N \gamma SLJJ_z | U^{(\lambda)}_{\varrho+q} | f^N \gamma' SL'J'J'_z > \tag{2.14}$$

where the energy denominator ΔE_{av}, the odd - k crystal-field parameters and the radial integrals are all incorporated into the parameters $Y(\lambda,q,\varrho)$. The $C^k_q | \phi_\beta > < \phi_\beta | C^{(1)}_\varrho$ are equivalent to $U^{(\lambda)}_{\varrho+q}$ (λ even).

The line strength S of a radiative transition from level a to level b, defined as the square of the electric dipole matrix elements for spontaneous transition probabilities, is therefore given by

$$S = | < \psi_a | \mathbf{P} | \psi_b > |^2 \tag{2.15}$$

and the spontaneous electric dipole transition probability W^R_{ab}, is of the form :

$$W^R_{ab} \, \alpha \, S$$

and therefore

$$W^R_{ab} \, \alpha \, \Big| \sum_{q,\lambda \text{ even}} Y(\lambda,q,\varrho) < f^N \gamma SLJJ_z | U^{(\lambda)}_{\varrho+q} | f^N \gamma' SL'J'J'_z > \Big|^2 . \tag{2.16}$$

The radiative decay time τ^R_{ab} for transitions from a level a to all the terminal levels b, is of the form

$$\frac{1}{\tau^R_{ab}} = \sum_b W^R_{ab} . \tag{2.17}$$

CHAPTER 3

EXPERIMENTAL

3.1 Crystal Preparation

Most of the crystals used in this study were grown by the author. For the CaF_2 and SrF_2 type crystals, a A.D. Little 38 KW radio frequency induction furnace was used while a Department built two-zone variable-gradient Bridgman furnace was used for growing the $CsCdBr_3$ type crystals. Both furnaces employ the Bridgman-Stockbarger technique of lowering the molten starting material through a temperature gradient.

A further two SrF_2:Ho^{3+} crystals with Ho^{3+} concentrations of 0.005% and 0.1% respectively, were purchased from Optovac Inc. for use as reference samples for the study of the additional centres found in SrF_2:Ho^{3+} crystals.

The crystal growing procedures will now be briefly described.

3.1.1 Fluorite type crystals

The starting material comprised CaF_2, SrF_2 and BaF_2 off-cuts supplied by Optovac Inc. and 99% pure HoF_3 obtained from Alfa Inorganics Inc.. For the crystals used for this study, the 10 to 12 g of off-cuts used for growing each crystal were crushed to smaller pieces. HoF_3 concentrations in the range 0.0005% to 0.1% were generally added with the 0.005% and 0.01% concentrations being used mostly for the CaF_2 and SrF_2 type crystals respectively, whose laser selective excitation spectra are presented here. The measured rare-earth and alkaline-earth fluorides were placed in a graphite crucible with a tight fitting lid. The graphite crucible had a bore 10 mm in diameter and 40 mm deep. The crucible was then mounted centrally within a graphite cylinder inside the R.F. furnace. Between the graphite cylinder and the induction coil of the furnace was a layer of Union Carbide Fibrefrax insulation of 96 kg/m^3 density.

The chamber of the furnace was evacuated to less than $2x10^{-5}$ torr before power was turned on. The furnace was then left at power settings of 0.6 A and 1.4 KV for at least four hours in order to bake out any moisture that may have accumulated while the starting material was being mounted. After this period, the power was then gradually increased to 2.0 A and 3.1 KV for CaF_2 or 2.2 A and 3.2 KV for SrF_2 type crystals, while monitoring the pressure in the chamber. Once the required power settings had been attained, the crucible was lowered through the temperature gradient at either 3.5 mm/h or 2.5 mm/h. The slower rate was adopted for growing crystals to be used for polarisation studies as such crystals resulted in better oriented samples. Crystals to be used for the general spectroscopic measurements were lowered at the faster rate of 3.5 mm/h. Growth times were either 24 or 30 hours depending on which of the two lowering rates was chosen. At the end of the growth period, the power was gradually reduced over a period of three hours. A mechanical device (installed during the second half of this study) automatically started winding the power down once the crucible reached the bottom of the furnace. The crystals obtained had up to 30 mm long usable sections.

For unoriented samples, 2 - 3 mm thick discs were cut off using a rotary diamond saw. These were then polished using Carborundum abrasive paper grades P280, P800 and P1200 in succession. Carborundum silicon carbide grain GRIT No. 800 mixed with a little water to make a paste was then used for an optical finish.

Samples to be used for polarisation studies had to be oriented in either the <100> or the <111> directions. As CaF_2 and SrF_2 crystals cleave along the (111) planes, these were used as the reference planes for the crystal orienting process. A cleavage plane was found by chipping off small bits from the edge of the crystal until the characteristic cleavage surface was identified. Once one such surface had been obtained, the second cleavage plane was easily identified as two cleavage planes intersect at an angle of 109.7° along a <110> axis. A brass rod having a wedge at this angle was found useful for identifying the second cleavage plane. Having identified the two intersecting cleavage planes, the crystal could be either <100> or <111> oriented as required.

For <100> oriented samples, the two intersecting (111) planes were glued into the fitting wedge of the brass rod using araldite epoxyl resin glue (from Ciba-Geigy) and left overnight to set. The brass rod was then tightly clamped to the diamond saw bench with the crystal aligned such that the <110> axis was parallel to the surface and perpendicular to the cutting edge of the blade.

Taking the axis of the brass rod perpendicular to both the surface of the blade and the <110> axis of the crystal as the zero angle (0°), the rod was rotated by a swivel joint through +45° and -45°, with a cut through the crystal being made at each angle. The new surfaces intersect at 90° and define the (100) planes of the crystal. Samples of 2 - 3 mm thicknesses were then cut parallel to one of the (100) planes to give two parallel (100) planes and a third, perpendicular. This third (100) face was reserved for laser entrance while the two parallel faces were for observation of the resulting fluorescence. Again a laser exit face had to be ground, using the P280 abrasive paper, parallel to the entrance face. The samples were then polished, with great care so as not to alter the orientation.

For <111> oriented samples, 2 - 3 mm thick slices were chipped off parallel to one of the (111) planes. This gave samples with two parallel (111) faces and a third (111) face at an angle of 109.7° to be used as the entrance face for the laser beam. An exit face for the laser beam had to be ground and polished using the abrasive paper and silicon carbide grain. The cleaved (111) surfaces did not need any polishing.

3.1.2 $CsCdBr_3$ crystals

Starting materials for $CsCdBr_3$ crystals were 99.9% pure CsBr obtained from Aldrich Chemical Company Inc. and 99% pure $CdBr_2$ from Hopkins and Williams. The dopants were Ho_2O_3(99.9% pure) from Semi-elements Inc. and NaBr(c.p. grade) from Riedel-De Haen. An oxide had to be used for the rare-earth dopant as the bromide was not available, but this would then be converted to a bromide during the HBr treatment described below. The chemicals were dried by baking in a vacuum oven for at least two days before use.

The U-shaped tube as in Figure 3.1, was made from 8 mm internal diameter Pyrex glass tubing. The tube has a 2 mm wide constriction about 15 mm from the tip. This is so that as the tube passes through the temperature gradient the molten starting mixture starts to crystallise at the pointed tip, many small crystals form in the bulb but only a single crystal grows past the constriction. Consequently while the material in the bulb part of the tube is in poly-crystalline form, the rest of the boule is made up of a single crystal. The U-shaped glass tube was dried overnight in a hot oven.

For $CsCdBr_3:Ho^{3+}$ crystals, Ho^{3+} concentrations of 0.01%, 0.1% and 0.3% were used while for $CsCdBr_3:Ho^{3+}:Na^+$ crystals the two crystals grown had $0.3\%Ho^{3+}:1\%Na^+$ and $0.05\%Ho^{3+}:0.2\%Na^+$ concentrations respectively. The Na^+ concentration was always higher to ensure preferential formation of Ho^{3+} - Na^+ pair centres.

Stoichiometric quantities of the starting chemicals were mixed and dried using the technique developed by Mr R. Ritchie of the Department. In this procedure, the chemicals are added to the sieve end of the U-shaped tube as shown in Figure 3.1. Hydrogen bromide (HBr) gas, pre-bubbled through concentrated sulphuric acid to dry, is allowed to flow through the mixture. Initially taps 1 and 2 of Figure 3.1 are closed while taps 3 and 4 are open, allowing the dry HBr gas to flow along the direction shown by the solid arrow in Figure 3.1. The electric furnace is then turned on and, through the furnace controller, set to heat up to 560 °C in $2\frac{1}{2}$ hours. This ensures that the chemicals are well dried in an HBr gas atmosphere before melting. At the end of the $2\frac{1}{2}$ hour period, the temperature is held at 560 °C for a further 30 minutes with the HBr gas bubbling through the molten mixture. The part of the glass tube below the furnace is then warmed up using a gas torch so that the molten mixture would trickle down to the

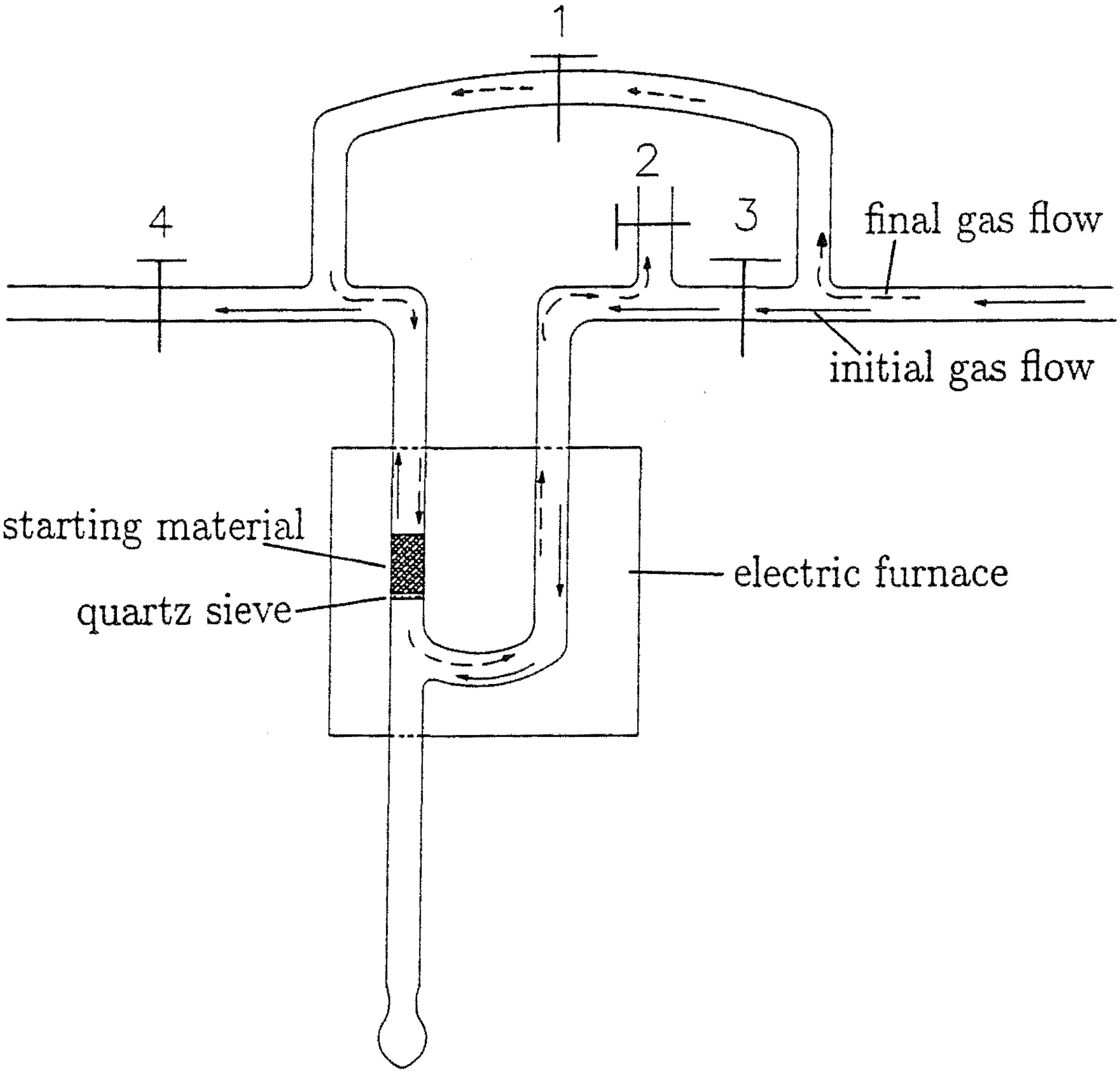

Figure 3.1: Set-up for mixing and drying the chemicals for growing $CsCdBr_3$ crystals.

bottom of the tube rather than solidify mid-way down the tube as it cools. To reverse the gas flow, taps 1 and 2 are opened and taps 3 and 4 closed so that the gas flows through the mixture as shown by the dashed arrows in Figure 3.1. This forces the molten mixture to trickle through the sieve to the bottom of the tube. Any that solidifies before reaching the bottom is melted with the gas torch before the ampule is carefully sealed off just above the mixture.

For the crystal growth, a Department built two-zone variable-gradient Bridgman furnace had its "cool" and "hot" zone temperatures set to 330 °C and 520 °C respectively. The temperatures took up to 10 minutes to stabilise. A motor was then set to lower the sealed off ampule through the temperature gradient at the rate of 0.86 mm/h. The growth period was 8 - 10 days, after which the crystal was annealed using the two-stage temperature control. Firstly, the "hot" zone temperature (520 °C) was lowered to match the "cool" zone temperature(330 °C) over a period of 15 hours. Both zone temperatures were then lowered from 330 °C to room temperature over 14 hours. Usable crystals of up to 30 mm in length were obtained.

Although $CsCdBr_3$ is not appreciably hygroscopic, the crystals were kept in a dry box in which the humidity was kept below 20% with drying pellets. As $CsCdBr_3$ crystals cleave easily in (1110) planes, samples for use were generally cleaved off the boule. The crystals are too soft and brittle to be easily polished.

3.2 Deuteration Treatment of the Fluorite Crystals

The Hall and Schumacher [44] method of hydrogenation was used with deuterium (D_2) gas. This involves heating a crystal in contact with aluminium metal in temperatures of up to 900 °C in a few cm of Hg pressure of D_2 for a set period of time. For their hydrogenated CaF_2 crystals, Hall and Schumacher [44] reported obtaining interstitial hydrogen ion densities of up to $10^{19}/cm^3$ by this method.

For the deuteration of crystals used in this study, flat coils of aluminium wire were wound to place against both surfaces of a polished crystal. Thin crystals of 1 - 1.5 mm thickness were deuterated so as to have a uniform D^- content across the whole width of the crystal. Thicker crystals tended to develop a D^- gradient with more towards the surfaces than in the centre of the crystal. Both the coils and the crystal were carefully cleaned with acetone before the crystal was inserted between the coils making sure that there was contact between the crystal and the aluminium coils. The crystal and coils assembly was then placed in a clean alumina crucible which was gently lowered to the bottom of a quartz tube. The quartz tube was placed centrally in an electric furnace and evacuated for a few hours using a vacuum backing pump. The furnace was then set to 100 °C and left for about 6 hours to remove any traces of water vapour. After this drying period, a mercury diffusion pump was used to attain a vacuum of better than 10^{-4} torr. Dry deuterium gas was then flushed through the system twice before a partial pressure of 20 mmHg of D_2 gas was introduced and the tube sealed off. The temperature of the furnace was then gradually raised to 850 °C over a period of $2\frac{1}{2}$ hours and maintained at this temperature for the desired duration of the deuteration period. The deuteration periods for the crystals measured here were between 4 and 24 hours.

At the end of the deuteration period, the crystals were quickly quenched to room temperature, by removal of the furnace whilst still at 850 °C, to minimise formation of cluster centres during cooling. Fragments of aluminium wire attached to the surface of the crystal during the deuteration process were etched off with dilute hydrochloric acid. The samples were then lightly polished again, using the P1200 abrasive paper and silicon carbide grain.

3.3 Cryogenic Aspects

The results reported here were performed at crystal temperatures ranging from 2 K to 77 K with most of the measurements being done at 10 K. Two types of cryostats were used, one covering temperatures from 10 K upwards while the other used liquid helium at 2 K. These are now separately discussed.

3.3.1 Closed-cycle cryostat

For the 10 K to 77 K experiments, a CTI-Cryogenics Model 21C Cryodyne two-stage closed-cycle conducting type cryostat with a water cooled compressor unit was used. Two types of crystal holders were used with this cryostat depending on whether optical absorption or laser selective excitation experiments were to be performed.

As absorption measurements require thicker samples than for laser spectroscopy, the crystal holder for optical absorption studies comprised a copper block 40 mm long and 15 mm wide attached to a circular copper plate by a shaft 10 mm long . The copper plate matched the cold head of the cryostat. This type of holder enabled samples of the same crystal of up to 40 mm thick to be mounted at the same time. For the laser spectral experiments, the crystal holder comprised a copper block 40 mm long and 15 mm wide attached to a circular copper plate which matched the cold head of the cryostat. The holder had two slots 4 mm wide and 14 mm apart and a single crystal could be mounted across each slot. Fluorescence could be observed from either side of, and at right angles to, the block.

Indium foil was used on both holders, between the samples and the copper block and between the circular copper plate and the cold head of the cryostat, to improve thermal contact. This was especially important for the Ho^{3+} work reported here as some new spectral lines started to appear at crystal temperatures of about 15 K. The temperature of the sample, as measured by a silicon diode attached to the base of the cold head, was monitored and controlled by a Palm Beach Cryophysics Inc. Model 4025 Cryogenic Thermometer/Controller. The base temperature of 9.5 K was usually attained in 40 minutes and the temperature of the sample could be raised by means of a heating element. When changing the crystal temperature to a new setting, say from 10 K to 20 K, 15 - 20 minutes was allowed for after the controller had reached that set temperature, for the crystal to reach thermal equilibrium.

3.3.2 Liquid helium cryostat

For the experiments conducted at liquid helium temperature a glass dewar as shown in Figure 3.2 was used, with the samples directly immersed in the superfluid helium. The dewar built in the Department is based on a design from Dr N.B. Manson of the Laser Physics Centre, Australian National University. Modifications were made to the liquid helium fill and sample rod access lines.

For the dewar built here, as shown in Figure 3.2, the helium fill line and sample rod were combined. The helium fill tube has small holes towards the bottom. The helium transfer tube fitted inside the fill tube and the liquid would trickle down the tube and out through the small holes into the glass dewar. The sample holders were thin (1 mm thick) copper plates 22 cm long and 11 mm wide attached to a brass rod. The end of the brass rod screwed onto the bottom of the helium fill tube. The copper plate had two circular slots 5 mm in diameter and 5 mm apart. Samples were glued across the slots with aeroldite glue. For absorption studies, samples could be glued across the whole width of the copper plate. The sample rod assembly could be moved up and down to access either sample with the optical beam.

The outer jacket of the dewar was evacuated over a period of at least 6 hours before being closed off. With the sample mounted and the inner chamber sealed, the outer chamber was filled with liquid nitrogen for periods ranging from 4 - 12 hours, prior to liquid helium being transferred to the dewar. The helium was then pumped to its super fluid state in about 5 minutes, with a Dynavac 450 ℓ/min pump.

The dewar has a 5ℓ capacity and, once pumped to superfluid state, the helium lasted for 5 - 6 hours. Refilling tended to cloud the windows and so the dewar was normally left to warm up to room temperature before another liquid helium transfer could be made. The outer jacket was evacuated before each

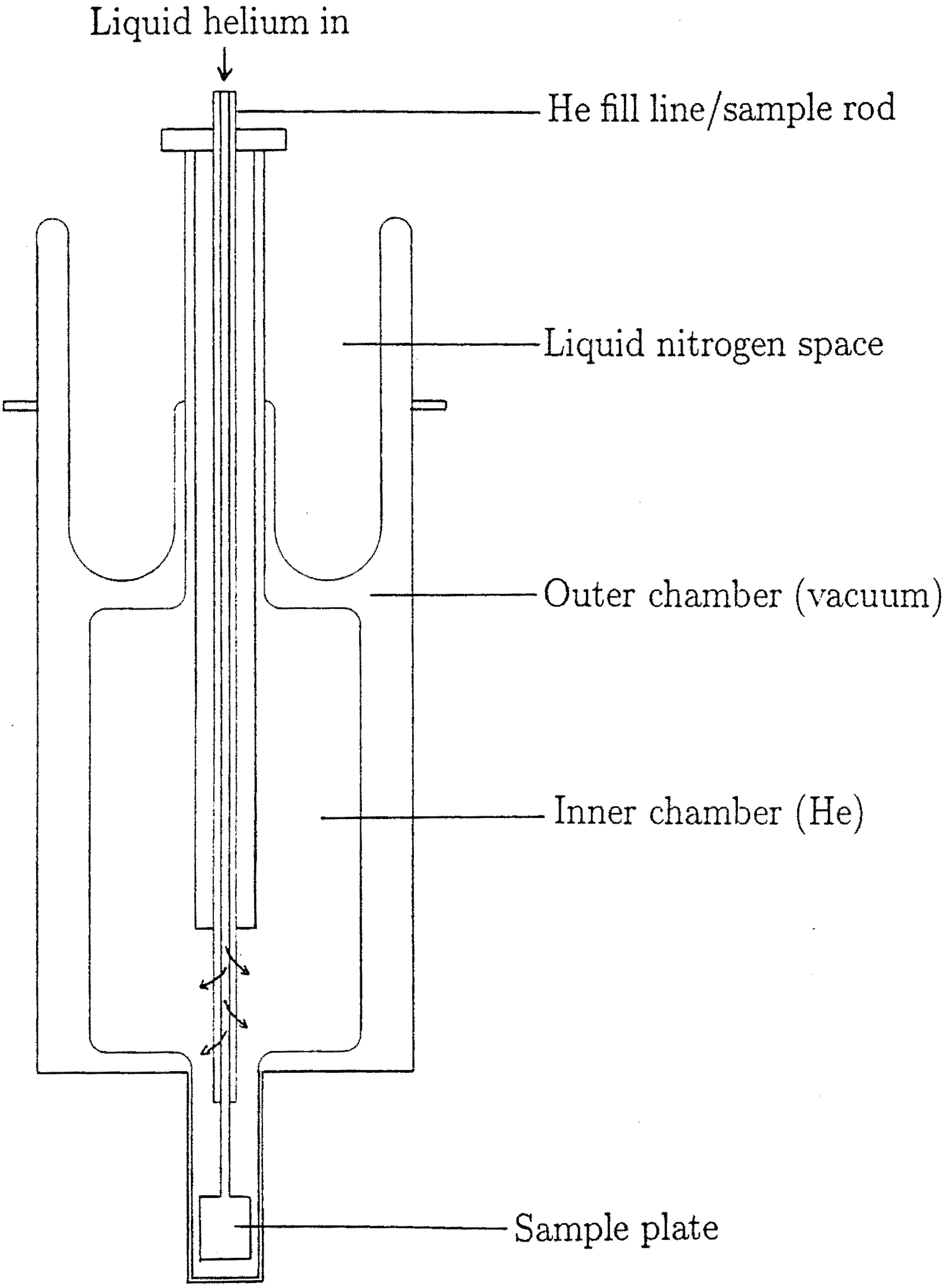

Figure 3.2: The immersion type liquid helium dewar.

helium usage.

3.4 Optical Absorption Spectral Techniques

For absorption spectroscopy a 100 W Tungsten halogen lamp with a 12 V regulated power supply was used as the light source. The absorption spectra were recorded photo-electrically using a Spex 1700 0.75 m single monochromator equipped with an EMI 9558 S20 photomultiplier tube. The photomultiplier tube was thermo-electrically cooled to -25 °C by a Products for Research Inc. Model TE-104 cooler. Output from the photomultiplier tube, as measured by a Keithley Instruments 610B electrometer, was passed through a Department-built active filter and variable offset device before being plotted out by a Sekonic SS250F chart recorder.

For the results presented here, crystal thicknesses of 10 - 30 mm were used for a satisfactory signal to noise ratio. Spectrometer slit widths of 45 - 60 μm were needed, and for a more uniform spectral response, the scrambler in front of the entrance slit of the spectrometer was removed.

3.5 Laser Selective Excitation Spectral Techniques

For the first half of this work, a Spectra Physics Model 171 15 W argon ion laser with a Model 270 exciter was used as the excitation source. Later, a Spectra Physics Model 2045E 15 W argon ion laser with a Model 2570E supply was installed. Argon laser powers in the range 1.5 - 5 W were used to pump a Spectra Physics model 375 dye laser. Two dyes, Coumarin 540 and Rhodamine 640 perchlorate, obtained from Exciton Chemical Company Inc. were used for the spectroscopic results presented here. The Coumarin 540 dye has a lasing range of 18100 - 19200 cm^{-1} when excited by the 488 nm laser line while the Rhodamine 640 dye lases in the range 14950 - 16100 cm^{-1} with excitation from the 514.5 nm argon laser line. These dye ranges cover the absorption spectral regions of the $E(^5S_2,^5F_4)$ and $D(^5F_5)$ multiplets respectively, of the Ho^{3+} ion.

For the Coumarin 540 dye typical output powers were in the range 18 - 60 mW. During the first 100 hours of dye use, an input laser power in the 3 - 3.5 W range would give an average of 50 mW of dye laser output power. Thereafter only 15 - 25 mW could be achieved for argon laser powers of up to 5 W. After about 150 hours of operation, 10 - 20 drops of cyclo-octatatraene(COT) (from Exciton Chemical Company) had to be added to the dye to improve the output power. The COT increased the dye laser power by 20 - 40 % for periods of up 30 hours of use. Dye changes were made after every 250 - 300 hours of use.

The Rhodamine 640 dye gave more output power than the Coumarin 540 dye. For the measurements presented here, dye laser output powers of 100 - 120 mW were used and this required only 1.5 W of argon laser input power. The dye also lasts longer than the Coumarin 540 dye.

A birefringent filter rotated by a model 375 stepper motor unit allowed the dye range to be scanned in small steps of 0.5 cm^{-1}. The drive unit gave dye energy positions reproducible to within 0.2 cm^{-1} for successive scans. The output from the dye laser had a linewidth of 0.5 cm^{-1} and a frequency drift of up to $\pm$ 1 cm^{-1} over 12 hours.

With crystals mounted for laser experiments, as set out in Section 3.3, one of two types of spectra could be recorded from the fluorescence observed in opposite directions perpendicular to the crystal. The first type of spectra, known as laser excitation (broadband) spectra were recorded using the Spex 1700 0.75 m single monochromator and EMI 9558 S20 photomultiplier tube. The Spex 1700 monochromator, set to zero order and equipped with Corning glass filters CS2-59, CS2-60, CS2-61 or CS2-64, was used to monitor all the fluorescence from the $D \rightarrow Z$ transitions in the 15000 cm^{-1} region. The output from the photomultiplier tube was displayed on the 610B electrometer and, through a voltage to frequency converter, was recorded on a frequency counter.

The second set of spectra to be measured were laser excited fluorescence spectra, for which a Spex 1403 0.85 m double monochromator and an RCA 31034 photomultiplier tube were used. The photomultiplier tube was thermo-electrically cooled to -25 °C. Depending on the intensity of the fluorescence being measured, slit widths of 10 - 200 μm were mostly used. The output from the photomultiplier tube was passed through a Princeton model 1121 amplifier/discriminator unit before being displayed on the Princeton Applied Research model 1112 photon counter.

Collection, display and storage of data was controlled by an Apple IIe microcomputer. The signal output from either the frequency counter (for broadband spectra) or the photon counter (for laser excited fluorescence spectra) was displayed on the computer screen, stored on floppy discs and plotted out by a Hewlett Packard HP7475A plotter.

For polarisation measurements, the configuration as in Figure 2.2 was used. The polarisation of the E vector of the laser could be changed between the y and z directions with a Spectra Physics 310 polarisation rotator. A polaroid sheet mounted between the collimating and focussing lenses (for the fluorescence detection) was used as the analyser. By rotating the polaroid sheet to the y or x directions as shown in Figure 2.2, the polarisation of the fluorescence to be measured could be chosen. Although the general nomenclature x(ab)z, where :

x is the direction of incidence of the laser;

a (= y or z) is the polarisation of the E vector of the laser;

b (= y or x) is the polarisation of the fluorescence;

and z is the direction of propagation of the fluorescence,

is usually adopted for describing the polarisation geometry, the (ab) only notation is used for all the results to be presented here, as x and z are the same throughout. Therefore, polarisation ratios are simply recorded as yy : yx rather than x(yy)z : x(yx)z.

3.6 Fluorescence Lifetime Measurements

For fluorescence lifetime measurements, a PRA model LN1000 nitrogen laser was used to excite a PRA model LN107 dye laser, both from Photochemical Research Associates Inc.. The dye laser was driven by a DD1790 drive unit. The nitrogen laser was specified to have an average energy of 1.1 mJ per pulse at 337.1 nm and a pulse duration of 800 ps while the dye laser was specified as having an average energy per pulse of 115 μJ.

The various dyes used for excitation of several Ho^{3+} multiplets as discussed in Chapter 8 are as follows :-

Dye	**Dye range(nm)**	**Ho^{3+} multiplets excited**
Rhodamine 640	620 - 670	D ($^5F_5$)
Coumarin 540A	520 - 580	E ($^5S_2$, $^5F_4$)
Coumarin 481	460 - 510	F($^5F_3$)
Stilbene 420	400 - 470	J ($^5G_5$)

The Spex 1700 0.75 m single monochromator and EMI 9558 S20 photomultiplier tube were used to record the fluorescence, with the spectrometer set to monitor a specific transition for a particular centre. The output from the photomultiplier tube was recorded by a Hitachi model VC 6275 digital storage oscilloscope triggered by the nitrogen laser pulse as monitored by an RCA 931A S11 photomultiplier tube. With an appropriate terminating load, the digital storage oscilloscope was used to average 256 sweeps of the whole transient.

A GW BASIC program written by K. Murdoch and updated by P. Wells of the Department was then used to transfer the resultant transient from the digital storage oscilloscope to an IBM PC microcomputer and store the data on floppy discs.

CHAPTER 4

SPECTROSCOPY OF Ho^{3+} IONS IN CaF_2 TYPE CRYSTALS

The first reported laser selective excitation study of CaF_2:Ho^{3+} was performed by Seelbinder and Wright [117]. Spectral and temporal measurements were presented for the two major single Ho^{3+} ion centres (labelled A and B) identified. Spectral measurements covered both absorption and fluorescence transitions between the $^5I_8$ and each of the $^5F_5$, $^5S_2$, $^5F_4$, $^5F_3$, $^3K_8$, $^5F_1$ and $^5G_6$ multiplets and fluorescence transitions between the $^5S_2$ and $^5I_7$ multiplets. Fluorescence lifetime measurements were also presented for transitions from the D($^5F_5$), E($^5S_2$) and F($^5F_3$) multiplets of both the A and B centres. Cluster centres in CaF_2:Ho^{3+}(0.2%) crystals, both pure and double doped with Ho^{3+} and Er^{3+}, were also studied through upconversion and pair interactions between similar and dissimilar ions. As the energy levels of Ho^{3+} and Er^{3+} lie in the same spectral region for most of the multiplets, it was difficult to discriminate between the transitions of Ho^{3+} - Er^{3+}, Ho^{3+} - Ho^{3+} and Er^{3+} - Er^{3+} centres. In such cases time resolved studies were sometimes helpful as the mixed Ho^{3+} - Er^{3+} centres were found to have much shorter fluorescence lifetimes than Ho^{3+} ion centres.

EPR measurements at 4.2 K on the tetragonal symmetry (A) centre in CaF_2:Ho^{3+}(0.1%) crystals were performed by Kornienko and Rybaltovskii in 1972 [66]. Using a microwave source in the range 70 - 75 GHz, a ground state splitting of 50.8 GHz was determined for the A centre. A more recent measurement of 60 GHz was reported by Hasan [47] from high resolution laser measurements.

Campbell [24] measured this ground state splitting to be 1.85 ± 0.2 cm^{-1} from the far infrared absorption spectrum of a 48 mm thick CaF_2:Ho^{3+}(0.05%) crystal.

Although the CaF_2:Ho^{3+} system has been studied in some detail as outlined above, energy levels for the two known single Ho^{3+} - F^- centres (A and B) have not yet been derived from the reported transition energies [117], nor have the symmetry irrep labels of the various Ho^{3+} energy levels been established. The site symmetries of the Ho^{3+} ions in these two centres were proposed [117] to be tetragonal and trigonal for the A and B centres respectively, on the basis of the similarity of the spectra of these centres to those of the corresponding Er^{3+} centres [122], but without definitive proof being given. A consequence of this is that, until recently [109], it was not known whether the ground state of Ho^{3+} in the A centre is a doublet or singlet level. Irrep label assignments made by the study reported here have helped explain the hyperfine structures observed for this centre [81]. The first section (4.1) of this chapter is mainly directed at (i) using polarisation measurements to substantiate earlier site symmetry assignments for the A and B centres, (ii) deriving energy levels for these two centres and (iii) assigning irrep labels to the various crystal-field energy levels derived.

As this work is concerned with the study of the spectroscopy of just the single Ho^{3+} ion centres, low Ho^{3+} dopant concentration of no more than 0.005% was chosen in order to have minimal formation of cluster centres. An understanding of the behavior of single ion centres is a prerequisite for the future study of cluster centres.

Additionally, results from a study of $CaF_2{:}Ho^{3+}$ crystals containing 1% of SrF_2 or BaF_2 are also presented with model assignments for the two new centres observed for each system. Although the results presented here for these mixed crystal centres are for 1% of Sr^{2+} and Ba^{2+}, the two centres were observed at lesser strength for dopant alkaline-earth concentrations down to 0.1%. The 1% concentration was chosen as it gave spectral lines of sufficient intensity for detailed study. Comparisons are made between these new centres and the A centre, as well as between the new centres themselves.

In Section 4.5, results from a study of deuterated $CaF_2{:}Ho^{3+}$ crystals are also presented. Although attempts to identify the exact D^- analogue of the F^- A centre were unsuccessful, two low symmetry D^- centres of A centre parentage and the D^- analogue of the B centre were found and their spectroscopy is described.

4.1 Spectroscopy of CaF_2:Ho^{3+} Crystals

Absorption Spectra

The most straight forward way of determining the distribution and relative concentrations of the various centres present in a given crystal system is by optical absorption spectroscopy. It is however necessary to systematically vary both the dopant concentration and crystal thickness in order to obtain transitions with a good signal to noise ratio.

For CaF_2:Ho^{3+}, a dopant concentration of 0.02% in 10 mm thick samples was found to give sufficiently intense and narrow absorption features representative of the two single Ho^{3+} ion centres (A and B) present in the low concentration Ho^{3+} crystals (Figure 4.1). The absorption lines were found to be ten times stronger for the transitions to the ${}^5S_2$,${}^5F_4$ multiplets in the 535 nm region compared to transitions to the ${}^5F_5$ multiplet in the 640 nm region.

Laser Selective Excitation Spectra

Laser excitation spectra in both the 18000 and 15000 cm^{-1} regions were obtained with monitoring all of fluorescence transitions in the 15000 cm^{-1} region simultaneously. These so-called broadband laser selective excitation spectra display the same features as the corresponding absorption spectra (Figures 4.2(a) and 4.3(a)). The transitions maintain the same relative intensities for Ho^{3+} concentrations over the range 0.0005% to 0.02%. Centres present for such low Ho^{3+} concentrations were attributed to single Ho^{3+} - F^- centres by Seelbinder and Wright [117], henceforth referred to as [SW]. A Ho^{3+} concentration of 0.005% was chosen for the laser selective excitation work reported here.

By laser selective excitation with monitoring of specific Ho^{3+} transitions, all observed transitions were found to belong to one of two centres denoted A and B, following the identifications of [SW]. The relevant excitation spectra are shown in Figures 4.2 (b),(c) and 4.3 (b),(c) for the $Z \rightarrow E$ and $Z \rightarrow D$ transitions respectively.

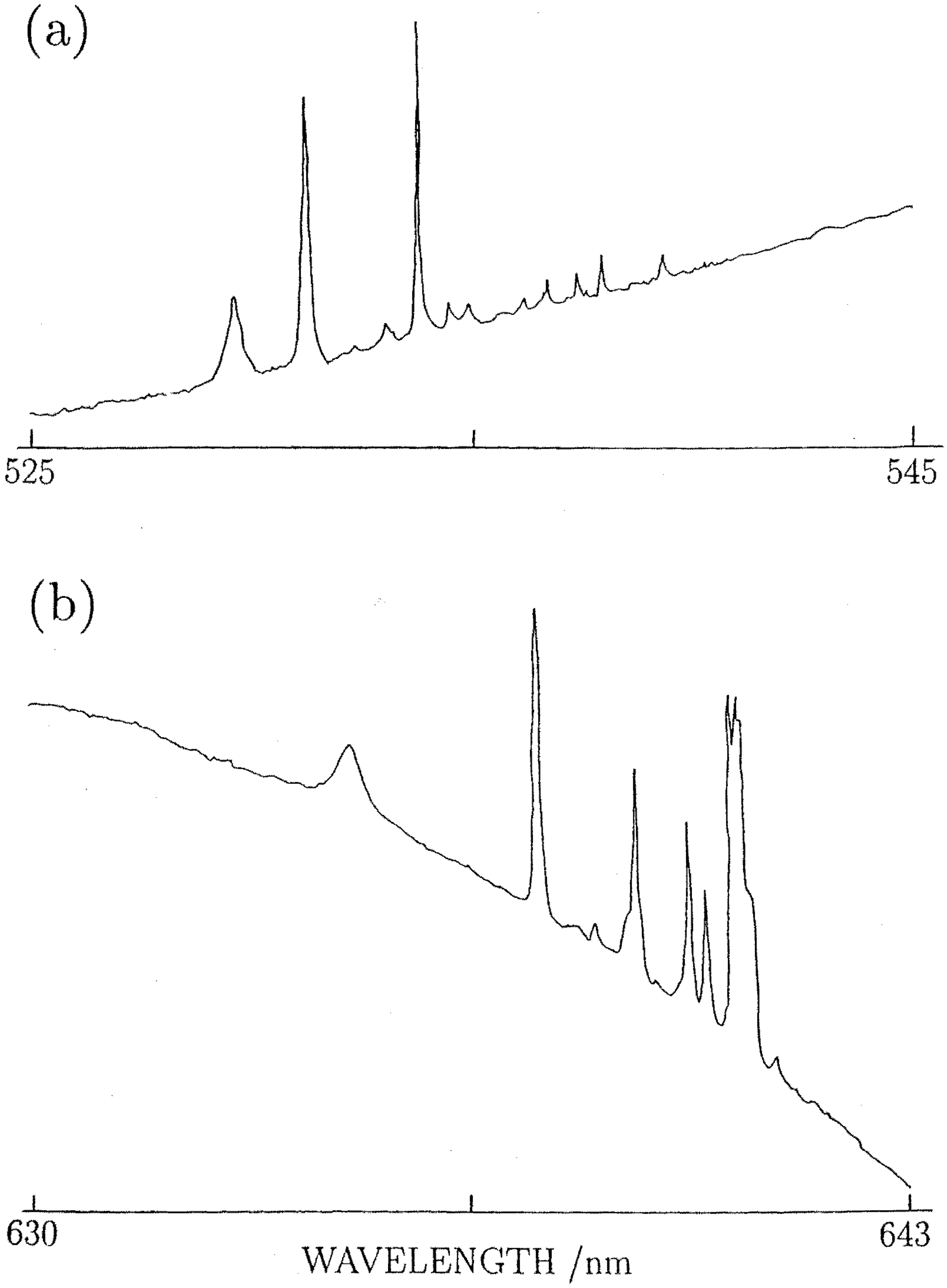

Figure 4.1: 10 K absorption spectra in $CaF_2:Ho^{3+}$ (0.02%) crystals :
(a) Z→E transitions;
(b) Z→D transitions.

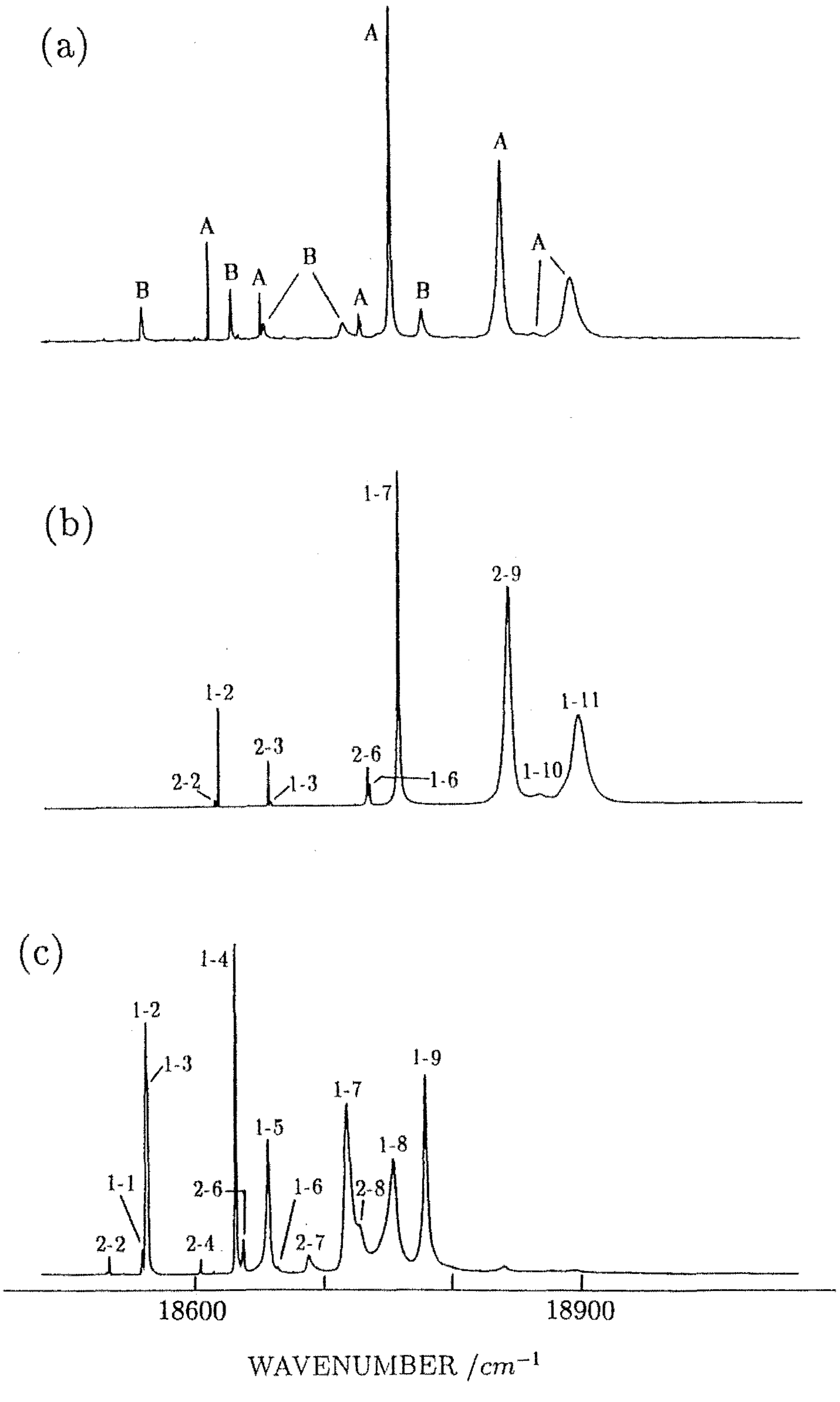

Figure 4.2: 10 K broadband and selective excitation spectra of the E multiplet in CaF_2:Ho^{3+}(0.005%) crystals :
(a) broadband excitation spectrum, monitoring all the D→Z transitions;
(b) A centre excitation spectrum, monitoring the $E_1 \rightarrow Z_4$ transition at 18483.5 cm^{-1};
(c) B centre excitation spectrum, monitoring the $E_2 \rightarrow Z_3$ transition at 18504.5 cm^{-1}.
Transitions are labelled by the appropriate lower and upper multiplet crystal-field level identifications.

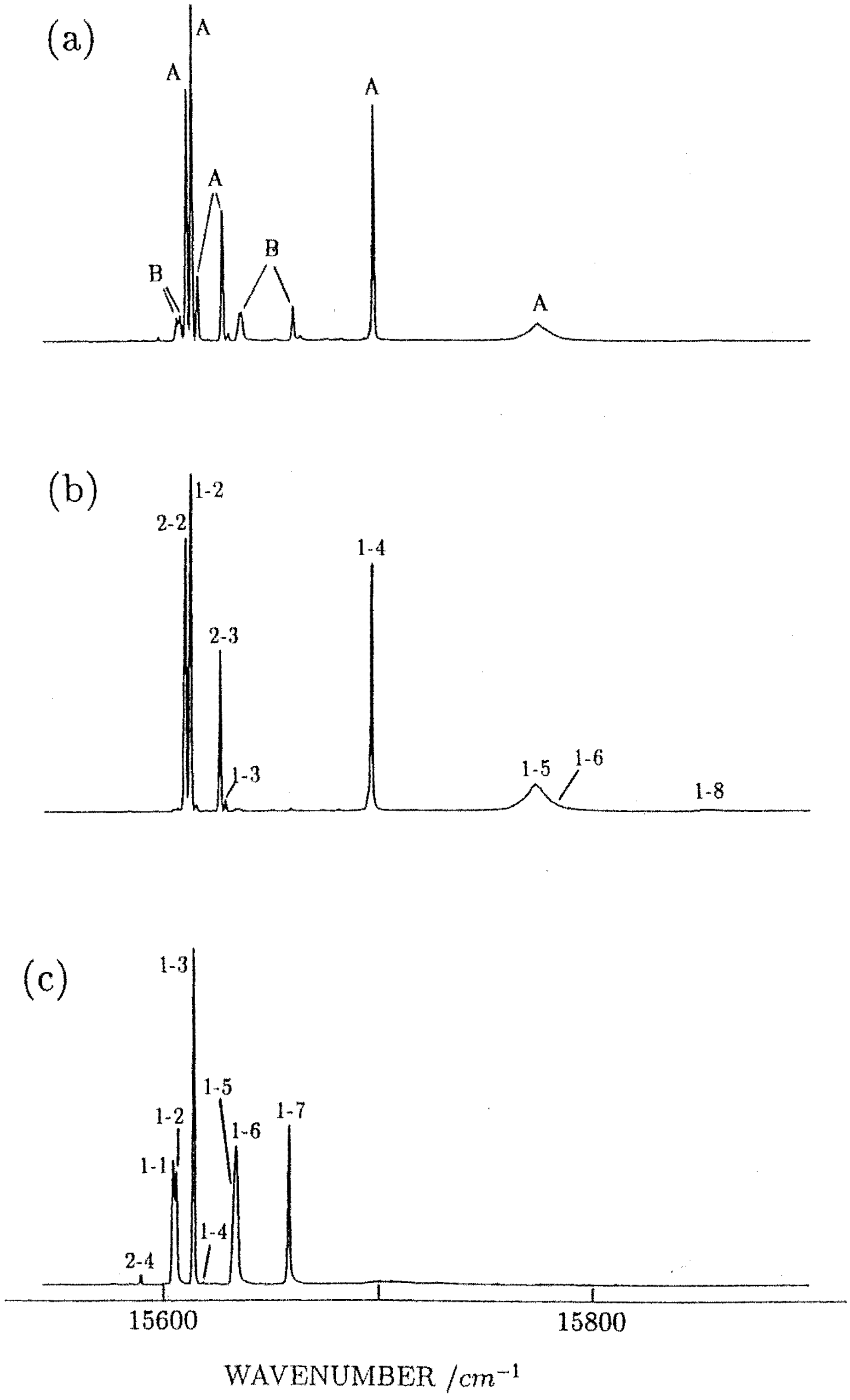

Figure 4.3: 10 K broadband and selective excitation spectra of the D multiplet in $CaF_2:Ho^{3+}$(0.005%) crystals :
(a) broadband excitation spectrum, monitoring all the D→Z transition;
(b) A centre excitation spectrum, monitoring all the $D_1 \rightarrow Z_3$ transitions at 15522.5 cm^{-1};
(c) B centre excitation spectrum, monitoring the $D_2 \rightarrow Z_3$ transition at 15541.0 cm^{-1}.

4.1.1 Spectroscopy of the A centre

In the Z → E excitation spectrum of the A centre (Figure 4.2(b)) transitions to seven upper levels are apparent. The three lowest and sharpest of these at 18613.2, 18655.1 and 18726.8 cm^{-1} show a common doublet splitting of 1.9 cm^{-1} on each line peak, which for the remaining broad transitions is not resolved. This 1.9 cm^{-1} splitting has previously been observed in EPR [66] and in high resolution laser spectroscopy [47] measurements and was attributed to the low-lying first excited state, Z_2, which is just 1.9 cm^{-1} above the ground state, Z_1. The two lowest transitions in the Z → D excitation spectrum (Figure 4.3(b)) also clearly show this splitting.

From the E → Z fluorescence spectrum (Figure 4.4(a)) the four transitions to the Z_3, Z_5, Z_{10} and Z_{12} levels were found to occur as pairs with a common separation of 14.0 cm^{-1}. As such patterns were not observed in either the excitation spectrum (Figure 4.2(b)) or for the E → Z_1,Z_2 fluorescence transitions, no level could be unambiguously identified as being 14.0 cm^{-1} above or below the lowest observed E multiplet level at 18613.2 cm^{-1}. To identify the missing unobserved E multiplet level, additional spectral measurements were carried out at 2 K. These indicate that there is a level 14.0 cm^{-1} below the lowest observed E level at 18613.2 cm^{-1}. The reasoning used is as follows :

When the E → Z fluorescence spectrum was measured at 2 K, (Figure 4.5(a)), only the lower energy transitions of each pair showing the 14.0 cm^{-1} separation were observed. As the temperature was raised from 10 K to 20 K, the higher energy transition of each pair as well as the transition at 18613.2 cm^{-1} were found to grow in intensity. Additional transitions at 18483.5, 18144.0 and 18121.0 cm^{-1} were found to be single, with the two at 18483.5 and 18144.0 cm^{-1} being present in the 2 K spectrum, while the 18121.0 cm^{-1} transition was absent. All these observations can be accounted for by a level at 18599.0 cm^{-1} (14.0 cm^{-1} lower in energy than 18613.2 cm^{-1}) which is inferred to be the lowest level E_1 of the E multiplet. The single transitions at 18483.5 and 18144.0 cm^{-1} originate from

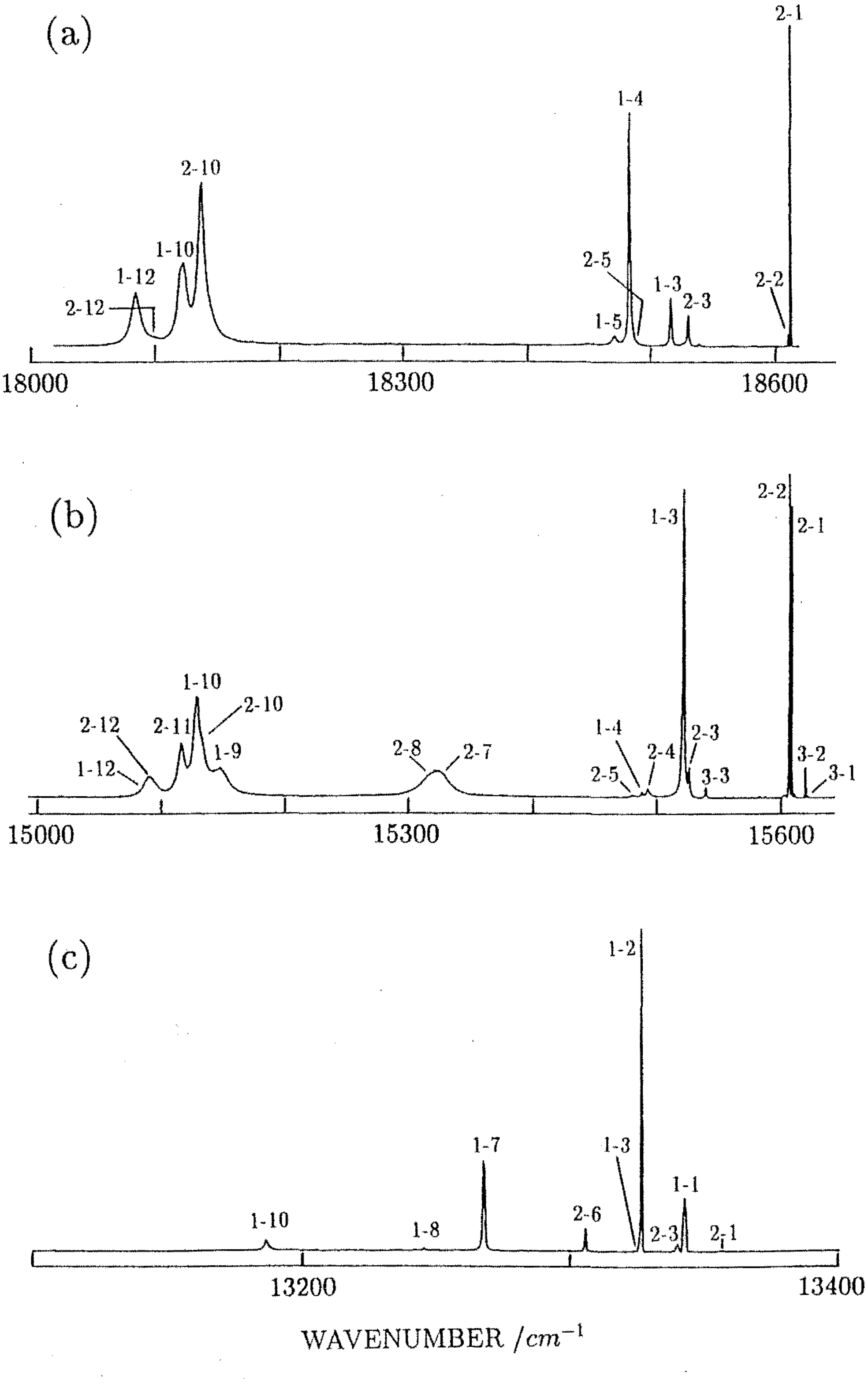

Figure 4.4: 10 K fluorescence spectra for the A centre in CaF$_2$:Ho^{3+}(0.005%) crystals :
(a) E→Z transitions, for excitation of the Z$_2$→E$_9$ transition at 18833.0 cm^{-1};
(b) D→Z transitions, for excitation of the Z$_1$→D$_4$ transition at 15682.0 cm^{-1};
(c) E→Y transitions, for excitation of the Z$_2$→E$_9$ transition at 18833.0 cm^{-1}.
Transitions are labelled by the appropriate upper and lower multiplet crystal-field level identifications.

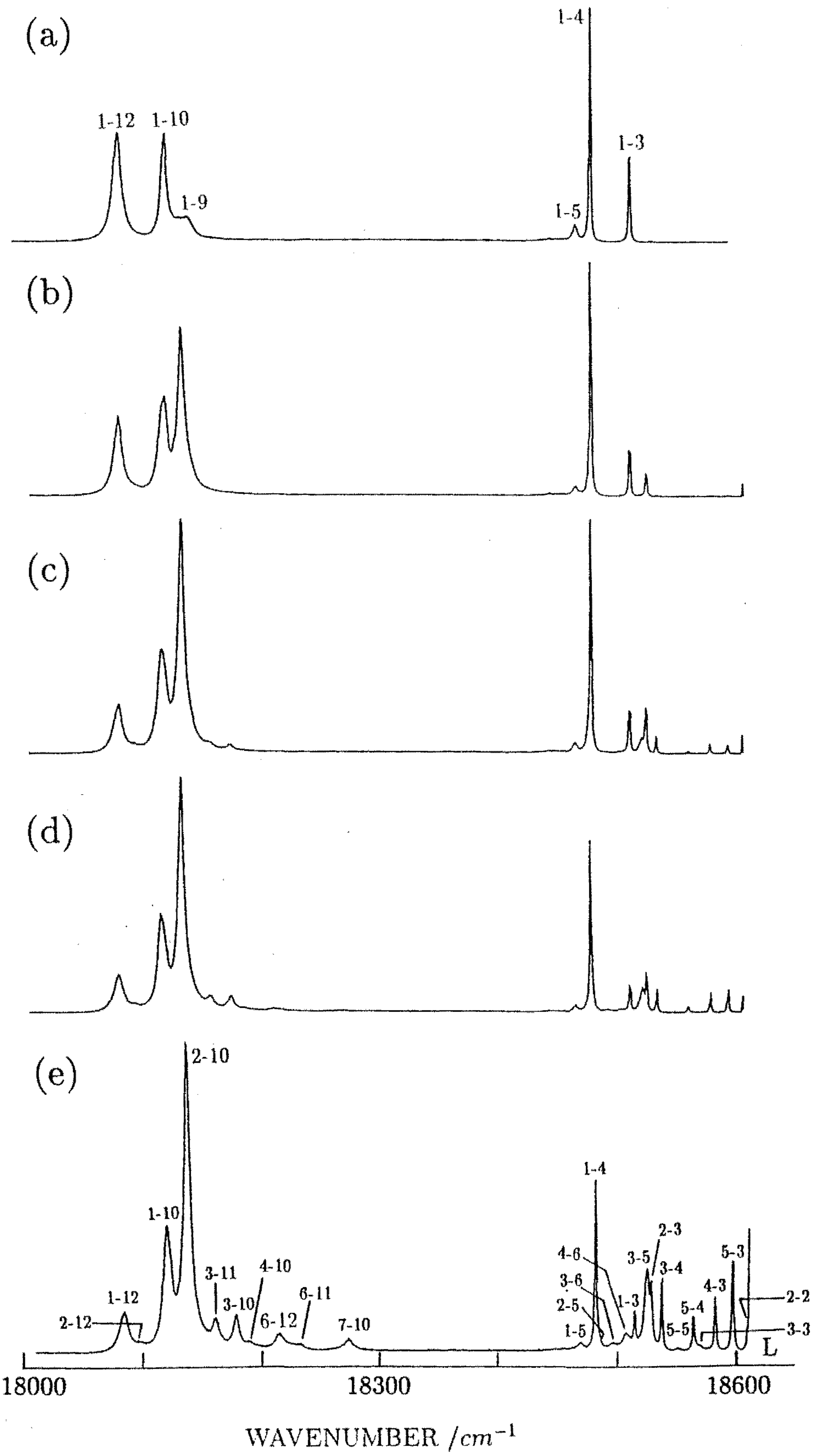

Figure 4.5: Variable temperature (2 K to 55 K) fluorescence spectra of the E→Z transitions for the A centre in CaF_2:Ho^{3+}(0.005%) crystals for excitation of the $Z_1 \rightarrow E_2$ transition at 18613.2 cm^{-1} :
(a) 2 K spectrum; (b) 10 K spectrum;
(c) 20 K spectrum; (d) 30 K spectrum;
(e) 55 K spectrum.

this level while that at 18121.0 cm^{-1} was assigned as originating from the E_2 level at 18613.2 cm^{-1}.

The E → Y spectrum (Figure 4.4(c)) has two sets of transition pairs with the same 14.0 cm^{-1} separation as observed for four pairs of the E → Z transitions. These were found to have the same temperature dependence behaviour as the transition pairs in the E → Z spectrum, with the higher component being frozen out at 2 K and having increased intensity in the 20 K spectra. The single transition at 13304.5 cm^{-1} was also absent at 2 K and increased in intensity as the temperature was raised, showing that this transition also originates from the E_2 level at 18613.2 cm^{-1}. The other single transitions at 13326.0, 13267.0, 13244.0 and 13186.0 cm^{-1} were all observed in the 2 K spectra and therefore originate from the E_1 level at 18599.0 cm^{-1}.

Above 15 K, further new transitions started to appear and gained intensity as the temperature was gradually raised to 55 K. As can be seen from Figure 4.5 for the E → Z fluorescence transitions, most of these new transitions were present by 20 K and became more intense with increasing temperature. There are no new transitions in the spectra above 30 K (Figure 4.5(d)) and for temperatures above 55 K, all the transitions became too broad with resulting overlapping of the A and B centre transitions. A further two E levels, E_4 and E_5 at 18666.5 and 18681.5 cm^{-1} respectively, were identified from these temperature dependence studies. As transitions to these levels were not observed in the 10 K excitation spectra, the $Z_1,Z_2 \rightarrow E_4,E_5$ transitions themselves must be forbidden for C_{4v} symmetry centres and the E_4 and E_5 levels must therefore have different irrep labels from either the Z_1 or Z_2 levels. Fluorescence transitions from either the E_4 or E_5 levels to any of the other Z levels would not be expected to be observed at 10 K as the E_4 and E_5 levels are sufficiently higher in energy than the E_1 and E_2 levels not to be originating levels at 10 K. At temperatures above 10 K however, both levels become sufficiently populated for emission and although their specific transitions to either the Z_1 or Z_2 levels are electric dipole forbidden and therefore not observed, transitions to the Z_3, Z_5 and Z_{10} levels, in particular, are observed (Figure 4.5(e)). Also although neither the $E_1 \rightarrow Z_6$ nor $E_2 \rightarrow Z_6$ transitions are observed, at temperatures above 10 K both the $E_3 \rightarrow Z_6$ and $E_4 \rightarrow Z_6$ transitions are observed, thus identifying the Z_6 level to be at 158.0 cm^{-1}.

The D → Z transitions observed for Z → E excitation are comparatively weak requiring integration times as long as 5 - 10 s for reasonable signal to noise ratios. In contrast, for direct Z → D excitation the fluorescence was just as strong as that observed for the E → Z transitions for direct excitation of the E multiplet. It is concluded that when the E multiplet is being excited, the population of the D multiplet which depends on multiphonon relaxation across the 3000 cm^{-1} E to D multiplet energy gap, is weakly fed, hence the weak fluorescence.

The D → Z spectrum (Figure 4.4(b)) was closely similar to that for E → Z except for the additional feature centred at 15322.0 cm^{-1} corresponding to two Z levels of 284.5 and 292.5 cm^{-1} energies respectively, which does not correspond to any of the observed E → Z transitions. Some of the D → Z transitions were also found to occur in pairs with a separation of 4.5 cm^{-1}, with the components having a similar temperature dependence behaviour to the previously discussed E → Z and E → Y transitions. From this, a level at 15605.0 cm^{-1} (4.5 cm^{-1} below the lowest observed D multiplet level at 15609.5 cm^{-1}) was inferred. At 2 K, transitions from the D_3 level at 15623.0 cm^{-1} were not apparent while the $D_2 \rightarrow Z_1,Z_2$ transitions were appreciably weaker than at 10 K but still observable because of the small energy separation (4.5 cm^{-1}) between the D_1 and D_2 levels. No other possible transitions from the D_2 level to the other Z levels were apparent. Transitions assigned to the D_1 level (15605.0 cm^{-1}) were strongest at 2 K and decreased in intensity with increasing temperature. The energy levels derived are presented in Table 4.1.

4.1.2 Polarisation study of the A centre

Polarisation results obtained in both the <100> and <111> oriented samples (Figure 4.6 and Table 4.2) were found to be fully consistent with a

Table 4.1: Energy levels (in cm^{-1}) of the Z, Y, D, E and F multiplets of the A centre and their symmetries, as derived from the 2 K to 55 K spectra of $\mathrm{CaF_2:Ho^{3+}}$(0.005%) crystals. Uncertainty is ± 0.5 cm^{-1} unless otherwise stated.

Level	**Z($^5I_8$)**	**Y($^5I_7$)**	**D($^5F_5$)**	**E($^5S_2$,$^5F_4$)**	**F($^5F_3$)**
1	0±0.2(γ_1)	5257.0(γ_5)	15605.0(γ_3)	18599.0(γ_3)	20741.6(γ_2)
2	1.9±0.2(γ_2)	5273.0(γ_3)	15609.5(γ_5)	18613.2(γ_1)	20781.6(γ_5)
3	83.0(γ_5)	5274.0(γ_5)	15623.0(γ_2)	18655.1(γ_5)	-
4	115.5(γ_3)	-	15682.0(γ_1)	18666.5(γ_4)	-
5	128.0(γ_5)	-	15752.2(γ_5)	18681.5(γ_3)	20924.5(γ_5)
6	158.0(γ_4)	5308.5(γ_1)	15756.1(γ_2)	18726.8(γ_5)	
7	284.5(γ_1)	5332.0(γ_5)	-	18750.1(γ_1)	
8	292.5(γ_2)	5355.0(γ_3)	15823.5(γ_5)	-	
9	455.0(γ_3)	-		18834.9(γ_2)	
10	475.0(γ_5)	5413.0(γ_5)		18859.5(γ_5)	
11	492.0(γ_1)	-		18888.3(γ_1)	
12	513.0(γ_5)				
13	-				

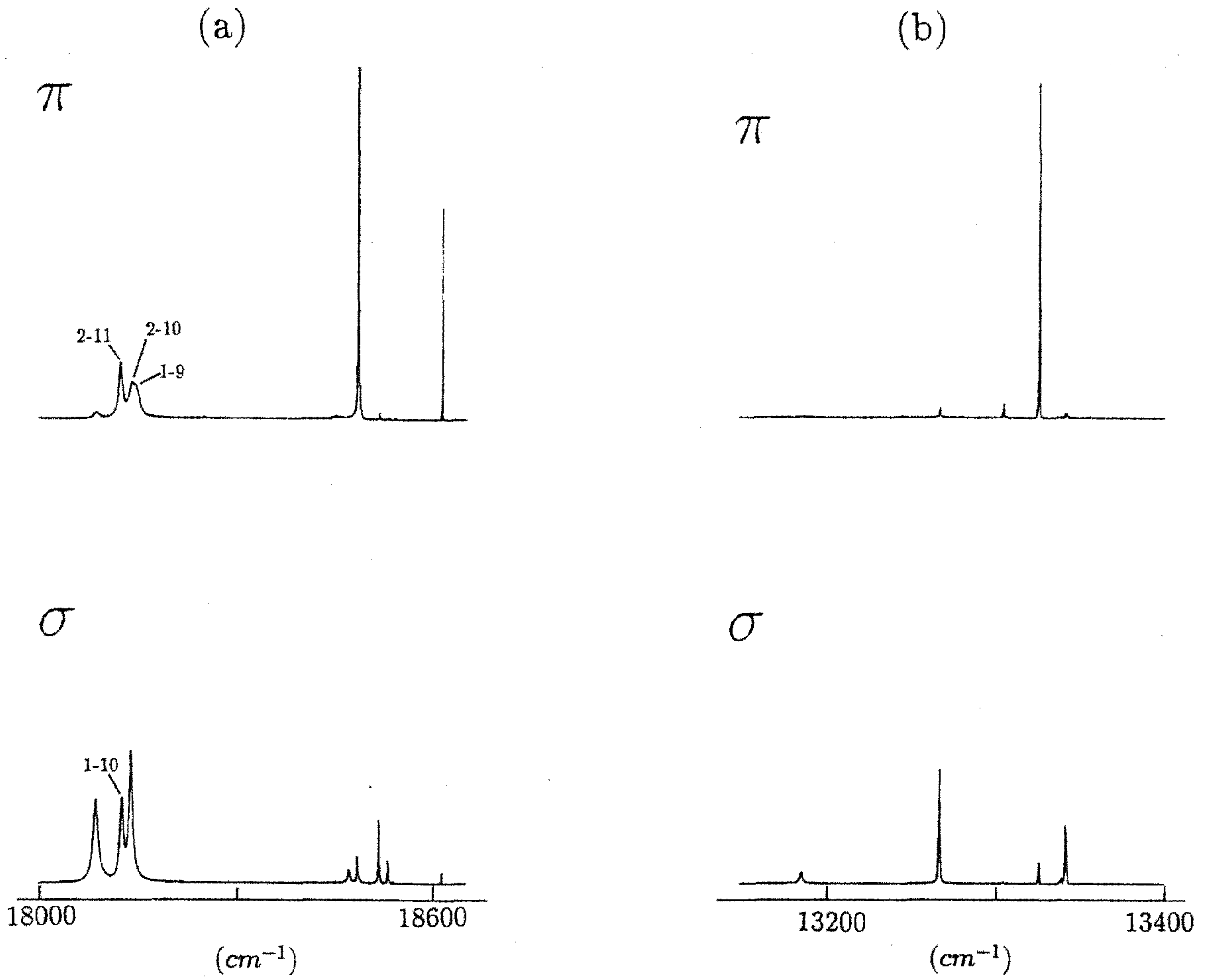

Figure 4.6: Polarisation of the 10 K fluorescence spectra of the E → Z and E → Y transitions of the A centre in CaF_2:Ho^{3+}(0.005%) crystals, for excitation of the Z_2→E_9 transition at 18833.0 cm^{-1}
(a) E → Z transitions (b) E → Y transitions
Transition labels are as in Figure 4.4

tetragonal symmetry assignment for the A centre. These ratios were distinct and consistent in the spectra to 55 K where new transitions appear. It can be seen from Figure 4.6(a),(b) and Table 4.2 that the transition pairs with the 14.0 cm^{-1} energy separation show the same polarisation behaviour for both components and which is indicative of transitions of the type $\gamma_{a'} \rightarrow \gamma_5$ (refer to Table 2.3) and therefore the common terminating Z level of both components of the pair has to be of γ_5 type. The Z_3, Z_5, Z_{10} and Z_{12} levels at 83.0, 128.0, 475.0 and 513.0 cm^{-1} respectively, are therefore all identified as γ_5 type levels. Since any $\gamma_{a'} \rightarrow \gamma_5$ transition is allowed by the C_{4v} symmetry selection rules, it can be deduced that the two lowest levels E_1 and E_2 of the E multiplet have different irrep labels, because the E_2 level at 18613.2 cm^{-1} is observable in absorption from the Z_1,Z_2 levels while the E_1 level at 18599.0 cm^{-1} is not observable by transitions from the Z_1,Z_2 levels. The single transitions at 18483.5, 18144.0 and 18121.0 cm^{-1} corresponding to the $E_1 \rightarrow Z_4$, $E_1 \rightarrow Z_9$ and $E_2 \rightarrow Z_{11}$ transitions respectively, are all principally π polarised showing that they are transitions of the type $\gamma_a \rightarrow \gamma_a$. Therefore the Z_4 and Z_9 levels at 115.5 and 455.0 cm^{-1} respectively, have the same irrep label as the E_1 level while the Z_{11} level at 492.0 cm^{-1} is necessarily of the same type as the E_2 level.

Several transitions, as shown in Figure 4.6, lie close to other transitions and could not be identified clearly in the unpolarised spectra, but are quite clearly apparent in the polarisation spectra. For example, the two transitions at 18144.0 and 18121.0 cm^{-1}, are masked by the close lying strong transitions at 18138.0 and 18124.0 cm^{-1} respectively (Figure 4.6(a)). It was possible to resolve these close lying transitions in such cases because a $\gamma_a \rightarrow \gamma_a$ type transition happens to occur next to a $\gamma_{a'} \rightarrow \gamma_5$ type transition and these have opposite polarisation behaviour. Likewise the $E_2 \rightarrow Z_5$ transition at 18485.0 cm^{-1} was also more evident in the σ polarisation spectrum because the adjacent and stronger transition at 18483.5 cm^{-1} is mainly π polarised (Figure 4.6(a)).

Excitation of any of the $Z_1 \rightarrow E_2$, $Z_1 \rightarrow E_7$, $Z_2 \rightarrow E_9$ and $Z_1 \rightarrow E_{11}$ transitions resulted in fluorescence with the same polarisation behaviour for each particular transition, consistent with a common $\gamma_a \rightarrow \gamma_a$ pump transition and either $\gamma_a \rightarrow \gamma_a$ or $\gamma_{a'} \rightarrow \gamma_5$ decay transitions. On the other hand, excitation of the $Z_1 \rightarrow E_3$ and $Z_1 \rightarrow E_6$ transitions gave polarisation ratios consistent with $\gamma_{a'} \rightarrow \gamma_5$ pump transitions and $\gamma_a \rightarrow \gamma_a$ or $\gamma_{a'} \rightarrow \gamma_5$ decay transitions in each case. The polarisation ratios observed for excitation of the $Z_1 \rightarrow E_{10}$ transition were indicative of a $\gamma_{a'} \rightarrow \gamma_5$ pump transition though partially masked by background fluorescence from both the E_9 and E_{11} levels.

By monitoring a transition of $\gamma_a \rightarrow \gamma_a$ type, for example the $E_1 \rightarrow Z_4$ transition at 18483.5 cm^{-1}, in the two possible analyser positions, polarised excitation spectra were observed (Figure 4.7). Such spectra distinguished clearly the γ_5 type levels of the upper E multiplet from those of the $\gamma_{a'}$ type, for transitions originating from the same lower multiplet Z level. In particular, the E_{10} level at 18859.5 cm^{-1} was positively identified in this manner (Figure 4.7).

Although the $^5S_2$ and $^5F_4$ multiplets are quite close in energy, levels belonging to the $^5S_2$ multiplet have been assigned to be the set lower in energy than those for the $^5F_4$ multiplet in both $LaF_3:Ho^{3+}$ [26] and $LaCl_3:Ho^{3+}$ [99]. It has therefore been assumed, in the following analysis, that the $^5S_2$ multiplet is lower in energy than the $^5F_4$ multiplet in the CaF_2 case too.

For the $^5S_2$ multiplet two upper levels E_2 and E_3 have been directly observed. The five remaining levels E_6, E_7, E_9, E_{10} and E_{11} observed are assigned to the $^5F_4$ multiplet and comprise two γ_5 and three $\gamma_{a'}$ irrep label type levels. The six levels observed for the $^5F_5$ multiplet comprise three γ_5 and three $\gamma_{a'}$ irrep label type levels. Examination of the summary of expected transition types in Table 2.1(a) shows that the ground multiplet levels Z_1 and Z_2 can only have γ_1 and γ_2 symmetry irrep labels to account for the number of observed levels in both the E and D multiplets. Further, the E_2 level can only have a γ_1 symmetry irrep label since a $J = 2$ multiplet such as $^5S_2$ does not possess any γ_2 type levels. The Z_{11} level is therefore assigned as of γ_1 type, the same as for the E_2 level. All the unobserved levels are those of either γ_3 or γ_4 symmetry.

Although from the C_{4v} symmetry selection rules, $\gamma_1 \leftrightarrow \gamma_2$ type transitions are not allowed, transitions from both the Z_1 and Z_2 levels to the E_2 level and vise versa are observed. With just a small (1.9 cm^{-1}) separation between the two singlet Z_1 and Z_2 levels, their electronic wavefunctions are sufficiently mixed by the hyperfine nuclear interaction (Chapter 9) to result in both transitions being allowed. In the absence of any hyperfine mixing, all transitions should be of pure $\gamma_1 \rightarrow \gamma_1$ or $\gamma_2 \rightarrow \gamma_2$ and $\gamma_{a'} \rightarrow \gamma_5$ (a′ = 1, 2) type only. A temperature of 2 K is not low enough to completely freeze out transitions involving the Z_2 level, which would result in the excitation of only those levels with the same irrep as the Z_1 level in addition to the always allowed γ_5 type levels. As the $Z_2 \leftrightarrow E_2$ transition is observed to be much weaker than $Z_1 \leftrightarrow E_2$, the Z_1 level is assigned to be of γ_1 type, the same as for the E_2 level, to give the observed strong $\gamma_1 \leftrightarrow \gamma_1$ transition. The Z_2 level is therefore assigned as a γ_2 type level.

The irrep label assignments of the $Z_1(\gamma_1)$, $Z_2(\gamma_2)$, $Z_3(\gamma_5)$, $Z_5(\gamma_5)$, $Z_{10}(\gamma_5)$ and $Z_{12}(\gamma_5)$ levels are all consistent with the earlier theoretical crystal-field calculations of Reid and Butler [109] for the case of their crystal-field parameter $X_{C_{4v}}$ being less than 365 cm^{-1}. There is further agreement with that analysis in that the Z_4 and Z_9 levels should have the same irrep label and likewise the Z_1 and Z_{11} levels, as observed. From comparison with their fit the Z_4 and Z_9 levels are assigned as γ_3 type levels while the Z_6 level is assigned as a γ_4 type level. This establishes the Z_1 level as a γ_1 type level and identifies the E_1 level as a γ_3 type level, the same as the Z_4 and Z_9 levels. With the E_3, E_6 and E_{10} levels already established as being of γ_5 type levels, the remaining three E levels, E_7, E_9 and E_{11} can only comprise the two γ_1 and one γ_2 type levels of the $^5F_4$ multiplet. The E_9 level at 18834.9 cm^{-1} is assigned as a γ_2 type level because the $Z_1,Z_2 \rightarrow E_9$ transition was found to be weaker at 2 K than at 10 K, compared to the corresponding transitions to the E_2, E_7 and E_{11} levels at the same temperatures which all maintained the same intensity ratios with temperature. This is

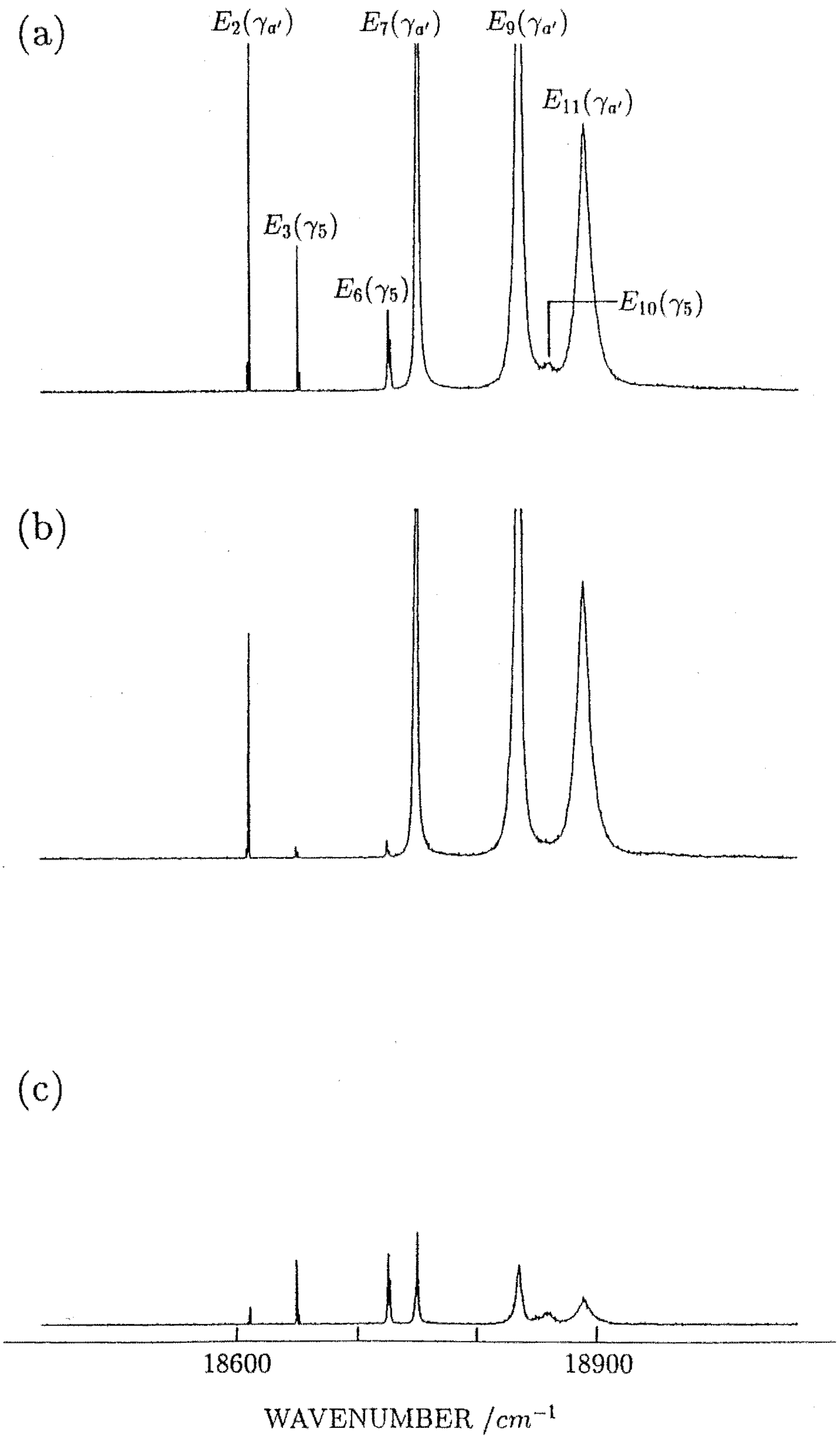

Figure 4.7: Polarisation of the 10 K selective excitation spectrum of the Z→E transitions of the A centre in CaF_2:Ho^{3+}(0.005%) crystals, monitoring the E_1→Z_4 transition at 18483.5 cm^{-1} :
(a) unpolarised spectrum showing the symmetries of the energy levels;
(b) π polarisation;
(c) σ polarisation.

Table 4.2: Observed and predicted intensity ratios for the polarised fluorescence transitions of the A centre in < 100 > and < 111 > oriented $CaF_2:Ho^{3+}$(0.005%) crystals, for excitation of the $Z_2 \rightarrow E_9$ transition at 18833.0 cm^{-1}.

Transition	**Wavenumber**	**Polarisation Ratios (±5%)**			
	(±0.5) cm^{-1}	**< 100 > orientation**		**< 111 > orientation**	
		[yy : yx]		**[y′y′/y′x′]**	
		Observed	**Expected**	**Observed**	**Expected**
* $E_7 \rightarrow Z_{10}$	18276.0	1 : 4.0	0 : 1		
* $E_6 \rightarrow Z_{11}$	18232.0	1 : 4.3	0 : 1		
* $E_6 \rightarrow Z_{12}$	18217.5	5.7 : 1	1 : 0		
* $E_5 \rightarrow Z_3$	18598.5	1 : 6.7	0 : 1		
* $E_5 \rightarrow Z_4$	18565.0	5.9 : 1	1 : 0		
* $E_5 \rightarrow Z_5$	18553.5	1 : 4.9	0 : 1		
* $E_4 \rightarrow Z_3$	18583.5	1 : 7.3	0 : 1		
* $E_4 \rightarrow Z_6$	18509.0	7.3 : 1	1 : 0		
* $E_4 \rightarrow Z_{10}$	18191.0	1 : 5.0	0 : 1		
* $E_3 \rightarrow Z_3$	18572.0	5.1 : 1	1 : 0		
* $E_3 \rightarrow Z_4$	18539.0	1 : 6.6	0 : 1		
* $E_3 \rightarrow Z_5$	18526.5	7.5 : 1	1 : 0		
* $E_3 \rightarrow Z_6$	18497.0	1 : 5.3	0 : 1		
* $E_3 \rightarrow Z_{10}$	18179.5	8.5 : 1	1 : 0		
* $E_3 \rightarrow Z_{11}$	18162.5	1 : 7.8	0 : 1		
$E_2 \rightarrow Z_1$	18613.2	18.4 : 1	1 : 0	3.1	3.0
$E_2 \rightarrow Z_2$	18611.3	17.5 : 1	1 : 0	2.9	3.0
$E_2 \rightarrow Z_3$	18530.0	1 : 11.6	0 : 1	$^{3.5}/_{5}$	$^{3}/_{5}$
$E_2 \rightarrow Z_5$	18485.0	1 : 10.5	0 : 1	$^{3.5}/_{5}$	$^{3}/_{5}$
$E_2 \rightarrow Z_{10}$	18138.0	1 : 10.0	0 : 1	$^{3.5}/_{5}$	$^{3}/_{5}$
$E_2 \rightarrow Z_{11}$	18121.0	10.6 : 1	1 : 0	2.6	3.0
$E_2 \rightarrow Z_{12}$	18100.0	1 : 8.3	0 : 1	$^{3.0}/_{5}$	$^{3}/_{5}$
$E_1 \rightarrow Z_3$	18516.0	1 : 12.5	0 : 1	$^{3.5}/_{5}$	$^{3}/_{5}$
$E_1 \rightarrow Z_4$	18483.5	12.3 : 1	1 : 0	3.1	3.0
$E_1 \rightarrow Z_5$	18471.0	1 : 9.0	0 : 1	$^{3.5}/_{5}$	$^{3}/_{5}$
$E_1 \rightarrow Z_9$	18144.0	8.2 : 1	1 : 0	2.6	3.0
$E_1 \rightarrow Z_{10}$	18124.0	1 : 11.6	0 : 1	$^{4.0}/_{5}$	$^{3}/_{5}$
$E_1 \rightarrow Z_{13}$	18086.0	1 : 11.7	0 : 1	$^{3.0}/_{5}$	$^{3}/_{5}$
* $E_5 \rightarrow Y_1$	13425.0	1 : 7.4	0 : 1		
* $E_5 \rightarrow Y_3$	13408.0	5.2 : 1	1 : 0		
* $E_5 \rightarrow Y_7$	13349.5	1 : 4.2	0 : 1		
* $E_5 \rightarrow Y_8$	13327.0	8.6 : 1	1 : 0		

cont...

Table 4.2 cont....

Transition	**Wavenumber** (±0.5) cm^{-1}	**Polarisation Ratios** (±5%)			
		< 100 > orientation [yy : yx]		**< 111 > orientation** [y′y′/y′x′]	
		Observed	**Expected**	**Observed**	**Expected**
* $E_4 \rightarrow Y_1$	13409.5	1 : 6.5	0 : 1		
* $E_4 \rightarrow Y_7$	13335.0	1 : 4.8	0 : 1		
* $E_4 \rightarrow Y_{10}$	13254.0	1 : 4.5	0 : 1		
* $E_3 \rightarrow Y_1$	13398.5	6.1 : 1	1 : 0		
* $E_3 \rightarrow Y_2$	13382.0	1 : 5.7	0 : 1		
* $E_3 \rightarrow Y_3$	13381.0	9.6 : 1	1 : 0		
* $E_3 \rightarrow Y_6$	13347.0	1 : 5.0	0 : 1		
* $E_3 \rightarrow Y_7$	13323.5	8.0 : 1	1 : 0		
* $E_3 \rightarrow Y_8$	13301.0	1 : 4.2	0 : 1		
* $E_3 \rightarrow Y_{10}$	13242.5	6.5 : 1	1 : 0		
$E_2 \rightarrow Y_1$	13356.0	1 : 10.4	0 : 1	$^{3.0}/_{5}$	$^{3}/_{5}$
$E_2 \rightarrow Y_3$	13339.0	1 : 10.9	0 : 1	$^{3.0}/_{5}$	$^{3}/_{5}$
$E_2 \rightarrow Y_6$	13304.5	10.3 : 1	1 : 0	2.7	3.0
$E_1 \rightarrow Y_1$	13342.0	1 : 12.4	0 : 1	$^{3.5}/_{5}$	$^{3}/_{5}$
$E_1 \rightarrow Y_2$	13326.0	16.0 : 1	1 : 0	2.7	3.0
$E_1 \rightarrow Y_3$	13325.0	1 : 7.5	0 : 1	-	$^{3}/_{5}$
$E_1 \rightarrow Y_7$	13267.0	1 : 13.5	0 : 1	$^{3.0}/_{5}$	$^{3}/_{5}$
$E_1 \rightarrow Y_8$	13244.0	14.1 : 1	1 : 0	2.7	3.0
$E_1 \rightarrow Y_{10}$	13186.0	1 : 10.7	0 : 1	$^{3.0}/_{5}$	$^{3}/_{5}$
$D_3 \rightarrow Z_1$	15623.0	10.8 : 1	1 : 0	2.0	3.0
$D_3 \rightarrow Z_2$	15621.0	11.6 : 1	1 : 0	1.9	3.0
$D_3 \rightarrow Z_3$	15540.5	1 : 13.4	0 : 1	$^{3.0}/_{5}$	$^{3}/_{5}$
$D_3 \rightarrow Z_8$	15330.5	6.5 : 1	1 : 0	2.0	3.0
$D_2 \rightarrow Z_1$	15609.5	1 : 9.1	0 : 1	$^{3.0}/_{5}$	$^{3}/_{5}$
$D_2 \rightarrow Z_2$	15607.5	1 : 8.9	0 : 1	$^{3.5}/_{5}$	$^{3}/_{5}$
$D_2 \rightarrow Z_3$	15527.0	8.4 : 1	1 : 0	2.3	3.0
$D_2 \rightarrow Z_4$	15494.5	1 : 11.6	0 : 1	$^{3.0}/_{5}$	$^{3}/_{5}$
$D_2 \rightarrow Z_5$	15483.0	9.6 : 1	1 : 0	1.9	3.0
$D_2 \rightarrow Z_7$	15325.0	1 : 8.8	0 : 1	$^{3.5}/_{5}$	$^{3}/_{5}$
$D_2 \rightarrow Z_8$	15317.5	1 : 7.4	0 : 1	$^{3.5}{}_{\cdot 5}$	$^{3}/_{5}$
$D_2 \rightarrow Z_{10}$	15135.0	7.1 : 1	1 : 0	2.1	3.0

cont...

Table 4.2 cont....

Transition	**Wavenumber (±0.5) cm^{-1}**	**Polarisation Ratios (±5%)**			
		<100> orientation [yy : yx]		**<111> orientation [y′y′/y′x′]**	
		Observed	**Expected**	**Observed**	**Expected**
$D_2 \rightarrow Z_{11}$	15117.5	1 : 7.1	0 : 1	$^{3.0}/_{5}$	$^{3}/_{5}$
$D_2 \rightarrow Z_{12}$	15095.5	6.3 : 1	1 : 0	1.9	3.0
$D_1 \rightarrow Z_3$	15522.5	1 : 8.9	0 : 1	$^{3.0}/_{5}$	$^{3}/_{5}$
$D_1 \rightarrow Z_4$	15489.5	12.0 : 1	1 : 0	2.3	3.0
$D_1 \rightarrow Z_9$	15148.0	7.2 : 1	1 : 0	2.3	3.0
$D_1 \rightarrow Z_{10}$	15129.0	1 : 7.3	0 : 1	$^{3.5}/_{5}$	$^{3}/_{5}$
$D_1 \rightarrow Z_{12}$	15091.0	1 : 7.2	0 : 1	$^{3.5}/_{5}$	$^{3}/_{5}$

* polarisation ratios measured at 55 K, with excitation of the $Z_1 \rightarrow E_2$ transition at 18613.2 cm^{-1}.

consistent with the $Z_2 \rightarrow E_9$ transition, being the principal transition, showing a decrease in intensity at 2 K arising from the decrease in the population of the Z_2 level at that temperature. The corresponding $Z_1 \rightarrow E_9$ transition should be much weaker, as observed, as it can only occur through the hyperfine interaction wavefunction mixing between the Z_1 and Z_2 levels and is therefore only weakly allowed.

From the polarisation measurements up to 55 K, irrep labels for those levels missing from the 10 K $E \leftrightarrow Z$ spectra (because their irrep labels are different from those of the Z_1 and Z_2 levels) were established. Polarisation studies at 55 K (Table 4.2) show the transitions assigned as $E_4 \rightarrow Z_3$, $E_5 \rightarrow Z_3$, $E_5 \rightarrow Z_5$, $E_3 \rightarrow Z_6$ and $E_4 \rightarrow Z_{10}$ have polarisation ratios of 0:1 while the $E_3 \rightarrow Z_3$, $E_5 \rightarrow Z_4$, $E_3 \rightarrow Z_5$ and $E_4 \rightarrow Z_6$ transitions are all polarised with ratios of 1:0. The polarisation ratios for the transitions from the E_3 level are consistent with the γ_5 assignment made for this level. Ratios for the transitions from the E_4 and E_5 levels to the Z_3, Z_5 and Z_{10} levels, all of which have γ_5 symmetry, require that the E_4 and E_5 levels be either of γ_3 or γ_4 symmetry. However the E_4 and E_5 levels cannot have the same irrep label because the only common transitions they have are to the γ_5 type levels. As the $E_4 \rightarrow Z_6$ transition is observed to be π polarised, consistent with a $\gamma_a \rightarrow \gamma_a$ type transition, the E_4 and Z_6 levels have the same irrep label γ_4. The $E_5 \rightarrow Z_4$ transition was also observed to be π polarised, therefore the E_5 and Z_4 levels necessarily have a common irrep label of γ_3. From the earlier assignments made for the Z_6 and Z_4 levels, the E_4 and E_5 levels are therefore assigned as γ_4 and γ_3 type levels respectively. From the $E \rightarrow Y$ polarisation spectra (Figure 4.6(b)), the transition pairs with the $E_1 - E_2$ energy separation of 14.0 cm^{-1} are all polarised with ratios of 0:1 for $Z_1,Z_2 \rightarrow E_9$ ($\gamma_a \rightarrow \gamma_a$) excitation. The single transitions at 13267.0 and 13186.0 cm^{-1} originating from the E_1 level are also observed to be of σ polarisation. The Y_1, Y_3, Y_7 and Y_{10} levels at 5257.0, 5274.0, 5332.0 and 5413.0 cm^{-1} respectively, are therefore all identified as γ_5 type levels. As the $E_2 \rightarrow Y_6$ transition at 13304.5 cm^{-1} is observed to be of π polarisation, the Y_6 level is a γ_1 type level, similar to the E_2 level. As the $E_1 \rightarrow Y_2$ and $E_1 \rightarrow Y_8$ transitions at 13326.0 and 13244.0 cm^{-1} respectively, are also observed to be of the same π polarisation, the Y_2 and Y_8 levels are assigned the same γ_3 irrep as for the E_1 level.

From the polarisation ratios observed for the $D \rightarrow Z$ transitions with $Z_1 \rightarrow E_9$ excitation (Table 4.2), the $D_1 \rightarrow Z_4$ and $D_1 \rightarrow Z_9$ transitions are both of π polarisation, consistent with $\gamma_a \rightarrow \gamma_a$ type fluorescence. The $D_3 \rightarrow Z_1$ and $D_3 \rightarrow Z_2$ transitions are also observed to be of π polarisation with the $D_3 \rightarrow Z_2$ transition being the stronger. The D_3 level is therefore assigned as of γ_2 symmetry consistent with the weakly allowed $Z_1 \leftrightarrow D_3$ transition of $\gamma_1 \leftrightarrow \gamma_2$ type, while the D_1 level is assigned as of the γ_3 type, the same as for the Z_4 and Z_9 levels. The D_2 level is assigned as a γ_5 type level for the following three reasons. Firstly, transitions to and from the Z_1 and Z_2 levels are of the same intensity as both transitions are allowed. Secondly, transitions to all the Z levels (except Z_{13}) are observed, which is characteristic of γ_5 type upper state. Thirdly, transitions from the D_2 level to all the γ_5 type levels (as identified from the $E \rightarrow Z$ fluorescence spectrum in Figure 4.4(a)) are observed to be of π polarisation while those to $\gamma_{a'}$ type levels are observed to be of σ polarisation, consistent with $\gamma_5 \rightarrow \gamma_5$ and $\gamma_5 \rightarrow \gamma_{a'}$ type fluorescence transitions respectively, for $\gamma_a \rightarrow \gamma_a$ excitation.

The feature centred at 15322.0 cm^{-1} is resolved into three transitions in the polarisation spectra, with the lower two transitions at 15317.5 and 15325.0 cm^{-1} polarised with a ratio of 0:1 and the third transition at 15330.5 cm^{-1} polarised with a ratio of 1:0. These three transitions have been assigned as the $D_2 \rightarrow Z_8$, $D_2 \rightarrow Z_7$ and $D_3 \rightarrow Z_8$ transitions respectively. The Z_8 level at 292.5 cm^{-1} must be a γ_2 irrep label type level since the $D_3 \rightarrow Z_8$ transition is observed to be of π polarisation ($\gamma_a \rightarrow \gamma_a$), leaving the Z_7 level at 284.5 cm^{-1} as the third and remaining γ_1 type level of the Z multiplet. Polarised excitation spectra as for the $Z \rightarrow E$ transitions were used to assign irrep labels to the D_4, D_5, D_6 and D_8 levels as γ_1, γ_5, γ_2 and γ_5 respectively.

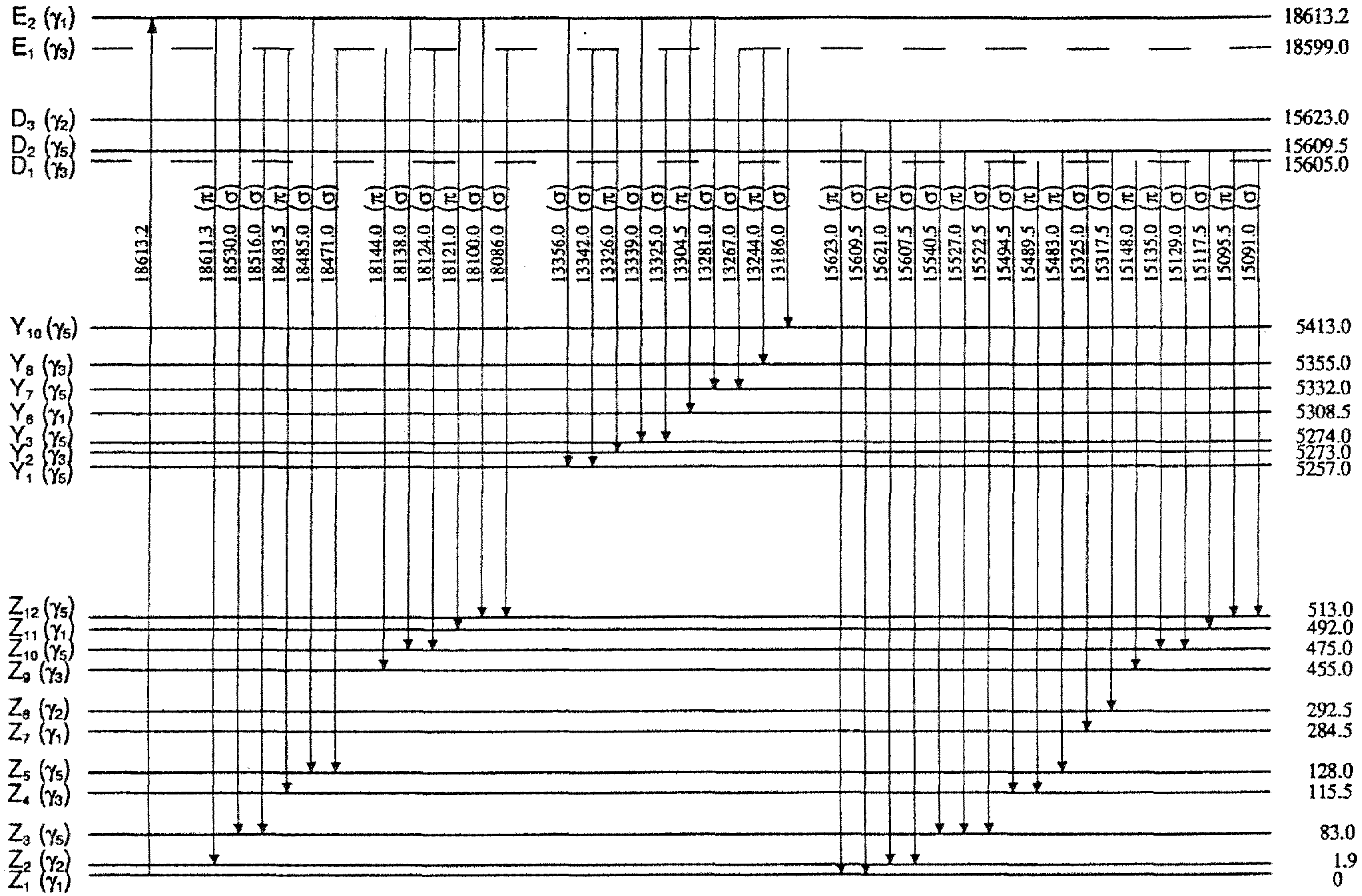

Figure 4.8: Energy level diagram for the A centre in CaF_2:Ho^{3+}(0.005%) crystals, for transitions as measured at 10 K.

With the Z_7 level being assigned as a γ_1 type level, it is not obvious why the $E_2 \rightarrow Z_7$ transition should be so weak, showing only as a small feature on a magnified scale.

An energy level scheme showing all the levels derived, together with their proposed irrep labels is presented in Figure 4.8 and Table 4.1. These data were used as the basis for the crystal-field calculations outlined in Chapter 7, where good crystal-field fits are reported.

4.1.3 Spectroscopy of the B centre

A total of nine transitions are identified from the ground Z_1 level to the E multiplet levels for the B centre. The Z → E excitation spectrum (Figure 4.2(c)) shows three close lying transitions at the low energy end of the spectrum. These have separations of 2.0 cm^{-1} and 1.0 cm^{-1} respectively between them. No other transitions in the Z → E excitation spectrum show such close energy separations. Transitions from the first excited Z_2 level at 27.0 cm^{-1} above the Z_1 level were also observed to most of the levels and are so identified. Although the $Z_1 \rightarrow E_6$ transition is weak, the $Z_2 \rightarrow E_6$ transition is strong and gives confidence in the identification of the upper multiplet E_6 level.

For Z → D excitation, seven levels were identified for the D multiplet (Figure 4.3(c)) with the D_1 and D_2 levels being only 1.5 cm^{-1} apart. The $D_1 \rightarrow Z_4$ transition was fairly weak, being only about 5% of the intensity of the $Z_1 \rightarrow D_3$ transition which is the strongest observed transition. The D_5 and D_6 levels were sufficiently overlapped to be indistinguishable in the excitation spectrum, with the combined $Z_1 \rightarrow D_5,D_6$ transition broader than any of the other transitions and of about the same linewidth as the overlapped $Z_1 \rightarrow D_1$ and $Z_1 \rightarrow D_2$ transitions. Since the $Z_1 \rightarrow D_7$ transition, about 20 cm^{-1} higher in energy than the $Z_1 \rightarrow D_5,D_6$ transitions, is narrower, the broadening of the $Z_1 \rightarrow D_5,D_6$ transitions could only be attributed to the overlap of two close lying transitions, giving an upper limit of 1 cm^{-1} for the D_5 - D_6 energy level separation. Transitions from the Z_2 level were observed to all the D levels with the $Z_2 \rightarrow D_4$ transition being particularly

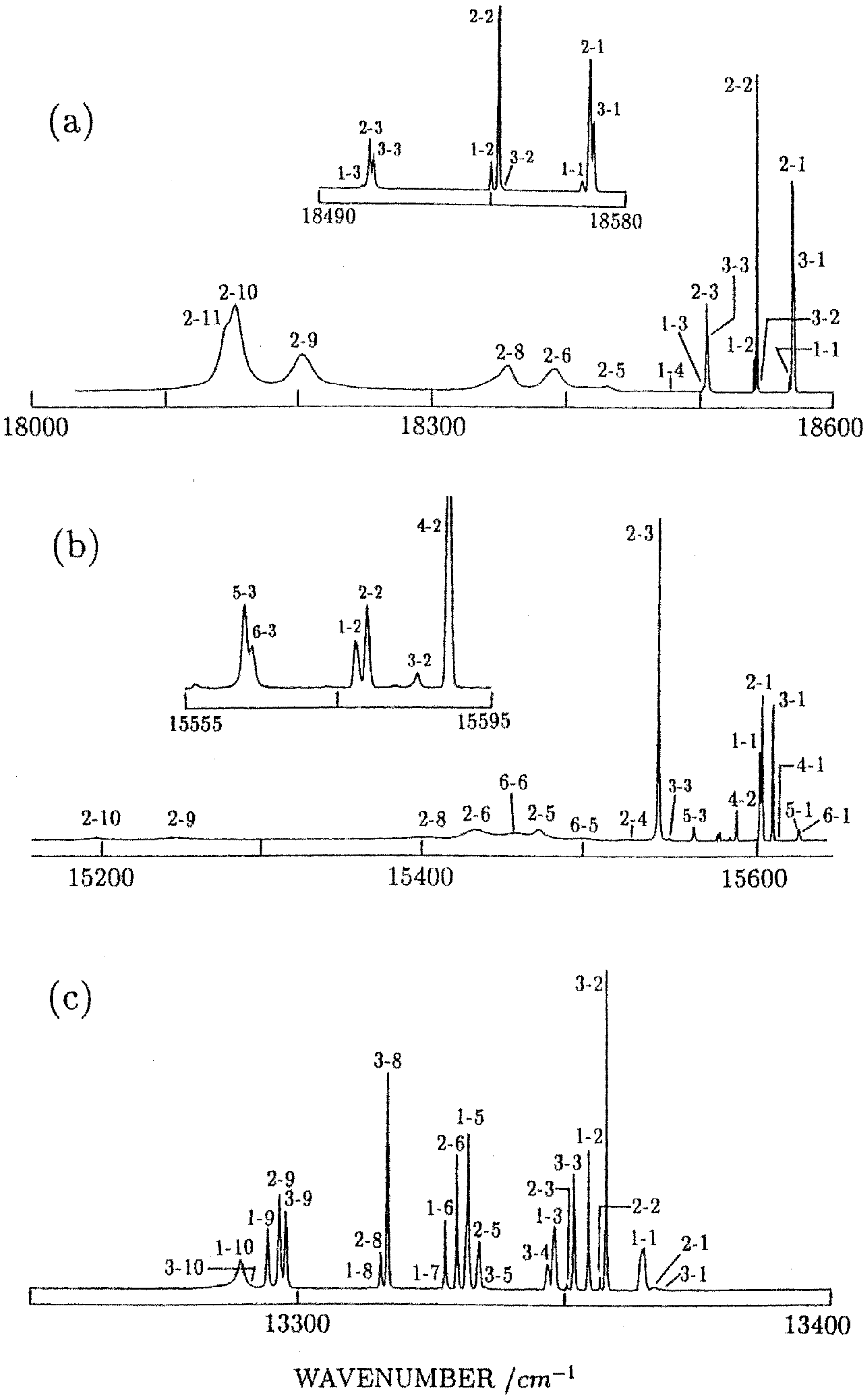

Figure 4.9: 10 K fluorescence spectra for the B centre in CaF_2:Ho^{3+}(0.005%) crystals :
(a) E→Z transitions, for excitation of the Z_1→E_4 transition at 18633.7 cm^{-1};
(b) D→Z transitions, for excitation of the Z_1→D_7 transition at 15647.0 cm^{-1};
(c) E→Y transitions, for excitation of the Z_1→E_4 transition at 18633.7 cm^{-1}.

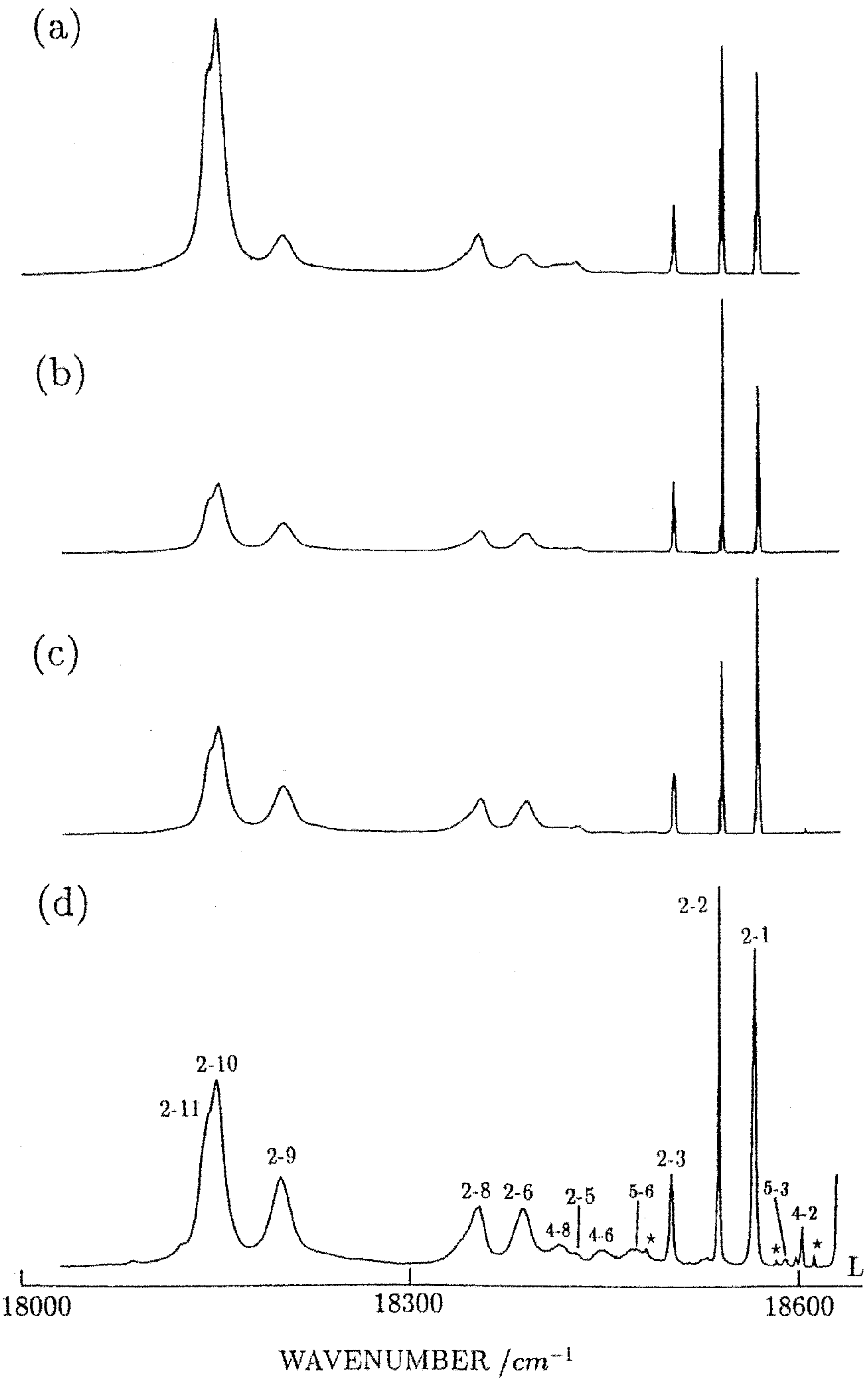

Figure 4.10: Variable temperature (2 K to 55 K) fluorescence spectra of the E→Z transitions for the B centre in $CaF_2:Ho^{3+}$(0.005%) crystals, for excitation of the $Z_1 \rightarrow E_4$ transition at 18633.7 cm^{-1} :
(a) 2 K spectrum; (b) 10 K spectrum;
(c) 30 K spectrum; (d) 55 K spectrum.

Transitions identified by * are for the A centre.

strong compared to the $Z_1 \rightarrow D_4$ transition.

For both the E and D multiplets, the B centre levels (Table 4.3) are much closer together than those for the A centre, being even more so for the D multiplet where the seven B centre levels span only a 45 cm^{-1} region compared to 220 cm^{-1} for the A centre. The barycentres of the energy level patterns are also lower for the B centre than for the A centre. Overall, the fluorescence is typically ten times stronger for the A centre than for the B centre, under comparable excitation conditions.

From the $E \rightarrow Z$ fluorescence spectrum (Figure 4.9(a)), transitions to the Z_1, Z_2 and Z_3 levels show the $E_1 - E_2 - E_3$ energy level separations of 2.0 and 1.0 cm^{-1} respectively (insert of Figure 4.9(a)). Transitions to the remaining Z levels are sufficiently broad not to reveal any such splittings.

The $E \rightarrow Y$ spectrum (Figure 4.9(c)) comprises transitions occurring either in the aforementioned triplets with 2.0 and 1.0 cm^{-1} separations or in pairs with a 3.0 cm^{-1} separation, identifying, respectively, transitions originating from either all of the E_1, E_2 and E_3 levels or just the E_1 and E_3 levels. Transitions from all the E_1, E_2 and E_3 levels were observed to the Y_1, Y_2, Y_3, Y_5, Y_6, Y_8 and Y_9 levels while transitions from just the E_1 and E_3 levels were observed to the Y_4, Y_7 and Y_{10} levels. Thus, all ten levels Y_1 - Y_{10} of the Y multiplet have been clearly identified (Table 4.3).

As for the A centre, fluorescence from the D multiplet was comparatively weak for $Z \rightarrow E$ excitation and quite strong for direct $Z \rightarrow D$ excitation. Transitions to the Z_1, Z_2 and Z_3 levels were found to be sharp and narrow while those to the remaining Z levels were weak and broad (Figure 4.9(b)). Transitions from the D_1 and D_2 levels to the Z_1 and Z_2 levels show the $D_1 - D_2$ energy level separation of 1.5 cm^{-1} while there is only one transition observed to the Z_3 level. Because the D levels are fairly close together, transitions to the Z_1 level through to the Z_6 level were observed from most upper D multiplet levels. The $D_5 - D_6$ energy level separation, measured to be 0.8 cm^{-1}, is very distinct in transitions to

Table 4.3: Energy levels (in cm^{-1}) of the Z, Y, D, E and F multiplets of the B centre and their symmetries, as derived from the 2 K to 55 K spectra of CaF_2:Ho^{3+}(0.005%) crystals. Uncertainty is ± 0.5 cm^{-1} unless otherwise stated.

Level	Z($^5I_8$)	Y($^5I_7$)	D($^5F_5$)	E($^5S_2$,$^5F_4$)	*F($^5F_3$)
1	0(γ_3)	5202.5(γ_3)	15604.0±0.2(γ_2)	18567.5±0.2(γ_3)	20715.0(γ_3)
2	27.0(γ_3)	5212.7(γ_1)	15605.5±0.2(γ_3)	18569.5±0.2(γ_1)	20722.4(γ_1)
3	65.0(γ_1)	5218.9(γ_3)	15613.0(γ_3)	18570.5±0.2(γ_3)	20749.5(γ_2)
4	81.0(γ_2)	5223.5(γ_2)	15618.0(γ_2)	18633.7(γ_3)	20779.3(γ_3)
5	138.5(γ_3)	5235.3(γ_3)	15627.7±0.2(γ_1)	18657.8(γ_1)	20800.8(γ_2)
6	178.5(γ_3)	5239.5(γ_1)	15628.5±0.2(γ_3)	18665.2(γ_2)	
7	-	5240.9(γ_2)	15647.0(γ_3)	18712.8(γ_3)	
8	213.5(γ_1)	5253.9(γ_3)		18751.0(γ_3)	
9	367.5(γ_3)	5272.9(γ_3)		18773.5(γ_1)	
10	417.5(γ_3)	5280.9(γ_2)			
11	423.5(γ_1)				

* Levels for the F multiplet were derived from the spectra of [SW], as no upconversion fluorescence was observed here.

the Z_3 level (insert of Figure 4.9(b)). Transitions to the Z_2 level also show this 0.8 cm^{-1} separation but are too weak to be observed clearly for the intensity scale used in Figure 4.9, while the transitions to the Z_1 level just show a single broad transition with a flat top. Transitions from either the D_1 or D_4 levels to the Z_3 level were not observed. The D → Z transitions identify the same levels of the Z multiplet as were found from the E → Z fluorescence transitions, yielding the Z_2 and Z_3 level energies as 27.0 and 65.0 cm^{-1} respectively.

At 2 K the fluorescence spectra were very similar to those at 10 K, except that fluorescence from the E_1 and D_1 levels was appreciably stronger than that from the E_2 and D_2 levels. As the temperature was raised above 10 K, transitions from higher E levels became apparent (Figure 4.10). Up to 30 K (Figure 4.10(c)), the $E_4 \rightarrow Z_2$ transition was the only new transition apparent that was absent at 10 K. However, at 55 K (Figure 4.10(d)) transitions from the E_4 and E_5 levels to all levels up to the Z_8 level, became apparent. The E_1 - E_2 - E_3 energy splittings were no longer obvious because of temperature broadening of the various transitions. For temperatures above 55 K, several A centre transitions started to appear as a result of the onset of overlap between the broadened A and B centre transitions and resulting simultaneous pumping occurring.

4.1.4 Polarisation study of the B centre

For a centre with exact C_{3v} symmetry, no polarisation effects are expected in <100> oriented samples. The fluorescence should therefore be independent of the polarisation used. In <111> oriented samples however, well defined polarisation ratios, as presented in Table 2.4, are expected for a centre with C_{3v} symmetry in CaF_2 type crystals. It is observed that for Z → E excitation, there is no significant change in intensity for the two analyser positions for any transitions in <100> oriented samples, indicative of a centre with exact trigonal symmetry. However, for Z → E excitation the fluorescence transitions did not show any well defined polarisation behaviour in the <111> crystal orientation geometry either, with most of the polarisation ratios being close to unity. This was found to be the

Table 4.4: Observed and predicted intensity ratios for the polarised D→Z fluorescence transitions of the B centre in <111> oriented $CaF_2:Ho^{3+}$(0.005%) crystals, for the excitation transitions shown.

Transition	Wavenumber (±0.5) (cm^{-1})	Polarisation ratios [y′y′/y′x′](±10%)						
		Observed	Expected	Observed				Expected
		$Z_1 \rightarrow D_1$		$Z_1 \rightarrow D_2$	$Z_1 \rightarrow D_3$	$Z_1 \rightarrow D_6$	$Z_1 \rightarrow D_7$	
$D_6 \rightarrow Z_1$	15628.6	0.62	$^{3}/_{7} - ^{15}/_{11}$	2.05	1.25	(laser)	0.99	arb
$D_6 \rightarrow Z_2$	15601.8	-	"	1.44	1.27	1.48	2.00	"
$D_6 \rightarrow Z_3$	15563.6	$^{14.1}/_{11}$	$^{15}/_{11}$	0.96	0.93	0.95	1.04	$^{3}/_{7} - ^{15}/_{11}$
$D_6 \rightarrow Z_5$	15491.0	1.10	$^{3}/_{7} - ^{15}/_{11}$	0.83	0.92	0.83	0.93	arb
$D_6 \rightarrow Z_6$	15450.5	1.05	"	0.99	0.88	0.83	0.56	"
$D_5 \rightarrow Z_2$	15601.2	$^{14.0}/_{11}$	$^{15}/_{11}$	0.70	0.66	0.68	0.65	$^{3}/_{7} - ^{15}/_{11}$
$D_5 \rightarrow Z_3$	15562.8	$^{3.2}/_{7}$	$^{3}/_{7}$	2.29	2.09	2.47	2.52	$^{3}/_{7}$ - 3.00
$D_4 \rightarrow Z_2$	15591.0	$^{14.3}/_{11}$	$^{15}/_{11}$	0.61	0.65	0.62	0.57	$^{3}/_{7} - ^{15}/_{11}$
$D_3 \rightarrow Z_1$	15613.0	0.76	$^{3}/_{7} - ^{15}/_{11}$	1.51	(laser)	1.61	1.85	arb
$D_3 \rightarrow Z_2$	15586.4	0.78	"	1.56	1.43	1.64	1.92	"
$D_3 \rightarrow Z_3$	15548.0	$^{14.2}/_{11}$	$^{15}/_{11}$	0.76	0.74	0.71	0.56	$^{3}/_{7} - ^{15}/_{11}$
$D_2 \rightarrow Z_1$	15605.5	-	$^{3}/_{7} - ^{15}/_{11}$	(laser)	1.66	2.04	2.13	arb
$D_2 \rightarrow Z_2$	15578.5	1.27	"	0.72	0.80	0.77	0.64	"
$D_2 \rightarrow Z_3$	15541.0	$^{14.0}/_{11}$	$^{15}/_{11}$	0.63	0.74	0.64	0.55	$^{3}/_{7} - ^{15}/_{11}$
$D_2 \rightarrow Z_5$	15467.0	1.04	$^{3}/_{7} - ^{15}/_{11}$	0.74	0.85	0.72	0.65	arb
$D_2 \rightarrow Z_6$	15427.5	0.90	"	1.22	1.05	1.37	1.44	"
$D_2 \rightarrow Z_8$	15392.0	$^{14.1}/_{11}$	$^{15}/_{11}$	0.60	0.66	0.58	0.62	$^{3}/_{7} - ^{15}/_{11}$

cont...

Table 4.4 cont...

Transition	**Wavenumber (±0.5) (cm^{-1})**	**Polarisation ratios [y′y′/y′x′] (±10%)**						
		Observed	**Expected**	**Observed**				**Expected**
		$Z_1 \rightarrow D_1$		**$Z_1 \rightarrow D_2$**	**$Z_1 \rightarrow D_3$**	**$Z_1 \rightarrow D_6$**	**$Z_1 \rightarrow D_7$**	
$D_2 \rightarrow Z_9$	15240.5	1.04	$^{3}/_{7}$ - $^{15}/_{11}$	0.72	0.82	0.79	0.64	arb
$D_2 \rightarrow Z_{10}$	15190.0	0.60	"	1.42	1.69	2.70	1.86	"
$D_1 \rightarrow Z_1$	15604.0	(laser)	$^{15}/_{11}$	-	0.53	0.61	0.50	$^{3}/_{7}$ - $^{15}/_{11}$
$D_1 \rightarrow Z_2$	15577.0	$^{14.3}/_{11}$	$^{15}/_{11}$	0.61	0.59	0.64	0.52	"

case irrespective of the particular $Z_1 \rightarrow E$ transition being excited. For $Z \rightarrow D$ excitation however, the well defined polarisation ratios presented in Table 4.4 and consistent with a trigonal symmetry assignment of the B centre were obtained for all the $D \rightarrow Z$ transitions. As can be seen from Table 4.4, exciting the $Z_1 \rightarrow D_2$, $Z_1 \rightarrow D_3$, $Z_1 \rightarrow D_6$ and $Z_1 \rightarrow D_7$ transitions gave similar polarisation ratios while the $Z_1 \rightarrow D_1$ transition gave a different set of ratios. Although the $Z_1 \rightarrow D_4$ transition was too weak to give conclusive results, its polarisation ratios were more comparable with those obtained for $Z_1 \rightarrow D_1$ excitation. From Table 2.4, the ratios obtained with $Z_1 \rightarrow D_1$ and $Z_1 \rightarrow D_4$ excitation were those expected from a $\gamma_a \leftrightarrow \gamma_3$ pump transition, while ratios from excitation of the $Z_1 \rightarrow D_2$, $Z_1 \rightarrow D_3$, $Z_1 \rightarrow D_6$ and $Z_1 \rightarrow D_7$ transitions were as expected for a $\gamma_3 \leftrightarrow \gamma_3$ pump transition. All these results conclusively confirm that the B centre is of exact trigonal symmetry.

Because the excitation spectra show transitions from the Z_1 level to all the expected upper levels of both E and D multiplets, the C_{3v} selection rules indicate that the ground state can only be a γ_3 irrep level. The E_1, E_2 and E_3 levels being the lowest three levels of the E multiplet, are levels of the $^5S_2$ multiplet. Since all transitions from the E_1, E_2 and E_3 levels were observed to the Z_1, Z_2 and Z_3 levels, the Z_2 and Z_3 levels cannot be of γ_2 symmetry because the $^5S_2$ multiplet does not have any γ_2 type level in C_{3v} symmetry. From the observed polarisation ratios for the $D \rightarrow Z$ transitions for $Z \rightarrow D$ excitation and from the assignment of the Z_1 level as of γ_3 symmetry, the D_2, D_3, D_6 and D_7 levels are all assigned to be γ_3 type levels as well. The remaining D_1, D_4 and D_5 levels therefore comprise the two γ_2 and one γ_1 type levels of the D multiplet. Because transitions from both the D_1 and D_4 levels to the Z_3 level were not observed while the $D_5 \rightarrow Z_3$ transition was observed, the D_1 and D_4 levels have the same irrep label type while the D_5 level has the same irrep as the Z_3 level. The D_1 and D_4 levels are therefore assigned as being γ_2 type levels, leaving the D_5 level as the only γ_1 level of the $^5F_5$ multiplet. The Z_3 level itself is also a γ_1 type level because the

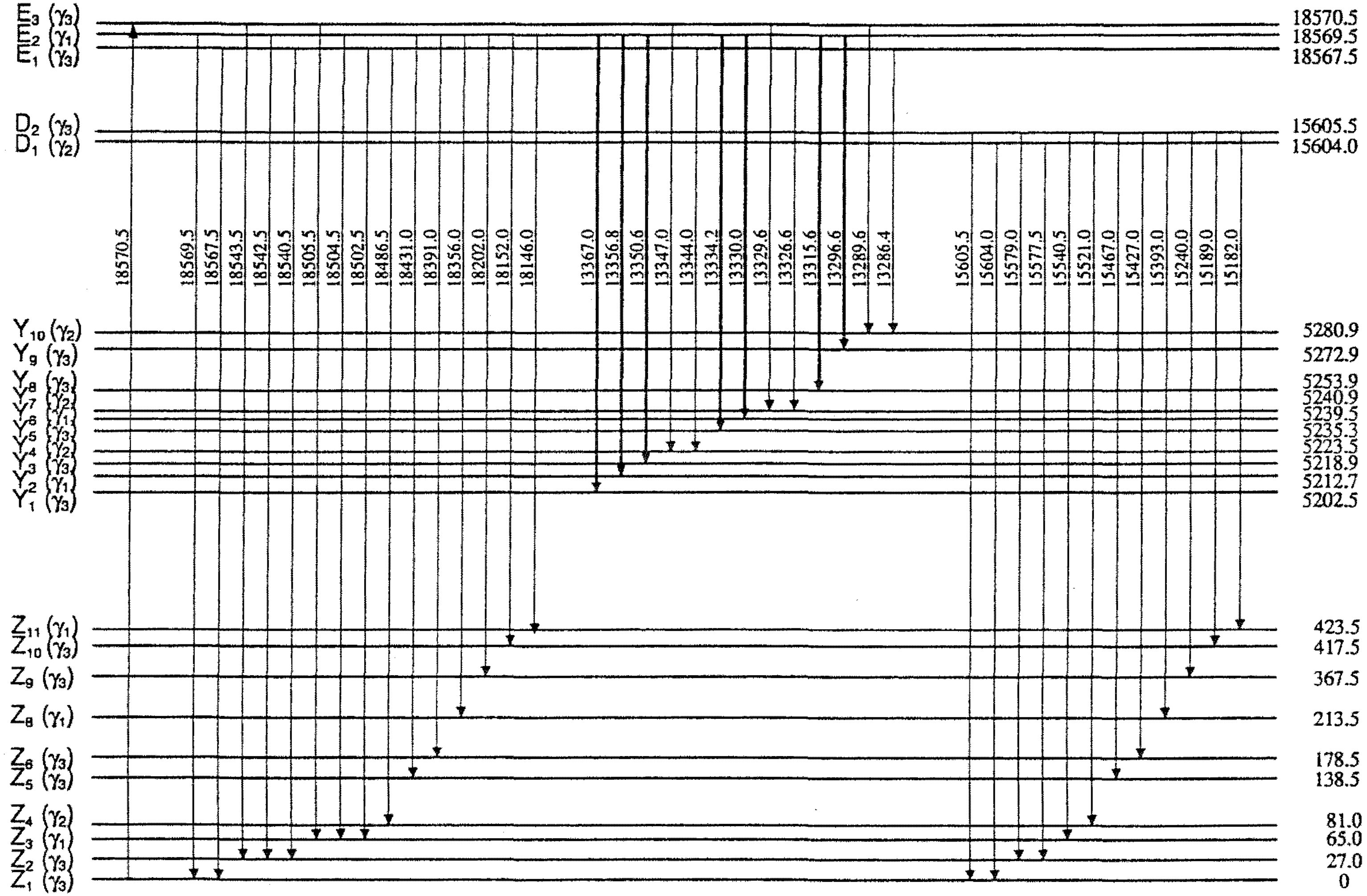

Figure 4.11: Energy level diagram for the B centre in CaF_2:Ho^{3+}(0.005%) crystals, for transitions as measured at 10 K. The bold lines represent a set of three transitions from the E_1, E_2 and E_3 levels to the particular Y multiplet level.

$D_5 \rightarrow Z_3$ transition is observed with ratios characteristic of a $\gamma_a \rightarrow \gamma_a$ fluorescence transition (Table 4.4). Finally, using Tables 2.1(b) and 2.4, the six levels Z_1, Z_2, Z_5, Z_6, Z_9 and Z_{10} are all assigned to be of γ_3 type as well.

Assignment of the Z_3 level as a γ_1 symmetry type level is consistent with one of the E_1, E_2 or E_3 levels having γ_1 symmetry. The E_6 level was assigned as of γ_2 type because the $E_6 \rightarrow Z_3$ transition was absent from the 20 - 55 K spectra (Figure 4.10).

For the E → Y transitions (Figure 4.9(c)), seven sets of three levels have the previously described E_1 - E_2 - E_3 energy level separations and the remaining three sets have just two levels 3.0 cm^{-1} apart. The transitions with the 3.0 cm^{-1} separations identify the three γ_2 type levels of the Y multiplet and the γ_3 type levels of the $^5S_2$ multiplet. As $\gamma_1 \leftrightarrow \gamma_2$ type transitions are forbidden, transitions from the $^5S_2$ multiplet levels to the γ_2 levels of the Y multiplet will necessarily only occur in pairs. Since transitions from the E_2 level to the Y_4, Y_7 and Y_{10} levels are all absent, the E_2 level is assigned as a γ_1 type level and the Y_4, Y_7 and Y_{10} levels are all γ_2 type levels of the Y multiplet. Hence the remaining levels Y_1, Y_2, Y_3, Y_5, Y_6, Y_8 and Y_9 comprise five of γ_3 symmetry and two of γ_1 symmetry types.

An energy level scheme showing all the levels derived and the proposed irrep labels is presented in Figure 4.11 and Table 4.3.

Because polarisation ratios could not be observed for Z → E excitation it is not possible to deduce from polarisation ratio measurements the irrep labels for any of the higher E multiplet levels. For such levels, irrep labels were assigned in accordance with the crystal-field calculations discussed in Chapter 7. There is confidence in such assignments because the irrep labels derived from the polarisation study here were found to agree completely with those predicted by the crystal-field calculations. For Z → E excitation, it appears that because of the small energy separations between the lowest three E levels, the polarisation ratios measured are always a superposition of the polarisation ratios of transitions from

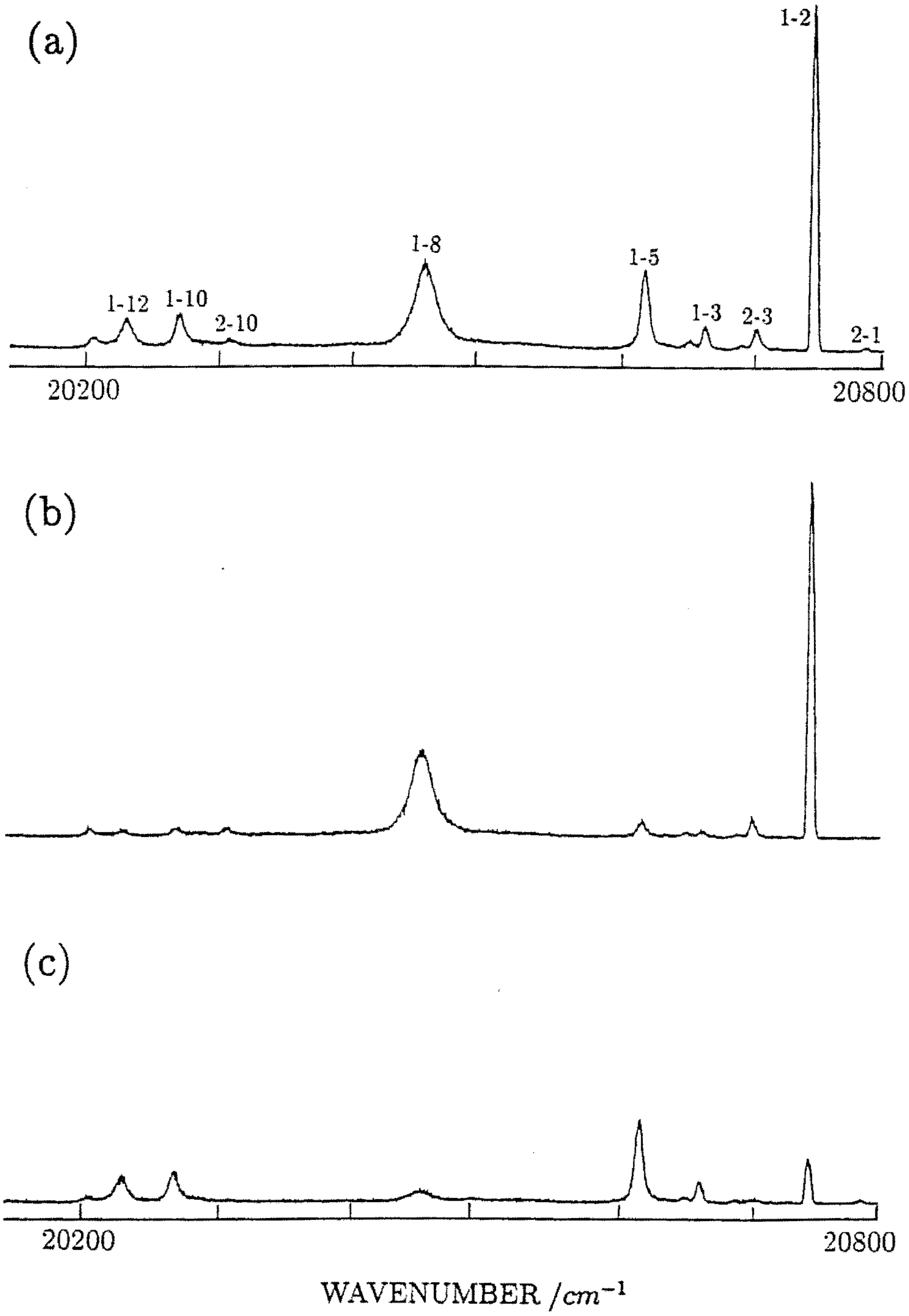

Figure 4.12: 10 K upconversion fluorescence spectrum of the F→Z transitions for the A centre in CaF_2:Ho^{3+}(0.005%) crystals, for excitation of the $Z_1 \rightarrow D_4$ transition at 15682.0 cm^{-1} :
(a) unpolarised; (b) π polarisation; (c) σ polarisation.

Table 4.5: Observed and predicted intensity ratios for the polarised F→Z fluorescence transitions of the A centre in < 100 > oriented CaF_2:Ho^{3+}(0.005%) crystals, for excitation of the Z_1→D_4 transition at 15682.0 cm^{-1}.

Transition	**Wavenumber (±0.5) cm^{-1}**	**Polarisation Ratios (±10%) [yy : yx]** Observed	Expected
F_2→Z_1	20781.5	1 : 4.6	0 : 1
F_2→Z_2	20779.5	1 : 4.3	0 : 1
F_2→Z_3	20698.0	4.1 : 1	1 : 0
F_2→Z_{10}	20305.5	6.1 : 1	1 : 0
F_1→Z_2	20739.5	7.9 : 1	1 : 0
F_1→Z_3	20659.5	1 : 3.7	0 : 1
F_1→Z_5	20614.0	1 : 4.6	0 : 1
F_1→Z_8	20441.0	7.0 : 1	1 : 0
F_1→Z_{10}	20268.0	1 : 3.9	0 : 1
F_1→Z_{12}	20227.5	1 : 3.7	0 : 1

two γ_3 type levels with a γ_1 level in-between to a particular Z or Y multiplet level. This would happen irrespective of the $Z_1 \rightarrow E$ transition pumped since the E_1, E_2 and E_3 levels are all originating levels for the observed fluorescence. Transitions from higher energy levels observed in the 20 - 55 K spectra were too weak to give any conclusive results as to polarisation ratio.

4.1.5 Upconversion fluorescence of the A and B centres

For the A centre, upconversion fluorescence was observed from both the $F(^5F_3)$ (Figure 4.12(a)) and E multiplets for $Z \rightarrow D$ excitation. The fluorescence was quite weak with that from the E multiplet being only 10^{-5} the intensity obtained for direct excitation of this multiplet.

This upconversion fluorescence was polarised identically to that observed for direct excitation in respect of the $E \rightarrow Z$ and $E \rightarrow Y$ transitions. From the polarisation spectra for the $F \rightarrow Z$ transitions presented in Figure 4.12(b),(c) and Table 4.5, the $F_1 \rightarrow Z_2$ and $F_1 \rightarrow Z_8$ transitions are observed to be principally π polarised, consistent with $\gamma_a \rightarrow \gamma_a$ fluorescence transitions for a $\gamma_a \rightarrow \gamma_a$ pump transition. This identifies the F_1 level as a γ_2 type level. Transitions to the Z_3, Z_5, Z_{10} and Z_{12} levels are all σ polarised as expected for $\gamma_{a'} \rightarrow \gamma_5$ fluorescence transitions. As the $F_2 \rightarrow Z_1,Z_2$ transitions at 20781.5, 20779.5 cm^{-1} respectively are both σ polarised while the $F_2 \rightarrow Z_3$ and $F_2 \rightarrow Z_{10}$ transitions at 20698.0 and 20305.5 cm^{-1} respectively, are observed to be π polarised, the F_2 level is assigned as a γ_5 type level.

For the B centre, no upconversion fluorescence for $Z \rightarrow D$ excitation was observable at all from either the E or F multiplets, giving an upper limit of well less than 10^{-7} of that for direct excitation for the E multiplet.

No upconversion fluorescence was observed for $Z \rightarrow E$ excitation for either the A or B centres setting an upper limit of 10^{-7} for both these cases.

4.2 Spectroscopy of $Ca_{0.99}Sr_{0.01}F_2:Ho^{3+}$(0.005%) Crystals

Laser excitation spectra of $Ca_{0.99}Sr_{0.01}F_2:Ho^{3+}$(0.005%) crystals monitoring all fluorescence transitions in the 15000 cm^{-1} region showed new transitions fairly close in energy to parent A centre transitions. By laser selective excitation of several of the new Z → E transitions, two distinct centres were identified. These are arbitrarily labelled as CS1 and CS2 in Figure 4.13. Because these transitions are weak, being only 5 - 10% of the intensity of the A centre transitions and quite close in energy to them, well discriminated selective excitation spectra, with minimal interference by neighbouring transitions of either the A or B centres, could only be obtained by monitoring the $E_2 \rightarrow Z_1$ transition of the appropriate centre in each case. Neither the CS1 nor CS2 centres could be selectively excited clearly in the D multiplet region because their transitions were much weaker and either overlapped or were so close to corresponding transitions of the A and B centres that simultaneous excitation of the different centres could not be avoided. Transitions corresponding to the CS1 and CS2 centres for Z → D excitation are so identified in the broadband excitation spectra given in Figure 4.14. These transitions were classified through their fluorescence spectra.

4.2.1 Spectroscopy of the CS1 centre

Both the excitation and fluorescence spectra for the CS1 centre (Figures 4.13(b) and 4.15) are similar to those for the A centre except for an overall shift of all the energy levels to lower energies. A Z_1 - Z_2 level splitting of 2.0 cm^{-1} is apparent in the transitions to the E_2, E_3 and E_6 levels. As found for the A centre, four sets of transition pairs are observed in the E → Z fluorescence spectrum for $Z_1 \rightarrow E_2$ excitation (Figure 4.15(a)). The E_1- E_2 energy level separation of 11.0 cm^{-1} for this centre is somewhat smaller than the 14.0 cm^{-1} found for the A centre. The four transition pairs are to the Z_3, Z_5, Z_{10} and Z_{12} levels identified as for the A centre. Three single transitions are observed at 18490.5, 18148.5 and 18128.0 cm^{-1} (in the 10 K spectra).

As for the A centre, spectra up to 30 K were recorded to determine the origin of the transition pairs. At 20 K, the higher energy transition in each pair as well as the single transition at 18128.0 cm^{-1} became more intense than at 10 K.

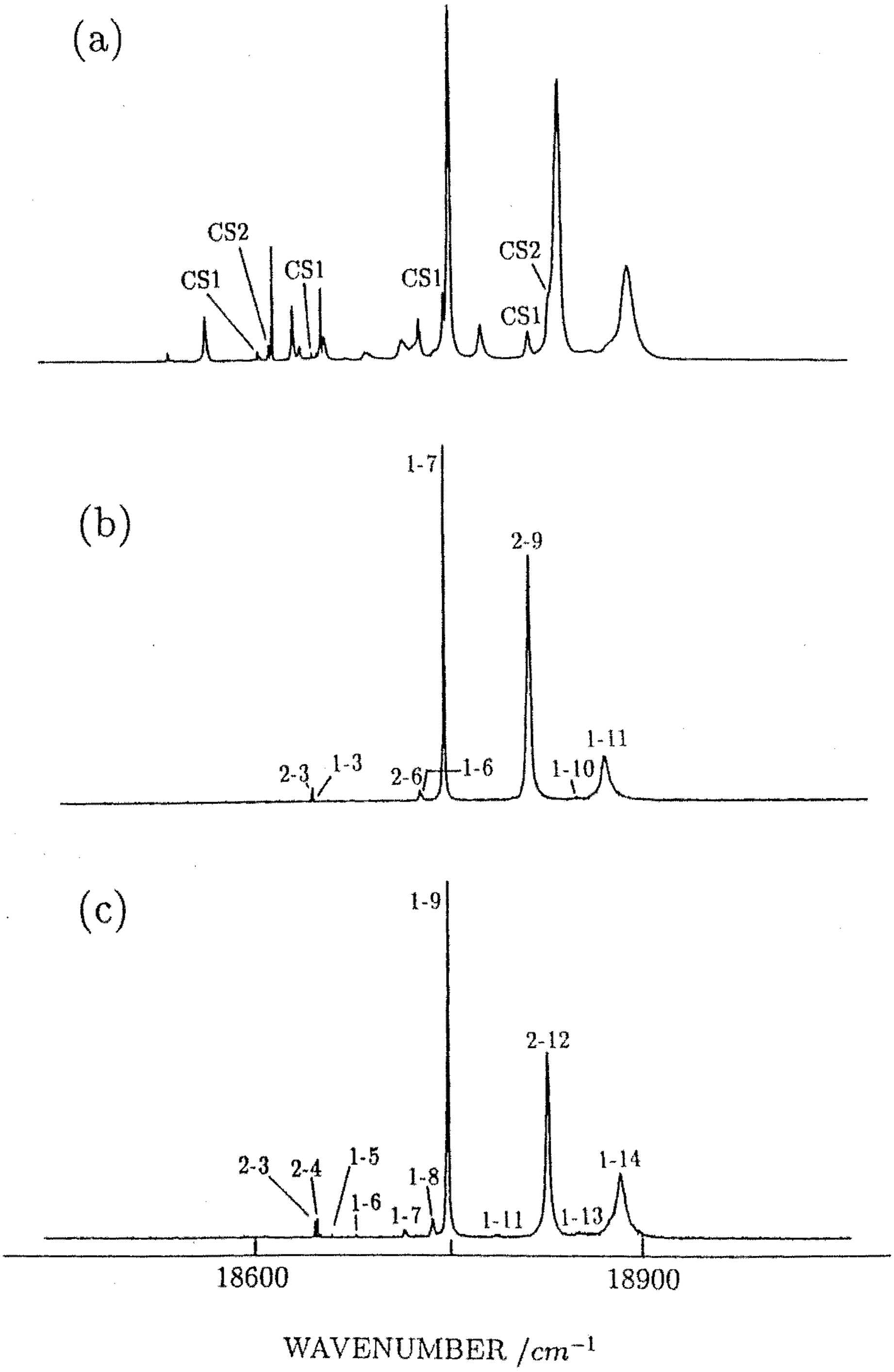

Figure 4.13: 10 K broadband and selective excitation spectra of the E multiplet in $Ca_{0.99}Sr_{0.01}F_2$:Ho^{3+}(0.005%) crystals :
(a) broadband excitation spectrum, monitoring all the D →Z transitions;
(b) CS1 centre excitation spectrum, monitoring the $E_2 \rightarrow Z_1$ transition at 18601.0 cm^{-1};
(c) CS2 centre excitation spectrum, monitoring the $E_2 \rightarrow Z_1$ transition at 18608.5 cm^{-1}.
Transitions are labelled by the appropriate lower and upper multiplet crystal-field level identifications.

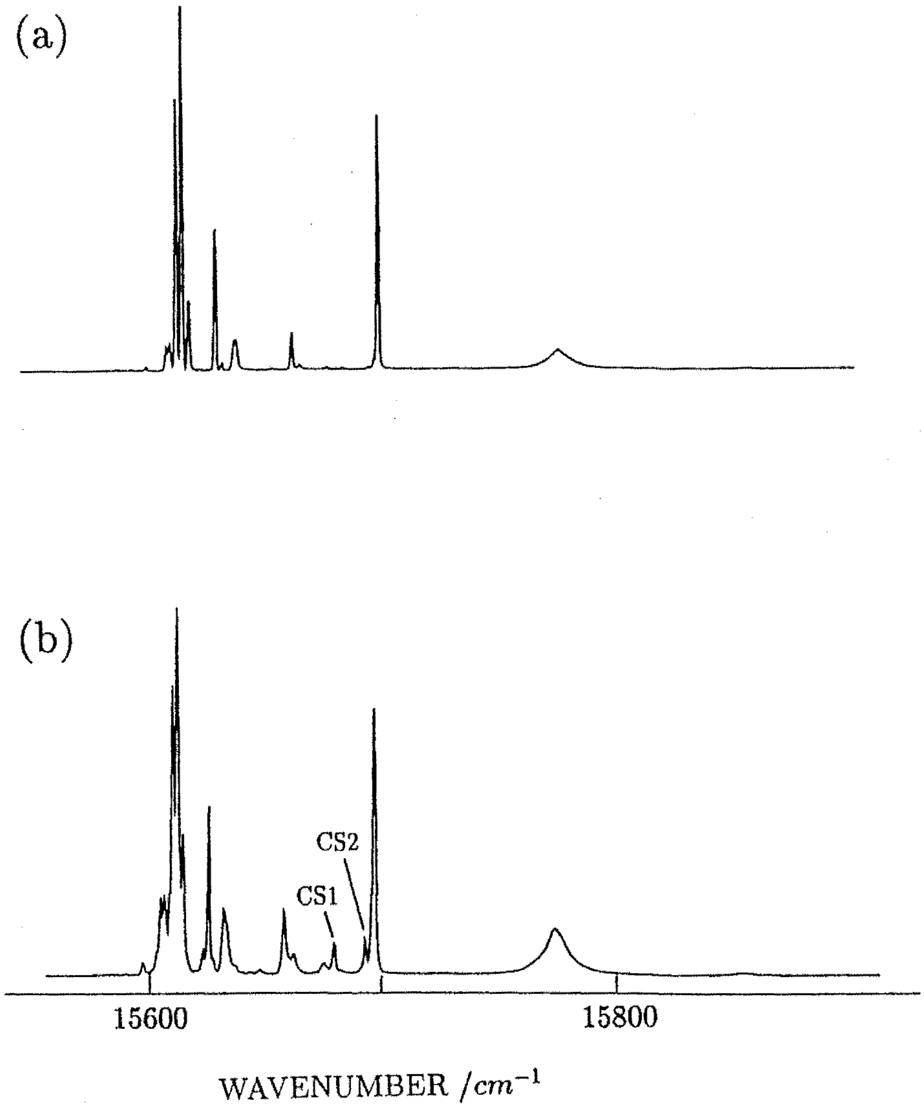

Figure 4.14: 10 K broadband excitation spectrum of the D multiplet in $Ca_{0.99}Sr_{0.01}F_2$:Ho^{3+}(0.005%) crystals :
(a) broadband spectrum in pure CaF_2:Ho^{3+}(0.005%);
(b) broadband spectrum in $Ca_{0.99}Sr_{0.01}F_2$:Ho^{3+}(0.005%).

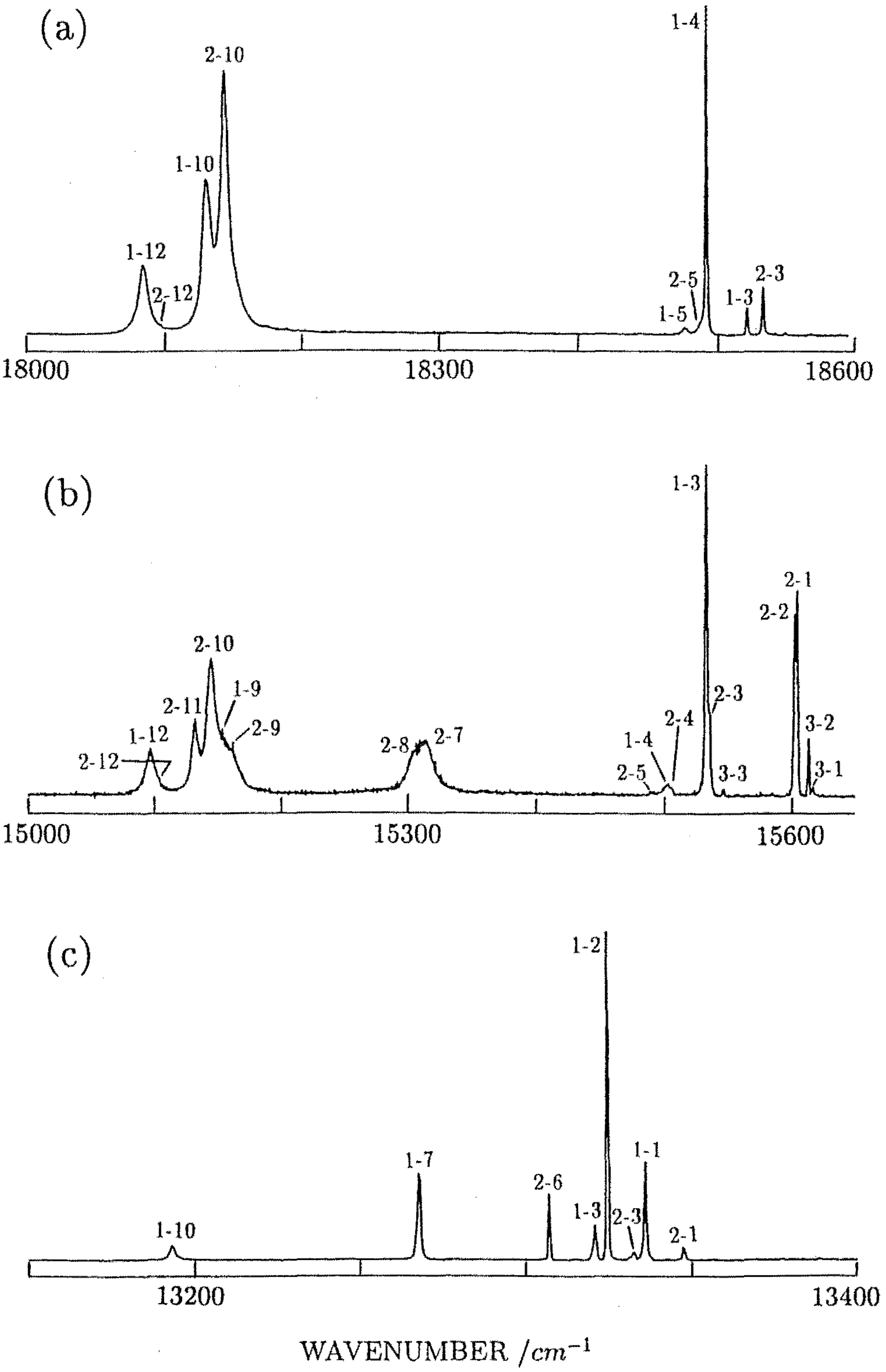

Figure 4.15: 10 K fluorescence spectra for the CS1 centre in $Ca_{0.99}Sr_{0.01}F_2:Ho^{3+}$(0.005%) crystals :
(a) E→Z transitions, for excitation of the $Z_1 \rightarrow E_2$ transition at 18601.0 cm^{-1};
(b) D→Z transitions, for excitation of the $Z_1 \rightarrow D_4$ transition at 15663.5 cm^{-1};
(c) E→Y transitions, for excitation of the $Z_1 \rightarrow E_2$ transition at 18601.0 cm^{-1}.
Transitions are labelled by the appropriate upper and lower multiplet crystal-field level identifications.

These transitions therefore originate from the lowest directly observed E_2 level at 18601.0 cm^{-1} while the remainder originate from a lower E_1 level whose energy is inferred as 18590.0 cm^{-1}, 11.0 cm^{-1} lower than the E_2 level. The transition pairs from the E_1 and E_2 levels identify the four levels Z_3, Z_5, Z_{10} and Z_{12} at 70.0, 115.0, 458.5 and 506.5 cm^{-1} respectively, as being γ_5 type levels. The single transitions at 18490.5, 18148.5 and 18128.0 cm^{-1} are assigned as the $E_1 \rightarrow Z_4$, $E_1 \rightarrow Z_9$ and $E_2 \rightarrow Z_{11}$ transitions respectively.

The E → Y spectrum (Figure 4.15(c)) has two sets of transition pairs with the E_1 - E_2 energy separation of 11.0 cm^{-1}. The higher energy transition in each pair was more intense at 20 K than at 10 K. Of the five single transitions at 13323.5, 13306.0, 13267.0, 13245.0 and 13192.0 cm^{-1}, only the transition at 13306.0 cm^{-1} was found to increase in intensity in going from 10 K to 20 K while the other four became weaker. The transition at 13306.0 cm^{-1} is therefore assigned as originating from the E_2 level, giving the Y_6 level energy as 5295.0 cm^{-1} while the transitions at 13323.5, 13267.0, 13245.0 and 13192.0 cm^{-1} all originate from the E_1 level to the Y multiplet levels Y_2, Y_7, Y_8 and Y_{10} at 5266.5, 5323.0, 5345.0 and 5398.0 cm^{-1} respectively.

From the D → Z spectrum (Figure 4.15(b)), the Z_1 - Z_2 energy level separation of 2.0 cm^{-1} is apparent in the sharpest fluorescence transitions from the D_2 and D_3 levels at 15603.0 and 15614.0 cm^{-1} respectively. The $D_1 \rightarrow Z_1,Z_2$ transitions were not observed, but transitions observed to the Z_3, Z_5, Z_{10} and Z_{12} levels place the D_1 level at 15600.0 cm^{-1}. The D_1 - D_2 energy level separation of 3.0 cm^{-1} found is slightly smaller than the 4.5 cm^{-1} determined for the A centre. The broad feature centred at 15310.0 cm^{-1} in the D → Z spectrum does not show clearly in the E → Z spectrum.

As raising the crystal temperature above 10 K resulted in unavoidable simultaneous excitation of the parent A centre, the higher energy E → Z transitions for the CS1 centre could not be identified. As a result, energies for the E_4, E_5 and Z_6 levels could not be determined as done for the A centre.

Table 4.6: Energy levels (in cm^{-1}) of the Z, Y, D and E multiplets of the CS1 centre and their symmetries, as derived from the 10 K spectra of $Ca_{0.99}Sr_{0.01}F_2:Ho^{3+}$(0.005%) crystals. Uncertainty is ± 0.5 cm^{-1}.

Level	Z($^5I_8$)	Y($^5I_7$)	D($^5F_5$)	E($^5S_2$,$^5F_4$)
1	0(γ_1)	5254.5(γ_5)	15600.0(γ_3)	18590.0(γ_3)
2	2.0(γ_2)	5266.5(γ_3)	15603.0(γ_5)	18601.0(γ_1)
3	70.0(γ_5)	5269.5(γ_5)	15614.0(γ_2)	18646.6(γ_5)
4	99.5(γ_3)	-	15663.5(γ_1)	-
5	115.0(γ_5)	-		-
6	-	5295.0(γ_1)		18725.6(γ_5)
7	296.0(γ_1)	5323.0(γ_5)		18744.3(γ_1)
8	301.0(γ_2)	5345.0(γ_3)		-
9	441.5(γ_3)	-		18808.5(γ_2)
10	458.5(γ_5)	5398.0(γ_5)		18848.0(γ_5)
11	473.0(γ_1)	-		18870.5(γ_1)
12	506.5(γ_5)			
13	-			

The energy levels derived for the CS1 centre are presented in Table 4.6.

4.2.2. Polarisation study of the CS1 centre

Polarisation measurements made on both <100> and <111> oriented crystals, as listed in Table 4.7, are fully consistent with a C_{4v} symmetry assignment for this centre.

For $Z_1 \rightarrow E_2$ excitation of the <100> oriented crystal, the $E \rightarrow Z$ transitions displayed the following polarisation behaviour :

(i) the transition pairs were all polarised 0:1, consistent with a γ_5 irrep label assignment for the Z_3, Z_5, Z_{10} and Z_{12} levels;

(ii) for the single transitions at 18490.5, 18148.5 and 18128.0 cm^{-1} the polarisation ratios of 1:0 observed indicate a $\gamma_a \rightarrow \gamma_a$ type transition. With the first two transitions identified as being the $E_1 \rightarrow Z_4$ and $E_1 \rightarrow Z_9$ transitions, a γ_3 irrep is assigned for the Z_4, Z_9 and E_1 levels. The transition at 18128.0 cm^{-1} corresponds to the $E_2 \rightarrow Z_{11}$ transition making the Z_{11} level a γ_1 type level, the same as the E_2 level.

This analysis gives an exact one to one correspondence between all the A and CS1 centre transitions. Again the $E_1 \rightarrow Z_9$ and $E_2 \rightarrow Z_{11}$ transitions are more easily separated in the polarised spectra (Figure 4.16(a)) for exactly the same reasons as discussed for the corresponding A centre transitions. Similar irrep label assignments were found for the D and Y levels. From the polarised excitation spectra (Figure 4.16(c)), the E_3, E_6 and E_{10} levels are all γ_5 type levels. Because the $D \rightarrow Z$ transitions were quite weak, polarisation ratios were only measurable for transitions up to the $D_1 \rightarrow Z_3$ transition at 15530.0 cm^{-1}, however these data were sufficient for assigning irrep labels to all the D multiplet levels.

The proposed model for this centre is for the Sr^{2+} ion to be located on the Ho^{3+} - F^- axis, on the opposite side of the interstitial F^- ion as shown in Figure 1.4(a). Such a configuration preserves the C_{4v} symmetry of the parent A centre but still has a sufficiently different crystal field at the Ho^{3+} ion site to cause an

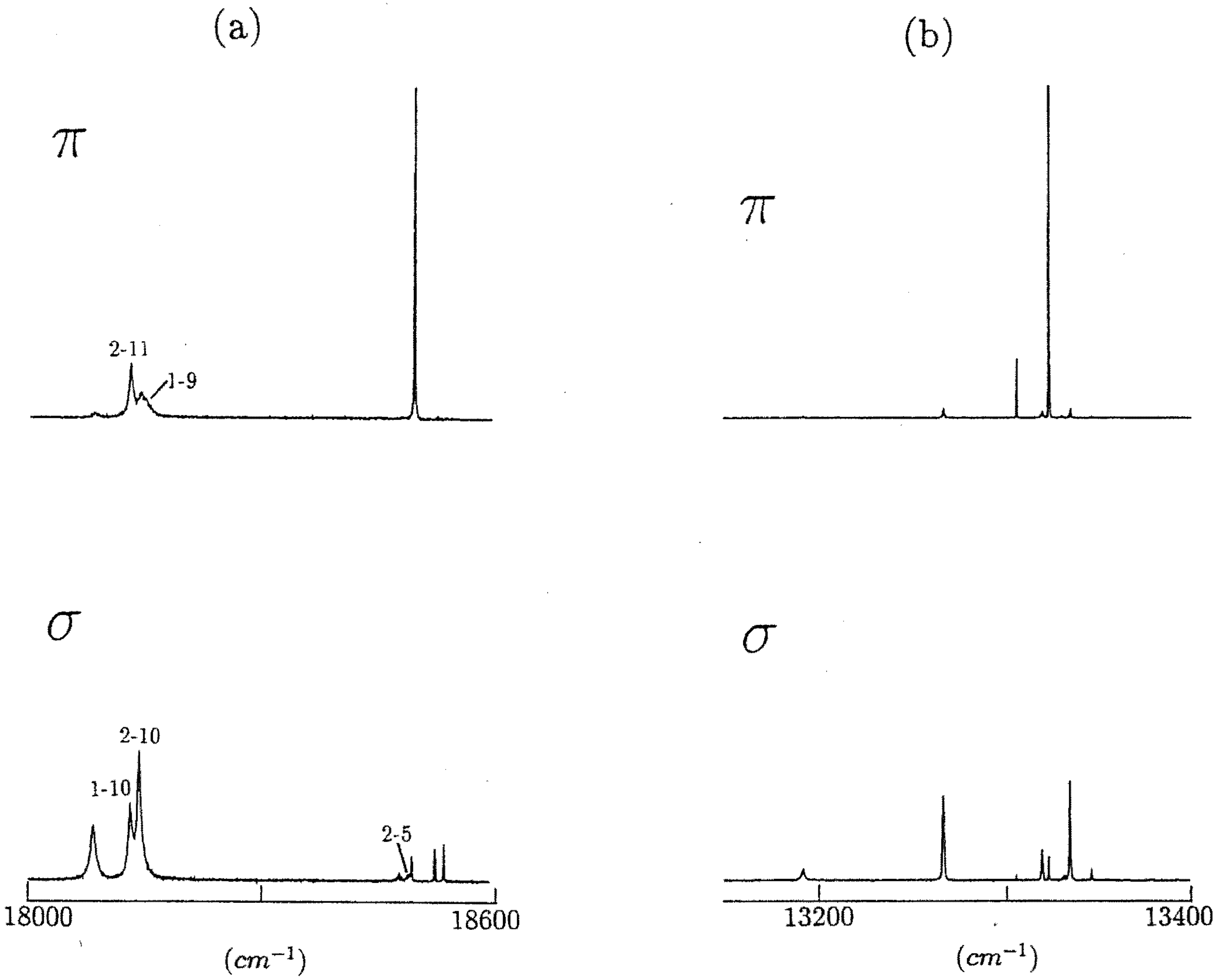
(a)
(b)
π
2-11
1-9
π
σ
2-10
1-10
2-5
σ
18000
18600
(cm⁻¹)
13200
13400
(cm⁻¹)

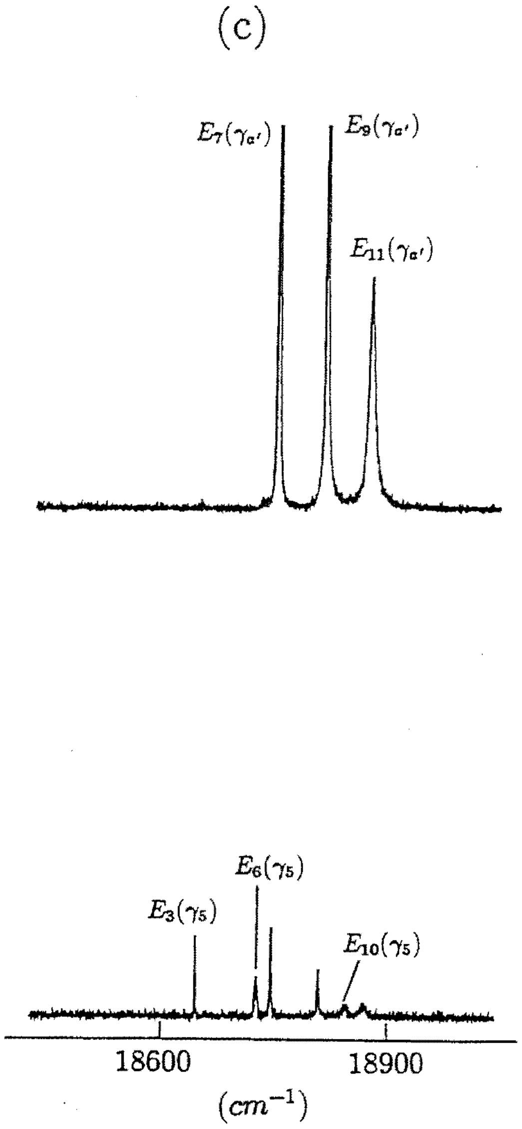

Figure 4.16: Polarisation of the 10 K selective excitation and fluorescence spectra of the CS1 centre in $Ca_{0.99}Sr_{0.01}F_2$:Ho^{3+}(0.005%) crystals :
(a) E→Z transitions, for excitation of the Z_1→E_2 transition at 18601.0 cm^{-1};
(b) E→Y transitions, for excitation of the Z_1→E_2 transition at 18601.0 cm^{-1};
(c) Z→E transitions, monitoring the E_2→Z_1 transition at 18601.0 cm^{-1}.
Transition labels are as in Figures 4.13(b) and 4.15.

Table 4.7: Observed and predicted intensity ratios for the polarised fluorescence transitions of the CS1 centre in < 100 > and < 111 > oriented $Ca_{0.99}Sr_{0.01}F_2$:Ho^{3+}(0.005%) crystals, for excitation of the $Z_1 \rightarrow E_2$ transition at 18601.0 cm^{-1}.

Transition	**Wavenumber** ($\pm$0.5) cm^{-1}	**Polarisation Ratios** ($\pm$10%) **< 100 > orientation** [yy : yx]		**< 111 > orientation** [y′y′/y′x′]	
		Observed	**Expected**	**Observed**	**Expected**
$E_2 \rightarrow Z_3$	18531.0	1 : 7.8	0 : 1	$^{3.5}/_{5}$	$^{3}/_{5}$
$E_2 \rightarrow Z_5$	18486.5	1 : 8.8	0 : 1	$^{3.0}/_{5}$	$^{3}/_{5}$
$E_2 \rightarrow Z_{10}$	18142.5	1 : 7.9	0 : 1	$^{3.5}/_{5}$	$^{3}/_{5}$
$E_2 \rightarrow Z_{11}$	18128.0	7.6 : 1	1 : 0	2.3	3.0
$E_1 \rightarrow Z_3$	18520.0	1 : 8.2	0 : 1	$^{3.5}/_{5}$	$^{3}/_{5}$
$E_1 \rightarrow E_4$	18490.5	14.9 : 1	1 : 0	2.3	3.0
$E_1 \rightarrow Z_5$	18475.0	1 : 9.0	0 : 1	$^{3.5}/_{5}$	$^{3}/_{5}$
$E_1 \rightarrow Z_9$	18148.5	5.5 : 1	1 : 0	-	3.0
$E_1 \rightarrow Z_{10}$	18130.5	1 : 8.6	0 : 1	$^{3.5}/_{5}$	$^{3}/_{5}$
$E_1 \rightarrow Z_{13}$	18083.5	1 : 7.7	0 : 1	$^{3.5}/_{5}$	$^{3}/_{5}$
$E_2 \rightarrow Y_1$	13346.5	1 : 6.8	0 : 1	$^{3.5}/_{5}$	$^{3}/_{5}$
$E_2 \rightarrow Y_3$	13331.5	1 : 3.6	0 : 1	$^{3.5}/_{5}$	$^{3}/_{5}$
$E_2 \rightarrow Y_6$	13306.0	18.5 : 1	1 : 0	2.2	3.0
$E_1 \rightarrow Y_1$	13335.0	1 : 9.8	0 : 1	$^{3.5}/_{5}$	$^{3}/_{5}$
$E_1 \rightarrow Y_2$	13323.5	13.0 : 1	1 : 0	2.3	3.0
$E_1 \rightarrow Y_3$	13320.0	1 : 4.1	0 : 1	$^{4.0}/_{5}$	$^{3}/_{5}$
$E_1 \rightarrow Y_7$	13267.0	1 : 8.2	0 : 1	$^{3.5}/_{5}$	$^{3}/_{5}$
$E_1 \rightarrow Y_{10}$	13192.0	1 : 5.6	0 : 1	$^{3.5}/_{5}$	$^{3}/_{5}$
$D_3 \rightarrow Z_2$	15612.0	6.7 : 1	1 : 0	2.1	3.0
$D_2 \rightarrow Z_1$	15603.0	1 : 8.7	0 : 1	$^{3.5}/_{5}$	$^{3}/_{5}$
$D_2 \rightarrow Z_2$	15601.0	1 : 8.1	0 : 1	$^{4.0}/_{5}$	$^{3}/_{5}$
$D_2 \rightarrow Z_3$	15533.0	7.7 : 1	1 : 0	2.3	3.0
$D_1 \rightarrow Z_3$	15530.0	1 : 6.1	0 : 1	$^{4.0}/_{5}$	$^{3}/_{5}$

overall shift of all levels to slightly lower energies. The complete energy level scheme together with the proposed irrep labels are presented in Table 4.6. The energy level diagram is closely similar to that given in Figure 4.8 for the A centre, except for the small shifts in energies, and therefore need not be separately reproduced here.

4.2.3 Spectroscopy of the CS2 centre

More transitions were observed in both the excitation and fluorescence spectra (Figures 4.13(c) and 4.17) for the CS2 centre than for either the CS1 or A centres. The main features of the spectra of the CS2 centre are :-

(i) the $Z_1,Z_2 \leftrightarrow E_1$ transitions which are unobserved for the CS1 and A centres are now observed;

(ii) the $E_1 - E_2$ energy separation of 13.5 cm^{-1} lies between the 11.0 cm^{-1} found for the CS1 centre and the 14.0 cm^{-1} for the A centre;

(iii) a $Z_1 - Z_2$ level separation of 2.0 cm^{-1} is apparent in the sharper transitions to the lowest energy levels of the E and D multiplets;

(iv) transition pairs are now observed for all transitions involving γ_5 (doublet) type levels of the C_{4v} symmetry centres;

(v) all possible transitions are allowed, as the maximum possible 17 levels are observed for the Z multiplet, 12 levels for the Y multiplet and 13 out of the possible 14 for the E multiplet;

(vi) the excitation transitions are all at least 5 cm^{-1} higher in energy than corresponding single transitions for the CS1 centre but lower in energy than those for the A centre. In general, the CS2 centre energies are closer to those of the A centre than to those of the CS1 centre.

From the E → Z spectrum shown in Figure 4.17(a), it can be seen that transitions that occur in pairs for the CS1 centre now consist of two sets of close energy pairs, with each pair having the $E_1 - E_2$ level separation of 13.5 cm^{-1}. For

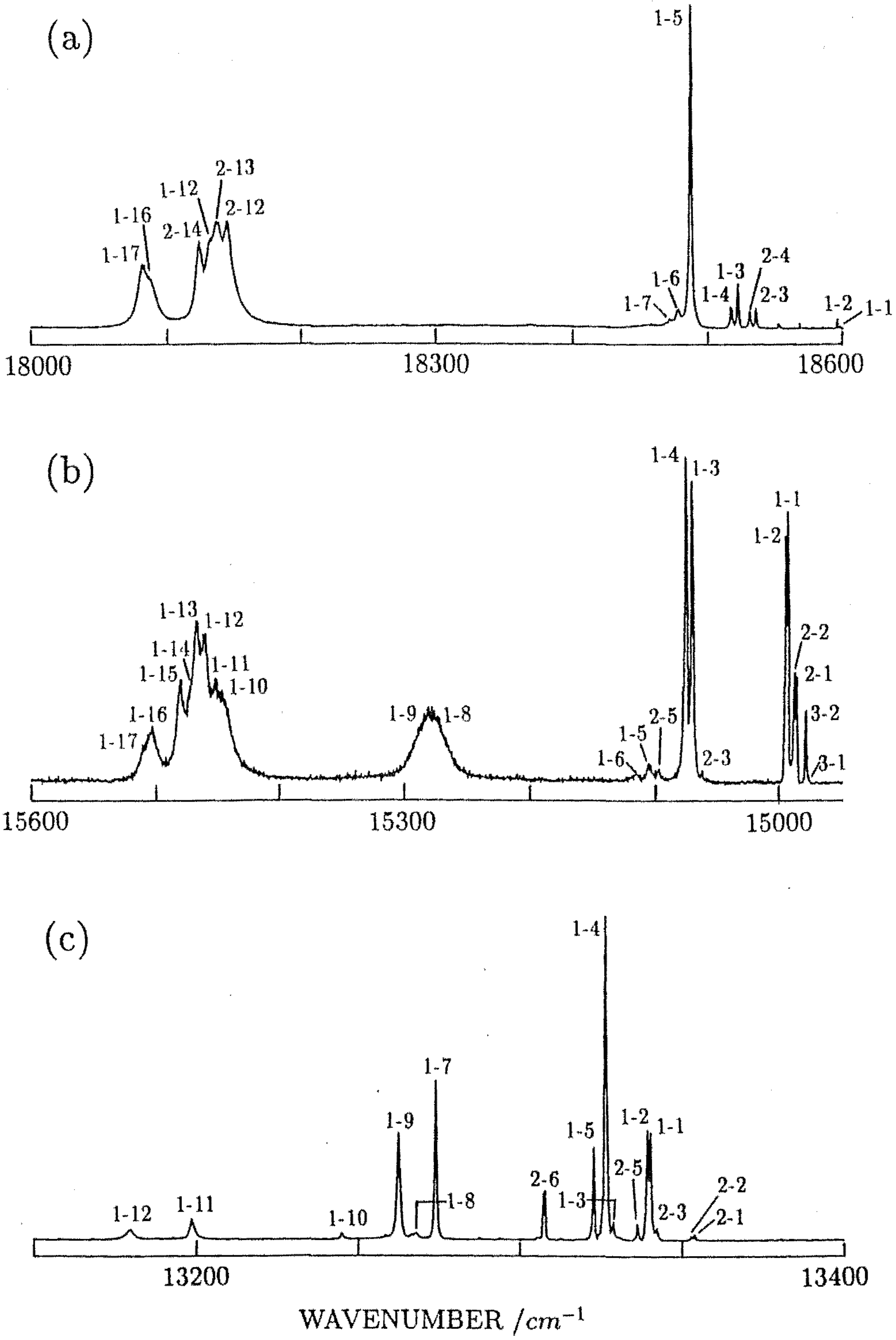

Figure 4.17: 10 K fluorescence spectra for the CS2 centre in $Ca_{0.99}Sr_{0.01}F_2$:Ho^{3+}(0.005%) crystals :
(a) E→Z transitions, for excitation of the $Z_1 \rightarrow E_2$ transition at 18608.5 cm^{-1};
(b) D→Z transitions, for excitation of the $Z_1 \rightarrow D_5$ transition at 15679.0 cm^{-1};
(c) E→Y transitions, for excitation of the $Z_1 \rightarrow E_2$ transition at 18608.5 cm^{-1}.
Transitions are labelled by the appropriate upper and lower multiplet crystal-field level identifications.

example, the CS1 centre transition pair at 18531.0 and 18520.0 cm^{-1} is now split in the CS2 centre to become four transitions at 18533.0, 18528.0, 18519.5 and 18515.0 cm^{-1}. These transitions can be classified as (i) a pair at 18533.0 and 18519.5 cm^{-1} and (ii) a pair at 18528.0 and 18515.0 cm^{-1}, with the separation within each pair being 13.5 cm^{-1} and the separation between these particular two pairs 4.5 cm^{-1}. The 4.5 cm^{-1} is assigned as the splitting of the Z_3 γ_5 (doublet) terminating level in the CS2 centre. This second separation will be distinctly different for each set of four transitions as different γ_5 terminating levels are involved. From the energy level scheme given in Figure 4.18, the Z_3, Z_5, Z_{10} and Z_{12} levels of the CS1 centre are split by 4.5, 6.0, 8.5 and 5.5 cm^{-1} respectively, for the CS2 centre. All four transitions in a particular group have comparable intensities while those transitions that were absent for the CS1 centre, for example the $E_1 \rightarrow Z_1,Z_2$ transitions, are still relatively weak. The three single transitions for this CS2 centre are observed at 18485.0, 18148.0 and 18123.0 cm^{-1} compared to the corresponding 18490.5, 18148.5 and 18128.0 cm^{-1} transitions respectively, found for the CS1 centre.

From the E → Y spectrum (Figure 4.17(c)), low symmetry splittings are also observed for transitions to the Y_1, Y_3, Y_7 and Y_{10} levels of the CS1 centre. Such splittings are measured to be 1.0, 2.0, 11.5 and 19.0 cm^{-1} respectively, being a range of both very small and very large values in comparison to the Z level splittings.

Splittings of the D → Z transitions (Figure 4.17(b)) are all the same as for the corresponding E → Z transitions, apart from the additional D_2 level splitting of 7.0 cm^{-1}.

The energy levels derived for the CS2 centre are presented in Table 4.8.

4.2.4 Polarisation study of the CS2 centre

Polarisation measurements obtained with either $Z_1 \rightarrow E_2$ excitation (Figure 4.19, Table 4.9) or $Z_2 \rightarrow E_4$ excitation (Figure 4.20, Table 4.10) are summarised below.

Table 4.8: Energy levels (in cm^{-1}) of the Z, Y, D and E multiplets of the CS2 centre and their symmetries, as derived from the 10 K spectra of $Ca_{0.99}Sr_{0.01}F_2$:Ho^{3+}(0.005%) crystals. Uncertainty is ±0.5 cm^{-1}.

Level	$Z(^5I_8)$	$Y(^5I_7)$	$D(^5F_5)$	$E(^5S_2, ^5F_4)$
1	0(γ_1)	5255.5(γ_2)	15604.0(γ_1)	18595.0(γ_1)
2	2.0(γ_2)	5256.5(γ_1)	15611.0(γ_2)	18608.5(γ_1)
3	75.5(γ_1)	5267.0(γ_2)	-	18650.5(γ_2)
4	80.0(γ_2)	5269.0(γ_1)	15621.0(γ_2)	18652.8(γ_1)
5	110.0(γ_1)	5272.5(γ_1)	15679.0(γ_1)	18660.0(γ_2)
6	119.0(γ_2)	5301.5(γ_1)		18677.6(γ_1)
7	125.0(γ_1)	5321.0(γ_2)		18713.0(γ_2)
8	277.0(γ_1)	5327.5(γ_2)		18736.4(γ_1)
9	285.0(γ_2)	5332.5(γ_1)		18748.2(γ_1)
10	447.0(γ_1)	5350.0(γ_1)		-
11	454.0(γ_1)	5396.5(γ_1)		18785.0(γ_2)
12	465.0(γ_2)	5415.5(γ_2)		18825.0(γ_2)
13	473.5(γ_1)			18849.5(γ_1)
14	485.5(γ_1)			18880.8(γ_1)
15	488.0(γ_2)			
16	509.0(γ_1)			
17	514.5(γ_2)			

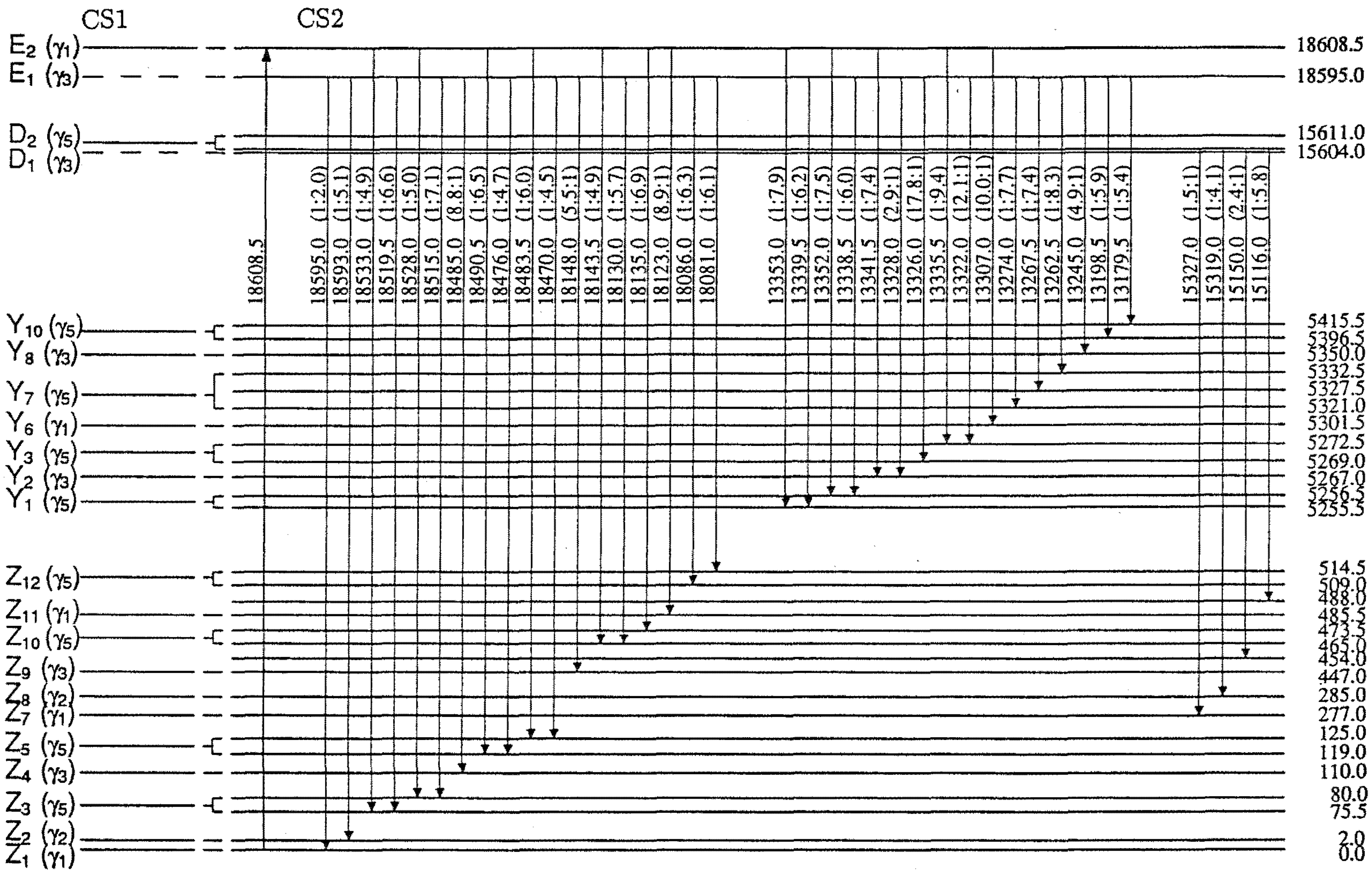

Figure 4.18: Energy level diagram for the CS2 centre in $Ca_{0.99}Sr_{0.01}F_2$:Ho^{3+}(0.005%) crystals, for the E → Z and E → Y transitions as measured at 10 K. For the particular Z levels not accessed by transitions from the E_1, E_2 levels, transitions from the D_1 level are shown. The energy levels on the left are those of the CS1 centre. Energy level irreps for the CS2 centre are presented in Table 4.8.

(a) For $Z_1 \rightarrow E_2$ ($\gamma_a \rightarrow \gamma_a$) excitation :-

(i) the $E \rightarrow Z$ transitions at 18485.0, 18148.0 and 18123.0 cm^{-1} were found to be π polarised (Figure 4.19(a)) just as were the $E_1 \rightarrow Z_4$, $E_1 \rightarrow Z_9$ and $E_2 \rightarrow Z_{11}$ transitions of the CS1 centre;

(ii) both sets of transitions from the E_1 and E_2 levels to split γ_5 levels were similarly polarised 0:1 with, for example, the four transitions at 18533.0, 18528.0, 18519.5 and 18515.0 cm^{-1} having measured polarisation ratios of 1:4.9, 1:5.0, 1:6.6 and 1:7.1 respectively (Table 4.9);

(iii) the $E_1 \rightarrow Z_1$ transition is found to be only slightly polarised with a ratio of 1:2 while the $E_1 \rightarrow Z_2$ transition is σ polarised with a ratio of 1:5.1 (Figure 4.19(a), Table 4.9);

(iv) all the $E \rightarrow Y$ transitions (Figure 4.19(b)) follow the same pattern as those for the CS1 centre except for the two transitions at 13335.5 and 13322.0 cm^{-1} which, although only 13.5 cm^{-1} apart, are polarised oppositely with ratios of 1:9.4 and 12.1:1 respectively (Table 4.9). The transition at 13328.0 cm^{-1} is only slightly π polarised while its partner at 13341.5 cm^{-1} is clearly σ polarised;

(v) polarisation ratios for $D \rightarrow Z$ transitions were as observed for the CS1 centre, characteristic of fluorescence from a pure γ_5 type upper level;

(vi) polarised $Z \rightarrow E$ excitation spectra show the transitions at 18748.2, 18825.0 and 18880.8 cm^{-1} being mainly π polarised while the remainder are all σ polarised (Figure 4.19(c));

(vii) with the E vector of the laser oriented along the z axis (laser polarised E_z), transitions that were polarised 1:0 for the E vector of the laser along the y axis (laser polarised E_y) are not observed. Fluorescence transitions that were polarised 0:1 for the laser polarised E_y are observed, but do not show any polarisation effects,

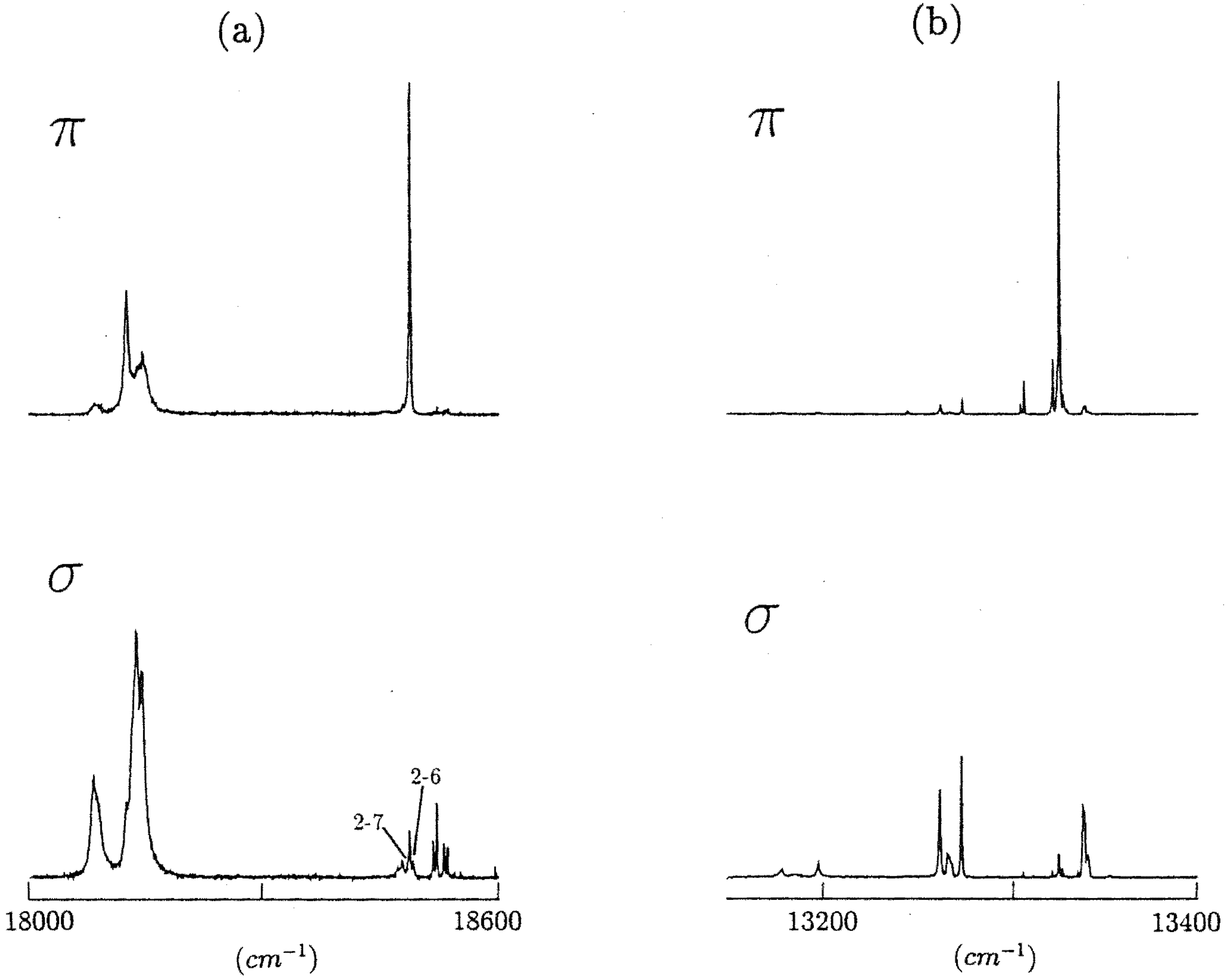
(a)
(b)
π
π
σ
σ
2-6
2-7
18000
18600
(cm^{-1})
13200
13400
(cm^{-1})

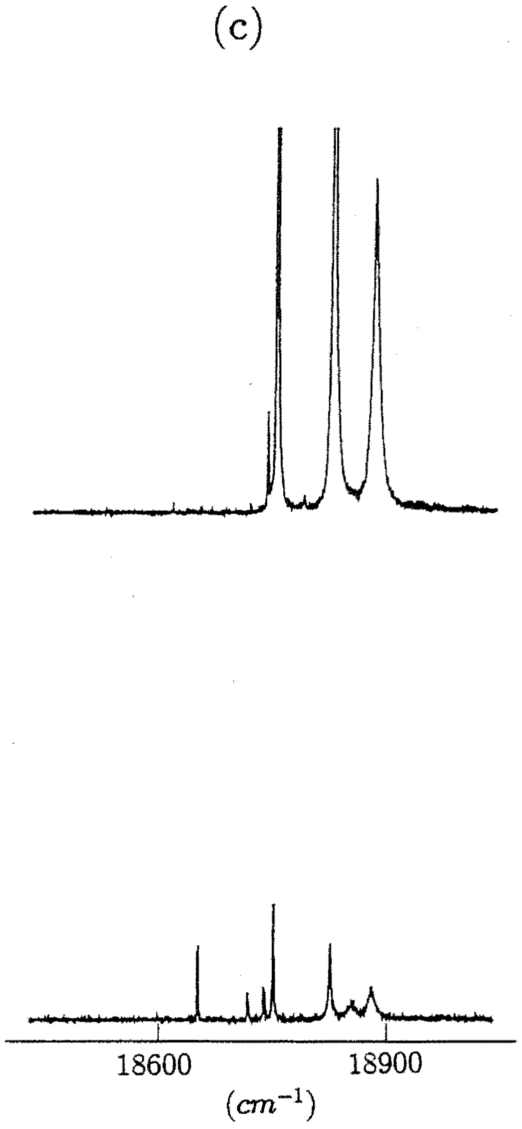

Figure 4.19: Polarisation of the 10 K selective excitation and fluorescence spectra of the CS2 centre in $Ca_{0.00}Sr_{0.01}F_2$:Ho^{3+}(0.005%) crystals :
(a) E→Z transitions, for excitation of the Z_1→E_2 transition at 18608.5 cm^{-1};
(b) Z→E transitions, monitoring the E_2→Z_1 transition at 18608.5 cm^{-1};
(c) Z→E transitions, monitoring the E_2→Z_1 transition at 18608.5 cm^{-1}.
Transition labels are as in Figures 4.13(c) and 4.17.

Table 4.9: Observed intensity ratios for the polarised fluorescence transitions of the CS2 centre in <100> and <111> oriented $Ca_{0.99}Sr_{0.01}F_2:Ho^{3+}$ (0.005%) crystals, for excitation of the $Z_1 \rightarrow E_2$ ($\gamma_1 \rightarrow \gamma_1$) transition at 18608.5 cm^{-1}.

Transition	**Wavenumber (±0.5) (cm^{-1})**	**Observed Polarisation Ratios (±5%)**	
		<100> orientation [yy : yx]	**<111> orientation** [y′y′/y′x′]
$E_2 \rightarrow Z_3$	18533.0	1 : 4.9	0.7
$E_2 \rightarrow Z_4$	18528.0	1 : 5.0	0.6
$E_2 \rightarrow Z_6$	18490.5	1 : 6.5	0.7
$E_2 \rightarrow Z_7$	18483.5	1 : 6.0	0.7
$E_2 \rightarrow Z_{12}$	18143.5	1 : 4.9	0.8
$E_2 \rightarrow Z_{13}$	18135.0	1 : 6.9	0.7
$E_2 \rightarrow Z_{14}$	18123.0	8.9 : 1	2.2
$E_1 \rightarrow Z_1$	18595.0	1 : 2.0	0.8
$E_1 \rightarrow Z_2$	18593.0	1 : 5.1	0.7
$E_1 \rightarrow Z_3$	18519.5	1 : 6.6	0.7
$E_1 \rightarrow Z_4$	18515.0	1 : 7.1	0.6
$E_1 \rightarrow Z_5$	18485.0	8.8 : 1	2.0
$E_1 \rightarrow Z_6$	18476.0	1 : 4.7	0.7
$E_1 \rightarrow Z_7$	18470.0	1 : 4.5	0.7
$E_1 \rightarrow Z_{10}$	18148.0	5.5 : 1	-
$E_1 \rightarrow Z_{12}$	18130.0	1 : 5.7	0.8
$E_1 \rightarrow Z_{16}$	18086.0	1 : 6.3	0.7
$E_1 \rightarrow Z_{17}$	18081.0	1 : 6.1	0.7
$E_2 \rightarrow Y_1$	13353.0	1 : 7.9	0.8
$E_2 \rightarrow Y_2$	13352.0	1 : 7.5	0.7
$E_2 \rightarrow Y_3$	13341.5	1 : 7.4	0.6
$E_2 \rightarrow Y_5$	13335.5	1 : 9.4	0.8
$E_2 \rightarrow Y_6$	13307.0	10.0 : 1	1.6
$E_1 \rightarrow Y_1$	13339.5	1 : 6.2	0.8
$E_1 \rightarrow Y_2$	13338.5	1 : 6.0	0.8
$E_1 \rightarrow Y_3$	13328.0	2.9 : 1	1.4
$E_1 \rightarrow Y_4$	13326.0	17.8 : 1	1.9
$E_1 \rightarrow Y_5$	13322.0	12.1 : 1	2.9
$E_1 \rightarrow Y_7$	13274.0	1 : 7.7	0.7
$E_1 \rightarrow Y_8$	13267.5	1 : 7.4	0.6
$E_1 \rightarrow Y_9$	13262.5	1 : 8.3	0.7
$E_1 \rightarrow Y_{10}$	13245.0	4.9 : 1	1.9
$E_1 \rightarrow Y_{11}$	13198.5	1 : 5.9	0.7
$E_1 \rightarrow Y_{12}$	13179.5	1 : 5.4	0.7
$D_3 \rightarrow Z_1$	15621.0	11.2 : 1	2.0
$D_3 \rightarrow Z_2$	15619.0	15.0 : 1	2.1
$D_2 \rightarrow Z_1$	15611.0	1 : 17.0	0.6
$D_2 \rightarrow Z_2$	15609.0	1 : 15.9	0.7
$D_2 \rightarrow Z_4$	15528.0	5.0 : 1	2.1
$D_1 \rightarrow Z_1$	15604.0	1 : 6.8	0.7
$D_1 \rightarrow Z_2$	15602.0	1 : 10.1	0.7
$D_1 \rightarrow Z_3$	15527.0	1 : 7.3	0.7
$D_1 \rightarrow Z_4$	15524.0	1 : 6.0	0.6
$D_1 \rightarrow Z_8$	15327.0	1.5 : 1	1.4
$D_1 \rightarrow Z_9$	15319.0	1 : 4.1	0.8
$D_1 \rightarrow Z_{11}$	15150.0	2.4 : 1	1.4
$D_1 \rightarrow Z_{15}$	15116.0	1 : 5.8	0.7

having isotropic polarisation ratios of exactly 1:1.

(b) For $Z_2 \rightarrow E_4$ ($\gamma_a \rightarrow \gamma_b$) excitation :-

(i) the transitions at 18485.0, 18148.0 and 18123.0 cm^{-1} were observed to be σ polarised (Figure 4.20(a), Table 4.10);

(ii) of the transitions from the E_1 and E_2 levels to split γ_5 levels, one member of the pair is π polarised while the other is σ polarised. Transitions from both the E_1 and E_2 levels to the higher energy component of the pair are polarised one way while transitions from both E levels to the lower component are oppositely polarised. As an example, considering the four levels at 18533.0, 18528.0, 18519.5 and 18515.0 cm^{-1} (Figure 4.20(a), Table 4.10), the pair of levels at 18533.0 and 18519.5 cm^{-1} (13.5 cm^{-1} apart) are both polarised 0:1 while the other two at 18528.0 and 18515.0 cm^{-1}, also 13.5 cm^{-1} apart, are both polarised 1:0. For transitions from the E_1 level to both components of the Z_{12} level, the higher transition is π polarised. There is no evident set pattern as to which component is polarised in a given way;

(iii) the $E_1 \rightarrow Z_1$ transition is σ polarised while the $E_1 \rightarrow Z_2$ transition is π polarised;

(iv) all the $E \rightarrow Y$ transitions (Figure 4.20(b), Table 4.10) show the same pattern as the $E \rightarrow Z$ transitions in that transitions from the same E level to the two components of a γ_5 level are oppositely polarised. Transitions that were polarised 1:0 for $Z_1 \rightarrow E_2$ excitation are now polarised 0:1. The transition pairs at 13335.5 and 13322.0 cm^{-1} and at 13328.0 and 13341.5 cm^{-1} both show opposite polarisations as observed for $Z_1 \rightarrow E_2$ excitation;

(v) For the laser polarised E_z, transitions that had ratios of 1:0 for the laser polarised E_y are not observed while transitions that were polarised 0:1 for the laser polarised E_y, are observed without any

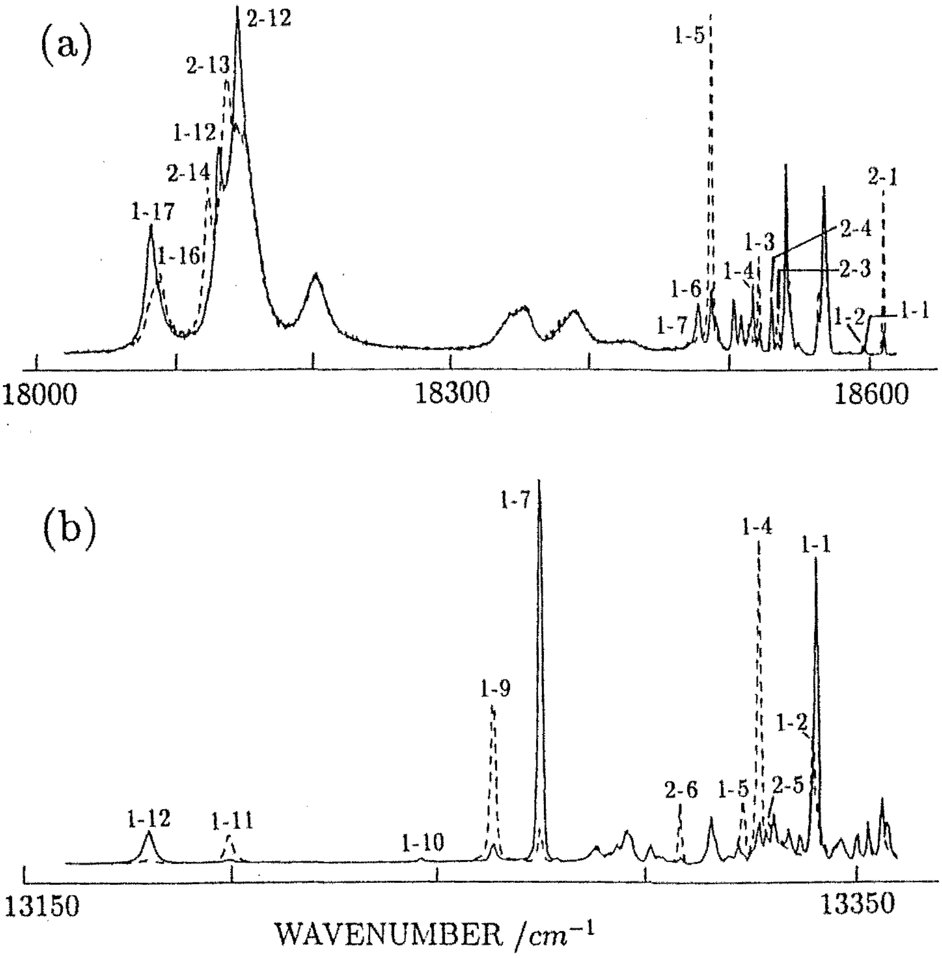

Figure 4.20: Polarisation of 10 K fluorescence spectra of the CS2 centre in $Ca_{0.99}Sr_{0.01}F_2$:Ho^{3+}(0.005%) crystals, for excitation of the $Z_2 \rightarrow E_4$ transition at 18650.8 cm^{-1} :
(a) E→Z transitions; (b) E→Y transitions;
———— π polarisation ---------- σ polarisation.
Transition labels are as in Figure 4.17.

Table 4.10: Observed and expected intensity ratios for the polarised fluorescence transitions of the CS2 centre in <100> oriented $Ca_{0.99}Sr_{0.01}F_2Ho^{3+}$(0.005%) crystals, for excitation of the $Z_2 \rightarrow E_4$ ($\gamma_2 \rightarrow \gamma_1$) transition at 18650.8 cm^{-1}.

Transition	Wavenumber (±0.5) (cm^{-1})	Polarisation Ratios (±5%) [yy : yx]	
		Observed	Expected
$E_2 \rightarrow Z_1$	18608.5	1 : 7.1	0 : 1
$E_2 \rightarrow Z_2$	18606.5	3.9 : 1	1 : 0
$E_2 \rightarrow Z_3$	18533.0	1 : 5.6	0 : 1
$E_2 \rightarrow Z4$	18528.0	6.2 : 1	1 : 0
$E_2 \rightarrow Z_6$	18490.5	5.1 : 1	1 : 0
$E_2 \rightarrow Z_7$	18483.5	1 : 5.2	0 : 1
$E_2 \rightarrow Z_{12}$	18143.5	5.9 : 1	1 : 0
$E_2 \rightarrow Z_{13}$	18135.0	1 : 7.0	0 : 1
$E_2 \rightarrow Z_{14}$	18123.0	1 : 8.1	0 : 1
$E_1 \rightarrow Z_1$	18595.0	1 : 6.9	0 : 1
$E_1 \rightarrow Z_2$	18593.0	6.4 : 1	1 : 0
$E_1 \rightarrow Z_3$	18519.5	1 : 5.2	0 : 1
$E_1 \rightarrow Z_4$	18515.0	5.0 : 1	1 : 0
$E_1 \rightarrow Z_5$	18485.0	1 : 7.2	0 : 1
$E_1 \rightarrow Z_6$	18476.0	7.1 : 1	1 : 0
$E_1 \rightarrow Z_7$	18470.0	1 : 5.4	0 : 1
$E_1 \rightarrow Z_{10}$	18148.0	1 : 4.9	0 : 1
$E_1 \rightarrow Z_{12}$	18130.0	6.8 : 1	1 : 0
$E_1 \rightarrow Z_{16}$	18086.0	1 : 6.0	0 : 1
$E_1 \rightarrow Z_{17}$	18081.0	7.6 : 1	1 : 0
$E_2 \rightarrow Y_3$	13341.5	1 : 4.4	0 : 1
$E_2 \rightarrow Y_5$	13335.5	9.1 : 1	1 : 0
$E_2 \rightarrow Y_6$	13307.0	1 : 9.0	0 : 1
$E_1 \rightarrow Y_1$	13339.5	11.2 : 1	1 : 0
$E_1 \rightarrow Y_2$	13338.5	1 : 10.4	0 : 1
$E_1 \rightarrow Y_3$	13328.0	5.1 : 1	1 : 0
$E_1 \rightarrow Y_4$	13326.0	1 : 8.0	0 : 1
$E_1 \rightarrow Y_5$	13322.0	1 : 6.1	0 : 1
$E_1 \rightarrow Y_7$	13274.0	11.6 : 1	1 : 0
$E_1 \rightarrow Y_8$	13267.5	4.4 : 1	1 : 0
$E_1 \rightarrow Y_9$	13262.5	1 : 8.6	0 : 1
$E_1 \rightarrow Y_{11}$	13198.5	1 : 6.3	0 : 1
$E_1 \rightarrow Y_{12}$	13179.5	7.3 : 1	1 : 0

preferred polarisation for the laser polarised E_z, with exact ratios of 1:1 being obtained;

(vi) the D → Z fluorescence was too weak to give any reliable polarisation results and no quantitative results were measured.

From the observation of transitions that were forbidden for both the A and CS1 centres as well as observation of splittings of the C_{4v} γ_5 type levels, the symmetry of the CS2 centre has to be lower than C_{4v} symmetry. The CS2 centre is therefore assigned as being a low symmetry C_s centre. Polarisation results obtained for $Z_1 \rightarrow E_2$ excitation (Table 4.9) show that the CS2 centre is certainly of C_{4v} symmetry parentage. The polarisation results for $Z_1 \rightarrow E_2$ excitation, as discussed above, do not distinguish between the so-called C_s(a) and C_s(b) configurations described by Khong [63], and shown here in Figure 1.4 (b) and (c), as the excitation transition is still of $\gamma_a \rightarrow \gamma_a$ type in C_s symmetry. To distinguish between the two possible C_s centre configurations, one needs to pump a transition of the type $\gamma_a \leftrightarrow \gamma_b$, for which the $\gamma_a \rightarrow \gamma_b$ fluorescence transition would have the different yy:yx ratios of 2:1 and 1:0 for the C_s(a) and C_s(b) configurations respectively, (Table 2.5). This was done as follows :-

The E_4 level observed at 18652.8 cm^{-1} arises from a low symmetry splitting of the E_3 level of both the CS1 and A centres. The $Z_2 \rightarrow E_4$ pump transition at 18650.8 cm^{-1} was appropriate to give fluorescence polarisation ratios as summarised in (b) above and in Table 4.10 which are consistent with the C_s(b) configuration. The resulting polarisation spectra for the E → Z and E → Y transitions are shown in Figure 4.20. The CS2 centre is therefore proposed to have the Sr^{2+} ion located off the Ho^{3+} - F^- axis as shown in Figure 1.4(b) to give a C_s symmetry centre with the C_s(b) configuration. Because the $Z_2 \rightarrow E_4$ transition is quite weak and close to the B centre $Z_1 \rightarrow E_5$ transition, some simultaneous excitation could not be avoided. The B centre transitions in Figure 4.20 are themselves not polarised.

From the predicted ratios of Table 2.5 and knowing that the E_1, E_2 and Z_1

levels are all γ_1 type levels in C_s symmetry while the Z_2 level has γ_2 symmetry, irrep labels for all the remaining levels could be deduced from the polarisation ratios obtained with $Z_2 \rightarrow E_4$ excitation. Given that the two possible irreps of the C_s symmetry are γ_1 and γ_2, and having established the $Z_2 \rightarrow E_4$ transition as a $\gamma_2 \rightarrow \gamma_1$ type transition, fluorescence transitions from the E_1 and E_2 levels that are polarised 1:0 ($\gamma_1 \rightarrow \gamma_2$) identify γ_2 terminating levels while those polarised 0:1 ($\gamma_1 \rightarrow \gamma_1$) identify γ_1 type lower multiplet levels.

For the E → Z spectra, two sets of transitions were found to be oppositely polarised, ((iv) in (a) and (b) above). It is likely that this arises from an overlap of two transitions to two levels lying within 0.5 cm^{-1} of each other or alternatively with a 14.0 cm^{-1} separation. In the first case, transitions from the same E level would be indistinguishable and the ratio measured would be for the stronger of the two transitions. In the latter case, a transition from the E_2 level to the higher energy Y level overlaps with that from the E_1 level to the lower energy Y level of the pair since the two sets of Y and E multiplet levels have almost the same separation. This overlap is highly likely given the many energy levels possible for the multiplets here and that all transitions are allowed in C_s symmetry.

All the derived energy levels, together with their proposed irrep labels are presented in Table 4.8. The energy level scheme presented in Figure 4.18 shows the relation between the CS1 and CS2 energy levels. The labelling of levels as Z_1, Z_2, Z_3 ....etc for the CS2 centre is necessarily different from that of the C_{4v} symmetry centres, for example, the Z_7 level of the CS2 centre does not correspond to the Z_7 level of the CS1 centre. The labelling adopted for the CS2 centre will also apply to the other C_s symmetry centres to be detailed later.

4.2.5 Upconversion fluorescence and spectra recorded above 20 K

Upconversion fluorescence was not observed for either the CS1 or CS2 centres for Z → E excitation. Some weak fluorescence, less than 10^{-6} the intensity of that for direct excitation, was observed from E and F multiplets, for Z → D excitation.

Raising the temperature of the crystal to above 20 K resulted in unintentional simultaneous excitation of the parent A centre. Any CS1 and CS2 fluorescence was swamped by that from the A centre and any additional high energy levels for the E multiplets of either the CS1 or CS2 centres could not be determined.

4.3 Spectroscopy of $Ca_{0.99}Ba_{0.01}F_2$:Ho^{3+}(0.005%) Crystals

For $Ca_{0.99}Ba_{0.01}F_2$:Ho^{3+}(0.005%) crystals, the laser excitation spectra for monitoring all fluorescence transitions in the 15000 cm^{-1} region while exciting either the Z → E or Z → D transitions had weak new features as shown in Figures 4.21 and 4.22 respectively. As for the $Ca_{0.99}Sr_{0.01}F_2$:Ho^{3+}(0.005%) crystals, two new centres arbitrarily labelled CB1 and CB2, with transition intensities of about 5% of corresponding transitions of the A centre, were identified. Completely discriminated selective excitation spectra, free from transitions of the A centre, could only be obtained by monitoring the $E_2 \rightarrow Z_1$ transition of the appropriate centre. Such completely selected excitation spectra for the Z → D transitions were not possible. Both the CB1 and CB2 centres have levels somewhat lower in energy than the corresponding CS1 and CS2 centres respectively, with the CB2 centre energy levels being slightly higher in energy than those of the CB1 centre.

4.3.1 Spectroscopy of the CB1 centre

From the excitation and fluorescence spectra of Figures 4.21(b) and 4.23, the CB1 centre is closely similar to both the A and CS1 centres. The Z_1 - Z_2 energy separation of 2.0 cm^{-1} is clearly apparent on the sharp transitions to the E_2, E_3 and E_6 levels.

In the E → Z fluorescence spectrum (Figure 4.23(a)), four pairs of transitions with a common energy interval of 10.5 cm^{-1} are observed. From these transition pairs, the energies inferred for the Z_3, Z_5, Z_{10} and Z_{12} levels are 63.5, 107.5, 451.5 and 503.5 cm^{-1} respectively. The E_1 level is deduced to be at

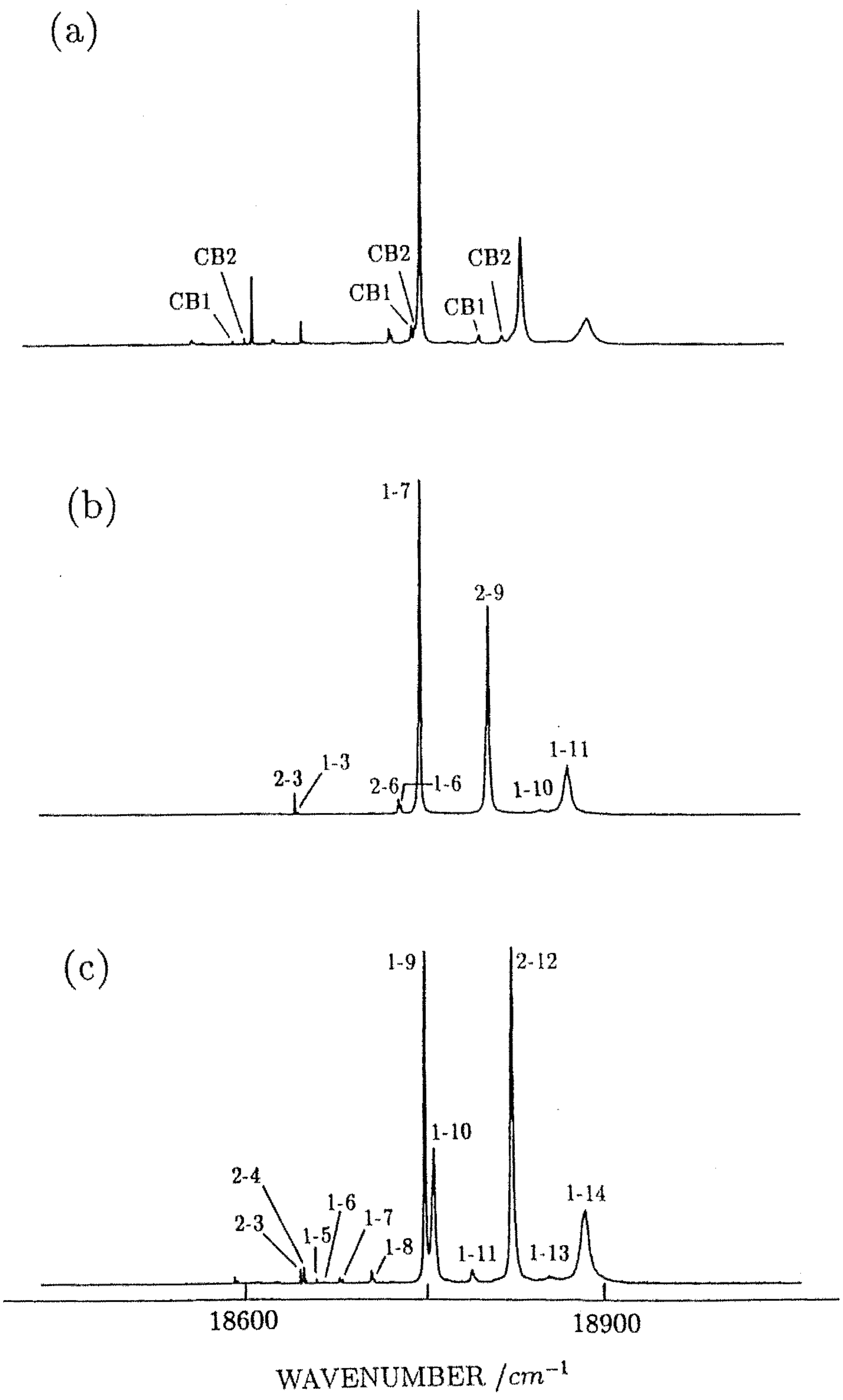

Figure 4.21: 10 K broadband and selective excitation spectra of the E multiplet in $Ca_{0.99}Ba_{0.01}F_2$:Ho^{3+}(0.005%) crystals :
(a) broadband excitation spectrum, monitoring all the D→Z transitions;
(b) CB1 centre excitation spectrum, monitoring the $E_2 \rightarrow Z_1$ transition at 18596.6 cm^{-1};
(c) CB2 centre excitation spectrum, monitoring the $E_2 \rightarrow Z_1$ transition at 18606.7 cm^{-1}.
Transitions are labelled by the appropriate lower and upper multiplet crystal-field level identifications.

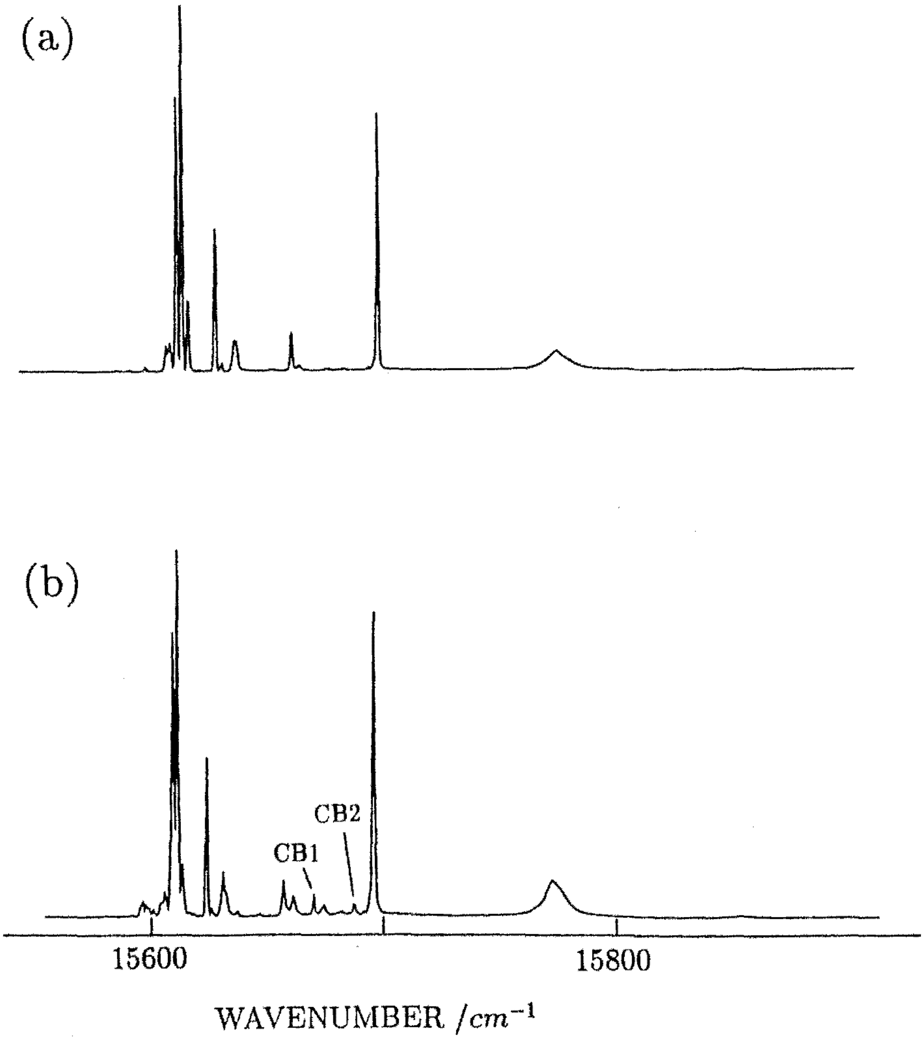

Figure 4.22: 10 K broadband excitation spectrum of the D multiplet in $Ca_{0.99}Ba_{0.01}F_2:Ho^{3+}$ (0.005%) crystals, monitoring all the D→Z transitions :
(a) broadband spectrum in pure $CaF_2:Ho^{3+}$(0.005%);
(b) broadband spectrum in $Ca_{0.99}Ba_{0.01}F_2:Ho^{3+}$(0.005%).

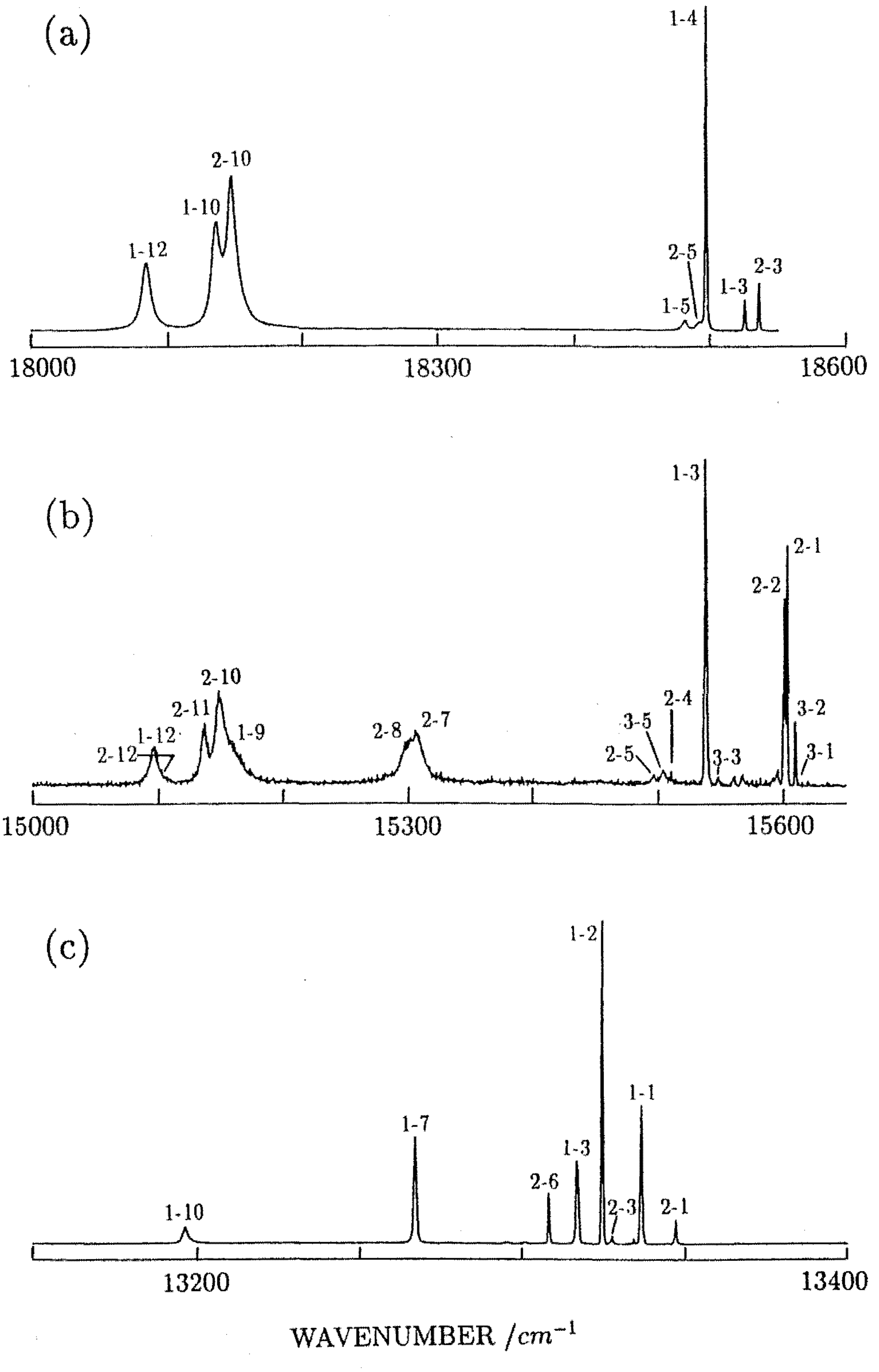

Figure 4.23: 10 K fluorescence spectra for the CB1 centre in $Ca_{0.99}Ba_{0.01}F_2$:Ho^{3+}(0.005%) crystals :
(a) E→Z transitions, for excitation of the Z_1→E_2 transition at 18596.6 cm^{-1};
(b) D→Z transitions, for excitation of the Z_1→D_4 transition at 15655.5 cm^{-1};
(c) E→Y transitions, for excitation of the Z_1→E_2 transition at 18596.6 cm^{-1};
Transitions are labelled by the appropriate upper and lower multiplet crystal-field level identifications.

18586.0 cm^{-1}, 10.5 cm^{-1} lower than the lowest observed E_2 level of the E multiplet at 18596.6 cm^{-1}. This E_1 - E_2 energy separation is quite similar to the 11.0 cm^{-1} found for the CS1 centre. Three single transitions are also observed at 18494.0, 18152.5 and 18132.5 cm^{-1}, all slightly higher than the corresponding transitions for the CS1 centre.

Spectra measured at 20 K show that the transitions at 18494.0 and 18152.5 cm^{-1} originate from the E_1 level while the transition at 18132.5 cm^{-1} originates from E_2, in an exactly analogous way to those found for both the A and CS1 centres.

The E → Y spectrum (Figure 4.23(c)), shows two sets of transitions with the same common E_1 - E_2 energy level separation of 10.5 cm^{-1}, yielding the Y_1 and Y_3 levels as being at 5250.0 and 5270.0 cm^{-1} respectively. Of the five single transitions at 13324.0, 13307.5, 13266.5, 13248.5 and 13195.5 cm^{-1}, the transition at 13307.5 cm^{-1} had more intensity at 20 K than at 10 K and is assigned as originating from the E_2 level while the remaining four transitions originate from the E_1 level.

The D → Z spectrum (Figure 4.23(b)) is similar to the E → Z spectrum, except for the specific additional feature centred at 15305.0 cm^{-1} which is only visible on a magnified scale in the E → Z spectrum. The Z_1 - Z_2 energy separation of 2.0 cm^{-1} is apparent in the sharpest transitions from the D_2 and D_3 levels at 15600.0 and 15608.5 cm^{-1} respectively. The D_1 level was deduced to be at 15598.5 cm^{-1} and the D_1 - D_2 energy level separation of 1.5 cm^{-1} is small compared to 3.0 and 4.5 cm^{-1} found for the CS1 and A centres, respectively.

The energy levels derived for the CB1 centre are presented in Table 4.11.

4.3.2 Polarisation study of the CB1 centre

From examination of the results of polarisation measurements on both < 100> and < 111> oriented crystals (Table 4.12), the CB1 centre clearly has C_{4v} symmetry. From measurements on the < 100> oriented crystals the following features were observed with Z_1 → E_2 excitation :-

Table 4.11: Energy levels (in cm^{-1}) of the Z, Y, D and E multiplets of the CB1 centre and their symmetries, as derived from the 10 K spectra of Ca$_{0.99}$Ba$_{0.01}$F$_2$:Ho^{3+}(0.005%) crystals. Uncertainty is ± 0.5 cm^{-1}.

Level	Z(^{5}I$_8$)	Y(^{5}I$_7$)	D(^{5}F$_5$)	E(^{5}S$_2$,^{5}F$_4$)
1	0(γ_1)	5250.0(γ_5)	15598.5(γ_3)	18586.0(γ_3)
2	2.0(γ_2)	5262.0(γ_3)	15600.0(γ_5)	18596.6(γ_1)
3	63.5(γ_5)	5270.0(γ_5)	15608.5(γ_2)	18644.1(γ_5)
4	92.0(γ_3)	-	15655.5(γ_1)	-
5	107.5(γ_5)	-		-
6	-	5289.0(γ_1)		18728.2(γ_5)
7	296.0(γ_1)	5319.5(γ_5)		18743.0(γ_1)
8	303.0(γ_2)	5337.5(γ_3)		-
9	433.5(γ_3)	-		18797.4(γ_2)
10	451.5(γ_5)	5390.5(γ_5)		18843.0(γ_5)
11	464.5(γ_1)	-		18864.9(γ_1)
12	503.5(γ_5)			
13	-			

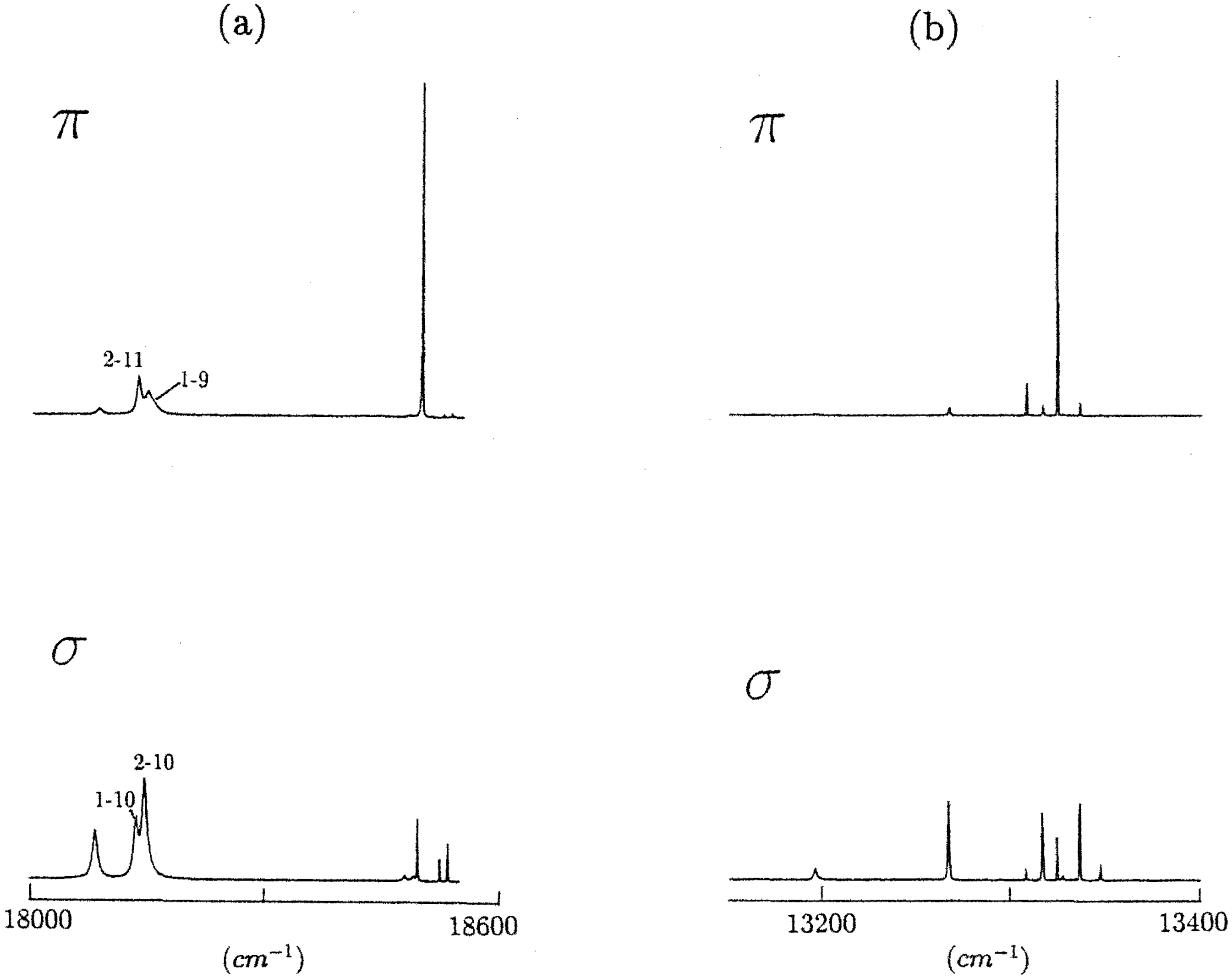
(a)
(b)
π
π
2-11
1-9
σ
σ
2-10
1-10
18000
18600
(cm^{-1})
13200
13400
(cm^{-1})

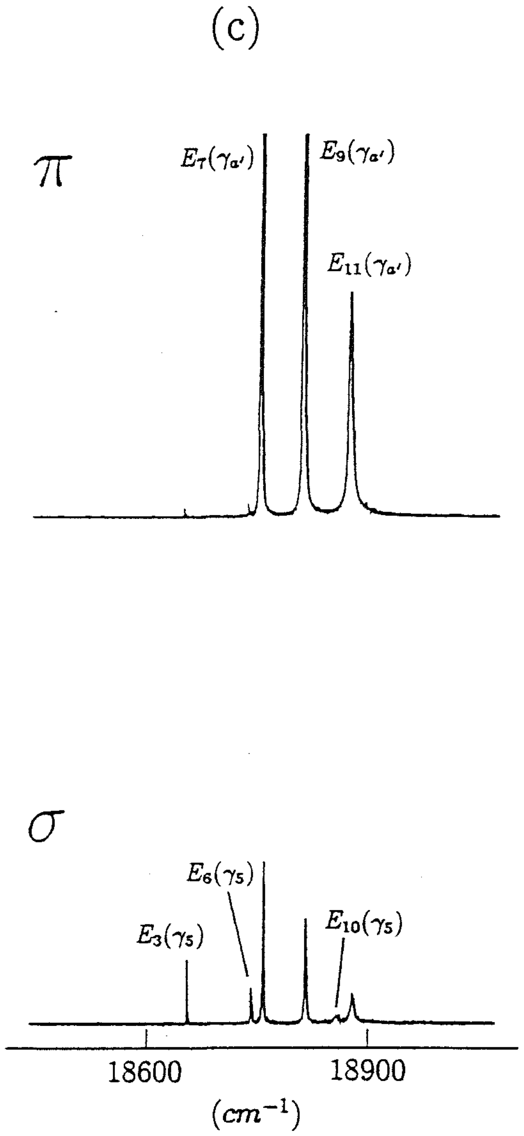

Figure 4.24: Polarisation of the 10 K selective excitation and fluorescence spectra of the CB1 centre in $Ca_{0.99}Ba_{0.01}F_2$:Ho^{3+}(0.005%) crystals :
(a) E→Z transitions, for excitation of the $Z_1 \rightarrow E_2$ transition at 18596.6 cm^{-1};
(b) E→Y transitions, for excitation of the $Z_1 \rightarrow E_2$ transition at 18596.6 cm^{-1};
(c) Z→E transitions, monitoring the $E_2 \rightarrow Z_1$ transition at 18596.6 cm^{-1}.
Transition labels are as in Figures 4.21(b) and 4.23.

(i) both transitions of a given pair (Figure 4.24(a)) were σ polarised as found for both the CS1 and A centres. The Z_3, Z_5, Z_{10} and Z_{12} levels are therefore necessarily of γ_5 symmetry;

(ii) as the $E_1 \rightarrow Z_4$, $E_1 \rightarrow Z_9$ and $E_2 \rightarrow Z_{11}$ transitions at 18494.0, 18152.5 and 18132.5 cm^{-1} respectively, are all π polarised (Figure 4.24(a), Table 4.12), the E_1, Z_4 and Z_9 levels are all assigned as γ_3 levels while the E_2 and Z_{11} levels are of γ_1 symmetry;

(iii) transitions to the Y_1, Y_3, Y_7 and Y_{10} levels are all σ polarised (Figure 4.24(b), Table 4.12) identifying these levels as γ_5 type levels;

(iv) as for the A and CS1 centres, the $E_2 \rightarrow Y_6$, $E_1 \rightarrow Y_2$ and $E_1 \rightarrow Y_8$ transitions are all π polarised, consistent with irrep labels of γ_1, γ_3 and γ_3 for Y_6, Y_2 and Y_8 energy levels respectively;

(v) polarisation ratios for the $D_2 \rightarrow Z$ transitions were all consistent with a γ_5 irrep label assignment for the D_2 level. Transitions from the D_1 and D_3 levels to the Z_4, Z_9 and Z_{11} levels were π polarised. Irrep labels could then be assigned based on whether or not a transition to the Z_4 level was observed and in the case of the D_3 level, also on the relative intensities of the transitions to the Z_1 and Z_2 levels, as discussed for the case of the A centre. The feature centred at 15305.0 cm^{-1} was resolved in the polarised spectra into three partially overlapped transitions corresponding to the $D_3 \rightarrow Z_8$, $D_2 \rightarrow Z_7$ and $D_2 \rightarrow Z_8$ transitions as found for the A centre;

(vi) irrep label assignments for the remaining upper E and D levels were based on polarised excitation spectra.

The energy levels together with the proposed irrep labels are presented in Table 4.11. Again, the energy level diagram is closely similar to that for the A centre (Figure 4.8), except for the shift of all the levels to lower energies and is therefore not reproduced specifically here. As for the the CS1 centre, the CB1

Table 4.12: Observed and predicted intensity ratios for the polarised fluorescence transitions of the CB1 centre in < 100> and < 111> oriented $Ca_{0.99}Ba_{0.01}F_2:Ho^{3+}$(0.005%) crystals, for excitation of the $Z_1 \rightarrow E_2$ transition at 18596.6 cm^{-1}.

Transition	**Wavenumber** ($\pm$**0.5**) $\mathbf{cm^{-1}}$	**Polarisation Ratios (±5%)** **<100> orientation** [yy : yx] **Observed**	**Expected**	**<111> orientation** [y′y′/y′x′] **Observed**	**Expected**
$E_2 \rightarrow Z_3$	18533.0	1 : 7.3	0 : 1	${}^{3.5}/_{5}$	${}^{3}/_{5}$
$E_2 \rightarrow Z_5$	18489.0	1 : 7.1	0 : 1	${}^{4.0}/_{5}$	${}^{3}/_{5}$
$E_2 \rightarrow Z_{10}$	18145.0	1 : 6.9	0 : 1	${}^{4.0}/_{5}$	${}^{3}/_{5}$
$E_2 \rightarrow Z_{11}$	18132.5	7.1 : 1	1 : 0	2.1	3.0
$E_1 \rightarrow Z_3$	18522.5	1 : 6.2	0 : 1	${}^{3.5}/_{5}$	${}^{3}/_{5}$
$E_1 \rightarrow Z_4$	18494.0	7.1 : 1	1 : 0	2.2	3.0
$E_1 \rightarrow Z_5$	18478.5	1 : 6.0	0 : 1	${}^{4.0}/_{5}$	${}^{3}/_{5}$
$E_1 \rightarrow Z_9$	18152.5	7.3 : 1	1 : 0	2.1	3.0
$E_1 \rightarrow Z_{10}$	18134.5	1 : 8.0	0 : 1	${}^{4.0}/_{5}$	${}^{3}/_{5}$
$E_1 \rightarrow Z_{13}$	18082.5	1 : 7.2	0 : 1	${}^{4.0}/_{5}$	${}^{3}/_{5}$
$E_2 \rightarrow Y_1$	13346.5	1 : 9.2	0 : 1	${}^{3.5}/_{5}$	${}^{3}/_{5}$
$E_2 \rightarrow Y_3$	13327.0	1 : 6.2	0 : 1	${}^{4.0}/_{5}$	${}^{3}/_{5}$
$E_2 \rightarrow Y_6$	13307.5	5.0 : 1	1 : 0	2.1	3.0
$E_1 \rightarrow Y_1$	13336.0	1 : 5.6	0 : 1	${}^{3.0}/_{5}$	${}^{3}/_{5}$
$E_1 \rightarrow Y_2$	13324.0	9.9 : 1	1 : 0	2.1	3.0
$E_1 \rightarrow Y_3$	13316.0	1 : 6.7	0 : 1	${}^{3.5}/_{5}$	${}^{3}/_{5}$
$E_1 \rightarrow Y_7$	13266.5	1 : 8.7	0 : 1	${}^{3.5}/_{5}$	${}^{3}/_{5}$
$E_1 \rightarrow Y_{10}$	13195.5	1 : 7.1	0 : 1	${}^{3.5}/_{5}$	${}^{3}/_{5}$
$D_2 \rightarrow Z_1$	15600.0	1 : 4.4	0 : 1	${}^{4.0}/_{5}$	${}^{3}/_{5}$
$D_2 \rightarrow Z_2$	15598.0	1 : 4.5	0 : 1	${}^{3.5}/_{5}$	${}^{3}/_{5}$
$D_2 \rightarrow Z_3$	15536.0	8.2 : 1	1 : 0	2.2	3.0
$D_1 \rightarrow Z_3$	15534.5	1 : 8.8	0 : 1	${}^{3.0}/_{5}$	${}^{3}/_{5}$

centre is proposed to comprise a Ba^{2+} ion on - axis with the Ho^{3+} - F^- pair, with the Ba^{2+} ion adjacent to the charge compensating interstitial F^- ion and on the opposite side from the Ho^{3+} ion, as shown in Figure 1.4(a).

4.3.3 Spectroscopy of the CB2 centre

Transitions for the CB2 centre (Figures 4.21(a) and 4.25) are slightly higher in energy than those for the CB1 centre. This centre is similar to the CS2 centre in that:-

(i) the $Z_1 - Z_2$ energy separation is 2.0 cm^{-1} and the $E_1 - E_2$ separation is 13.5 cm^{-1} (Figure 4.25), slightly larger than the 10.5 cm^{-1} found for the CB1 centre;

(ii) the $Z_1,Z_2 \leftrightarrow E_1$ transition is observed for the CB2 centre but not for the CB1 centre;

(iii) splittings are apparent on all transitions to levels that correspond to the γ_5 type levels of the CB1 centre. Again the observed splittings vary among the various transitions without any simple trend being apparent.

The splittings of the γ_5 type levels are all larger than those for the CS2 centre, being more than twice as large in most cases (Figures 4.18 and 4.26). The Z_3 level splitting, for example, is 9.5 cm^{-1} for the CB2 centre (Figure 4.26) and only 4.5 cm^{-1} for the CS2 centre (Figure 4.18). Likewise, the D_2 level is split by 14.0 cm^{-1} in the CB2 centre and only 7.0 cm^{-1} in the CS2 centre. Low symmetry splittings for the Y_1 and Y_3 levels are more than three times those found for corresponding levels of the CS2 centre, with the Y_7 level being split by about the same amount in both centres while the Y_{10} level is split by 43.0 cm^{-1} for the CB2 centre and only 19.0 cm^{-1} for the CS2 centre. The energy levels derived are presented in Table 4.13.

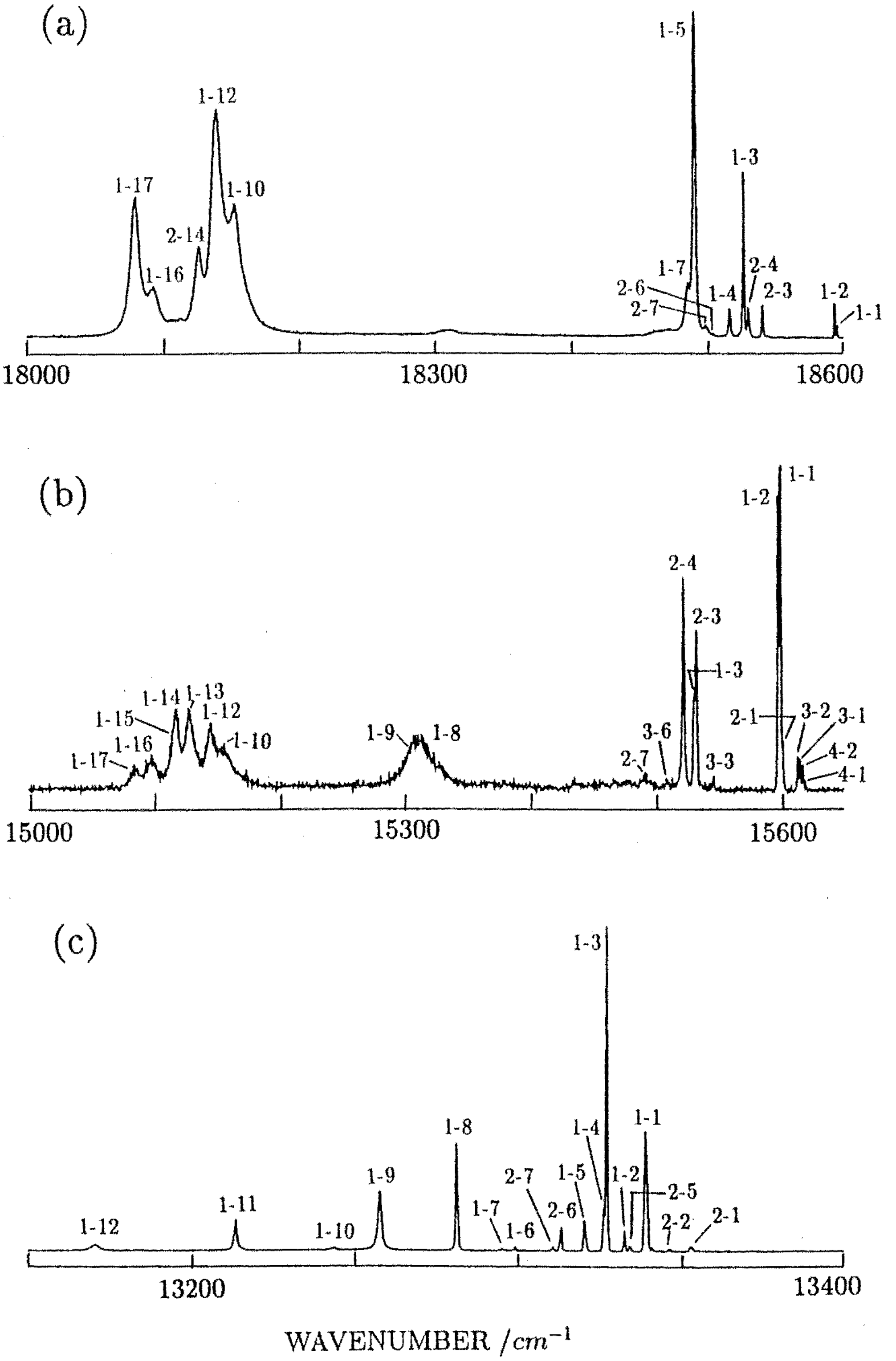

Figure 4.25: 10 K fluorescence spectra for the CB2 centre in $Ca_{0.99}Ba_{0.01}F_2:Ho^{3+}$(0.005%) crystals :
(a) $E \rightarrow Z$ transitions, for excitation of the $Z_1 \rightarrow E_2$ transition at 18606.7 cm^{-1};
(b) $D \rightarrow Z$ transitions, for excitation of the $Z_1 \rightarrow D_5$ transition at 15676.0 cm^{-1};
(c) $E \rightarrow Y$ transitions, for excitation of the $Z_1 \rightarrow E_2$ transition at 18606.7 cm^{-1}.

Table 4.13: Energy levels (in cm^{-1}) of the Z, Y, D and E multiplets of the CB2 centre and their symmetries, as derived from the 10 K spectra of Ca$_{0.99}$Ba$_{0.0}$F$_2$:Ho^{3+}(0.005%) crystals. Uncertainty is ±0.5 cm^{-1}.

Level	Z($^5I_8$)	Y($^5I_7$)	D($^5F_5$)	E($^5S_2$,$^5F_4$)
1	0(γ_1)	5254.5(γ_1)	15600.0(γ_1)	18593.1(γ_1)
2	2.0(γ_2)	5261.0(γ_2)	15601.5(γ_2)	18606.7(γ_1)
3	69.0(γ_2)	5266.5(γ_1)	15615.5(γ_1)	18651.5(γ_2)
4	79.5(γ_1)	5267.5(γ_2)	15619.5(γ_2)	18654.2(γ_1)
5	105.5(γ_1)	5273.5(γ_1)	15676.0(γ_1)	18660.7(γ_2)
6	103.5(γ_2)	5295.0(γ_1)		18664.5(γ_1)
7	110.0(γ_1)	5297.5(γ_2)		18673.4(γ_1)
8	283.0(γ_1)	5312.5(γ_1)		18704.1(γ_2)
9	293.5(γ_2)	5336.0(γ_2)		18746.6(γ_1)
10	442.5(γ_1)	5350.0(γ_1)		18753.4(γ_2)
11	-	5380.5(γ_2)		18784.2(γ_2)
12	456.0(γ_1)	5423.5(γ_1)		18818.3(γ_1)
13	472.5(γ_2)			18849.0(γ_2)
14	482.5(γ_1)			18883.1(γ_1)
15	485.0(γ_2)			
16	504.0(γ_2)			
17	515.5(γ_1)			

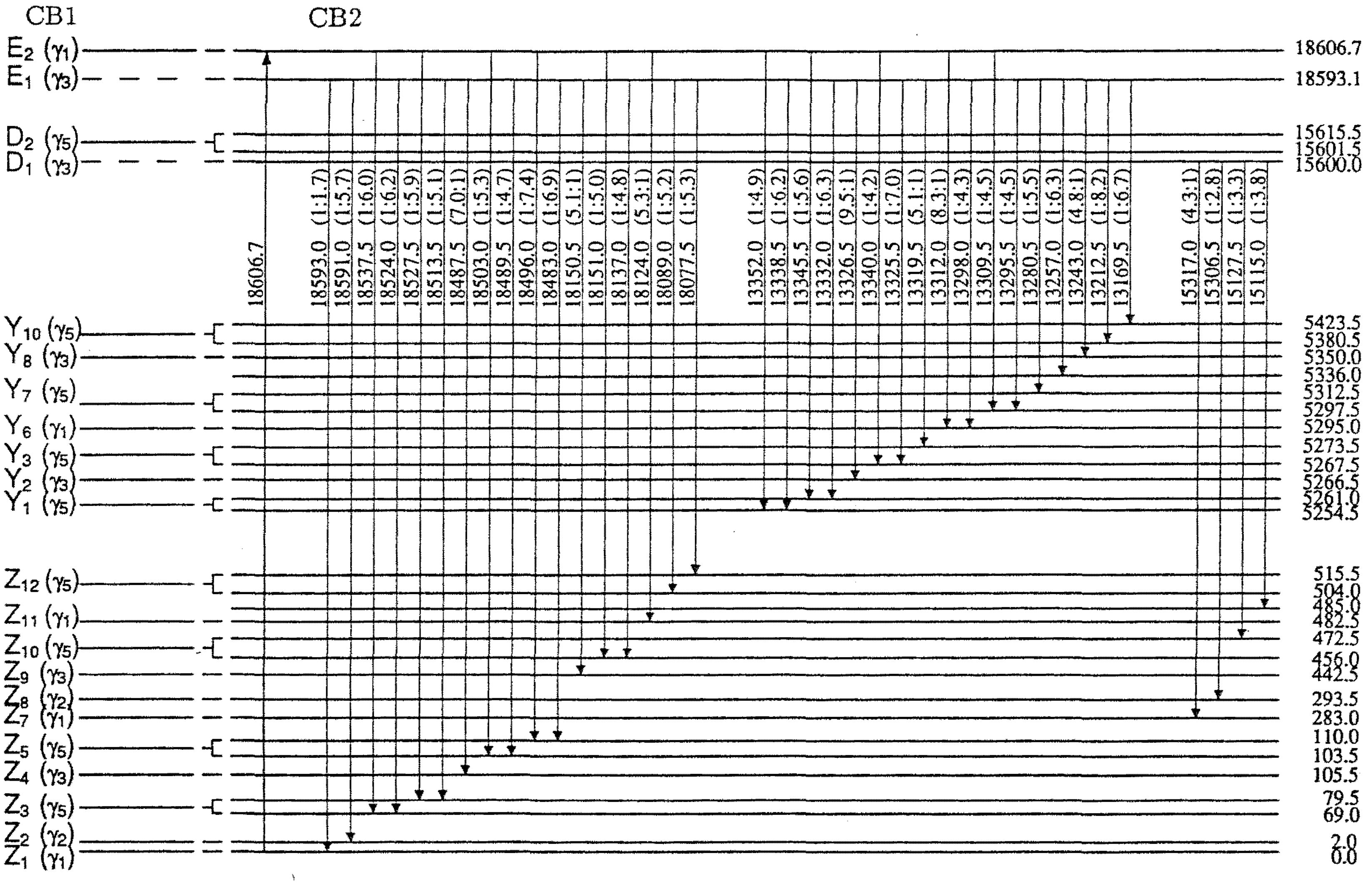

Figure 4.26: Energy level diagram for the CB2 centre in $Ca_{0.99}Ba_{0.01}F_2$:Ho^{3+}(0.005%) crystals, for the E → Z and E → Y transitions as measured at 10 K. For the particular Z levels not accessed by transitions from the E_1, E_2 levels, transitions from the D_1 level are shown. The energy levels on the left are those for the CB1 centre. Energy level irreps for the CB2 centre are presented in Table 4.12.

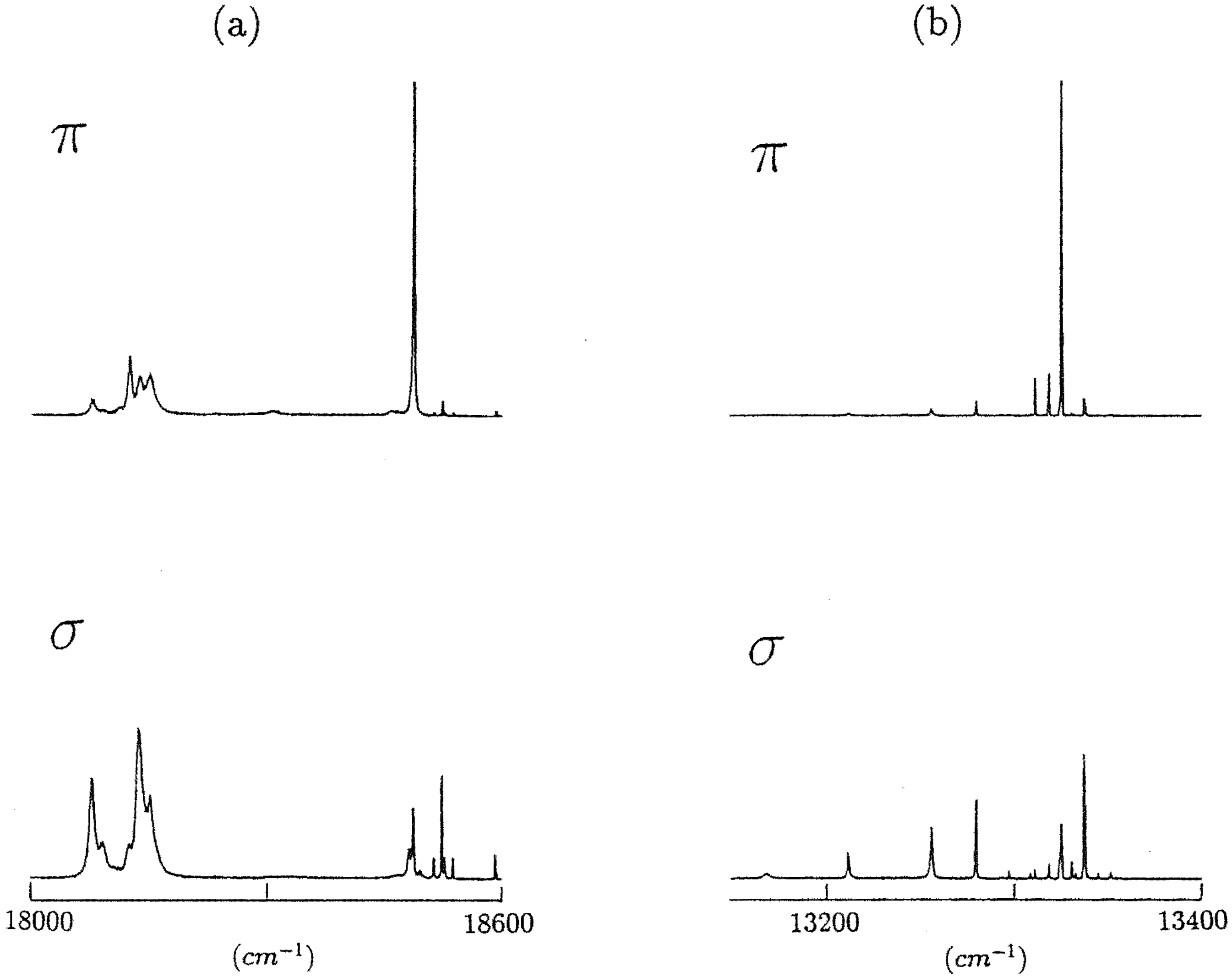
(a)
(b)
π
π
σ
σ
18000
18600
(cm^{-1})
13200
13400
(cm^{-1})

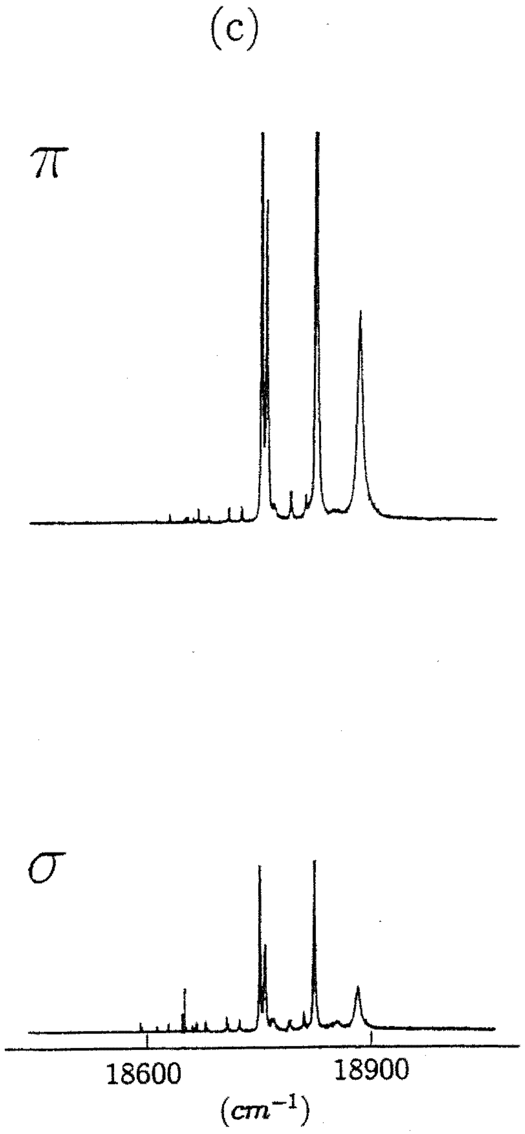

Figure 4.27: Polarisation of the 10 K selective excitation and fluorescence spectra of the CB2 centre in $Ca_{0.99}Ba_{0.01}F_2$:Ho^{3+}(0.005%) crystals :
(a) E→Z transitions, for excitation of the Z_1→E_2 transition at 18606.7 cm^{-1};
(b) E→Y transitions, for excitation of the Z_1→E_2 transition at 18606.7 cm^{-1};
(c) Z→E transitions, monitoring the E_2→Z_1 transition at 18606.7 cm^{-1}.
Transition labels are as in Figures 4.21(c) and 4.25.

Table 4.14: Observed and expected intensity ratios for the polarised fluorescence transitions of the CB2 centre in <100> and <111> oriented $Ca_{0.99}Ba_{0.01}F_2$:Ho^{3+}(0.005%) crystals, for excitation of the $Z_1 \rightarrow E_2$ ($\gamma_1 \rightarrow \gamma_1$) transition at 18606.7 cm^{-1}.

Transition	**Wavenumber (±0.5) (cm^{-1})**	**Observed Polarisation Ratios (±5%)**	
		<100>orientation [yy : yx]	**<111>orientation** [y′y′/y′x′]
$E_2 \rightarrow Z_3$	18537.5	1 : 6.0	0.6
$E_2 \rightarrow Z_4$	18527.5	1 : 5.9	0.7
$E_2 \rightarrow Z_6$	18503.0	1 : 5.3	0.7
$E_2 \rightarrow Z_7$	18496.0	1 : 7.4	0.7
$E_2 \rightarrow Z_{12}$	18151.0	1 : 5.0	0.8
$E_2 \rightarrow Z_{14}$	18124.0	5.3 : 1	2.0
$E_1 \rightarrow Z_1$	18593.0	1 : 1.7	0.8
$E_1 \rightarrow Z_2$	18591.0	1 : 5.7	0.7
$E_1 \rightarrow Z_3$	18524.0	1 : 6.2	0.7
$E_1 \rightarrow Z_4$	18513.5	1 : 5.1	0.7
$E_1 \rightarrow Z_5$	18487.5	7.0 : 1	2.0
$E_1 \rightarrow Z_6$	18489.5	1 : 4.7	0.8
$E_1 \rightarrow Z_7$	18483.0	1 : 6.9	0.7
$E_1 \rightarrow Z_{10}$	18150.5	5.1 : 1	2.0
$E_1 \rightarrow Z_{12}$	18137.0	1 : 4.8	0.8
$E_1 \rightarrow Z_{16}$	18089.0	1 : 5.2	0.8
$E_1 \rightarrow Z_{17}$	18077.5	1 : 5.3	0.8
$E_2 \rightarrow Y_1$	13352.0	1 : 4.9	0.7
$E_2 \rightarrow Y_2$	13345.5	1 : 5.6	0.7
$E_2 \rightarrow Y_4$	13340.0	1 : 4.2	0.7
$E_2 \rightarrow Y_5$	13333.5	1 : 9.5	0.6
$E_2 \rightarrow Y_6$	13312.0	8.3 : 1	2.1
$E_2 \rightarrow Y_7$	13309.5	1 : 4.5	0.7
$E_1 \rightarrow Y_1$	13338.5	1 : 6.2	0.7
$E_1 \rightarrow Y_2$	13332.0	1 : 6.3	0.8
$E_1 \rightarrow Y_3$	13326.5	9.5 : 1	2.6
$E_1 \rightarrow Y_4$	13325.5	1 : 7.0	0.7
$E_1 \rightarrow Y_5$	13319.5	5.1 : 1	2.0
$E_1 \rightarrow Y_6$	13298.0	1 : 4.3	0.8
$E_1 \rightarrow Y_7$	13295.5	1 : 4.5	0.8
$E_1 \rightarrow Y_8$	13280.5	1 : 5.5	0.7
$E_1 \rightarrow Y_9$	13257.0	1 : 6.3	0.7
$E_1 \rightarrow Y_{10}$	13243.0	4.8 : 1	2.0
$E_1 \rightarrow Y_{11}$	13212.5	1 : 8.2	0.7
$E_1 \rightarrow Y_{12}$	13169.5	1 : 6.7	0.6
$D_3 \rightarrow Z_1$	15615.5	5.2 : 1	2.2
$D_3 \rightarrow Z_2$	15613.5	5.0 : 1	2.0
$D_2 \rightarrow Z_1$	15601.5	1 : 5.9	0.5
$D_2 \rightarrow Z_3$	15532.5	1 : 6.0	0.8
$D_2 \rightarrow Z_4$	15522.5	1 : 4.9	0.6
$D_1 \rightarrow Z_1$	15600.0	1 : 6.2	0.7
$D_1 \rightarrow Z_2$	15598.0	1 : 5.8	0.7
$D_1 \rightarrow Z_3$	15531.0	5.9 : 1	2.6
$D_1 \rightarrow Z_4$	15521.0	4.7 : 1	1.9
$D_1 \rightarrow Z_8$	15317.0	4.3 : 1	2.4
$D_1 \rightarrow Z_9$	15306.5	1 : 2.8	0.8
$D_1 \rightarrow Z_{13}$	15127.5	1 : 3.3	0.8
$D_1 \rightarrow Z_{15}$	15115.0	1 : 3.8	0.8

4.3.4 Polarisation study of the CB2 centre

As for the CS2 centre, polarisation ratios were obtained with excitation of both the $Z_1 \rightarrow E_2$ and $Z_2 \rightarrow E_4$ transitions (Figures 4.27 and 4.28 respectively) with the following results :-

(a) For $Z_1 \rightarrow E_2(\gamma_a \rightarrow \gamma_a)$ excitation :

(i) the pairs of transitions to the split γ_5 type levels are polarised 0:1, with the exception of the transition at 13319.5 cm^{-1} which is mainly π polarised (Figure 4.27);

(ii) the single transitions corresponding to $\gamma_a \rightarrow \gamma_a$ type transitions of the CB1 centre are π polarised. Although the transition at 13298.0 cm^{-1} has been correlated to that at 13312.0 cm^{-1}, they have opposite polarisations. It may be coincidental that the two Y levels have the same energy separation as the E_1 - E_2 energy level separation as proposed for the CS2 centre;

(iii) the $E_1 \rightarrow Z_1$ transition is almost unpolarised with a polarisation ratio of just 1:1.7 while the $E_1 \rightarrow Z_2$ transition is σ polarised with a ratio of 1:5.7 (Table 4.14);

(iv) with the laser polarised E_z, all the transitions that were polarised 1:0 for the laser E_y are not observed while those that were polarised 0:1 for the laser polarised E_y are observed for the laser polarised E_z, but without any net polarisation.

(b) For $Z_2 \rightarrow E_4$ $(\gamma_a \rightarrow \gamma_b)$ excitation :-

(i) fluorescence from $\gamma_a \rightarrow \gamma_a$ type transitions was found to be polarised 0:1 while that by $\gamma_a \rightarrow \gamma_b$ type transitions was polarised 1:0 (Figure 4.28, Table 4.15). The two transition components from those transitions involving C_{4v} γ_5 type levels had opposite polarisation ratios;

(ii) the $E_1 \rightarrow Z_1$ transition is now mainly σ polarised while the $E_1 \rightarrow Z_2$ transition is π polarised (Table 4.15);

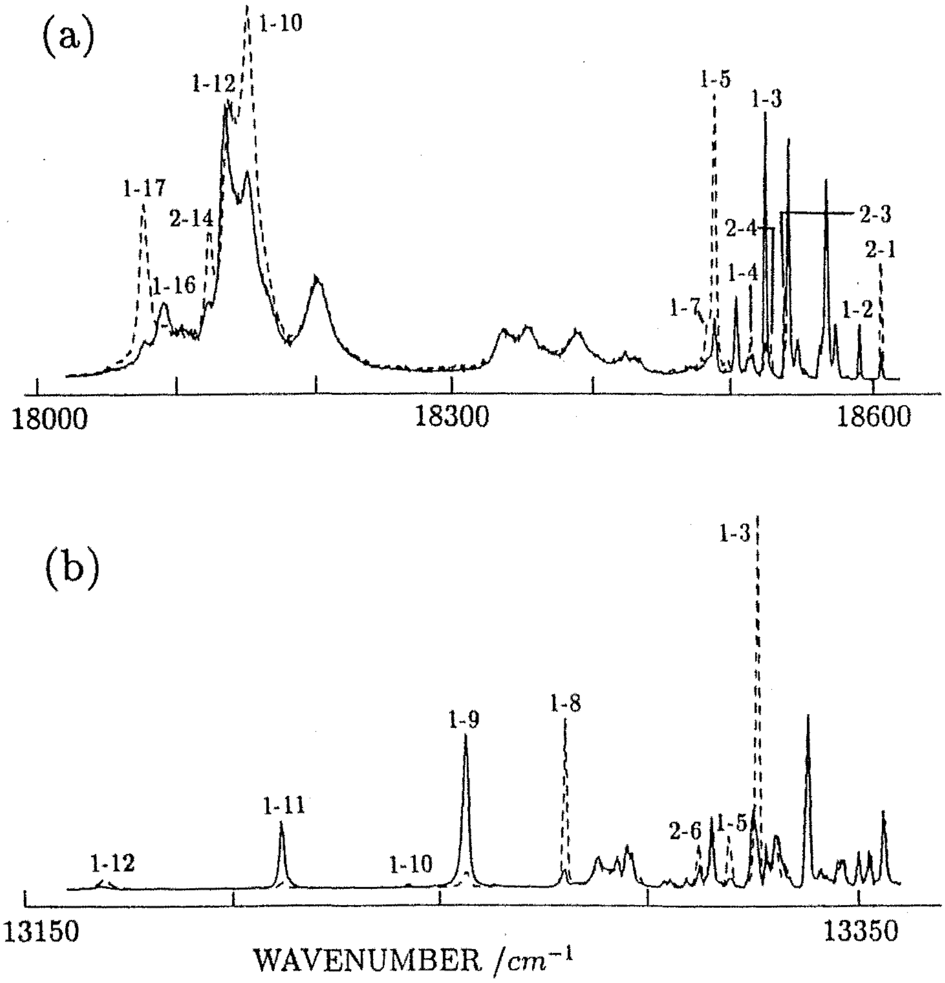

Figure 4.28: Polarisation of the 10 K fluorescence spectra of the CB2 centre in $Ca_{0.99}Ba_{0.01}F_2:Ho^{3+}$(0.005%) crystals, for excitation of the $Z_2 \rightarrow E_4$ transition at 18652.2 cm^{-1} :
(a) $E \rightarrow Z$ transitions (b) $E \rightarrow Y$ transitions
———— π polarisation - - - - - σ polarisation.
Transition labels as in Figure 4.25.

Table 4.15: Observed and expected intensity ratios for the polarised fluorescence transitions of the CB2 centre in <100> oriented $Ca_{0.99}Ba_{0.01}F^2$:Ho^{3+}(0.005%) crystals, for excitation of the $Z_2 \rightarrow E_4$ ($\gamma_2 \rightarrow \gamma_1$) transition at 18652.2 cm^{-1}.

Transition	**Wavenumber (±0.5) (cm^{-1})**	**Polarisation Ratios (±5%) [yy : yx] Observed**	**Expected**
$E_2 \rightarrow Z_1$	18606.7	1 : 5.5	0 : 1
$E_2 \rightarrow Z_2$	18604.7	4.1 : 1	1 : 0
$E_2 \rightarrow Z_3$	18537.5	6.1 : 1	1 : 0
$E_2 \rightarrow Z_4$	18527.5	1 : 7.0	0 : 1
$E_2 \rightarrow Z_7$	18496.0	1 : 5.7	0 : 1
$E_2 \rightarrow Z_{12}$	18151.0	1 : 5.8	0 : 1
$E_2 \rightarrow Z_{14}$	18124.0	1 : 8.2	0 : 1
$E_1 \rightarrow Z_1$	18593.0	1 : 4.9	0 : 1
$E_1 \rightarrow Z_2$	18591.0	7.0 : 1	1 : 0
$E_1 \rightarrow Z_3$	18524.0	6.7 : 1	1 : 0
$E_1 \rightarrow Z_4$	18513.5	1 : 5.2	0 : 1
$E_1 \rightarrow Z_5$	18487.5	1 : 6.3	0 : 1
$E_1 \rightarrow Z_7$	18483.0	1 : 5.4	0 : 1
$E_1 \rightarrow Z_{10}$	18150.5	1 : 6.6	0 : 1
$E_1 \rightarrow Z_{12}$	18137.0	1 : 6.0	0 : 1
$E_1 \rightarrow Z_{16}$	18089.0	7.2 : 1	1 : 0
$E_1 \rightarrow Z_{17}$	18077.5	1 : 8.8	0 : 1
$E_2 \rightarrow Y_6$	13312.0	1 : 4.9	0 : 1
$E_1 \rightarrow Y_3$	13326.5	1 : 6.9	0 : 1
$E_1 \rightarrow Y_4$	13325.5	5.2 : 1	1 : 0
$E_1 \rightarrow Y_5$	13319.5	1 : 5.4	0 : 1
$E_1 \rightarrow Y_8$	13280.5	1 : 8.7	0 : 1
$E_1 \rightarrow Y_9$	13257.0	9.3 : 1	1 : 0
$E_1 \rightarrow Y_{10}$	13243.0	1 : 6.4	0 : 1
$E_1 \rightarrow Y_{11}$	13212.5	8.5 : 1	1 : 0
$E_1 \rightarrow Y_{12}$	13169.5	1 : 5.0	0 : 1

(iii) fluorescence transitions that were π polarised for the laser polarised E_y are absent when the laser polarisation is rotated to E_z. Transitions that were σ polarised for E_y are observed for E_z but with no net preferred polarisation (i.e. ratios of 1:1).

Figure 4.26 shows the CB2 centre levels in relation to the CB1 centre levels. Irrep labels have been assigned based on the polarisation ratios obtained with $Z_2 \rightarrow E_4$ excitation as described in Section 4.2.4 for the CS2 centre and are given in Table 4.13.

The CB2 centre is therefore believed to be of C_s(b) symmetry with the Ba^{2+} ion in the (100) plane as shown in Figure 1.4(b). This is identical to the model proposed for the CS2 centre.

4.3.5 Upconversion fluorescence and spectra recorded above 20 K

As for the CS1 and CS2 centres, some upconversion fluorescence was observed for Z → D excitation but was too weak to measure while no upconversion fluorescence was observed for Z → E excitation.

Attempts at identifying other high energy E multiplet levels by measuring up to 55 K spectra were unsuccessful due to unavoidable simultaneous excitation of A centre transitions.

4.4 Discussion of the Centres

This section collects together and summarises the main features of the various centres(A, B, CS1, CS2, CB1 and CB2) in CaF_2. In Chapter 5 these centres will be further compared to those in $SrF_2:Ho^{3+}$ crystals.

From polarisation studies, the A and B centres in $CaF_2:Ho^{3+}$ have been shown conclusively to have exact C_{4v} and C_{3v} symmetry respectively, as first proposed by [SW]. All the transitions reported by [SW] have been confirmed, and extended with observation of additional transitions such as the $Z_{1,2} \rightarrow E_{10}$ and $Z_1 \rightarrow D_4$ transitions for the A and B centres respectively. The major contribution from the study here has been the determination of a complete set of energy levels and the assignment of irrep labels to all levels for both centres. The spectral measurements up to 55 K were helpful for identifying some additional levels and confirming the various $E_2 \rightarrow Z$ and $E_2 \rightarrow Y$ level transition assignments. Measurements at 2 K were essential for inferring the presence of the lowest E_1 level of the E multiplet and transitions to and from it. The crystal-field calculations of Reid and Butler were helpful as aids to determining irrep label assignments.

For all the centres, nearly all the energy levels for the Z, Y, D and E multiplets and some for the F multiplet have been identified with irrep labels assigned, giving reliable energy level schemes.

Comparison of the energy levels of the four new centres observed in both $Ca_{0.99}Sr_{0.01}F_2{:}Ho^{3+}$(0.005%) and $Ca_{0.99}Ba_{0.01}F_2{:}Ho^{3+}$(0.005%) with those of the parent A centre yields the following relationships:

(i) the two C_{4v} symmetry centres, CS1 and CB1, have E_1 - E_2 energy level separations of 11.0 and 10.5 cm^{-1} respectively, both somewhat smaller than the A centre value of 14.0 cm^{-1};

(ii) the two C_s symmetry centres, CS2 and CB2, have an E_1 - E_2 energy level separation of 13.5 cm^{-1}, closely comparable to that for the A centre;

(iii) for each crystal system, the C_{4v} symmetry centre has lower energy transitions than the corresponding C_s symmetry centre;

(iv) all additional transitions observed for the C_s centres could be fully accounted for through low symmetry splittings of C_{4v} γ_5 type levels or through the presence of transitions strictly forbidden for exact C_{4v} symmetry;

(v) the transitions that were forbidden under exact C_{4v} symmetry selection rules have generally quite weak intensity for the C_s symmetry centres.

Model assignments were made on the basis of choosing positions for the dopant alkaline-earth cation that were as close as possible to the Ho^{3+} ion while being consistent with the assigned Ho^{3+} site symmetry determined from the polarisation of the spectra (either the C_{4v} or C_s(b) arrangement). Other choices involving more remote placements of the dopant alkaline-earth ion would have their transitions within the linewidths of the parent A centre transitions. For the CS1 and CB1 C_{4v} symmetry centres, the model given in Figure 1.4(a) is the one with the most altered Ho^{3+} ion environment. Because the only other possibilities all involve the dopant alkaline-earth cation being at least two lattice spacings away from the Ho^{3+} ion, such substitutions would not influence the environment around the rare-earth ion to any great extent. It is to be expected that they would only give rise to transitions within the linewidth of the transitions of the parent C_{4v} symmetry centre. A dopant alkaline-earth cation located in the position shown in Figure 1.4(a) however would create the largest distortion through possible repositioning of both the interstitial F^- ion and the four F^- ions located between the interstitial F^- ion and the dopant alkaline-earth cation, with resulting maximum effect on the Ho^{3+} ion environment. As the region around the interstitial F^- ion is already spatially extended there is not much difference between having a new cation, Sr^{2+} or Ba^{2+}, in the neighbouring cube, hence the almost identical energies observed for the CS1 and CB1 centres. As exact analogues of each other, both the CS1 and CB1 centres have been assigned to this same specific model.

Similarly, for the two C_s symmetry centres, it is the dopant alkaline-earth cation closest to the Ho^{3+} ion that would give the maximum change to the Ho^{3+} site environment. The two models given in Figure 1.4 (b) and (c) are equally likely configurations that satisfy C_s symmetry. Distinction between the two is possible through polarisation studies with $\gamma_a \rightarrow \gamma_b$ type pump transitions, as per Table 2.5. The C_s configuration of Figure 1.4(b) has been assigned to both the CS2 and CB2 centres because the polarisation results for $Z_2 \rightarrow E_4$ excitation of each centre were found to unequivocally indicate the C_s(b) symmetry assignment.

Although the CS2 and CB2 centres have quite similar energy level patterns, the low symmetry splittings for corresponding transitions were found to be much larger for the CB2 centre than for the CS2 centre. This is reasonable as the Ba^{2+} ion, being larger than the Sr^{2+} ion, would alter the surrounding host lattice F^- ions more, resulting in larger low symmetry splittings of the γ_5 levels.

The CS1 and CB1 centres are analogous to the so-called A2 centre reported for the Pr^{3+} ion in $CaSrF_2$ and $CaBaF_2$ crystals while the CS2 and CB2 centres are equivalent to the so-called A1 centre of Pr^{3+} in the same crystals [63].

4.5 Spectroscopy of Deuterated CaF_2:Ho^{3+} Crystals

Deuterated centres were studied in preference to the hydrogenated centres as it is well established that D^- centres, in general, have stronger fluorescence than the corresponding H^- centres [107]. The reduction of fluorescence intensity in all hydrogenic type centres is through non-radiative quenching effects involving the hydride or deuteride local modes. For Ho^{3+}, the effects appeared to be quite severe, sufficient to preclude a detailed determination of the energy levels of even the D^- analogue of the A centre described earlier. It was found, from the onset, that although the D^- centre transitions were comparatively strong in absorption, they had weak fluorescence under laser excitation.

The main experimental problem in studying the Ho^{3+} - D^- centres was that the transitions did not show up as well in the broadband excitation spectra, in marked contrast to the other rare-earths previously studied viz, Er^{3+} [32] and Pr^{3+} [90]. For the Ho^{3+} case, one had to start off with a search of approximate positions derived from the absorption spectrum, find a fluorescence transition to monitor and then try to optimise the fluorescence signal. This procedure was laborious, time consuming and required careful tuning because most of the D^- transitions were quite close to F^- centre transitions. Even setting the spectrometer to monitor the vibronic transitions of the D^- transitions 500 cm^{-1} lower in energy than the electronic transitions and hence well removed from any

F^- centre electronic transitions did not provide any better discrimination. The coupling between the F^- and D^- centres by radiation coupling and by cross-pumping appears to be quite strong for Ho^{3+}.

Additional information on these centres may have been obtained from comparable studies on hydrogenated and tritiated samples, but, in view of the much weaker fluorescence from H^- centres compared to D^- centres, such studies were not attempted because of the already weak D^- fluorescence for all three D^- centres observed.

The centres in deuterated CaF_2:Ho^{3+} crystals were first studied by an Honours III student, M. Paris [95]. The high Ho^{3+} concentration adopted (0.05%) combined with the long deuteration periods of up to 90 hours resulted in very rich absorption spectra. Classifying the absorption transitions to the various centres was found to be difficult because of considerable overlap between different D^- centre transitions and between the D^- and F^- centre transitions. Of the fifteen D^- centre transitions pumped, none had a common fluorescence spectrum. There were only a few common transitions for some spectra, which is not sufficient for assigning transitions to particular centres. None of the spectra measured correlated to the D^- analogues of the F^- A and B centres.

In the study here, Ho^{3+} concentrations of 0.005% were used in conjunction with short deuteration periods of just 4 to 12 hours, in order to obtain just a few of the simpler D^- centres. Only a few new transitions were observed in the absorption spectra of such samples (Figure 4.29).

Because the D^- transitions are relatively weak under laser excitation, selective excitation spectra well discriminated from F^- centres could not be obtained. The fluorescence was weak, being only 0.5 - 1% of that of the F^- A centre. From comparison of several fluorescence spectra, three D^- centres were identified. Of these, one is analogous to the F^- B centre and has been labelled the D^- B centre while the other two are low symmetry centres related to the F^- A centre. These two centres are arbitrarily labelled D1 and D2. A careful search

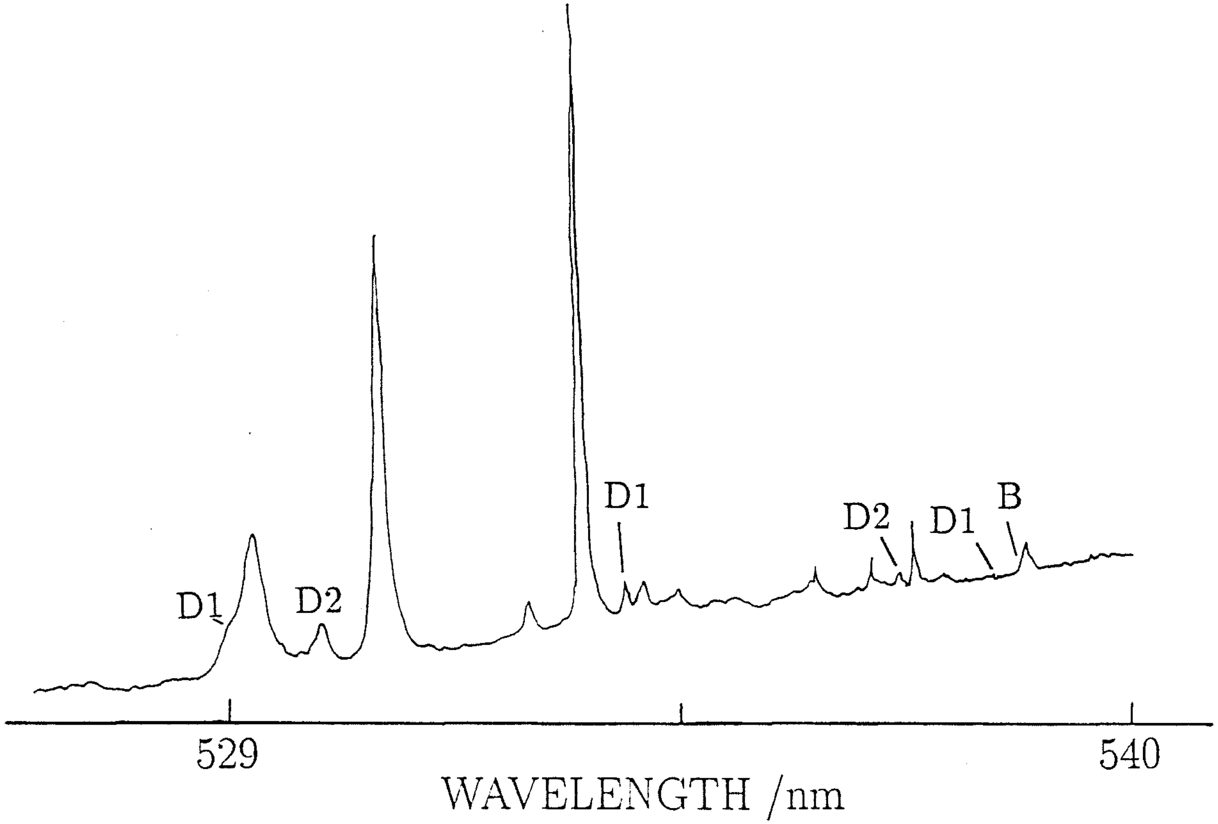

Figure 4.29: 10 K absorption spectrum of the Z→E transitions in CaF_2:Ho^{3+}(0.005%) crystals deuterated for 4 hours.

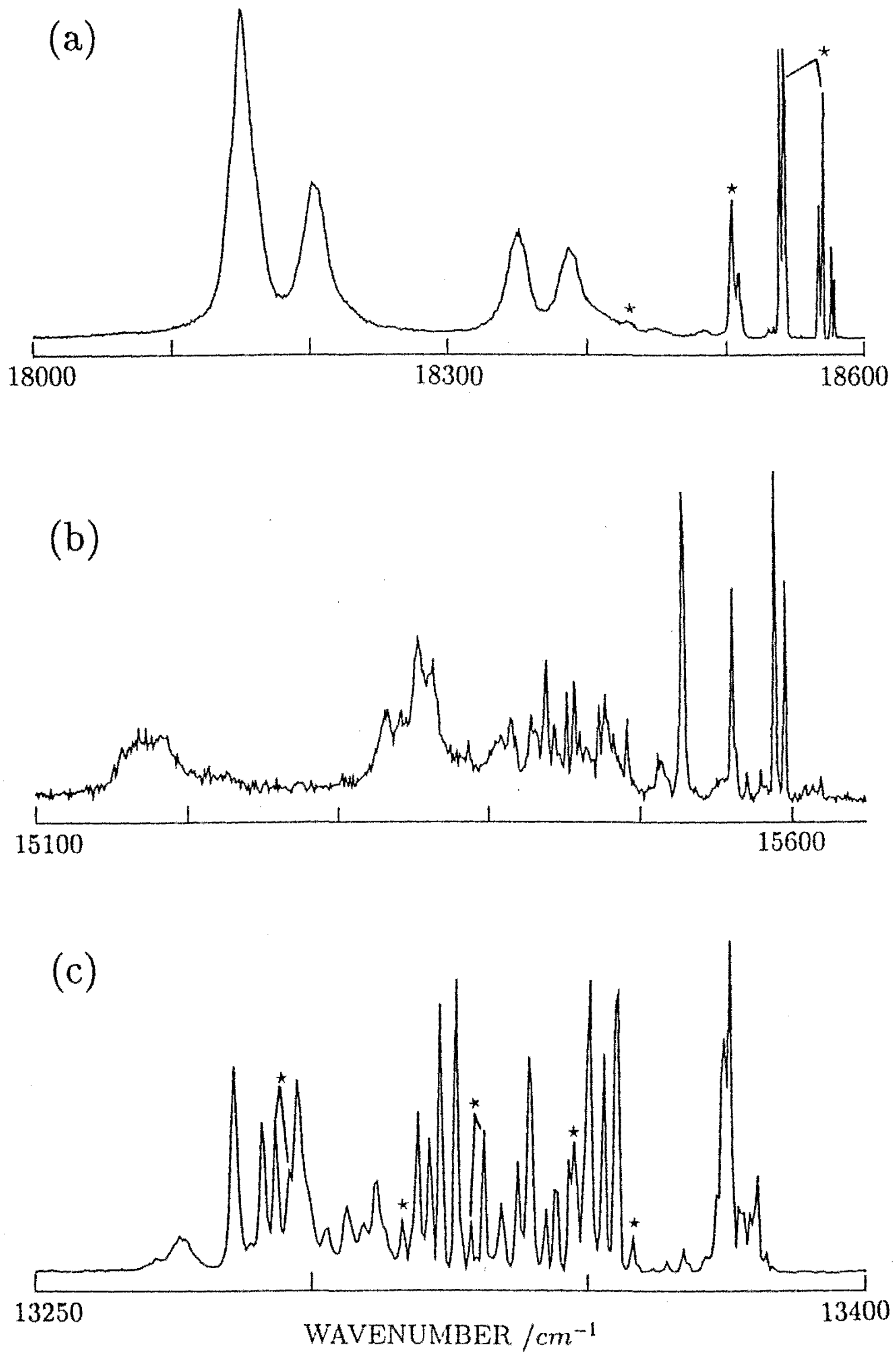

Figure 4.30: 10 K fluorescence spectra for the D^- B centre in CaF_2:Ho^{3+}(0.005%) crystals after 4 hours of deuteration, for excitation of the transition at 18571.7 cm^{-1} :
(a) E→Z transitions;
(b) D→Z transitions;
(c) E→Y transitions.
Transitions identified by * are for the F^- B centre.

Table 4.16: Energies (in cm^{-1}) of the E→Z, D→Z and E→Y transitions observed for the D$^-$ B centre in CaF$_2$:Ho^{3+}(0.005%) crystals, after 4 hours deuteration. Uncertainty is ± 1 cm^{-1}.

E→Z transitions	D→Z transitions	E→Y transitions
18571.7	15596.0	13380.5
18538.0	15589.0	13377.0
18504.5	15561.0	13375.5
18483.0	15528.0	13374.5
18449.0	15364.0	13373.0
18387.0	15354.0	13355.5
18352.0	15334.0	13353.0
18202.0	15170.0	13350.5
18150.0		13346.5
18144.0		13344.0
		13342.0
		13339.5
		13337.0
		13334.5
		13326.5
		13323.5
		13321.5
		13319.5
		13312.0
		13309.5
		13306.5
		13303.0
		13297.5
		13291.0
		13286.0
		13276.0

for the D^- analogue of the F^- A centre was unsuccessful. The three centres are now briefly discussed in turn.

4.5.1 The D^- B centre

Excitation of the transition at 18571.7 cm^{-1} (Figure 4.29), resulted in fluorescence spectra (Figure 4.30) similar to those for the F^- B centre except for a shift in energy of the transitions. As this pump transition is only 1.2 cm^{-1} higher than the $Z_1 \rightarrow E_3$ transition for the F^- B centre, fluorescence from the latter centre could not be completely eliminated. The E_1 - E_2 - E_3 energy level separations of this D^- centre could not be resolved, though the transitions to the Z_2 and Z_3 levels did show some structure. As for the F^- B centre, only transitions to the Z_1, Z_2 and Z_3 levels at 0, 33.5 and 63.0 cm^{-1} respectively, are sharp in the $E \rightarrow Z$ spectrum (Figure 4.30(a)).

The $E \rightarrow Y$ spectrum (Figure 4.30(c)), also shows transitions for both the F^- B and D^- B centres. The D^- centre transitions span a larger spectral range than the F^- centre transitions. Because of low fluorescence signal as well as appreciable overlap with the F^- B centre transitions, the E_1 - E_2 - E_3 energy level separations could not be deduced from this spectrum as done for the F^- centre.

The $D \rightarrow Z$ transitions (Figure 4.30(b)) were quite weak. Any small D_1 - D_2 energy level separation as found for the F^- centre was not apparent.

Since only one level for the E and D multiplets has been identified, transition energies rather than energy levels are presented in Table 4.16. The $E \rightarrow Z$ transitions identify closely similar Z levels for this D^- centre as corresponding transitions for the F^- centre.

4.5.2 The D1 and D2 centres

Both these centres show more transitions than can be accommodated by an exact C_{4v} symmetry centre and are assigned as being C_s symmetry centres.

For the D1 centre, the $E \rightarrow Z$ and $D \rightarrow Z$ transitions occur in two groups (Figure 4.31(a) and (b)). The pump transition at 18584.4 cm^{-1}, as well as the fluorescence transition at 18550.0 cm^{-1}, shows a 2.0 cm^{-1} splitting. It is not clear

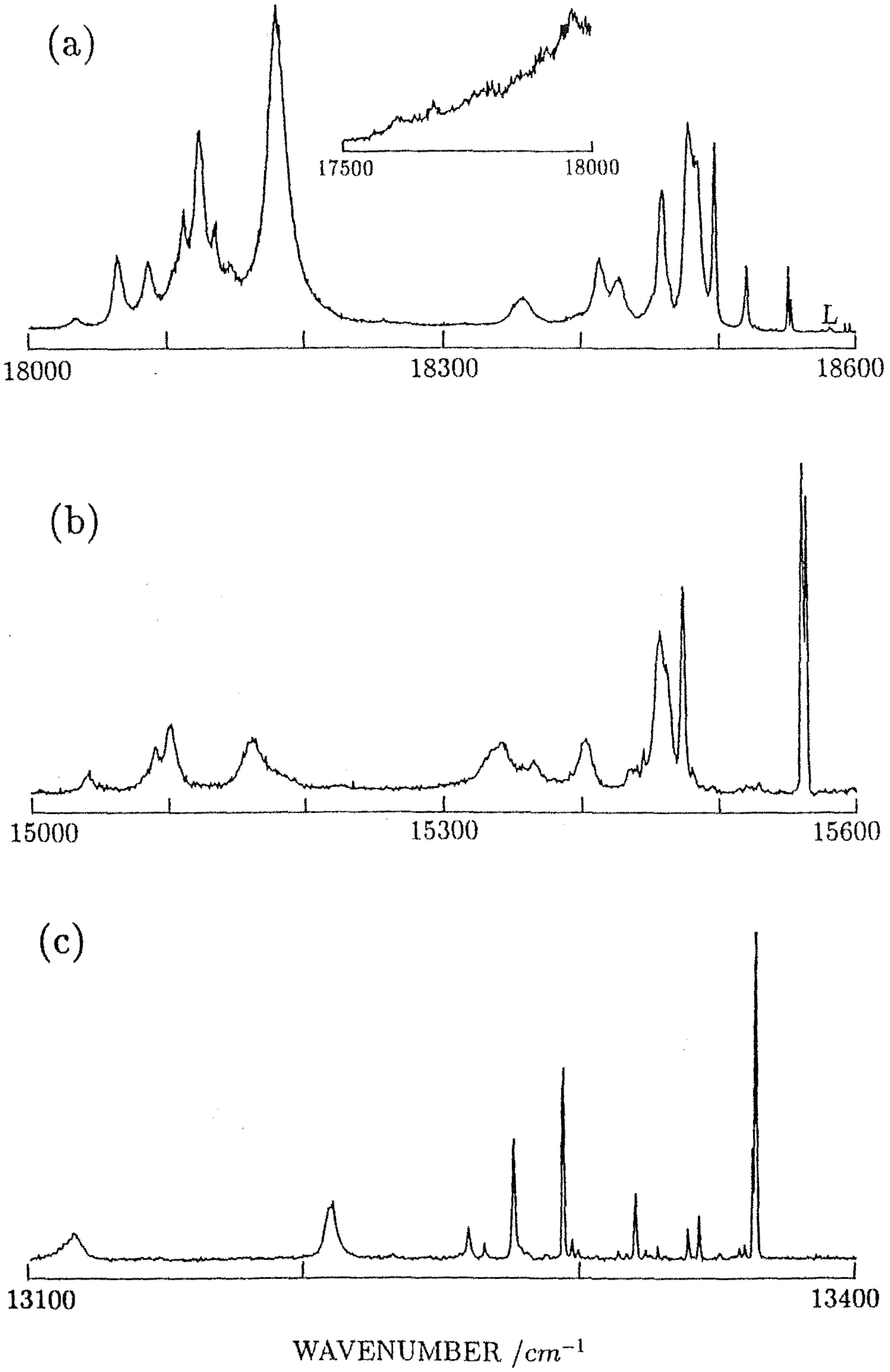

Figure 4.31: 10 K fluorescence spectra for the D1 centre in $CaF_2:Ho^{3+}$(0.005%) crystals after 4 hours deuteration, for excitation of the transition at 18584.4 cm^{-1} :
(a) E→Z transitions;
(b) D→Z transitions;
(c) E→Y transitions.

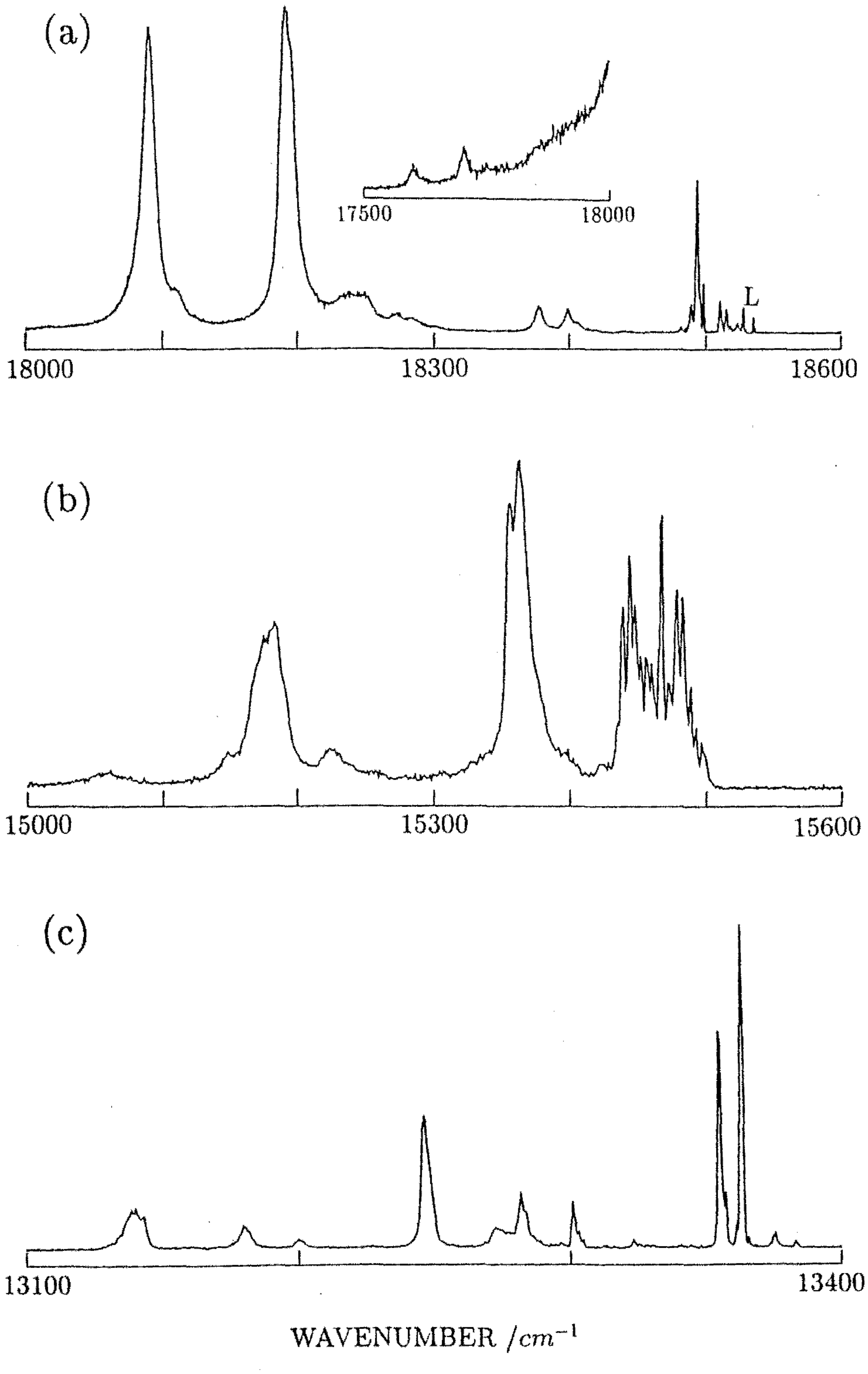

Figure 4.32: 10 K fluorescence spectra for the D2 centre in CaF_2:Ho^{3+}(0.005%) crystals after 4 hours deuteration, for excitation of the transition at 18620.8 cm^{-1} :

(a) E→Z transitions;
(b) D→Z transitions;
(c) E→Y transitions.

Table 4.17: Energies (in cm^{-1}) of the E→Z, D→Z and E→Y transitions observed for the D1 and D2 centres in CaF_2:Ho^{3+}(0.005%) crystals, after 4 hours deuteration. Uncertainty is ± 1 cm^{-1}.

Transitions	D1	D2
E→Z	18900.9	18861.9
	18733.9	18620.8
	18584.4	18532.6
	18582.5	18512.0
	18550.0	18507.5
	18548.0	18495.5
	18494.0	18491.5
	18482.0	18487.0
	18475.5	18396.0
	18457.0	18376.0
	18425.0	18193.0
	18410.0	18189.5
	18355.0	18106.5
	18178.5	18088.5
	18121.0	
	18110.0	
	18062.5	
D→Z	15561.0	15495.0
	15558.0	15487.0
	15527.0	15481.0
	15478.0	15477.0
	15471.0	15470.0
	15460.0	15466.0
	15455.0	15458.0
	15443.0	15454.0
	15434.0	15450.0
	15401.0	15446.0
	15363.0	15442.0
	15339.0	15437.0
	15160.0	15364.0
	15100.0	15361.0
	15089.0	15354.0
	15040.0	15222.0
		15189.0
		15181.0
		15173.0

cont...

Table 4.17 cont...

Transitions	**D1**	**D2**
E→Y	13364.0	13383.5
	13362.5	13376.0
	13343.0	13363.0
	13339.0	13357.5
	13328.0	13355.0
	13320.0	13323.5
	13294.0	13301.0
	13276.0	13282.0
	13265.0	13273.0
	13259.5	13246.5
	13210.5	13200.5
	13115.5	13180.0
		13140.0
Vibronic	18143.0	17884.0
	18132.5	17702.0
	18084.0	17598.0
	18029.5	
	17960.0	
	17908.0	
	17678.0	
	17608.0	

whether this is indeed the Z_1 - Z_2 splitting because it would give an E_1 - E_2 energy level separation of 33.0 cm^{-1} which is not apparent on any of the E → Z and E → Y transitions. Also, although the transition at 15561.0 cm^{-1} in the D → Z spectrum has a 2.0 cm^{-1} splitting, all transitions in the D → Z spectrum correspond to some transition in the E → Z spectrum, if the levels at 18584.4 and 15561.0 cm^{-1} are assumed to be the corresponding upper multiplet emitting levels. The transition at 18550.0 cm^{-1} cannot, therefore, be to the Z_1 and Z_2 levels as there are no transitions observed to the higher Z levels. The other transition at 18733.9 cm^{-1} belonging to this centre gives fluorescence that is almost wholly swamped by that for F^- A centre. The vibronic transitions are relatively strong with the transitions at 18084.0 and 18029.5 cm^{-1} (Figure 4.31(a)) being comparable in intensity to the electronic transitions. These vibronic transitions correspond to local mode phonon energies of 500.0 and 518.0 cm^{-1}.

The D2 centre is characterised by E → Z and D → Z fluorescence transitions occurring in three groups (Figure 4.32(a) and (b)). Two transitions at 18620.8 and 18532.6 cm^{-1} in the absorption spectrum belong to this centre. The correspondence between the E → Z and D → Z transitions is not very apparent and indeed the number of emitting levels for the upper E and D multiplets is not clear as some of the higher energy transitions have a common 4.0 cm^{-1} energy separation. From this occurrence, it is difficult to deduce whether this is actually a Z_1 - Z_2 energy level separation or just similar E and D low energy level separations. Only two vibronic transitions were observed at 17701.5 and 17597.0 cm^{-1} (insert of Figure 4.32(a)), corresponding to the two strong electronic transitions at 18193.0 and 18088.5 cm^{-1} respectively. These two vibronic transitions are weak compared to those for the D1 centre and give a common phonon energy of 491.5 cm^{-1}. As already mentioned, monitoring these vibronic transitions to determine the D2 centre excitation transitions did not result in any better discrimination from the F^- centre transitions.

Observed transition energies for both centres are summarised in Table 4.17.

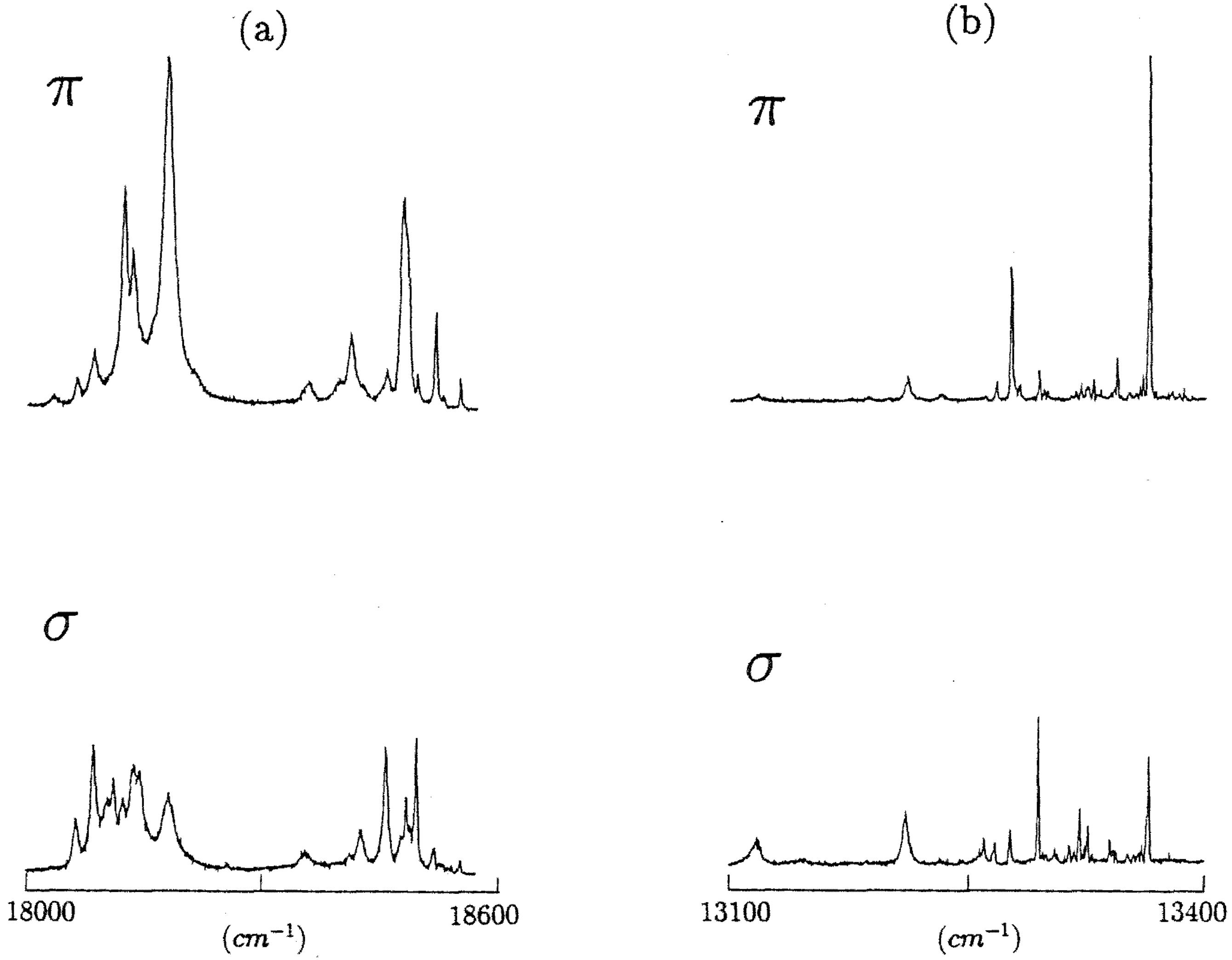

Figure 4.33: Polarisation of the 10 K fluorescence spectra of the D1 centre in CaF_2:Ho^{3+}(0.005% crystals deuterated for 4 hours, for excitation of the transition at 18584.4 cm^{-1} :
(a) E→Z transitions;
(b) E→Y transitions.

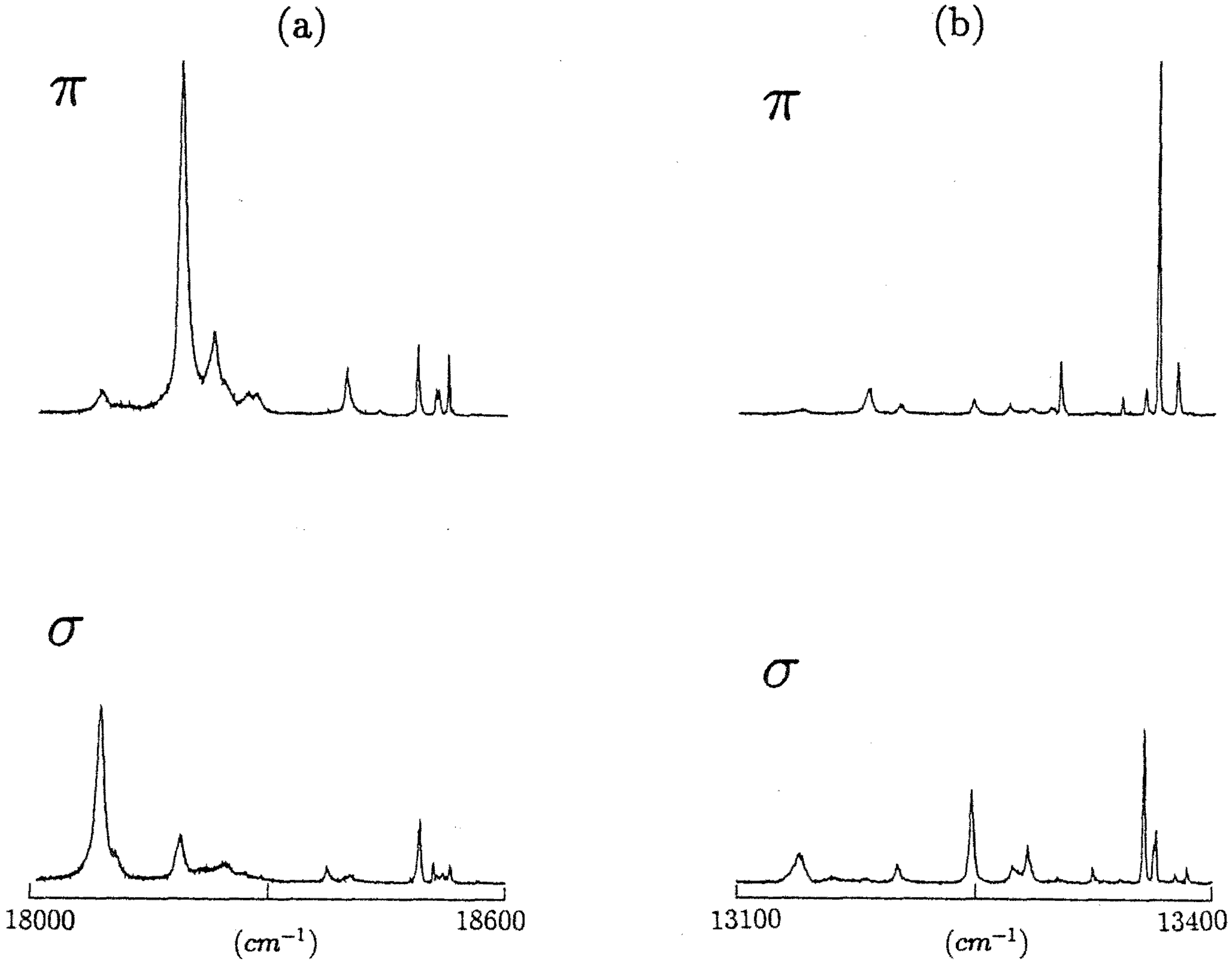

Figure 4.34: Polarisation of the 10 K fluorescence spectra of the D2 centre in CaF_2:Ho^{3+}(0.005%) crystals deuterated for 4 hours, for excitation of the transition at 18620.8 cm^{-1} :
(a) E→Z transitions;
(b) E→Y transitions.

Transitions for both the D1 and D2 centres were polarised showing polarisation ratios similar to those for C_{4v} symmetry centres in the <100> oriented crystals (Figures 4.33 and 4.34) and both centres should therefore be derived from the C_{4v} symmetry centre.

4.5.3 Discussion of the D^- centres

The D^- A centre could not be detected at all. It is possible that its transitions are completely swamped by overlap with transitions for one of the F^- centres, resulting in undetectable excitation and fluorescence transitions for this centre. From comparison with other rare-earths (Er^{3+}, Nd^{3+} and Pr^{3+}), there is no reason why there should not be a D^- A centre for Ho^{3+} even for the low deuteration periods used here. Furthermore, infrared local modes of the D^- C_{4v} centre have been reported [55].

The D^- B centre has similar characteristics to the F^- B centre and is therefore assigned as a C_{3v} symmetry centre with an analogous configuration to the F^- B centre. Due to feeble fluorescence intensity for this centre, wide monochromator slits of 100 to 200 μm (1 - 2 cm^{-1} resolution) were used and any E_1 - E_2 - E_3 or D_1 - D_2 energy level separations could not be measured.

The D1 and D2 centres are believed to be modifications of the D^- A centre. Vibronic transitions were relatively strong for the D1 centre. The most likely model for the D1 centre is the modified C_{4v} symmetry Ho^{3+} - D^- centre reduced to C_s symmetry by a D^- substitution for one of the eight F^- ions in the first coordinate shell which is the configuration proposed for the $C_s(1)$ centre found in deuterated CaF_2:Pr^{3+} crystals [105]. For the D2 centre both the spectral pattern and observation of a related low vibronic transition interval of 491.5 cm^{-1} suggests that the configuration is significantly different from that of the D1 centre. The observed polarisation ratios suggest a C_{4v} parentage for this centre as well. It is possible that there are more D^- ions involved in this centre, as was proposed for the $C_s(2)$ centre of Pr^{3+} [105].

Neither the D1 nor the D2 centre exhibits any bleaching phenomena, reversible or otherwise, such as that reported for C_s symmetry centres in Nd^{3+}[45], Pr^{3+}[105, 106] and Er^{3+}[32] doped crystals. In all, the hoped for characterisation of the deuteride analogue centre of the F^- A centre and of the observation of reversible bleaching for the C_s symmetry centres was completely precluded by the relative weakness of the Ho^{3+} fluorescence in D^- centres, the considerable overlap of D^- transitions with those of the F^- centres and the apparent complete absence of any simple D^- centres even at low deuteration levels.

CHAPTER 5

SPECTROSCOPY OF Ho^{3+} IONS IN SrF_2 TYPE CRYSTALS

The most striking feature of the spectroscopy of rare-earth ions introduced into SrF_2 and BaF_2 crystals at low concentrations is the observed change in the symmetry of the principal rare-earth ion centre from a tetragonal symmetry configuration at the beginning of the rare-earth series to a trigonal symmetry one towards the end [18]. Such a symmetry change does not occur in CaF_2 crystals.

From various EPR measurements in SrF_2 crystals, the change over is determined to occur in the vicinity of the rare-earth ions Dy^{3+} and Ho^{3+}. Of the rare-earth ions studied, Ce^{3+} [18], Nd^{3+} [15] and Sm^{3+} [7] ions have only tetragonal symmetry RE^{3+} centres, Gd^{3+} [119] and Dy^{3+} [6, 39] ions have both tetragonal and trigonal symmetry RE^{3+} centres present, while Er^{3+} [8, 18] and Yb^{3+} [104] ions have only trigonal and cubic symmetry RE^{3+} centres present. For Tb^{3+} ions in SrF_2 crystals, two types of tetragonal symmetry centres were observed [9]. The EPR results reported for SrF_2:Ho^{3+}(0.1%) crystals [103] indicate that the principal centre has trigonal symmetry. These particular measurements were done at both X band (~10 GHz) and K band (~35 GHz) frequencies and the spectra obtained were solely for Ho^{3+} ions in sites of C_{3v} symmetry, with EPR resonances of neither cubic nor tetragonal symmetry centres being detected. It was concluded from these studies that the principal Ho^{3+} ion centre in SrF_2 is of C_{3v} symmetry.

For rare-earth ions in BaF_2 crystals, the ions at the beginning of the series have a principal centre of tetragonal symmetry while for those ions towards the end of the series, the principal centre is of trigonal symmetry. The change over in the principal centre symmetry from tetragonal to trigonal is expected to occur in the vicinity of the Pr^{3+} and Nd^{3+} ions [18].

The aforementioned EPR results for Ho^{3+} ions in SrF_2 crystals [103] are not in agreement with the spectroscopic results presented here where the principal centre has been found to be of tetragonal symmetry, with the trigonal symmetry centre being at only 2% of the tetragonal symmetry centre concentration. Possible resolution of this principal centre symmetry anomaly is presented in Section 5.6.

An argon ion laser excitation study of $SrF_2:Ho^{3+}(1\%)$ has been reported [70]. Using the 457.9, 465.9, 472.7, 476.5, 488.0 and 514.5 nm argon laser lines, three fluorescence groups were observed in the 530.0 - 561.5 nm, 635.0 - 662.5 nm and 745.0 - 770.0 nm regions. The group in the 530.0 - 561.5 nm region was assigned as $^5F_4,^5S_2 \rightarrow {}^5I_8$ fluorescence transitions, that in the 635.0 - 662.5 nm region was assigned as arising from the overlapped $^5F_3 \rightarrow {}^5I_7$ and $^5F_5 \rightarrow {}^5I_8$ fluorescence transitions while the group in the 745.0 - 770.0 nm region was ascribed to the $^5F_4,^5S_2 \rightarrow {}^5I_7$ transitions. The study however did not elucidate any centre distributions and symmetries nor present any energy level assignments.

The spectroscopic results presented here for Ho^{3+} ions in SrF_2 crystals are based on 2 K, 10 K and up to 55 K spectral measurements and related polarisation studies. As such, the study of Ho^{3+} ion centres in SrF_2 crystals here parallels that for the A and B centres in $CaF_2:Ho^{3+}$ crystals as presented in Chapter 4. The similarities and differences between the spectra of Ho^{3+} ions in SrF_2 and CaF_2 crystals will be high-lighted. Additionally, three other centres labelled here SC1, SC2, and SB1 arising from the presence of small amounts of Ca^{2+} and Ba^{2+} ions in the SrF_2 starting material are described.

In a similar previous laser selective excitation study of Er^{3+} ions in $SrF_2:Er^{3+}(0.05\%)$ crystals [30, 68], four centres were found, and arbitrarily labelled J, N1, N2 and N3. Of these, the J centre was proposed to be of exact trigonal symmetry and N3 was assigned as a tetragonal symmetry centre, with the N1 and N2 centres as slight modifications thereof.

An additional four centres, associated with deuterium ions, found in weakly deuterated $SrF_2:Ho^{3+}(0.005\%)$ crystals, are described in Section 5.7. All these four centres have some resemblance to the F^- A centre but none of them was the exact D^- analogue. These four D^- centres have been arbitrarily labelled D1, D2, D3 and D4.

Absorption Spectra

Although Ho^{3+} absorption transitions were readily observed in 10 mm thick $CaF_2:Ho^{3+}$(0.02%) crystals, none could be observed at measurable intensity in similar thicknesses of SrF_2 crystals. Both the Ho^{3+} concentration and crystal thickness had to be gradually increased until sufficient intensity absorption transitions were observed for 0.1% Ho^{3+} concentration crystals of 25 - 30 mm thickness.

The transitions are many and rather broad which is not unexpected as, at such high Ho^{3+} concentrations, both single Ho^{3+} - F^- ion centres and cluster centres would be present. The $Z \rightarrow E$ and $Z \rightarrow D$ absorption spectra for $SrF_2:Ho^{3+}$(0.1%) crystals, as recorded at 10 K, are presented in Figure 5.1. The absorption transitions ascribed to the $Z \rightarrow D$ transitions were found to be much weaker than those for the $Z \rightarrow E$ transitions.

Laser Selective Excitation Spectra

In contrast to optical absorption measurements where concentrations of 0.1% were needed, broadband excitation spectra measured in 0.005% and 0.01% Ho^{3+} concentrations show narrow and intense features, which maintained the same relative intensities for Ho^{3+} concentrations over the range 0.001% to 0.02%. Both the $Z \rightarrow E$ and $Z \rightarrow D$ broadband excitation spectra have fewer transitions than the absorption spectra measured in $SrF_2:Ho^{3+}$(0.1%) crystals, as only single Ho^{3+} ion centres are present in the lower Ho^{3+} concentration crystals. However, the broadband excitation spectra measured for 0.1%Ho^{3+} doped crystals are closely similar to the absorption spectra of Figure 5.1.

As fluorescence intensities in $SrF_2:Ho^{3+}$ crystals were found to be typically 20 times less than those in $CaF_2:Ho^{3+}$ crystals for the same Ho^{3+} dopant concentration, a Ho^{3+} concentration of 0.01% was chosen for the $SrF_2:Ho^{3+}$ studies reported here.

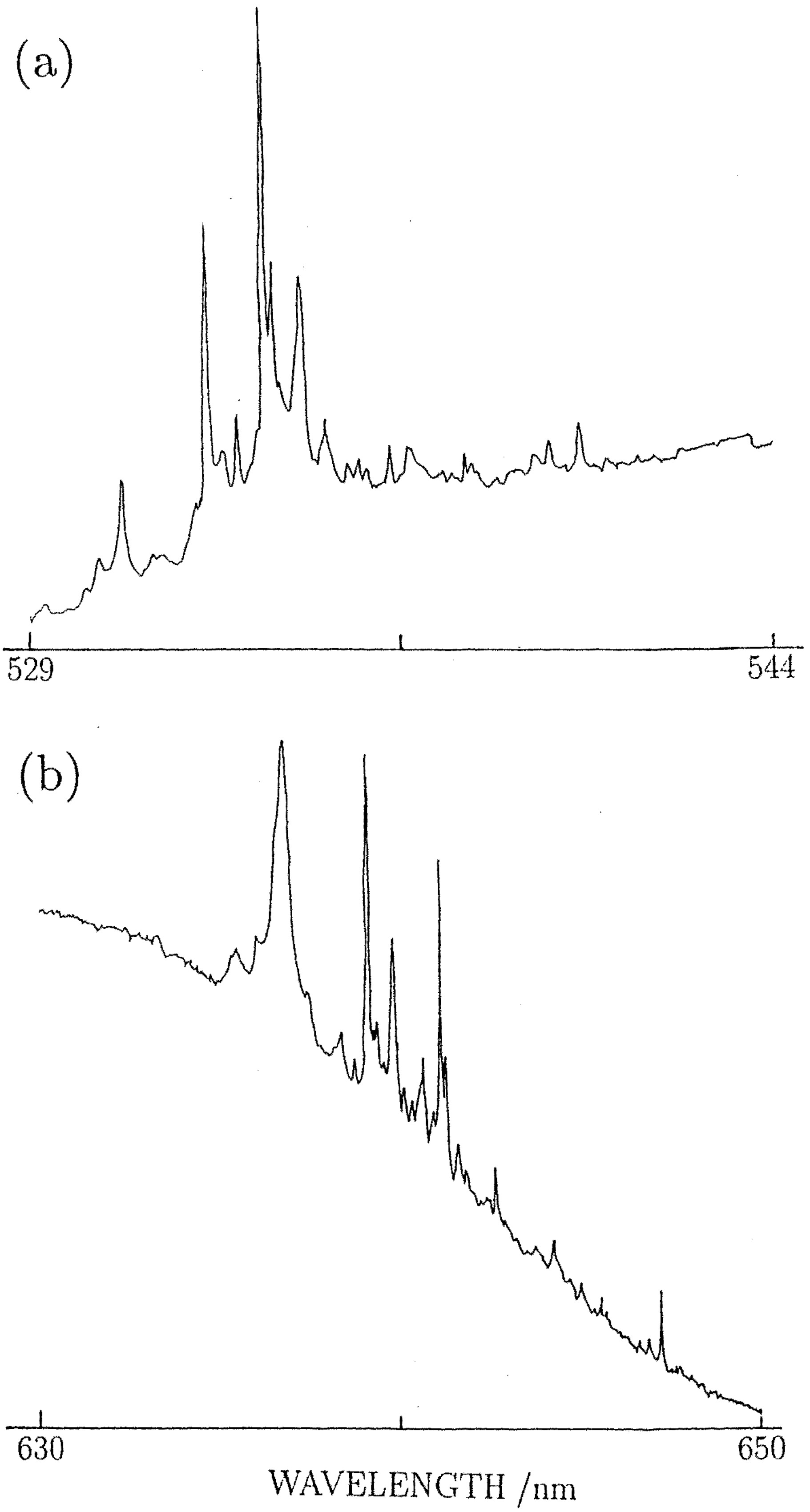

Figure 5.1: 10 K absorption spectra in SrF_2:Ho^{3+}(0.1%) crystals :
(a) Z→E transitions;
(b) Z→D transitions.

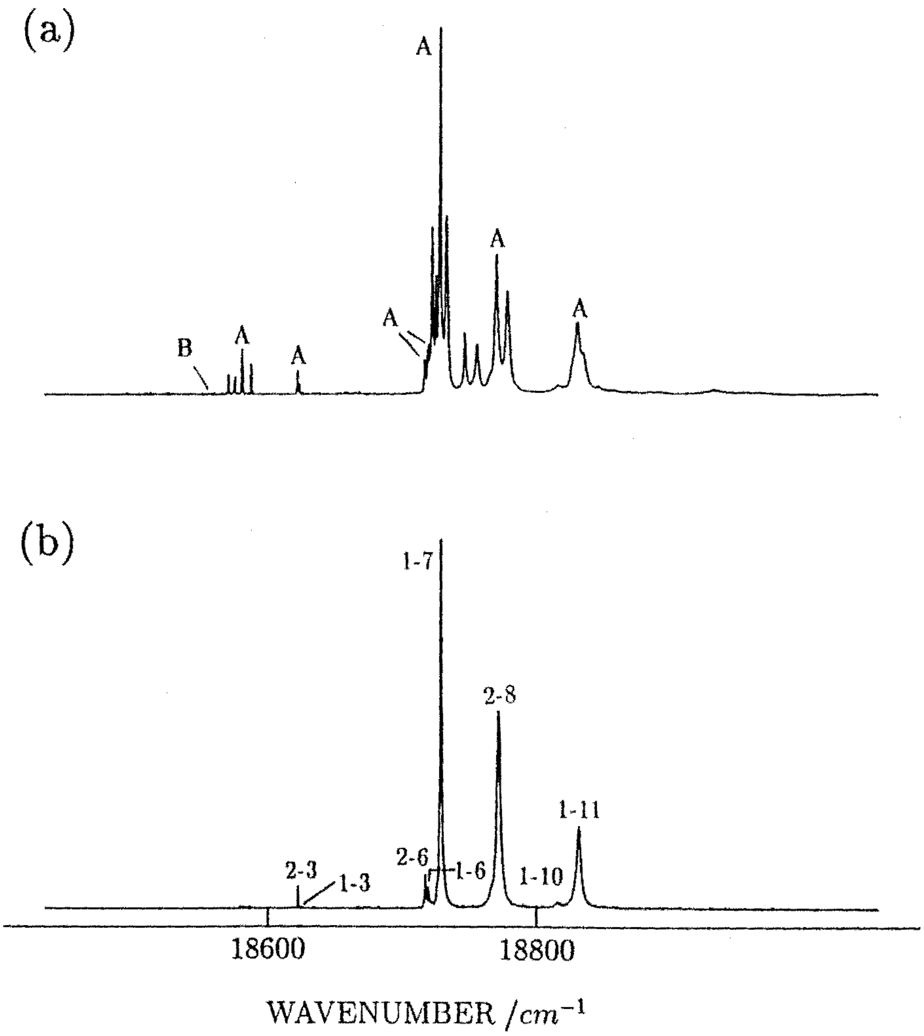

Figure 5.2: 10 K broadband and selective excitation spectra for the E multiplet of the A centre in SrF_2:Ho^{3+}(0.01%) crystals :
(a) broadband excitation spectrum, monitoring all the D→Z transitions;
(b) SrF_2 A centre excitation spectrum, monitoing the $E_2 \rightarrow Z_1$ transition at 18585.7 cm^{-1}.
Transitions are labelled by the appropriate lower and upper multiplet crystal-field level identifications.

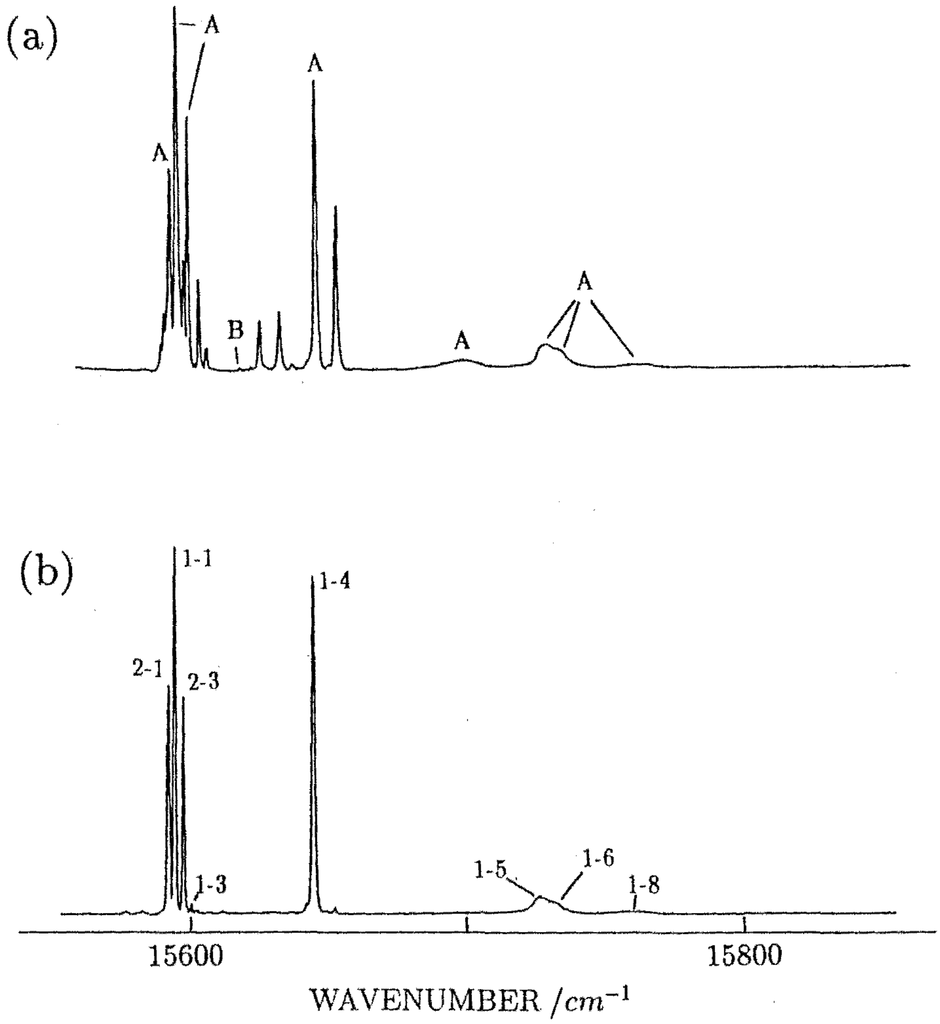

Figure 5.3: 10 K broadband and selective excitation spectra for the D multiplet of the A centre in $SrF_2:Ho^{3+}$ (0.01%) crystals :
(a) broadband excitation spectrum, monitoring all the D→Z transitions;
(b) SrF_2 A centre excitation spectrum, monitoring the $D_1 \rightarrow Z_3$ transition at 15539.5 cm^{-1}.

By laser selective excitation, five distinct centres, labelled A, B, SC1, SC2 and SB1 in Figures 5.2, 5.3, 5.10, 5.11, 5.13 and 5.14 were identified. The concentrations of the SC1, SC2 and SB1 centres, as judged by excitation intensity, which depends on fluorescence efficiency, was about half that of the A centre while the B centre was found to be present only at 2% of the concentration of the A centre. As in the case of the CS1, CS2, CB1 and CB2 centres, it was only possible to obtain completely discriminated selective excitation spectra for each of the A , SC1, SC2 and SB1 centres by monitoring the respective $E_2 \rightarrow Z_1$ transition of each centre. Because of its comparative weakness, it was not possible to obtain any completely discriminated excitation spectrum for the B centre. The spectroscopy of the various centres are now discussed in turn.

5.1 The A and B Centres in SrF_2:Ho^{3+}(0.01%) Crystals

5.1.1 Spectroscopy of the SrF_2 A centre

Selective excitation spectra for both the $Z \rightarrow E$ and $Z \rightarrow D$ transitions are presented in Figures 5.2 and 5.3 respectively and the fluorescence spectra in Figure 5.4. The spectra of this centre were found to be closely similar in both excitation and fluorescence to those of the A centre of CaF_2, with an overall shift in all the levels to lower energies. The transitions to the E_2, E_3 and E_6 levels in the excitation spectrum have a common Z_1 - Z_2 spacing of 2.7 cm^{-1}, which is larger than the 1.9 cm^{-1} observed for the CaF_2 A centre. The A centre's first excited level Z_2 is therefore slightly higher in SrF_2 than in CaF_2.

The $E \rightarrow Z$ fluorescence spectrum (Figure 5.4(a)) has four sets of transition pairs with a common separation of 6.0 cm^{-1}, compared to 14.0 cm^{-1} for the CaF_2 A centre. The E_1 level for this centre is thus at 18579.5 cm^{-1}, some 6.0 cm^{-1} lower than the E_2 level at 18585.7 cm^{-1} which is the lowest directly observed level of the E multiplet. Three single transitions were observed at 18504.0, 18202.5 and 18182.5 cm^{-1}. When the temperature of the crystal was raised to 20 K the particular transition at 18182.5 cm^{-1} as well as the higher energy transition of each transition pair increased in intensity. These transitions must therefore originate from the E_2 level while the remaining single transitions at 18504.0 and 18202.5 cm^{-1} and the lower energy transition of each pair originate from the E_1 level.

At 30 K, transitions from the E_3 level at 18624.8 cm^{-1} became apparent while transitions from the E_5 through to E_{11} levels were still scarcely visible. By 40 K, all the additional transitions had appeared clearly and increased further in intensity as the temperature was gradually raised to 55 K. The fluorescence spectrum for the E → Z transitions at 55 K is shown in Figure 5.5. A further E level at 18671.5 cm^{-1} was identified from these high temperature transitions. This E_5 level does not show any transitions to the Z_1 and Z_2 levels, but is revealed through its well defined transitions to the Z_3, Z_4 and Z_{10} energy levels.

The E → Y spectrum (Figure 5.4(c)) has two sets of transition pairs having the same E_1 - E_2 energy level separation of 6.0 cm^{-1}. Of the five single transitions observed at 13348.5, 13330.0, 13296.0, 13276.0 and 13231.0 cm^{-1}, only the transition at 13330.0 cm^{-1} gained intensity as the crystal temperature was raised to 20 K. This transition therefore originates from the E_2 level and is to the Y_6 level at 5255.5 cm^{-1} (Table 5.1). The remaining four transitions from the E_1 level to the Y_3, Y_7, Y_8 and Y_{10} levels at 5231.0, 5283.5, 5303.5 and 5348.5 cm^{-1} respectively (Table 5.1), were all weaker in the 20 K spectrum than in the 10 K spectrum. This is the same behaviour as observed for the E → Y transitions of the CaF_2 A centre.

In the D → Z spectrum (Figure 5.4(b)), transitions from the D_1 and D_3 levels to the Z_1 and Z_2 levels show the 2.7 cm^{-1} Z_1 - Z_2 energy level separation. The D → Z spectrum is closely similar to that for the E → Z transitions except for the additional feature centred at 15330.5 cm^{-1} whose analogue is very weak in the E → Z spectrum. As observed for the CaF_2 A centre, the fluorescence from the D multiplet was strong for direct Z → D excitation and weak for Z → E excitation. The D_1 level has transitions clearly distinguishable to most of the Z levels while

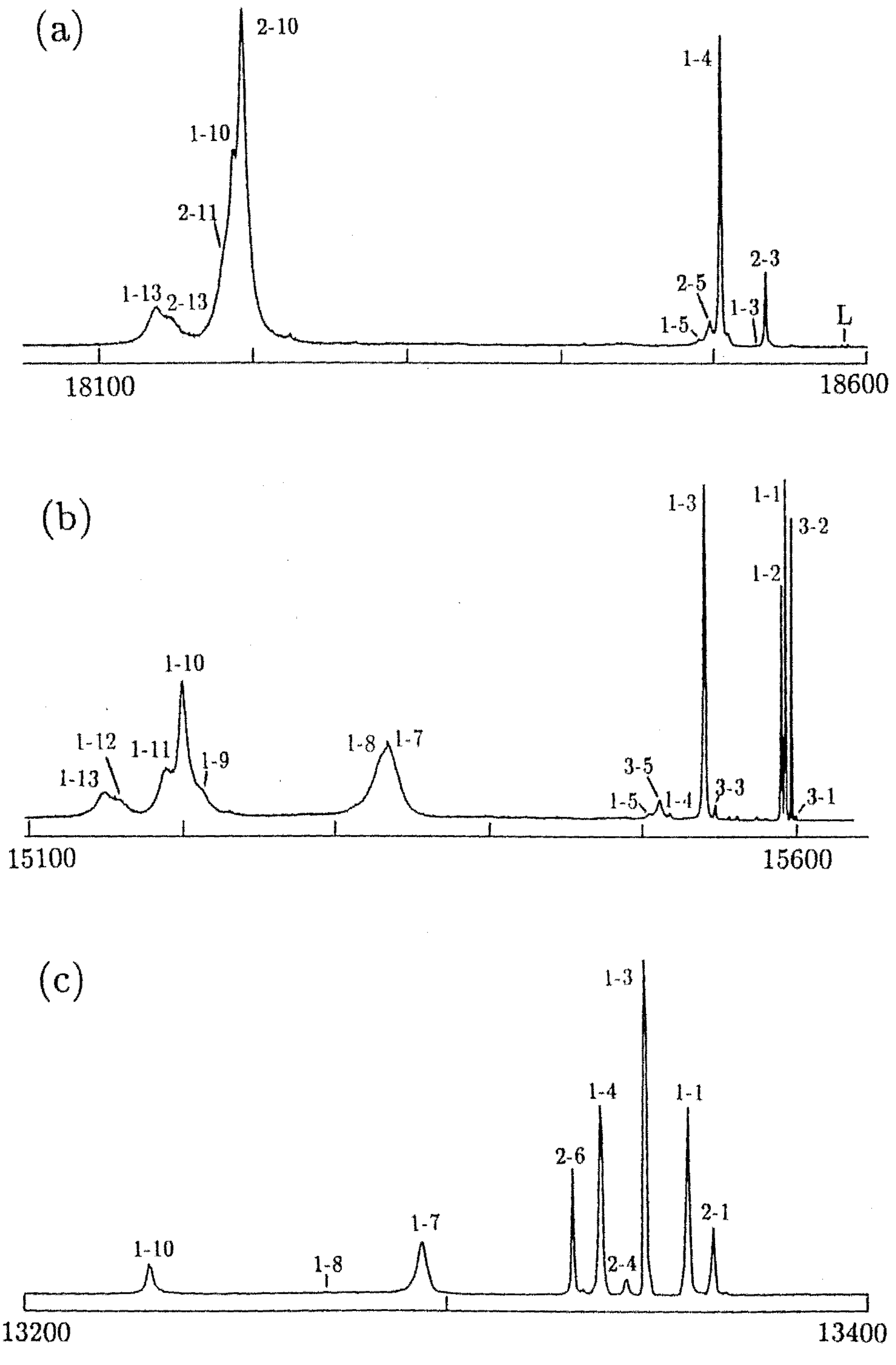

Figure 5.4: 10 K fluorescence spectra for the A centre in $SrF_2:Ho^{3+}$(0.01%) crystals :
(a) E→Z transitions, for excitation of the $Z_1 \to E_2$ transition at 18585.7 cm^{-1};
(b) D→Z transitions, for excitation of the $Z_1 \to D_4$ transition at 15642.3 cm^{-1};
(c) E→Y transitions, for excitation of the $Z_1 \to E_2$ transition at 18585.7 cm^{-1}.
Transitions are labelled by the appropriate upper and lower multiplet crystal-field level identifications. The laser position is identified by "L".

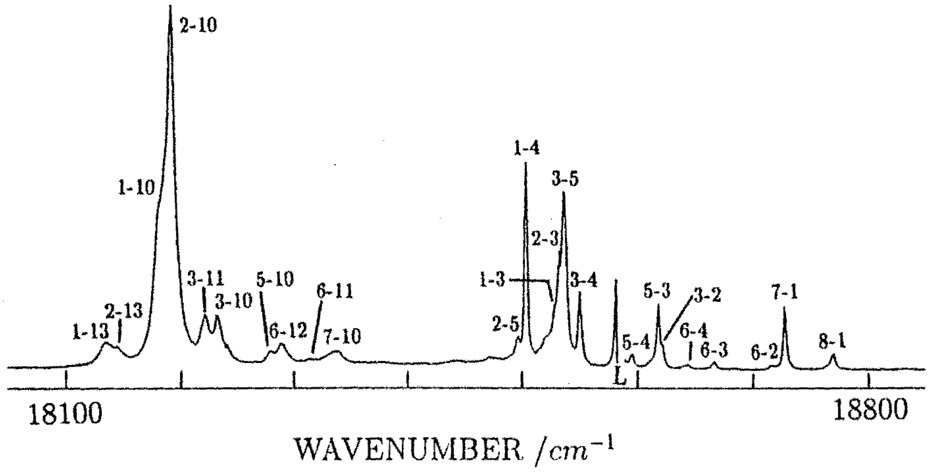

Figure 5.5: 55 K fluorescence spectrum of the E→Z transitions for the A centre in $SrF_2:Ho^{3+}$(0.01%) crystals, for excitation of the $Z_1 \rightarrow E_2$ transition at 18585.7 cm^{-1}.

Transitions are labelled by the appropriate upper and lower multiplet crystal-field level identifications. The laser position is identified by "L".

Table 5.1 : Energy levels (in cm^{-1}) of the Z, Y, D, E and F multiplets of the SrF_2 A centre and their symmetries, as derived from the 2 K to 55 K spectra of SrF_2:Ho^{3+}(0.01%) crystals. Uncertainty is ± 0.5 cm^{-1} unless otherwise indicated.

Level	Z($^5I_8$)	Y($^5I_7$)	D($^5F_5$)	E($^5S_2$,$^5F_4$)	F($^5F_3$)
1	0±0.2(γ_1)	5220.5(γ_5)	15593.0(γ_5)	18579.5(γ_3)	20735.5(γ_2)
2	2.7±0.2(γ_2)	-	-	18585.7(γ_1)	20756.5(γ_5)
3	52.5(γ_5)	5231.0(γ_3)	15599.0(γ_2)	18624.8(γ_5)	-
4	75.5(γ_3)	5241.5(γ_5)	15642.3(γ_1)	-	-
5	89.0(γ_5)	-	15727.8(γ_5)	18671.5(γ_3)	-
6	-	5255.5(γ_1)	15735.1(γ_2)	18718.7(γ_5)	
7	255.5(γ_1)	5283.5(γ_5)	-	18729.0(γ_1)	
8	265.5(γ_2)	5303.5(γ_3)	15764.1(γ_5)	18771.0(γ_2)	
9	377.0(γ_3)	-		-	
10	393.0(γ_5)	5348.5(γ_5)		18817.5(γ_5)	
11	403.0(γ_1)	-		18833.7(γ_1)	
12	430.0(γ_4)				
13	443.0(γ_5)				

the D_3 level does not have any transitions to the Z_4, Z_9 and Z_{11} levels. Transitions to the Z_1, Z_3, Z_5, Z_{10} and Z_{13} levels all show the D_1 - D_3 energy level separation of 6.0 cm^{-1}. In CaF_2 the energy of the lowest D multiplet level was inferred to be lower than the lowest directly observed level through observation of transition pairs with a constant energy separation of 4.5 cm^{-1}, but no such pairing was observed here for SrF_2. All the observed transitions have been found to originate from just the two levels at 15593.0 and 15599.0 cm^{-1}. The level at 15593.0 cm^{-1} is therefore the lowest energy level D_1 of the D multiplet.

The energy levels derived are presented in Table 5.1.

5.1.2 Polarisation study of the SrF_2 A centre

Polarisation ratios were measured for both <100> and <111> oriented crystals. Results obtained for $E \rightarrow Z$ and $E \rightarrow Y$ transitions with $Z_1 \rightarrow E_2$ excitation (Figure 5.6) and for $D \rightarrow Z$ transitions with $Z_1 \rightarrow D_4$ excitation are presented in Table 5.2. Only the <100> orientation results will be discussed here as the same conclusions can be reached from the results from either orientation.

In both the $E \rightarrow Z$ and $E \rightarrow Y$ spectra (Figure 5.6 (a) and (b)), the transition pairs are polarised with a 0:1 ratio. This is consistent with a γ_5 irrep label assignment for the Z_3, Z_5, Z_{10} and Z_{13} levels at 52.5, 89.0, 393.0 and 443.0 cm^{-1} respectively, as well as for the Y_1 and Y_4 levels at 5220.5 and 5241.5 cm^{-1} respectively. The single transitions at 18504.0, 18202.5 and 18182.5 cm^{-1} were all measured to be π polarised and are therefore assigned to be $\gamma_a \rightarrow \gamma_a$ type transitions. The $E \rightarrow Y$ transitions at 13348.5, 13330.0 and 13276.0 cm^{-1} were also π polarised, while the two transitions at 13296.0 and 13231.0 were σ polarised. These last two transitions identify the Y_7 and Y_{10} levels as γ_5 type levels. Using the same arguments as applied in the analysis for the CaF_2 A centre, the E_1 and E_2 levels have γ_3 and γ_1 symmetry irrep labels respectively. The Y_6 level is also of γ_1 symmetry while the Y_3 and Y_8 levels have γ_3 symmetry labels. Similarly the Z_4 and Z_9 levels are both γ_3 type levels and the Z_{11} level is of γ_1 symmetry.

The $D_1 \rightarrow Z_1$ and $D_1 \rightarrow Z_2$ transitions at 15593.0 and 15590.3 cm^{-1}

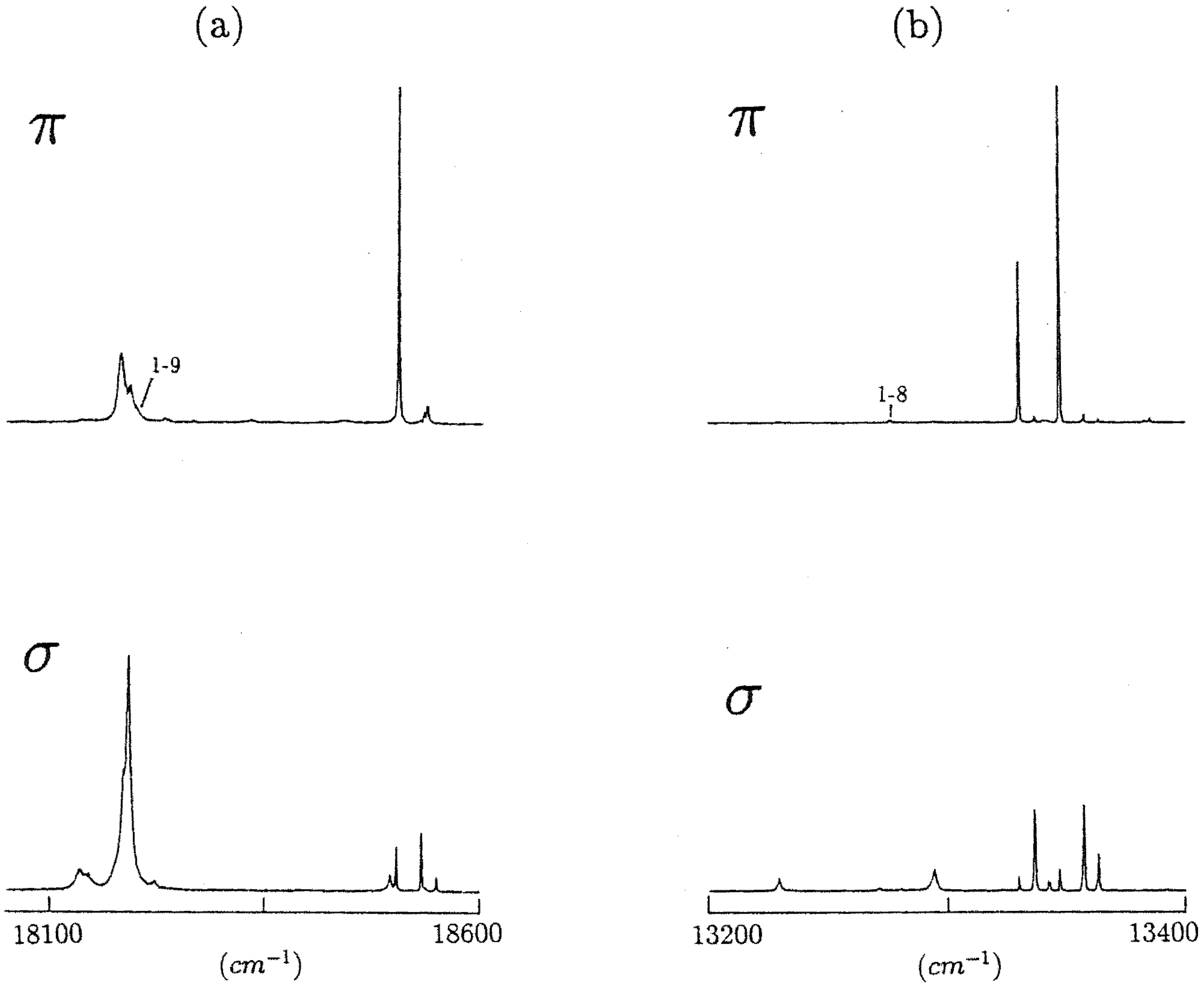
(a)
(b)
π
1-9
π
1-8
σ
σ
18100
18600
(cm⁻¹)
13200
13400
(cm⁻¹)

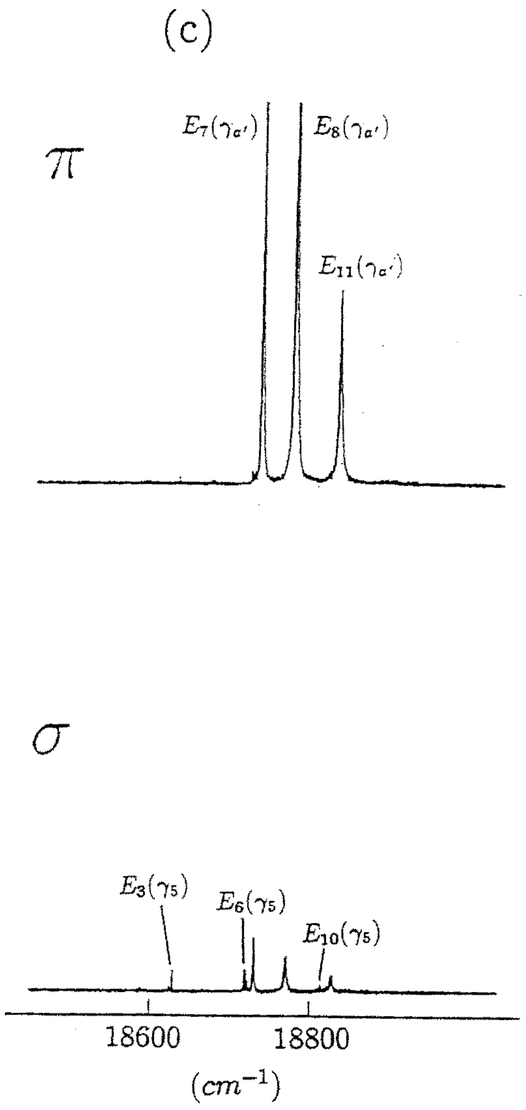

Figure 5.6: Polarisation of the 10 K selective excitation and fluorescence spectra of the A centre in SrF_2:Ho^{3+}(0.01%) crystals :
(a) E→Z transitions, for excitation of the Z_1→E_2 transition at 18585.7 cm^{-1};
(b) E→Y transitions, for excitation of the Z_1→E_2 transition at 18585.7 cm^{-1};
(c) Z→E transitions, monitoring the E_2→Z_1 transition at 18585.7 cm^{-1}.
Transition labels are as in Figures 5.2(b) and 5.4.

Table 5.2: Observed and predicted intensity ratios for the polarised fluorescence transitions of the A centre in <100> and <111> oriented $SrF_2:Ho^{3+}$(0.01%) crystals, for excitation of the $Z_1 \to E_2$ transition at 18585.7 cm^{-1}.

Transition	**Wavenumber**	**Polarisation Ratios (±5%)**			
	(±0.5) cm^{-1}	**<100> orientation**		**<111> orientation**	
		[yy : yx]		**[y′y′/y′x′]**	
		Observed	**Expected**	**Observed**	**Expected**
$E_2 \to Z_3$	18533.0	1 : 7.8	0 : 1	$^{3.0}/_{5}$	$^{3}/_{5}$
$E_2 \to Z_5$	18497.0	1 : 10.7	0 : 1	$^{3.5}/_{5}$	$^{3}/_{5}$
$E_2 \to Z_{10}$	18192.5	1 : 12.7	0 : 1	$^{3.5}/_{5}$	$^{3}/_{5}$
$E_2 \to Z_{11}$	18182.5	11.3 : 1	1 : 0	2.2	3.0
$E_2 \to Z_{13}$	18142.5	1 : 10.7	0 : 1	$^{3.5}/_{5}$	$^{3}/_{5}$
$E_1 \to Z_3$	18527.0	1 : 7.4	0 : 1	$^{4.0}/_{5}$	$^{3}/_{5}$
$E_1 \to Z_4$	18504.0	9.5 : 1	1 : 0	2.5	3.0
$E_1 \to Z_5$	18490.5	1 : 10.1	0 : 1	$^{4.0}/_{5}$	$^{3}/_{5}$
$E_1 \to Z_9$	18202.5	9.3 : 1	1 : 0	-	3.0
$E_1 \to Z_{10}$	18187.0	1 : 12.7	0 : 1	$^{4.0}/_{5}$	$^{3}/_{5}$
$E_1 \to Z_{13}$	18136.0	: 10.7	0 : 1	$^{3.5}/_{5}$	$^{3}/_{5}$
$E_2 \to Y_1$	13365.0	1 : 10.8	0 : 1	$^{4.0}/_{5}$	$^{3}/_{5}$
$E_2 \to Y_4$	13344.0	1 : 8.3	0 : 1	$^{4.0}/_{5}$	$^{3}/_{5}$
$E_2 \to Y_6$	13330.0	18.5 : 1	1 : 0	2.7	3.0
$E_1 \to Y_1$	13359.0	1 : 9.7	0 : 1	$^{3.5}/_{5}$	$^{3}/_{5}$
$E_1 \to Y_3$	13348.5	19.7 : 1	1 : 0	2.7	3.0
$E_1 \to Y_4$	13338.0	1 : 12.7	0 : 1	$^{3.5}/_{5}$	$^{3}/_{5}$
$E_1 \to Y_7$	13296.0	1 : 11.1	0 : 1	$^{4.0}/_{5}$	$^{3}/_{5}$
$E_1 \to Y_8$	13276.0	11.3 : 1	1 : 0	2.2	3.0
$E_1 \to Y_{10}$	13231.0	1 : 8.1	0 : 1	$^{4.0}/_{5}$	$^{3}/_{5}$
$D_3 \to Z_1$	15599.0	8.2 : 1	1 : 0	2.1	3.0
$D_3 \to Z_2$	15596.3	9.7 : 1	1 : 0	2.3	3.0
$D_3 \to Z_3$	15546.5	1 : 7.4	0 : 1	$^{3.5}/_{5}$	$^{3}/_{5}$
$D_3 \to Z_5$	15511.0	1 : 8.0	0 : 1	$^{2.5}/_{5}$	$^{3}/_{5}$

Cont....

Table 5.2 cont....

Transition	**Wavenumber (±0.5) cm^{-1}**	**Polarisation Ratios (±5%)**			
		<100> orientation [yy : yx]		**<111> orientation [y′y′/y′x′]**	
		Observed	**Expected**	**Observed**	**Expected**
$D_3 \rightarrow Z_8$	15334.0	8.8 : 1	1 : 0	2.0	3.0
$D_3 \rightarrow Z_{13}$	15156.0	1 : 6.5	0 : 1	$^{4.0}/_{5}$	$^{3}/_{5}$
$D_1 \rightarrow Z_1$	15593.0	1 : 8.0	0 : 1	$^{3.5}/_{5}$	$^{3}/_{5}$
$D_1 \rightarrow Z_2$	15590.3	1 : 8.5	0 : 1	$^{3.0}/_{5}$	$^{3}/_{5}$
$D_1 \rightarrow Z_3$	15539.5	9.2 : 1	1 : 0	2.4	3.0
$D_1 \rightarrow Z_4$	15518.0	1 : 7.5	0 : 1	$^{3.5}/_{5}$	$^{3}/_{5}$
$D_1 \rightarrow Z_5$	15504.5	6.8 : 1	1 : 0	2.0	3.0
$D_1 \rightarrow Z_7$	15337.5	1 : 7.0	0 : 1	$^{4.0}/_{5}$	$^{3}/_{5}$
$D_1 \rightarrow Z_8$	15327.5	1 : 6.9	0 : 1	$^{4.0}/_{5}$	$^{3}/_{5}$
$D_1 \rightarrow Z_9$	15213.0	1 : 6.8	0 : 1	$^{4.0}/_{5}$	$^{3}/_{5}$
$D_1 \rightarrow Z_{10}$	15200.0	7.2 : 1	1 : 0	2.3	3.0
$D_1 \rightarrow Z_{11}$	15189.0	1 : 6.6	0 : 1	$^{3.5}/_{5}$	$^{3}/_{5}$
$D_1 \rightarrow Z_{12}$	15163.0	1 : 6.0	0 : 1	$^{4.0}/_{5}$	$^{3}/_{5}$
$D_1 \rightarrow Z_{13}$	15150.0	6.2 : 1	1 : 0	2.0	3.0

respectively, were both σ polarised while the $D_3 \rightarrow Z_1$ and $D_3 \rightarrow Z_2$ transitions at 15599.0 and 15596.3 cm^{-1} respectively, were found to be π polarised. Given that the Z_1 and Z_2 levels are γ_1 and γ_2 type levels respectively, the D_1 level is of γ_5 symmetry while the D_3 level is of $\gamma_{a'}$ symmetry. As the $D_3 \rightarrow Z_1$ transition is weak compared to the $D_3 \rightarrow Z_2$ transition, the D_3 level is assigned to be of γ_2 symmetry. The $D_3 \rightarrow Z_1$ transition is then only allowed through the hyperfine mixing of the Ho^{3+} electronic wavefunctions of the Z_1 and Z_2 levels, hence its weak intensity. Transitions from the D_1 level to the γ_5 type Z levels are all π polarised while transitions to the Z_4, Z_9, Z_{11} and Z_{12} levels are all σ polarised. The broader feature centred at 15330.5 cm^{-1} was resolved in the polarisation spectra to three transitions at 15334.0, 15327.5 and 15337.5 cm^{-1}. The first two transitions correspond to the $D_3 \rightarrow Z_8$ and $D_1 \rightarrow Z_8$ transitions respectively, while the 15337.5 cm^{-1} line is the $D_1 \rightarrow Z_7$ transition. Of these, the $D_1 \rightarrow Z_7$ and $D_1 \rightarrow Z_8$ transitions were both σ polarised, consistent with being $\gamma_5 \rightarrow \gamma_{a'}$ type transitions, while the $D_3 \rightarrow Z_8$ transition was π polarised ($\gamma_a \rightarrow \gamma_a$ type transition) identifying the Z_8 level at 265.5 cm^{-1} as a γ_2 type level. The previously undetected Z_7 level at 255.5 cm^{-1} is therefore of γ_1 symmetry.

From the polarised excitation spectra, the $\gamma_{a'} \rightarrow \gamma_5$ transitions in both the E (Figure 5.6(c)) and D multiplets were found to be σ polarised with monitoring of the $E_2 \rightarrow Z_1$ transition at 18585.7 cm^{-1} or the $D_1 \rightarrow Z_3$ transition at 15539.5 cm^{-1} respectively. The $\gamma_{a'}$ transitions could then be assigned as either γ_1 or γ_2 in an analogous way to that done for the CaF_2 A centre. The transition at 18768.0 cm^{-1} was relatively weak at 2 K compared to 10 K, consistent with its being a $Z_2 \rightarrow E_8$ transition rather than a $Z_1 \rightarrow E_8$ transition. The E_8 level is therefore of γ_2 symmetry, with the strong $\gamma_2 \rightarrow \gamma_2$ and weak $\gamma_1 \rightarrow \gamma_2$ transitions. As the $Z_1 \rightarrow D_4$ transition is much stronger than the $Z_2 \rightarrow D_4$ transition in the 10 K excitation spectrum (Figure 5.3(b)), the D_4 level is assigned as a γ_1 type level.

All these polarisation results for both <100> (Figure 5.6) and <111> oriented crystals (Table 5.2) support an exact C_{4v} symmetry assignment for this

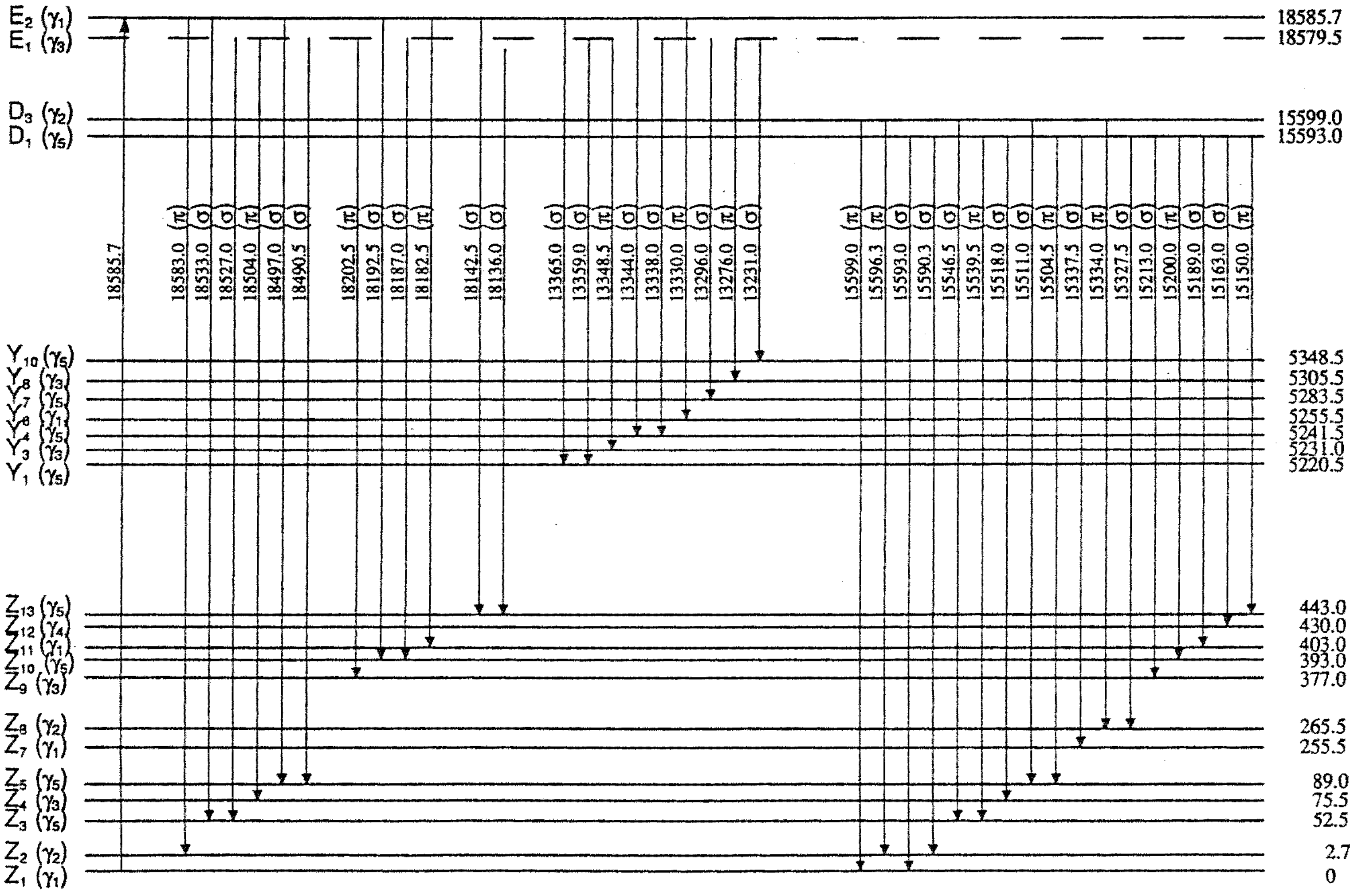

Figure 5.7: Energy level diagram for the A centre in $SrF_2:Ho^{3+}$(0.01%) crystals, for transitions as measured at 10 K.

centre. The centre has therefore been labelled the SrF_2 A centre in analogy to the CaF_2 A centre. An energy level diagram showing all the observed fluorescence transitions and their polarisation for the <100> orientation is presented in Figure 5.7. Energy levels for the Z, Y, D, E and F multiplets, as presented in Table 5.1, were used for the crystal-field calculations reported in Chapter 7.

5.1.3 Spectroscopy of the SrF_2 B centre

The B centre is so labelled because of the similarities of the fluorescence spectra of this centre with those of the earlier discussed CaF_2 B centre. Because the fluorescence was comparatively weak, being only 2% of the A centre fluorescence, the spectroscopic results presented in Figure 5.8 were measured in SrF_2 crystals with a Ho^{3+} concentration of 0.05% rather than the 0.01% used in the spectroscopic measurements for the other four centres. Well discriminated selective excitation spectra could not be obtained and higher energy levels for this centre could only be identified through comparison of fluorescence spectra. Transitions for this centre are so labelled in the broadband excitation spectra presented in Figures 5.2 and 5.3.

From the E → Z spectrum (Figure 5.8(a)), the $E_1 - E_2 - E_3$ energy level separations are apparent in transitions to the Z_2 and Z_3 levels. The separations were measured to be 2.4 and 1.6 cm^{-1} respectively, about 0.5 cm^{-1} larger than those found for the CaF_2 B centre. For excitation of the $Z_1 \rightarrow E_2$ transition at 18564.0 cm^{-1}, the fluorescence spectra obtained are closely similar to those for the CaF_2 B centre (Figure 4.9). The Z_2 level at 26.5 cm^{-1} is almost exactly the same energy as for the Z_2 level in CaF_2 but the Z_3 level at 52.5 cm^{-1} is lower than the corresponding level at 65.0 cm^{-1} in CaF_2. In general, all B centre energy levels are appreciably lower in SrF_2 (Table 5.3) than in CaF_2 (Table 4.3) crystals.

The E → Y spectrum (Figure 5.8(c)) has transitions occurring in groups of either three or two. There are seven groups of three transitions with the characteristic $E_1 - E_2 - E_3$ energy level separations of 2.5 and 1.5 cm^{-1}

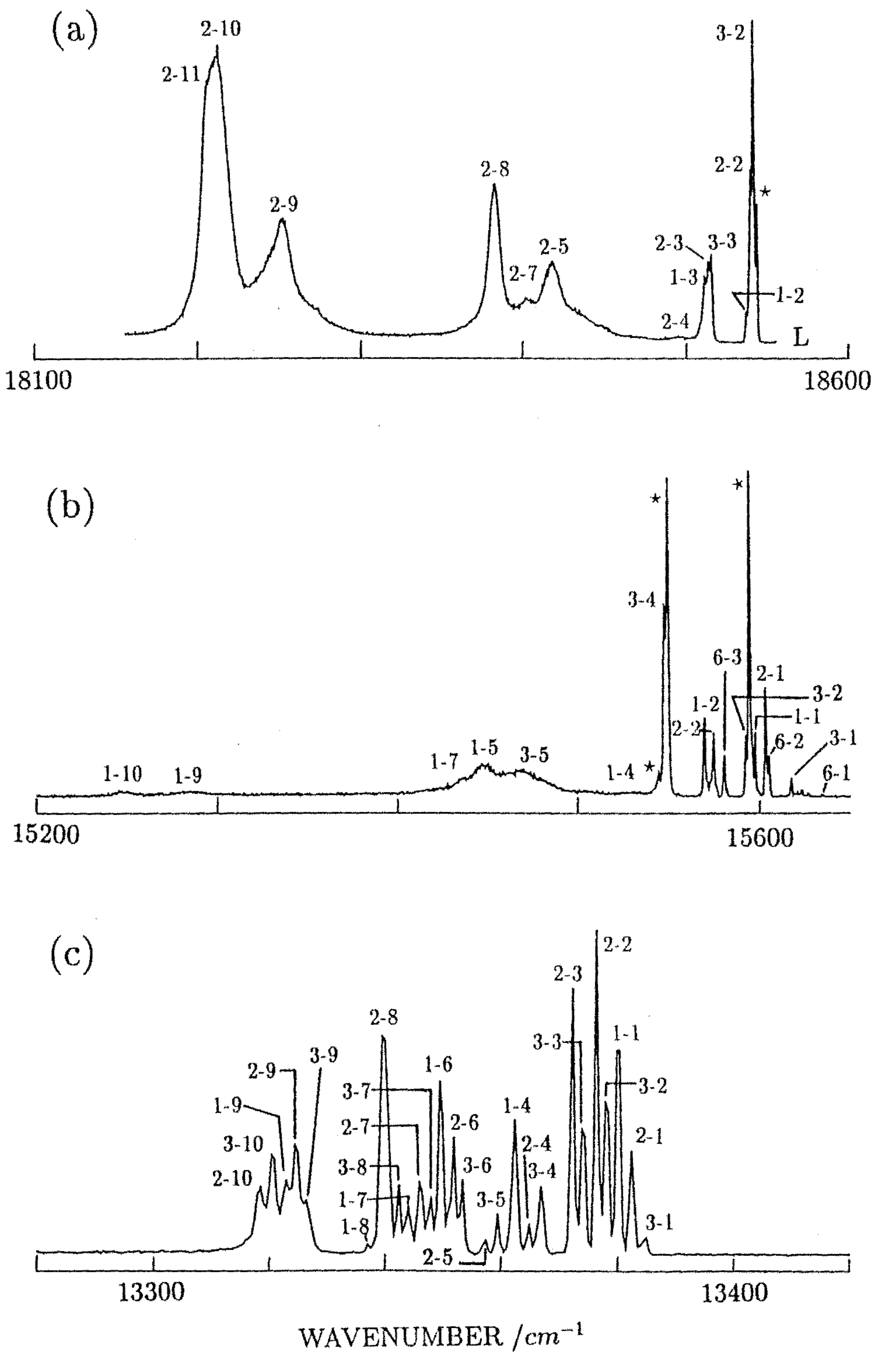

Figure 5.8: 10 K fluorescence spectra for the B centre in SrF_2:Ho^{3+}(0.05%) crystals :
(a) E→Z transitions, for excitation of the Z_1→E_2 transition at 18564.0 cm^{-1};
(b) D→Z transitions, for excitation of the Z_1→D_3 transition at 15615.5 cm^{-1};
(c) E→Y transitions, for excitation of the Z_1→E_2 transition at 18564.0 cm^{-1}.

Transitions identified by * are for a different centre.

Table 5.3 : Energy levels (in cm^{-1}) of the Z, Y, D and E multiplets of the SrF_2 B centre and their symmetries, as derived from the 10 K to 55 K spectra of SrF_2:Ho^{3+}(0.05%) crystals. Uncertainty is ± 0.5 cm^{-1}.

Level	$Z(^5I_8)$	$Y(^5I_7)$	$D(^5F_5)$	$E(^5S_2,^5F_4)$
1	$0(\gamma_3)$	$5183.0(\gamma_3)$	$15595.5(\gamma_2)$	$18561.6(\gamma_1)$
2	$26.5(\gamma_3)$	$5189.0(\gamma_2)$	$15601.5(\gamma_3)$	$18564.0(\gamma_3)$
3	$52.5(\gamma_1)$	$5193.5(\gamma_3)$	$15615.5(\gamma_2)$	$18565.6(\gamma_3)$
4	$70.0(\gamma_2)$	$5200.5(\gamma_1)$	-	-
5	$148.0(\gamma_3)$	$5208.5(\gamma_1)$	-	$18666.7(\gamma_1)$
6	-	$5214.0(\gamma_2)$	$15630.5(\gamma_1)$	-
7	$163.0(\gamma_3)$	$5219.5(\gamma_3)$	-	-
8	$184.0(\gamma_1)$	$5226.0(\gamma_3)$		$18736.5(\gamma_3)$
9	$315.0(\gamma_3)$	$5241.0(\gamma_3)$		$18767.2(\gamma_1)$
10	$354.0(\gamma_3)$	$5247.0(\gamma_2)$		
11	$359.5(\gamma_1)$			

respectively, and three groups of two transitions with the E_2 - E_3 energy level separation of 1.5 cm^{-1}. Comparison with the closely similar CaF_2 B centre transitions requires that the E_1 level be of γ_1 symmetry and the E_2 and E_3 levels be γ_3 symmetry type levels. The E → Y transition pairs would then be to the γ_2 type levels of the Y multiplet.

Again the D → Z spectrum (Figure 5.8(b)) is closely similar to that found for the CaF_2 B centre both in energy level pattern and in the weakness of the low energy transitions. The four D multiplet levels D_1, D_2, D_3 and D_6 at 15595.5, 15601.5, 15615.5 and 15630.5 cm^{-1} respectively (Table 5.3) were identified by fluorescence transitions originating from them, but neither the $D_1 \rightarrow Z_3$ nor $D_3 \rightarrow Z_3$ transitions were observed here. The D_1 - D_2 energy level separation of 6.0 cm^{-1} is large compared to the 1.5 cm^{-1} observed for the CaF_2 case.

5.1.4 Polarisation study of the SrF_2 B centre

Polarisation measurements were made for some of the stronger D → Z transitions (Table 5.4), for $Z_1 \rightarrow D_3$ excitation. The $Z_1 \rightarrow D_3$ transition was the only one well separated from corresponding transitions of the other four centres, so additional Z → D excitation measurements could not be made for comparison. From the polarisation ratios in Table 2.4, the $D_1 \rightarrow Z_1$ and $D_1 \rightarrow Z_2$ transitions are of the form $\gamma_a \rightarrow \gamma_3$ while the $D_2 \rightarrow Z_1$ and $D_2 \rightarrow Z_2$ transitions are of the $\gamma_3 \rightarrow \gamma_3$ type. The Z_1 and Z_2 levels are therefore γ_3 type levels. Because the $D_3 \rightarrow Z_1$ and $D_3 \rightarrow Z_2$ transitions are also of $\gamma_a \rightarrow \gamma_3$ type while the $D_3 \rightarrow Z_4$ transition is of $\gamma_a \rightarrow \gamma_a$ type, the D_3 and Z_4 levels have the same irrep label (either γ_1 or γ_2) and the D_2 level is of γ_3 symmetry.

Since the $E_1 \rightarrow Z_3$ transition is observed, but the D_1, $D_3 \rightarrow Z_3$ transitions are not, the D_1 and D_3 levels are assigned as γ_2 type levels and the Z_3 level as a γ_1 level. The polarisation ratio observed for the $D_3 \rightarrow Z_4$ transition requires that the Z_4 level be of γ_2 symmetry as well. The D_6 level is assigned as a γ_1 level because the $D_6 \rightarrow Z_3$ transition is observed while the $D_6 \rightarrow Z_4$ transition is not.

Irrep label assignments for the remaining E, Y and Z levels are derived

Table 5.4: Observed and predicted intensity ratios for the polarised D → Z fluorescence transitions of the B centre in <111> oriented SrF_2:Ho^{3+}(0.05%) crystals, for excitation of the $Z_1 \rightarrow D_3$ transition at 15615.5 cm^{-1}.

Transition	Wavenumber (±0.5) (cm^{-1})	Polarisation ratios [y′y′/y′x′] (±10%)	
		Observed	Expected
$D_3 \rightarrow Z_1$	15615.5	(laser)	$^{15}/_{11}$
$D_3 \rightarrow Z_2$	15590.0	$^{14.0}/_{11}$	$^{15}/_{11}$
$D_3 \rightarrow Z_4$	15545.0	$^{3.2}/_{7}$	$^{3}/_{7}$
$D_2 \rightarrow Z_1$	15601.5	1.01	$^{3}/_{7}$ - $^{15}/_{11}$
$D_2 \rightarrow Z_2$	15573.5	1.05	$^{3}/_{7}$ - $^{15}/_{11}$
$D_1 \rightarrow Z_1$	15595.5	$^{14.3}/_{11}$	$^{15}/_{11}$
$D_1 \rightarrow Z_2$	15568.5	$^{14.0}/_{11}$	$^{15}/_{11}$

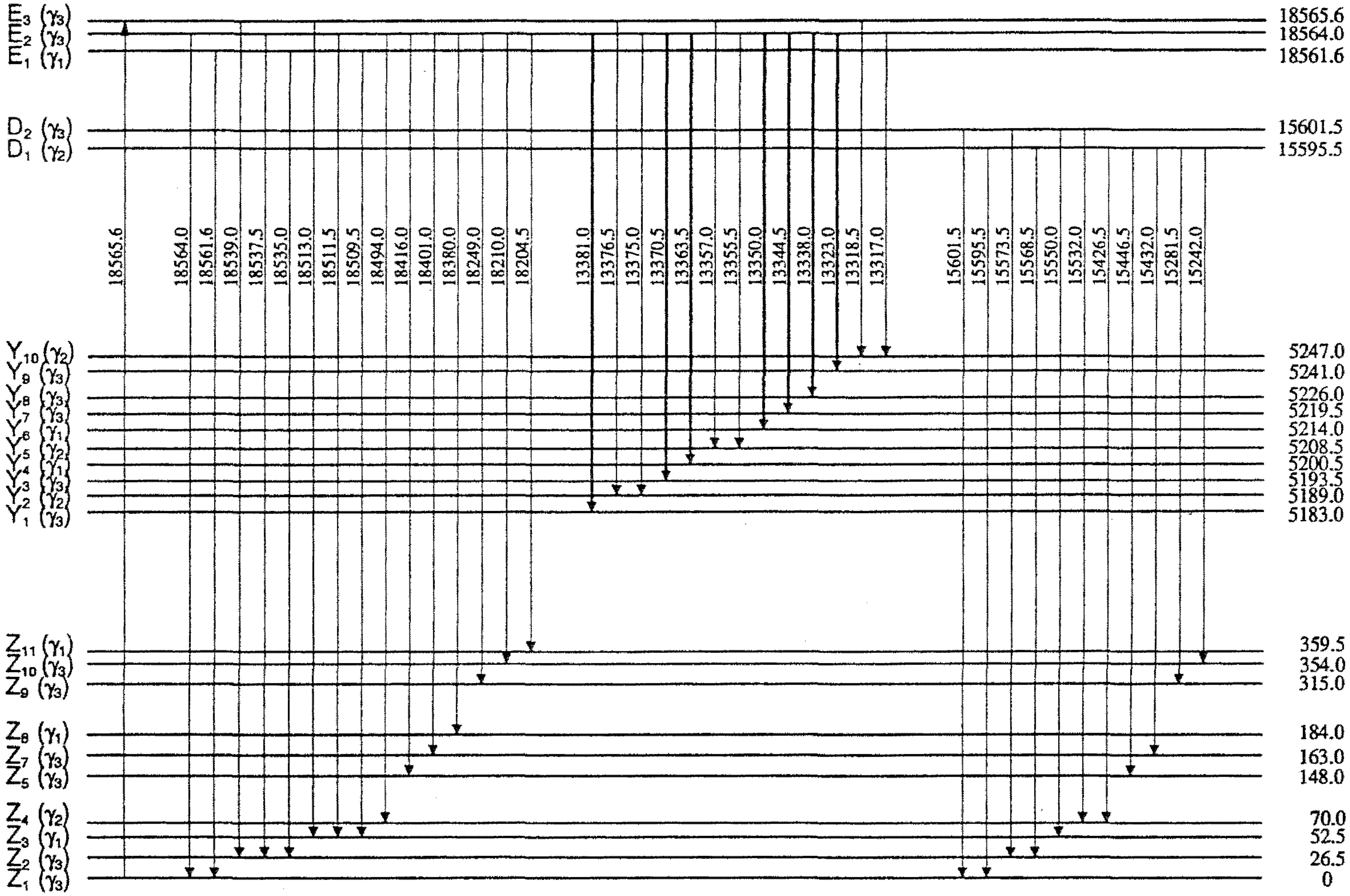

Figure 5.9: Energy level diagram for the B centre in $SrF_2:Ho^{3+}$(0.05%) crystals, for transitions as measured at 10 K. The bold lines represent a set of three transitions from the E_1, E_2 and E_3 levels of the particular Y multiplet level.

from the crystal-field analysis just as done for the CaF_2 B centre. The polarisation ratios obtained (Table 5.4) are consistent with an exact C_{3v} symmetry assignment for this centre.

The energy level scheme showing all the observed transitions is presented in Figure 5.9 and all the levels derived for the Z, Y, D and E multiplets are presented in Table 5.3.

5.2 The SC1, SC2 and SB1 Centres in $SrF_2:Ho^{3+}$(0.01%) Crystals

In addition to transitions of the A and B centres, transitions of three other minor centres were also observed in $SrF_2:Ho^{3+}$(0.01%) crystals. Intensities of transitions of these centres were found to vary with temperature with those of the SB1 centre being about 30% and those of the SC1 and SC2 centres only 5 - 10% of those of the A centre at 2 K. At 10 K all three centre transitions were about 40% of the A centre transition intensities. The model configurations of the SC1, SC2 and SB1 centres will be discussed in Section 5.5.

All three centres have some spectral similarity with the SrF_2 A centre. The $E_2 \rightarrow Z_1$ and $D_1 \rightarrow Z_3$ transitions of each centre were monitored in turn to obtain well discriminated $Z \rightarrow E$ and $Z \rightarrow D$ excitation spectra respectively, for each centre.

5.2.1 Spectroscopy of the SC1 centre

Transitions to the E_2 and E_3 levels of the SC1 centre (Figure 5.10(c)) show a common spacing of 2.5 cm^{-1} from the Z_1 - Z_2 energy level separation, about the same as the 2.7 cm^{-1} observed for the SrF_2 A centre.

As transition pairs observed in the $E \rightarrow Z$ fluorescence spectrum (Figure 5.12(a)) have a common separation of 4.5 cm^{-1}, the E_1 and E_2 levels are concluded to be separated by 4.5 cm^{-1} for this centre, a slightly smaller value compared to the 6.0 cm^{-1} determined for the A centre. Of the three single transitions observed at 18513.5, 18202.5 and 18178.5 cm^{-1}, only the two transitions at 18513.5 and 18202.5 cm^{-1} were still present in the 2 K spectrum and are

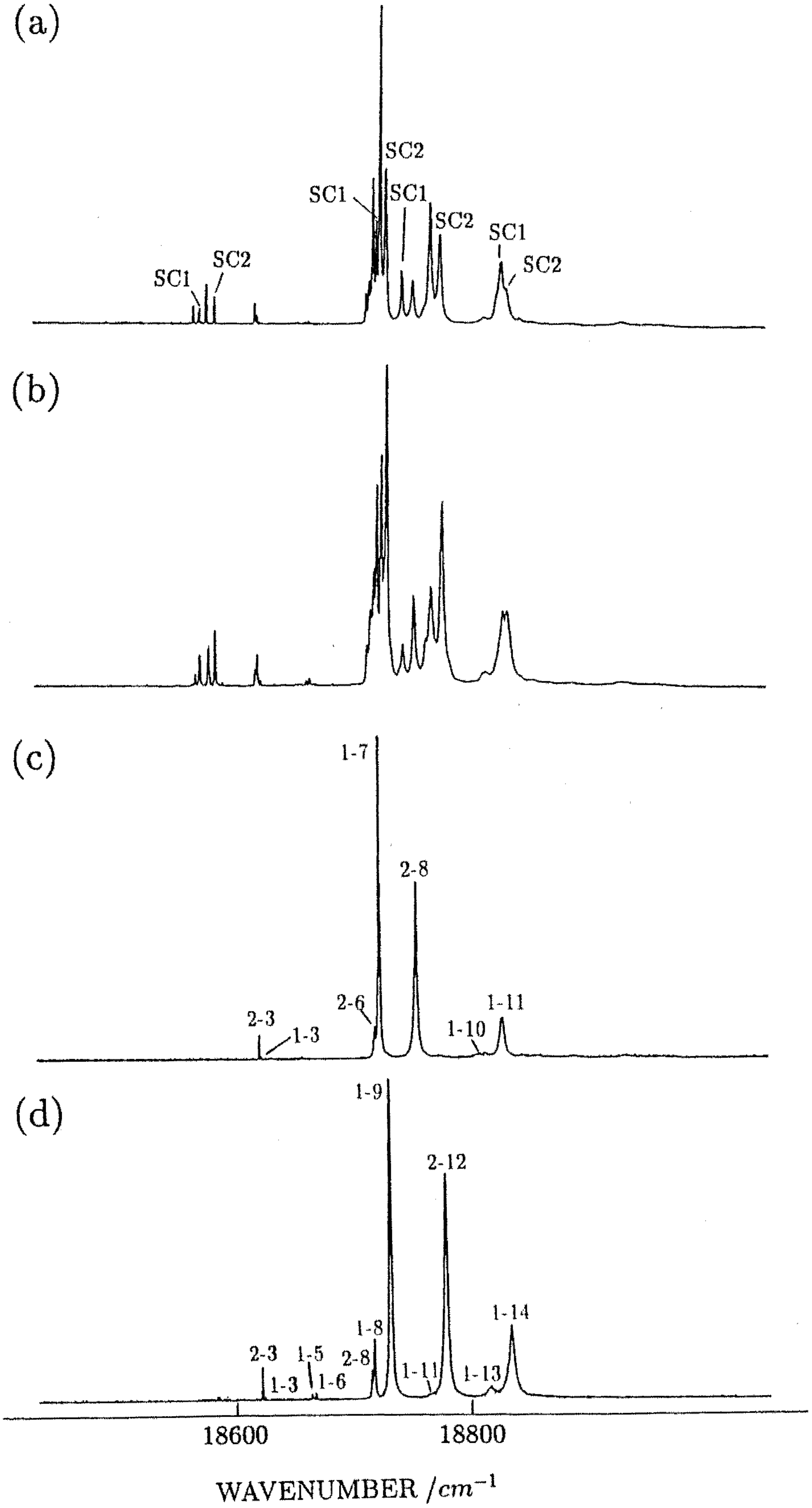

Figure 5.10: 10 K broadband and selective excitation spectra for the E multiplets of the SC1 and SC2 centres in $SrF_2:Ho^{3+}$(0.01%) and $Sr_{0.99}Ca_{0.01}:Ho^{3+}$(0.01%) crystals :
(a) broadband excitation spectrum in $SrF_2:Ho^{3+}$(0.01%), monitoring all the D → Z transitions;
(b) broadband excitation spectrum in $Sr_{0.99}Ca_{0.01}F_2:Ho^{3+}$(0.01%), monitoring all the D → Z transitions;
(c) SC1 centre excitation spectrum, monitoring the $E_2 \rightarrow Z_1$ transition at 18579.9 cm^{-1};
(d) SC2 centre excitation spectrum, monitoring the $E_2 \rightarrow Z_1$ transition at 18590.1 cm^{-1}

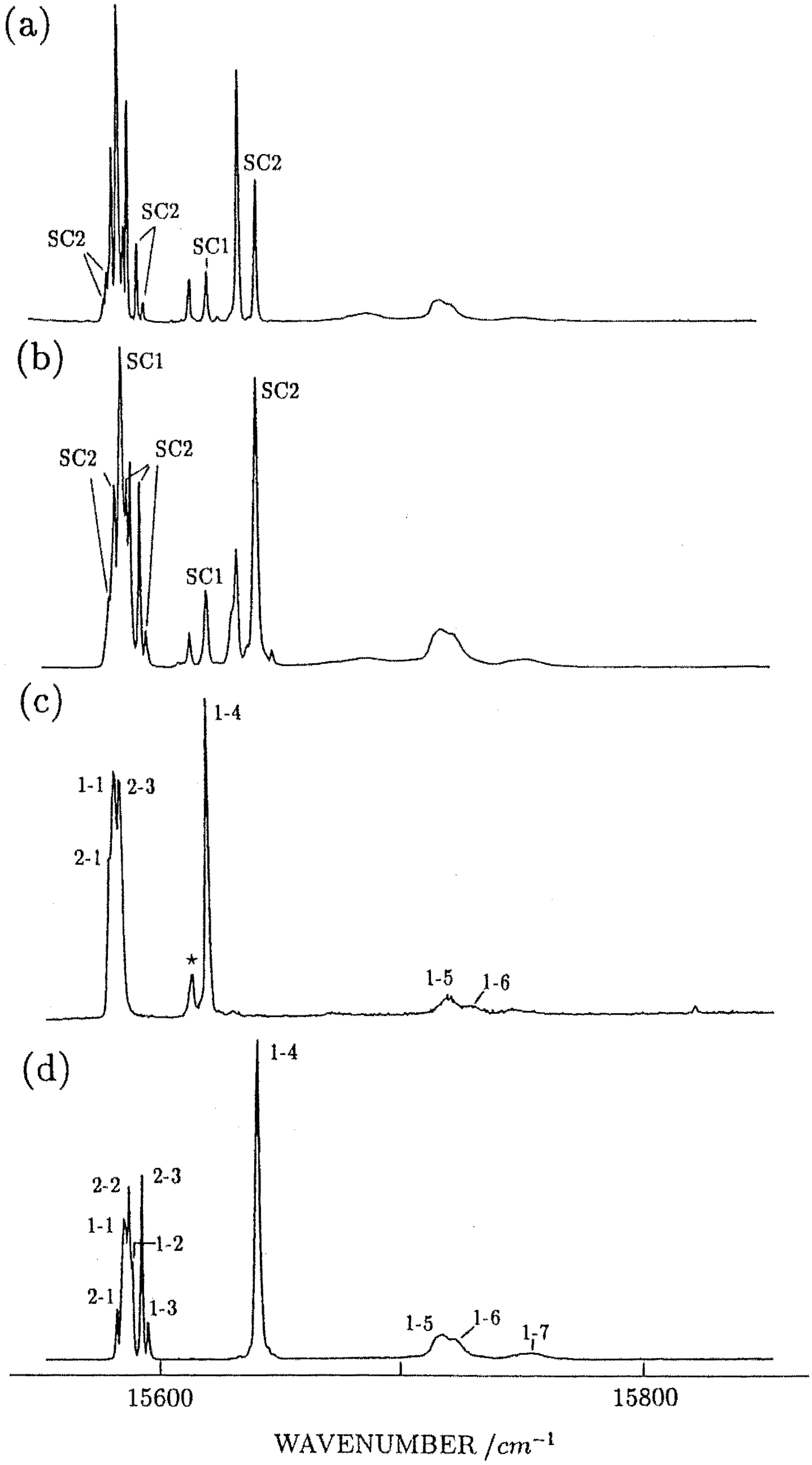

Figure 5.11: 10 K broadband and selective excitation spectra for the D multiplets of the SC1 and SC2 centres in SrF_2:Ho^{3+}(0.01%) and $Sr_{0.99}Ca_{0.01}F_2$:Ho^{3+}(0.01%) crystals :
(a) broadband excitation spectrum in SrF_2:Ho^{3+}(0.01%), monitoring all the D→Z transitions;
(b) broadband excitation spectrum in $Sr_{0.99}Ca_{0.01}F_2$:Ho^{3+}(0.01%), monitoring all the D→Z transitions;
(c) SC1 centre excitation spectrum, monitoring the $D_1 \rightarrow Z_3$ transition at 15548.5 cm^{-1};
(d) SC2 centre excitation spectrum, monitoring the $D_1 \rightarrow Z_4$ transition at 15534.5 cm^{-1}.

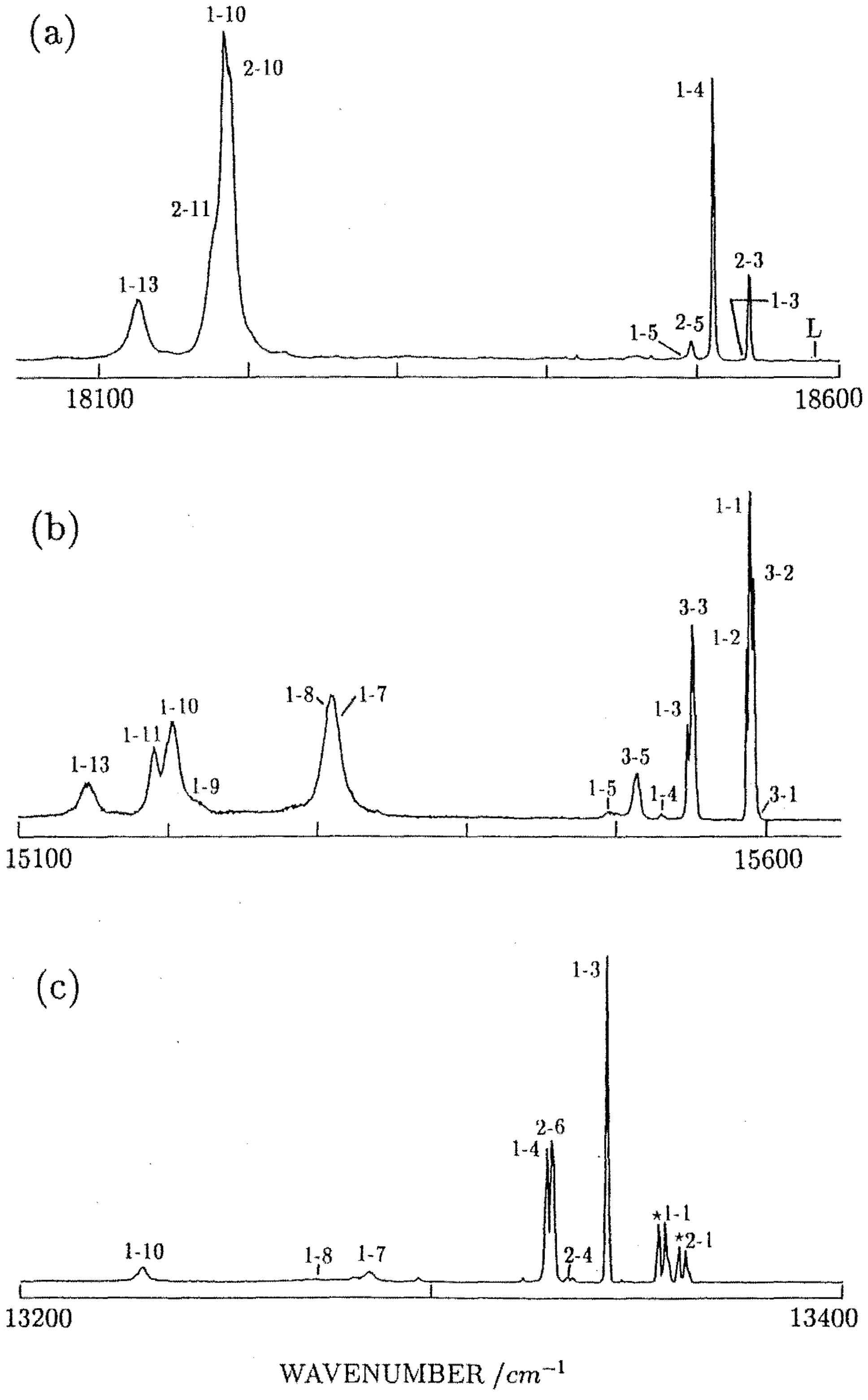

Figure 5.12: 10 K fluorescence spectra for the SC1 centre in SrF_2:Ho^{3+}(0.01%) crystals :
(a) E→Z transitions, for excitation of the Z_1→E_2 transition at 18579.9 cm^{-1};
(b) D→Z transitions, for excitation of the Z_1→D_4 transition at 15630.0 cm^{-1};
(c) E→Y transitions, for excitation of the Z_1→E_2 transition at 18579.9 cm^{-1}.
Transitions are labelled by the appropriate upper and lower multiplet crystal-field level identifications. The laser position is identified by "L". Transitions marked * in (c) are for the SB1 centre.

Table 5.5 : Energy levels (in cm^{-1}) of the Z, Y, D, E and F multiplets of the SC1 centre and their symmetries, as derived from the 2 K to 55 K spectra of $SrF_2:Ho^{3+}$(0.01%) crystals. Uncertainty is ± 0.5 cm^{-1}.

Level	Z($^5I_8$)	Y($^5I_7$)	D($^5F_5$)	E($^5S_2$,$^5F_4$)	F($^5F_3$)
1	0(γ_1)	5217.0(γ_5)	15590.0(γ_5)	18574.5(γ_3)	20736.0(γ_2)
2	2.5(γ_2)	-	-	18579.9(γ_1)	20750.0(γ_5)
3	41.5(γ_5)	5231.5(γ_3)	15594.5(γ_2)	18626.4(γ_5)	-
4	61.0(γ_3)	5246.0(γ_5)	15630.0(γ_1)	-	-
5	80.0(γ_5)	-	15735.4(γ_5)	18672.0(γ_3)	-
6	-	5249.5(γ_1)	15742.4(γ_2)	18725.5(γ_5)	
7	279.0(γ_1)	5289.0(γ_5)	-	18725.1(γ_1)	
8	282.0(γ_2)	5302.5(γ_3)	15767.7(γ_5)	18757.2(γ_2)	
9	372.0(γ_3)	-		-	
10	389.0(γ_5)	5345.0(γ_5)		18817.3(γ_5)	
11	401.0(γ_1)	-		18831.0(γ_1)	
12	430.0(γ_4)				
13	445.5(γ_5)				

assigned as originating from the E_1 level at 18574.5 cm^{-1}. The remaining transition at 18178.5 cm^{-1} was only present in the 10 K and higher temperature (to 55 K) spectra and therefore originates from the E_2 level at 18579.9 cm^{-1}.

The E → Y spectrum (Figure 5.12(c)) comprises two sets of transition pairs with the 4.5 cm^{-1} E_1 - E_2 energy level separation and five single transitions. Of the five single transitions only that at 13330.0 cm^{-1} was not observed in the 2 K spectrum and therefore must originate from the E_2 level.

From the D → Z spectrum (Figure 5.12(b)), transitions to the Z_1, Z_2 and Z_3 levels occur as pairs with a 4.5 cm^{-1} energy separation which is assigned as the D_1 - D_3 energy level separation. Transitions are observed from the D_1 level to almost all of the Z levels. Fewer transitions are observed from the D_3 level with the $D_3 \rightarrow Z_1$ transition having only about 5% of the intensity of the $D_3 \rightarrow Z_2$ transition.

Energy levels derived for the SC1 centre are presented in Table 5.5.

5.2.2 Spectroscopy of the SB1 centre

The SB1 centre (Figures 5.13, 5.14 and 5.15) has the following specific features in common with the SC1 centre just discussed :

(i) an Z_1 - Z_2 energy level splitting of 2.5 cm^{-1} is apparent on transitions to both the E_2 and E_3 levels;

(ii) four sets of transition pairs occur in the E → Z spectrum (Figure 5.15(a)) and two sets in the E → Y spectrum (Figure 5.15(c)). The E_1 - E_2 energy level separation deduced from the common separation is 5.0 cm^{-1} which is almost the same as for the SC1 centre;

(iii) three single transitions occur in the E → Z spectrum and five in the E → Y spectrum. Of these, the transitions at 18181.5 and 13328.5 cm^{-1} are assigned as originating from the E_2 level;

(iv) the D_1 - D_3 energy level separation is 5.0 cm^{-1}. Transitions from the D_1 level are observed to most of the Z levels and a few are

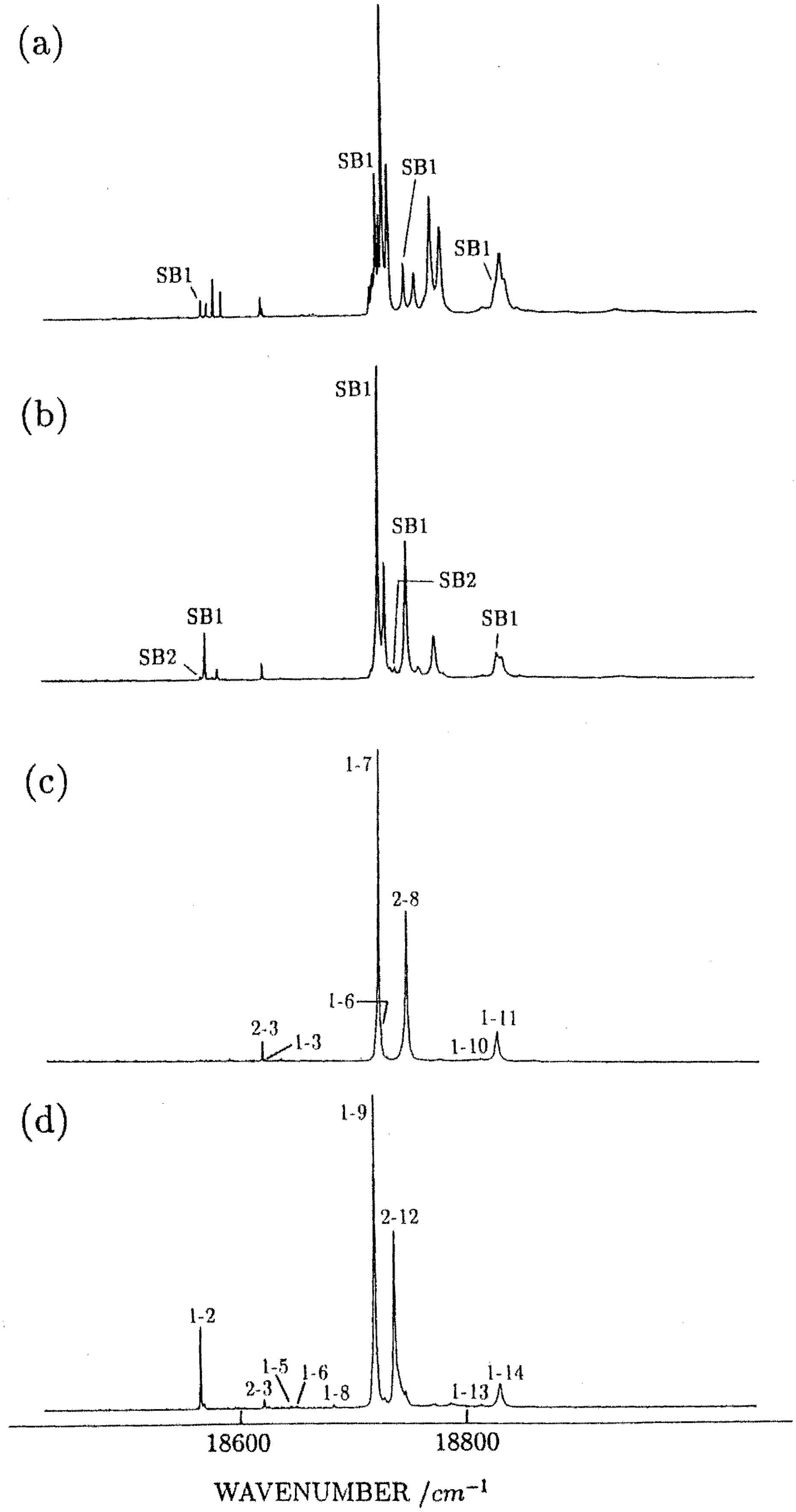

Figure 5.13: 10 K broadband and selective excitation spectra for the E multiplets of the SB1 and SB2 centres in $SrF_2:Ho^{3+}(0.01\%)$ and $Sr_{0.99}Ba_{0.01}F_2:Ho^{3+}(0.01\%)$ crystals :
(a) broadband excitation spectrum in $SrF_2:Ho^{3+}(0.01\%)$, monitoring all the D→Z transitions;
(b) broadband excitation spectrum in $Sr_{0.99}Ba_{0.01}F_2:Ho^{3+}(0.01\%)$, monitoring all the D→Z transitions;
(c) SB1 centre excitation spectrum, monitoring the $E_2 \rightarrow Z_1$ transition at 18575.8 cm^{-1};
(d) SB2 centre excitation spectrum, monitoring the transition at 18525.4 cm^{-1}.

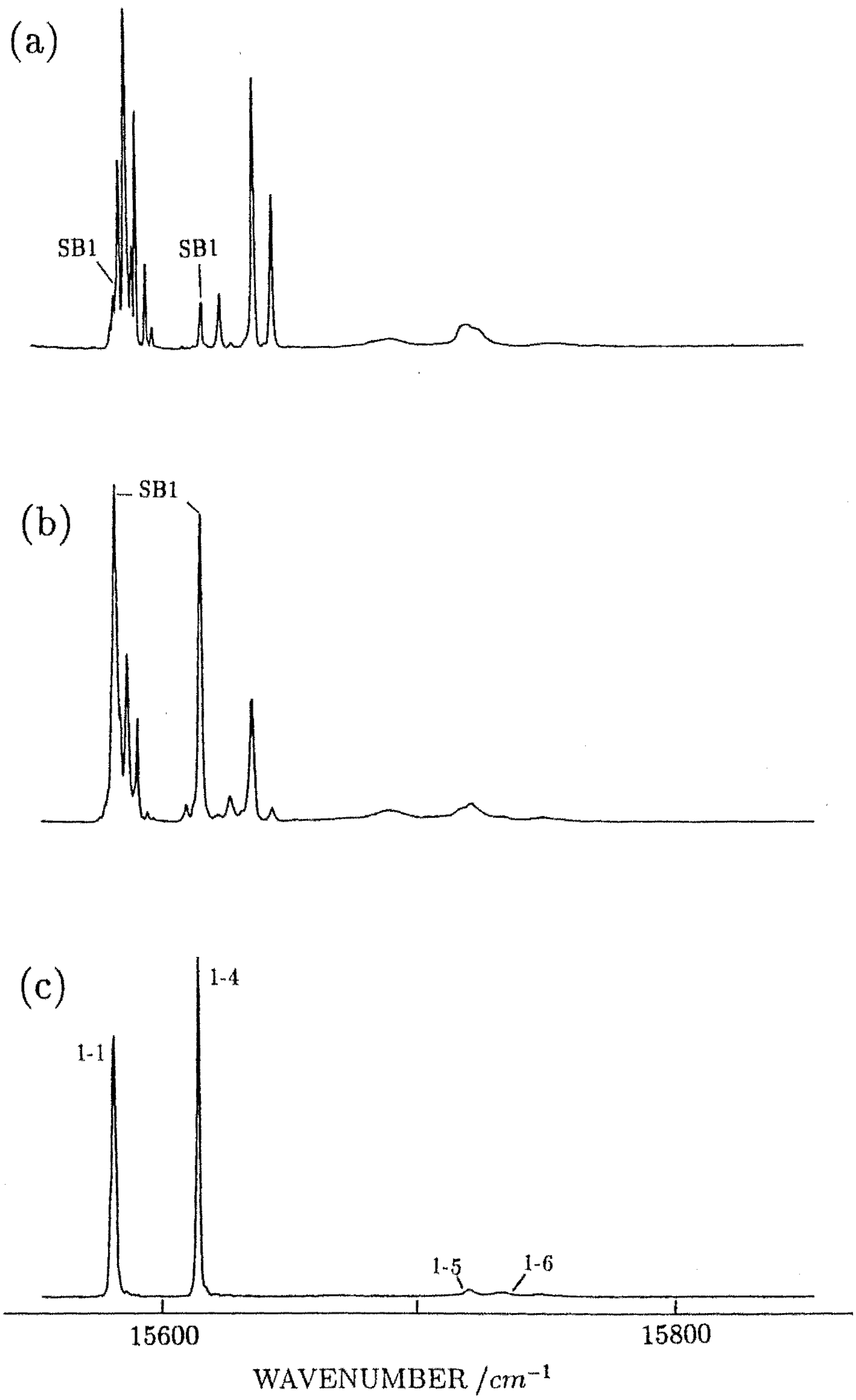

Figure 5.14: 10 K broadband and selective excitation spectra for the D multiplet of the SB1 centre in $SrF_2:Ho^{3+}(0.01\%)$ and $Sr_{0.99}Ba_{0.01}F_2:Ho^{3+}(0.01\%)$ crystals :
(a) broadband excitation spectrum in $SrF_2:Ho^{3+}(0.01\%)$, monitoring all the $D \rightarrow Z$ transitions;
(b) broadband excitation spectrum in $Sr_{0.99}Ba_{0.01}F_2:Ho^{3+}(0.01\%)$, monitoring all the $D \rightarrow Z$ transitions;
(c) SB1 centre excitation spectrum, monitoring the $D_1 \rightarrow Z_3$ transition at 15552.0 cm^{-1}.

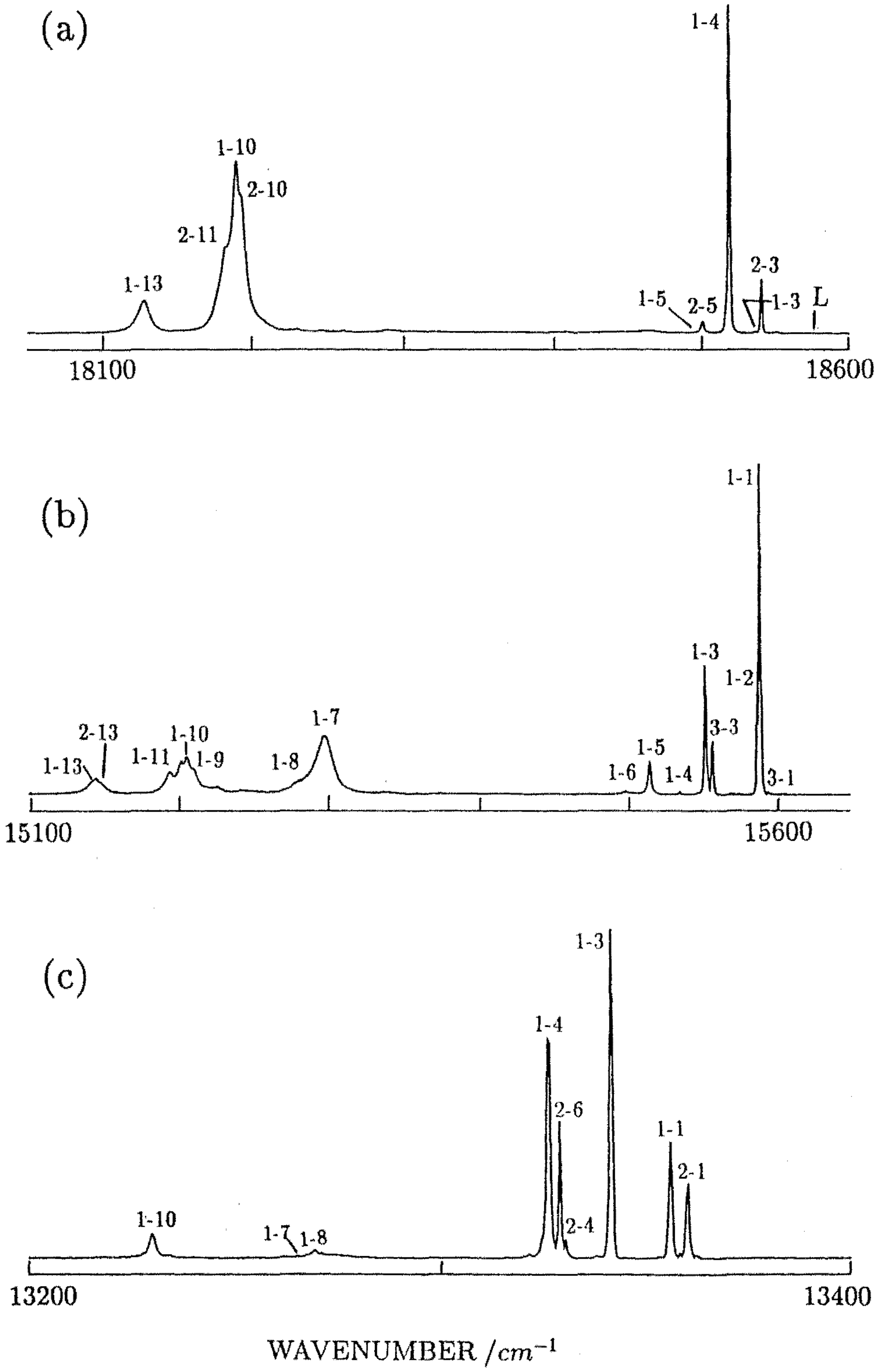

Figure 5.15: 10 K fluorescence spectra for the SB1 centre in SrF_2:Ho^{3+}(0.01%) crystals :
(a) E→Z transitions, for excitation of the Z_1→E_2 transition at 18575.8 cm^{-1};
(b) D→Z transitions, for excitation of the Z_1→D_4 transition at 15624·0 cm^{-1};
(c) E→Y transitions, for excitation of the Z_1→E_2 transition at 18575.8 cm^{-1}.
Transitions are labelled by the appropriate upper and lower multiplet crystal-field level identifications. The laser position is identified by "L".

Table 5.6 : Energy levels (in cm^{-1}) of the Z, Y, D, E and F multiplets of the SB1 centre and their symmetries, as derived from the 2 K to 55 K spectra of SrF$_2$:Ho^{3+}(0.01%) crystals. Uncertainty is ± 0.5 cm^{-1}.

Level	**Z(^{5}I$_8$)**	**Y(^{5}I$_7$)**	**D(^{5}F$_5$)**	**E(^{5}S$_2$,^{5}F$_4$)**	**F(^{5}F$_3$)**
1	0(γ_1)	5215.5(γ_5)	15588.0(γ_5)	18571.0(γ_3)	20737.0(γ_2)
2	2.5(γ_2)	-	-	18575.8(γ_1)	20746.0(γ_5)
3	37.0(γ_5)	5230.5(γ_3)	15593.0(γ_2)	18625.2(γ_5)	-
4	54.0(γ_3)	5245.5(γ_5)	15624.0(γ_1)	-	-
5	76.0(γ_5)	-	15733.6(γ_5)	18671.0(γ_3)	-
6	91.0(γ_4)	5247.0(γ_1)	15750.5(γ_2)	18723.8(γ_5)	
7	291.0(γ_1)	5305.0(γ_5)	-	18722.1(γ_1)	
8	305.0(γ_2)	5301.5(γ_3)	15770.9(γ_5)	18747.8(γ_2)	
9	378.0(γ_3)	-		-	
10	383.5(γ_5)	5341.5(γ_5)		18815.0(γ_5)	
11	394.0(γ_1)	-		18829.1(γ_1)	
12	430.0(γ_4)				
13	445.5(γ_5)				

observed from the D_3 level (Figure 5.15(b)). The $D_3 \rightarrow Z_1$ transition is much weaker than the $D_3 \rightarrow Z_2$ transition.

Energy levels for the SB1 centre (Table 5.6) are generally lower in energy than those for the SC1 centre (Table 5.5) which are, in turn, lower in energy than those of the SrF_2 A centre (Table 5.1).

5.2.3 Polarisation studies of the SC1 and SB1 centres

Polarisation results obtained for $Z_1 \rightarrow E_2$ excitation for each centre are summarised in Tables 5.7 and 5.8. Results for the <100> orientation (Figures 5.16 and 5.17 respectively) are summarised as follows :-

(i) transition pairs in both E → Z and E → Y spectra were polarised with a ratio of 0:1. These identify the Z_3, Z_5, Z_{10}, Z_{13}, Y_1 and Y_4 levels as γ_5 type levels;

(ii) single transitions in the E → Z spectrum were polarised 1:0 and the Z_4, Z_9 and Z_{11} levels derived from these transitions are assigned the same irrep labels as the corresponding energy levels for the SrF_2 A centre;

(iii) Of the five single transitions in the E → Y spectra, two are polarised with a ratio of 0:1 and are therefore to γ_5 type levels. The three remaining transitions are of $\gamma_a \rightarrow \gamma_a$ type giving the Y_6 level as of γ_1 symmetry and the Y_3 and Y_8 levels as of γ_3 symmetry;

(iv) as the transitions from the D_1 level to the Z_3, Z_5, Z_{10} and Z_{13} levels were π polarised, the D_1 level is certainly a γ_5 type level as for the A centre. Transitions from the D_3 level yield a $\gamma_{a'}$ irrep for this level with γ_2 being chosen on the basis of the relative intensities of transitions to the Z_1 and Z_2 levels;

(v) all excitation transitions (Figures 5.16(c) and 5.17(c)) were well polarised and irrep labels could be assigned along similar lines to that done for the SrF_2 A centre. For both the SC1 and SB1 centres, the γ_5 type level of the E_6 and E_7 energy level pair was

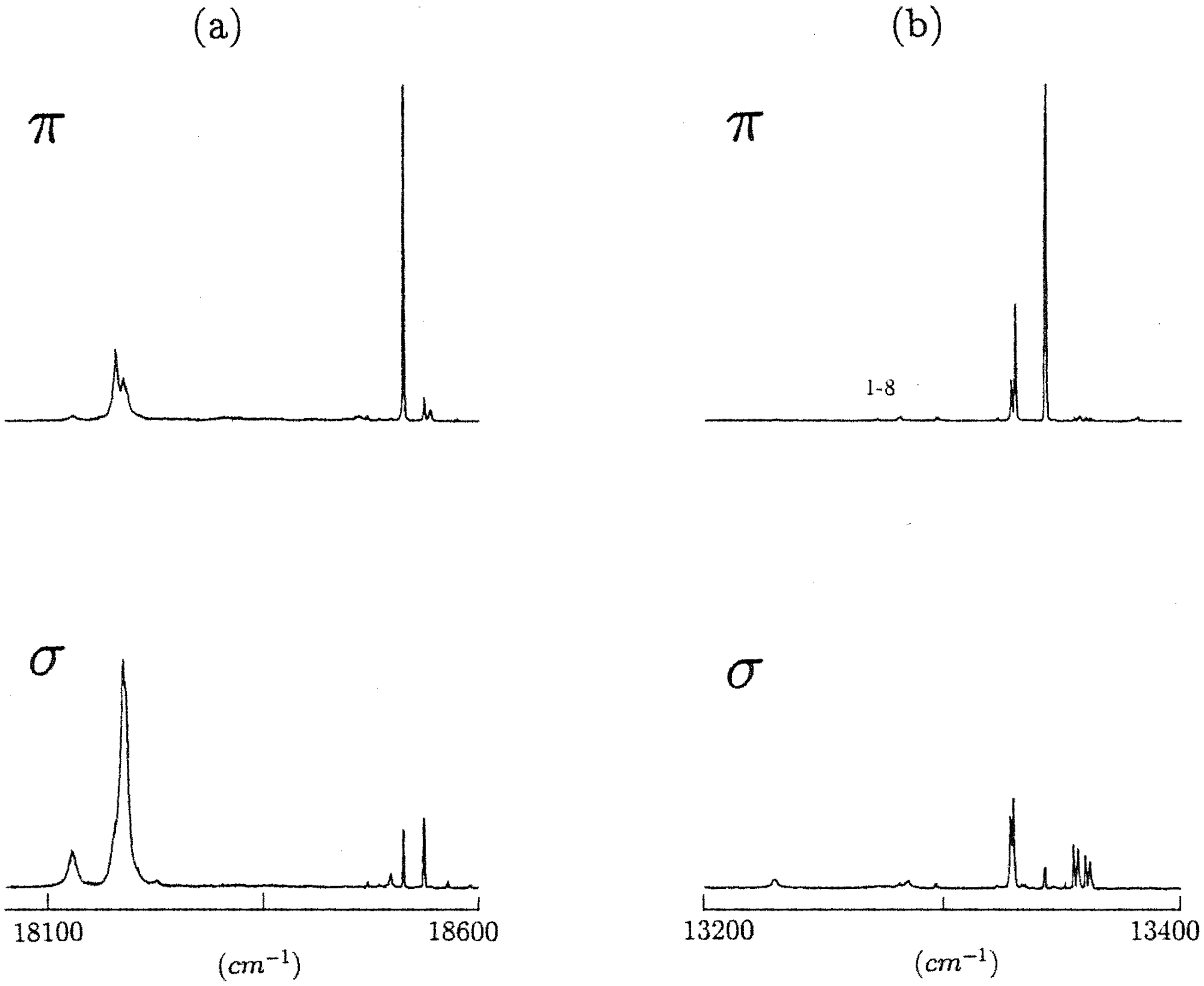
(a)
(b)
π
π
1-8
σ
σ
18100
18600
(cm⁻¹)
13200
13400
(cm⁻¹)

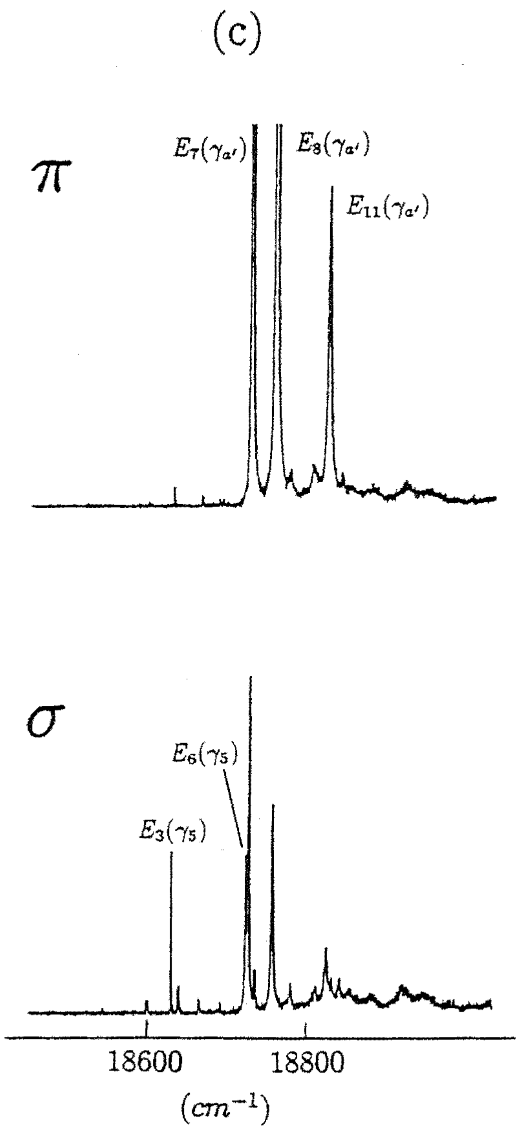

Figure 5.16: Polarisation of the 10 K selective excitation and fluorescence spectra of the SC1 centre in $SrF_2:Ho^{3+}(0.01\%)$ crystals :
(a) E→Z transitions, for excitation of the $Z_1 \rightarrow E_2$ transition at 18579.9 cm^{-1} ;
(b) E→Y transitions, for excitation of the $Z_1 \rightarrow E_2$ transition at 18579.9 cm^{-1} ;
(c) Z→E transitions, monitoring the $E_2 \rightarrow Z_1$ transition at 18579.9 cm^{-1}.
Transition labels are as in Figures 5.10(c) and 5.12.

Table 5.7: Observed and predicted intensity ratios for the polarised fluorescence transitions of the SC1 centre in <100> and <111> oriented $SrF_2:Ho^{3+}$(0.001%) crystals, for excitation of the $Z_1 \rightarrow E_2$ transition at 18579.7 cm^{-1}.

Transition	**Wavenumber ($\pm$0.5) cm^{-1}**	**Polarisation Ratios ($\pm$5%)**			
		<100> orientation [yy : yx]		**<111> orientation [y′y′/y′x′]**	
		Observed	**Expected**	**Observed**	**Expected**
$E_2 \rightarrow Z_3$	18538.0	1 : 6.2	0 : 1	$^{3.5}/_5$	$^3/_5$
$E_2 \rightarrow Z_5$	18499.5	1 : 6.9	0 : 1	$^{4.0}/_5$	$^3/_5$
$E_2 \rightarrow Z_{10}$	18190.5	1 : 13.5	0 : 1	$^{4.0}/_5$	$^3/_5$
$E_2 \rightarrow Z_{11}$	18178.5	15.0 : 1	1 : 0	2.3	3.0
$E_1 \rightarrow Z_3$	18533.0	1 : 5.2	0 : 1	$^{4.0}/_5$	$^3/_5$
$E_1 \rightarrow Z_4$	18513.5	7.3 : 1	1 : 0	2.6	$^3/_5$
$E_1 \rightarrow Z_5$	18494.5	1 : 5.0	0 : 1	$^{3.0}/_5$	$^3/_5$
$E_1 \rightarrow Z_9$	18202.5	5.9 : 1	1 : 0	2.0	3.0
$E_1 \rightarrow Z_{10}$	18187.5	1 : 15.2	0 : 1	$^{4.0}/_5$	$^3/_5$
$E_1 \rightarrow Z_{13}$	18129.0	1 : 7.5	0 : 1	$^{4.0}/_5$	$^3/_5$
$E_2 \rightarrow Y_1$	13362.5	1 : 7.2	0 : 1	$^{3.0}/_5$	$^3/_5$
$E_2 \rightarrow Y_4$	13333.5	1 : 5.5	0 : 1	$^{4.0}/_5$	$^3/_5$
$E_2 \rightarrow Y_6$	13330.0	5.5 : 1	1 : 0	2.1	3.0
$E_1 \rightarrow Y_1$	13357.5	1 : 6.0	0 : 1	$^{3.0}/_5$	$^3/_5$
$E_1 \rightarrow Y_3$	13343.0	20.1 : 1	1 : 0	2.6	3.0
$E_1 \rightarrow Y_4$	13328.5	1 : 6.8	0 : 1	$^{4.0}/_5$	$^3/_5$
$E_1 \rightarrow Y_7$	13285.5	1 : 7.3	0 : 1	$^{4.0}/_5$	$^3/_5$
$E_1 \rightarrow Y_8$	13272.0	7.5 : 1	1 : 0	2.3	3.0
$E_1 \rightarrow Y_{10}$	13229.5	1 : 5.0	0 : 1	$^{4.0}/_5$	$^3/_5$
$D_3 \rightarrow Z_1$	15594.5	6.1 : 1	1 : 0	2.1	3.0
$D_3 \rightarrow Z_2$	15592.0	6.9 : 1	1 : 0	2.3	3.0
$D_3 \rightarrow Z_3$	15553.0	1 : 5.9	0 : 1	$^{3.5}/_5$	$^3/_5$
$D_3 \rightarrow Z_5$	15514.5	1 : 5.5	0 : 1	$^{4.0}/_5$	$^3/_5$
$D_1 \rightarrow Z_1$	15590.0	1 : 7.1	0 : 1	$^{3.5}/_5$	$^3/_5$
$D_1 \rightarrow Z_2$	15597.5	1 : 7.0	0 : 1	$^{3.5}/_5$	$^3/_5$
$D_1 \rightarrow Z_3$	15548.5	6.9 : 1	1 : 0	2.2	3.0

Cont...

Table 5.7 cont...

Transition	**Wavenumber (±0.5) cm^{-1}**	**Polarisation Ratios (±5%)** **<100> orientation** **[yy : yx]** **Observed**	**Expected**	**<111> orientation** **[y′y′/y′x′]** **Observed**	**Expected**
$D_1 \rightarrow Z_4$	15529.0	1 : 5.5	0 : 1	$^{4.0}/_{5}$	$^{3}/_{5}$
$D_1 \rightarrow Z_7$	15311.0	1 : 5.0	0 : 1	$^{3.5}/_{5}$	$^{3}/_{5}$
$D_1 \rightarrow Z_8$	15308.0	1 : 5.2	0 : 1	$^{4.0}/_{5}$	$^{3}/_{5}$
$D_1 \rightarrow Z_9$	15218.0	1 : 5.0	0 : 1	$^{4.0}/_{5}$	$^{3}/_{5}$
$D_1 \rightarrow Z_{10}$	15201.5	6.0 : 1	1 : 0	2.0	3.0
$D_1 \rightarrow Z_{11}$	15190.0	1 : 5.5	0 : 1	$^{4.0}/_{5}$	$^{3}/_{5}$
$D_1 \rightarrow Z_{13}$	15147.0	5.2 : 1	1 : 0	2.1	3.0

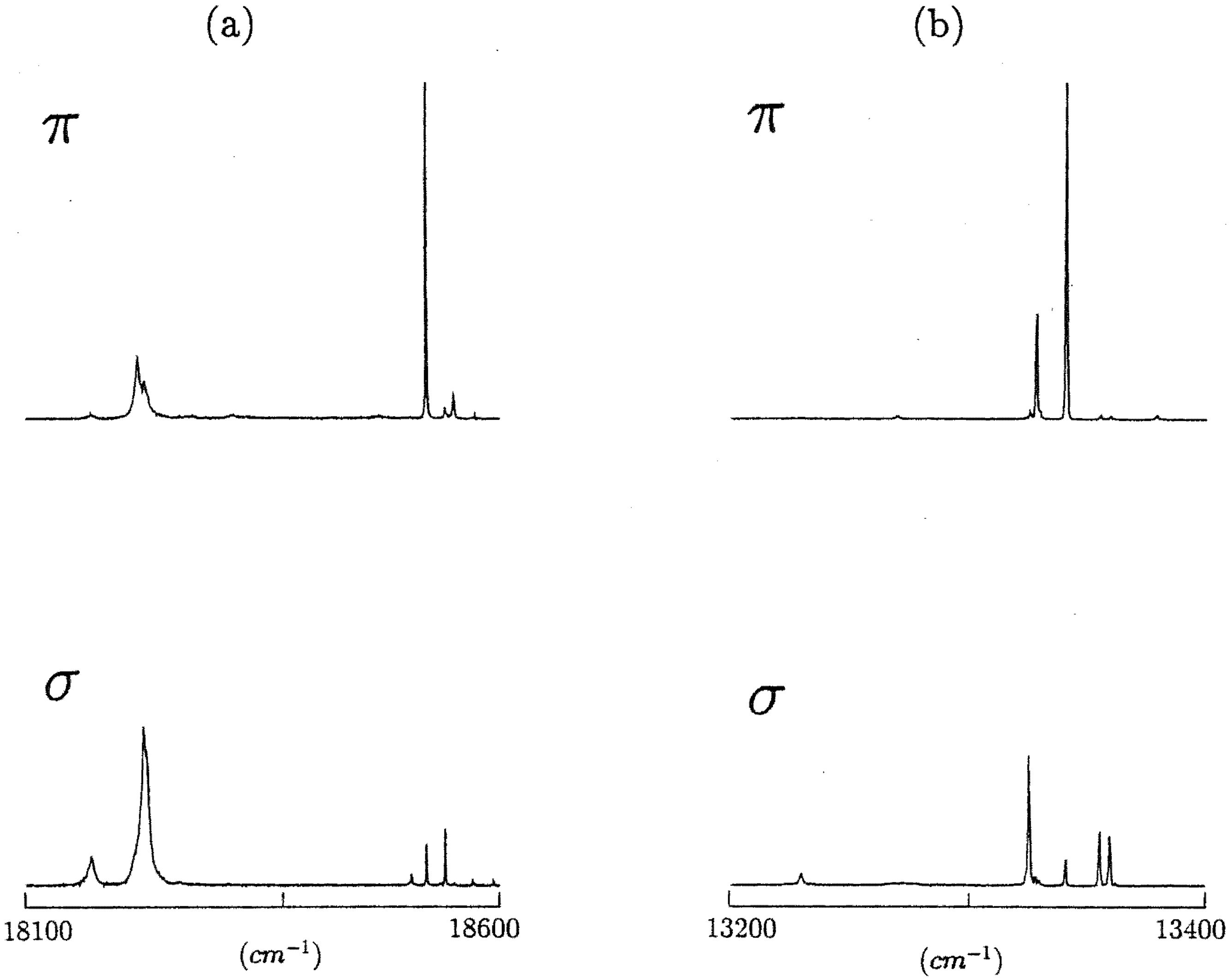
(a)
(b)
π
π
σ
σ
18100
18600
(cm^{-1})
13200
13400
(cm^{-1})

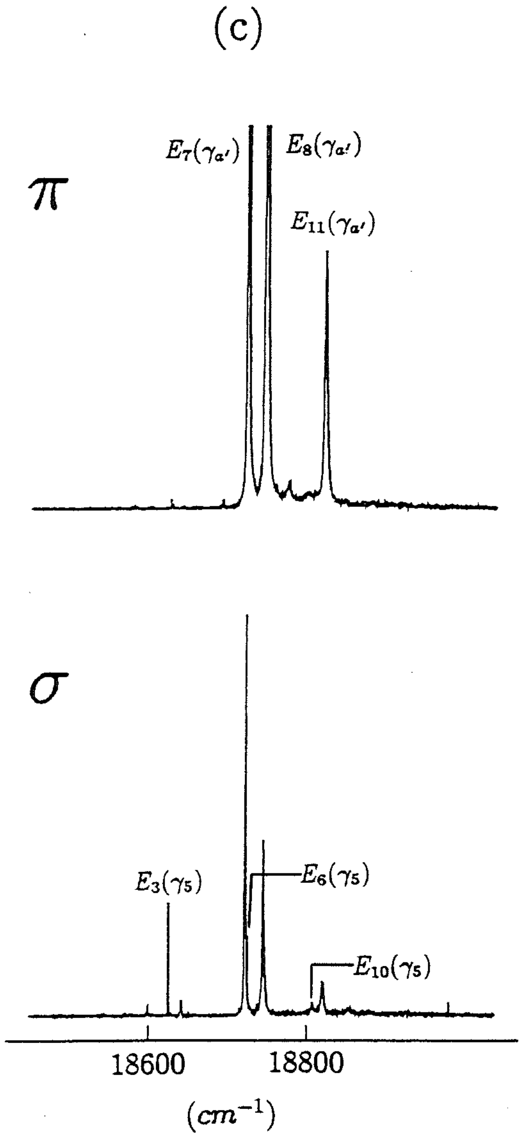

Figure 5.17 Polarisation of the 10 K selective excitation and fluorescence spectra of the SB1 centre in SrF_2:Ho^{3+}(0.01%) crystals :
(a) E→Z transitions, for excitation of the Z_1→E_2 transition at 18575.8 cm^{-1};
(b) E→Y transitions, for excitation of the Z_1→E_2 transition at 18575.8 cm^{-1};
(c) Z→E transitions, monitoring the E_2→Z_1 transition at 18575.8 cm^{-1}.
Transition labels are as in Figures 5.13(c) and 5.15.

Table 5.8: Observed and predicted intensity ratios for the polarised fluorescence transitions of the SB1 centre in <100> and <111> oriented $SrF_2:Ho^{3+}(0.005\%)$ crystals, for excitation of the $Z_1 \rightarrow E_2$ transition at 18575.8 cm^{-1}.

Transition	**Wavenumber (±0.5) cm^{-1}**	**Polarisation Ratios (±5%)** **<100> orientation [yy : yx]**		**<111> orientation [y′y′/y′x′]**	
		Observed	**Expected**	**Observed**	**Expected**
$E_2 \rightarrow Z_3$	18538.5	1 : 5.2	0 : 1	${}^{3.5}/_5$	${}^{3}/_5$
$E_2 \rightarrow Z_5$	18499.5	1 : 11.4	0 : 1	${}^{3.5}/_5$	${}^{3}/_5$
$E_2 \rightarrow Z_{10}$	18192.5	1 : 8.9	0 : 1	${}^{4.0}/_5$	${}^{3}/_5$
$E_2 \rightarrow Z_{11}$	18181.5	9.9 : 1	1 : 0	2.7	3.0
$E_1 \rightarrow Z_3$	18534.0	1 : 5.7	0 : 1	${}^{4.0}/_5$	${}^{3}/_5$
$E_1 \rightarrow Z_4$	18517.0	10.4 : 1	1 : 0	2.5	3.0
$E_1 \rightarrow Z_5$	18495.0	1 : 5.5	0 : 1	${}^{3.5}/_5$	${}^{3}/_5$
$E_1 \rightarrow Z_9$	18193.0	8.0 : 1	1 : 0	2.4	3.0
$E_1 \rightarrow Z_{10}$	18187.5	1 : 9.3	0 : 1	${}^{4.0}/_5$	${}^{3}/_5$
$E_1 \rightarrow Z_{13}$	18125.5	1 : 5.8	0 : 1	${}^{4.0}/_5$	${}^{3}/_5$
$E_2 \rightarrow Y_1$	13360.0	1 : 12.3	0 : 1	${}^{3.5}/_5$	${}^{3}/_5$
$E_2 \rightarrow Y_4$	13330.0	1 : 6.2	0 : 1	${}^{3.5}/_5$	${}^{3}/_5$
$E_2 \rightarrow Y_6$	13328.5	14.8 : 1	1 : 0	2.3	3.0
$E_1 \rightarrow Y_1$	13355.5	1 : 9.9	0 : 1	${}^{4.0}/_5$	${}^{3}/_5$
$E_1 \rightarrow Y_3$	13340.5	16.6 : 1	1 : 0	2.7	3.0
$E_1 \rightarrow Y_4$	13325.5	1 : 12.5	0 : 1	${}^{3.5}/_5$	${}^{3}/_5$
$E_1 \rightarrow Y_7$	13266.0	1 : 5.2	0 : 1	${}^{4.0}/_5$	${}^{3}/_5$
$E_1 \rightarrow Y_8$	13269.5	8.3 : 1	1 : 0	2.3	3.0
$E_1 \rightarrow Y_{10}$	13229.5	1 : 8.6	0 : 1	${}^{3.5}/_5$	${}^{3}/_5$
$D_3 \rightarrow Z_1$	15593.0	5.5 : 1	1 : 0	2.0	3.0
$D_3 \rightarrow Z_2$	15590.5	5.2 : 1	1 : 0	2.2	3.0
$D_3 \rightarrow Z_3$	15556.0	1 : 5.7	0 : 1	${}^{3.5}/_5$	${}^{3}/_5$
$D_1 \rightarrow Z_1$	15588.0	1 : 6.0	0 : 1	${}^{3.5}/_5$	${}^{3}/_5$
$D_1 \rightarrow Z_2$	15585.5	1 : 6.3	0 : 1	${}^{3.0}/_5$	${}^{3}/_5$
$D_1 \rightarrow Z_3$	15552.0	6.8 : 1	1 : 0	2.4	3.0
$D_1 \rightarrow Z_4$	15534.5	1 : 6.0	0 : 1	${}^{4.0}/_5$	${}^{3}/_5$
$D_1 \rightarrow Z_5$	15513.0	1 : 5.8	0 : 1	${}^{3.5}/_5$	${}^{3}/_5$
$D_1 \rightarrow Z_6$	15497.0	1 : 5.0	0 : 1	${}^{4.0}/_5$	${}^{3}/_5$
$D_1 \rightarrow Z_7$	15297.0	1 : 5.4	0 : 1	${}^{4.0}/_5$	${}^{3}/_5$

Cont...

Table 5.8 cont....

Transition	Wavenumber (±0.5) cm^{-1}	Polarisation Ratios (±5%)			
		<100> orientation [yy : yx]		<111> orientation [y′y′/y′x′]	
		Observed	Expected	Observed	Expected
$D_1 \rightarrow Z_8$	15283.0	1 : 5.2	0 : 1	$^{4.0}/_{5}$	$^{3}/_{5}$
$D_1 \rightarrow Z_9$	15210.5	1 : 4.9	0 : 1	$^{3.5}/_{5}$	$^{3}/_{5}$
$D_1 \rightarrow Z_{10}$	15205.5	6.9 : 1	1 : 0	2.2	3.0
$D_1 \rightarrow Z_{11}$	15195.0	1 : 5.0	0 : 1	$^{3.0}/_{5}$	$^{3}/_{5}$
$D_1 \rightarrow Z_{13}$	15144.0	5.9 : 1	1 : 0	2.1	3.0

higher in energy than the γ_1 level whereas the opposite is true for these same levels of the SrF_2 A centre.

Both the SC1 and SB1 centres show polarisation ratios characteristic of exact C_{4v} symmetry centres and have been assigned as such. The possible configuration for these centres is proposed to be analogous to that proposed for the CS1 and CB1 centres and will be discussed in Sections 5.5 and 5.6.

Energy level diagrams for both centres are quite similar to that for the SrF_2 A centre (Figure 5.7) except for changes in transition energies as listed in Tables 5.7 and 5.8 respectively. Energy levels obtained for the Z, Y, D, E and F multiplets are presented in Tables 5.5 and 5.6 for the SC1 and SB1 centres respectively.

5.2.4 Spectroscopy of the SC2 centre

Both the excitation and fluorescence spectra for this centre (Figures 5.10(d), 5.11(d) and 5.18) are significantly different from those for the SC1 and SB1 centres, with more transitions being observed for the SC2 centre. The main features of the spectra of this centre are :

(i) a $Z_1 - Z_2$ energy level splitting of 2.5 cm^{-1} was apparent on transitions to low energy levels of both the E and D multiplets (Figures 5.10(d) and 5.11(d)) respectively;

(ii) both the $E_1 \rightarrow Z_1$ and $E_1 \rightarrow Z_2$ transitions were observed for this centre (Figure 5.18(a)). The $E_1 - E_2$ energy level separation was measured to be 6.5 cm^{-1} which is similar to that for the SrF_2 A centre and slightly larger than that for both the SC1 and SB1 centres;

(iii) level pairs were observed in all cases for levels derived from the γ_5 type levels of the SC1 and SB1 centres. As observed for the CS2 and CB2 centres, these γ_5 type level splittings range in magnitude from as small as 2.5 cm^{-1} for the Y_1 level to 39.0 cm^{-1} for the Y_7

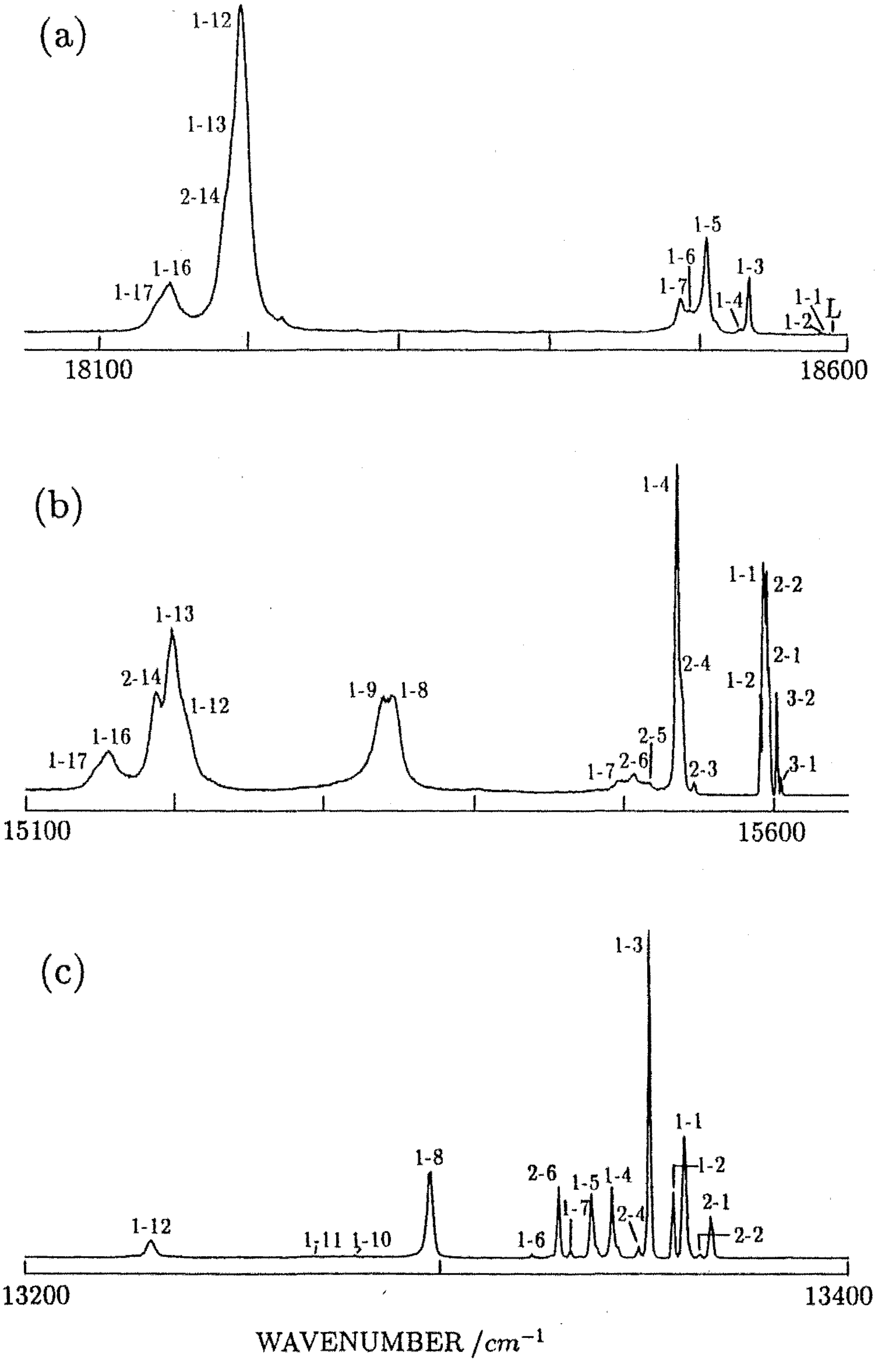

Figure 5.18: 10 K fluorescence spectra for the SC2 centre in SrF_2:Ho^{3+}(0.01%) crystals :
(a) E→Z transitions, for excitation of the Z_1→E_2 transition at 18590.1 cm^{-1};
(b) D→Z transitions, for excitation of the Z_1→D_4 transition at 15650.5 cm^{-1};
(c) E→Y transitions, for excitation of the Z_1→E_2 transition at 18590.1 cm^{-1}.

Table 5.9 : Energy levels (in cm^{-1}) of the Z, Y, D and E multiplets of the SC2 centre and their symmetries, as derived from the 2 K to 55 K spectra of $SrF_2:Ho^{3+}$(0.01%) crystals. Uncertainty is ± 0.5 cm^{-1}.

Level	$Z(^5I_8)$	$Y(^5I_7)$	$D(^5F_5)$	$E(^5S_2,^5F_4)$
1	$0(\gamma_1)$	$5223.5(\gamma_2)$	$15593.0(\gamma_1)$	$18583.5(\gamma_1)$
2	$2.5(\gamma_2)$	$5226.0(\gamma_1)$	$15597.0(\gamma_2)$	$18590.1(\gamma_1)$
3	$52.5(\gamma_2)$	$5232.0(\gamma_1)$	$15604.0(\gamma_1)$	$18627.6(\gamma_2)$
4	$58.0(\gamma_1)$	$5241.0(\gamma_1)$	$15650.5(\gamma_2)$	$18636.0(\gamma_1)$
5	$80.0(\gamma_1)$	$5246.0(\gamma_2)$	$15730.8(\gamma_1)$	$18666.7(\gamma_2)$
6	$89.5(\gamma_2)$	$5260.5(\gamma_1)$	$15738.5(\gamma_2)$	$18669.6(\gamma_1)$
7	$97.5(\gamma_1)$	$5251.0(\gamma_1)$	$15765.1(\gamma_2)$	-
8	$250.0(\gamma_1)$	$5285.0(\gamma_2)$		$18718.9(\gamma_2)$
9	$255.0(\gamma_2)$	-		$18734.0(\gamma_1)$
10	-	$5309.5(\gamma_1)$		-
11	-	$5314.0(\gamma_1)$		$18765.8(\gamma_2)$
12	$390.0(\gamma_1)$	$5353.0(\gamma_2)$		$18778.7(\gamma_2)$
13	$396.5(\gamma_2)$			$18818.9(\gamma_1)$
14	$409.0(\gamma_1)$			$18837.8(\gamma_1)$
15	-			
16	$439.0(\gamma_1)$			
17	$445.5(\gamma_2)$			

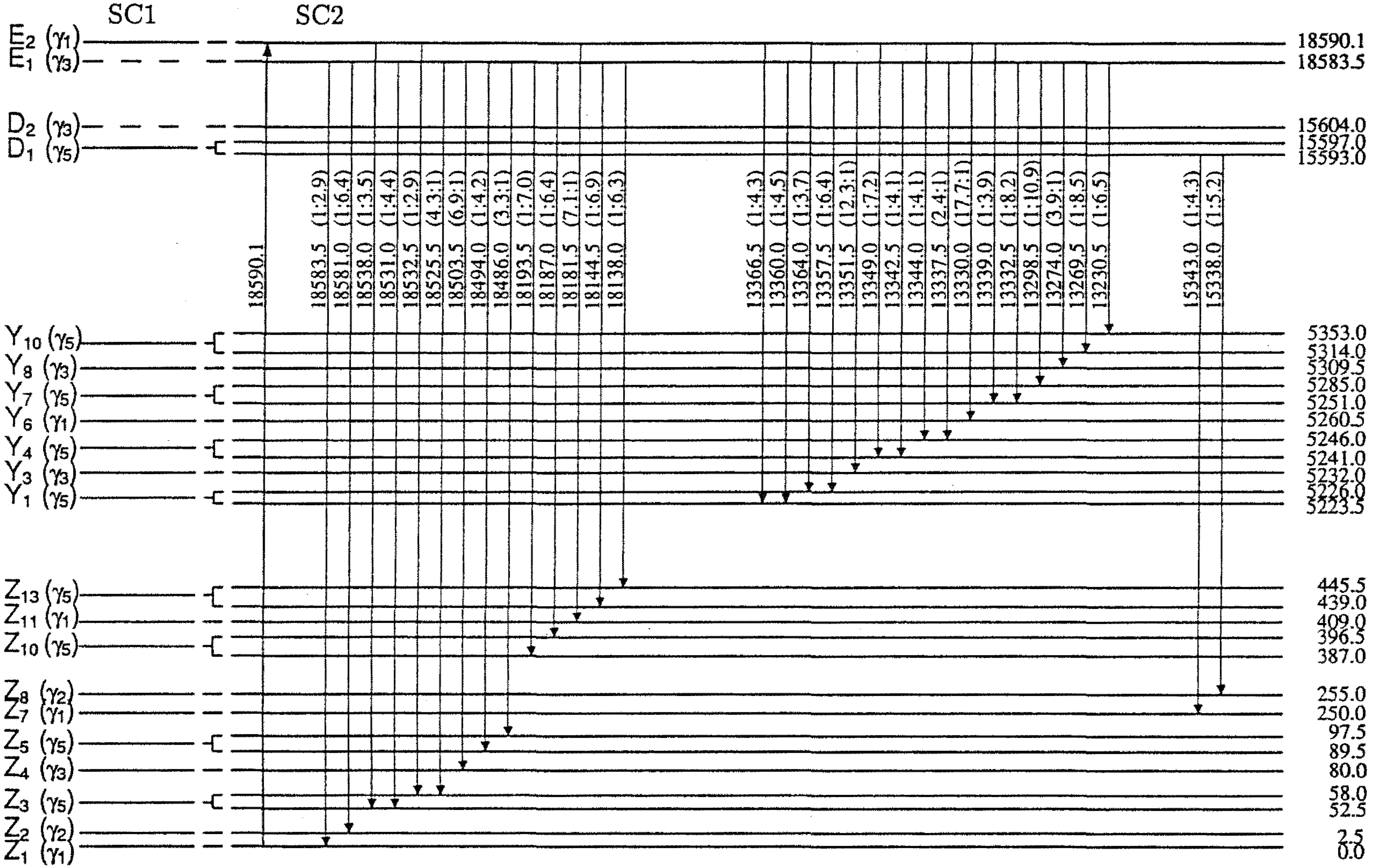

Figure 5.19: Energy level diagram for the SC2 centre in $SrF_2:Ho^{3+}$(0.01%) crystals, for the E → Z and E → Y transitions as measured at 10 K. For the particular Z levels not accessed by transitions from the E_1, E_2 levels, transitions from the D_1 level are shown. The energy levels on the left are those for the SC1 centre. Energy level irreps for the SC2 centre are presented in Table 5.9.

level (Figure 5.19). Splittings for the Z levels range from 5.5 cm^{-1} for the Z_3 level to 9.5 cm^{-1} for the Z_{10} level, while that for the D_1 level is just 4.0 cm^{-1};

(iv) two single transitions were observed at 18503.5 and 18181.5 cm^{-1} in the E → Z spectrum (Figure 5.18(a)) and three at 13351.5, 13330.0 and 13274.0 cm^{-1} in the E → Y spectrum (Figure 5.18(c));

(v) transitions corresponding to the $D_1 \rightarrow Z_7$ and $D_1 \rightarrow Z_8$ transitions in the SC1 and SB1 centres were well separated in the unpolarised spectra of the SC2 centre by 4.5 cm^{-1} (Figure 5.18(b));

(vi) all excitation transitions were found to be higher in energy than those of corresponding transitions of the SrF_2 A, SC1 and SB1 centres.

Observations (i) through to (v) are as found for the CS2 and CB2 centres in the $Ca_{0.99}Sr_{0.01}F_2$:Ho^{3+}(0.005%) and $Ca_{0.99}Ba_{0.01}F_2$:Ho^{3+}(0.005%) crystals respectively. For both the CS2 and CB2 centres though, their excitation transitions were lower in energy than for the CaF_2 A centre whereas, for the SC2 centre here, the excitation transitions are higher in energy than even those of the SrF_2 A centre.

Energy levels derived for the SC2 centre are presented in Table 5.9.

5.2.5 Polarisation study of the SC2 centre

Although transitions for this centre were not as well polarised as those for the other centres just discussed, the ratios obtained still show evidence of a parent C_{4v} symmetry centre. As for the CS2 and CB2 centres, polarisation ratios were measured for $Z_1 \rightarrow E_2$ ($\gamma_a \rightarrow \gamma_a$) excitation in both <100> and <111> oriented samples (Table 5.10) and for $Z_2 \rightarrow E_6$ ($\gamma_a \rightarrow \gamma_b$) excitation in the <100> orientation. Polarisation ratios measured in the <100> orientation (Figure 5.20) are summarised below.

(a) For $Z_1 \rightarrow E_2$ excitation :-

(i) the transition pairs to split γ_5 levels were σ polarised, except for three transitions at 18525.5, 18486.0 and 13337.5 cm^{-1} which were π polarised. It is believed that these differences come from having overlapping levels and transitions as discussed for the CS2 and CB2 centres;

(ii) the single transitions at 18503.5, 18181.5, 13351.5, 13330.0 and 13274.0 cm^{-1} were all π polarised. The $E_1 \rightarrow Z_1$ transition was partially polarised with a ratio of 1:2.9 while the $E_1 \rightarrow Z_2$ transition was completely σ polarised. The difference in polarisation for these two transitions was also observed for the CS2 and CB2 centres;

(iii) transitions from both components of the split D_1 level were polarised, as for the SC1 centre, with ratios characteristic of a γ_5 irrep, for both components;

(iv) with the E vector of the laser along the z axis (laser polarised E_z) all transitions that were π polarised with the E vector of the laser along the y axis (laser polarised E_y) were now not observed while transitions that were σ polarised with the laser polarised E_y were observed for the laser polarised E_z, but with polarisation ratios of unity.

(b) For $Z_2 \rightarrow E_6$ excitation, transitions that were π polarised for $Z_1 \rightarrow E_2$ excitation were now found to be σ polarised while transitions that were σ polarised for $Z_1 \rightarrow E_2$ excitation were now found to be π polarised. The $E_1 \rightarrow Z_1$ transition was σ polarised and the $E_1 \rightarrow Z_2$ transition was π polarised. Component transitions from a given E level to a split γ_5 level were always of opposite polarisations.

As all these results are as found for the CS2 and CB2 centres, the SC2 centre is proposed to be a C_s(b) symmetry centre with the exact configuration to be further discussed in Sections 5.5 and 5.6. An energy level diagram showing the SC2 energy levels in relation to the SC1 levels is presented in Figure 5.19. Energy levels derived for the Z, Y, D and E multiplets are given in Table 5.9. These are

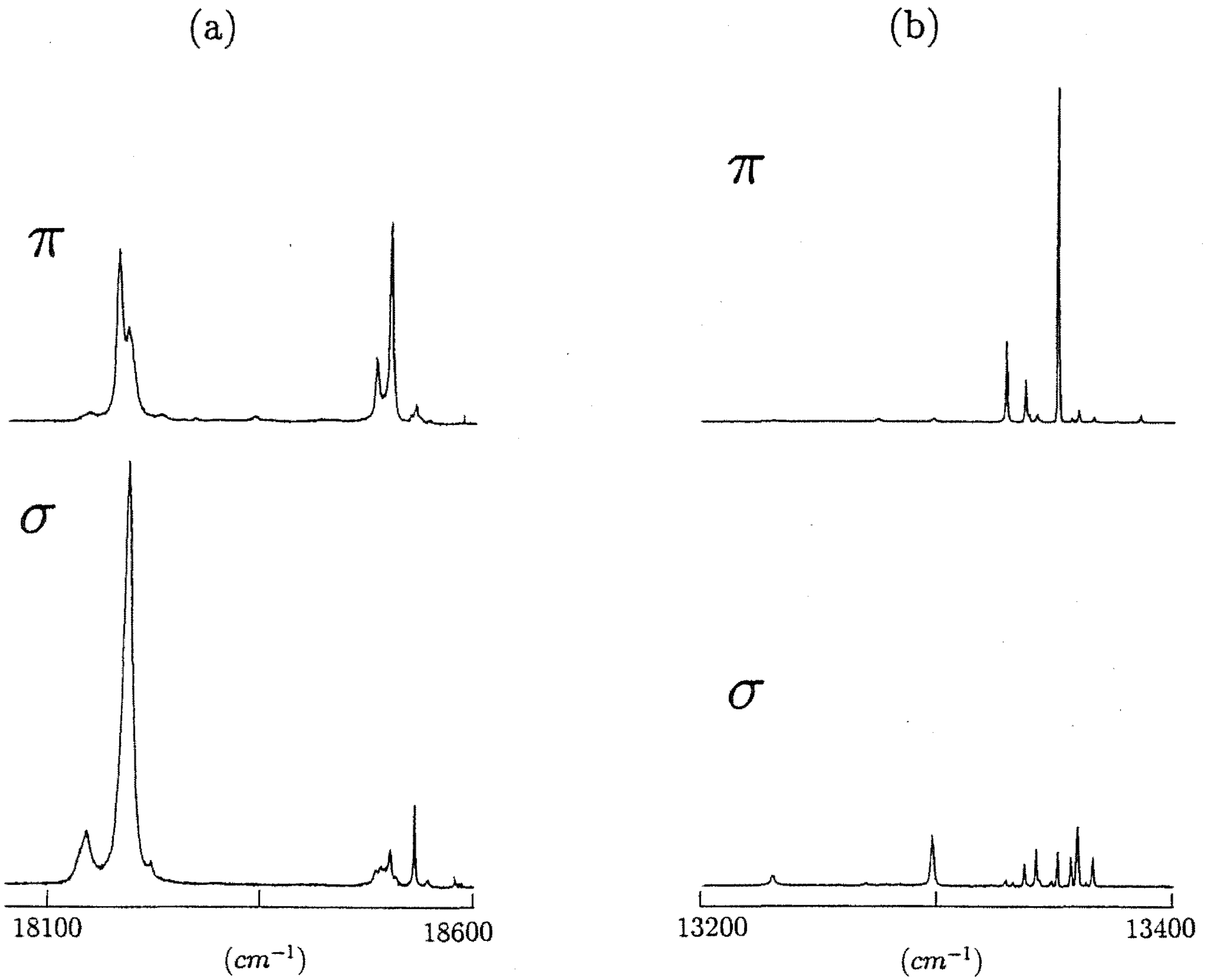
(a)
(b)
π
σ
π
σ
18100
18600
(cm⁻¹)
13200
13400
(cm⁻¹)

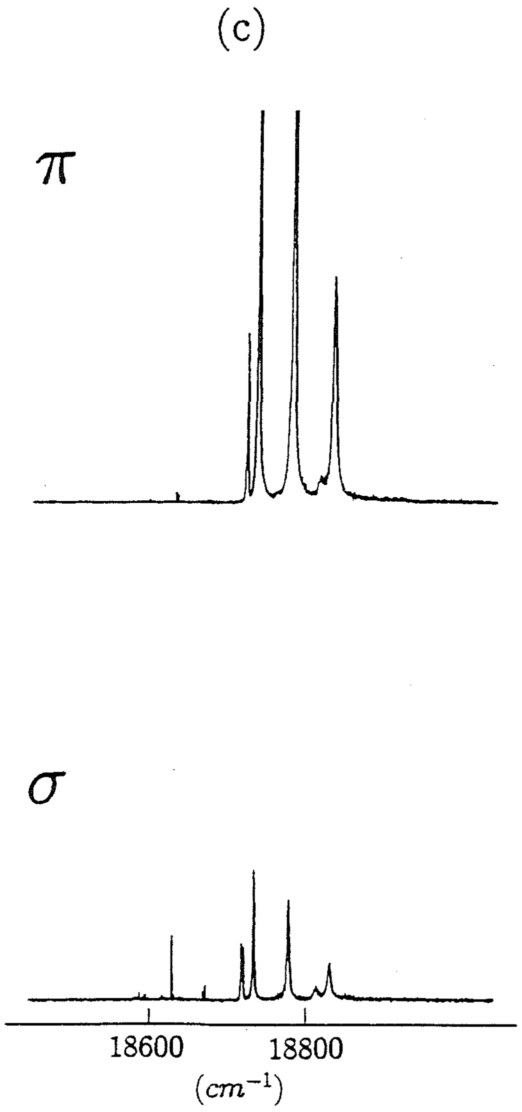

Figure 5.20: Polarisation of the 10 K selective excitation and fluorescence spectra of the SC2 centre in $SrF_2:Ho^{3+}$(0.01%) crystals :
(a) E→Z transitions, for excitation of the $Z_1 \rightarrow E_2$ transition at 18590.1 cm^{-1};
(b) E→Y transitions, for excitation of the $Z_1 \rightarrow E_2$ transition at 18590.1 cm^{-1};
(c) Z→E transitions, monitoring the $E_2 \rightarrow Z_1$ transition at 18590.1 cm^{-1}.
Transition labels are as in Figures 5.10(d) and 5.18.

Table 5.10 : Observed intensity ratios for the polarised fluorescence transitions of the SC2 centre in <100> and <111> oriented $Sr_{0.99}Ca_{0.01}F_2:Ho^{3+}$(0.005%) crystals, for excitation of the $Z_1 \rightarrow E_2$ transition at 18590.1 cm^{-1}.

Transition	**Wavenumber (± 0.5) (cm^{-1})**	**Observed Polarisation Ratios (± 5%)**	
		<100> orientation [yy : yx]	**<100> orientation [y′y′/y′x′]**
$E_2 \rightarrow Z_3$	18538.0	1 : 3.5	0.7
$E_2 \rightarrow Z_4$	18532.5	1 : 2.9	0.8
$E_2 \rightarrow Z_{14}$	18181.5	7.1 : 1	2.1
$E_1 \rightarrow Z_1$	18583.5	1 : 2.9	0.8
$E_1 \rightarrow Z_2$	18581.0	1 : 6.4	0.8
$E_1 \rightarrow Z_3$	18531.0	1 : 4.4	0.7
$E_1 \rightarrow Z_4$	18525.5	4.3 : 1	2.0
$E_1 \rightarrow Z_5$	18503.5	6.9 : 1	2.3
$E_1 \rightarrow Z_6$	18494.0	1 : 4.2	0.8
$E_1 \rightarrow Z_7$	18486.0	3.3 : 1	2.2
$E_1 \rightarrow Z_{12}$	18193.5	1 : 7.0	0.8
$E_1 \rightarrow Z_{13}$	18187.0	1 : 6.4	0.7
$E_1 \rightarrow Z_{16}$	18144.5	1 : 6.9	0.7
$E_1 \rightarrow Z_{17}$	18138.0	1 : 6.3	0.7
$E_2 \rightarrow Y_1$	13366.5	1 : 4.3	0.6
$E_2 \rightarrow Y_2$	13364.0	1 : 3.7	0.8
$E_2 \rightarrow Y_4$	13349.0	1 : 7.2	0.6
$E_2 \rightarrow Y_5$	13344.0	1 : 4.1	0.7
$E_2 \rightarrow Y_7$	13339.0	1 : 3.9	0.7
$E_2 \rightarrow Y_6$	13330.0	17.7 : 1	1.8
$E_1 \rightarrow Y_1$	13360.0	1 : 4.5	0.6
$E_1 \rightarrow Y_2$	13357.0	1 : 6.4	0.5
$E_1 \rightarrow Y_3$	13351.5	12.3 : 1	1.6
$E_1 \rightarrow Y_4$	13342.5	1 : 4.1	0.6
$E_1 \rightarrow Y_5$	13337.5	2.4 : 1	1.1
$E_1 \rightarrow Y_7$	13332.5	1 : 8.2	0.7
$E_1 \rightarrow Y_8$	13298.5	1 : 10.9	0.6
$E_1 \rightarrow Y_{10}$	13274.0	3.9 : 1	1.9
$E_1 \rightarrow Y_{11}$	13269.5	1 : 8.5	0.5
$E_1 \rightarrow Y_{12}$	13230.5	1 : 6.5	0.6

labelled in an analogous manner to that done for the CS2 and CB2 centres.

5.3 Upconversion Fluorescence of the SrF_2 A, B, SC1, SC2 and SB1 Centres

For Z → E excitation, no upconversion fluorescence was observed for any of the five centres.

For $Z_1 \rightarrow D_4$ excitation, weak upconversion fluorescence was observed from the E and F multiplets for just the A, SC1 and SB1 centres. Fluorescence from the E multiplet was 10^{-5} times weaker than that obtained from direct excitation and that from the F multiplet was about ten times weaker than that from the E multiplet. As for the CaF_2 case, the E → Z fluorescence was polarised exactly as found for direct excitation while polarisation ratios for the F → Z transitions were not measurable because the fluorescence was just too weak. The Z level pattern for each centre was clearly apparent and completely consistent with the Z levels derived from the D → Z and E → Z transitions. Spectra for the F → Z transitions are shown in Figure 5.21 (a), (b) and (c) for the SrF_2 A, SC1 and SB1 centres respectively.

For the SC2 and B centres, no upconversion fluorescence was detected, setting an upper limit of 10^{-7} of the intensity of the principal $D_1 \rightarrow Z_3$ and $D_1 \rightarrow Z_2$ transitions respectively, for any such fluorescence.

5.4 Spectra Recorded up to 55 K for the SC1, SC2 and SB1 Centres

For $Z_1 \rightarrow E_2$ excitation, fluorescence spectra of the E → Z transitions were recorded for temperatures up to 55 K for the SC1, SC2 and SB1 centres. Some levels whose transitions from the Z_1 and Z_2 levels or from the E_1 and E_2 levels are absent in the 10 K spectra could be identified from such spectra.

Fluorescence spectra recorded at 55 K for each of the three centres are presented in Figure 5.22. As in the $CaF_2{:}Ho^{3+}$ case, all new transitions had appeared by 30 K and increased in intensity as the temperature was raised further

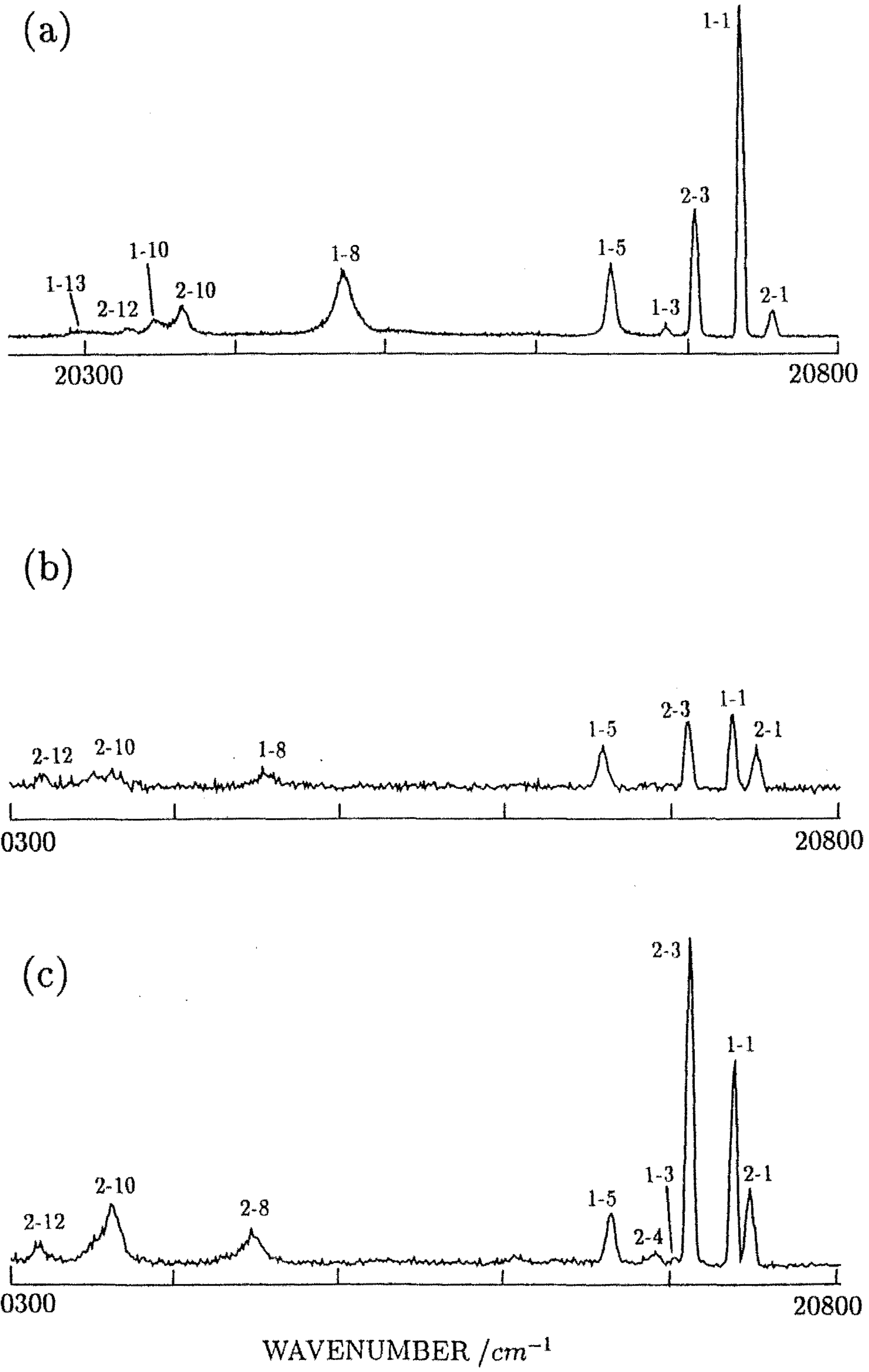

Figure 5.21: 10 K upconversion fluorescence spectra of the F→Z transitions for the A, SC1 and SB1 centres in SrF_2:Ho^{3+}(0.01%) crystals, for Z→D excitation :
(a) SrF_2 A centre spectrum, for excitation of the $Z_1 \rightarrow D_4$ transition at 15642.3 cm^{-1};
(b) SC1 centre spectrum, for excitation of the $Z_1 \rightarrow D_4$ transition at 15630.0 cm^{-1};
(c) SB1 centre spectrum, for excitation of the $Z_1 \rightarrow D_4$ transition at 15624.0 cm^{-1}.

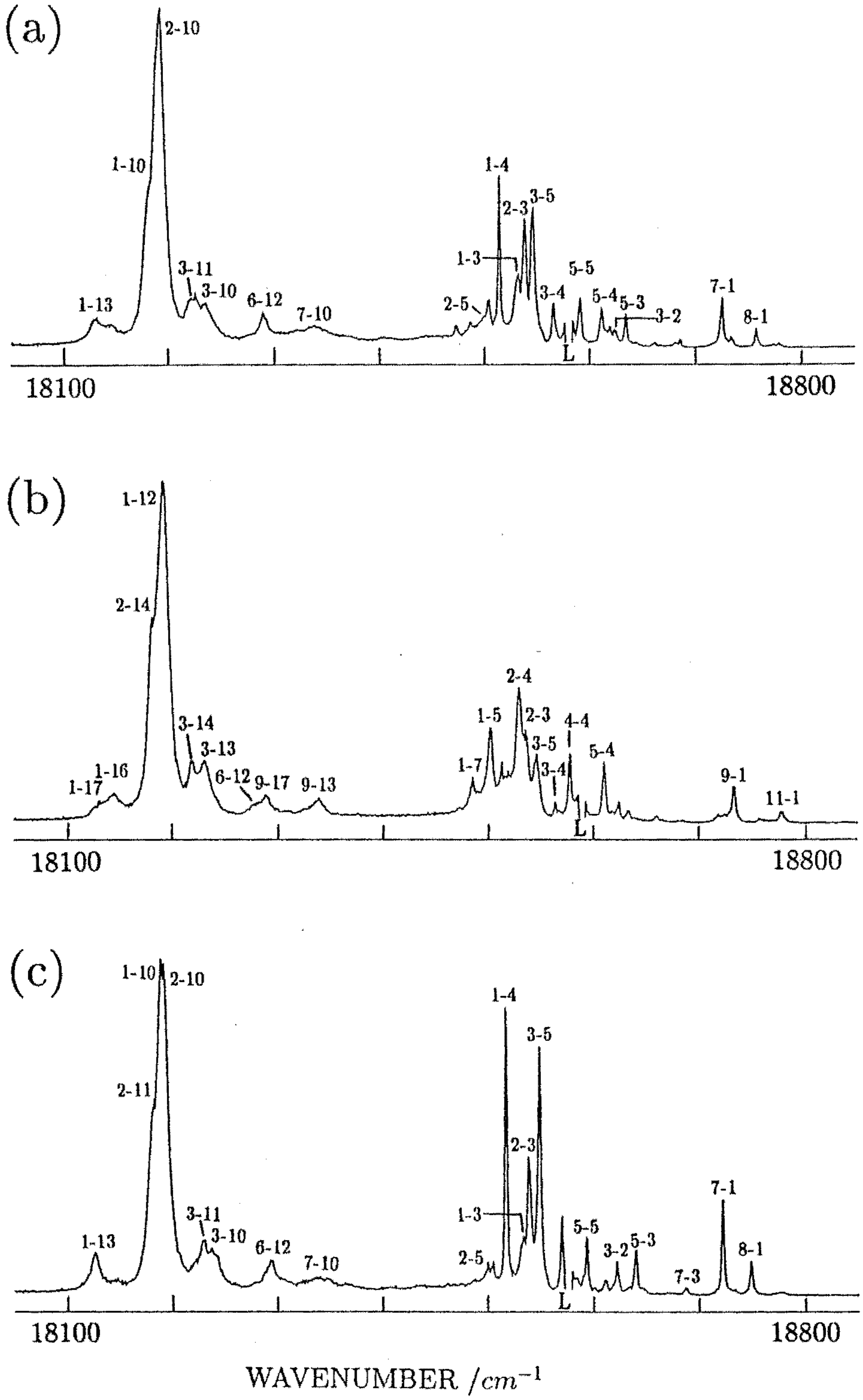

Figure 5.22: 55 K fluorescence spectra of the E→Z transitions for the SC1, SC2 and SB1 centres in SrF_2:Ho^{3+}(0.01%) crystals :
(a) SC1 centre spectrum, for excitation of the Z_1→E_2 transition at 18579.9 cm^{-1};
(b) SC2 centre spectrum, for excitation of the Z_1→E_2 transition at 18590.1 cm^{-1};
(c) SB1 centre spectrum, for excitation of the Z_1→E_2 transition at 18575.8 cm^{-1}.
Transition labels are as in Figure 5.5.

to 55 K. Above 55 K there was overlap from fluorescence transitions from other centres, as the respective pump transitions began to overlap.

5.5 Configurations of the SC1, SC2 and SB1 Centres

It was initially rather surprising that the centres SC1 and SB1 had the same symmetry as the SrF_2 A centre. From the $CaF_2:Ho^{3+}$ study, it has been established that additional C_{4v} symmetry centres could arise from an on-axis substitution of the host cation by a dopant cation, while a dopant cation located off the Ho^{3+} - F^- axis would reduce the symmetry to give a low symmetry C_s centre. The observation that the two centres SC1 and SB1 have the same features as the CS1 and CB1 centres while the SC2 centre is more like the CB2 centre, led to the conclusion that there must be small amounts of Ca^{2+} and Ba^{2+} ions in the host SrF_2 crystals used here.

Hence, $SrF_2:Ho^{3+}$(0.01%) crystals containing 1% of either CaF_2 of BaF_2 were grown and studied. Broadband excitation spectra for the $Sr_{0.99}Ca_{0.01}F_2:Ho^{3+}$(0.01%) crystals as shown in Figures 5.10(b) and 5.11(b), show transitions assigned to the SC1 and SC2 centres become more intense than those assigned to the A and SB1 centres. Transitions from the SC1 and SC2 centres were of comparable intensity to those of the SrF_2 A centre in the same crystal. Transitions for the SB1 centre were observed to be 30 - 50% weaker in the mixed $Sr_{0.99}Ca_{0.01}F_2:Ho^{3+}$(0.01%) crystal than in the parent $SrF_2:Ho^{3+}$(0.01%) crystal.

From broadband excitation spectra for $Sr_{0.99}Ba_{0.01}F_2:Ho^{3+}$(0.01%) crystals, Figures 5.13(b) and 5.14(b), transitions due to the SB1 centre were found to increase by three to five times over those found in the parent $SrF_2:Ho^{3+}$(0.01%) crystals, with the SC1 and SC2 centre transitions barely visible and the A centre at least twice as weak as in the parent crystal. A fourth centre labelled SB2 in Figure 5.13(b), also appeared in this crystal. As the transition at 18571.9 cm^{-1} for this SB2 centre was close to the $Z_2 \rightarrow E_2$ transition for the SB1 centre at 18573.0 cm^{-1}, fluorescence transitions for the SB2 centre could not be obtained well discriminated from those of the SB1 centre. The E → Z spectrum for the SB2 centre is quite similar to those for the SC1, SC2 and SB1 centres. The strong transition at 18525.4 cm^{-1} in the E → Z fluorescence spectrum (Figure 5.23(a)) is clearly from this centre. Monitoring this transition gave a well discriminated excitation spectrum (Figure 5.13(d)) which had just as many transitions as did the SC2 centre. The D → Z and E → Y spectra shown in Figure 5.23 (b) and (c), also show transitions for the SB1 centre as well as those for the SB2 centre. Unfortunately because of the unavoidable overlap with transitions of the SB1 centre, it could not be established whether or not any low symmetry splittings of the C_{4v} symmetry γ_5 type levels were present. Nevertheless, this centre is proposed to be the Ba^{2+} analogue of the SC2 centre. As its energy level scheme could not be established, only transition energies of this centre are listed in Table 5.11.

Two SrF_2 crystals with Ho^{3+} concentrations of 0.005% and 0.1% respectively, were purchased from Optovac Inc. as reference crystals to verify the source of the Ca^{2+} and Ba^{2+} ions present in the SrF_2:Ho^{3+} crystals grown here from Optovac stock SrF_2 off-cuts. The Optovac crystals were also found to have all the SC1, SC2, SB1 and SB2 centres presented above in the same relative intensities as found here. The only difference is that crystals grown here were found to have slightly lower Ho^{3+} concentration than those from Optovac for the same dopant level, most likely due to some segregation of Ho^{3+} ions during growth of those crystals grown here.

By comparison of the relative fluorescence intensities, the Ca^{2+} and Ba^{2+} concentration in the nominally pure SrF_2 starting material is about 0.2%. The centres SC1, SC2 and SB1 are therefore ascribed to the presence of small amounts of Ca^{2+} and Ba^{2+} ions respectively in the nominally pure starting SrF_2 material. It could be that the N1 and N2 centres in SrF_2:Er^{3+} are from similar levels of Ca^{2+} and Ba^{2+} ions in the SrF_2 used for the SrF_2:Er^{3+} crystals.

The SC1 and SB1 centres are assigned as having a Ca^{2+} and Ba^{2+} ion

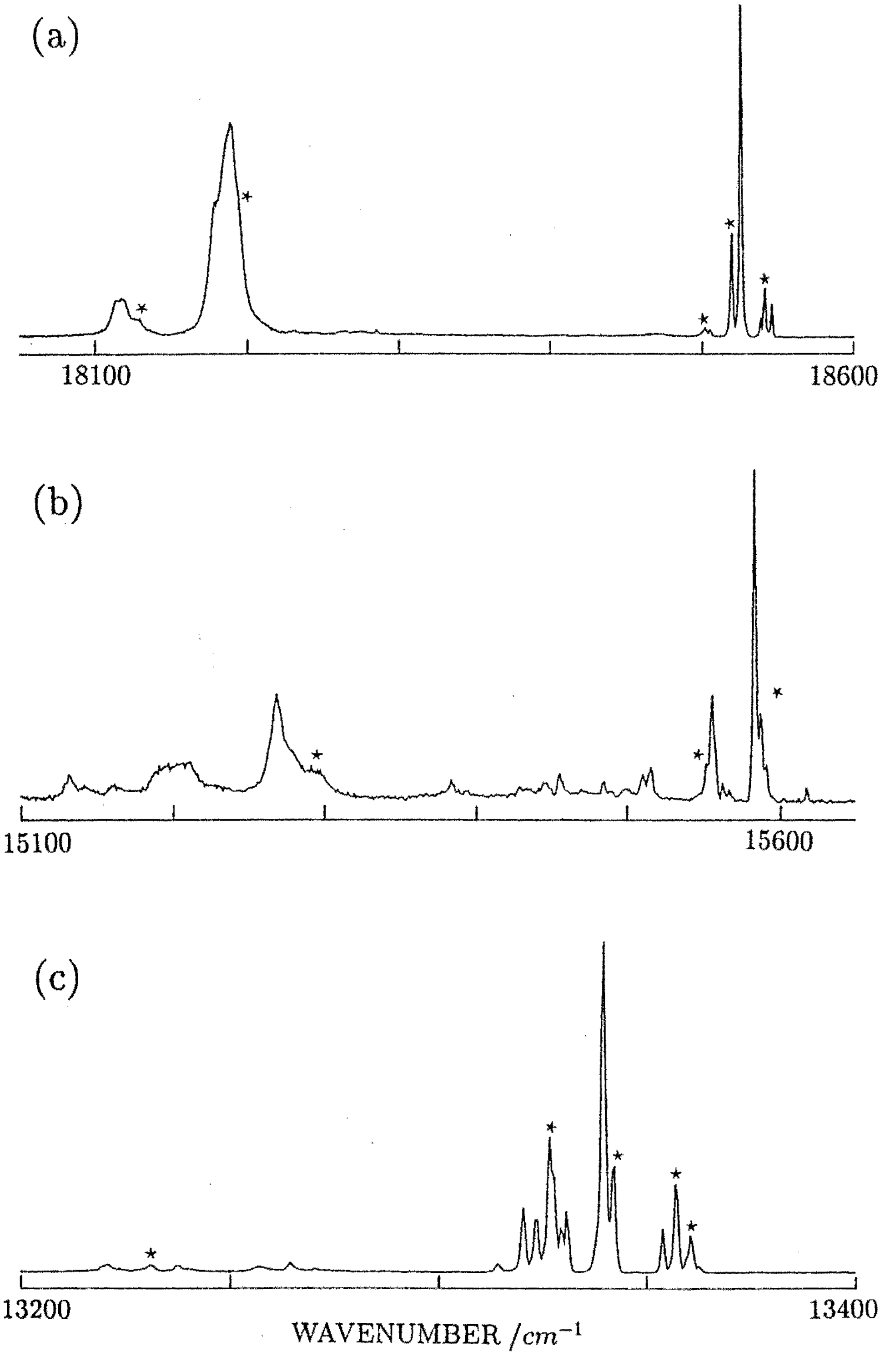

Figure 5.23: 10 K fluorescence spectra for the SB2 centre in $Sr_{0.99}Ba_{0.01}F_2$:Ho^{3+}(0.01%) crystals, for excitation of the transition at 18573.0 cm^{-1} :
(a) E→Z transitions;
(b) D→Z transitions;
(c) E→Y transitions.
Transitions marked by * are for the SB1 centre.

Table 5.11 : Energies (in cm^{-1}) of the Z → E, E → Z, D → Z and E → Y transitions observed for the SB2 centre in $Sr_{0.99}Ba_{0.01}F_2$:Ho^{3+}(0.01%) crystals at 10 K. Uncertainty is ± 0.5 cm^{-1}.

Z → E transitions	**E → Z transitions**	**D → Z transitions**	**E → Y transitions**
18833.1	18546.0	15618.0	13362.5
18816.6	18538.5	15584.0	13354.0
18791.0	18525.4	15556.0	13340.0
18777.5	18505.5	15456.0	13331.0
18739.8	18189.0	15280.0	13328.0
18720.9	18180.5	15269.0	13323.5
18684.4	18117.0	15162.0	13320.5
18654.9	18112.0	15132.0	13314.5
18650.3			13264.5
18629.3			13257.5
18622.5			13237.5
18573.0			13220.5

respectively, located adjacent to the interstitial F^- ion on the Ho^{3+} - F^- axis, giving a C_{4v} symmetry centre with the same configuration as proposed for the CS1 and CB1 centres (Figure 1.4(a)). The SC2 centre is assigned as having a Ca^{2+} ion located in the same position relative to the Ho^{3+} ion, as was the Ba^{2+} of the CB2 centre, giving a C_s(b) symmetry centre (Figure 1.4(b)). By qualitative comparison, it is believed that the SB2 centre has the same C_s(b) symmetry configuration.

5.6 Discussion of the Centres

Although CaF_2:Ho^{3+} has been well studied by EPR, fluorescence and lifetime measurements, relatively little had been reported on SrF_2:Ho^{3+}. This study therefore gives the first detailed analysis of the five centres present at the 0.01% Ho^{3+} concentration level, together with model assignments based on spectral polarisation measurements.

Although the Sr^{2+} ion is intermediate in ionic size to the Ca^{2+} and Ba^{2+} ions, there does not appear to be any special manifestation of these relative sizes in the spectra of the SC1 and SB1 centres. The only noticeable difference is that levels for the SB1 centre have lower energies than for the SC1 centre just as the CB1 centre also has lower energy levels than the CS1 centre. In both cases these differences follow from the slightly expanded lattice for Ba^{2+} ions present. In all cases the C_{4v} symmetry centres having a different interstitial alkaline-earth cation always have slightly lower energies than the parent A centre for both CaF_2 and SrF_2 type crystals. The E_1 - E_2 and D_1 - D_3 energy level separations are closely similar for the modified C_{4v} symmetry centres in the same host. The close similarity in the energy level patterns and irrep label assignments for the modified C_{4v} symmetry centres compared to the parent C_{4v} (A) centre gives confidence in the model assignments made.

The SC2 centre is different from the CaF_2 type C_s symmetry centres in that its energy levels are higher than those of the parent SrF_2 A centre. The γ_5 type level splittings follow the same pattern as for the CS2 and CB2 centre energy levels in having a combination of the smallest and largest splittings in the Y multiplet and in-between sizes for the Z and D multiplet levels. The C_s symmetry centre of each case has the same $E_1 - E_2$ energy level separation as the corresponding parent A centre. The component transitions of some pairs have opposite polarisations, for excitation of the $Z_1 \rightarrow E_2$ transition of the SC2 centre and it is always the case that the mainly π polarised component of the pair has a polarisation ratio close to unity which may be an indication of a partial overlap of oppositely polarised transitions. This would account for some of the unobserved levels since all transitions are allowed in C_s symmetry.

For all the centres, the $Z_1 - Z_2$ energy level splitting does not change much between the A and respective mixed crystal centres. The small difference of up to 0.2 cm^{-1} in the measured positions of the Z_2 level in different centres might not be a real effect but merely better resolution for the case of the A centre.

The principal A centre has been shown to have Ho^{3+} ions in sites of C_{4v} symmetry while the C_{3v} symmetry B centre is quite weak. This is in contradiction to the EPR measurements which predict a principal Ho^{3+} centre of C_{3v} symmetry in $SrF_2:Ho^{3+}$ [103]. A possible reason for this is that the Z_1 and Z_2 levels of the A centre have both been determined to be crystal-field singlets with an energy separation of 2.7 cm^{-1}. This centre therefore would not give rise to any EPR resonances at either X band (9.5 GHz) or K band (35 GHz). EPR measurements at about 75 GHz, as done for $CaF_2:Ho^{3+}$ [66] would be required to detect the presence of any EPR resonances of this C_{4v} symmetry centre and to measure the corresponding $Z_1 - Z_2$ energy level splitting. On the other hand, the trigonal centre, although having much weaker optical transitions, would give rise to EPR resonances at both X and K bands because the ground state is a γ_3 (doublet) level. Hence the principal centre anomaly can be reasonably accounted for.

The observation of both C_{4v} and C_{3v} symmetry centres in $SrF_2:Ho^{3+}$ is not too surprising. Although Er^{3+} ions in SrF_2 crystals have a purely trigonal centre, Dy^{3+} ion in SrF_2 on the other side of Ho^{3+} in the rare-earth series has both C_{4v}

and C_{3v} symmetry centres. It could very well be that the change in symmetry of the principal centre from mainly tetragonal to mainly trigonal symmetry does occur between the Ho^{3+} and Er^{3+} ions.

5.7 Spectroscopy of the D^- Centres in SrF_2:Ho^{3+}(0.005%) Crystals

Hydrogenic centres in SrF_2 crystals have been studied through infrared and EPR spectroscopy for all rare-earths [36]. A hydrogenic centre of C_{4v} symmetry was reported for all rare-earths up to Ho^{3+} in the rare-earth series but was absent for ions from Er^{3+} onwards. Additional rhombic centres were identified for the RE^{3+} ions from La^{3+} to Ho^{3+} while low symmetry centres were found for the remaining six small ionic radii rare-earths from Dy^{3+} onwards.

For optical studies, deuterated rather than hydrogenated crystals were chosen as fluorescence from the deuterated centres is much stronger than that from hydrogenated centres. As for the CaF_2 case, the crystals were only lightly deuterated with typical deuteration periods of 12 - 24 hours. For the parent F^- A centre, sufficient intensity absorption lines could only be obtained for thick (30 mm) samples at high Ho^{3+} concentrations of about 0.1%, hence transitions for cluster centres were expected to be present too. The broadband excitation spectrum for SrF_2:Ho^{3+}(0.005%) after 24 hours deuteration had only a few new weak features at lower energies than those of the F^- centres (Figure 5.24).

With SrF_2 fluorescence already being weaker than for CaF_2 for the parent A centre, the fluorescence of the new deuterated centres was very weak, being about 1% of the SrF_2 F^- A centre intensity. Transitions for the D^- analogue of the F^- A centre were searched for but not found. Instead four centres with some similarity to the SrF_2 A centre were identified. These centres have been arbitrarily labelled D1, D2, D3 and D4. Transitions energies for the four centres are listed in Table 5.12.

For the D2 centre, both the E → Z and E → Y fluorescence transitions were measured (Figure 5.25). For the D1, D3 and D4 centres only the E → Z

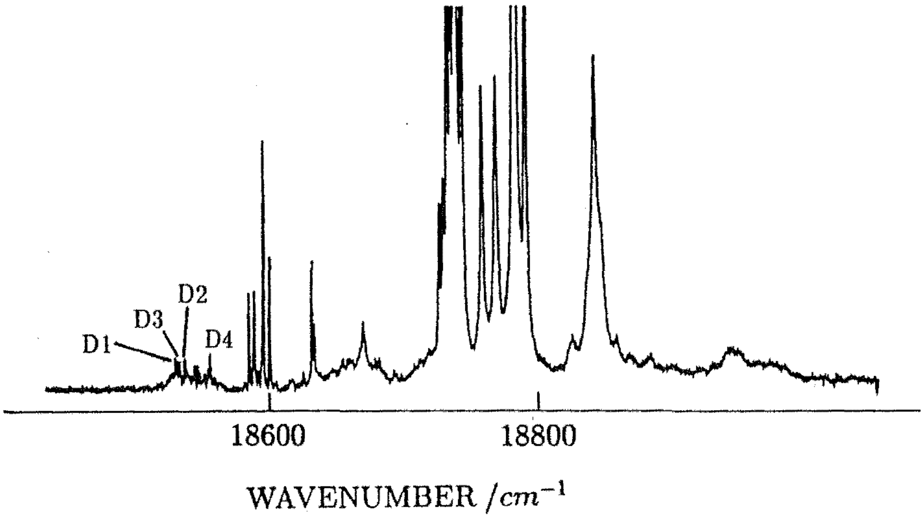

Figure 5.24: 10 K broadband excitation spectrum of the E multiplet in SrF_2:Ho^{3+}(0.005%) crystals after 24 hours deuteration.

fluorescence transitions were strong enough to be recorded (Figure 5.26). The Raman line of SrF_2 at 290.0 cm^{-1}[†] was apparent in all the 10 K E → Z fluorescence spectra (Figures 5.25 and 5.26), indicating the relative weakness of the fluorescence.

Spectra for the D1 and D2 centres are similar to those for the D1 and D2 centres in CaF_2:Ho^{3+}:D^-. The transition at 18150.0 cm^{-1} in the E → Z spectrum for the D1 centre appears to be a vibronic transition, but local mode phonon energies could not be deduced as no other vibronic transitions were found. It is likely that the D1 centre is derived from the SrF_2 A centre and has the same configuration as the corresponding D1 centre in deuterated CaF_2 crystals. The D2, D3 and D4 centres are quite likely to be derived from the SC1, SB1 and SC2 centres respectively.

[†] Denham P., Field G.R., Morse P.L.R. and Wilkinson G.R., Proc. Roy. Soc. (Lond.) **A317**, 55 (1970)

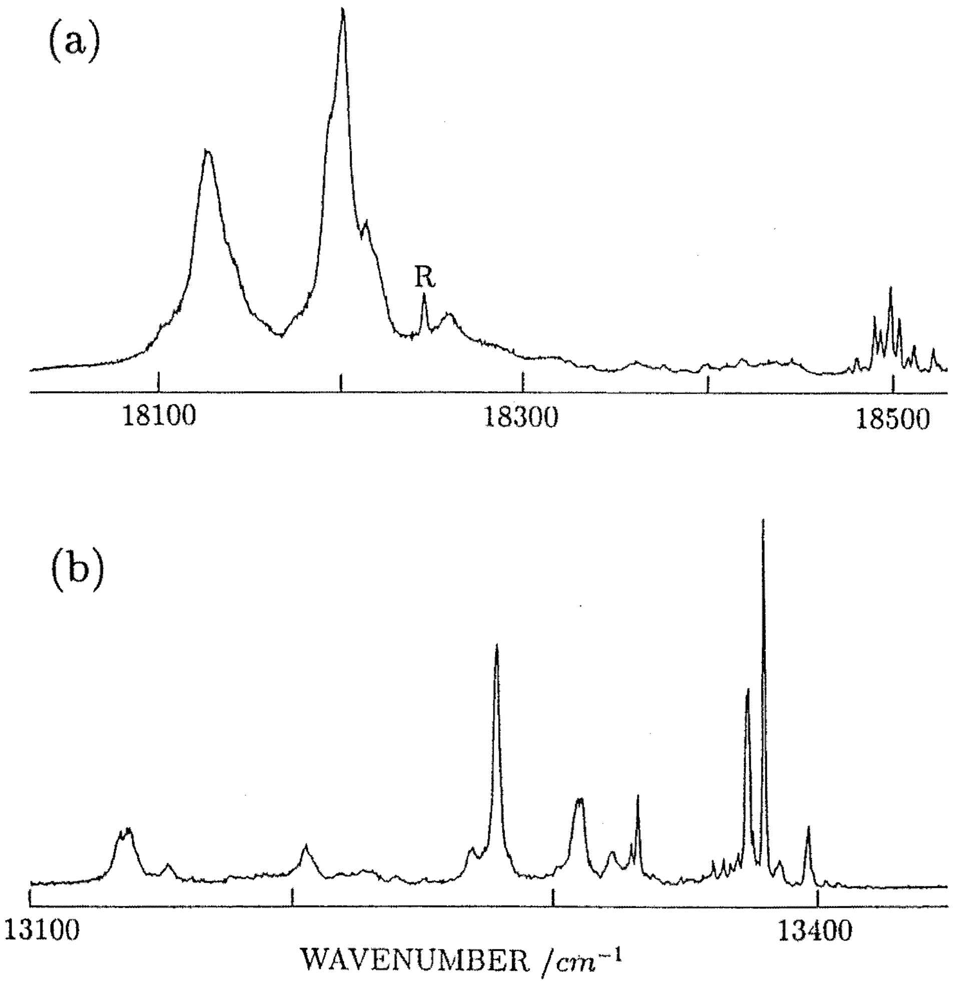

Figure 5.25: 10 K fluorescence spectra for the D2 centre in SrF_2:Ho^{3+}(0.005%) crystals after 24 hours deuteration, for excitation of the transition at 18536.3 cm^{-1} :
(a) E→Z transitions;
(b) E→Y transitions.

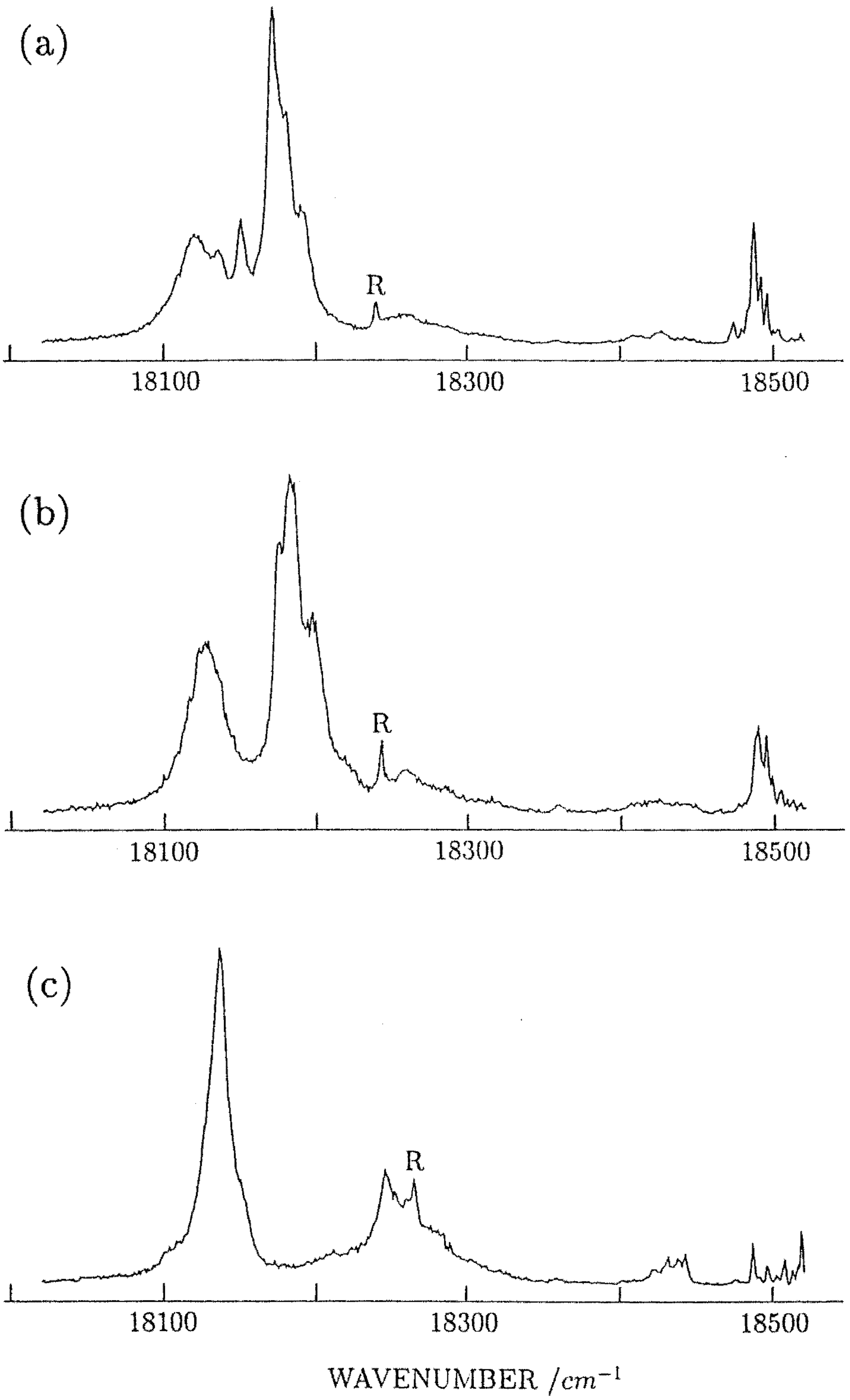

Figure 5.26: 10 K fluorescence spectra of the E →Z transitions for the D1, D3 and D4 centres in SrF$_2$:Ho^{3+}(0.005%) crystals after 24 hours deuteration :
(a) D1 centre spectrum, for excitation of the transition at 18528.3 cm^{-1};
(b) D3 centre spectrum, for excitation of the transition at 18531.5 cm^{-1};
(c) D4 centre spectrum, for excitation of the transition at 18553.5 cm^{-1}.

Table 5.12 : Energies (in cm^{-1}) of the transitions observed for the D1, D2, D3 and D4 centres in SrF$_2$:Ho^{3+}(0.005%) crystals, after 24 hours deuteration. Uncertainty is ± 1 cm^{-1}.

Transitions	D1	D2	D3	D4
E → Z	18528.3	18536.3	18531.5	18553.5
	18495.0	18522.5	18494.0	18518.0
	18491.0	18512.0	18489.0	18507.0
	18486.0	18503.5	18197.0	18495.0
	18473.0	18499.0	18182.0	18486.0
	18189.0	18493.5	18175.0	18245.0
	18180.0	18490.0	18126.0	18136.0
	18171.0	18260.0		
	18150.0*	18214.5		
	18135.0	18201.0		
	18119.0	18194.5		
		18127.0		
E → Y		13396.5		
		13385.5		
		13379.5		
		13374.0		
		13332.0		
		13329.5		
		13322.0		
		13310.0		
		13279.0		
		13269.0		
		13205.5		
		13152.0		
		13135.5		

* Vibronic transition

CHAPTER 6

SPECTROSCOPY OF Ho^{3+} IONS IN $CsCdBr_3$ CRYSTALS

$CsCdBr_3$ is an ideal host for study of dimer centres as these form even at low (0.01%) dopant concentrations. This is in contrast to other host crystals such as CaF_2 and $LiYF_4$, which require dopant concentrations of several % to produce appreciable concentrations of cluster centres, because of the randomness of the dopant distribution. More importantly, in $CsCdBr_3$ the two ions of a dimer centre have a well defined separation as well as identical crystalline environments.

Interest in this particular host stemmed from a study of $CsCdBr_3$:Er^{3+}(0.7%) by Cockroft et al. [28, 31]. Of the centres present in this crystal, only the principal dimer centre was studied in any detail [31] and found to exhibit upconversion fluorescence, with such transitions having intensities of up to 30% of the intensity of the strongest $E_1 \rightarrow Z_3$ transition, for excitation of the E multiplet. Energy levels of the multiplets of Er^{3+} up to 36000 cm^{-1} were inferred. In addition, small splittings of typically 0.5 cm^{-1} were observed on some of the sharper transitions and were attributed to interactions between the two Er^{3+} ions of a dimer centre. In two separate subsequent studies [29, 85] the dynamics of the upconversion fluorescence for the various multiplets has been studied through fluorescence lifetime measurements. In the 1%Er^{3+} doped crystal studied by Cockroft, Jones and Nguyen [29], eight minor centres were also present, six of which were found to exhibit upconversion.

Other trivalent rare-earth ions in $CsCdBr_3$ that have been studied by laser spectroscopy include Tb^{3+} [13, 72], Nd^{3+} [10, 11, 12], Pr^{3+} [27, 41, 90, 101, 102], Ce^{3+} [14] and Ce^{3+} - Tm^{3+} pairs [82].

For Tb^{3+}, luminescence ascribed to the principal Tb^{3+} - Tb^{3+} dimer centre was measured at both 4.2 K and room temperatures [72] and the cross relaxation mechanism pertaining to the $^5D_3$ and $^5D_4$ multiplets discussed [13]. The temperature dependence of the relaxation rate was proposed to be due to the population of the higher energy levels of both the $^7F_6$ and the $^5D_3$ multiplets, for temperatures approaching 75 K. Thermal population of the higher lying energy levels would result in better matching of the energy gaps between the various multiplets. The decrease in the relaxation rate for temperatures above 75 K was ascribed to increases in the energy mismatch for the relevant multiplets as the even higher energy levels of the $^7F_6$ and $^5D_3$ multiplets become populated.

In $CsCdBr_3:Nd^{3+}$ [11, 12], two centres were identified as having respectively single Nd^{3+} ions and Nd^{3+} ion pairs with upconversion fluorescence observed for the pair centre. Nd^{3+} ions co-doped with one of the monovalent (M^+) ions Li^+, Na^+ and Ag^+ give rise to centres of the form Cd^{2+} - Nd^{3+} - M^+ - Cd^{2+}, and these were also studied [11]. The transitions for such centres were found to be satellite lines either close to or within the linewidth of the principal Cd^{2+} - Nd^{3+} - V - Nd^{3+} - Cd^{2+} dimer centre transitions. However, for some multiplets the fluorescence lifetimes of the Nd^{3+} - M^+ centre were much longer than those of the regular Nd^{3+} - Nd^{3+} dimer centre, and time resolved studies could be used to distinguish between the centres [11]. Fluorescence lifetime measurements for several multiplets of both centres highlighted the various relaxation channels available. From a further study of the 0.3% Nd^{3+} doped crystals [12], the spectroscopy and dynamics for a new centre proposed to be of the form Cd^{2+} - Nd^{3+} - Nd^{3+} - V - Cd^{2+} were presented. Though present at a much weaker concentration than the more usual dimer centre, this centre was found to increase in intensity with increasing Nd^{3+} concentration.

In $CsCdBr_3:Pr^{3+}$, eight centres were identified for Pr^{3+} concentrations of either 0.1% or 0.3% [41]. Two of these centres were found to exhibit significant upconversion fluorescence. The principal dimer centre has also been studied through high resolution laser and Zeeman spectroscopy [27, 101, 102]. Current studies of double doped $CsCdBr_3:Tm^{3+}(0.5\%):Pr^{3+}(0.1\%)$ [90] show evidence of overlapping between the Tm^{3+} - Tm^{3+} and Tm^{3+} - Pr^{3+} pair centre transitions.

For the Ce^{3+} ion [14], emission in the 580 - 650 nm and 380 - 435 nm regions was reported for ultraviolet excitation, for the Ce^{3+} - Ce^{3+} dimer, Ce^{3+} - Li^{+} dimer and single Ce^{3+} ion centres.

Energy transfer mechanisms between heterogeneous rare-earth ion centres have also been studied for the Ce^{3+} - Tm^{3+} centre [82] which shows efficient energy transfer from Ce^{3+} to Tm^{3+} for excitation of the 4f - 5d transition of Ce^{3+} at about 27800 cm^{-1}.

Spectroscopic study of crystals doped with two different rare-earths seemed a logical extension. With energy exchange occurring between the two different rare-earth ions of the resulting centre, further insight into the energy transfer mechanisms might be gained. Hence, crystals doubly doped with 0.3% Er^{3+} and 1% of one of Yb^{3+}, Ce^{3+} or Lu^{3+} were grown and studied. These ions were chosen as they would give rise to different Er^{3+} - RE^{3+} centres without complicating the spectra too much as they, themselves, have at most transitions to and from a single excited multiplet in the infrared region of the spectrum.

In all three cases, there were no distinct transitions observed in either the absorption or excitation spectra that could be attributed to an Er^{3+} ion coupled to a Yb^{3+}, Ce^{3+} or Lu^{3+} ion nearby. It is quite possible that the transitions from such heterogeneous pairs lie within the linewidth of the homogeneous Er^{3+} dimer pair centre transitions. As the fluorescence from the Er^{3+} - Er^{3+} dimer centre was found to be about ten times weaker in the doubly doped crystals compared to the parent Er^{3+} only crystals, this is indirect evidence that the second rare-earth dopant was incorporated in the crystal. However, fluorescence from Yb^{3+} ions was searched for in the 10000 cm^{-1} region of the expected $^2F_{5/2} \rightarrow {}^2F_{7/2}$ transitions, with $Z \rightarrow E$ excitation of the Er^{3+} ion, without success. As the Er^{3+} fluorescence in this same region for the $^4I_{11/2} \rightarrow {}^4I_{15/2}$ transitions is quite strong, it appears that the Yb^{3+} fluorescence could be strongly quenched by the Er^{3+} ions. Another reason could be that energy transfer is relatively inefficient between Er^{3+} and Yb^{3+} because the phonon energies of $CsCdBr_3$ of up to 163 cm^{-1} [96] are too low to bridge the energy gap between the $^4I_{11/2}$ energy levels of Er^{3+} and the $^2F_{5/2}$

energy levels of Yb^{3+}. Because of these problems in detecting the Er^{3+} - Yb^{3+} dimer centre transitions, attention was directed to characterising Ho^{3+} dimer centre transitions in the single Ho^{3+} doped $CsCdBr_3$ crystal host.

Following the study of Ho^{3+} ions in fluorite type crystals, a study of the $CsCdBr_3$:Ho^{3+} system seemed appropriate for investigation of Ho^{3+} ion pair interactions and upconversion fluorescence processes. The spectroscopy of Ho^{3+} ions in $CsCdBr_3$ had not been done before and would supplement the knowledge of the behaviour of trivalent rare-earth ions in this crystal host. Similarities with the Er^{3+} case were expected, as well as some differences, arising from the spectral and energy irrep label differences between Kramer's and non-Kramer's ions.

Absorption Spectra

Optical absorption spectra, as measured in 15 - 20 mm thick crystals of $CsCdBr_3$:Ho^{3+}(0.3%), show strong absorption features for both the Z → E and Z → D transitions (Figure 6.1). These strong transitions were classified as belonging to just one centre, the well established dimer centre, which is the major centre in these crystals.

Laser Selective Excitation

Laser excitation spectra measured with monitoring of all fluorescence transitions in the 15000 cm^{-1} region in $CsCdBr_3$ crystals containing 0.3% and 0.1% Ho^{3+} ions had the same features as the absorption spectra. Because there were no observable differences between the spectra measured for 0.3% and 0.1% Ho^{3+} concentrations, apart from the slightly narrower transitions observed for the 0.1% crystals, the 0.3% Ho^{3+} doped samples were studied in most cases. The relevant broadband excitation spectra for the Z → E and Z → D transitions are presented in Figures 6.2, 6.3 and 6.4. By laser selective excitation, transitions for the major dimer centre were distinguished from those of the minor centre, which is arbitrarily labelled the L centre. This L centre (transitions marked by L in Figures 6.3(a) and 6.4(a)) will be discussed in Section 6.2.1.

In $CsCdBr_3$ crystals containing 0.01% Ho^{3+}, transitions belonging to the L

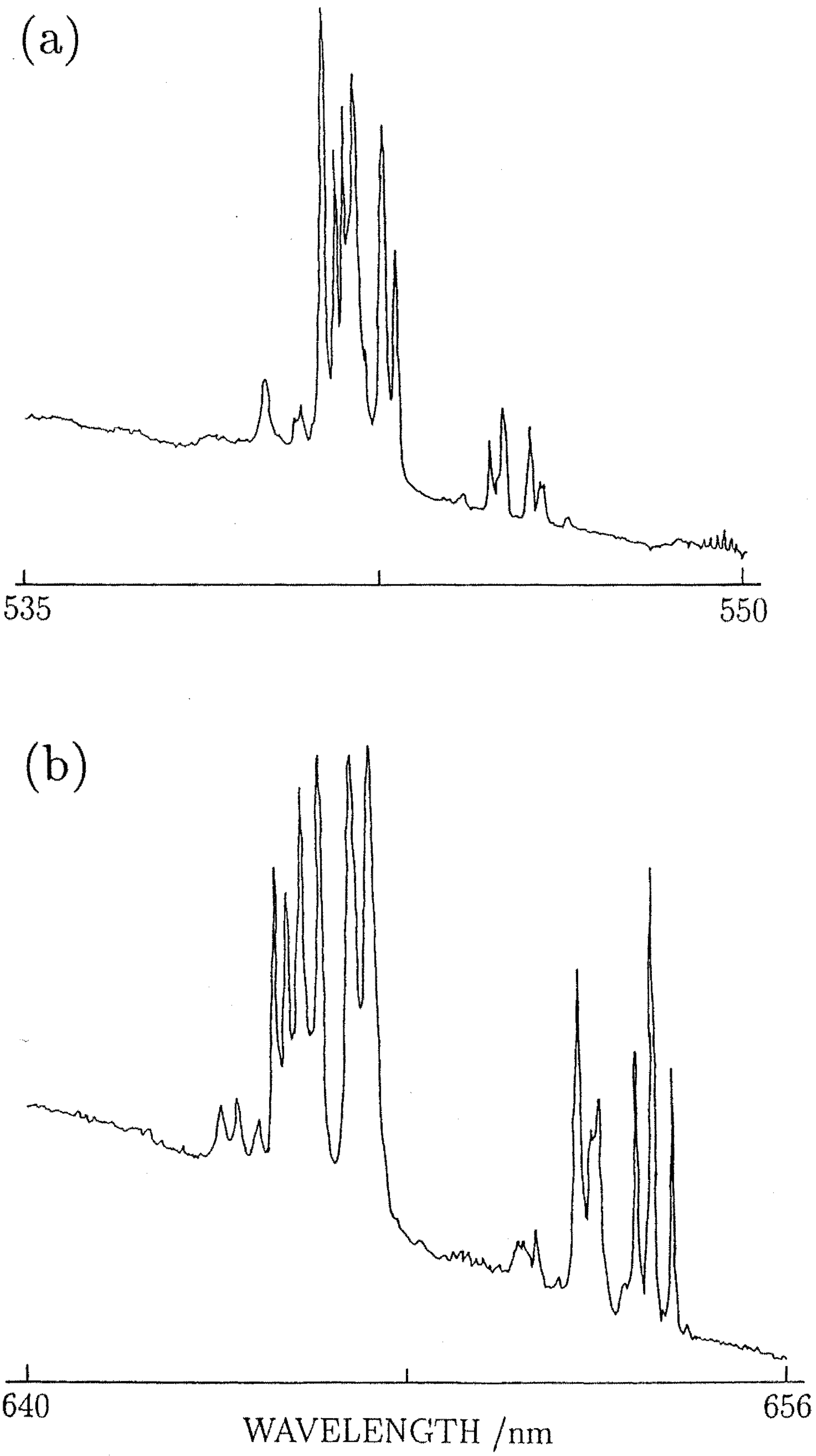

Figure 6.1: 10 K absorption spectra in CsCdBr$_3$:Ho^{3+}(0.3%) crystals :
(a) Z→E transitions;
(b) Z→D transitions.

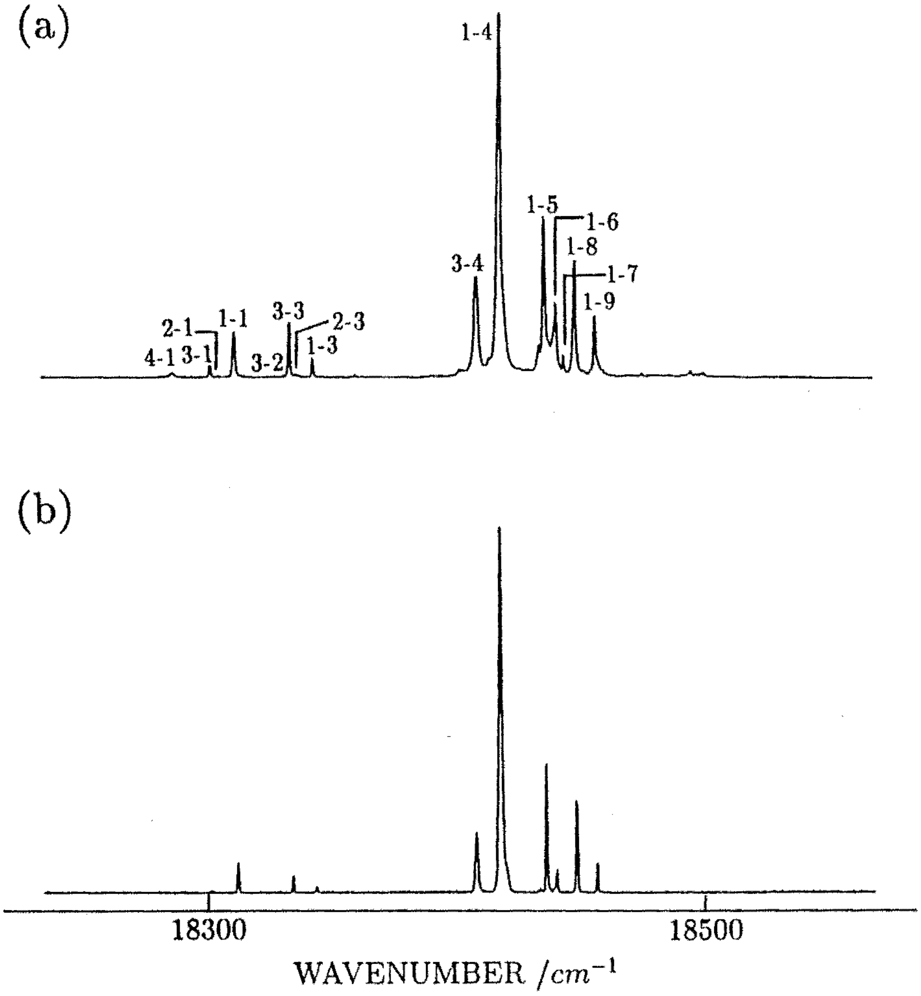

Figure 6.2: 10 K broadband and selective excitation spectra of the E multiplet in <111> oriented $CsCdBr_3:Ho^{3+}$(0.3%) crystals :
(a) broadband excitation spectrum, monitoring all the D→Z transitions;
(b) excitation spectrum for the principal dimer centre, monitoring the $P_1' \to C_1$ transition at 17330.0 cm^{-1}.

Transitions are labelled by the appropriate lower and upper multiplet crystal-field level identifications.

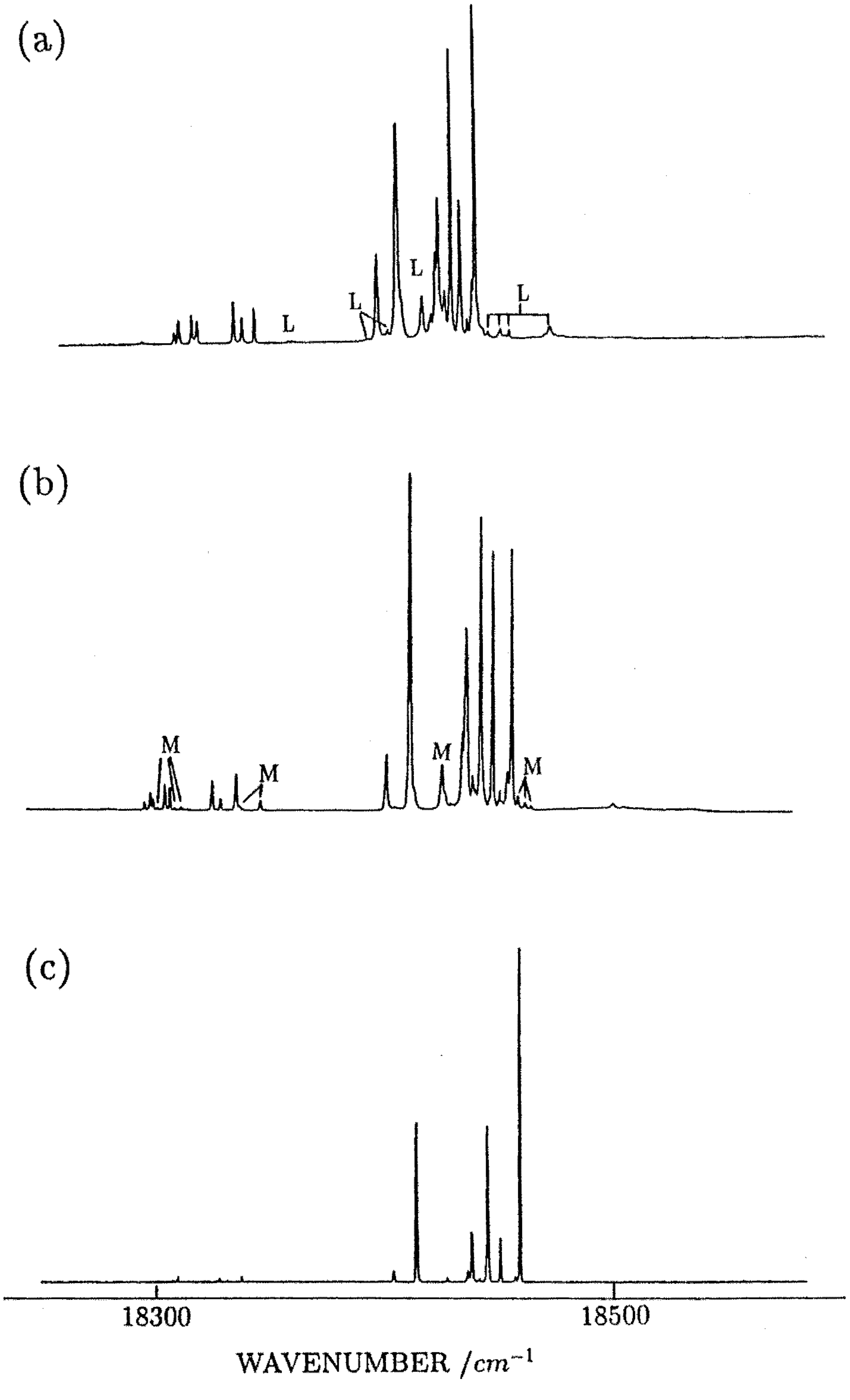

Figure 6.3: 10 K broadband excitation spectra of the E multiplet in unoriented CsCdBr$_3$:Ho^{3+}(0.3%) and CsCdBr$_3$(0.01%) crystals, monitoring all the D→Z transitions :
(a) broadband spectrum in unoriented CsCdBr$_3$:Ho^{3+}(0.3%) crystals showing the L centre transitions;
(b) broadband spectrum in unoriented CsCdBr$_3$:Ho^{3+}(0.01%) crystals showing the M centre transitions;
(c) excitation spectrum of the principal dimer centre in unoriented CsCdBr$_3$:Ho^{3+}(0.01%) crystals, monitoring the $F_1 \rightarrow Z_2$ transition at 20384.5 cm^{-1}.

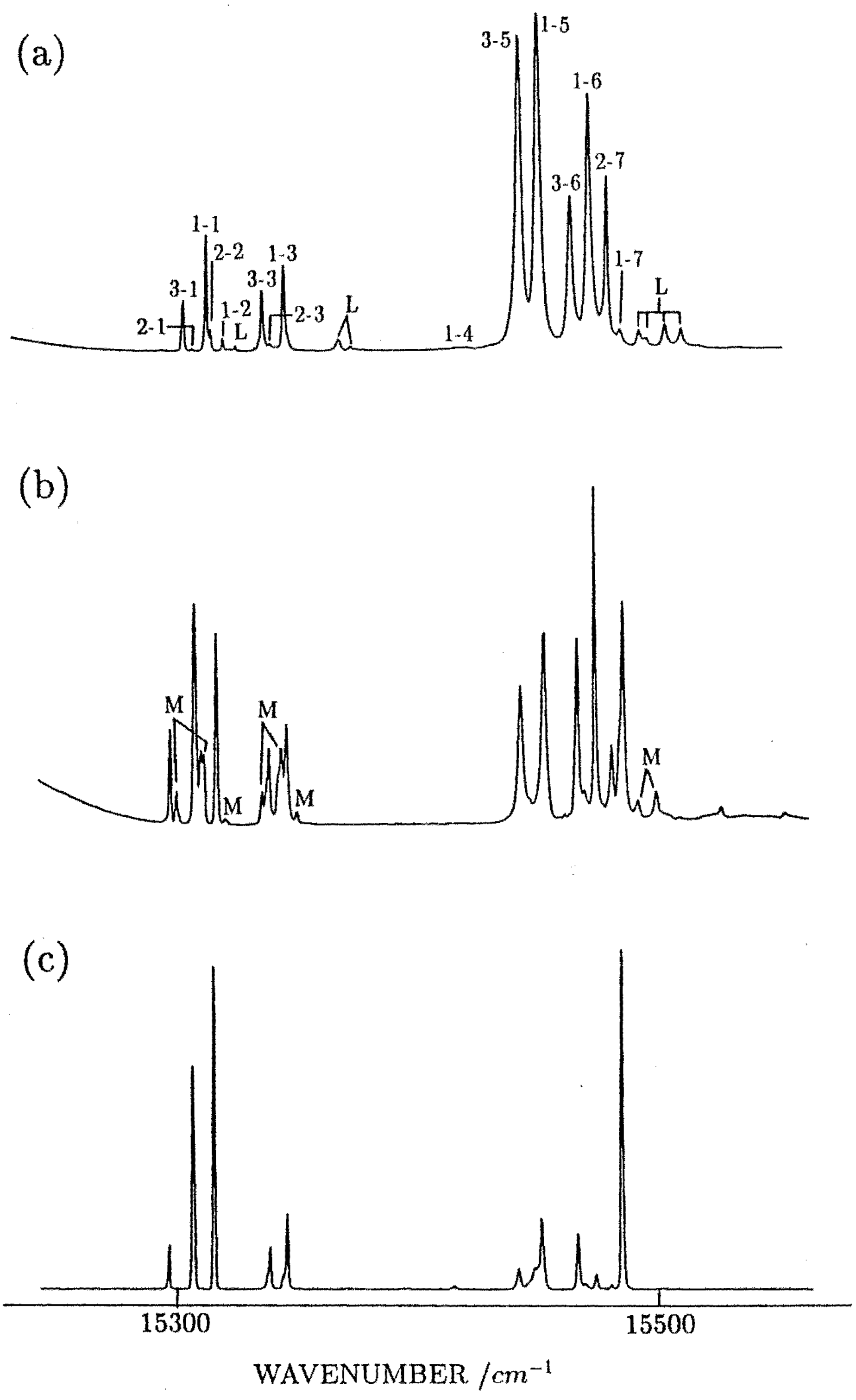

Figure 6.4: 10 K broadband and selective excitation spectra of the D multiplet in $CsCdBr_3:Ho^{3+}$(0.3%) and $CsCdBr_3:Ho^{3+}$(0.01%) crystals :
(a) broadband excitation spectrum in <111> oriented $CsCdBr_3:Ho^{3+}$(0.3%) crystals, monitoring the D→Z transitions;
(b) broadband excitation spectrum in unoriented $CsCdBr_3:Ho^{3+}$(0.01%) crystals, monitoring all the D→Z transitions;
(c) excitation spectrum of the principal dimer centre in unoriented $CsCdBr_3:Ho^{3+}$(0.01%) crystals, monitoring the $F_1 \rightarrow Z_2$ transition at 20384.5 cm^{-1}.

centre, which were clearly present in the 0.1 - 0.3% samples, were wholly absent. Transitions assigned to the dimer centre still dominate while several other new transitions are now apparent. These new transitions occur at quite different energies from those of the L centre and are attributed to another centre, arbitrarily labelled the M centre (Figures 6.3(b) and 6.4(b)), to be discussed in Sections 6.2.2 to 6.2.4.

An additional centre found in $CsCdBr_3$ crystals doubly doped with Ho^{3+} and Na^+ ions which has been arbitrarily labelled the N centre, will be discussed in Section 6.2.5.

Because the lowest three levels of the Z multiplet, Z_1, Z_2 and Z_3, are quite close in energy for all the centres found here, being separated by just 5.5 and 3.5 cm^{-1} respectively for the principal dimer centre, both the absorption and excitation spectra recorded at 10 K show transitions originating from all three levels. At 2 K, transitions from the Z_1 level only were observed. The results presented here are mostly as measured at 10 K since the measurements at 2 K were used just to confirm the lowest energy level and transition assignments for each of the Z, D and E multiplets.

6.1 The Dimer Centre in $CsCdBr_3$:Ho^{3+}(0.3%) Crystals

6.1.1 Spectroscopy of the dimer centre

With excitation of the $Z_1 \rightarrow E_4$ transition at 18416.3 cm^{-1}, thirty groups of fluorescence transitions were observed in the 11000 - 30000 cm^{-1} spectral range accessible with the Spex 1403 double monochromator used here. In some cases, such as for the $D \rightarrow Z$ and $F \rightarrow Y$ transitions, there was some overlap of transitions between the different multiplet pairs. Analysis of such spectra was aided by comparison with other transitions from different upper multiplets to the same lower multiplet. Energy levels up to the 35522.5 cm^{-1} (U_2) level of the $^3F_2$ multiplet were derived. The small splittings apparent on some of the observed transitions will be discussed in Section 6.1.2.

For excitation of the $Z_1 \rightarrow D_5$ transition at 15442.2 cm^{-1}, the same fluorescence spectra as for $Z \rightarrow E$ excitation were obtained, except for the absence of any transitions from the U ($^3F_2$) multiplet. This is to be expected as energy transfer between the two ions of a dimer centre, for $Z \rightarrow D$ excitation, would not be sufficient to reach the U multiplet energy levels at about 35500 cm^{-1}, which is more than twice the pump energy.

The fluorescence spectra, labelled with transition assignments between the various multiplets, are presented in Figures 6.5 to 6.11.

Upconversion fluorescence was strong for both $Z \rightarrow E$ and $Z \rightarrow D$ excitation (Table 6.1). In particular, the $F_1 \rightarrow Z_2$ transition was found to be 29% of the intensity of the $E_1 \rightarrow Z_7$ transition for $Z_1 \rightarrow E_4$ excitation and 6.7% of the intensity of the $D_1 \rightarrow Z_{10}$ transition for $Z_1 \rightarrow D_5$ excitation, these being the highest efficiencies measured. Upconversion fluorescence intensities for all the other transitions were found to be less than 2% of either the $E_1 \rightarrow Z_7$ or $D_1 \rightarrow Z_{10}$ transition, which is much lower than those found for the $F_1 \rightarrow Z_2$ transition. In general, overall relative upconversion efficiencies are found to be higher for $Z \rightarrow E$ than for $Z \rightarrow D$ excitation.

The $F_1 \rightarrow Y_5$ transition was about 75% of the intensity of the $D_1 \rightarrow Z_{10}$ transition for $Z_1 \rightarrow E_4$ excitation but only 0.5% of the same transition for $Z_1 \rightarrow D_5$ excitation. The weak intensity observed for $D \rightarrow Z$ excitation (Figure 6.5(a)) is partially accounted for by the lower upconversion efficiency to the F multiplet (29% with $Z \rightarrow E$ excitation and 6.7% with $Z \rightarrow D$ excitation). The intensity ratios of the $F_1 \rightarrow Z_2$ to $F_1 \rightarrow Y_5$ transitions and $E_1 \rightarrow Z_7$ to $E_1 \rightarrow Y_1$ fluorescence transitions are about the same for both excitations.

The two weak transition groups found in the 14000 and 11000 cm^{-1} regions (Figure 6.12) remain unassigned. These transitions could be from some higher energy multiplets which were not identified in this study. It is not clear though as to what the terminating multiplets could be because the energy separations of the transitions in both groups do not resemble separations between the energy levels

Table 6.1: Relative intensities of peak transitions in the fluorescence spectra of the principal dimer centre in <111> oriented $CsCdBr_3$:Ho^{3+}(0.3%) crystals, as measured at 10 K with excitation of the $Z_1 \rightarrow E_4$ and $Z_1 \rightarrow D_5$ transitions respectively. Intensities are relative to the $E_1 \rightarrow Z_7$ and $D_1 \rightarrow Z_{10}$ transitions, for excitation to the E and D multiplets respectively.

Transition	**Wavenumber (± 0.5) (cm^{-1})**	**Relative Intensities**	
		$Z_1 \rightarrow E_4$	**$Z_1 \rightarrow D_5$**
$D_1 \rightarrow Z_{10}$	15090.5	26.9	1000
$E_1 \rightarrow Z_7$	18137.0	1000	2.83
$F_1 \rightarrow Z_2$	20384.5	290	67.4
$J_1 \rightarrow Z_5$	23501.5	2.35	0.110
$M_1 \rightarrow Z_{10}$	27030.5	0.0235	-
$E_1 \rightarrow Y_1$	13222.0	950	2.27
$F_1 \rightarrow Y_5$	15207.5	19.6	5.04
$M_1 \rightarrow Y_1$	22154.5	8.54	0.0329
$Q_1 \rightarrow Y_1$	27751.0	0.129	-
$F_1 \rightarrow A_3$	11765.5	1.24	0.0210
$K_1 \rightarrow A_1$	17002.0	1.33	0.0318
$M_2 \rightarrow A_1$	18656.5	0.538	-
$P_1 \rightarrow A_1$	21553.0	2.69	0.0483
$Q_2 \rightarrow A_6$	24166.0	0.172	
$Q_2 \rightarrow B_2$	21676.0	4.24	0.0266
$P'_1 \rightarrow C_1$	17330.0	1.31	0.0262
$Q_2 \rightarrow C_1$	19632.0	4.42	0.0145
$Q_2 \rightarrow D_1$	17540.00	0.956	-
$Q_2 \rightarrow E_1$	14530.5	1.12	0.0214
$U_1 \rightarrow E_1$	17181.5	0.789	-

Figure 6.5: 10 K fluorescence spectra of transitions to the Z multiplet levels for the principal dimer centre in $CsCdBr_3:Ho^{3+}$(0.3%) crystals, for excitation of either the $Z_1 \rightarrow E_4$ transition at 18416.3 cm^{-1} or the $Z_1 \rightarrow D_5$ transition at 15442.2 cm^{-1} :
(a) D→Z transitions (for $Z_1 \rightarrow D_5$ excitation);
(b) E→Z transitions;
(c) F→Z transitions;
(d) J→Z transitions;
(e) K→Z transitions, with the overlapping P′→Y transitions as shown;
(f) M→Z transitions;
(g) O→Z transitions;
(h) P→Z transitions.
Transitions are labelled by the appropriate upper and lower multiplet crystal-field level identifications.

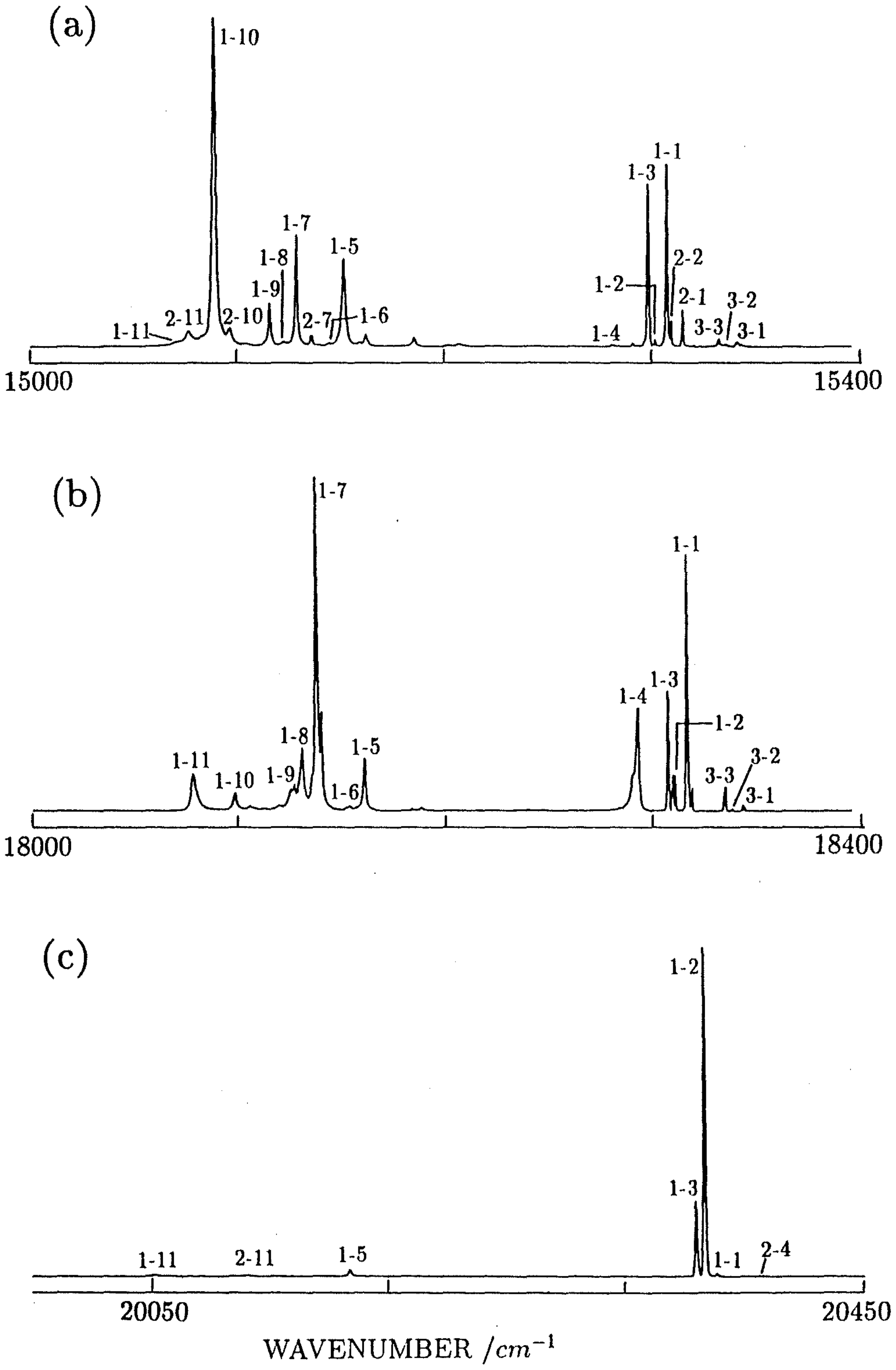
(a)
1-10
1-1
1-3
1-7
1-5
1-8
1-9
2-2
1-2
2-1
3-2
1-6
2-10
2-7
2-11
1-11
3-3
3-1
1-4
15000
15400
(b)
1-7
1-1
1-3
1-4
1-2
1-8
1-5
1-11
3-2
3-3
1-10
1-9
1-6
3-1
18000
18400
(c)
1-2
1-3
1-11
2-11
1-5
1-1
2-4
20050
20450
WAVENUMBER /cm⁻¹

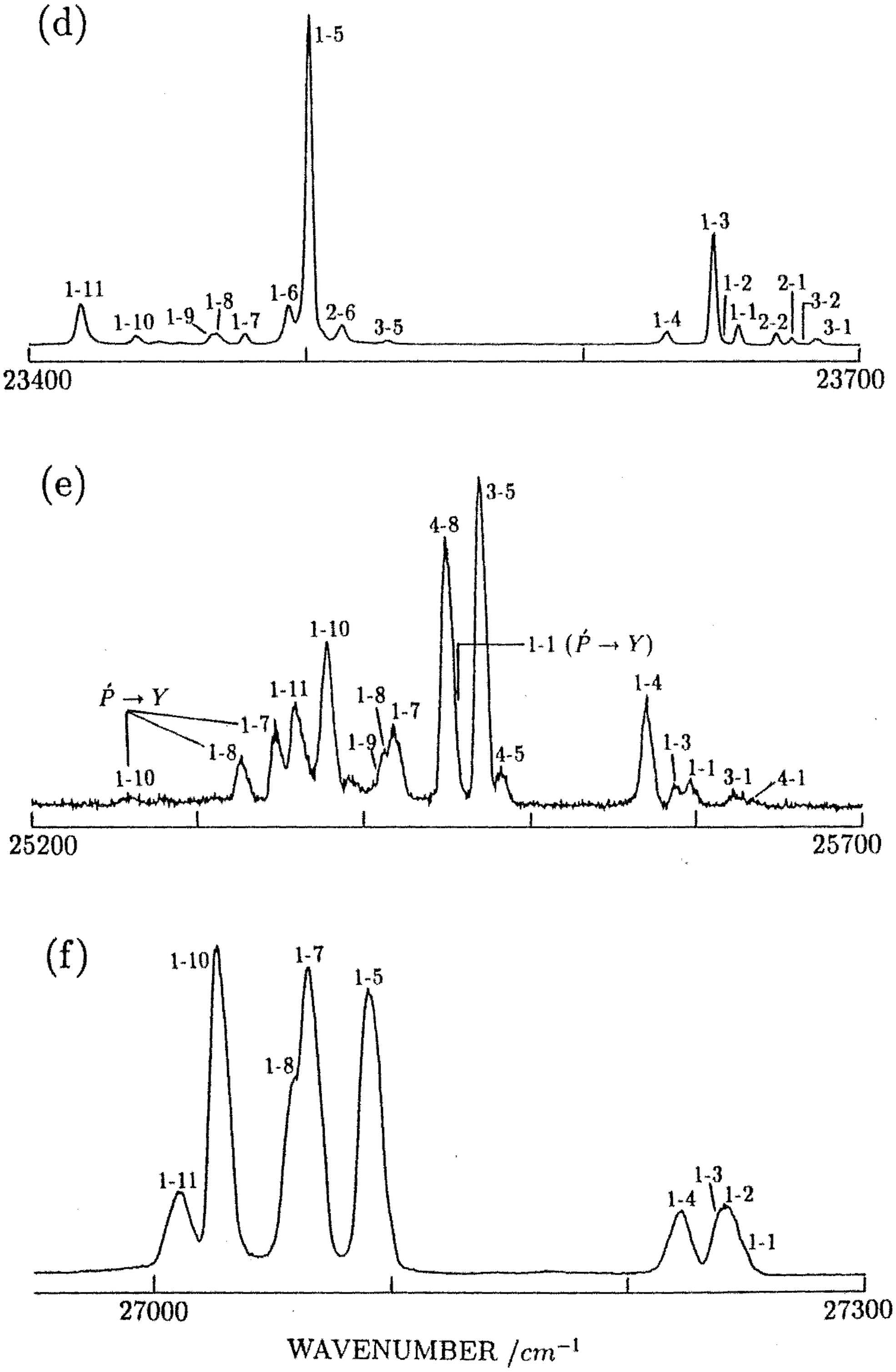
(d)
1-5
1-11
1-10
1-9
1-8
1-7
1-6
2-6
3-5
1-4
1-3
1-2
1-1
2-1
2-2
3-2
3-1
23400
23700
(e)
3-5
4-8
1-1 (Ṕ → Y)
1-10
1-11
Ṕ → Y
1-7
1-8
1-10
1-8
1-7
1-9
4-5
1-4
1-3
1-1
3-1
4-1
25200
25700
(f)
1-10
1-7
1-5
1-8
1-11
1-3
1-4
1-2
1-1
27000
27300
WAVENUMBER /cm⁻¹

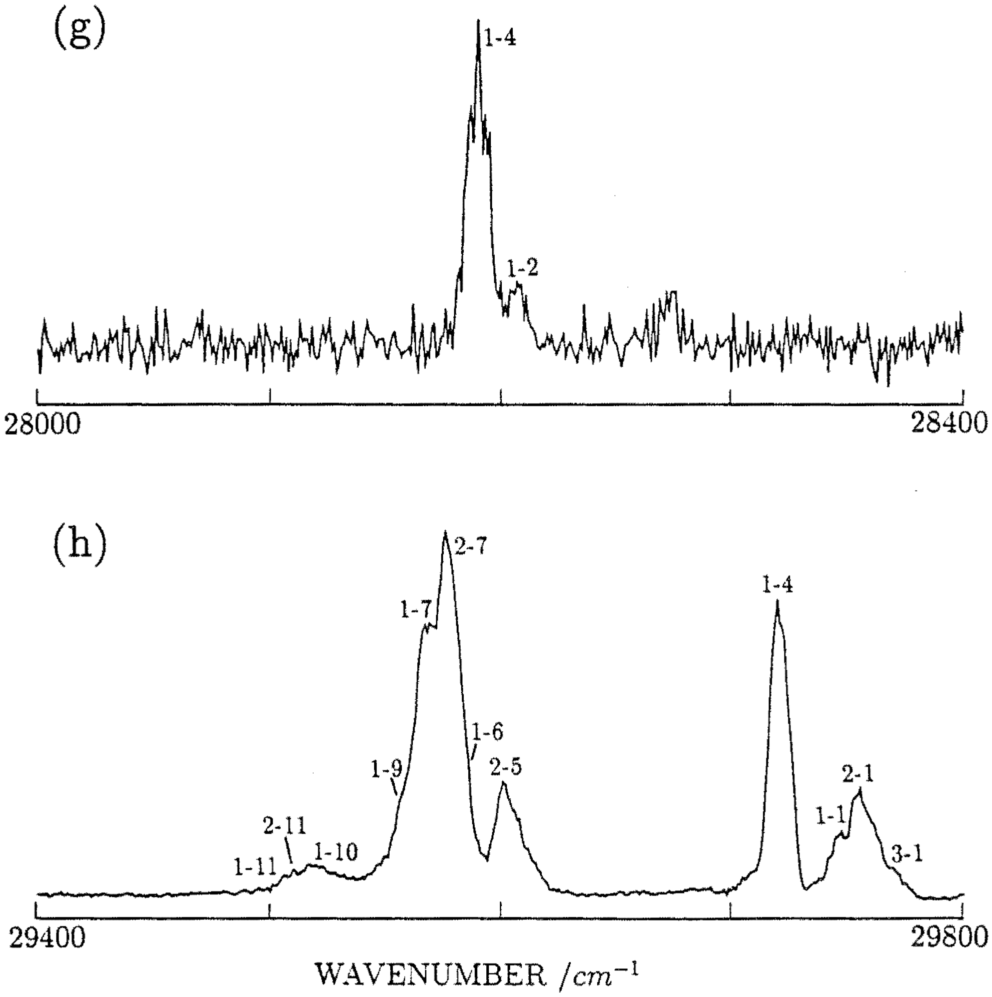
(g)
1-4
1-2
28000
28400
(h)
2-7
1-7
1-4
1-6
1-9
2-5
2-1
1-1
2-11
1-10
1-11
3-1
29400
29800
WAVENUMBER $/cm^{-1}$

Figure 6.6: 10 K fluorescence spectra of transitions to the Y multiplet levels for the principal dimer centre in $CsCdBr_3:Ho^{3+}$(0.3%) crystals, for excitation of either the $Z_1 \rightarrow E_4$ or the $Z_1 \rightarrow D_5$ transition :

(a) E→Y transitions, with the overlapping C→Z transitions as shown;

(b) F→Y transitions, unlabelled transitions are for D→Z as in Figure 6.5(a);

(c) M→Y transitions;

(d) P→Y transitions;

(e) Q→Y transitions.

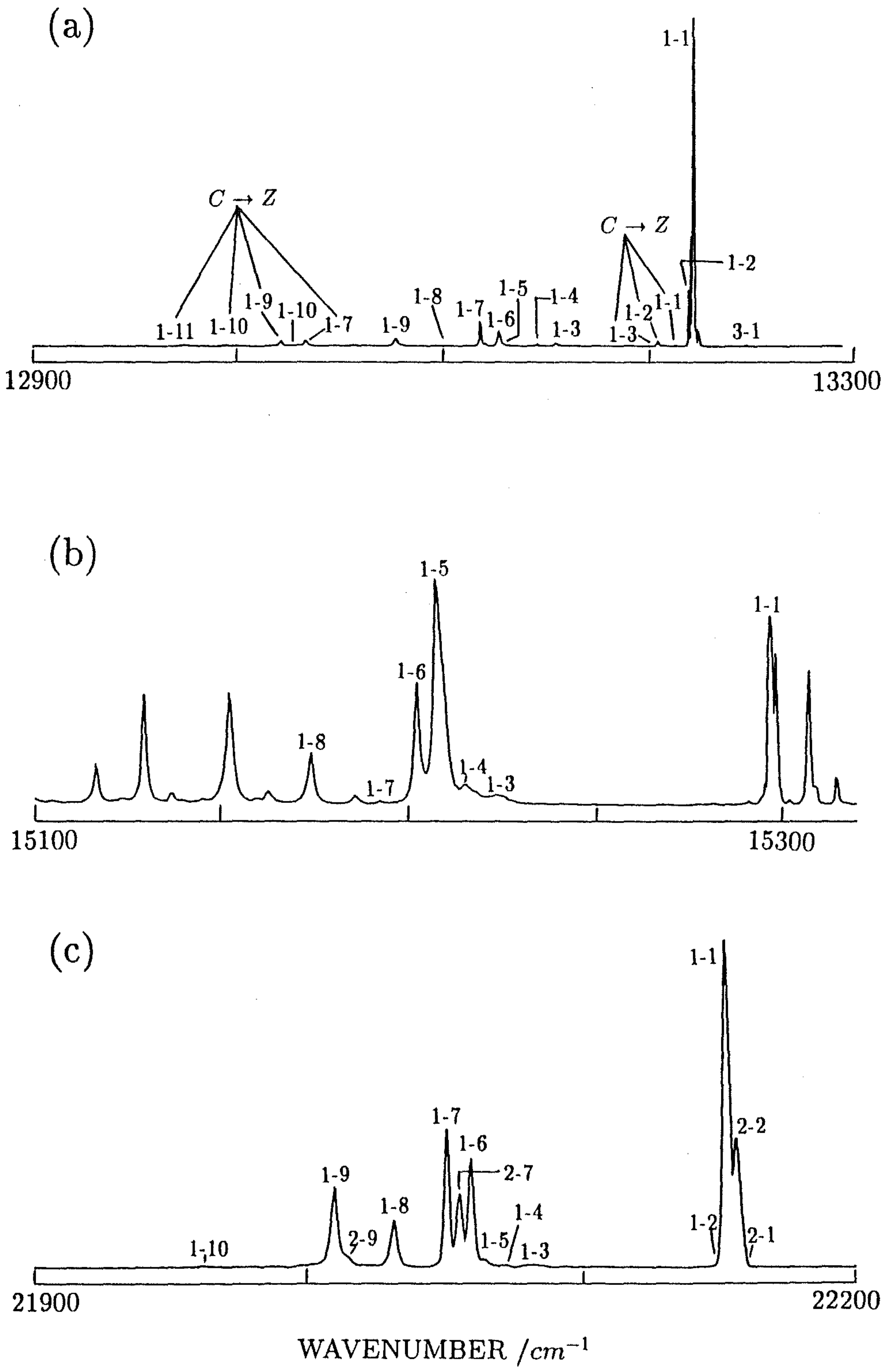
(a)
C → Z
1-11
1-10
1-9
1-10
1-7
1-9
1-8
1-7
1-6
1-5
1-4
1-3
C → Z
1-3
1-2
1-1
1-2
1-1
3-1
12900
13300
(b)
1-5
1-6
1-8
1-7
1-4
1-3
1-1
15100
15300
(c)
1-10
1-9
2-9
1-8
1-7
1-6
2-7
1-5
1-4
1-3
1-1
2-2
1-2
2-1
21900
22200
WAVENUMBER /cm^{-1}

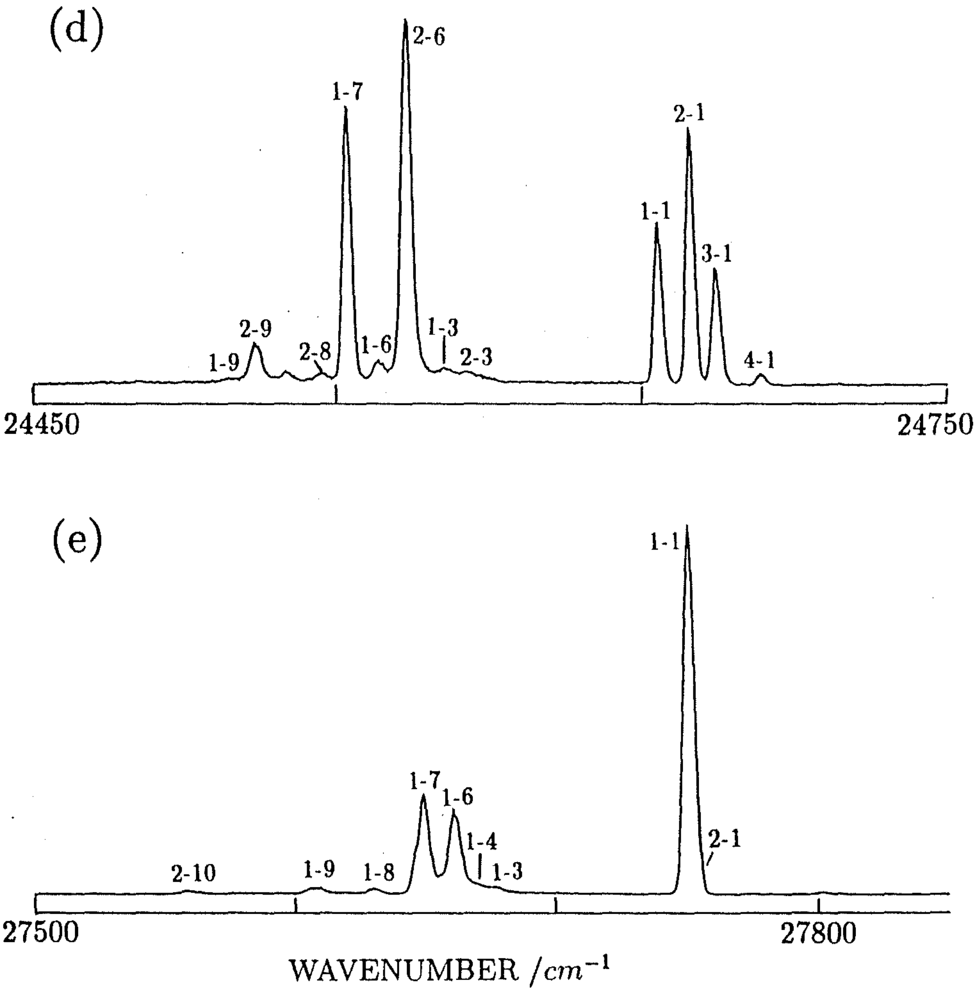
(d)
2-6
1-7
2-1
1-1
3-1
2-9
1-9
2-8
1-6
1-3
2-3
4-1
24450
24750
(e)
1-1
1-7
1-6
1-4
2-1
2-10
1-9
1-8
1-3
27500
27800
WAVENUMBER /cm⁻¹

of any of the multiplets identified here. The group in the 11600 - 11000 cm^{-1} region extends below 11000 cm^{-1} which is the limit of the spectrometer used here. The spectrum for the group of transitions in the 14100 - 13300 cm^{-1} region, as shown in Figure 6.12(a), in general resembles the spectra reported for Sm^{2+} ions in CaF$_2$, SrF$_2$ and BaF$_2$ crystals [130]. It is therefore possible that some of the broader transitions in this region are due to Sm^{2+} ions. A study of CsCdBr$_3$:Sm^{2+} crystals would help establish whether or not any of these transitions are due to Sm^{2+} ions, as trace amounts of Sm^{2+} are often present in the starting rare-earth materials for growing crystals.

The energy levels derived for the Ho^{3+} dimer centre are presented in Table 6.2. A total of 86 levels for 18 multiplets have been identified. Most of the multiplets below 35000 cm^{-1} have been found to be originating multiplets for fluorescence transitions and this is possible because the low phonon energies of up to 163 cm^{-1} for CsCdBr$_3$ [96], compared to 465 cm^{-1} for CaF$_2$ [38] and 360 cm^{-1} for SrF$_2$ [112], result in less non-radiative quenching between close-lying multiplets. As most of the Ho^{3+} multiplets are separated by at least 2000 cm^{-1}, it would require about twenty phonons to bridge such an energy gap during multiphonon assisted decay. Decay processes requiring many phonons are quite improbable. It has been found, for the principal Nd^{3+} dimer centre [11], that only multiplets lying within 1000 cm^{-1} of each other are appreciably populated by multiphonon relaxation processes.

With an energy gap of 3000 cm^{-1} between the E and D multiplets of Ho^{3+}, the population of the D multiplet following Z → E excitation is not through multiphonon relaxation but by energy transfer between the two ions of a dimer centre. Considering the two equivalent Ho^{3+} ions of a centre, both absorb a 18416.3 cm^{-1} photon (pump transition) and may relax to the lowest level E$_1$ of the E multiplet at 18315.2 cm^{-1}. Energy transfer occurs in such a way that one ion loses some 3000 cm^{-1} of energy and the other gains about a similar amount. After this transfer, the donor Ho^{3+} ion will be in the excited D multiplet while the

Figure 6.7: 10 K fluorescence spectra of transitions to the A multiplet levels for the principal dimer centre in $CsCdBr_3:Ho^{3+}$(0.3%) crystals, for excitation of either the $Z_1 \rightarrow E_4$ or the $Z_1 \rightarrow D_5$ transition :
(a) F→A transitions;
(b) H→A transitions;
(c) J→A transitions, unlabelled transitions are for D→Z as in Figure 6.5(a);
(d) K→A transitions;
(e) M→A transitions;
(f) P→A transitions, with the overlapping H→Z transitions as shown;
(g) Q→A transitions;
(h) U→A transitions (for $Z_1 \rightarrow E_4$ excitation).

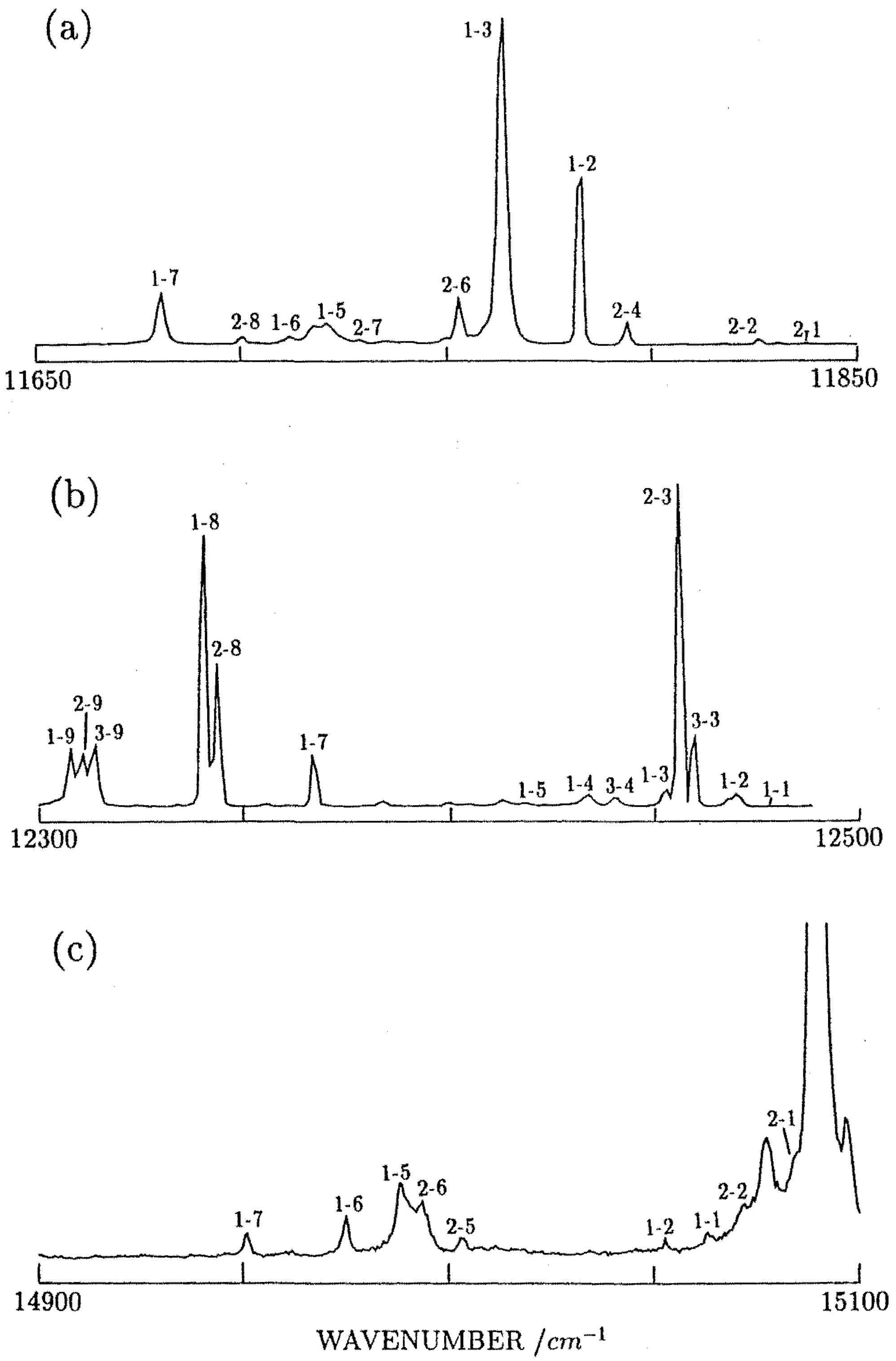
(a)
1-3
1-2
1-7
2-6
2-8
1-6
1-5
2-7
2-4
2-2
2-1
11650
11850
(b)
1-8
2-8
2-9
1-9
3-9
1-7
2-3
3-3
1-5
1-4
3-4
1-3
1-2
1-1
12300
12500
(c)
2-1
2-2
1-5
2-6
1-6
1-7
2-5
1-2
1-1
14900
15100
WAVENUMBER /cm^{-1}

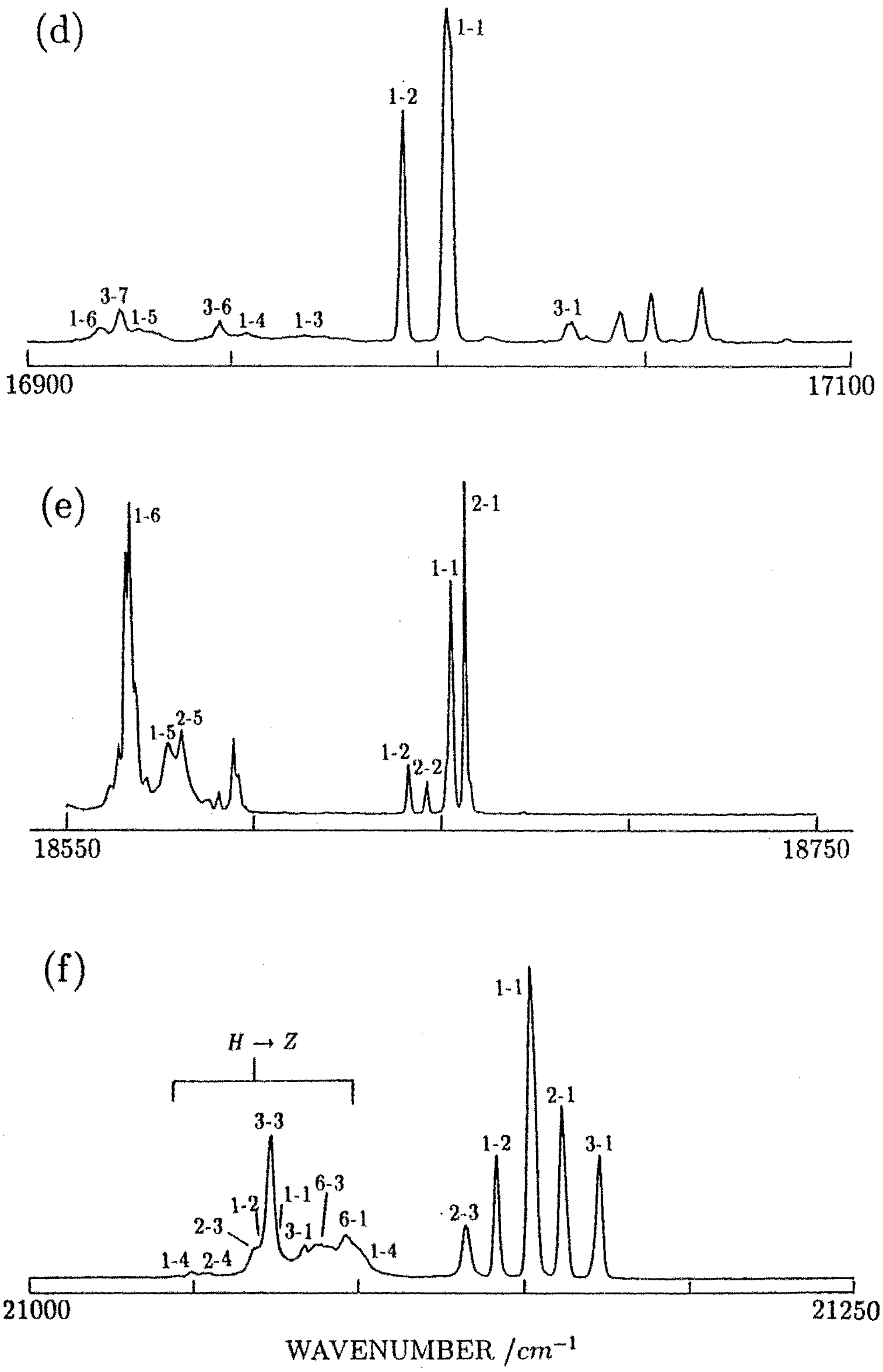
(d)
1-1
1-2
1-6
3-7
1-5
3-6
1-4
1-3
3-1
16900
17100
(e)
1-6
2-1
1-1
1-5
2-5
1-2
2-2
18550
18750
(f)
1-1
H → Z
2-1
3-3
1-2
3-1
1-1
6-3
1-2
2-3
3-1
6-1
2-3
1-4
2-4
1-4
21000
21250
WAVENUMBER /cm⁻¹

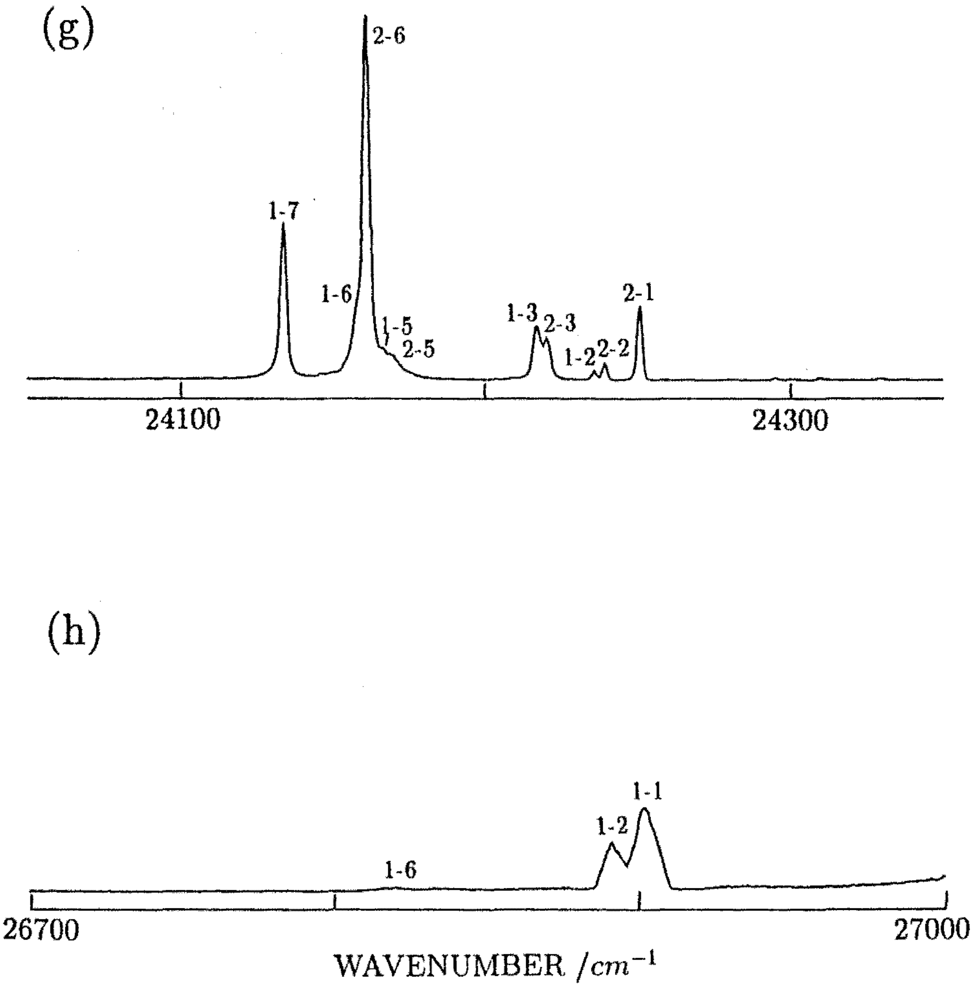
(g)
2-6
1-7
1-6
1-5
2-5
1-3
2-3
1-2
2-2
2-1
24100
24300
(h)
1-1
1-2
1-6
26700
27000
WAVENUMBER /cm⁻¹

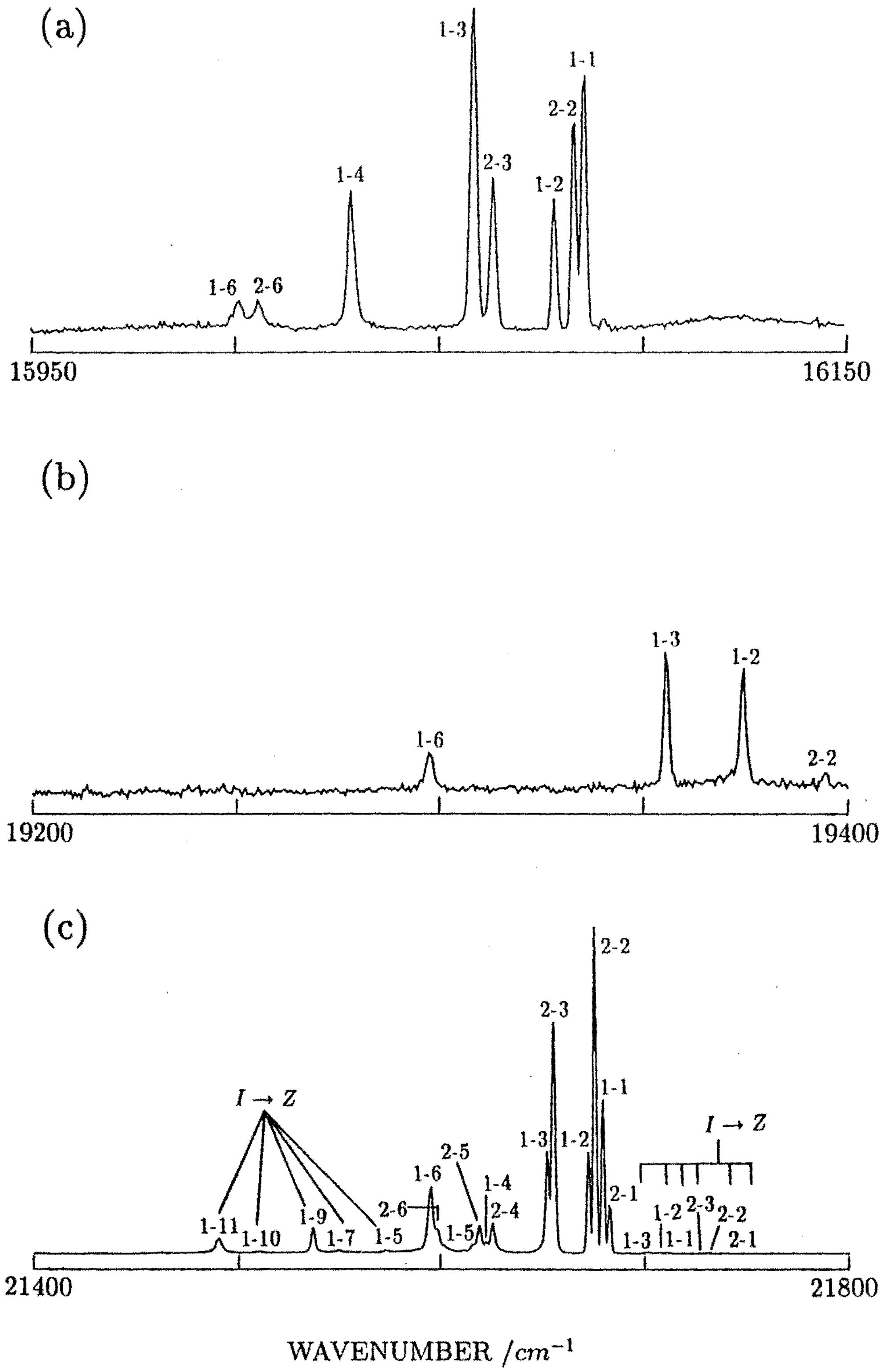

Figure 6.8: 10 K fluorescence spectra of transitions to the B multiplet levels, for the principal dimer centre in $CsCdBr_3:Ho^{3+}$(0.3%) crystals, for excitation of either the $Z_1 \to E_4$ or the $Z_1 \to D_5$ transition :
(a) M→B transitions;
(b) P′→B transitions;
(c) Q→B transitions, with the overlapping I→Z transitions as shown.

acceptor Ho^{3+} ion can be in either of the higher energy $H(^3K_8)$ or $I(^5G_6)$ multiplets. This would account for the fluorescence observed from all three multiplets, D, H and I.

The F multiplet would be populated through multiphonon relaxation from either the H or I multiplets as they are relatively close-lying. There are minimal non-radiative decay processes from the F multiplet to the next E multiplet as this latter multiplet lies about 2000 cm^{-1} lower in energy than the F multiplet. Because of the weak quenching processes in $CsCdBr_3$, the fluorescence from the F multiplet is expected to be quite strong while that from either the H or the I multiplets is relatively weak, as observed. Further evidence of this particular decay process is in the observation of the same rise time for monitoring both the $D_1 \rightarrow Z_{10}$ and the $F_1 \rightarrow Z_2$ fluorescence transitions (Chapter 8).

Similar decay channels that explain the observation of fluorescence from higher energy levels than those excited include :

$[E ; E] \longrightarrow [C ; J]$
$[E ; E] \longrightarrow [B ; K]$
$[E ; E] \longrightarrow [A ; O, M]$
$[E ; E] \longrightarrow [Y ; P', P]$
$[E ; E] \longrightarrow [Z ; U]$

where the first set of brackets shows the initial state of the two Ho^{3+} ions of the pair and the second set shows the final states of the same two Ho^{3+} ions after the energy transfer. Other non-radiative relaxation processes are also possible.

For the particular $[E ; E] \longrightarrow [A ; O, M]$ process above, the actual energy transfer involves the A and O multiplets only in the final state. The M multiplet would be populated by later multiphonon relaxation since there is an energy separation of only about 965 cm^{-1} between the M and O multiplets. Fluorescence from the O multiplet was found to be much weaker than that from the M multiplet, consistent with substantial non-radiative decay from it to the lower-lying M multiplet. Similarly for the $[E ; E] \longrightarrow [Y ; P', P]$ process, the energy transfer

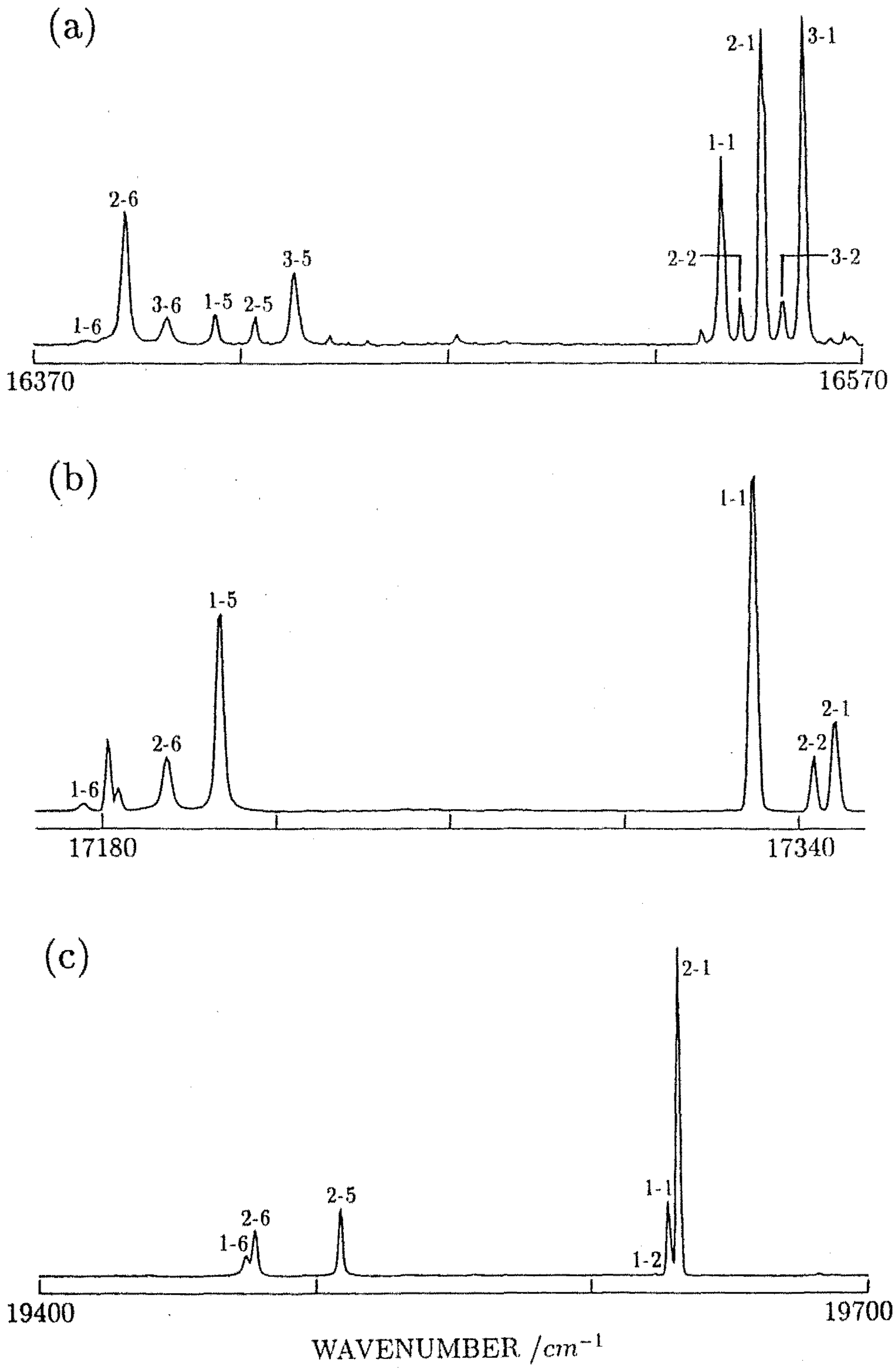

Figure 6.9: 10 K fluorescence spectra of transitions to the C multiplet levels for the principal dimer centre in CsCdBr$_3$:Ho^{3+}(0.3%) crystals, for excitation of either the $Z_1 \rightarrow E_4$ or the $Z_1 \rightarrow D_5$ transition :
(a) P→C transitions;
(b) P′→C transitions, unlabelled transitions are for U→E as in Figure 6.11(c);
(c) Q→C transitions.

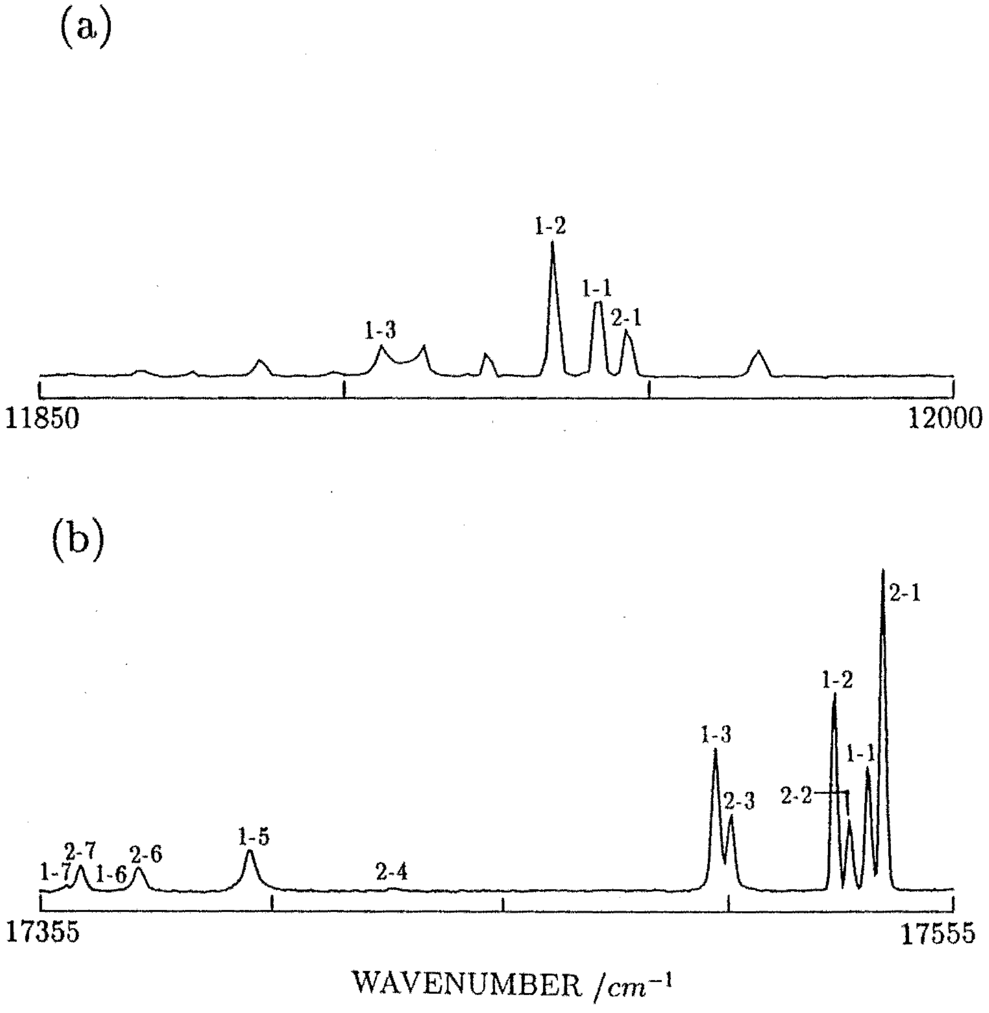

Figure 6.10: 10 K fluorescence spectra of transitions to the D multiplet levels, for the principal dimer centre in $CsCdBr_3:Ho^{3+}$(0.3%) crystals, for excitation of either the $Z_1 \rightarrow E_4$ or the $Z_1 \rightarrow D_5$ transition :
(a) M→D transitions;
(b) Q→D transitions.

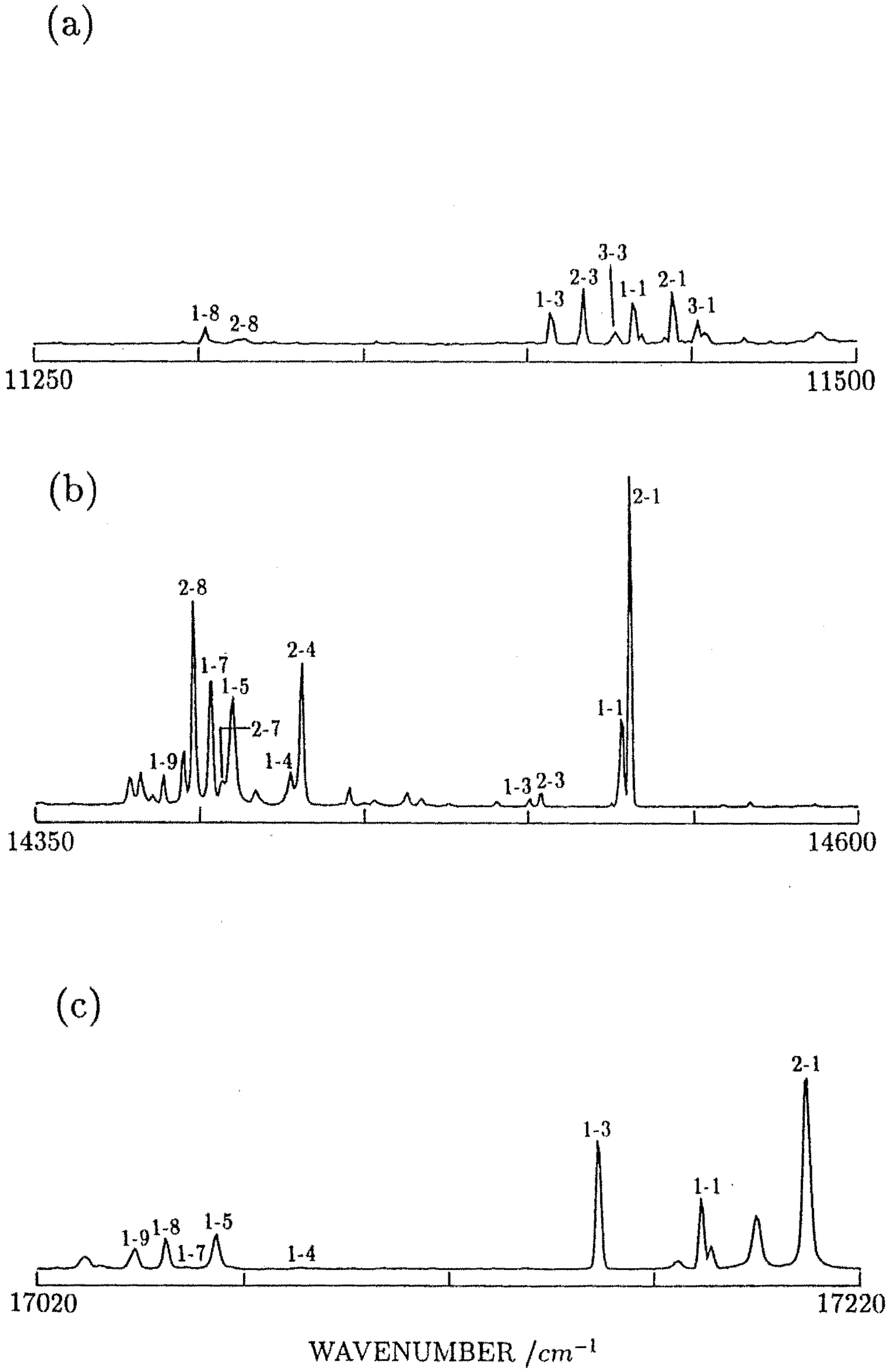

Figure 6.11: 10 K fluorescence spectra of transitions to the E multiplet levels, for the principal dimer centre in CsCdBr$_3$:Ho^{3+}(0.3%) crystals, for excitation of either the $Z_1 \to E_4$ or the $Z_1 \to D_5$ transition :
(a) $P \to E$ transitions;
(b) $Q \to E$ transitions;
(c) $U \to E$ transitions (for $Z_1 \to E_4$ excitation), unlabelled transitions are for $P' \to C$ as in Figure 6.9(b).

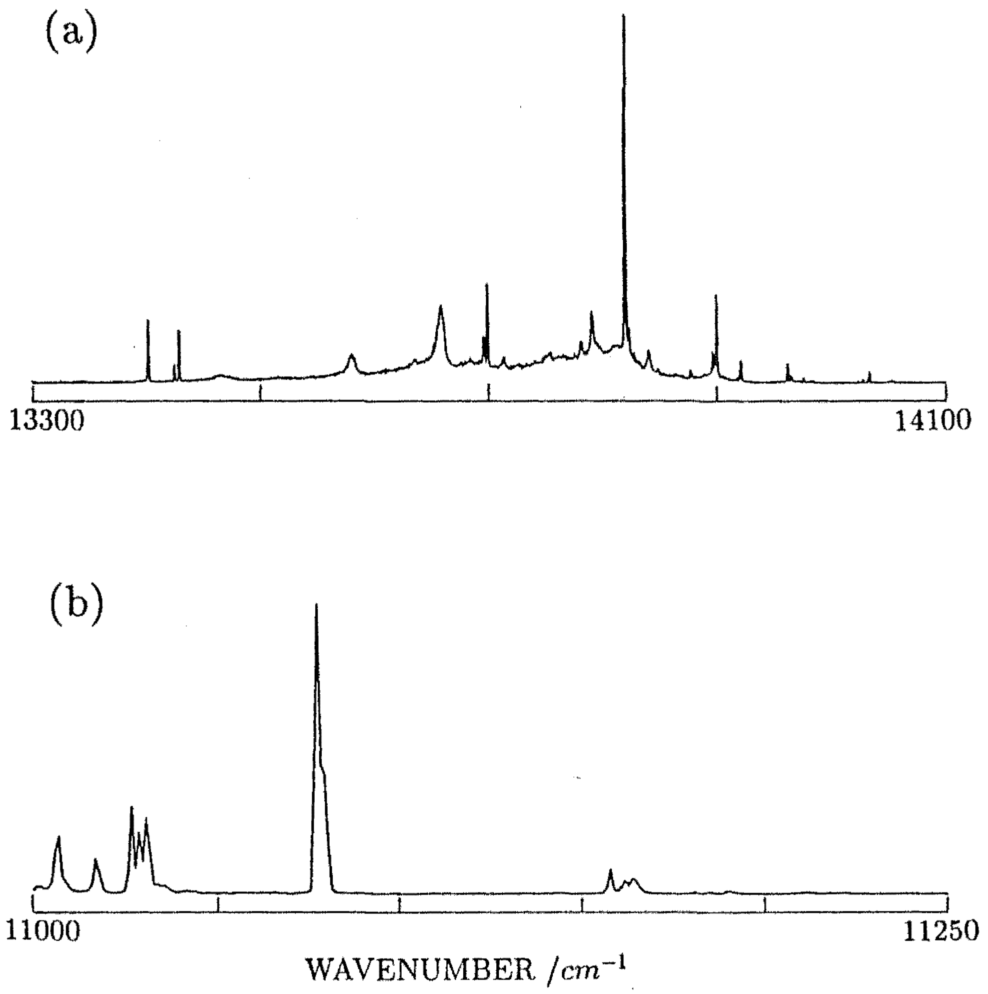

Figure 6.12: Unassigned fluorescence transitions observed for excitation of either the $Z_1 \rightarrow E_4$ or the $Z_1 \rightarrow D_5$ transition of the principal dimer centre in $CsCdBr_3:Ho^{3+}$(0.3%) crystals.

involves only the Y and P′ multiplets. As the P multiplet, being only 800 cm^{-1} lower in energy than the P′ multiplet is fed by multiphonon relaxation, the fluorescence from the P′ multiplet is expected to be weaker than that from the P multiplet, as observed. The [E ; E] ⟶ [Z ; U] process involves the Z and V ($^3G_5$) multiplets initially, followed by a subsequent relaxation to the U multiplet. In this case, fluorescence by transitions originating from the V multiplet was not observed.

Using the same analysis some of the possible relaxation pathways for the alternative Z → D excitation are :

[D ; D] ⟶ [A ; I, H, F]
[D ; D] ⟶ [Z ; P′, P]
[D ; D] ⟶ [Y ; K]
[D ; D] ⟶ [B ; E]

In identifying possible decay channels, the particular process resulting in the population of the Q multiplet at ~32850 cm^{-1} appears to be special and more complicated than any of the above. In the first instance, this Q multiplet being at ~32850 cm^{-1} had not been expected to fluoresce at all with Z → D excitation, as 30900 cm^{-1} is the upper limit for upconversion from a simple dimer pair ion interaction. Fluorescence from the Q multiplet to the Y, A, B, C, D and E multiplets was observed for both Z → E and Z → D excitations. There appears to be no direct way of populating the Q multiplet from excitation of just two Ho^{3+} ions especially with the single frequency laser excitation carried out here. From energy considerations, one requires at least an ion in an E multiplet level to interact with another in a D multiplet level, as upconversion in this case would result in the donor ion relaxing to the ground multiplet while the acceptor ion is excited to either the R or the S multiplets at about 33600 cm^{-1}. Multiphonon relaxation could then lead to the population of the Q multiplet just 800 cm^{-1} lower in energy than the R multiplet. Although there is no direct way for the [E ; E] ⟶ [D ; E] or the [D ; D] ⟶ [D ; E] decay processes to occur, the

Table 6.2 : Energy levels (in cm^{-1}) for 18 multiplets of the principal dimer centre and their symmetries, as derived from the 2 K and 10 K spectra of $CsCdBr_3:Ho^{3+}$ (0.3%) crystals. Uncertainty is ± 0.5 cm^{-1}.

Level	$Z(^5I_8)$	$Y(^5I_7)$	$A(^5I_6)$	$B(^5I_5)$	$C(^5I_4)$	$D(^5F_5)$	$E(^5S_2, {}^5F_4)$
1	0.0(γ_3)	5092.8(γ_3)	8595.5(γ_1)	11164.0(γ_2)	13215.5(γ_3)	15307.5(γ_3)	18315.2(γ_3)
2	5.5(γ_2)	5095.0(γ_1)	8606.0(γ_3)	11171.5(γ_3)	13221.0(γ_2)	15314.5(γ_2)	18340.5(γ_1)
3	9.0(γ_3)	5166.0(γ_3)	8624.5(γ_2)	11191.5(γ_3)	-	15341.5(γ_3)	18342.5(γ_3)
4	26.0(γ_1)	5174.0(γ_2)	8641.0(γ_1)	11221.5(γ_3)	-	15411.5(γ_1)	18416.3(γ_3)
5	155.0(γ_3)	5182.5(γ_2)	8670.5(γ_3)	11227.5(γ_2)	13338.0(γ_1)	15442.2(γ_3)	18434.9(γ_3)
6	162.0(γ_3)	5187.0(γ_3)	8681.5(γ_3)	11248.5(γ_3)	13369.5(γ_3)	15471.0(γ_3)	18439.2(γ_1)
7	178.0(γ_3)	5195.5(γ_3)	8708.0(γ_2)			15483.0(γ_2)	18443.1(γ_2)
8	188.5(γ_1)	5215.0(γ_2)	8735.5(γ_3)				18448.2(γ_1)
9	190.5(γ_1)	5236.5(γ_3)	8768.5(γ_1)				18457.2(γ_3)
10	217.0(γ_2)	5285.5(γ_1)					
11	237.0(γ_3)						

Cont....

Table 6.2 (p.2) cont....

Level	**F($^5F_3$)**	**H($^3K_8$)**	**I($^5G_6$)**	**J($^5G_5$)**	**K($^5G_4$)**	**M($^3H_5$)**	**O($^5G_3$)**
1	20390.0(γ_2)	21076.5(γ_3)	21727.5(γ_3)	23656.5(γ_3)	25597.0(γ_3)	27247.5(γ_3)	28214.0(γ_3)
2	20435.0(γ_3)	21079.5(γ_1)	21738.0(γ_2)	23675.5(γ_2)	-	27251.5(γ_1)	
3		21083.5(γ_3)		23684.0(γ_3)	25626.5(γ_3)		
4		-			-		
5		-			25637.5(γ_3)		
6		21096.5(γ_3)					

Cont...

Table 6.2 (p.3) cont....

Level	**$P(^3K_6)$**	**$P'(^3D_2)$**	**$Q(^3D_3)$**	**$U(^3F_2)$**
1	29748.5(γ_1)	30546.0(γ_1)	32844.0(γ_2)	35499.0(γ_3)
2	29758.0(γ_3)	30564.5(γ_3)	32847.5(γ_3)	35522.5(γ_1)
3	29769.0(γ_3)		32866.0(γ_1)	
4	29786.0(γ_2)		32894.0(γ_3)	
5	29806.5(γ_2)			

[D ; E] $\longrightarrow$ [Z ; Q] process seems to be the only reasonable one that can account for the observed fluorescence from the Q multiplet. One possibility is that two sets of pairs of Ho^{3+} ions are involved in getting the two Ho^{3+} ions in a dimer from either of the two excited states (E or D) to the [D ; E] stage required to account for emission from the Q multiplet. Two laser excitation experiments and concentration dependence studies would help verify whether or not such complex double ion pair processes do occur. Another possibility is that since the fluorescence lifetime of the F multiplet is about half the fluorescence lifetimes of the E and D multiplets (Chapter 8), the acceptor ion in the F multiplet (from the [E ; E] $\longrightarrow$ [D ; F] scheme above) could decay to the ground state and be re-excited to the E multiplet whilst the donor ion is still in the D multiplet, giving a hetero-excited pair. In this way the ions in the E and D multiplets are from the same pair but in different excited states and co-operative upconversion would give either ion the required energy to reach the Q multiplet. This is possible since the lifetimes of fluorescence transitions from both the D and E multiplets are comparatively long and quite similar. This upconversion process would be independent of which of the two multiplets E or D is being excited provided the lifetime of the fluorescence from the intermediate B multiplet (for the [D ; D] $\longrightarrow$ [B ; E] scheme) is relatively shorter than that for the E multiplet. These two possibilities will be further discussed in Section 6.3.

6.1.2 Splittings on some sharp transitions of the Ho^{3+} dimer centre

Two different kinds of splittings were observed in the $CsCdBr_3$:Ho^{3+} spectra. These have been classified as either low symmetry crystal-field splittings or pair splittings depending on whether they are greater or less than 0.5 cm^{-1} respectively, and will be discussed in turn :

(a) Low symmetry splittings

Ho^{3+} ions in centres of C_{3v} symmetry have energy levels necessarily transforming as one of the irreps γ_1, γ_2 or γ_3 of the C_{3v} group, with the γ_1 and γ_2 irreps being of single dimension while the γ_3 irrep is of double dimension. Any change in the crystal field around the Ho^{3+} ion from exact C_{3v} symmetry would split the γ_3 (doublet) levels, thereby removing the degeneracy. Splittings resulting from such lifting of the γ_3 type level degeneracy have been termed low symmetry crystal-field splittings and have been used to identify the parent C_{3v} symmetry γ_3 type levels for the Ho^{3+} dimer centre.

As can be seen from the spectra in Figures 6.13 to 6.16, the observed splittings range in magnitude from 1.2 cm^{-1} to 2.5 cm^{-1}. Specific cases will now be discussed in turn :

(i) *Transitions between the E and Z multiplet levels*

From the $Z \rightarrow E$ excitation spectra (Figure 6.13), splittings of 2.5 cm^{-1}, 1.6 cm^{-1} and 1.9 cm^{-1} can be seen on the $Z_1 \rightarrow E_1$, $Z_1 \rightarrow E_5$ and $Z_1 \rightarrow E_9$ transition lines respectively (Figure 6.13 (b) and (e)). In each case, one component of the split transition is purely σ polarised while the other is nearly π polarised. For the E_1 and E_5 energy levels, the σ polarised component is the higher energy member of the pair while for the E_9 energy level, the σ polarised component is of lower energy than the π component.

As the $Z_1 \rightarrow E_3$ and $Z_1 \rightarrow E_4$ transitions are broad, they cannot be expected to show any resolvable splittings. With the spectral resolution limit being set at 0.5 cm^{-1} by the linewidth of the laser, splittings of less than 1 cm^{-1} could not be observed in the excitation spectra. The fact that transitions to the E_3 and E_4 levels are broad could be taken as an indication of the presence of incipient splittings approaching 1 cm^{-1}.

In the fluorescence spectra (Figure 6.14), transitions from the E_1 level to the Z_1, Z_3, Z_4, Z_5, Z_7, Z_8, Z_9 and Z_{11} levels all show a common splitting measured to be 2.5 cm^{-1} while the $E_1 \rightarrow Z_6$ transition (Figure 6.14(c)) has a smaller splitting of 1.3 cm^{-1}. The $E_1 \rightarrow Z_2$ and $E_1 \rightarrow Z_{10}$ transitions (Figure 6.14 (a) and (e)) do not show any splittings at all, with the two transitions being purely σ polarised.

Of the nine $E_1 \rightarrow Z$ transitions showing splittings, the lower energy components of the $E_1 \rightarrow Z_4$, $E_1 \rightarrow Z_8$ and $E_1 \rightarrow Z_9$ transitions (Figure 6.14 (b) and

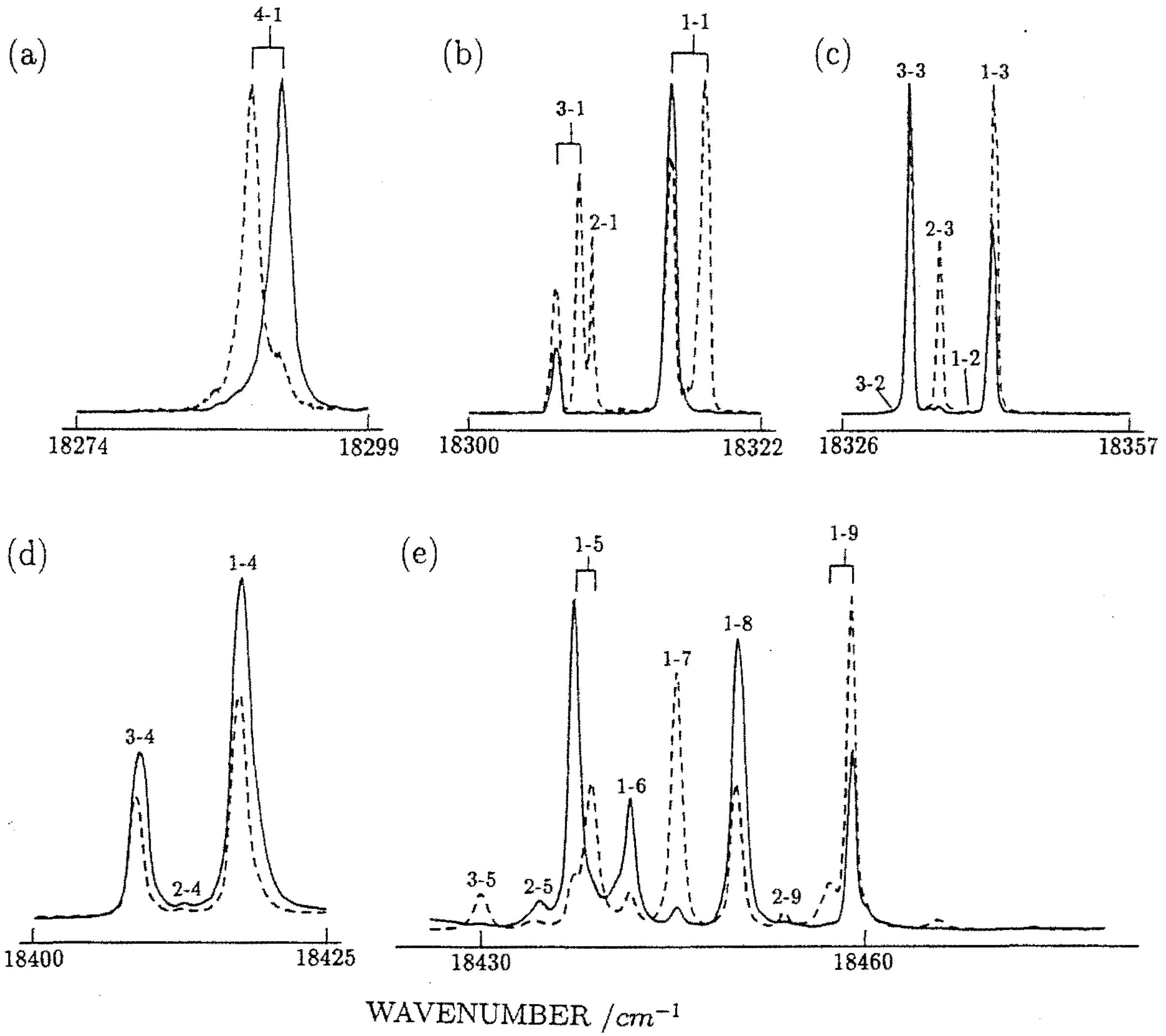

Figure 6.13 Polarisation of the 10 K selective excitation spectrum of the Z →E transitions of the principal dimer centre in $CsCdBr_3{:}Ho^{3+}$(0.3%) crystals, monitoring the $E_1 \rightarrow Z_7$ transition at 18137.0 cm^{-1}. Transitions to the E_1, E_5 and E_9 energy levels show splittings of 2.5, 1.6 and 1.9 cm^{-1} respectively.

———— π polarisation - - - - - - - σ polarisation (d)) are purely σ polarised while the higher energy components are mainly π polarised. The remaining five transitions showing the 2.5 cm^{-1} low symmetry splitting have the higher energy component purely σ polarised and the lower mainly π polarised. The $E_1 \rightarrow Z_6$ transition has both components stronger in σ polarisation than in π.

From the C_{3v} group selection rules, the number of levels of γ_1, γ_2 or γ_3 type irrep labels expected for each multiplet are as set out in Table 2.1(b). For the Z multiplet there are three levels of γ_1 type symmetry, two of γ_2 and six of γ_3 type symmetry.

Based on the above analysis of the behaviour of the splittings on the $E_1 \rightarrow Z$ transitions under polarisation, the Z_2 and Z_{10} energy levels are assigned as γ_2 type levels because they are the only two with the common characteristics of no splittings in transitions from the E_1 level and in having purely σ polarised transitions from the E_1 level. The Z_4, Z_8 and Z_9 levels are all assigned as γ_1 type levels because the split components are polarised identically in their transitions from the E_1 level. The remaining six levels Z_1, Z_3, Z_5, Z_6, Z_7 and Z_{11} are assigned to be of γ_3 symmetry. Since the splitting of 2.5 cm^{-1} is common to five of the six levels, the E_1 level is assigned as being a γ_3 type level with a low symmetry crystal-field splitting of 2.5 cm^{-1}. The assignment of a γ_3 type label to the Z_1 level follows from the total number of levels (nine for the E multiplet and seven for the D multiplet) observed in the excitation spectra.

Although the γ_3 symmetry levels of the Z multiplet are also expected to show splittings, such splittings appear to be less than the E_1 splitting and not resolvable. The reduced overall splitting observed for the $E_1 \rightarrow Z_6$ transition is an indication of two possible sets of overlapping splittings.

In the same way as for the E_1 level, the E_3, E_4, E_5 and E_9 levels are also assigned as γ_3 symmetry levels as transitions from the Z_1 level to these E multiplet levels either show a splitting or are broad. The $Z_1 \rightarrow E_7$ transition is not split at all and is purely σ polarised and hence the E_7 level at 18443.1 cm^{-1} is assigned as

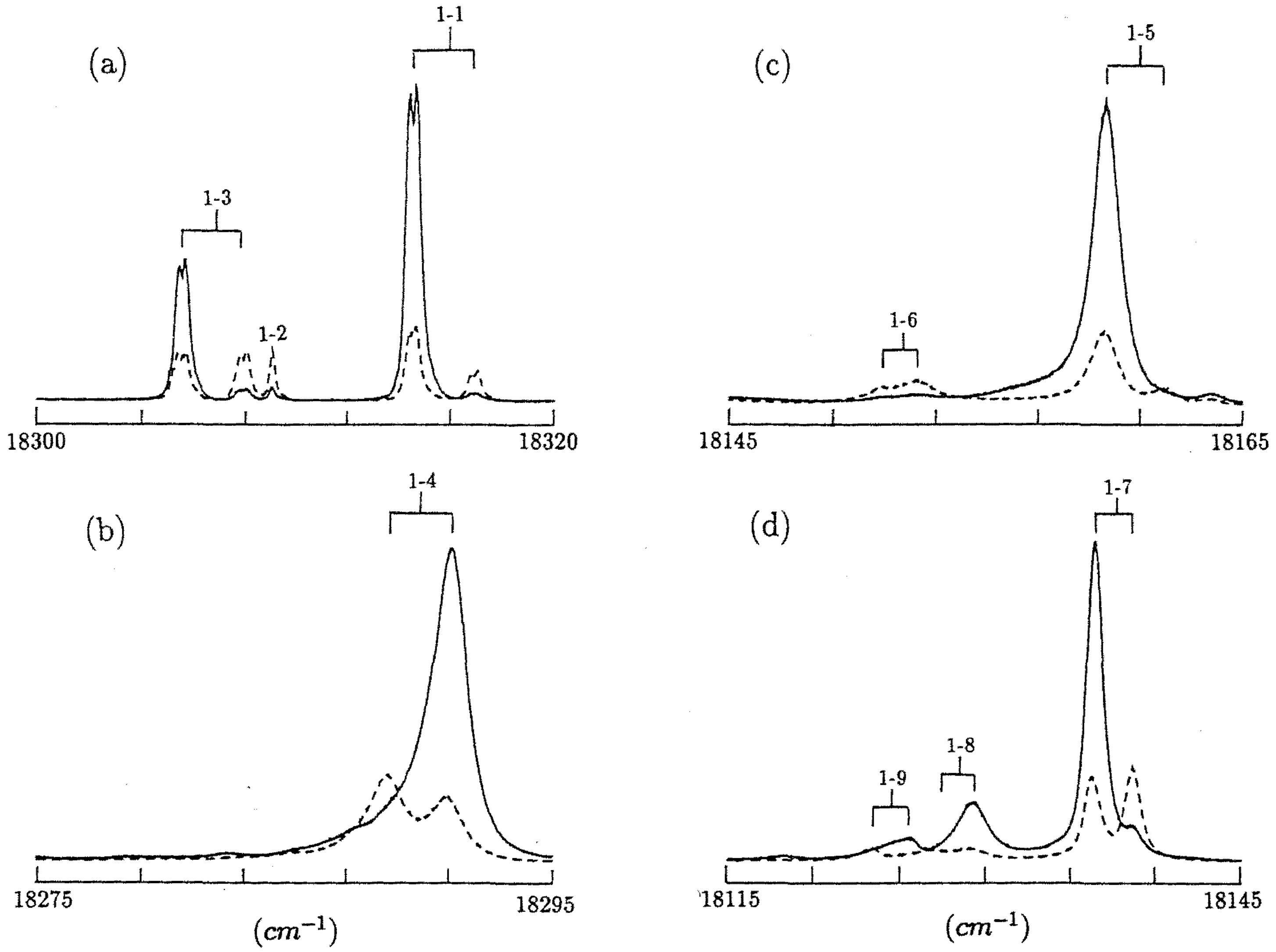
(a)
1-1
1-3
1-2
18300
18320
(b)
1-4
18275
18295
(cm^{-1})
(c)
1-5
1-6
18145
18165
(d)
1-7
1-8
1-9
18115
18145
(cm^{-1})

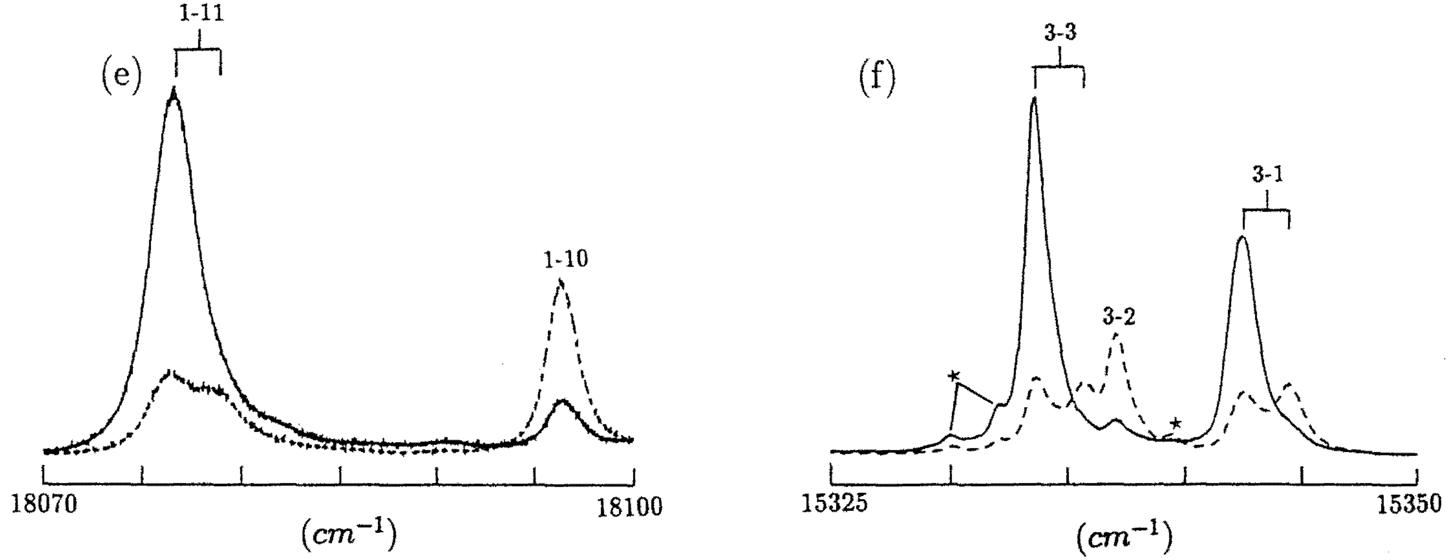

Figure 6.14: Polarisation behaviour of the two components of each split $E_1 \rightarrow Z$ and $D_3 \rightarrow Z$ transition in the 10 K fluorescence spectra of the principal dimer centre in $CsCdBr_3:Ho^{3+}$(0.3%) crystals.

(a) $E_1 \rightarrow Z_{1,2,3}$	(b) $E_1 \rightarrow Z_4$
(c) $E_1 \rightarrow Z_{5,6}$	(d) $E_1 \rightarrow Z_{7,8,9}$
(e) $E_1 \rightarrow Z_{10,11}$	(f) $D_3 \rightarrow Z_{1,2,3}$
———— π polarisation	- - - - - - - σ polarisation

Transitions identified by * are for the L centre.

of γ_2 symmetry, consistent with the criteria for the similar assignment for the Z_2 and Z_{10} levels. As the $Z_1 \rightarrow E_2$, $Z_1 \rightarrow E_6$ and $Z_1 \rightarrow E_8$ transitions do not show any splittings and are principally π polarised, the E_2, E_6 and E_8 levels are all assigned the γ_1 irrep label.

(ii) *Transitions between the D and Z multiplet levels*

As can be seen from the $Z \rightarrow D$ excitation spectra in Figure 6.15, the only observable splitting is for the $Z_1 \rightarrow D_3$ and the $Z_3 \rightarrow D_3$ transitions. This was measured to be 1.9 cm^{-1} for both transitions. Transitions to the D_1, D_5 and D_6 levels are all fairly broad and incipient splittings approaching 1 cm^{-1} cannot be ruled out.

As the D_2 and D_7 levels at 15314.5 cm^{-1} and 15483.0 cm^{-1} respectively, have transitions from the Z_1 and Z_3 levels that are not split and are σ polarised, and have transitions from the Z_2 level that are π polarised, the D_2 and D_7 levels are assigned as γ_2 irrep levels, the same as for the Z_2 and Z_{10} levels. The D_1, D_3, D_5 and D_6 levels are all γ_3 type levels. The $Z_1 \rightarrow D_4$ transition at 15411.5 cm^{-1} is very weak and the D_4 level is assigned as being the only γ_1 type level of the D multiplet.

All the $D \rightarrow Z$ fluorescence transitions show no other splittings, apart from the aforementioned 1.9 cm^{-1} apparent on the $D_3 \rightarrow Z_1$ and $D_3 \rightarrow Z_3$ transitions (Figure 6.14(f)). The observed polarisation ratios for all the $D_1 \rightarrow Z$ transitions (Table 6.3) are in agreement with the irrep label assignments made from the polarisation of the $E_1 \rightarrow Z$ fluorescence transitions, except for the two levels Z_2 and Z_{10}. The $E_1 \rightarrow Z_2$ and $E_1 \rightarrow Z_{10}$ transitions were found to be purely σ polarised while the $D_1 \rightarrow Z_2$ and $D_1 \rightarrow Z_{10}$ transitions were mainly π polarised. Since the D_1 level is definitely a γ_3 type level because transitions to all Z levels are observed, the transitions to the Z_2 and Z_{10} levels were expected to be mainly σ polarised in accordance with the C_{3v} selection rules, and not π. This anomalous polarisation observed for the $D_1 \rightarrow Z_2$ and the $D_1 \rightarrow Z_{10}$ transitions cannot be accounted for.

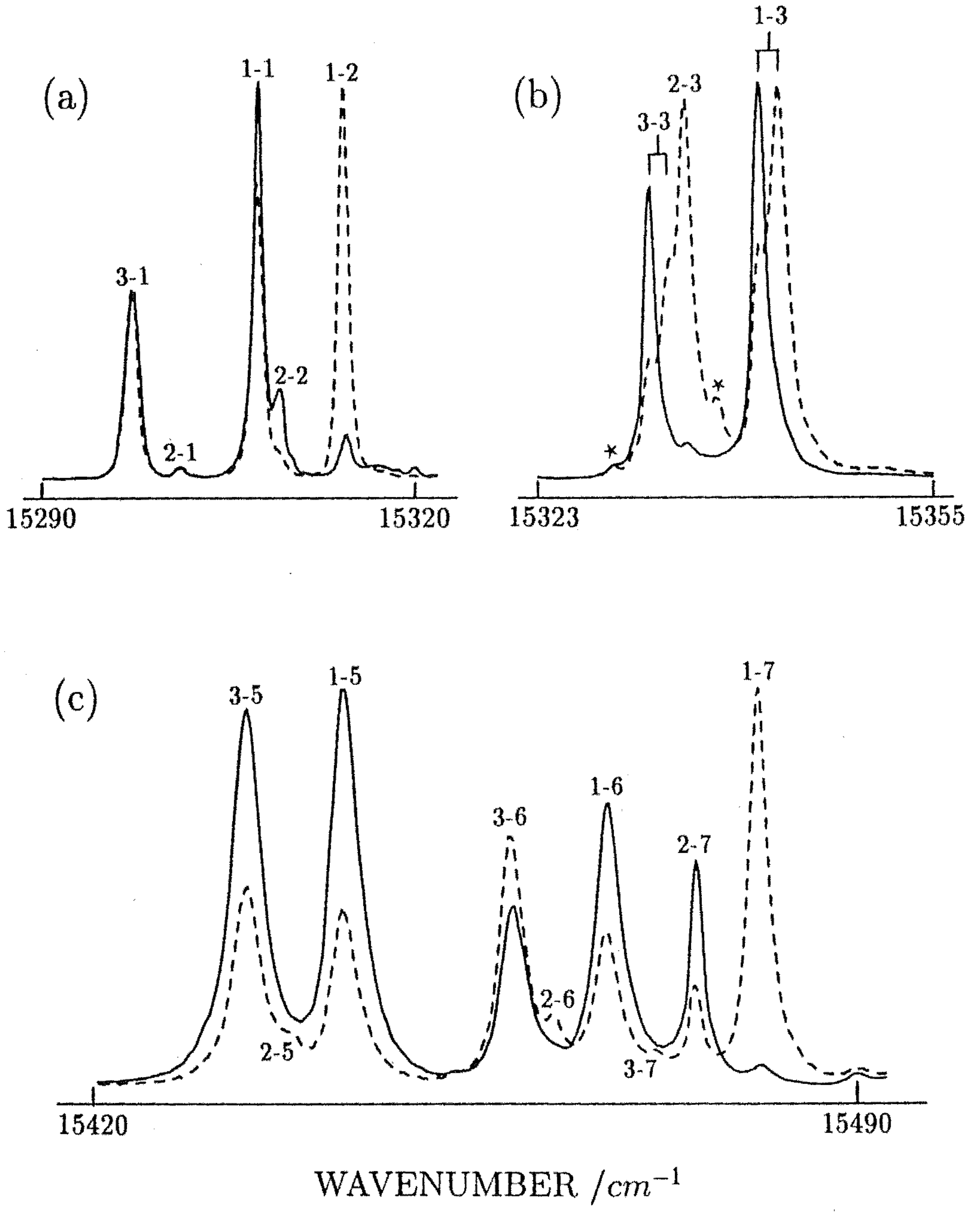

Figure 6.15: Polarisation of the 10 K selective excitation spectrum of the Z→D transitions of the principal dimer centre in $CsCdBr_3:Ho^{3+}$(0.3%) crystals, monitoring the $D_1 \to Z_{10}$ transition at 15090.5 cm^{-1}. Transitions to the D_3 level show a splitting of 1.9 cm^{-1}.
———— π polarisation - - - - - σ polarisation.

Transitions identified by * are for the L centre.

(iii) *Transitions from the E_1, F_1 and M_1 levels to the Y multiplet levels*

The $E_1 \rightarrow Y_1$ and $E_1 \rightarrow Y_2$ transitions are quite close giving a Y_1 - Y_2 energy level separation of 2.2 cm^{-1} while the Y_1 level is itself split by 1.2 cm^{-1}. The spectrum for the $E_1 \rightarrow Y_1,Y_2$ transitions (Figure 6.16(a)) is therefore rendered complicated by the superposition of the 2.5 cm^{-1} splitting of the E_1 level, the 1.2 cm^{-1} splitting in the Y_1 level and the close proximity of the Y_1 and Y_2 levels. Additional pair splittings, as discussed later in Section 6.1.2(b), are also present. The $E_1 \rightarrow Y_6$ and $E_1 \rightarrow Y_7$ transitions clearly show the 2.5 cm^{-1} splitting associated with the E_1 level. The $E_1 \rightarrow Y_7$ transition has an additional splitting of 1.1 cm^{-1} which is ascribed to a splitting of the Y_7 level itself. Because the $E_1 \rightarrow Y_6$ transition is quite broad any up to 1 cm^{-1} splitting could have been masked. The $E_2 \rightarrow Y_7$ transition shows the 1.1 cm^{-1} splitting assigned to the Y_7 level without any accompanying E_1 level splitting of 2.5 cm^{-1} which further supports the conclusion that the E_1 and Y_7 levels are split by 2.5 and 1.1 cm^{-1} respectively. The $E_2 \rightarrow Y_6$ transition is broad and does not show any noticeable splittings.

From the $F_1 \rightarrow Y_1$ spectrum in Figure 6.16(b), the 1.2 cm^{-1} splitting of the Y_1 level is apparent as well as the pair splittings for both the F_1 and Y_1 levels to be discussed in Section 6.1.2(b). Since the $F_1 \rightarrow Y_2$ transition is absent, the F_1 and Y_2 levels must have different irrep labels (γ_1 or γ_2) resulting in a forbidden $\gamma_1 \leftrightarrow \gamma_2$ type transition.

The $M_1 \rightarrow Y_1,Y_2$ and $M_2 \rightarrow Y_1,Y_2$ transitions as shown in Figure 6.16(c) all have separations in accordance with the Y_1 - Y_2 energy level separation of 2.2 cm^{-1}. Although the $M_1 \rightarrow Y_1,Y_2$ and $M_2 \rightarrow Y_1,Y_2$ transitions are fairly broad, the Y_1 splitting of 1.2 cm^{-1} is still apparent but any splittings attributable to the M_1 and M_2 levels were not observed. As the $M_2 \rightarrow Y_2$ transition is purely π polarised, the M_2 and Y_2 levels have the same irrep label.

(iv) *Weak fluorescence transitions*

Low symmetry splittings were not observed for any of the J → Z, Q → B or Q → C transitions. Most of these transitions are broad, with linewidths of

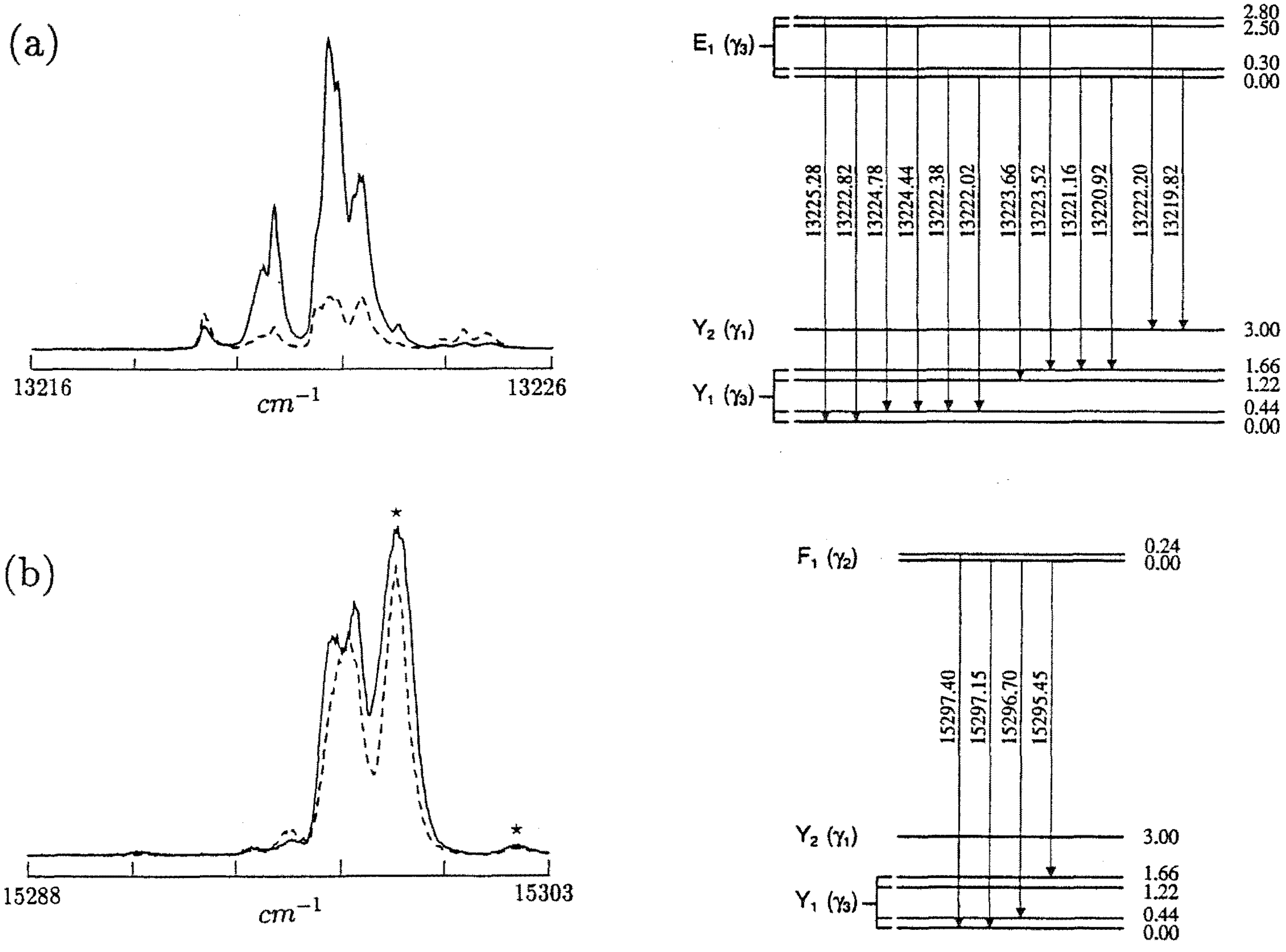
(a)
13216
13226
cm^{-1}
E$_1$ (γ_3)
Y$_2$ (γ_1)
Y$_1$ (γ_3)
2.80
2.50
0.30
0.00
3.00
1.66
1.22
0.44
0.00
13225.28
13222.82
13224.78
13224.44
13222.38
13222.02
13223.66
13223.52
13221.16
13220.92
13222.20
13219.82
(b)
15288
15303
cm^{-1}
★
★
F$_1$ (γ_2)
Y$_2$ (γ_1)
Y$_1$ (γ_3)
0.24
0.00
3.00
1.66
1.22
0.44
0.00
15297.40
15297.15
15296.70
15295.45

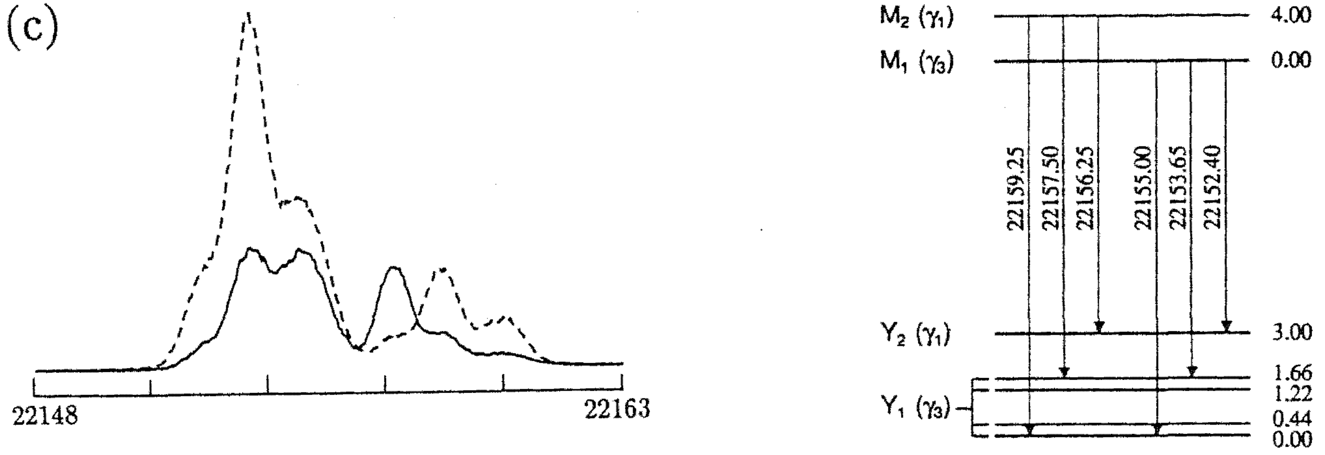

Figure 6.16: Polarisation of the 10 K fluorescence transitions from the E_1, F_1, M_1 and M_2 levels to the Y_1 and Y_2 levels of the principal dimer centre in $CsCdBr_3:Ho^{3+}$(0.3%) crystals, for excitation of the $Z_1 \rightarrow E_4$ transition at 18416.3 cm^{-1}. The energy level diagrams on the right show transitions between components of the upper and lower multiplet levels, corresponding to the spectra on the left.

(a) $E_1 \rightarrow Y_{1,2}$

(b) $F_1 \rightarrow Y_1$, transitions marked * are $D_1 \rightarrow Z_2$ and $D_1 \rightarrow Z_3$ as in Figure 6.15(a)

(c) $M_{1,2} \rightarrow Y_{1,2}$

———— π polarisation - - - - - - - σ polarisation

1 - 5 cm^{-1}, and any splittings could be easily masked. The remaining transitions were too weak for any splittings to be detected. Any upconversion fluorescence transitions whose intensities were less than 0.2% of the main $E_1 \rightarrow Z_7$ or $D_1 \rightarrow Z_{10}$ transition for $Z_1 \rightarrow E_4$ and $Z_1 \rightarrow D_5$ excitation respectively, were not examined in detail for evidence of low symmetry splittings.

(b) Pair splittings

In addition to the low symmetry splittings discussed in (a) above, a further set of smaller splittings in the range 0.20 - 0.44 cm^{-1} was observed on several of the sharper transitions. Only the most intense and sharpest transitions were searched for such splittings as spectrometer slit widths of just 10 μm for the entrance and exit slits of the spectrometer were required to achieve better than 0.2 cm^{-1} resolution.

These so-called pair splittings were measured for the $E_1 \rightarrow Z_1,Z_3$ transitions (Figure 6.17(a)) as 0.30 cm^{-1} while the $E_1 \rightarrow Z_2$ transition does not show any splitting. The $E_3 \rightarrow Z_1,Z_3$ transitions (Figure 6.17(b)) show quite similar splittings measured to be 0.20 cm^{-1}. These splittings are assigned to the upper E_1 and E_3 levels respectively, since splittings in the Z levels should be common to both the $E_1 \rightarrow Z_1,Z_3$ and $E_3 \rightarrow Z_1,Z_3$ as well as $D \rightarrow Z$ transitions. Both the $F_1 \rightarrow Z_1$ and $F_1 \rightarrow Z_3$ transitions were found to have a splitting of 0.24 cm^{-1} (Figure 6.17(c)). Likewise, the $E_1 \rightarrow Y_1$ and $F_1 \rightarrow Y_1$ transitions show a common pair splitting of 0.44 cm^{-1} (Figure 6.16 (a) and (b)) which is additional to the 0.30 and 0.24 cm^{-1} attributed to the E_1 and F_1 levels respectively. The pair splitting for the Y_1 level is therefore inferred as 0.44 cm^{-1}.

For each transition showing a pair splitting, both components have the same polarisation, either π or σ. These pair splittings are attributed to the coupling between the two Ho^{3+} ions of a dimer centre. Similar splittings have been reported for Er^{3+} ions in the same crystal host [31].

6.1.3 Polarisation of the fluorescence transitions

All irrep label assignments have been based on polarisation measurements.

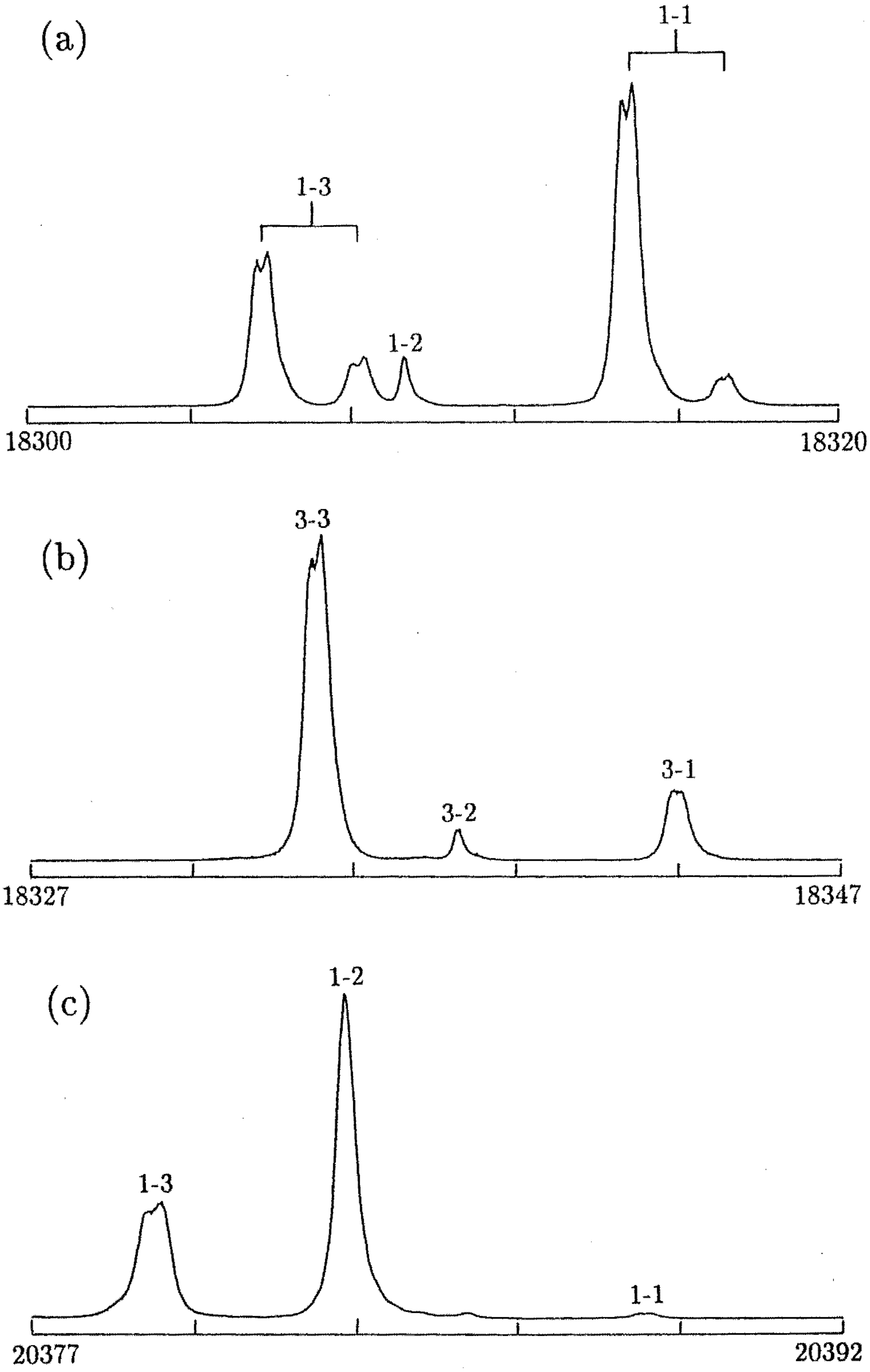

Figure 6.17: 10 K fluorescence spectra of the transitions from the E_1, E_3 and F_1 levels to the Z_1, Z_2 and Z_3 levels of the principal dimer centre in $CsCdBr_3:Ho^{3+}$(0.3%) crystals, for excitation of the $Z_1 \rightarrow E_4$ transition at 18416.3 cm^{-1}. Transitions to the Z_1 and Z_3 levels show additional small splittings :
(a) $E_1 \rightarrow Z_{1,2,3}$; (b) $E_3 \rightarrow Z_{1,2,3}$; (c) $F_1 \rightarrow Z_{1,2,3}$.

For purposes of the following discussion the polarisation results have been grouped according to the particular terminating multiplet. Although the results are presented for transitions from the lowest level of the upper multiplet in each case, the same arguments were applied to assign irrep labels for the higher energy levels of a given multiplet.

(i) *Transitions from the D_1, E_1, F_1 and J_1 levels to the Z multiplet levels*

Polarisation results for the $D_1 \rightarrow Z$ and $E_1 \rightarrow Z$ transitions have already been discussed in detail in Section 6.1.2(a) above, so attention here will be directed to the $F_1 \rightarrow Z$ and $J_1 \rightarrow Z$ transitions.

The $F_1 \rightarrow Z_2$ transition was almost wholly π polarised with a polarisation ratio of 22:1 (Table 6.3). This is an indication of a $\gamma_a \rightarrow \gamma_a$ (a = 1 or 2) type transition and, since the Z_2 level has already been assigned as of γ_2 symmetry, the F_1 level is assigned to be the same. This assignment is supported by there being no transitions from the F_1 level to the γ_1 type levels Z_1, Z_8 and Z_9. Although the $F_1 \rightarrow Z_2$ transition has the highest upconversion intensity of all measured transitions, all the other $F_1 \rightarrow Z$ transitions were quite weak making their polarisation character uncertain. The $F_1 \rightarrow Z_{10}$ transition was slightly σ polarised when it should have been π polarised. The assignment of the F_1 level as a γ_2 type level has been made on the stringent criteria of a completely polarised $F_1 \rightarrow Z_2$ transition and the total number of $F_1 \rightarrow Z$ transitions observed.

Since all the Z levels have been identified through transitions from the J_1 level, this J_1 level can only be a γ_3 type level. The polarisation results for all transitions except the $J_1 \rightarrow Z_2$ and $J_1 \rightarrow Z_{10}$ transitions are fully consistent with this assignment. The $J_1 \rightarrow Z_2$ and $J_1 \rightarrow Z_{10}$ transitions, although weak, were stronger in π polarisation with ratios of 1.2:1 and 1.5:1 respectively, while both were expected to be mainly σ polarised since they are $\gamma_3 \rightarrow \gamma_2$ type transitions. This polarisation anomaly is as found for the $D_1 \rightarrow Z_2$ and $D_1 \rightarrow Z_{10}$ transitions (Section 6.1.2(a)).

Table 6.3: Observed intensity ratios for the polarised fluorescence transitions from the E_1, D_1, J_1, and F_1 levels to the Z multiplet levels of the principal dimer centre in <111> oriented $CsCdBr_3$:Ho^{3+}(0.3%) crystals, for excitation of the $Z_1 \rightarrow E_4$ transition at 18416.3 cm^{-1}. For the split transitions, polarisation ratios for both components are given. Uncertainty is ±15%.

	$E_1(\gamma_3)$	**$D_1(\gamma_3)$**	**$J_1(\gamma_3)$**	**$F_1(\gamma_2)$**
$Z_1(\gamma_3)$	1 : 5.0 5.0 : 1	2.4 : 1	1 : 1.3	1 : 4.0
$Z_2(\gamma_2)$	1 : 5.0	1.7 : 1	1.2 : 1	22.7 : 1
$Z_3(\gamma_3)$	1 : 4.7 2.4 : 1	1.1 : 1	5.7 : 1	1 : 4.0
$Z_4(\gamma_1)$	4.9 : 1 1 : 4.4	1 : 1.7	1 : 3.7	N/A
$Z_5(\gamma_3)$	1 : 3.9 4.4 : 1	3.3 : 1	5.2 : 1	1 : 4.6
$Z_6(\gamma_3)$	1 : 3.2 1 : 3.0	1 : 3.0	1 : 2.7	1 : 1.6
$Z_7(\gamma_3)$	1 : 4.2 4.5 : 1	8.8 : 1	1 : 1.7	1.7 : 1
$Z_8(\gamma_1)$	4.9 : 1 1 : 3.7	1 : 2.0	1 : 2.0	N/A
$Z_9(\gamma_1)$	4.2 : 1 1 : 4.7	1 : 6.3	1 : 2.2	N/A
$Z_{10}(\gamma_2)$	1 : 3.1	8.1 : 1	1.5 : 1	1 : 1.5
$Z_{11}(\gamma_3)$	1 : 3.9 4.6 : 1	2.3 : 1	5.1 : 1	1 : 4.7

Table 6.4: Observed intensity ratios for the polarised fluorescence transitions from the E_1, M_1, F_1, Q_1 and P_1 levels to the Y multiplet levels of the principal dimer centre in <111> oriented $CsCdBr_3:Ho^{3+}(0.3\%)$ crystals, for excitation of the $Z_1 \rightarrow E_4$ transition at 18416.3 cm^{-1}. For the split transitions, polarisation ratios for both components are given. Uncertainty is ±15%.

	$E_1(\gamma_3)$	$M_1(\gamma_3)$	$F_1(\gamma_2)$	$Q_1(\gamma_2)$	$P_1(\gamma_1)$
$Y_1(\gamma_3)$	6.3 : 1 6.2 : 1	1 : 3.0	1 : 2.7	1 : 2.0	1 : 1.2
$Y_2(\gamma_1)$	1 : 2.2	1 : 4.5	N/A	N/A	3.7 : 1
$Y_3(\gamma_3)$	4.7 : 1	1 : 1.1	1 : 3.1	1 : 1.8	1.5 : 1
$Y_4(\gamma_2)$	1 : 2.4	1 : 2.4	3.9 : 1	2.0 : 1	N/A
$Y_5(\gamma_2)$	1 : 2.9	1 : 2.1	5.5 : 1	2.9 : 1	N/A
$Y_6(\gamma_3)$	3.3 : 1	1.9 : 1	1 : 4.2	1 : 1.9	1 : 1.8
$Y_7(\gamma_3)$	1.5 : 1 1 : 2.8	2.9 : 1	1 : 3.2	1 : 2.2	1 : 2.1
$Y_8(\gamma_2)$	1 : 3.3	1 : 3.5	6.3 : 1	1.5 : 1	N/A
$Y_9(\gamma_3)$	7.4 : 1	1 : 3.9	1 : 2.4	1 : 1.8	( )
$Y_{10}(\gamma_1)$	1 : 3.1	1 : 2.0	N/A	N/A	( )

( ) transition too weak to measure polarisation ratios

(ii) *Transitions from the E_1, F_1, M_1, P_1 and Q_1 levels to the Y multiplet levels*

From the E → Y transitions, the Y_1, Y_6 and Y_7 levels are all γ_3 type levels because they all possess low symmetry crystal-field splittings.

Non-observance of the $F_1 \rightarrow Y_2$ and $F_1 \rightarrow Y_{10}$ transitions establishes the Y_2 and Y_{10} levels to be γ_1 type levels since the F_1 level is already assigned to be of γ_2 symmetry. As transitions from the F_1 level to the Y_4, Y_5 and Y_8 levels are largely π polarised, these three levels have γ_2 type symmetry labels. The Y_3 and Y_9 levels are assigned as γ_3 type levels.

Transitions from the M_1 level to all ten Y levels were observed therefore the M_1 level is necessarily a γ_3 type level. The polarisation ratios (Table 6.4) are consistent with both these M_1 and Y multiplet level assignments.

As transitions from the P_1 level to the three levels Y_4, Y_5 and Y_8 were not observed, the P_1 level is likely to be a γ_1 level. The polarisation spectra although weak, did show the $P_1 \rightarrow Y_2$ transition to be principally π polarised ($\gamma_1 \rightarrow \gamma_1$) with transitions to γ_3 type levels being slightly σ polarised.

The $Q_1 \rightarrow Y_2$ and $Q_1 \rightarrow Y_{10}$ transitions were not observed. As the observed $Q_1 \rightarrow Y$ transitions had similar polarisation ratios to those for the $F_1 \rightarrow Y$ transitions the F_1 and Q_1 levels are likely to have the same γ_2 irrep label, therefore the Q_1 level has been assigned as a γ_2 type level.

(iii) *Transitions from the F_1, K_1, M_1, P_1, Q_1 and U_1 levels to the A multiplet levels*

From the measured polarisation ratios of transitions to the first seven levels identified for the A multiplet (Table 6.5), the six energy levels F_1, K_1, M_1, P_1, Q_1 and U_1 can be subdivided into three different categories, with the F_1 and Q_1 levels in one, the K_1, M_1 and U_1 levels in the other and the P_1 level in the third. Each category will now be discussed separately :

Transitions to the A_1 and A_4 levels were not observed from either the F_1 or Q_1 levels. Transitions from both the F_1 and Q_1 levels to the A_3 and A_7 levels were much stronger in π polarisation than in σ while transitions to the A_2, A_5 and A_6 levels were principally σ polarised. Since the F_1 and Q_1 levels are both γ_2 type levels, the A_3 and A_7 levels are also γ_2 while the A_1 and A_4 levels are γ_1 and the A_2, A_5 and A_6 levels are γ_3 type levels.

Although the polarisation ratios for the transitions from the K_1, M_1 and U_1 levels to the A multiplet levels are not particularly consistent, all three have been assigned as γ_3 type levels because transitions to most of the nine A multiplet levels A_1 to A_9, as derived from the F → A, P → A and Q → A transitions, have been observed in each case.

The $P_1 \rightarrow A_3$ and $P_1 \rightarrow A_7$ transitions were not observed. The $P_1 \rightarrow A_1$ and $P_1 \rightarrow A_4$ transitions were π polarised while the $P_1 \rightarrow A_2$, $P_1 \rightarrow A_5$ and $P_1 \rightarrow A_6$ transitions were mainly σ polarised. All these results are consistent with the γ_1 assignment made in (ii) above for the P_1 level.

(iv) *Transitions from the P_1' and Q_1 levels to the B multiplet levels*

Six energy levels have been identified for the B multiplet. Transitions from the Q_1 (γ_2) level to all the six B multiplet levels were observed and so the only irrep labels applicable are γ_2 and γ_3. The $Q_1 \rightarrow B_1$ and $Q_1 \rightarrow B_5$ transitions were mainly π polarised while the remaining four transitions were mainly σ polarised (Table 6.6). The B_1 and B_5 levels are therefore assigned as γ_2 type levels while the B_2, B_3, B_4 and B_6 levels are all of γ_3 symmetry.

As no transitions to either the B_1 or B_5 levels were observed from the P_1' level while transitions to the B_2, B_3, B_4 and B_6 levels were observed to be principally σ polarised, the P_1' level is a γ_1 type level. Although the $M_1 \rightarrow$ B level transitions were too weak for any polarisation ratio measurements, the observance of transitions from the M_1 level to all six B levels is fully consistent with the earlier γ_3 symmetry assignment for this level ((iii) above).

(v) *Transitions from the P_1, P_1' and Q_1 levels to the C multiplet levels*

Four levels have been identified for the C multiplet. Of the transitions observed from the Q_1 level, the $Q_1 \rightarrow C_5$ transition is absent, the $Q_1 \rightarrow C_2$ transition

Table 6.5: Observed intensity ratios for the polarised fluorescence transitions from the F_1, Q_1, K_1, M_1, U_1 and P_1 levels to the A multiplet levels of the principal dimer centre in <111> oriented $\mathrm{CsCdBr_3:Ho^{3+}}$(0.3%) crystals, for excitation of the $\mathrm{Z}_1 \rightarrow \mathrm{E}_4$ transition at 18416.3 $\mathrm{cm^{-1}}$. Uncertainty is ±15%.

	$\mathbf{F_1(\gamma_2)}$	$\mathbf{Q_1(\gamma_2)}$	$\mathbf{K_1(\gamma_3)}$	$\mathbf{M_1(\gamma_3)}$	$\mathbf{U_1(\gamma_3)}$	$\mathbf{P_1(\gamma_1)}$
$\mathrm{A_1}(\gamma_1)$	N/A	N/A	1 : 4.1	1.5 : 1	1 : 1.5	3.4 : 1
$\mathrm{A_2}(\gamma_3)$	1 : 4.7	1 :3.0	1 : 6.5	2.5 : 1	1 : 5.0	1 : 4.3
$\mathrm{A_3}(\gamma_2)$	5.8 : 1	5.1 : 1	1 : 3.2	( )	( )	N/A
$\mathrm{A_4}(\gamma_1)$	N/A	N/A	1 : 1.2	( )	( )	2.2 : 1
$\mathrm{A_5}(\gamma_3)$	1 : 1.3	1 : 1	1 : 3.9	1.7 : 1	( )	1 : 2.5
$\mathrm{A_6}(\gamma_3)$	1 : 4.0	1 : 1	( )	1 : 1.1	( )	1 : 3.5
$\mathrm{A_7}(\gamma_2)$	5.4 : 1	4.8 : 1	( )	( )	( )	N/A

Table 6.6: Observed intensity ratios for the polarised fluorescence transitions from the Q_1, Q_2 and $\mathrm{P'}_1$ levels to the B multiplet levels of the principal dimer centre in <111> oriented $\mathrm{CsCdBr_3:Ho^{3+}}$(0.3%) crystals, for excitation of the $\mathrm{Z}_1 \rightarrow \mathrm{E}_4$ transition at 18416.3 $\mathrm{cm^{-1}}$. Uncertainty is ±15%.

	$\mathbf{Q_1(\gamma_2)}$	$\mathbf{Q_2(\gamma_3)}$	$\mathbf{P'_1(\gamma_1)}$
$\mathrm{B_1}(\gamma_2)$	4.8 : 1	1 : 6.9	N/A
$\mathrm{B_2}(\gamma_3)$	1 : 6.5	1 : 1.9	1 : 2.4
$\mathrm{B_3}(\gamma_3)$	1 : 3.4	1.7 : 1	1 : 3.8
$\mathrm{B_4}(\gamma_3)$	1 : 3.3	1 : 1.1	( )
$\mathrm{B_5}(\gamma_2)$	3.2 : 1	1 : 2.5	N/A
$\mathrm{B_6}(\gamma_3)$	1 : 3.7	2.0 : 1	1 : 3.4

( ) transition too weak to measure polarisation ratios

Table 6.7: Observed intensity ratios for the polarised fluorescence transitions from the Q_1, P_1, P'_1 and P'_2 levels to the C multiplet levels of the principal dimer centre in <111> oriented $CsCdBr_3:Ho^{3+}$(0.3%) crystals, for excitation of the $Z_1 \rightarrow E_4$ transition at 18416.3 cm^{-1}. Uncertainty is ±15%.

	$Q_1(\gamma_2)$	$P_1(\gamma_1)$	$P'_1(\gamma_1)$	$P'_2(\gamma_3)$
$C_1(\gamma_3)$	1 : 3.8	1 : 1.3	1 : 1.8	1.3 : 1
$C_2(\gamma_2)$	2.5 : 1	N/A	N/A	1 : 4.0
$C_5(\gamma_1)$	N/A	3.8 : 1	5.7 : 1	( )
$C_6(\gamma_3)$	1 : 2.3	( )	1 : 2.7	1 : 2.5

( ) transition too weak to measure polarisation ratios.

Table 6.8: Observed intensity ratios for the polarised fluorescence transitions from the Q_1, Q_2 and U_1 levels to the D and E multiplet levels respectively, of the principal dimer centre in <111> oriented $CsCdBr_3:Ho^{3+}$(0.3%) crystals, for excitation of the $Z_1 \rightarrow E_4$ transition at 18416.3 cm^{-1}. Uncertainty is ±15%

	$Q_1(\gamma_2)$	$Q_2(\gamma_3)$
$D_1(\gamma_3)$	1 : 4.7	1 : 4.7
$D_2(\gamma_2)$	5.4 : 1	1 : 2.1
$D_3(\gamma_3)$	1 : 4.6	2.4 : 1
$D_5(\gamma_3)$	1 : 3.0	4.1 : 1

	$U_1(\gamma_3)$
$E_1(\gamma_3)$	1 : 5.0 5.4 : 1
$E_3(\gamma_3)$	1 : 5.0
$E_4(\gamma_3)$	1 : 5.0
$E_5(\gamma_3)$	4.8 : 1
$E_8(\gamma_3)$	1 : 4.8

is mainly π polarised while the $Q_1 \rightarrow C_1$ and $Q_1 \rightarrow C_6$ transitions are mainly σ polarised (Table 6.7). Because the Q_1 level has already been assigned as of γ_2 symmetry, the C_2 level is also a γ_2 symmetry level, the C_5 level a γ_1 symmetry level and the C_1 and C_6 levels are γ_3 symmetry levels.

Transitions from the P_1' and P_1 levels to the C_2 level were absent while those to the C_5 level were π polarised in both cases. This agrees with the irrep labels already assigned to both the P_1' and P_1 levels (in (iii) and (iv) above).

(vi) *Remaining unassigned transitions*

Both the transitions in the 14100 - 13300 cm^{-1} region which could be due to Sm^{2+} ions and those in the 11160 - 11000 cm^{-1} region whose origin is as yet not established were found to be well polarised, just like most of the transitions for the dimer centre.

6.1.4 Irrep label assignments for the weak transitions

In assigning irrep labels, polarisation results have been used in conjunction with the total numbers of transitions observed between any two multiplets. Some transitions, $O \rightarrow Z$ for example (Figure 6.5(g)), are too weak for polarisation studies. However, since the Z_2 and Z_4 levels have been established to be γ_2 and γ_1 type levels respectively, the presence or absence of transitions to such levels could be used to deduce the irrep labels of the upper multiplet energy levels. As transitions from the O_1 level to both the Z_2 and Z_4 levels were observed, O_1 was assigned to be a γ_3 type level. Similarly as the $I_1 \rightarrow Z_2$ and $I_1 \rightarrow Z_4$ transitions were both observed (Figure 6.8(c)), the I_1 level was assigned as a γ_3 type level.

These energy levels and the proposed irrep labels have been used in the crystal-field calculations to be described in Chapter 7.

6.2 The Minority Centres in $CsCdBr_3$:Ho^{3+} Crystals

In addition to the dominant dimer centre transitions in the excitation spectra of Figures 6.3 and 6.4, other weaker centre transitions are also present. For the 0.1% and 0.3% Ho^{3+} doped $CsCdBr_3$ crystals studied here, these weak transitions have been found to belong to a single centre arbitrarily labelled the L centre. This L centre to be described in Section 6.2.1, has similar characteristics to the principal dimer centre in that transition energies are closely similar and upconversion fluorescence is observed for both the principal dimer and L centres.

In the 0.01% Ho^{3+} doped $CsCdBr_3$ crystals, transitions of a different minority centre are observed as shown in Figures 6.3(b) and 6.4(b) and have significantly different energies from the L centre transitions. Transitions for this new centre which has been arbitrarily labelled the M centre, occur at up to 8 cm^{-1} higher energies than corresponding transitions for the principal dimer centre. Unlike the L centre, the M centre does not exhibit any upconversion fluorescence, but shows similar low symmetry crystal-field splittings to those found for the dimer centre.

A further minority centre arbitrarily labelled the N centre, was found in $CsCdBr_3$ crystals doubly doped with Ho^{3+} and Na^+ ions. The N centre is therefore assigned as a Ho^{3+} - Na^+ pair. It was found to display similar spectral features to the M centre of the weakly doped $CsCdBr_3$:Ho^{3+}(0.01%) crystals.

The three minority centres will now be described in turn :

6.2.1 Spectroscopy of the L centre

Transitions for this centre are shown by L in Figures 6.3(a) and 6.4(a). Although some of the L centre transitions could be easily identified in the excitation spectra, fluorescence transitions varied from being completely overlapped with those of the principal dimer centre transitions to being only separated by about 3 cm^{-1} (Figure 6.18). Transitions unique to the L centre are listed in Table 6.9, as they were insufficient to allow an energy level scheme to be derived.

Upconversion fluorescence was observed from the F multiplet (Figure 6.18(a)) for $Z \rightarrow E$ excitation, and from both the F and E multiplets for $Z \rightarrow D$ excitation.

It is not clear whether any splittings as observed for the dimer centre occur

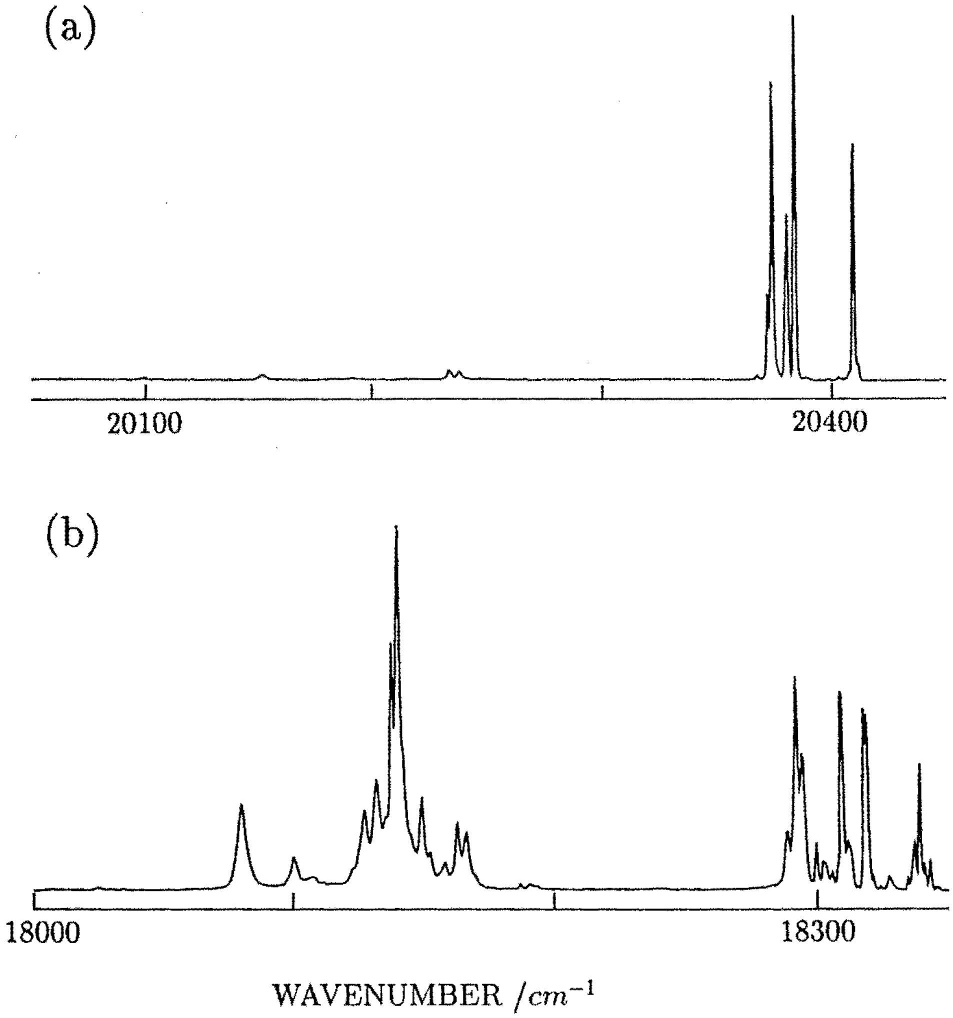
(a)
20100
20400
(b)
18000
18300
WAVENUMBER /cm⁻¹

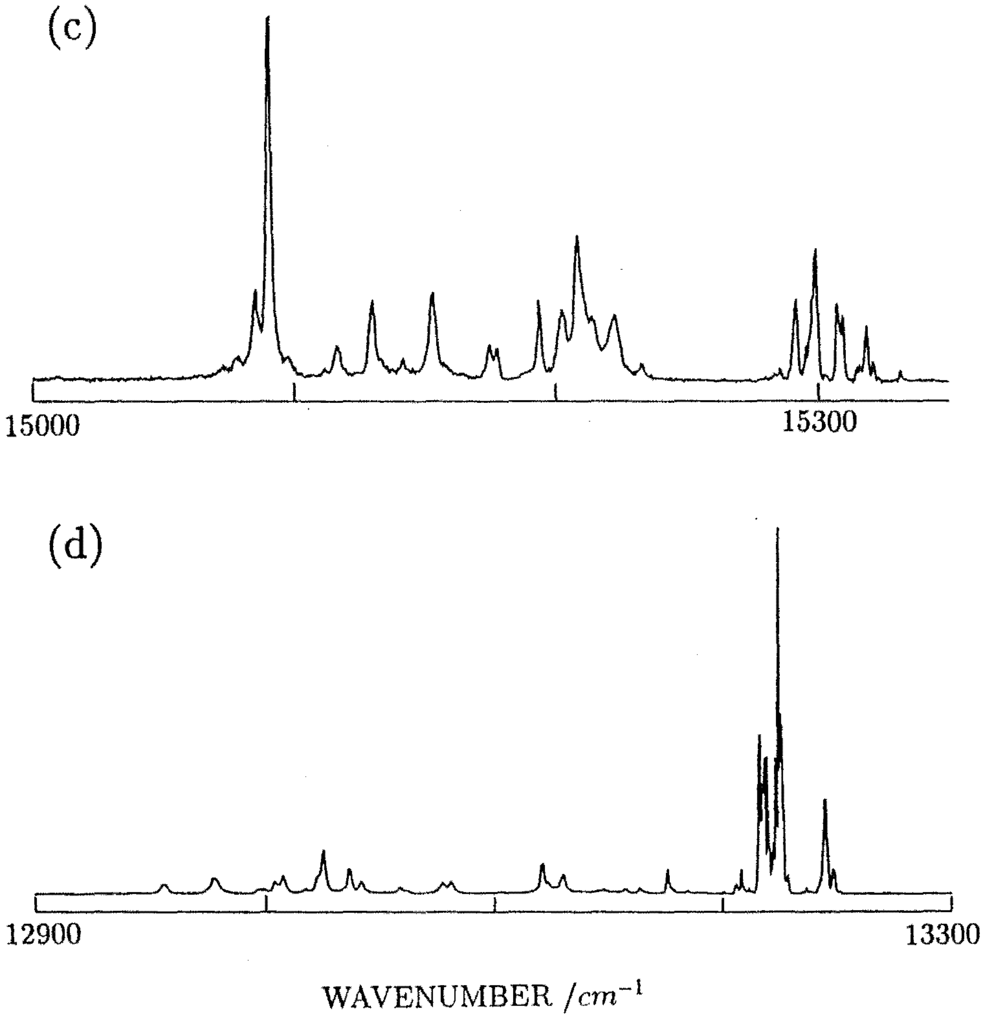

Figure 6.18: 10 K fluorescence spectra of the L centre in $CsCdBr_3$:Ho^{3+}(0.3%) crystals, for excitation of the transition at 18362.6 cm^{-1} :
(a) F→Z transitions;
(b) E→Z transitions;
(c) D→Z and F→Y transitions;
(d) E→Y transitions.

Table 6.9 : Energies (in cm^{-1}) of the transitions observed for the L centre in $CsCdBr_3$:Ho^{3+} (0.3%) crystals, as measured at 10 K. Uncertainty is ± 0.5 cm^{-1}.

Z→E	**E→Z**	**Z→D**	**D→Z**	**F→Z**	**E→Y**
18496.9	18340.5	15510.9	15320.0	20407.0	13246.5
18476.8	18336.5	15503.7	15316.5	20400.5	13243.5
18472.5	18332.0	15493.5	15293.5	20371.0	13235.0
18465.2	18324.5	15490.4	15290.0	20369.0	13218.0
18432.6	18316.0	15366.1	15231.0	20364.5	13217.0
18412.2	18305.5	15360.9	15220.5	20235.5	13215.0
18403.5	18299.5	15320.2	15191.5	20097.0	13183.5
18362.6	18297.0	15290.1	15175.5		13174.5
18360.5	18286.0		15083.0		13162.5
	18149.5		15070.5		13076.0
	18147.0				13040.5
	18135.5				13016.0
					13006.0
					13002.5
					12995.0
					12954.0

in any of the L centre transitions because transitions for this centre could not be distinguished sufficiently from those for the dimer centre. Polarisation studies could not be carried out for this centre because the fluorescence was too weak to give any conclusive results and the centre could not be selectively excited.

Since the L centre which is only found in the 0.1% and 0.3% Ho^{3+} doped crystals and is absent from the 0.01% Ho^{3+} doped crystal exhibits upconversion, it is not likely to be a single Ho^{3+} ion centre. The observation of relatively strong upconversion fluorescence strongly suggests that there is more than one Ho^{3+} ion in this centre. It is therefore tentatively supposed that the L centre is of the form $Cd^{2+} - Ho^{3+} - Ho^{3+} - V - Cd^{2+}$ similar to the B centre reported for $CsCdBr_3$:Nd^{3+}(0.3%) crystals [12]. This Nd^{3+} B dimer centre was characterised by energy transfer rates ten times greater than those obtained for the principal Nd^{3+} dimer centre. For the $^4G_{5/2}$ multiplet of Nd^{3+} for example, the energy transfer rates for the principal dimer and the B centres were calculated to be $2x10^5\ s^{-1}$ [11] and $14x10^6\ s^{-1}$ [12] respectively. It was concluded from such fluorescence lifetime measurements that the B centre Nd^{3+} ions are more strongly coupled and hence closer together than the Nd^{3+} ions in the principal dimer centre. Although fluorescence measurements could not be done in this study for the Ho^{3+} L centre, this Ho^{3+} L centre is assigned as of the same configuration as the Nd^{3+} B centre, on the basis of observation of upconversion fluorescence and the Ho^{3+} concentration dependence of the L centre intensity.

6.2.2 Spectroscopy of the M centre

This M centre was only found in the 0.01% Ho^{3+} concentration crystal and not in either the 0.1% or 0.3% Ho^{3+} concentration crystals. Transitions for the M centre are shown by M in Figures 6.3(b) and 6.4(b).

Fluorescence transitions for E → Z and E → Y (Figure 6.19 (a) and (c)) were found to be well separated from those of the dimer centre. Although the D → Z spectrum (Figure 6.19(b)) also includes some dimer centre transitions, such transitions are relatively weak and easily distinguished from those of the M centre.

For excitation of either the $Z_1 \rightarrow E_3$ or $Z_1 \rightarrow E_4$ transitions at 18350.9 cm^{-1} and 18428.3 cm^{-1} respectively, only the E → Z and E → Y fluorescence (Figure 6.19 (a) and (c)) was observed, without any upconversion or D → Z fluorescence being observed. For excitation of the $Z_1 \rightarrow D_1$ transition at 15309.5 cm^{-1} or the $Z_1 \rightarrow D_3$ transition at 15348.8 cm^{-1}, only the D → Z fluorescence (Figure 6.19(b)) was observed with no upconversion fluorescence at all.

Because there is no upconversion fluorescence observed for excitation of either the E or D multiplets for this centre, the M centre is assigned to be a single Ho^{3+} ion centre. The configuration of the single Ho^{3+} ion M centre could be either

(i) a Ho^{3+} ion near a vacancy or a Cd^{2+} ion, with the second Ho^{3+} ion too far away for any interaction to occur;

or (ii) a Ho^{3+} ion charge compensated by some monovalent ion, present as an impurity in the starting chemicals.

Absence of any D → Z fluorescence for Z → E excitation is consistent with the earlier proposition that the population of the D multiplet only occurs through upconversion mechanisms (as discussed for the dimer centre (Section 6.1.1)) rather than through phonon assisted decay from the E to the D multiplet as is the case in the CaF_2 type crystals.

Although no excitation spectra for the M centre transitions could be obtained well discriminated from those of the principal dimer centre, excitation spectra for the dimer centre well discriminated from any of the minority centre transitions were obtained by monitoring the $F_1 \rightarrow Z_2$ transition obtained from upconversion. The remaining transitions were then pumped and found to all belong to the M centre.

Fluorescence spectra for all three spectral regions (18000, 15000 and 13000 cm^{-1}) for the M centre closely resemble those for the dimer centre apart from an overall shift in all transitions to lower energies. The $E_1 \rightarrow Z_7$ transition is the strongest transition for both the M and dimer centres, with that for the M

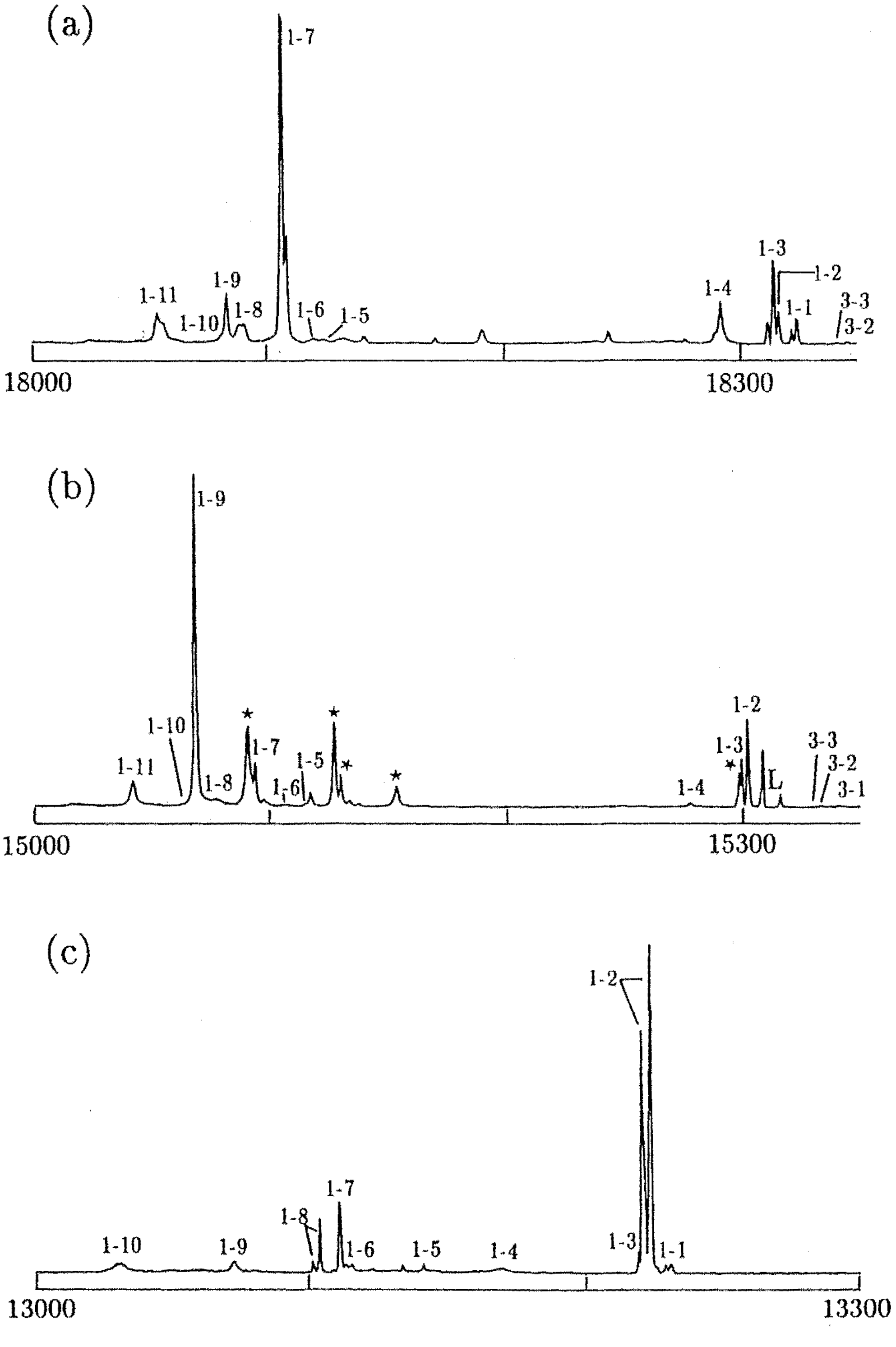

Figure 6.19: 10 K fluorescence spectra of the single Ho^{3+} M centre in $CsCdBr_3:Ho^{3+}(0.01\%)$ crystals :
(a) E→Z transitions, for excitation of the $Z_1 \rightarrow E_3$ transition at 18350.9 cm^{-1};
(b) D→Z transitions, for excitation of the $Z_1 \rightarrow D_1$ transition at 15309.5 cm^{-1};
(c) E→Y transitions, for excitation of the $Z_1 \rightarrow E_3$ transition at 18350.9 cm^{-1}.
The laser position is identified by "L".

Transitions identified by * are for the principal dimer centre.

Table 6.10 : Energies (in cm^{-1}) of the Z, Y, D and E multiplets of the M single ion centre and their symmetries, as derived from the 10 K spectra of CsCdBr$_3$:Ho^{3+} (0.01%) crystals. Uncertainty is ± 0.5 cm^{-1}.

Level	Z($^5I_8$)	Y($^5I_7$)	D($^5F_5$)	E($^5S_2$, $^5F_4$)
1	0.0(γ_3)	5093.0(γ_1)	15309.5(γ_3)	18320.1(γ_3)
2	7.5(γ_2)	5102.0(γ_3)	15318.1(γ_2)	-
3	10.0(γ_3)	5105.0(γ_2)	15348.8(γ_3)	18350.9(γ_3)
4	32.5(γ_1)	5155.0(γ_3)	-	18428.3(γ_3)
5	197.5(γ_3)	5183.0(γ_2)	15470.8(γ_3)	-
6	204.5(γ_3)	5208.5(γ_3)	15481.8(γ_2)	18437.0(γ_2)
7	215.5(γ_3)	5213.0(γ_2)	15497.9(γ_3)	18440.8(γ_3)
8	233.5(γ_1)	5220.5(γ_3)		18461.7(γ_3)
9	241.0(γ_1)	5249.5(γ_3)		18465.3(γ_1)
10	247.0(γ_2)	5291.5(γ_1)		
11	269.0(γ_3)			

centre being only 5% of the intensity of the dimer centre transition. The energy levels derived for the Z, Y, D and E multiplets of the M centre are presented in Table 6.10.

6.2.3 Low symmetry splittings of transitions of the M centre

Splittings assigned as low symmetry crystal-field splittings for the dimer centre were also observed for the M centre. On the whole, such transition splittings were smaller for this centre than for corresponding transitions of the dimer centre.

The E_1 to Z_1, Z_3, Z_4, Z_6, Z_7, Z_8, Z_9 and Z_{11} transitions all show a common splitting of 2.0 cm^{-1}, 0.5 cm^{-1} less than the 2.5 cm^{-1} found for the dimer centre. The $E_1 \rightarrow Z_2$ and $E_1 \rightarrow Z_{10}$ transitions do not show any splitting, while the $E_1 \rightarrow Z_5$ has a smaller splitting of 1.0 cm^{-1}, giving the same overall pattern as found for the dimer centre. All the $D \rightarrow Z$ transitions do not show any splittings.

Transitions from the E_1 level to the Y_1, Y_2, Y_6 and Y_8 levels show the 2.0 cm^{-1} splitting assigned to the E_1 level. Transitions to the Y_2 and Y_8 levels had further splittings of 1.5 cm^{-1} and 0.5 cm^{-1} respectively which are assigned as the respective low symmetry crystal-field splittings for the Y_2 and Y_8 levels of this centre.

6.2.4 Polarisation of the M centre transitions

As for the dimer centre, the measured polarisation ratios were well defined being mostly either 2:1 or 1:3 (Table 6.11). The $E_1 \rightarrow Z_2$ and $E_1 \rightarrow Z_{10}$ transitions were principally σ polarised, while the high energy components of the $E_1 \rightarrow Z_4$, $E_1 \rightarrow Z_8$ and $E_1 \rightarrow Z_9$ transitions were mainly π polarised and the low energy components σ polarised. For transitions to the Z_1, Z_3, Z_6, Z_7 and Z_{11} levels, the low energy components were principally π polarised and the higher energy σ polarised. This is an identical polarisation pattern to that found for the dimer centre.

The $D_1 \rightarrow Z_2$ and $D_1 \rightarrow Z_{10}$ transitions of the M centre did not show any definite polarisation with ratios being close to unity in both cases. This is not

Table 6.11: Observed intensity ratios for the polarised fluorescence transitions from the E and D multiplets of the M single ion centre in <111> oriented $CsCdBr_3:Ho^{3+}$(0.01%) crystals, for excitation of the $Z_1 \rightarrow E_3$ transition at 18350.9 cm^{-1}. For the split transitions, polarisation ratios for both components are given.

Transition	Wavenumber (±0.5) (cm^{-1})	Polarisation Ratios (±15%) [y′y′ : y′x′]
$E_3 \rightarrow Z_2$	18343.5	1 : 2.1
$E_3 \rightarrow Z_3$	18341.0	2.0 : 1
$E_1 \rightarrow Z_1$	18322.0	1 : 2.7
	18320.0	2.9 : 1
$E_1 \rightarrow Z_2$	18314.5	1 : 2.5
$E_1 \rightarrow Z_3$	18312.0	3.2 : 1
	18310.0	3.0 : 1
$E_1 \rightarrow Z_4$	18289.5	2.0 : 1
	18287.5	1 : 3.0
$E \rightarrow Z_5$	18124.5	2.0 : 1
	18123.5	1.8 : 1
$E_1 \rightarrow Z_6$	18118.0	1 : 2.0
	18116.0	2.0 : 1
$E_1 \rightarrow Z_7$	18106.5	1 : 2.2
	18104.5	3.1 : 1
$E_1 \rightarrow Z_8$	18088.5	2.0 : 1
	18086.5	1 : 2.9
$E_1 \rightarrow Z_9$	18081.0	1.5 : 1
	18079.0	1 : 2.4
$E_1 \rightarrow Z_{10}$	18075.0	1 : 3.0
$E_1 \rightarrow Z_{11}$	18053.0	1 : 2.2
	18051.0	2.0 : 1
$D_1 \rightarrow Z_2$	15302.0	1 : 1.1
$D_1 \rightarrow Z_3$	15299.5	1.9 : 1
$D_1 \rightarrow Z_4$	15277.5	1 : 1.3
$D_1 \rightarrow Z_5$	15113.0	1.3 : 1
$D_1 \rightarrow Z_6$	15105.5	1 : 1.2
$D_1 \rightarrow Z_7$	15094.0	1 : 1.4
$D_1 \rightarrow Z_8$	15077.0	1.1 : 1
$D_1 \rightarrow Z_9$	15068.5	1 : 2.0
$D_1 \rightarrow Z_{10}$	15064.0	1 : 1
$D_1 \rightarrow Z_{11}$	15040.5	1.6 : 1
$E_1 \rightarrow Y_1$	13229.0	1 : 3.0
		1 : 2.7
$E_1 \rightarrow Y_2$	13221.5	1 : 3.6
	13219.5	2.1 : 1

Cont....

Table 6.11 cont....

$E_1 \rightarrow Y_3$	13217.0	1 : 3.9
$E_1 \rightarrow Y_4$	13167.0	2.4 : 1
$E_1 \rightarrow Y_5$	13139.0	1 : 2.2
$E_1 \rightarrow Y_6$	13113.5	1 : 1.6
	13111.5	1 : 1.5
$E_1 \rightarrow Y_7$	13109.0	1 : 2.6
$E_1 \rightarrow Y_8$	13101.5	1.7 : 1
	13099.5	5.0 : 1
$E_1 \rightarrow Y_9$	13072.5	1 : 3.0
$E_1 \rightarrow Y_{10}$	13030.5	1.6 : 1

consistent with either the $E_1 \to Z_2$ and $E_1 \to Z_{10}$ transition results for this centre or the corresponding results for the same transitions of the dimer centre where the same two transitions were found to be principally π polarised. Although the ratios obtained for the $D \to Z$ transitions are not as good as for $E \to Z$ transitions, probably due to overlap with transitions from the dimer centre, it is difficult to explain why the $D_1 \to Z_2$ and $D_1 \to Z_{10}$ transitions are almost unpolarised. Corresponding transitions for the dimer centre did not match with the ratios obtained from the $E \to Z$ and $F \to Z$ transitions. The remaining $D \to Z$ transitions of the M centre were polarised the same as corresponding transitions for the dimer centre.

Both components of the $E_1 \to Y_1$ and $E_1 \to Y_6$ transitions were mainly σ polarised. Transitions to the Y_3, Y_5, Y_7 and Y_9 levels were all σ polarised while transitions to the Y_2 and Y_8 levels have oppositely polarised components, with the higher energy component from the E_1 level being mainly π polarised. Transitions to the Y_4 and Y_{10} levels were broad and mainly π polarised.

Irrep label assignments were made using the same analysis as that described for the dimer centre.

6.2.5 Spectroscopy of the N centre

The N centre was identified in both the $CsCdBr_3$:Ho^{3+}(0.3%):Na^+(1%) and the $CsCdBr_3$:Ho^{3+}(0.05%):Na^+(0.2%) crystals and is proposed to be a single Ho^{3+} - single Na^+ centre of the form Cd^{2+} - Ho^{3+} - Na^+ - Cd^{2+}. Most of the transitions for this centre were found to have almost identical energies to those of the M (single ion) centre and could not be resolved from these. Evidence for the presence of Na^+ ions in the sample was found in the relative increase in intensity of the M centre transitions in this crystal compared to those in the parent crystal. The Ho^{3+} - Na^+ centre has the same characteristics as the single Ho^{3+} M centre in that there is no upconversion fluorescence observed for either $Z \to E$ or $Z \to D$ excitation and there is no $D \to Z$ fluorescence observed for $Z \to E$ excitation. There is overlap from dimer centre transitions in the spectra presented here which

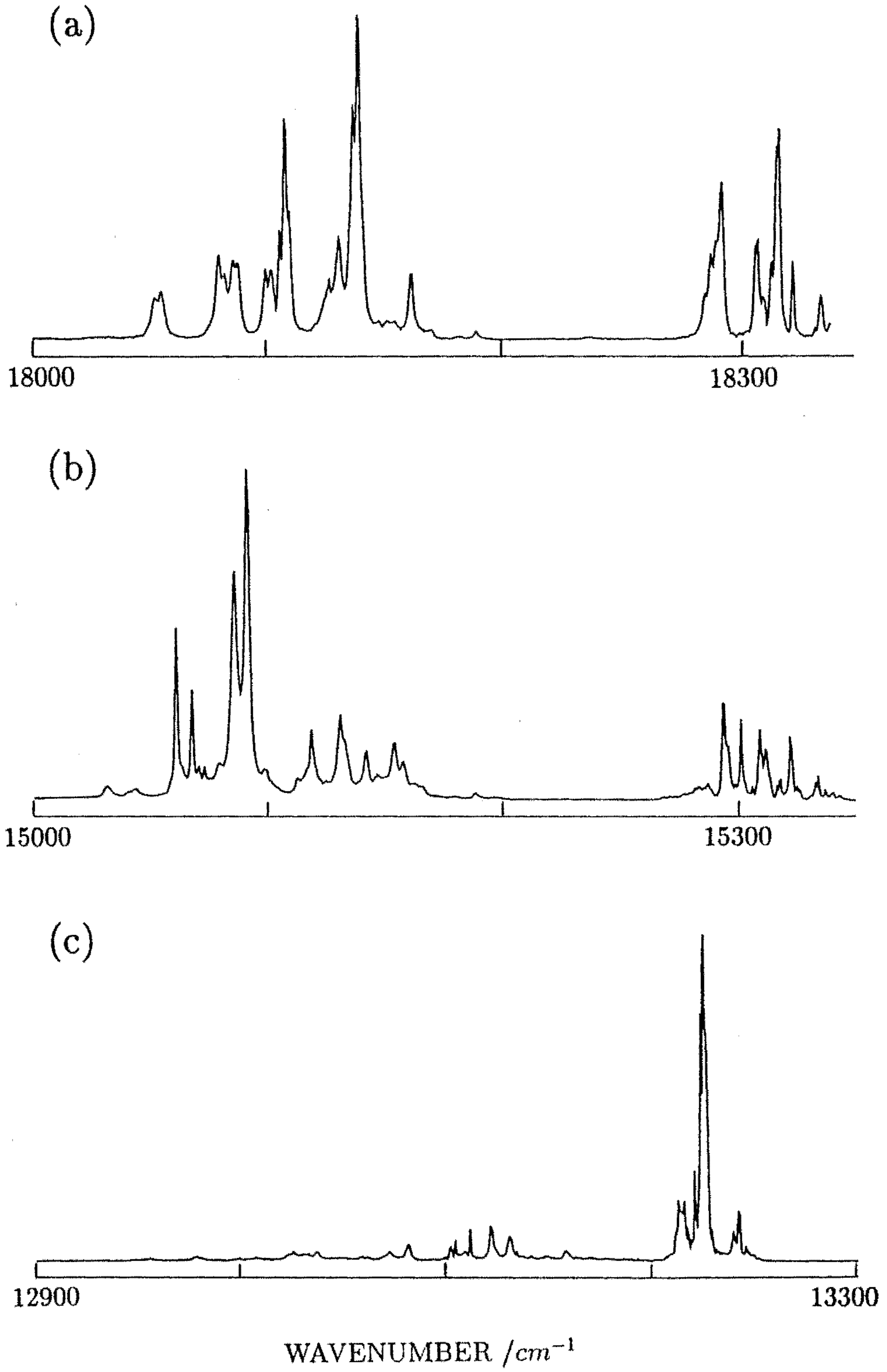

Figure 6.20: 10 K fluorescence spectra of the N centre in $CsCdB_3$:Ho^{3+}(0.3%):Na^{+}(1%) crystals :
(a) E→Z transitions, for excitation of the transition at 18351.4 cm^{-1};
(b) D→Z transitions, for excitation of the transition at 15502.7 cm^{-1};
(c) E→Y transitions, for excitation of the transition at 18351.4 cm^{-1}.

were measured in the 0.3%Ho^{3+}:1%Na^{+} doped crystals. Although the spectra from the lower concentration (0.05%Ho^{3+}:0.2%Na^{+}) doped samples were better able to be discriminated, the resulting fluorescence was too weak to show any splittings clearly.

Like the M and dimer centres, the N centre transitions also have some low symmetry crystal-field splittings measured to be 2.7 cm^{-1} for the E → Z transitions. This is larger than the 2.0 cm^{-1} found for the M centre but close to the 2.5 cm^{-1} found for the dimer centre. Though clearly similar, the M and N single Ho^{3+} ion centres are not the same because the crystal field at the Ho^{3+} ion site is different for the two centres, as evidenced by the difference in the low symmetry crystal-field splittings.

As no distinct transitions could be identified for this centre because of overlap with the M centre transitions, the energy level schemes for the M and N centres are proposed to be almost identical. Typical spectra are presented in Figure 6.20. No polarisation measurements were possible.

6.3 Discussion of the Ho^{3+} Centres in $CsCdBr_3$ Crystals

From the study of the spectral transitions of the principal dimer centre, an energy level scheme complete with irrep label assignments has been obtained, as done for the other rare-earths ions Er^{3+}, Nd^{3+} and Pr^{3+} already studied in the same crystal host. Observation of pair splittings is as for the Er^{3+} dimer centre. While low symmetry crystal-field splittings would not occur for the Kramer's ions Nd^{3+} and Er^{3+}, such splittings have not been reported for Pr^{3+}, the other even electron rare-earth ion studied so far. Observation of low symmetry crystal-field splittings in this study of Ho^{3+} gives evidence that the Ho^{3+} and probably other rare-earth ions, in $CsCdBr_3$ crystals, are displaced from sites of exact C_{3v} symmetry.

The observation of fluorescence from the Q multiplet at ~32850 cm^{-1} with excitation of both the Z → E and Z → D transitions can be accounted for by one of two processes :-

(i) that not only do the two ions making up a dimer centre interact to give upconversion but also ions from neighbouring pairs may interact. This long range interaction would result in the observation of fluorescence originating from higher energy levels than can be accounted for by the simple dimer cooperative upconversion processes.

Any such long range interaction between different ion pairs would be dependent on the dopant concentration. For the 0.1% and 0.3% Ho^{3+} concentrations used here, there did not seem to be any such increase in intensity of fluorescence from the Q multiplet at the higher concentration.

Also, for interaction of different pairs of ions one would expect a different final result for excitation of different multiplets as the paired ions do not necessarily have to have the E and D multiplets as intermediate states for the different excitations. Different higher energy multiplets should be accessible with excitation of different multiplets. There is no evidence of this in the fluorescence spectra measured here with $Z \rightarrow E$ and $Z \rightarrow D$ excitation.

(ii) There could be a manifestation of significant differences in the lifetimes of the final states (multiplets) of the donor and acceptor ions in a pair whereby an initially homo-excited pair eventually behaves more like a hetero-excited pair. In such cases, fluorescence would also be observed from more and higher energy multiplets than can be accounted for by simple direct upconversion process.

This latter process is quite probable for the case encountered here for Ho^{3+}, for two reasons. Firstly, lifetime measurements (to be discussed in Chapter 8) show the same rise time for the F and D multiplets. The transient obtained for monitoring the $D_1 \rightarrow Z_{10}$ transition also shows the F multiplet fluorescence lifetime forming part of that rise time. Secondly, assuming the process to be lifetime dependent, all that is required is that one of the multiplets after the first energy exchange has a shorter lifetime than the other. The process would then be independent of both dopant concentration and which of the E and D multiplets is being excited, as observed here.

Based on the evidence from the fluorescence lifetime measurements, and the lack of concentration dependence for the fluorescence from the Q multiplet, it is proposed that the latter process (as in (ii) above) is responsible for the population of this Q multiplet.

Polarisation measurements have been useful for irrep label assignments to the various levels. It is not clear why the $D_1 \rightarrow Z_2$, $D_1 \rightarrow Z_{10}$, $J_1 \rightarrow Z_2$ and $J_1 \rightarrow Z_{10}$ transitions are mainly π polarised when they are expected to be σ polarised, for the level assignments given. The $E_1 \rightarrow Z_2$ and $E_1 \rightarrow Z_{10}$ transitions indicate a strict selection rule which allows transitions between only one component of the C_{3v} symmetry γ_3 level and a γ_2 symmetry level but allows transitions between both components and γ_1 type levels.

The highest upconversion ratio of 29% obtained for the $F_1 \rightarrow Z_2$ transition in Ho^{3+} is comparable to the 31% reported for the $G_1 \rightarrow Z_3$ transition in Er^{3+} [31]. Such strongest upconversion fluorescence transitions originate from the same spectral region (20400 - 20100 cm^{-1}) for both Ho^{3+} and Er^{3+} ions.

Two main results emerge from the study of the Ho^{3+} minority centres in $CsCdBr_3$ crystals. Firstly, the minority centres are not always single Ho^{3+} ion centres but, depending on the dopant concentration, could be either Ho^{3+} cluster or single Ho^{3+} ion centres. Secondly, the crystal-field environment at the rare-earth ion site in the single Ho^{3+} ion centre is not too different from that in the Ho^{3+} dimer centre, with both centres not being of exact C_{3v} symmetry. The change in the dimer centre environment though, is sufficiently large to shift levels by at least 2 cm^{-1} to lower energies from the single ion levels as well as give larger low symmetry crystal-field splittings.

The N centre transitions could not be clearly distinguished from those of the M centre, showing that the energy levels of the single Ho^{3+} centre and those of the Ho^{3+} - Na^+ centre are close enough to be indistinguishable. The Na^+ ion therefore, has minimal influence on the crystalline environment at the rare-earth ion site. For Nd^{3+} ions co-doped with one of Li^+, Na^+ and Ag^+ [11], transitions for the Nd^{3+} - Li^+, Nd^{3+} - Na^+ and Nd^{3+} - Ag^+ centres were found to be within the linewidth of the single Nd^{3+} ion centre.

Since the L centre exhibits upconversion fluorescence and shows a concentration dependence similar to that of the Nd^{3+} B centre [12], it is proposed that this L centre is a dimer centre of the form Cd^{2+} - Ho^{3+} - Ho^{3+} - V - Cd^{2+}. Because the Ho^{3+} ions in this centre are closer together than those in the well established Cd^{2+} - Ho^{3+} - V - Ho^{3+} - Cd^{2+} dimer centre, energy transfer processes are likely to be more efficient for the L centre than for the principal dimer centre. Ho^{3+} concentrations of 0.5 - 1.0% might be more suitable for the study of this L centre as it is likely to have stronger fluorescence at higher concentrations, although the principal dimer centre will still dominate. Characterisation of the upconversion fluorescence transitions and the respective lifetimes would help establish whether or not the mechanism by which the Q multiplet is populated is the same for both centres. Such measurements could easily be done if the intensity of the L centre fluorescence could be at least double that from the 0.3% Ho^{3+} doped crystals and the transitions better discriminated from those of the principal dimer centre. At the 0.3% concentration, upconversion fluorescence could be measured only for the F and E multiplets. It is hoped that at the higher Ho^{3+} concentrations, fluorescence from the higher energy multiplets would be strong enough to do both spectral and fluorescence lifetime measurements. Upconversion mechanisms and energy transfer rates could then be compared between the two centres.

It is unlikely that co-doping two different rare-earth ions would yield any more information about the dimer centre, unless the dopants have reasonably close energy levels such as for Er^{3+} and Ho^{3+} for example. Heterogeneous rare-earth ion pair studies have been successful only in the case of the Ce^{3+} - Tm^{3+} pair centre [82] because the 4f - 5d transitions of Ce^{3+} at about 27800 cm^{-1} overlap with the $^1D_2$ multiplet of Tm^{3+}. The relative positions of the multiplets of the two different rare-earth ions in the dimer centre is of importance in the $CsCdBr_3$ crystal host, because of the low phonon energies. This is also shown by the absence of any new transitions that could be ascribed to the Er^{3+} - Yb^{3+} pair centre in the $CsCdBr_3$:Er^{3+}:Yb^{3+} crystals studied here, as discussed earlier (at the beginning of this Chapter). The Ho^{3+} and Er^{3+} ions would therefore be suitable as co-dopants because they have several overlapping multiplets. Such a choice however would require careful sorting of the Er^{3+} - Ho^{3+} centre transitions from those of Er^{3+} - Er^{3+} and Ho^{3+} - Ho^{3+} pair centres, as transitions for the latter two centres could easily be simultaneously excited. A heavier and larger monovalent ion co-dopant such as K^+ or Rb^+ might give different low symmetry splittings and even shift all energy levels from those of the single ion centre if the crystal field at the rare-earth ion site is significantly altered by the presence of the larger neighbouring monovalent ion. Other AMX_3 type hosts like $CsMgCl_3$ are obvious alternative hosts for studying the Ho^{3+} dimer and single ion centres.

CHAPTER 7

CRYSTAL-FIELD ANALYSES OF Ho^{3+} IONS IN SITES OF C_{4v} AND C_{3v} SYMMETRY

Crystal-field calculations have been done for Ho^{3+} ions in LaF_3 [25, 26], $LiYF_4$ [98] and $LaCl_3$ [33, 99] crystals among other hosts. In all cases, there were reported good fits of the theoretical energy levels to those measured experimentally. For the C_2 symmetry Ho^{3+} site in LaF_3:Ho^{3+}, 204 experimental levels from 35 multiplets were fitted with an overall standard deviation of only 10 cm^{-1} [25]. Although this standard deviation is small, individual levels have differences of up to 25 cm^{-1} between observed and calculated energies. In $LiYF_4$:Ho^{3+}, correlated and spin-correlated crystal-field effects were included in the calculations with significant improvement to the fits to the levels of the $^3K_{8,7}$, $^5G_{5,4,2}$ and $^3H_{6,5}$ multiplets [98]. For the C_{3h} symmetry Ho^{3+} site in $LaCl_3$ [33], 128 levels were fitted using twenty free parameters resulting in an overall standard deviation of 5.2 cm^{-1}, again with differences for individual levels of up to 34 cm^{-1}. Inclusion of spin-correlated crystal-field effects [108] was found to improve the fit to the $^3K_8$ multiplet levels, reducing the standard deviation for this multiplet $\sigma(^3K_8)$ from 15.5 cm^{-1} to 3.5 cm^{-1}.

For the C_{4v} centre in CaF_2:Ho^{3+}, Reid and Butler [109], using the point group basis representation, derived the relative positions of the levels of the $^5I_8$ multiplet and traced the C_{4v} levels and their irrep labels back to their respective cubic level origins. Because of insufficient experimental data, their scheme was based on crystal-field parameters interpolated from those of the other RE^{3+} (Ce^{3+}, Nd^{3+}, Er^{3+} and Yb^{3+}) ions. Neither the C_{3v} centre in CaF_2 nor any centre in SrF_2 or $CsCdBr_3$ have received any attention, because their energy levels had not been well established to date. Having determined, in the work reported here, a fair number of the possible energy levels for the two major centres and two modified C_{4v} symmetry centres in both CaF_2:Ho^{3+} and SrF_2:Ho^{3+} crystals and for a further two centres in $CsCdBr_3$:Ho^{3+} crystals, it was appropriate to attempt some crystal-field fittings, to try to establish how the spectroscopic similarities and differences between the particular centres would appear in the respective crystal-field parameters. Crystal-field fits were also performed to provide an independent check on the irrep label assignments made from polarisation measurements.

The crystal-field routine used here was that supplied by Dr M.F. Reid of the University of Hong Kong. The crystal-field Hamiltonian used is of the form

$$H = H_o + H_{el} + H_{so} + H_{cf} ,$$

where

(i) H_o is the spherically symmetric part of the free ion Hamiltonian comprising the kinetic energy of the $4f^{10}$ electrons and their central-field Coulomb interaction with the nucleus;

(ii) $$H_{el} = \sum_{k=0,2,4,6} f_k F^k + \alpha L(L+1) + \beta G(G_2) + \gamma G(R_7) + \sum_{i=2,3,4,6,7,8} t_i T^i$$

The first term is the usual electrostatic interaction between the ten 4f electrons while the higher order terms are the electrostatic correlation terms for two-body and three-body configuration interactions respectively. The F^k are the electrostatic integrals and the f_k form the angular part of the electrostatic interaction. α, β and γ are the two body parameters, $G(G_2)$ and $G(R_7)$ are Casimir's operators for the groups G_2 and R_7 respectively and L is the total orbital angular momentum. T^i and t_i are the three body parameters and operators respectively;

(iii) $$H_{so} = A_{so}\zeta + \sum_{f=2,4,6} p_f P^f + \sum_{h=0,2,4} m_h M^h$$

where the first term is the usual spin-orbit interaction term and the other two are the magnetically correlated (spin-spin and spin-other-orbit) and electrostatically correlated spin-orbit terms respectively. Here ζ is the spin-orbit integral and A_{so} is the angular part of the spin-orbit interaction. The M^h (Marvin integrals) and P^f are the magnetic and electrostatic correlation parameters respectively with m_h and p_f as corresponding parameters;

(iv) $$H_{cf} = \sum_{k,q,i} B^k_q(C^{(k)}_q)_i + V_{ccf} + V_{sccf}$$

The first term is the usual crystal-field Hamiltonian. Correlation and spin correlation crystal-field effects (V_{ccf} amd V_{sccf} respectively) can also be added as higher order terms. These have not been written out in full as they are not used in the crystal-field analysis attempted here. The B^k_q are the crystal-field parameters and $C^{(k)}_q$ are Racah tensor operators which transform as corresponding spherical harmonics. For C_{4v} and C_{3v} symmetry centres studied here, the respective crystal fields of the form given in Chapter 2 have been used.

The free ion parameters are adopted from the analysis of $LaCl_3$:Ho^{3+} [33] and the crystal-field parameters from the crystal-field analysis of CaF_2:Er^{3+} [30, 42] have been used as a starting point for the fitting procedure. The standard deviation σ for the crystal-field fit of the levels of each centre was calculated from

$$\sigma = \sum [(\Delta E_i)^2 / (n-p)]^{\frac{1}{2}} ,$$

where ΔE_i is the difference between experimental and theoretical energies for each particular level, n is the total number of experimental energy levels used for the particular fit and p is the number of parameters that were varied.

As the crystal-field fitting program was used with a $4f^4$ rather than a $4f^{10}$ configuration, all the crystal-field (B^k_q), spin-orbit (ζ) and three-body (T^i) parameters obtained from the fits have opposite signs to those expected for a $4f^{10}$ configuration. The parameters reported here (Tables 7.4, 7.7, 7.10, 7.13, 7.16 and

Table 7.1: The free ion parameters adopted from $LaCl_3$:Ho^{3+}[33] and not varied here (all quantities in cm^{-1})

Parameter	**Value**
α	17.3
β	-624
γ	2084
T^2	287
T^3	37
T^4	98
T^6	-313
T^7	421
T^8	359
M^0	3.04
P^2	528

7.17) have been corrected accordingly for this sign change.

7.1 Centres in CaF_2 and SrF_2 Type Crystals

There were four aims to this crystal-field analysis :-

(i) to establish trends in parameters in going from A to the modified C_{4v} symmetry centres;

(ii) to compare parameters for the CaF_2 and SrF_2 host crystals for both the A and B centres;

(iii) to compare parameters for the A and B centres for Ho^{3+} to those previously determined for Er^{3+} as these two ions are expected to have similar crystal-field parameters;

(iv) to establish irrep labels for some of the levels for the B centres in CaF_2 and SrF_2.

7.1.1 The A and B centres

The fitted energy levels and corresponding irrep labels for the A and B centres in CaF_2:Ho^{3+} and SrF_2:Ho^{3+} crystals are presented in Tables 7.2, 7.3, 7.5 and 7.6. For both the A and B centres of Ho^{3+}, the corresponding crystal-field parameters for Er^{3+} are given in brackets for each host (Tables 7.4 and 7.7).

The Er^{3+} parameters given here for the A centre have been derived from those of Freeth et al. [42, 43] by using equations 2.7(c), which give the relationship between the C_{4v} symmetry crystal-field Hamiltonian used here and that used by Freeth et al. [42, 43]. Such a conversion was necessary for a direct comparison to be made between the crystal-field parameters of Ho^{3+} and Er^{3+} ions in the same C_{4v} symmetry centre. For the Er^{3+} B and J centres, the crystal-field parameters given here are those of Cockcroft et al. [30].

For the CaF_2 A centre, 39 levels were fitted with a standard deviation of 3.9 cm^{-1} (Tables 7.2 and 7.4) and for the CaF_2 B centre 41 levels were fitted with a standard deviation of 3.3 cm^{-1} (Tables 7.5 and 7.7). There is good agreement with Er^{3+} parameters for both the A and B centres (Tables 7.4 and 7.7). For the

Table 7.2: C_{4v} symmetry crystal-field level fits to the $^5I_8$(Z), $^5I_7$(Y), $^5F_5$(D), $^5S_2$(E), $^5F_4$(E) and $^5F_3$(F) multiplets of the A centre in CaF_2:Ho^{3+} crystals. All quantities are in cm^{-1} in air.

Multiplet	State	Symmetry	Calculated	Observed	Difference
$^5I_8$	Z_1	γ_1	-2.3	0.0	2.3
	Z_2	γ_2	-1.4	1.9	3.3
	Z_3	γ_5	84.6	83.0	-1.6
	Z_4	γ_3	117.9	115.5	-2.4
	Z_5	γ_5	133.7	128.0	-5.7
	Z_6	γ_4	162.2	158.0	-4.2
	Z_7	γ_1	288.0	284.5	-3.5
	Z_8	γ_2	292.3	292.5	0.2
	Z_9	γ_3	450.1	455.0	4.9
	Z_{10}	γ_5	472.3	475.0	2.7
	Z_{11}	γ_1	494.5	492.0	-2.5
	Z_{12}	γ_5	510.9	513.0	2.1
	Z_{13}	γ_4	512.1	-	
$^5I_7$	Y_1	γ_5	5255.6	5257.0	1.4
	Y_2	γ_3	5272.0	5273.0	1.0
	Y_3	γ_5	5270.2	5274.0	3.8
	Y_4	γ_2	5274.1	-	
	Y_5	γ_4	5281.0	-	
	Y_6	γ_1	5305.7	5308.5	2.8
	Y_7	γ_5	5333.2	5332.0	-1.2
	Y_8	γ_3	5356.9	5355.0	-1.9
	Y_9	γ_4	5406.9	-	
	Y_{10}	γ_5	5416.7	5413.0	-3.7
	Y_{11}	γ_2	5424.4	-	
$^5F_5$	D_1	γ_3	15606.1	15605.0	-1.1
	D_2	γ_5	15609.2	15609.5	0.3
	D_3	γ_2	15623.3	15623.0	-0.3
	D_4	γ_1	15673.1	15682.0	8.9
	D_5	γ_5	15756.8	15752.2	-4.6
	D_6	γ_2	15759.6	15756.1	-3.5
	D_7	γ_4	15771.7	-	
	D_8	γ_5	15823.2	15823.5	0.3
$^5S_2$,$^5F_4$	E_1	γ_3	18606.2	18599.0	-7.2
	E_2	γ_1	18615.4	18613.2	-2.2
	E_3	γ_5	18657.3	18655.1	-2.2
	E_4	γ_4	18660.9	18666.5	5.6
	E_5	γ_3	18673.7	18681.5	7.8
	E_6	γ_5	18730.2	18726.8	-3.4
	E_7	γ_1	18749.0	18750.1	1.1
	E_8	γ_4	18790.2	-	
	E_9	γ_2	18833.1	18834.9	1.8
	E_{10}	γ_5	18859.5	18859.5	0
	E_{11}	γ_1	18889.6	18888.3	-1.3
$^5F_3$	F_1	γ_2	20741.0	20741.6	0.6
	F_2	γ_5	20780.6	20781.6	1.0
	F_3	γ_3	20846.1	-	
	F_4	γ_4	20862.7	-	
	F_5	γ_5	20925.9	20924.5	-1.4

Table 7.3: C_{4v} symmetry crystal-field level fits to the $^5I_8$(Z), $^5I_7$(Y), $^5F_5$(D), $^5S_2$(E), $^5F_4$(E) and $^5F_3$(F) multiplets of the A centre in SrF_2:Ho^{3+} crystals. All quantities are in cm^{-1} in air.

Multiplet	State	Symmetry	Calculated	Observed	Difference
$^5I_8$	Z_1	γ_1	-3.1	0.0	3.1
	Z_2	γ_2	-1.6	2.7	4.3
	Z_3	γ_5	54.2	52.5	-1.7
	Z_4	γ_3	79.2	75.5	-3.7
	Z_5	γ_5	96.5	89.0	-7.5
	Z_6	γ_4	119.4	-	
	Z_7	γ_1	261.4	255.5	-5.9
	Z_8	γ_2	266.2	265.5	-0.7
	Z_9	γ_3	377.6	377.0	-0.6
	Z_{10}	γ_5	389.8	393.0	3.2
	Z_{11}	γ_1	403.0	403.0	0
	Z_{12}	γ_4	429.2	430.0	0.8
	Z_{13}	γ_5	438.2	443.0	4.8
$^5I_7$	Y_1	γ_5	5221.4	5220.5	-0.9
	Y_2	γ_2	5222.8	-	
	Y_3	γ_3	5233.2	5231.0	-2.2
	Y_4	γ_5	5241.2	5241.5	0.3
	Y_5	γ_4	5247.9	-	
	Y_6	γ_1	5252.7	5255.5	2.8
	Y_7	γ_5	5285.5	5283.5	-2.0
	Y_8	γ_3	5301.4	5303.5	2.1
	Y_9	γ_4	5341.9	-	
	Y_{10}	γ_5	5347.9	5348.5	0.6
	Y_{11}	γ_2	5353.5	-	
$^5F_5$	D_1	γ_5	15591.4	15593.0	1.6
	D_2	γ_3	15592.0	-	
	D_3	γ_2	15598.2	15599.0	0.8
	D_4	γ_1	15636.0	15642.3	6.3
	D_5	γ_5	15730.5	15727.8	-2.7
	D_6	γ_2	15737.8	15735.1	-2.7
	D_7	γ_4	15746.0	-	
	D_8	γ_5	15766.9	15764.1	-2.8
$^5S_2$,$^5F_4$	E_1	γ_3	18582.6	18579.5	-3.1
	E_2	γ_1	18586.4	18585.7	-0.7
	E_3	γ_5	18624.0	18624.8	0.8
	E_4	γ_4	18627.6	-	
	E_5	γ_3	18664.5	18671.5	7.0
	E_6	γ_5	18722.6	18718.7	-3.9
	E_7	γ_1	18724.4	18729.0	4.6
	E_8	γ_2	18772.1	18771.0	-1.1
	E_9	γ_4	18773.3	-	
	E_{10}	γ_5	18818.6	18817.5	-1.1
	E_{11}	γ_1	18837.1	18833.7	-3.4
$^5F_3$	F_1	γ_2	20736.0	20735.5	-0.5
	F_2	γ_5	20755.5	20756.5	1.0
	F_3	γ_3	20823.5	-	
	F_4	γ_4	20845.5	-	
	F_5	γ_5	20882.6	-	

Table 7.4: Free ion and crystal-field parameters for the C_{4v} symmetry centres in $CaF_2:Ho^{3+}$ and $SrF_2:Ho^{3+}$ crystals. Parameters for the Er^{3+} A centre in $CaF_2:Er^{3+}$ are given in brackets (all quantities (except n) are in cm^{-1}).

Parameter	CaF_2 A centre	SrF_2 A centre
F^2	95961±26	96009±15
F^4	66875±19	66868±19
F^6	47099±38	46886±37
ζ	2139±2(2390)	2139±2
B^2_A	685±9(608)	338±9
B^4_A	356±9(409)	297±9
B^6_A	419±7(403)	325±8
B^4_C	-1085±8(-1172)	-1030±8
B^6_C	557±4(505)	488±4
n	39	36
σ	3.9	3.7

A centre, the Ho^{3+} parameters are within 10% of the Er^{3+} parameters with the fourth degree axial and cubic parameters being smaller in magnitude for Ho^{3+} while both the second and the sixth degree axial parameters are larger than for Er^{3+}. For the B centre, corresponding Ho^{3+} and Er^{3+} parameter values lie within 25% of each other, except for the fourth degree cubic parameter which is 45% smaller for Ho^{3+} than for Er^{3+}.

For the SrF_2 A centre, 36 levels were fitted with a standard deviation of 3.7 cm^{-1} (Tables 7.3 and 7.4). The resulting second degree axial crystal-field parameter B^2_A, is about half that for the CaF_2 A centre. Corresponding to this change in the crystal-field parameter B^2_A, is the observed energy separations between the lowest levels of a given multiplet (except Z) which are reduced by about 50% in going from CaF_2 to SrF_2. The higher degree axial and cubic crystal-field parameters are all reduced in SrF_2 by up to 25% of the CaF_2 values. For the B centre, the second degree axial crystal-field parameter B^2_A in SrF_2 is reduced by 75% from that in CaF_2 while the fourth degree axial crystal-field parameter B^4_A is 2.5 times larger. The sixth degree axial and cubic crystal-field parameters are decreased by up to 35% in SrF_2 compared to CaF_2. As for the CaF_2 B centre, the axial and cubic components of the crystal field are of comparable magnitude for the Ho^{3+} B centre (Table 7.7). Both the previously discussed polarisation results and the crystal-field parameters found here, suggest the same C_{3v} configuration for the SrF_2 B centre as for the CaF_2 B centre.

In SrF_2:Er^{3+} crystals, the principal centre labelled J, was found by both EPR [8, 18] and laser selective excitation [30, 68] measurements, to be of C_{3v} symmetry. This J centre was proposed to have a different configuration from that of the B centre in CaF_2:Er^{3+}, although they both have the C_{3v} symmetry. For the B centre, a model configuration in which the eight-fold symmetry from the cubic arrangement of the nearest neighbour lattice F^- ions around the Er^{3+} ion, was broken by the presence of a vacancy at one of the F^- sites was proposed [30, 75, 128], while the J centre was assigned the more usual next nearest neighbour F^-

Table 7.5: C_{3v} symmetry crystal-field level fits to the $^5I_8$(Z), $^5I_7$(Y), $^5F_5$(D), $^5S_2$(E), $^5F_4$(E) and $^5F_3$(F) multiplets of the B centre in CaF_2:Ho^{3+} crystals. All quantities are in cm^{-1} in air.

Multiplet	State	Symmetry	Calculated	Observed	Difference
$^5I_8$	Z_1	γ_3	-2.9	0.0	2.9
	Z_2	γ_3	28.2	27.0	-1.2
	Z_3	γ_1	64.5	65.0	0.5
	Z_4	γ_2	79.4	81.0	1.6
	Z_5	γ_3	144.5	138.5	-6.0
	Z_6	γ_3	178.9	178.5	-0.4
	Z_7	γ_2	183.3	-	
	Z_8	γ_1	214.1	213.5	-0.6
	Z_9	γ_3	365.7	367.5	1.8
	Z_{10}	γ_3	413.6	417.5	3.9
	Z_{11}	γ_1	422.9	423.5	0.6
$^5I_7$	Y_1	γ_3	5202.2	5202.5	0.3
	Y_2	γ_1	5216.2	5212.7	-3.5
	Y_3	γ_3	5224.2	5218.9	-5.3
	Y_4	γ_2	5221.1	5223.5	2.4
	Y_5	γ_3	5234.8	5235.3	0.5
	Y_6	γ_1	5237.8	5239.5	1.7
	Y_7	γ_2	5238.3	5240.9	2.6
	Y_8	γ_3	5252.5	5253.9	1.4
	Y_9	γ_3	5274.2	5272.9	-1.3
	Y_{10}	γ_2	5282.2	5280.9	-1.3
$^5F_5$	D_1	γ_2	15608.4	15604.0	-4.4
	D_2	γ_3	15606.0	15605.5	-0.5
	D_3	γ_3	15613.2	15613.0	-0.2
	D_4	γ_2	15617.8	15618.0	0.2
	D_5	γ_1	15629.9	15627.7	-2.2
	D_6	γ_3	15631.7	15628.5	-3.2
	D_7	γ_3	15649.0	15647.0	-2.0
$^5S_2$,$^5F_4$	E_1	γ_3	18566.4	18567.5	1.1
	E_2	γ_1	18566.8	18569.5	2.7
	E_3	γ_3	18569.6	18570.5	1.0
	E_4	γ_3	18627.9	18633.7	5.8
	E_5	γ_1	18654.9	18657.8	2.9
	E_6	γ_2	18657.4	18665.2	7.8
	E_7	γ_3	18717.4	18712.8	-4.6
	E_8	γ_3	18750.9	18751.0	0.1
	E_9	γ_1	18772.3	18773.5	1.2
$^5F_3$	F_1	γ_3	20718.8	20715.0	-3.8
	F_2	γ_1	20719.9	20722.4	2.5
	F_3	γ_2	20751.1	20749.5	-1.6
	F_4	γ_3	20780.4	20779.3	-1.1
	F_5	γ_2	20802.9	20800.8	-2.1

Table 7.6: C_{3v} symmetry crystal-field level fits to the $^5I_8$(Z), $^5I_7$(Y), $^5F_5$(D), $^5S_2$(E) and $^5F_4$(E) multiplets of the B centre in SrF_2:Ho^{3+} crystals. All quantities are in cm^{-1} in air.

Multiplet	State	Symmetry	Calculated	Observed	Difference
$^5I_8$	Z_1	γ_3	4.5	0.0	-4.5
	Z_2	γ_3	20.6	26.5	5.9
	Z_3	γ_1	55.5	52.5	-3.0
	Z_4	γ_2	67.8	70.0	2.2
	Z_5	γ_3	144.2	148.0	3.8
	Z_6	γ_2	158.8	-	
	Z_7	γ_3	167.6	163.0	-4.6
	Z_8	γ_1	184.2	184.0	-0.2
	Z_9	γ_3	313.5	315.0	1.5
	Z_{10}	γ_3	353.2	354.0	0.8
	Z_{11}	γ_1	361.4	359.5	-1.9
$^5I_7$	Y_1	γ_3	5184.7	5183.0	-1.7
	Y_2	γ_2	5187.7	5189.0	1.3
	Y_3	γ_3	5196.0	5193.5	-2.5
	Y_4	γ_1	5200.3	5200.5	0.2
	Y_5	γ_1	5211.8	5208.5	-3.3
	Y_6	γ_2	5213.0	5214.0	1.0
	Y_7	γ_3	5217.5	5219.5	2.0
	Y_8	γ_3	5222.8	5226.0	3.2
	Y_9	γ_3	5241.2	5241.0	-0.2
	Y_{10}	γ_2	5247.1	5247.0	-0.1
$^5F_5$	D_1	γ_2	15596.0	15595.5	-0.5
	D_2	γ_3	15601.8	15601.5	-0.3
	D_3	γ_2	15613.0	15615.5	2.5
	D_4	γ_3	15615.0	-	
	D_5	γ_3	15627.0	-	
	D_6	γ_1	15632.0	15630.5	-1.5
	D_7	γ_3	15640.3	-	
$^5S_2$,$^5F_4$	E_1	γ_1	18560.7	18561.6	0.9
	E_2	γ_3	18564.1	18564.0	-0.1
	E_3	γ_3	18566.2	18565.6	-0.6
	E_4	γ_3	18639.6	-	
	E_5	γ_1	18667.3	18666.7	-0.6
	E_6	γ_2	18673.4	-	
	E_7	γ_3	18718.6	-	
	E_8	γ_3	18735.1	18736.5	1.4
	E_9	γ_1	18767.8	18767.2	-0.6

Table 7.7: Free ion and crystal-field parameters for the C_{3v} symmetry centres in $CaF_2:Ho^{3+}$ and $SrF_2:Ho^{3+}$ crystals. Parameters for the Er^{3+} B and J centers are given in brackets in the respective columns (quantities in cm^{-1}).

Parameter	**CaF_2 B centre**	**SrF_2 B centre**
F^2	95896±20	95382±31
F^4	67035±16	67182±17
F^6	47029±29	45527±45
ζ	2140±2	2136±2
B^2_A	197±7(140.6)	52±8(189.0)
B^4_A	-72±9(-76.7)	-184±10(-246.8)
B^6_A	223±8(-341.6)	-149±7(-280.4)
$\hat{B}^6_A$	-676±6(-530.7)	-526±6(103.6)
B^4_C	46±6(82.8)	-58±7(1113.0)
B^6_C	681±5(581.0)	605±5(986.7)
n	41	30
σ	3.3	2.9

interstitial configuration of Figure 1.2(b) [30, 75]. This difference in the configurations for the two Er^{3+} centres is apparent in the crystal-field parameters obtained for the two centres [30] which are included in Table 7.7. For the Er^{3+} B centre, the axial and cubic crystal-field parameters are comparable whereas for the J centre, the axial crystal-field parameters are much smaller than the cubic crystal-field parameters.

There is not much resemblance between the Ho^{3+} SrF_2 B centre and the Er^{3+} J centre parameters, with the fourth degree cubic crystal-field parameter B^4_c for the Ho^{3+} B centre being only 5% of that for the Er^{3+} J centre. Therefore, although the Er^{3+} J centre of SrF_2 does not have the same configuration as the Er^{3+} B centre of CaF_2, the B centres in CaF_2 and SrF_2 for Ho^{3+} are expected to have the same configuration as the Er^{3+} B centre because all the crystal-field parameters are comparable for the Ho^{3+} centres.

For the energy levels of both the C_{4v} and the C_{3v} symmetry centres in $CaF_2:Ho^{3+}$and $SrF_2:Ho^{3+}$, irrep label assignments based on crystal-field calculations (Tables 7.2, 7.3, 7.5 and 7.6) were in agreement with those based on polarisation measurements (Tables 4.1, 4.3, 5.1 and 5.3). For the C_{3v} symmetry centres, irrep labels (γ_1 and γ_3) for some of the levels were identified by these crystal-field calculations as the polarisation data were insufficient for a complete assignment.

7.1.2 The modified C_{4v} symmetry centres (CS1, CB1, SC1 and SB1)

The fitted energy levels for the CS1 and CB1 centres are presented in Tables 7.8 and 7.9 respectively, while those for the SC1 and SB1 centres are presented in Tables 7.11 and 7.12 respectively. The resulting crystal-field parameters are presented in Table 7.10 for the CS1 and CB1 centres and Table 7.13 for the SC1 and SB1 centres.

The relative magnitudes of the crystal-field parameters obtained for the modified C_{4v} symmetry centres in $CaF_2:Ho^{3+}$ and $SrF_2:Ho^{3+}$ crystals, with respect to the corresponding A centre, are shown schematically in Figures 7.1 and 7.2

Table 7.8: C_{4v} symmetry crystal-field level fits to the $^5I_8$(Z), $^5I_7$(Y), $^5F_5$(D), $^5S_2$(E) and $^5F_4$(E) multiplets of the CS1 centre in $Ca_{0.99}Sr_{0.01}F_2:Ho^{3+}$ crystals. All quantities are in cm^{-1} in air.

Multiplet	**State**	**Symmetry**	**Calculated**	**Observed**	**Differnce**
	Z_1	γ_1	-1.8	0.0	1.8
	Z_2	γ_2	-0.1	2.0	2.1
	Z_3	γ_5	70.3	70.0	-0.3
	Z_4	γ_3	100.4	99.5	-0.9
	Z_5	γ_5	118.8	115.0	-3.8
	Z_6	γ_4	143.1	-	
	Z_7	γ_1	296.0	296.0	0
	Z_8	γ_2	301.9	301.0	-0.9
	Z_9	γ_3	441.5	441.5	0
	Z_{10}	γ_5	458.0	458.5	0.5
	Z_{11}	γ_1	474.6	473.0	-1.6
	Z_{12}	γ_5	503.8	506.5	2.7
	Z_{13}	γ_4	499.3	-	
$^5I_7$	Y_1	γ_5	5252.7	5254.5	1.8
	Y_2	γ_3	5265.0	5266.5	1.5
	Y_3	γ_5	5268.7	5269.5	0.8
	Y_4	γ_2	5257.8	-	
	Y_5	γ_4	5278.9	-	
	Y_6	γ_1	5293.7	5295.0	1.3
	Y_7	γ_5	5323.4	5323.0	-0.4
	Y_8	γ_3	5343.8	5345.0	1.2
	Y_9	γ_4	5395.4	-	
	Y_{10}	γ_5	5402.6	5398.0	-4.6
	Y_{11}	γ_2	5409.0	-	
$^5F_5$	D_1	γ_3	15601.8	15600.0	-1.8
	D_2	γ_5	15603.0	15603.0	0
	D_3	γ_2	15614.0	15614.0	0
	D_4	γ_1	15660.8	15663.5	2.7
	D_5	γ_5	15761.8	-	
	D_6	γ_2	15766.3	-	
	D_7	γ_4	15778.4	-	
	D_8	γ_5	15813.0	-	
$^5S_2$,$^5F_4$	E_1	γ_3	18593.6	18590.0	-3.6
	E_2	γ_1	18600.8	18601.0	0.2
	E_3	γ_5	18644.9	18646.6	1.7
	E_4	γ_4	18648.0	-	
	E_5	γ_3	18668.5	-	
	E_6	γ_5	18729.8	18725.6	-4.2
	E_7	γ_1	18740.9	18744.3	3.4
	E_8	γ_4	18790.9	-	
	E_9	γ_2	18805.2	18808.5	3.3
	E_{10}	γ_5	18848.1	18848.0	-0.1
	E_{11}	γ_1	18872.0	18870.5	-1.5

Table 7.9: C_{4v} symmetry crystal-field level fits to the $^5I_8(Z)$, $^5I_7(Y)$, $^5F_5(D)$, $^5S_2(E)$ and $^5F_4(E)$ multiplets of the CB1 centre in $Ca_{0.99}Ba_{0.01}F_2:Ho^{3+}$ crystals. All quantities are in cm^{-1} in air.

Multiplet	State	Symmetry	Calculated	Observed	Difference
$^5I_8$	Z_1	γ_1	-2.7	0.0	2.7
	Z_2	γ_2	-0.8	2.0	2.8
	Z_3	γ_5	64.5	63.5	-1.0
	Z_4	γ_3	93.7	92.0	-1.7
	Z_5	γ_5	111.5	107.5	-4.0
	Z_6	γ_4	136.4	-	
	Z_7	γ_1	297.4	296.0	-1.4
	Z_8	γ_2	303.6	303.0	-0.6
	Z_9	γ_3	434.8	433.5	-1.3
	Z_{10}	γ_5	449.9	451.5	1.6
	Z_{11}	γ_1	465.7	464.5	-1.2
	Z_{12}	γ_5	499.8	503.5	3.7
	Z_{13}	γ_4	491.4	-	
$^5I_7$	Y_1	γ_5	5248.0	5250.0	2.0
	Y_2	γ_3	5261.6	5262.0	0.4
	Y_3	γ_5	5269.6	5270.0	0.4
	Y_4	γ_2	5250.4	-	
	Y_5	γ_4	5277.6	-	
	Y_6	γ_1	5286.9	5289.0	2.1
	Y_7	γ_5	5319.8	5319.5	-0.3
	Y_8	γ_3	5338.1	5337.5	-0.6
	Y_9	γ_4	5388.3	-	
	Y_{10}	γ_5	5394.8	5390.5	-4.3
	Y_{11}	γ_2	5400.9	-	
$^5F_5$	D_1	γ_3	15599.8	15598.5	-1.3
	D_2	γ_5	15599.7	15600.0	0.3
	D_3	γ_2	15608.7	15608.5	-0.2
	D_4	γ_1	15653.3	15655.5	2.2
	D_5	γ_5	15761.3	-	
	D_6	γ_2	15767.9	-	
	D_7	γ_4	15778.6	-	
	D_8	γ_5	15806.8	-	
$^5S_2$,$^5F_4$	E_1	γ_3	18590.1	18586.0	-4.1
	E_2	γ_1	18596.7	18596.6	-0.1
	E_3	γ_5	18642.0	18644.1	2.1
	E_4	γ_4	18645.1	-	
	E_5	γ_3	18669.0	-	
	E_6	γ_5	18731.2	18728.2	-3.0
	E_7	γ_1	18738.6	18743.0	4.4
	E_8	γ_4	18791.4	-	
	E_9	γ_2	18794.6	18797.4	2.8
	E_{10}	γ_5	18844.7	18843.0	-1.7
	E_{11}	γ_1	18866.3	18864.9	-1.4

Table 7.10: Free ion and crystal-field parameters for the modified C_{4v} symmetry centres in $Ca_{0.99}Sr_{0.01}F_2:Ho^{3+}$ and $Ca_{0.99}Ba_{0.01}F_2:Ho^{3+}$ crystals (quantities in cm^{-1}).

Parameter	**CS1 centre**	**CB1 centre**
F^2	96887±29	96796±31
F^4	66522±17	66553±18
F^6	49005±43	48786±46
ζ	2143±2	2142±2
B^2_A	508±6	428±7
B^4_A	367±7	356±7
B^6_A	376±5	370±6
B^4_C	-1169±6	-1196±7
B^6_C	557±3	556±3
n	30	30
σ	2.6	2.8

Table 7.11. C_{4v} symmetry crystal field level fits to the $^5I_8$(Z), $^5I_7$(Y), $^5F_5$(D), $^5S_2$(E), $^4F_4$(E) and $^5F_3$(F) multiplets of the SC1 centre in $Sr_{0.99}Ca_{0.01}F_3$:Ho^{3+} crystals. All quantities are in cm^{-1} in air.

Multiplet	State	Symmetry	Calculated	Observed	Difference
$^5I_8$	Z_1	γ_1	-3.4	0.0	3.4
	Z_2	γ_2	-1.8	2.5	4.3
	Z_3	γ_5	44.0	41.5	-2.5
	Z_4	γ_3	65.7	61.0	-4.7
	Z_5	γ_5	87.3	80.0	-7.3
	Z_6	γ_4	108.4	-	
	Z_7	γ_1	278.5	279.0	0.5
	Z_8	γ_2	283.8	282.0	-1.8
	Z_9	γ_3	375.3	372.0	-3.3
	Z_{10}	γ_5	386.7	389.0	2.3
	Z_{11}	γ_1	398.7	401.0	2.3
	Z_{12}	γ_4	430.9	430.0	-0.9
	Z_{13}	γ_5	442.5	445.5	3.0
$^5I_7$	Y_1	γ_5	5217.3	5217.0	-0.3
	Y_2	γ_2	5216.6	-	
	Y_3	γ_3	5232.3	5231.5	-0.8
	Y_4	γ_5	5245.0	5246.0	1.0
	Y_5	γ_4	5249.6		
	Y_6	γ_1	5247.9	5249.5	1.6
	Y_7	γ_5	5292.2	5289.0	-3.2
	Y_8	γ_3	5300.7	5302.5	1.8
	Y_9	γ_4	5339.2	-	
	Y_{10}	γ_5	5344.9	5345.0	0.1
	Y_{11}	γ_2	5350.2	-	
$^5F_5$	D_1	γ_5	15587.4	15590.0	2.6
	D_2	γ_3	15591.0	-	
	D_3	γ_2	15591.8	15594.5	2.7
	D_4	γ_1	15625.8	15630.0	4.2
	D_5	γ_5	15735.2	15735.4	0.2
	D_6	γ_2	15747.6	15742.4	-5.2
	D_7	γ_4	15751.1	-	
	D_8	γ_5	15769.0	15767.7	-1.3
$^5S_2$,$^5F_4$	E_1	γ_3	18578.6	18574.5	-4.1
	E_2	γ_1	18582.1	18579.9	-2.2
	E_3	γ_5	18624.2	18626.4	2.2
	E_4	γ_4	18627.3	-	
	E_5	γ_3	18668.9	18672.0	3.1
	E_6	γ_5	18726.1	18725.5	-0.6
	E_7	γ_1	18719.6	18725.1	5.5
	E_8	γ_2	18760.5	18757.2	-3.3
	E_9	γ_4	18780.3	-	
	E_{10}	γ_5	18817.9	18817.3	-0.6
	E_{11}	γ_1	18836.1	18831.0	-5.1
$^5F_3$	F_1	γ_2	20735.2	20736.0	0.8
	F_2	γ_5	20748.7	20750.0	1.3
	F_3	γ_3	20829.1	-	
	F_4	γ_4	20849.8	-	
	F_5	γ_5	20879.8	-	

Table 7.12: C_{4v} symmetry crystal-field level fits to the $^5I_8$(Z), $^5I_7$(Y), $^5F_5$(D), $^5S_2$(E), $^5F_4$(E) and $^5F_3$(F) multiplets of the SB1 centre in $Sr_{0.99}Ba_{0.01}F_2:Ho^{3+}$ crystals. All quantities are in cm^{-1} in air.

Multiplet	State	Symmetry	Calculated	Observed	Difference
$^5I_8$	Z_1	γ_1	-1.1	0.0	1.1
	Z_2	γ_2	1.0	2.5	1.5
	Z_3	γ_5	36.9	37.0	0.1
	Z_4	γ_3	54.7	54.0	-0.7
	Z_5	γ_5	82.6	76.0	-6.6
	Z_6	γ_4	97.2	91.0	-6.2
	Z_7	γ_1	293.3	291.0	-2.1
	Z_8	γ_2	300.9	305.0	4.1
	Z_9	γ_3	376.0	378.0	2.0
	Z_{10}	γ_5	382.4	383.5	1.1
	Z_{11}	γ_1	391.5	394.0	2.5
	Z_{12}	γ_4	431.9	430.0	-1.9
	Z_{13}	γ_5	443.9	445.5	1.6
$^5I_7$	Y_1	γ_5	5214.4	5215.5	1.1
	Y_2	γ_2	5212.5	-	
	Y_3	γ_3	5230.0	5230.5	0.5
	Y_4	γ_5	5246.9	5245.5	-1.4
	Y_5	γ_4	5250.9	-	
	Y_6	γ_1	5247.5	5247.0	-0.5
	Y_7	γ_5	5299.9	5305.0	5.1
	Y_8	γ_3	5301.4	5301.5	0.1
	Y_9	γ_4	5340.5	-	
	Y_{10}	γ_5	5344.9	5341.5	-3.4
	Y_{11}	γ_2	5348.8	-	
$^5F_5$	D_1	γ_5	15583.0	15588.0	5.0
	D_2	γ_3	15587.9	-	
	D_3	γ_2	15585.6	15593.0	7.4
	D_4	γ_1	15619.7	15624.0	4.3
	D_5	γ_5	15736.6	15733.6	-3.0
	D_6	γ_2	15756.2	15750.5	-5.7
	D_7	γ_4	15757.3	-	
	D_8	γ_5	15770.4	15770.9	0.5
$^5S_2$,$^5F_4$	E_1	γ_3	18575.6	18571.0	-4.6
	E_2	γ_1	18578.6	18575.8	-2.8
	E_3	γ_5	18623.8	18625.2	1.4
	E_4	γ_4	18626.5	-	
	E_5	γ_3	18671.4	18671.0	-0.4
	E_6	γ_5	18728.4	18723.8	-4.6
	E_7	γ_1	18715.6	18722.1	6.5
	E_8	γ_2	18750.5	18747.8	-2.7
	E_9	γ_4	18787.2		
	E_{10}	γ_5	18815.3	18815.0	-0.3
	E_{11}	γ_1	18834.7	18829.1	-5.6
$^5F_3$	F_1	γ_2	20737.2	20737.0	-0.2
	F_2	γ_5	20740.7	20746.0	5.3
	F_3	γ_3	20828.4	-	
	F_4	γ_4	20852.5	-	
	F_5	γ_5	20878.8	-	

Table 7.13: Free ion and crystal-field parameters for the modified C_{4v} symmetry centres in $Sr_{0.99}Ca_{0.01}F_2:Ho^{3+}$ and $Sr_{0.99}Ba_{0.01}F_2:Ho^{3+}$ crystals (quantities in cm^{-1}).

Parameter	**SC1 centre**	**SB1 centre**
F^2	96129±26	96272±30
F^4	66844±19	66830±22
F^6	47148±37	47487±43
ζ	2140±2	2141±3
B_A^2	235±9	153±10
B_A^4	261±10	271±10
B_A^6	287±7	229±8
B_C^4	-1119±8	-1185±8
B_C^6	502±4	509±5
n	36	37
σ	3.6	4.2

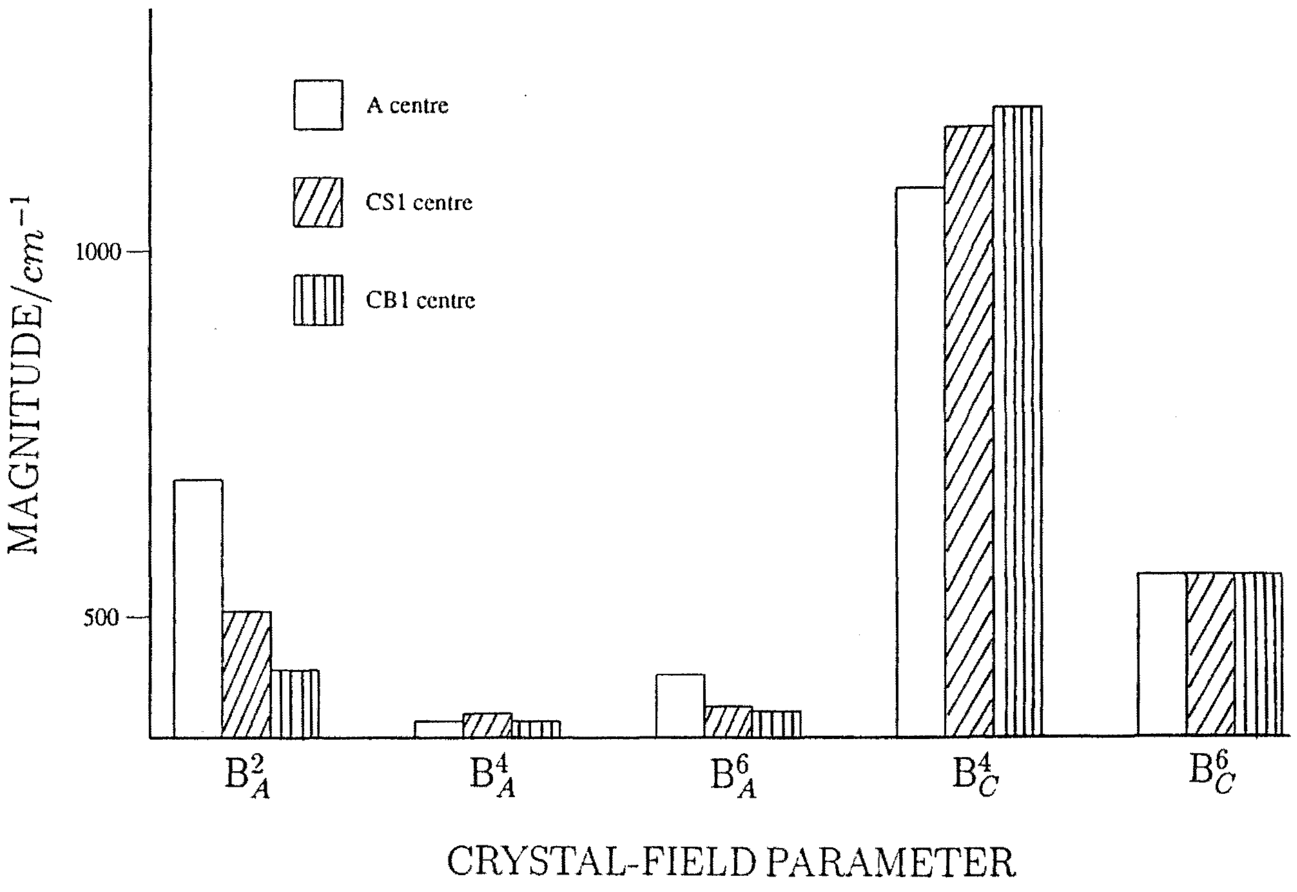

Figure 7.1: Relative magnitudes of the crystal-field parameters for the A, CS1 and CB1 centres in $CaF_2:Ho^{3+}$ type crystals.

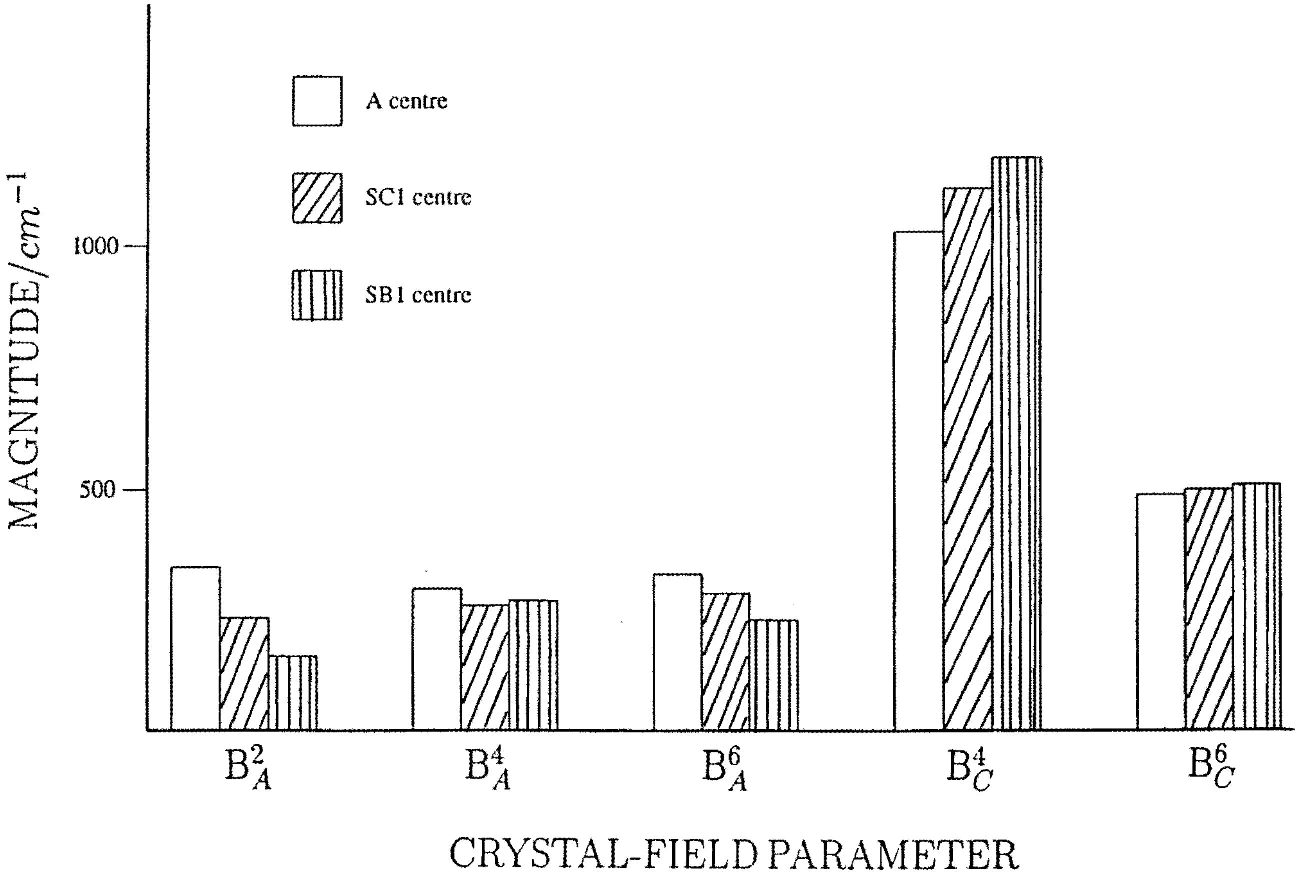

Figure 7.2: Relative magnitudes of the crystal-field parameters for the A, SC1 and SB1 centres in $SrF_2:Ho^{3+}$ type crystals.

respectively.

In general, there is a decrease in the second degree axial crystal-field parameter in going from the A centre to the modified centres, with the Ba^{2+} centre having the lowest values in both CaF_2 and SrF_2. The cubic part of the field (which is derived from the eight neighbouring F^- ions) is the same in the parent and modified centres while the axial components are markedly altered in the modified centres. This is to be expected as, from the C_{4v} model assigned to these centres, the dopant cation is most likely to have some effect on the interstitial F^- ion but, being two lattice spacings away from the Ho^{3+} ion, is unlikely to have any effect on the eight F^- ions surrounding the Ho^{3+} ion, which give the main contribution to the cubic crystal field.

For all centres, irrep labels determined from the crystal-field analysis (Tables 7.8, 7.9, 7.11 and 7.12) are in agreement with those from polarisation studies (Tables 4.6, 4.11, 5.5 and 5.6).

7.2 The Dimer and M (single ion) Centres in $CsCdBr_3$:Ho^{3+} Crystals

Pr^{3+} and Nd^{3+} are among the most widely studied rare-earths in $CsCdBr_3$. For Pr^{3+} [102], it was found that the octahedral part of the field at the rare-earth ion site was appreciably larger than the axial part. It was concluded that the rare-earth ions in $CsCdBr_3$ crystals were in a mainly octahedral field with an additional weak trigonal distortion. For Nd^{3+} [10] a crystal-field analysis of the 48 levels derived gave a standard deviation of 15 cm^{-1}, although differences were up to 117 cm^{-1} between observed and calculated energies for individual levels. The crystal field of the Nd^{3+} ions of the dimer centre was concluded to be largely cubic.

For the Ho^{3+} dimer centre here, 86 levels were used for the crystal-field fit which gave a standard deviation of 21 cm^{-1}, with differences of up to 50 cm^{-1} between the observed and calculated energies for individual levels. For the M (single ion) centre a standard deviation of 16 cm^{-1} was obtained for 34 levels.

The levels are presented in Table 7.14 for the dimer centre and Table 7.15 for the M centre. Fewer levels were available for the M centre as it does not exhibit any upconversion fluorescence which precludes identification of levels of higher energy multiplets than the E multiplet. For the M centre, there was not much difference in the crystal-field fit resulting from setting α, β and γ to either the $LaCl_3$ values or the dimer centre values, but the dimer centre values were chosen for the results presented here, for consistency with that centre. Parameters for both centres are presented in Table 7.16.

There is little change in the parameters between the dimer and the M single ion centre, except for the fourth degree axial and the sixth degree cubic crystal-field parameters, B^4_A and B^4_C, which for the M centre are larger than those for the principal dimer centre.

From the possible model configurations of the M centre given in Chapter 6 (Section 6.2.2), this M centre is either of the form Cd^{2+} - Ho^{3+} - Cd^{2+} - Cd^{2+} with the second Ho^{3+} ion further away along the chain, or of the form Cd^{2+} - Ho^{3+} - M^+ - Cd^{2+} where M^+ is a monovalent ion. In either configuration , the Ho^{3+} ion does not have any neighbouring vacant site and this accounts for the axial component of the crystal field being stronger for the M centre, than for the dimer centre where there is a neighbouring vacant site. For the dimer centre, the presence of the vacant site also induces the repositioning of the six Br^- ions around each Ho^{3+} ion. The Br^- ions in the dimer centre are likely to be further out spatially compared to those around the Ho^{3+} ion of the M centre, thereby causing some reduction in the cubic crystal field at the Ho^{3+} site in the dimer centre. Both these effects are manifested in the following two observations made about the energy levels :-

(i) levels for the dimer centre have somewhat lower energies than for the single ion centre;

and (ii) the observed low symmetry crystal-field splittings are larger for the dimer centre than for the M single ion centre.

Table 7.14: C_{3v} symmetry crystal-field level fits to 18 multiplets of the dimer centre in $CsCdBr_3:Ho^{3+}$ crystals. All quantities are in cm^{-1} in air.

Multiplet	State	Symmetry	Calculated	Observed	Difference
$^5I_8$(Z)	Z_1	γ_3	10.2	0	-10.2
	Z_2	γ_2	36.1	5.5	-30.6
	Z_3	γ_3	19.6	9.0	-10.6
	Z_4	γ_1	55.3	26.0	-29.3
	Z_5	γ_3	135.1	155.0	19.9
	Z_6	γ_3	167.1	162.0	-5.1
	Z_7	γ_3	208.5	178.0	-30.5
	Z_8	γ_1	175.5	188.5	13.0
	Z_9	γ_1	190.6	190.5	-0.1
	Z_{10}	γ_2	226.1	217.0	-9.1
	Z_{11}	γ_3	224.8	237.0	12.2
$^5I_7$(Y)	Y_1	γ_3	5109.7	5092.8	-16.9
	Y_2	γ_1	5114.2	5095.0	-19.2
	Y_3	γ_3	5115.6	5166.0	50.4
	Y_4	γ_2	5131.0	5174.0	43.0
	Y_5	γ_2	5193.3	5182.5	-10.8
	Y_6	γ_3	5170.6	5187.0	16.4
	Y_7	γ_3	5221.1	5195.5	-22.6
	Y_8	γ_2	5206.7	5215.0	8.3
	Y_9	γ_3	5234.8	5236.5	1.7
	Y_{10}	γ_1	5239.7	5285.5	45.8
$^5I_6$(A)	A_1	γ_1	8617.1	8595.5	-21.6
	A_2	γ_3	8621.4	8606.0	-15.4
	A_3	γ_2	8619.8	8624.5	4.7
	A_4	γ_1	8646.2	8641.0	-5.2
	A_5	γ_3	8634.9	8670.5	35.6
	A_6	γ_3	8701.7	8681.5	-20.2
	A_7	γ_2	8687.1	8708.0	20.9
	A_8	γ_3	8721.6	8735.5	13.9
	A_9	γ_1	8729.7	8768.5	38.8
$^5I_5$(B)	B_1	γ_2	11170.5	11164.0	-6.5
	B_2	γ_3	11181.5	11171.5	-10.0
	B_3	γ_3	11192.6	11191.5	-1.1
	B_4	γ_3	11225.1	11221.5	-3.6
	B_5	γ_2	11238.4	11227.5	-10.9
	B_6	γ_3	11259.3	11248.5	-10.8
	B_7	γ_1	11269.7	-	
$^5I_4$(C)	C_1	γ_3	13184.5	13215.5	31.0
	C_2	γ_2	13230.9	13221.0	-9.9
	C_3	γ_1	13252.6	-	
	C_4	γ_3	13282.8	-	
	C_5	γ_1	13365.2	13338.0	-27.2
	C_6	γ_3	13366.3	13369.5	3.2

cont....

Table 7.14 (p.2) cont....

Multiplet	**State**	**Symmetry**	**Calculated**	**Observed**	**Difference**
$^5F_5$(D)	D_1	γ_3	15322.8	15307.5	-15.3
	D_2	γ_2	15312.4	15314.5	2.1
	D_3	γ_3	15359.5	15341.5	-18.0
	D_4	γ_1	15386.3	15411.5	25.2
	D_5	γ_3	15455.6	15442.2	-13.4
	D_6	γ_3	15476.5	15471.0	-5.5
	D_7	γ_2	15456.8	15483.0	26.2
$^5S_2$(E)	E_1	γ_3	18317.9	18315.2	-2.7
	E_2	γ_1	18327.0	18340.5	13.5
	E_3	γ_3	18332.2	18342.5	10.3
$^5F_4$(E)	E_4	γ_3	18416.2	18416.3	0.1
	E_5	γ_3	18438.2	18434.9	-3.3
	E_6	γ_1	18396.3	18439.2	42.9
	E_7	γ_2	18439.4	18443.1	3.7
	E_8	γ_1	18480.2	18448.2	-32.0
	E_9	γ_3	18481.2	18457.2	-24.0
$^5F_3$(F)	F_1	γ_2	20401.2	20390.0	-11.2
	F_2	γ_3	20467.7	20435.0	32.7
	F_3	γ_3	20508.3	-	
	F_4	γ_1	20529.6	-	
	F_5	γ_2	20563.3	-	
$^3K_8$(H)	H_1	γ_3	21075.6	21076.5	0.9
	H_2	γ_1	21076.1	21079.5	3.4
	H_3	γ_3	21081.3	21083.5	2.2
	H_4	γ_1	21089.2	-	
	H_5	γ_1	21094.3	-	
	H_6	γ_3	21099.1	21096.5	-2.6
	H_7	γ_3	21112.8	-	
	H_8	γ_2	21141.0	-	
	H_9	γ_2	21151.5	-	
	H_{10}	γ_3	21156.4	-	
	H_{11}	γ_3	21159.1	-	
$^5G_6$(I)	I_1	γ_3	21729.5	21727.5	-2.0
	I_2	γ_2	21716.3	21738.0	21.7
	I_3	γ_3	21755.5	-	
	I_4	γ_2	21758.9	-	
	I_5	γ_1	21805.4	-	
	I_6	γ_1	21856.3	-	
	I_7	γ_3	21898.9	-	
	I_8	γ_3	21928.7	-	
	I_9	γ_1	21934.8	-	
$^5G_5$(J)	J_1	γ_3	23682.9	23656.5	-26.4
	J_2	γ_2	23677.2	23675.5	-1.7
	J_3	γ_3	23703.3	23684.0	-19.3
	J_4	γ_1	23745.1	-	
	J_5	γ_2	23748.1	-	
	J_6	γ_3	23765.2	-	
	J_7	γ_3	23783.1	-	

cont....

Table 7.14 (p.3) cont....

Multiplet	**State**	**Symmetry**	**Calculated**	**Observed**	**Difference**
$^5G_4$(K)	K_1	γ_3	25577.7	25597.0	19.3
	K_2	γ_1	25541.7	-	
	K_3	γ_3	25609.7	25626.5	16.8
	K_4	γ_2	25622.1	-	
	K_5	γ_3	25628.9	25637.5	8.6
	K_6	γ_1	25629.8	-	
$^3H_5$(M)	M_1	γ_3	27242.4	27247.5	5.1
	M_2	γ_1	27258.3	27251.5	-6.8
	M_3	γ_3	27285.7	-	
	M_4	γ_3	27323.7	-	
	M_5	γ_2	27341.0	-	
	M_6	γ_3	27355.1	-	
	M_7	γ_2	27363.5	-	
$^5G_3$(O)	O_1	γ_3	28196.5	28214.0	17.5
	O_2	γ_1	28189.4	-	
	O_3	γ_3	28214.1	-	
	O_4	γ_2	28226.4	-	
	O_5	γ_2	28331.4	-	
$^3K_6$(P)	P_1	γ_1	29765.5	29748.5	-17.0
	P_2	γ_3	29774.3	29758.0	-16.3
	P_3	γ_3	29778.9	29769.0	-9.9
	P_4	γ_2	29785.6	29786.0	0.4
	P_5	γ_2	29802.4	29806.5	4.1
	P_6	γ_3	29804.6	-	
	P_7	γ_1	29814.5	-	
	P_8	γ_3	29816.6	-	
	P_9	γ_1	29832.2	-	
$^3D_2$(P′)	P'_1	γ_1	30551.0	30546.0	-5.0
	P'_2	γ_3	30573.2	30564.5	-8.7
	P'_3	γ_3	30594.0	-	
$^3D_3$(Q)	Q_1	γ_2	32812.8	32844.0	31.2
	Q_2	γ_3	32845.8	32847.5	1.7
	Q_3	γ_1	32868.7	32866.0	-2.7
	Q_4	γ_3	32881.0	32894.0	13.0
	Q_5	γ_2	32948.1	-	
$^3F_2$(U)	U_1	γ_3	35511.9	35499.0	-12.9
	U_2	γ_1	35523.6	35522.5	-1.1
	U_3	γ_3	35591.5	-	

Table 7.15: C_{3v} symmetry crystal-field level fits to the $^5I_8$(Z), $^5I_7$(Y), $^5S_2$(E), and $^5F_4$(E) multiplets of the M single ion centre of $CsCdBr_3:Ho^{3+}$ crystals. All quantities are in cm^{-1} in air.

Multiplet	State	Symmetry	Calculated	Observed	Difference
$^5I_8$	Z_1	γ_3	-3.5	0.0	-3.5
	Z_2	γ_2	22.6	7.5	-15.1
	Z_3	γ_3	22.1	10.0	-12.1
	Z_4	γ_1	27.4	32.5	5.1
	Z_5	γ_3	197.1	197.5	0.4
	Z_6	γ_3	211.9	204.5	-7.4
	Z_7	γ_3	233.5	215.5	-18.0
	Z_8	γ_1	212.1	233.5	21.4
	Z_9	γ_1	221.2	241.0	19.8
	Z_{10}	γ_2	229.9	247.0	17.1
	Z_{11}	γ_3	268.4	269.0	0.6
$^5I_7$	Y_1	γ_1	5105.3	5093.0	-12.3
	Y_2	γ_3	5114.3	5102.0	-12.3
	Y_3	γ_2	5107.2	5105.0	-2.2
	Y_4	γ_3	5123.5	5155.0	31.5
	Y_5	γ_2	5199.5	5183.0	-16.5
	Y_6	γ_3	5202.1	5208.5	6.4
	Y_7	γ_2	5214.1	5213.0	-1.1
	Y_8	γ_3	5235.7	5220.5	-15.2
	Y_9	γ_3	5257.7	5249.5	-8.2
	Y_{10}	γ_1	5262.6	5291.5	28.9
$^5F_5$	D_1	γ_3	15308.4	15309.5	1.1
	D_2	γ_2	15294.0	15318.1	24.1
	D_3	γ_3	15353.6	15348.8	-4.8
	D_4	γ_1	15342.5	-	
	D_5	γ_3	15471.1	15470.8	0.3
	D_6	γ_2	15487.9	15481.8	-6.1
	D_7	γ_3	15515.6	15497.9	-17.7
$^5S_2$	E_1	γ_3	18330.2	18320.1	-10.1
	E_2	γ_1	18321.1	-	
	E_3	γ_3	18345.6	18350.9	5.3
$^5F_4$	E_4	γ_3	18413.9	18428.3	14.4
	E_5	γ_1	18381.7	-	
	E_6	γ_2	18438.7	18437.0	-1.7
	E_7	γ_3	18443.8	18440.8	-3.0
	E_8	γ_3	18464.1	18461.7	-2.4
	E_9	γ_1	18464.4	18465.3	0.9

Table 7.16: Free ion and crystal-field parameters for the dimer and M single ion centres in $CsCdBr_3:Ho^{3+}$ crystals (quantities in cm^{-1}).

Parameter	**Dimer Centre**	**M Single Ion Centre**
F^2	93661±50	93734±167
F^4	62833±112	63676±111
F^6	45144±82	46242±244
α	9±4	9*
β	-516±21	-516*
γ	2784±50	2784*
ξ	2136±6	2135±12
B^2_A	443±39	387±39
B^4_A	-674±42	-1317±39
B^6_A	412±41	387±33
$\hat{B}^6_A$	30±37	74±38
B^4_C	482±33	384±36
B^6_C	24±34	-171±32
n	86	34
σ	21	16

* α, β and γ were not varied for the M single ion centre.

Table 7.17: Free ion and crystal-field parameters for the Nd^{3+} and Er^{3+} dimer centres in $CsCdBr_3$ crystals (quantities in cm^{-1}).

Parameter	**Nd^{3+}**	**Er^{3+}**
F^2	70807	97772±67
F^4	51875	70366±80
F^6	35144	48154±82
α	21.9	17.7
β	-670	-582
γ	1586	1800
ξ	875	2363±8
B^2_A	-302	-148±52
B^4_A	-1474	-992±53
B^6_A	206	254±46
$\hat{B}^6_A$	392	101±53
B^4_C	496	472±44
B^6_C	8	14±39
n	48	46
σ	15	22

Parameters for Nd^{3+} were derived from Fit B of Barthem, Buisson and Cone [10] by using equations 2.8(c).

(i) would be a direct result of a more expanded arrangement of the Br^- ligands around the Ho^{3+} ion of the dimer centre, giving reduced Coulomb and crystal-field interactions. As Cd^{2+} is larger than Ho^{3+} (or any other rare-earth), it is possible that the Ho^{3+} ion is not centrally placed in the same way as the Cd^{2+}, but is slightly shifted off centre and probably off the c axis as well. Such a shift would be larger for the Ho^{3+} ion of the dimer centre that for the Ho^{3+} ion of the M single ion centre because of the vacancy, hence the larger low symmetry crystal-field splittings observed for the dimer centre ((ii) above). The Ho^{3+} ions in both centres are not in sites of exact C_{3v} symmetry.

The crystal-field parameters for the Nd^{3+} dimer centre derived from those of Barthem et al. [10] by using equations 2.8(c), and those for the Er^{3+} dimer centre obtained from a calculation done here using the energy level data of Cockroft et al. [29] are presented in Table 7.17.

From comparison of the parameters for the Ho^{3+}, Nd^{3+} and Er^{3+} dimer centre crystal-field parameters (Tables 7.16 and 7.17), it can be seen that the cubic crystal-field parameters are comparable to the axial crystal-field parameters for all three centres. This is contrary to the conclusion made by Barthem et al. [10] that the crystal-field at the Nd^{3+} ion site is approximately cubic. In their calculations, the crystal-field Hamiltonian used is that of equation 2.8(b), and for this Hamiltonian, the crystal field would be largely cubic if the relations

$$B^4_3 = -1.195\, B^4_0$$
$$B^6_3 = 0.604\, B^6_0$$
$$B^6_6 = 0.633\, B^6_0$$

hold for the crystal-field parameters obtained [54]. From the crystal-field parameters of their Fit B [10], the following relations are obtained

$$B^4_3 = -1.237\, B^4_0$$
$$B^6_3 = 0.638\, B^6_0$$
$$B^6_6 = 0.140\, B^6_0 .$$

However, parameters constrained to satisfy the cubic symmetry relations of

Hutchings [54] above, (Fit C of Barthem et al. [10]) were also found to give a satisfactory crystal-field fit, leading to the conclusion that the crystal-field at the Nd^{3+} ion site is largely cubic.

The results obtained here (Tables 7.16 and 7.17) show the cubic crystal-field parameters being comparable to the axial crystal-field parameters, and the crystal-field at the Ho^{3+}, Nd^{3+} and Er^{3+} ion sites cannot be said to be largely cubic.

CHAPTER 8

FLUORESCENCE LIFETIME MEASUREMENTS

In addition to the spectroscopic results presented in Chapters 4, 5 and 6, fluorescence lifetimes were measured for the Ho^{3+} centres in the CaF_2 and SrF_2 type crystals, and for the Ho^{3+} dimer centre in $CsCdBr_3$. Fluorescence lifetime measurements are important for evaluating ion-lattice and ion-ion interactions for particular host and dopant systems. Such knowledge is required for an understanding of fluorescence processes and relaxation mechanisms for rare-earth ions in excited electronic states.

The fluorescence lifetimes measured are determined by the combined effects of the two main processes of radiative and non-radiative decay. The latter includes relaxation by phonon emission and energy transfer processes resulting from ion-ion coupling. Radiative relaxation includes pure electronic and phonon-assisted emission transitions. These processes depend on several aspects, including the particular ion and lattice involved, magnitudes of the various energy gaps, the temperature and the nature of coupling between ions.

The general expression for the observed transient of an excited state a is of the form :

$$\frac{1}{\tau_{ab}} = \sum_b W^R_{ab} + \sum_b W^{NR}_{ab} , \qquad 8.1$$

for transitions from a to all final states b. Here τ_{ab} is the measured lifetime, W^R_{ab} is the radiative decay probability and W^{NR}_{ab} is the non-radiative probability. W^R_{ab} and W^{NR}_{ab} can vary from being of comparable magnitude to being widely different. For systems of essentially uncoupled ions, such as dilute systems, the contribution to W^{NR}_{ab} is wholly from multiphonon emission processes.

The least squares fitting routine GUSCOR used to fit the fluorescence lifetime transients observed here was written by Dr. J.B. Ward of the Department.

Depending on the shape of the transients observed, one of two expressions could be used to obtain either just the fluorescence decay time of a state or both the fluorescence rise and decay times.

Transients without a rise time were fitted to the expression

$$I = A + Be^{-t/d}, \tag{8.2}$$

where d is the lifetime of the particular multiplet and A and B are the base-line and amplitude parameters respectively.

Transients showing a rise time were fitted to the expression

$$I = A + B(e^{-t/d} - e^{-t/f}), \tag{8.3}$$

where d and f are the fluorescence decay and rise times respectively.

Expression 8.3 is applicable to the upconversion fluorescence transients observed for the dimer centre in $CsCdBr_3:Ho^{3+}$ crystals while expression 8.2 is for transients obtained from direct excitation of the respective multiplets in $CaF_2:Ho^{3+}$, $SrF_2:Ho^{3+}$ and $CsCdBr_3:Ho^{3+}$ crystals.

8.1 Centres in CaF_2 and SrF_2 Type Crystals

In 1978, fluorescence lifetime measurements for the A and B centres in $CaF_2:Ho^{3+}$, for Ho^{3+} concentrations in the range 0.01 - 0.1% and for temperatures varied between 80 K and 573 K were reported [71]. As expected, the fluorescence lifetimes were found to decrease with increase in both the Ho^{3+} concentration and the temperature. Later, Seelbinder and Wright [117] presented low temperature (10 K) fluorescence lifetime measurements for $CaF_2:Ho^{3+}$(0.01%) crystals. Fluorescence decay times for the D, E and F multiplets for both the A and B centres, and for the D multiplet of the C, D and E cluster centres were reported. More recently, Tang et al. [123] used fluorescence lifetime measurements to distinguish between transitions for the A and B centres in a laser excitation study of $CaF_2:Ho^{3+}$(0.01%) crystals at 77 K.

Riseberg and Moos [113] measured multi-phonon relaxation rates for the F and E multiplets of Ho^{3+} in $SrF_2:Ho^{3+}$(1%) crystals, among other systems.

Multi-phonon relaxation processes were found to depend on the crystal host (both through the respective phonon cut-off frequency and magnitude of the static crystal field), the relevant energy gaps between the multiplets and the temperature. The spontaneous multi-phonon emission transition rate was found to have an exponential dependence on the energy gap separating an emitting multiplet from the next lower energy multiplet.

8.1.1 Temporal results

Fluorescence lifetimes measured here for the E and D multiplets of the A and B centres in $CaF_2:Ho^{3+}$(0.005%) are in exact agreement with those obtained by Seelbinder and Wright for their 0.01% doped crystals. For the E multiplet, the A centre has a longer fluorescence lifetime than the B centre, while for the D multiplet the B centre has the longer lifetime. The temporal transients are presented in Figure 8.1 and the corresponding fluorescence lifetimes listed in Table 8.1.

For the modified centres found in $Ca_{0.99}Sr_{0.01}F_2:Ho^{3+}$ and $Ca_{0.99}Ba_{0.01}F_2:Ho^{3+}$ crystals, the fluorescence lifetimes are close to those measured for the A centre, indicating a parent A centre origin for the four centres CS1, CS2, CB1 and CB2. The transients are presented in Figures 8.2 and 8.3, and the resulting fluorescence decay times also listed in Table 8.1.

In $SrF_2:Ho^{3+}$ fluorescence lifetimes were measured for the A, SC1, SC2 and SB1 centres while fluorescence for the B and SB2 centres was just too weak to give any reliable lifetime results. The transients for the A, SB1, SC1 and SC2 are presented in Figures 8.4 and 8.5, while the measured fluorescence lifetimes are included in Table 8.1.

The relative magnitudes of the observed fluorescence lifetimes for the E and D multiplets of the A and the respective modified centres in both CaF_2 and SrF_2 type crystals are shown schematically in Figures 8.6 and 8.7 respectively.

8.1.2 Dependence of fluorescence lifetimes on crystal-field parameters

The analysis here is a preliminary attempt to understand the fluorescence

Figure 8.1: 10 K temporal transients for the A and B centres in $CaF_2:Ho^{3+}$(0.005%) crystals :

(a) the A centre $E \rightarrow Z$ fluorescence, with excitation of the $Z_1 \rightarrow E_2$ transition at 18613.2 cm^{-1} and monitoring the $E_1 \rightarrow Z_4$ transition at 18483.5 cm^{-1};

(b) the B centre $E \rightarrow Z$ fluorescence, with excitation of the $Z_1 \rightarrow E_4$ transition at 18633.7 cm^{-1} and monitoring the $E_2 \rightarrow Z_2$ transition at 18542.5 cm^{-1};

(c) the A centre $D \rightarrow Z$ fluorescence, with excitation of the $Z_1 \rightarrow D_2$ transition at 15609.5 cm^{-1} and monitoring the $D_1 \rightarrow Z_3$ transition at 15522.5 cm^{-1};

(d) the B centre $D \rightarrow Z$ fluorescence, with excitation of the $Z_1 \rightarrow D_4$ transition at 15618.0 cm^{-1} and monitoring the $D_2 \rightarrow Z_3$ transition at 15541.0 cm^{-1}.

The solid curves give the best fits to the temporal transient data with the resulting decay times as presented in Table 8.1

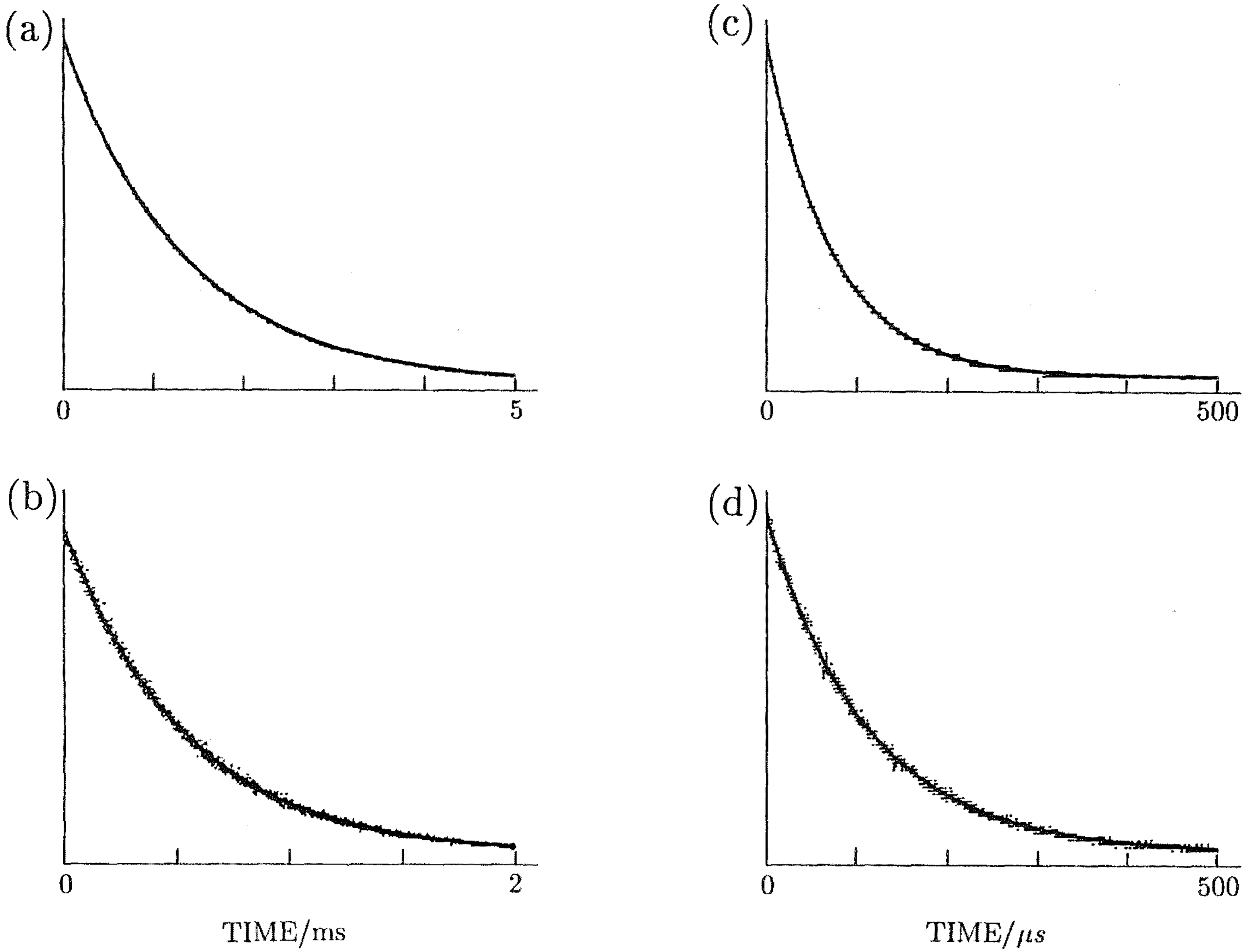
(a)
0
5
(c)
0
500
(b)
0
2
TIME/ms
(d)
0
500
TIME/μs

Figure 8.2: 10 K temporal transients for the CS1 and CS2 centres in $Ca_{0.99}Sr_{0.01}F_2$:Ho^{3+}(0.005%) crystals :

(a) the CS1 centre $E \rightarrow Z$ fluorescence, with excitation of the $Z_1 \rightarrow E_2$ transition at 18601.0 cm^{-1} and monitoring the $E_1 \rightarrow Z_4$ transition at 18490.5 cm^{-1};

(b) the CS2 centre $E \rightarrow Z$ fluorescence, with excitation of the $Z_1 \rightarrow E_2$ transition at 18608.5 cm^{-1} and monitoring the $E_1 \rightarrow Z_5$ transition at 18485.0 cm^{-1};

(c) the CS1 centre $D \rightarrow Z$ fluorescence, with excitation of the $Z_1 \rightarrow D_4$ transition at 15663.5 cm^{-1} and monitoring the $D_1 \rightarrow Z_3$ transition at 15530.0 cm^{-1};

(d) the CS2 centre $D \rightarrow Z$ fluorescence, with excitation of the $Z_1 \rightarrow D_5$ transition at 15679.0 cm^{-1} and monitoring the $D_1 \rightarrow Z_4$ transition 15524.0 cm^{-1}.

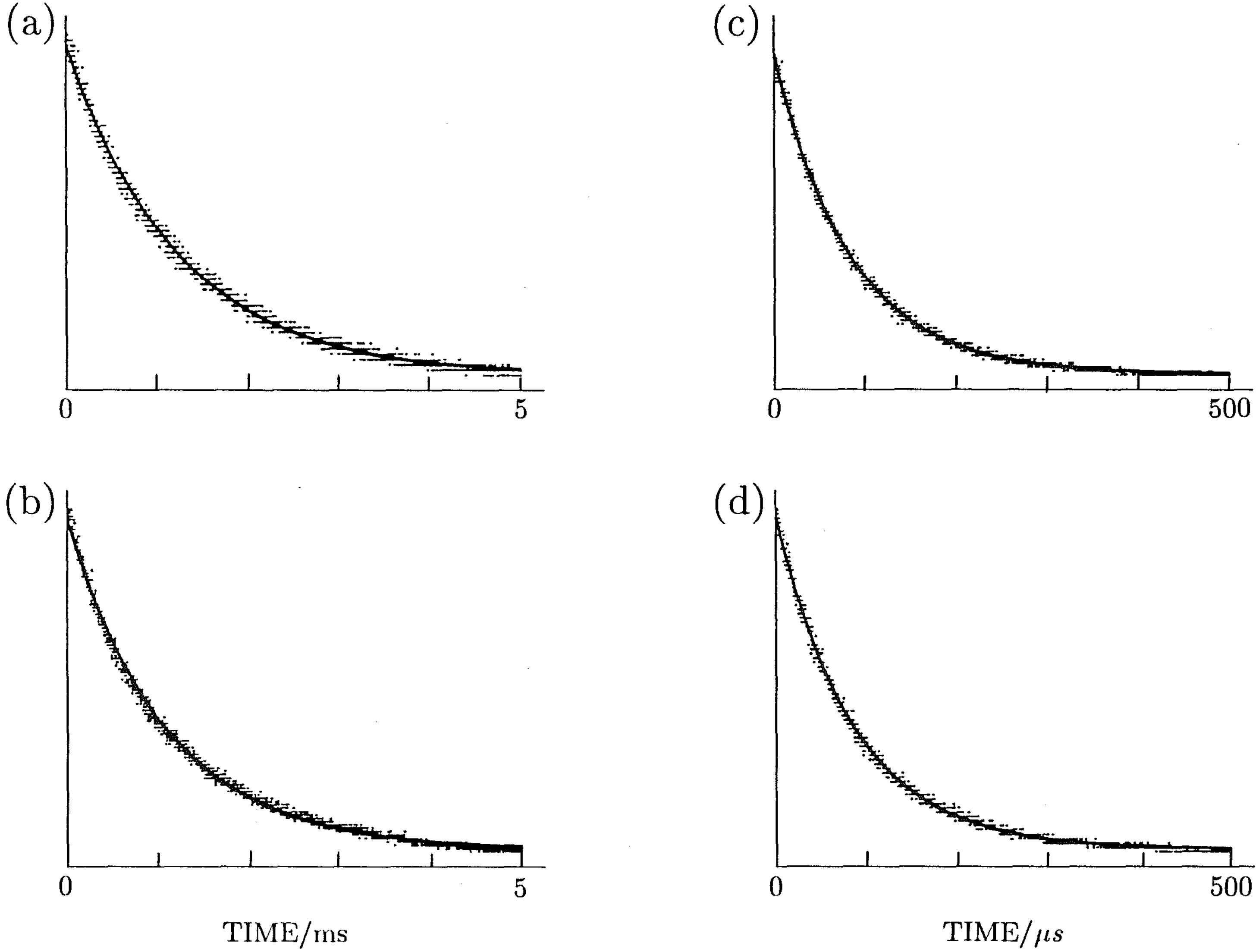
(a)
0
5
(c)
0
500
(b)
0
5
TIME/ms
(d)
0
500
TIME/μs

Figure 8.3: 10 K temporal transients for the CB1 and CB2 centres in $Ca_{0.99}Ba_{0.01}F_2:Ho^{3+}$(0.005%) crystals :
(a) the CB1 centre E →Z fluorescence, with excitation of the $Z_1 \rightarrow E_2$ transition at 18596.6 cm^{-1} and monitoring the $E_1 \rightarrow Z_4$ transition at 18494.0 cm^{-1};
(b) the CB2 centre E →Z fluorescence, with excitation of the $Z_1 \rightarrow E_2$ transition at 18606.7 cm^{-1} and monitoring the $E_1 \rightarrow Z_5$ transition at 18487.5 cm^{-1};
(c) the CB1 centre D →Z fluorescence, with excitation of the $Z_1 \rightarrow D_4$ transition at 15655.5 cm^{-1} and monitoring the $D_1 \rightarrow Z_3$ transition at 15534.5 cm^{-1};
(d) the CB2 centre D →Z fluorescence, with excitation of the $Z_1 \rightarrow D_5$ transition at 15676.0 cm^{-1} and monitoring the $D_1 \rightarrow Z_4$ transition at 15521.0 cm^{-1}.
The solid curves give the best fits to the temporal transient data with the resulting decay times as presented in Table 8.1

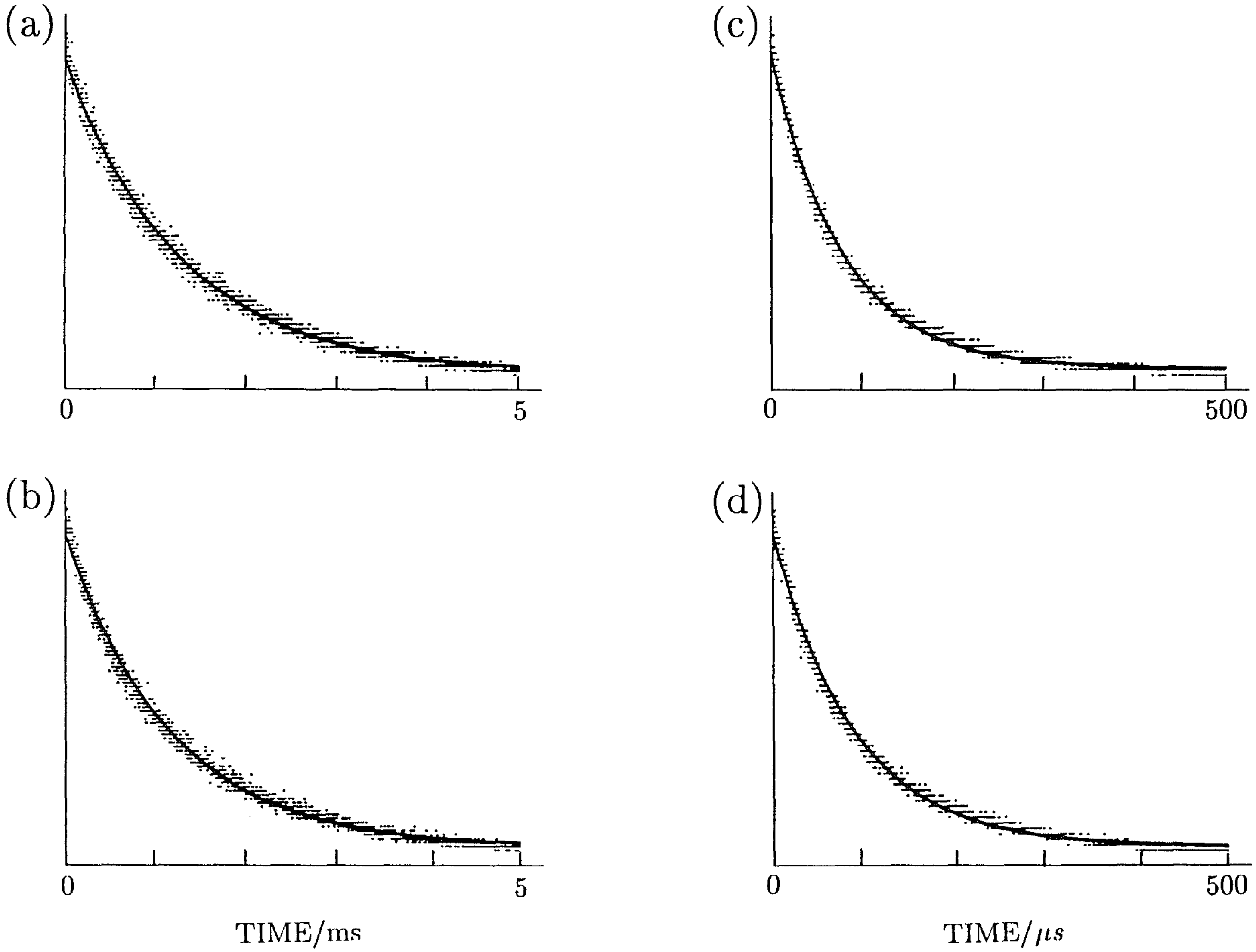
(a)
0
5
(c)
0
500
(b)
0
5
TIME/ms
(d)
0
500
TIME/μs

lifetime trends without attempting a detailed transition probability calculation.

In Chapter 2 (Section 2.5) it is shown that the radiative transition probability W^R_{ab} from a level a with wavefunction $|\gamma SLJJ_z>$ to all the terminating levels b whose wavefunctions are $|\gamma' SL'J'J'_z>$, is given by the expression

$$W^R_{ab} \; \alpha \; \Big| \sum_{q,\lambda \; \mathrm{even}} Y(\lambda,q,\varrho) < \gamma SLJJ_z \mid U^{(\lambda)}_{\varrho+q} \mid \gamma' SL'J'J_z' > \Big|^2 ,$$

where $Y(\lambda, q, \varrho)$ includes the odd-parity crystal-field terms.

As the parameters of the odd terms in the crystal-field expansion are not known, any trends in the spontaneous emission transition probabilities, and therefore the corresponding radiative fluorescence lifetimes of the various centres are established using the same approach as used by Reeves [105], in which the following assumptions are made :

(i) for centres of the same symmetry, the wavefunctions of corresponding energy levels are almost similar;

(ii) there is direct correspondence between the even and the odd terms of the crystal-field expansion among similar centres and the parameters for the odd terms of the crystal-field expansion are scaled up or down from the even term parameters determined from the crystal-field.

The spontaneous emission transition probability is therefore proportional to the square of the appropriate even-term crystal-field parameter and, for two centres of the same symmetry, the A and CS1 centres in CaF_2 type crystals for example, the relative magnitude of the radiative fluorescence lifetime is given by :

$$\frac{\tau(A)}{\tau(CS1)} = \left| \frac{B^k_q(CS1)}{B^k_q(A)} \right|^2 ,$$

where $\tau(A)$ and $\tau(CS1)$ are the radiative fluorescence lifetimes of the A and CS1 centres and the B^k_q are the crystal-field parameters from Chapter 7.

This approach is no more than qualitatively valid, and can only hold for particular crystal-field parameters giving dominant contributions. So far, it has

Figure 8.4: 10 K temporal transients for the SrF_2 A and SB1 centres in SrF_2:Ho^{3+}(0.01%) and $Sr_{0.99}Ba_{0.01}F_2$:Ho^{3+}(0.01%) crystals respectively :

(a) the SrF_2 A centre E→Z fluorescence, with excitation of the $Z_1 \rightarrow E_2$ transition at 18585.7 cm^{-1} and monitoring the $E_1 \rightarrow Z_4$ transition at 18504.0 cm^{-1};

(b) the SB1 centre E→Z fluorescence, with excitation of the $Z_1 \rightarrow E_2$ transition at 18575.8 cm^{-1} and monitoring the $E_1 \rightarrow Z_4$ transition at 18517.0 cm^{-1};

(c) the SrF_2 A centre D→Z fluorescence, with excitation of the $Z_1 \rightarrow D_4$ transition at 15642.3 cm^{-1} and monitoring the $D_1 \rightarrow Z_3$ transition at 15539.5 cm^{-1};

(d) the SB1 centre D→Z fluorescence, with excitation of the $Z_1 \rightarrow D_4$ transition at 15624.0 cm^{-1} and monitoring the $D_1 \rightarrow Z_3$ transition at 15552.0 cm^{-1}.

The solid curves give the best fits to the temporal transient data with the resulting decay times as presented in Table 8.1

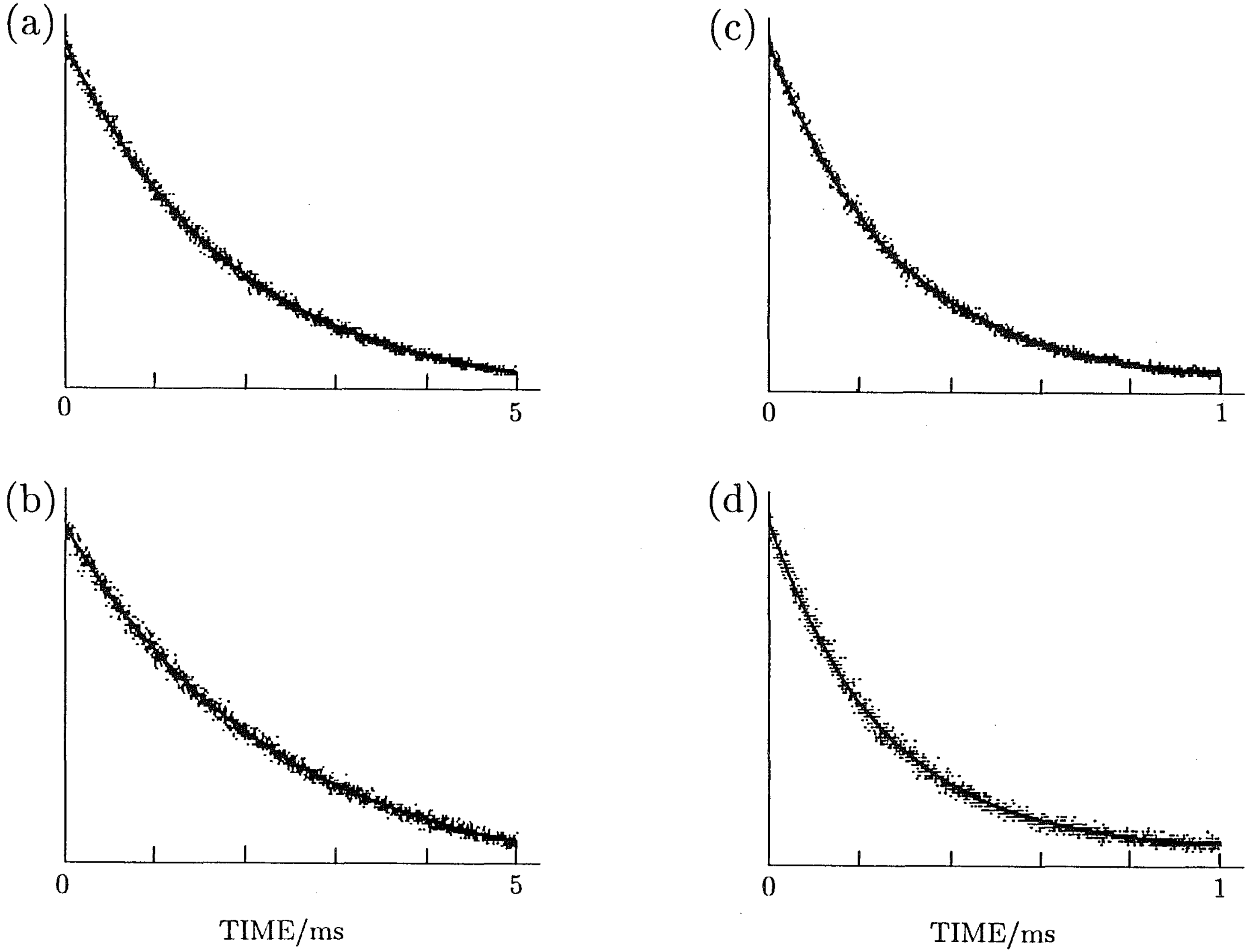
(a)
0
5
(b)
0
5
TIME/ms
(c)
0
1
(d)
0
1
TIME/ms

Figure 8.5: 10 K temporal transients for the SC1 and SC2 centres in $Sr_{0.99}Ca_{0.01}F_2:Ho^{3+}$(0.01%) crystals :
(a) the SC1 centre E → Z fluorescence, with excitation of the $Z_1 \rightarrow E_2$ transition at 18579.9 cm^{-1} and monitoring the $E_1 \rightarrow Z_4$ transition at 18513.5 cm^{-1};
(b) the SC2 centre E → Z fluorescence, with excitation of the $Z_1 \rightarrow E_2$ transition at 18590.1 cm^{-1} and monitoring the $E_1 \rightarrow Z_5$ transition at 18503.5 cm^{-1};
(c) the SC1 centre D → Z fluorescence, with excitation of the $Z_1 \rightarrow D_4$ transition at 15630.0 cm^{-1} and monitoring the $D_1 \rightarrow Z_3$ transition at 15548.5 cm^{-1};
(d) the SC2 centre D → Z fluorescence, with excitation of the $Z_1 \rightarrow D_4$ transition at 15650.5 cm^{-1} and monitoring the $D_1 \rightarrow Z_4$ transition at 15535.0 cm^{-1}.
The solid curves give the best fits to the temporal transient data, with the resulting decay times as presented in Table 8.1.

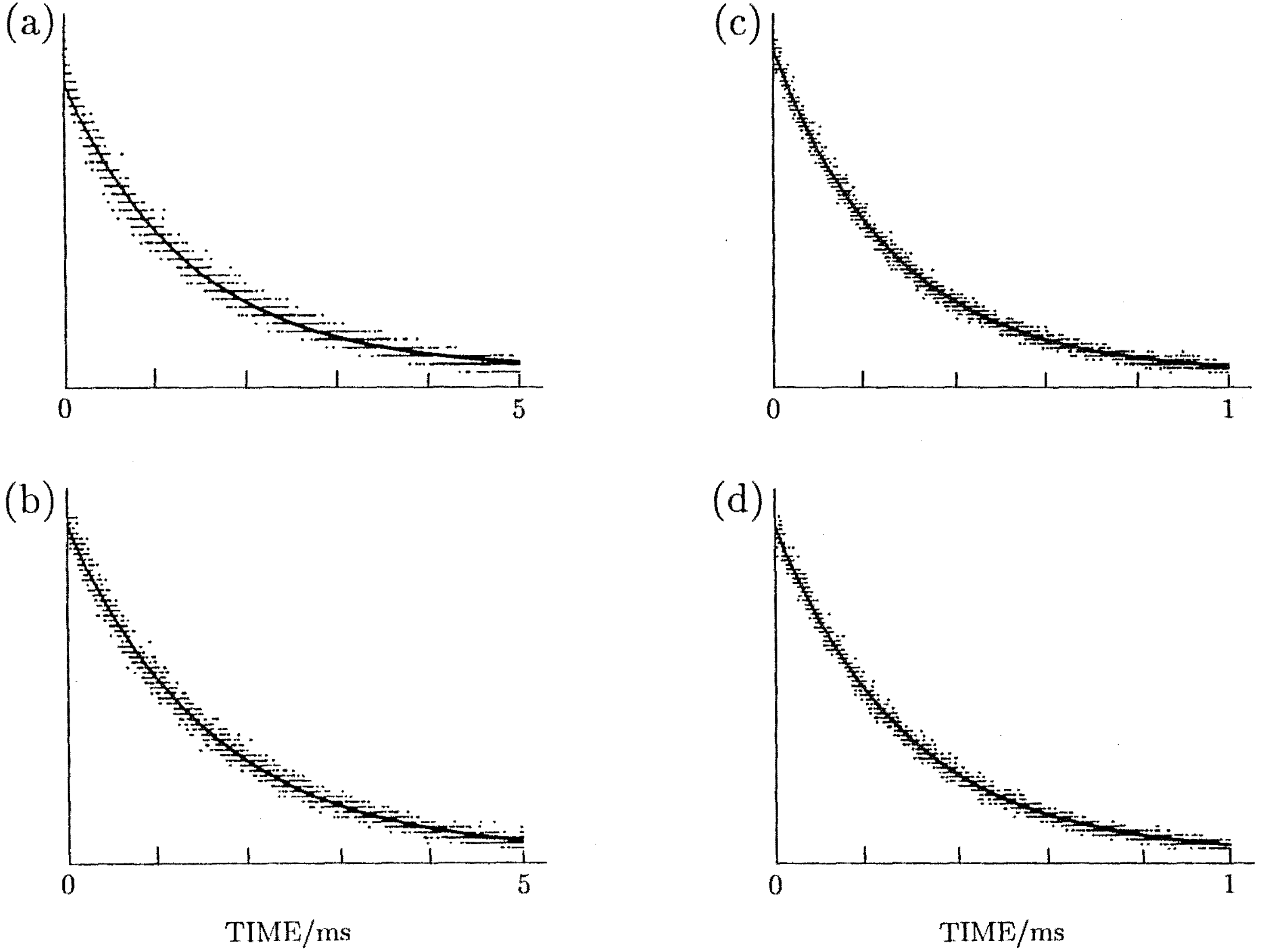
(a)
0
5
(b)
0
5
TIME/ms
(c)
0
1
(d)
0
1
TIME/ms

been found useful for analysis of the fluorescence lifetimes of the H^- and D^- charge compensated C_{4v} symmetry centres in Pr^{3+} [105, 106] and Nd^{3+} [45] in relation to the corresponding fluorescence lifetime for the F^- C_{4v} centre. Changes in the measured fluorescence lifetimes were largely reflected in the variations in the second degree axial parameter B^2_A.

Assuming further that the fluorescence lifetimes measured here for the Ho^{3+} centres are wholly from radiative relaxation processes, the single crystal-field parameter for each centre whose change, compared to the corresponding parameter of the respective A centre, can account for the change in the fluorescence lifetime measured for the centre is established. Although more than one parameter is expected to have some effect on the resultant fluorescence lifetime, the parameters chosen have the most effect in each case.

For the A centres in CaF_2:Ho^{3+} and SrF_2:Ho^{3+} crystals, the E multiplet fluorescence lifetime τ_E seems to follow on the crystal-field parameter B^4_A while that for the D multiplet (τ_D) follows changes in the crystal-field parameter B^2_A. Relative changes in the fluorescence lifetimes and the corresponding parameters are shown in Table 8.2(a).

The general trend for the modified C_{4v} symmetry centres in both the CaF_2 and SrF_2 type crystals is that the fourth degree parameters can account for changes in τ_E while changes in the sixth degree parameters appear to be responsible for changes in τ_D in going from the parent C_{4v} symmetry centre to the modified C_{4v} symmetry centres, as shown in Table 8.2(b).

For the two C_s symmetry centres, CS2 and CB2, τ_E is shorter while τ_D is longer than the corresponding lifetimes for the CS1 and CB1 centres respectively. For the SC2 centre however both τ_E and τ_D are longer than for the SC1 centre. Mixed centres for Pr^{3+} [63] were found to have longer fluorescence lifetimes than the parent C_{4v} centre and for these Pr^{3+} centres, the changes in energy levels and crystal-field parameters were more pronounced in going from the parent C_{4v} symmetry centre to the mixed crystal centres.

Table 8.1: 10 K fluorescence lifetimes for the Ho^{3+} centres present in $CaF_2:Ho^{3+}$(0.005%), $SrF_2:Ho^{3+}$(0.01%) and related mixed crystals for direct excitation of the respective multiplet.

Crystal host	Centre	Lifetimes (μs)	
		$E(^5S_2)$	$D(^5F_5)$
CaF_2	A	1328±27	73.1±0.7
	B	532±10	114±1
$Ca_{0.99}Sr_{0.01}F_2$	CS1	1236±25	84.2±0.8
	CS2	1080±22	87.8±0.9
$Ca_{0.99}Ba_{0.01}F_2$	CB1	1282±26	81.2±1.6
	CB2	1228±25	90.9±1.8
SrF_2	A	1863±37	270±5
$Sr_{0.99}Ca_{0.01}F_2$	SC1	1314±26	263±5
	SC2	1611±32	286±6
$Sr_{0.99}Ba_{0.01}F_2$	SB1	2363±47	248±5

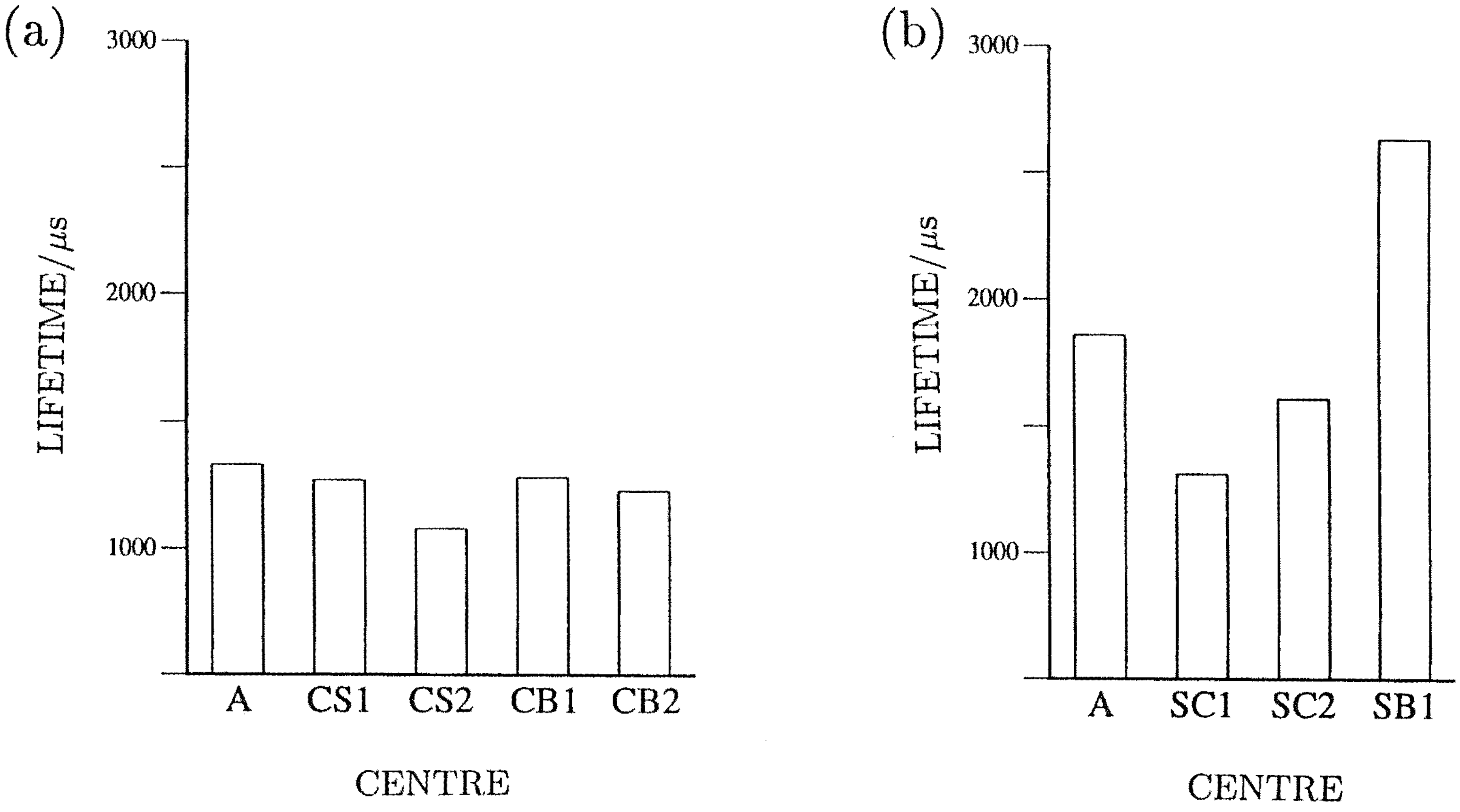

Figure 8.6: Comparison of the fluorescence lifetime data for the E→Z transitions of:
(a) the centres in $CaF_2:Ho^{3+}$ type crystals;
(b) the centres in $SrF_2:Ho^{3+}$ type crystals.

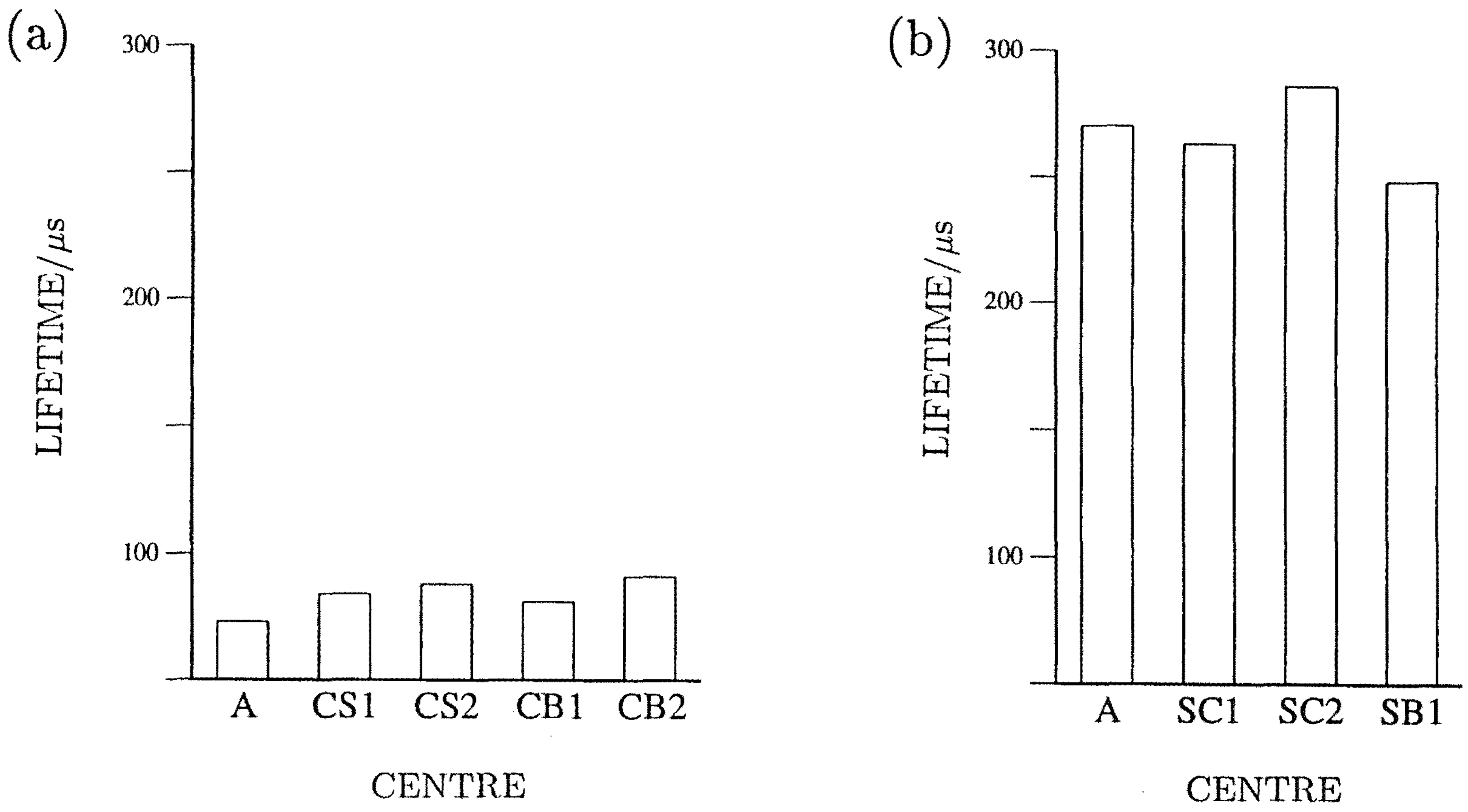

Figure 8.7: Comparison of the fluorescence lifetime data for the D→Z transitions of:-
(a) the centres in CaF_2:Ho^{3+} type crystals;
(b) the centres in SrF_2:Ho^{3+} type crystals.

Table 8.2: Correspondence between the changes in the fluorescence lifetimes and the relative magnitudes of the crystal-field parameters for (a) the C_{4v} symmetry SrF_2 A centre and (b) the modified C_{4v} symmetry centres in the $CaF_2{:}Ho^{3+}$(0.005%) and $SrF_2{:}Ho^{3+}$(0.01%) type crystals

(a)

Multiplet	$\frac{\tau(\mathrm{SrF_2\ A\ centre})}{\tau(\mathrm{CaF_2\ A\ centre})}$	Relevant B^k_q	$\left\lvert\frac{B^k_q(\mathrm{CAF_2\ A\ centre})}{B^k_q(\mathrm{SrF_2\ A\ centre})}\right\rvert^2$
E	1.40	B^4_A	1.44
D	3.69	B^2_A	4.11

(b)

Multiplet	CaF₂				SrF₂			
	Centre	$\frac{\tau(\mathrm{centre})}{\tau(\mathrm{A\ centre})}$	Relevant B^k_q	$\left\lvert\frac{B^k_q(\mathrm{A\ centre})}{B^k_q(\mathrm{centre})}\right\rvert^2$	Centre	$\frac{\tau(\mathrm{centre})}{\tau(\mathrm{SrF_2\ A\ centre})}$	Relevant B^k_q	$\left\lvert\frac{B^k_q(\mathrm{SrF_2\ A\ centre})}{B^k_q(\mathrm{centre})}\right\rvert^2$
E	CS1	0.93	B^4_A	0.94	SC1	0.71	B^4_C	0.85
	CB1	0.97	B^4_A	1.00	SB1	1.27	B^4_A	1.20
D	CS1	1.15	B^6_A	1.24	SC1	0.97	B^6_C	0.92
	CB1	1.11	B^6_A	1.28	SB1	0.92	B^6_C	0.92

8.2 The Dimer Centre in $CsCdBr_3:Ho^{3+}$ Crystals

Fluorescence lifetime measurements for the principal dimer centre give insight into the possible upconversion mechanisms for dimer centres in $CsCdBr_3$ crystals. For the Nd^{3+} [11] dimer centre, the Nd^{3+} ions were found to have much shorter fluorescence lifetimes than those in the single Nd^{3+} ion centres. Various decay channels for the $^4F_{7/2}$, $^4F_{9/2}$ and $^4G_{5/2}$ multiplets of Nd^{3+} were derived from relative magnitudes of the lifetimes and transition intensities observed for the fluorescence from these and other lower energy multiplets.

For Er^{3+}, Cockroft et al. [29] carried out a detailed analysis of the dynamics of the upconversion from the Er^{3+} dimer centre. They were able to deduce energy transfer rates between pairs from the rise and decay times following the analysis of Buisson and Vial [20] for Pr^{3+} ions in LaF_3 crystals. Also for Er^{3+}, McPherson and Meyerson [85], using the transients obtained for emission from the $^4G_{9/2}$ and $^4G_{11/2}$ multiplets showed that multi-phonon relaxations were a more probable process than either energy transfer or radiative relaxation processes.

The analysis of Buisson and Vial [20] was also used here to obtain upconversion energy transfer rates from the rise times measured for the Ho^{3+} dimer centre. For an initial population of N_d pairs of ions excited by the laser pulse, the time variation of N_d is given by

$$\dot{N}_d = -2W_2N_d - W_tN_d \, , \qquad 8.4$$

where W_2 is the radiative decay rate of the excited multiplet and W_t is the upconversion energy transfer rate. Upconversion will result in N_3 ions being excited to a higher energy state than pumped. The time evolution of N_3 is given by

$$\dot{N}_3 = W_tN_d - W_3N_3 \, , \qquad 8.5$$

where W_3 is the radiative decay rate for the higher energy state.

Solving for N_3 from 8.4 and 8.5 yields

$$N_3 = \frac{N_d^0 W_t}{(W_3-(2W_2+W_t))} \left[e^{-(2W_2+W_t)t} - e^{-W_3t} \right] , \qquad 8.6$$

where N_d^0 is the population of excited dimers soon after the laser pulse. The rise is the greater of the two rates $(2W_2+W_t)$ and W_3 and the decay rate is the lesser.

The results for the Ho^{3+} principal dimer centre give the following correspondence between the decay and rise times of equations 8.3 and 8.6:-

$$d = 1/W_3 \tag{8.7(a)}$$

and

$$f = 1/\{2W_2 + W_t\}\ . \tag{8.7(b)}$$

For weakly coupled pairs, W_t would approach zero and the rise time would then be equal to half the fluorescence lifetime of the pumped state. For rapid transfer rates and small radiative decay rates as observed for the Ho^{3+} dimer centre here, the rise time measured is almost equal to the upconversion energy transfer time.

8.2.1 Temporal results for Ho^{3+} ions in $CsCdBr_3$ crystals

Attempts to measure fluorescence lifetimes for the minority L, N and the single Ho^{3+} ion (M) centres here were unsuccessful because the fluorescence was too weak to monitor under pulse laser excitation. Results for the principal dimer centre only are presented here.

Fluorescence lifetimes for the Ho^{3+} dimer centre presented here have been measured for three different excitation cases:-

(i) direct excitation to the J, F, E and D multiplets for measuring the respective multiplet fluorescence lifetimes;

(ii) with Z → E excitation, for measuring upconversion fluorescence rise and decay times;

(iii) with Z → D excitation, for measuring upconversion fluorescence transients, as in (ii) above.

The temporal transients obtained are presented in Figures 8.8 to 8.12, while the fluorescence rise and decay times are given in Table 8.3. The same fluorescence lifetime results were obtained for Ho^{3+} concentrations of 0.3%, 0.1% and 0.01%. The three excitation cases are now discussed separately :

(i) Only fluorescence lifetimes for the J, F, E and D multiplets could

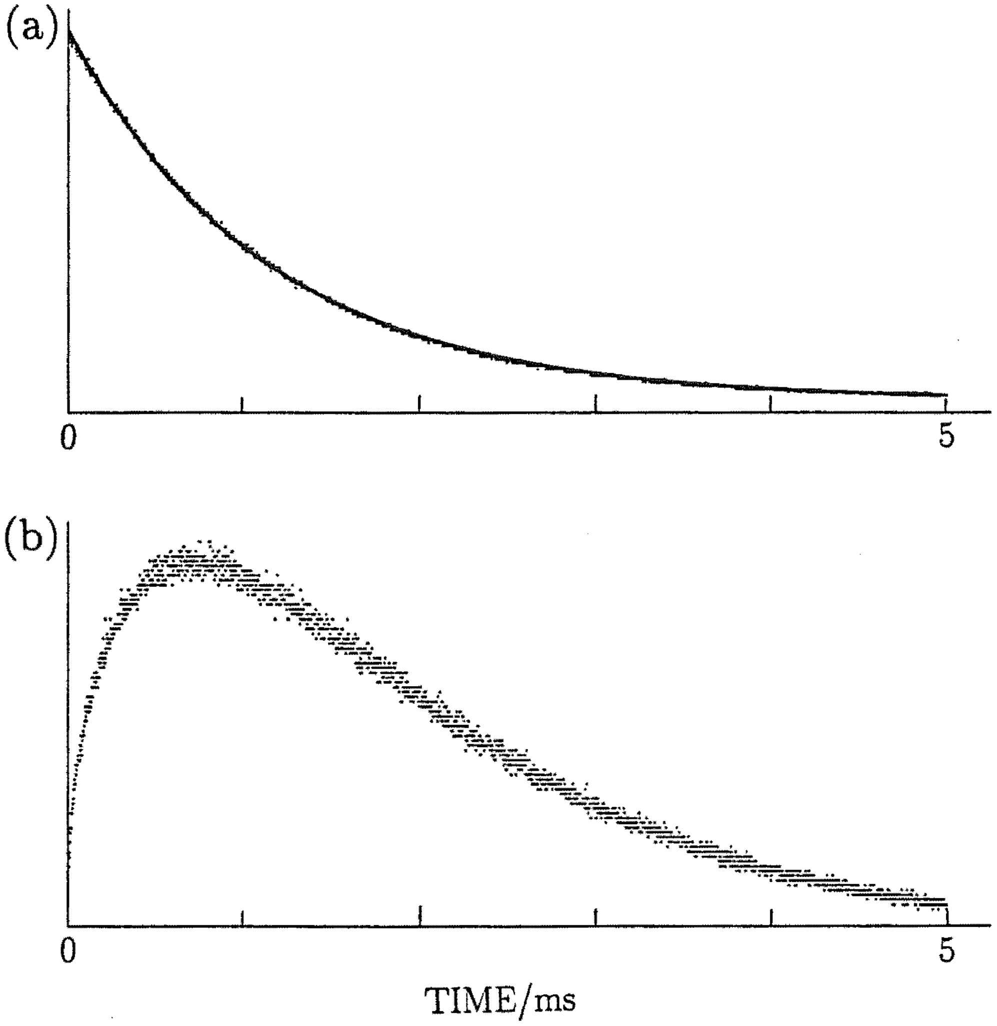

Figure 8.8: 10 K temporal transients for the fluorescence from the D multiplet of the dimer centre in $CsCdBr_3:Ho^{3+}$ crystals for monitoring the $D_1 \rightarrow Z_{10}$ transition at 15090.5 cm^{-1} and excitation of :
(a) the $Z_1 \rightarrow D_5$ transition at 15442.2 cm^{-1};
(b) the $Z_1 \rightarrow E_4$ transition at 18416.3 cm^{-1}.
The solid curve gives the best fit to the data, with the resulting lifetimes as presented in Table 8.3.

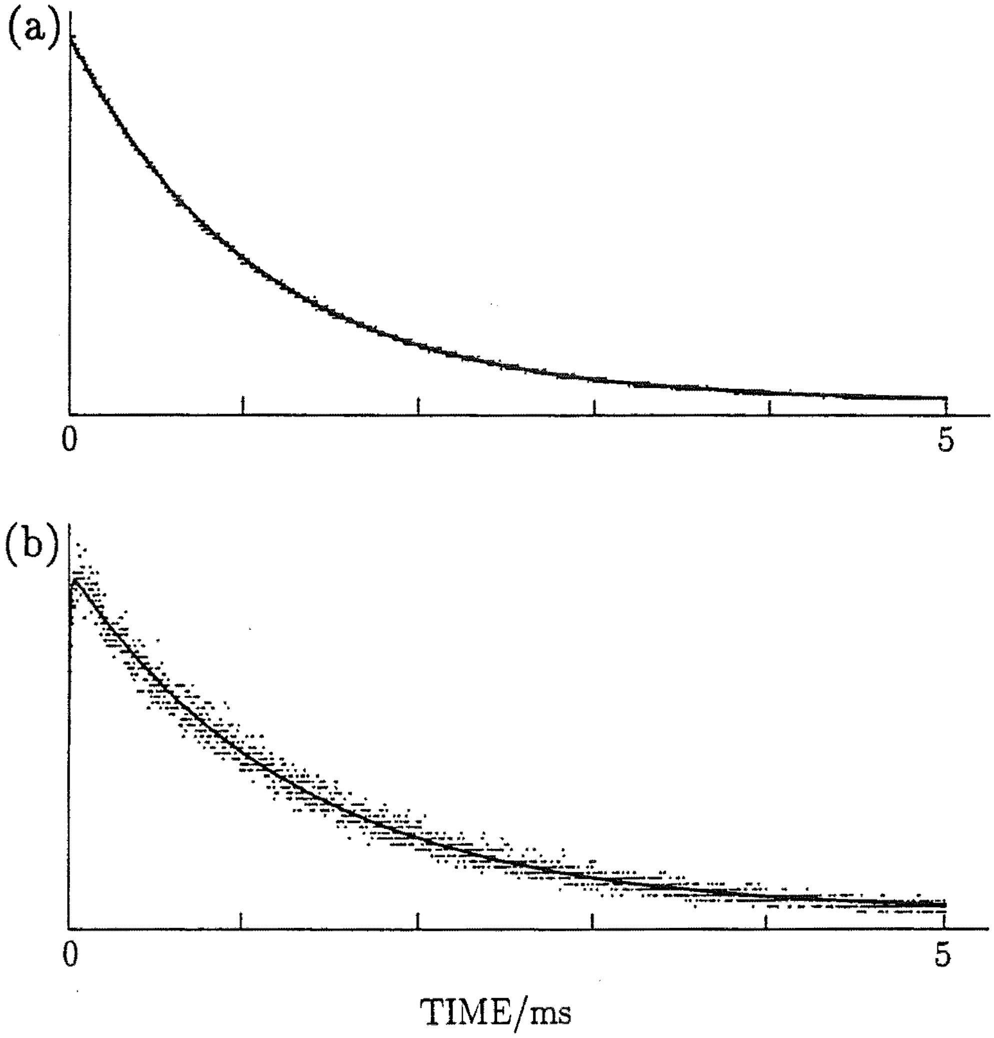

Figure 8.9: 10 K temporal transients for the fluorescence from the E multiplet of the dimer centre in $CsCdBr_3:Ho^{3+}$ crystals, for monitoring the $E_1 \rightarrow Z_7$ transition at 18137.0 cm^{-1} and excitation of :
(a) the $Z_1 \rightarrow E_4$ transition at 18416.3 cm^{-1} ;
(b) the $Z_1 \rightarrow D_5$ transition at 15442.2 cm^{-1}.
The solid curves give the best fits to the data, with the resulting lifetimes as presented in Table 8.3.

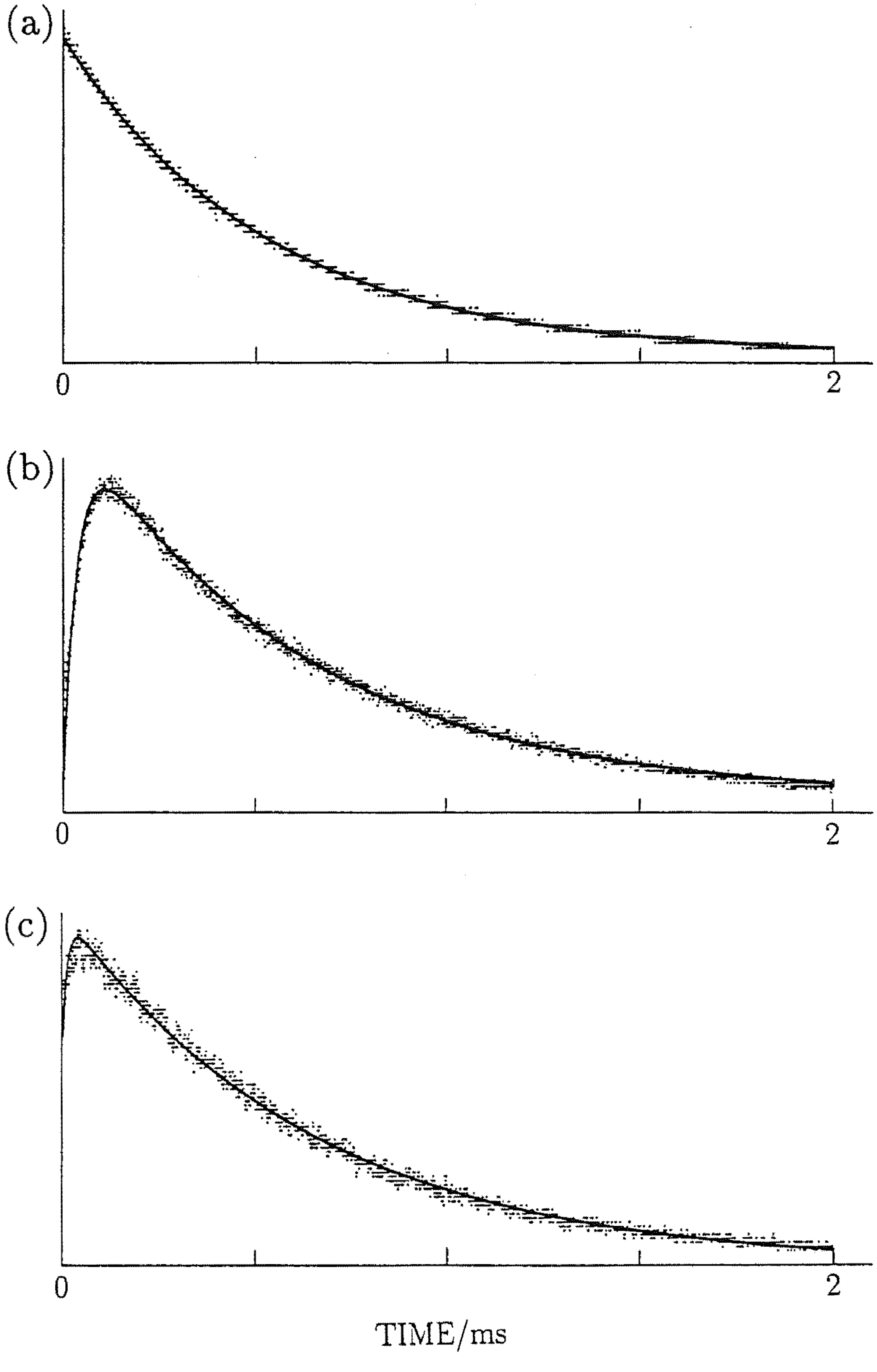

Figure 8.10: 10 K temporal transients for the fluorescence from the F multiplet of the dimer centre in $CsCdBr_3:Ho^{3+}$ crystals, for monitoring the $F_1 \rightarrow Z_2$ transition at 20384.5 cm^{-1} and excitation of :
(a) the $Z_1 \rightarrow F_2$ transition at 20435.0 cm^{-1};
(b) the $Z_1 \rightarrow E_4$ transition at 18416.3 cm^{-1};
(c) the $Z_1 \rightarrow D_5$ transition at 15442.2 cm^{-1}.
The solid curves give the best fits to the data, with the resulting lifetimes as presented in Table 8.3.

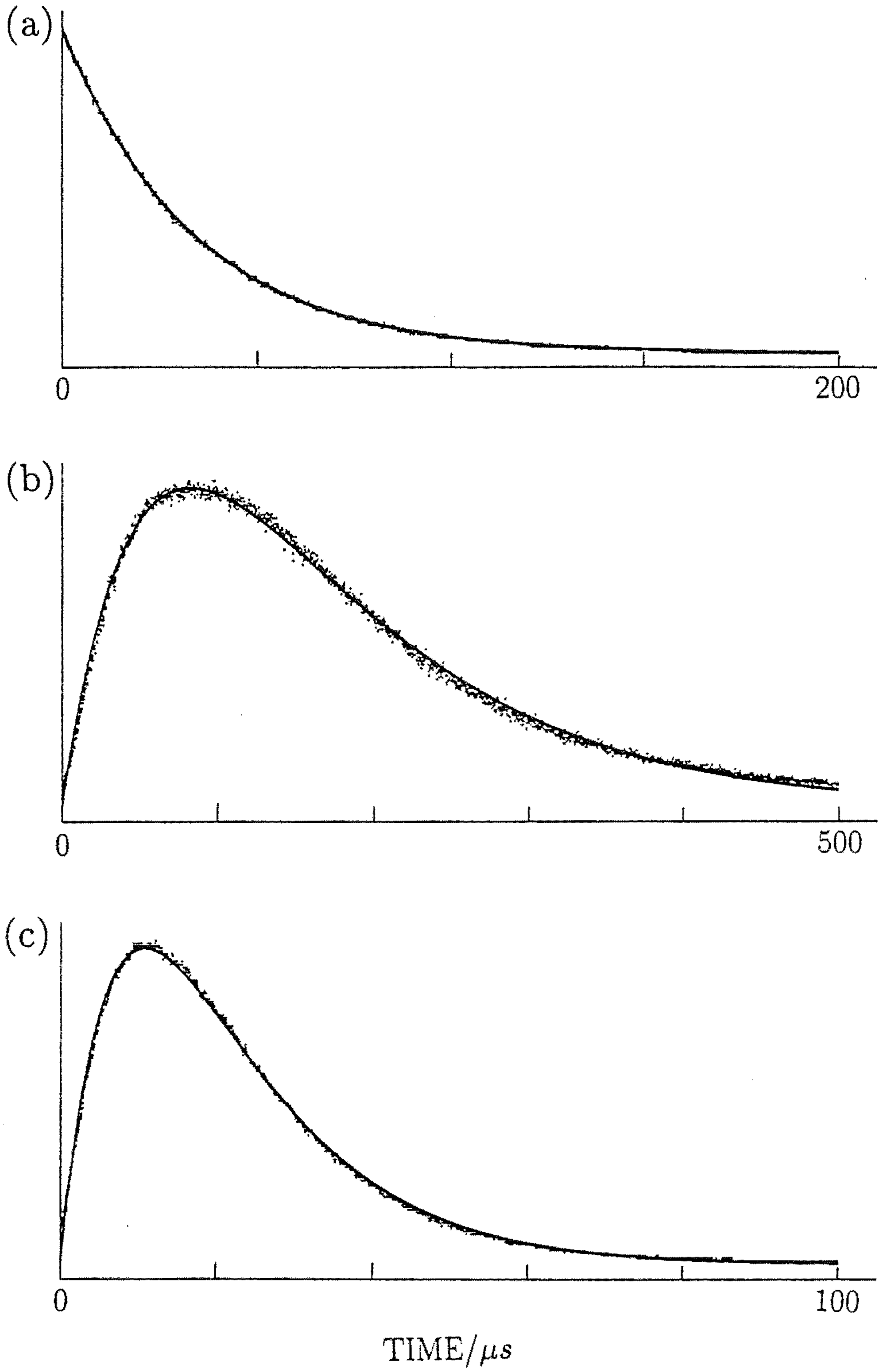

Figure 8.11: 10 K temporal transients for the fluorescence from the J multiplet of the dimer centre in CsCdBr$_3$:Ho^{3+} crystals, for monitoring the $J_1 \rightarrow Z_{10}$ transition at 23439.5 cm^{-1} and excitation of :
(a) the $Z_1 \rightarrow J_1$ transition at 23656.5 cm^{-1};
(b) the $Z_1 \rightarrow E_4$ transition at 18416.3 cm^{-1};
(c) the $Z_1 \rightarrow D_5$ transition at 15442.2 cm^{-1}.
The solid curves give the best fits to the data, with the resulting lifetimes as presented in Table 8.3.

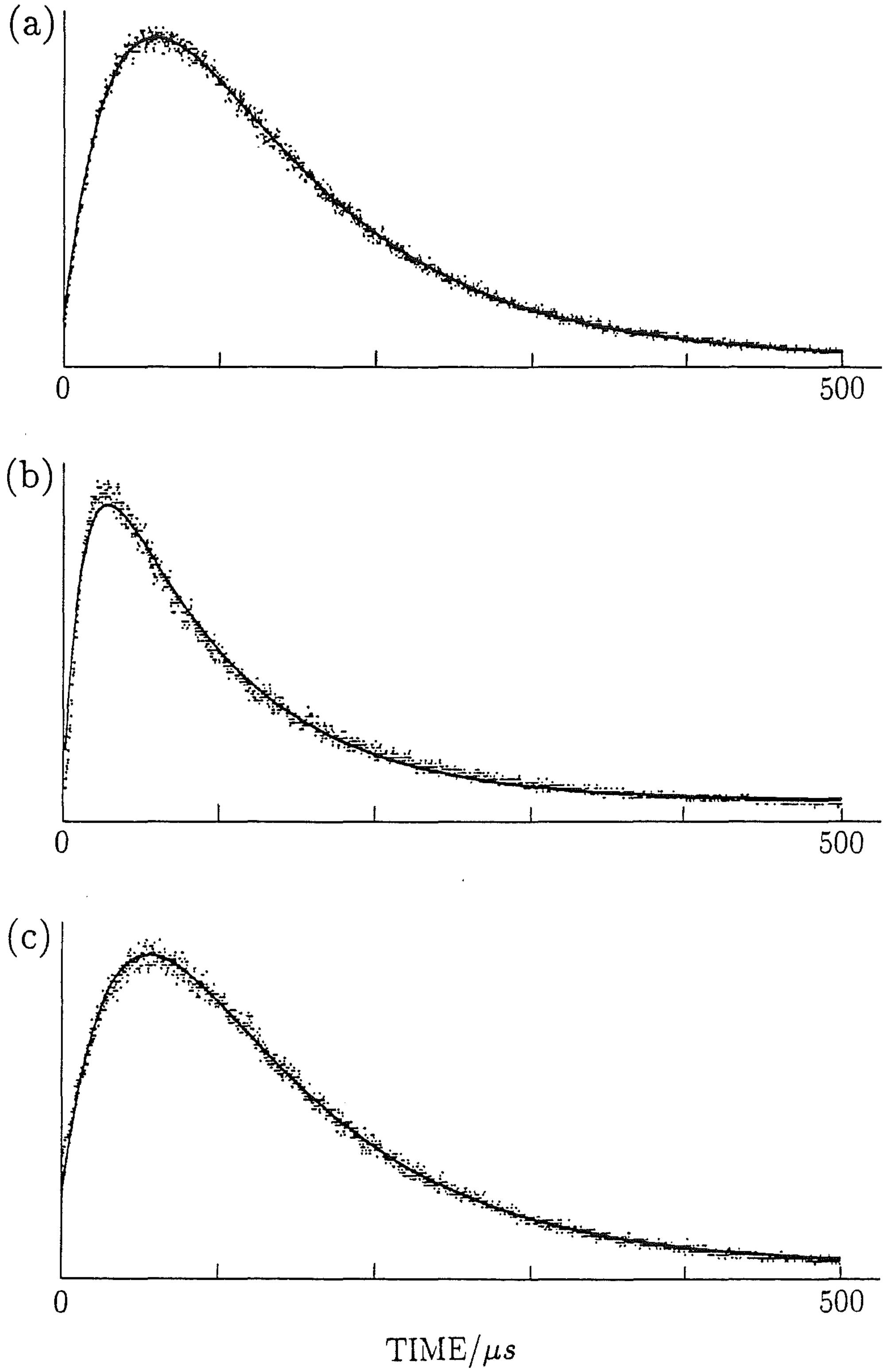

Figure 8.12: 10 K temporal transients for the fluorescence from the M, P and Q multiplets of the dimer centre in $CsCdBr_3$:Ho^{3+} crystals, for excitation of the $Z_1 \rightarrow E_4$ transition at 18416.3 cm^{-1} and monitoring :
(a) the $M_1 \rightarrow Y_1$ transition at 22154.0 cm^{-1};
(b) the $P_1 \rightarrow A_1$ transition at 21153.0 cm^{-1};
(c) the $Q_1 \rightarrow B_1$ transition at 21672.5 cm^{-1}.
The solid curves give the best fits to the data, with the resulting lifetimes as presented in Table 8.3.

be measured with direct excitation as available dyes only covered their respective regions. The fluorescence lifetimes for the E and D multiplets were found to be comparatively long, being 1086 μs and 1116 μs respectively, while that for the F multiplet was about half these E and D lifetime values, being 535 μs. The J multiplet had a relatively short lifetime of only 33.7 μs. Since the next lower energy multiplet I($^5G_6$) is about 1900 cm^{-1} lower than the J multiplet, it is unlikely that non-radiative relaxation to this lower multiplet is responsible for shortening the lifetime for the J multiplet. Also as fluorescence from the J multiplet was appreciably stronger than that from the I multiplet, the J multiplet must be a more efficiently fluorescing multiplet than the I multiplet.

(ii) With Z → E excitation, rise times were observed for the D, F, J, M, P and Q multiplets. For the D and F multiplets, the decay times were similar to the lifetimes measured with direct excitation to the respective multiplets. The F, M and Q multiplets have a common rise time of about 37.6 μs, the P multiplet has a shorter rise time of 13.1 μs, and the J multiplet a longer rise time of 63.1 μs. The decay time of 109.2 μs observed for the J multiplet for Z → E excitation is three times longer than that obtained from direct excitation.

The fluorescence transient obtained for monitoring the D → Z emission, with Z → E excitation, was rather different in that the transient was found to have two different rise times. The first rise time measured to be 37.2 μs was obtained from fitting data points of the first 100 μs of the transient. The second rise time of 562 μs fits data points for the remainder of the rise part of the transient. The two rise times were obtained from fitting the corresponding part of the "rise" transient separately with the same decay transient. Using either of the 37.2 μs and 562 μs rise times gave similar values of 1348 μs and 1298 μs respectively for the decay time, which are close to the fluorescence lifetime of the D multiplet of 1116 μs. As the composite temporal transient could not be fitted in its entirety using the expression 8.3, only the measured transient is presented in Figure 8.8(b).

(iii) For Z → D excitation, temporal transients were obtained only for the E, F and J multiplets as the fluorescence from the other multiplets was too weak to measure. For both the E and F multiplets, the decay times were comparable to the fluorescence lifetimes as measured with direct excitation of the respective multiplet. The decay time for the J multiplet was found to be about three times shorter than that for direct excitation. Rise times were measured to be 6.1, 13.0 and 10.6 μs for the E, F and J multiplets respectively (Table 8.3).

8.2.2 Discussion of the decay and rise times

For the D, E and F multiplets, the decay times observed from the upconversion fluorescence are just the fluorescence lifetimes of the corresponding upper multiplets. For the F multiplet, the decay times obtained for both Z → E and Z → D excitation were found to be similar to the fluorescence lifetime obtained from direct excitation of that multiplet. Decay times measured for the J multiplet are different for each excitation, with the times for Z → E and Z → D excitations being three times longer and three times shorter respectively, than that obtained from direct excitation.

Since the fluorescence lifetime for the J multiplet is 33.7 μs for direct excitation (Table 8.3), it had been expected that the decay times from the transients obtained for both Z → E and Z → D excitation would be of the same magnitude. Instead, the decay times of 109.2 μs obtained for Z → E excitation

Table 8.3: 10 K fluorescence lifetime data for the Ho^{3+} dimer centre in $CsCdBr_3$:Ho^{3+}(0.3%) crystals.

Upper multiplet of fluorescence transition measured	Fluorescence lifetime		Energy transfer time(μs)	Absorption transition being pumped
	Rise(μs)	Decay(μs)		
$^5F_5$(D)	*	1116±22	-	$Z_1 \rightarrow D_5$
	37.2±1.1	1348±27	39.9±2.0	$Z_1 \rightarrow E_4$
	562±1.7	1298±26		
$^5S_2$(E)	*	1086±22	-	$Z_1 \rightarrow E_4$
	6.1±0.1	1303±26	6.2±0.3	$Z_1 \rightarrow D_5$
$^5F_3$(F)	*	535±11	-	$Z_1 \rightarrow F_1$
	36.0±0.7	612±12	38.6±1.2	$Z_1 \rightarrow Z_4$
	13.0±0.3	650±13	13.3±0.6	$Z_1 \rightarrow D_5$
$^5G_5$(J)	*	33.7±0.7	—	$Z_1 \rightarrow J_1$
	63.1±1.3	109.2±2.2	71.4±2.2	$Z_1 \rightarrow E_4$
	10.6±0.2	13.2±0.3	10.8±0.5	$Z_1 \rightarrow D_5$
$^3H_5$(M)	37.6±0.8	104.5±2.1	40.4±1.8	$Z_1 \rightarrow E_4$
$^3K_6$(P)	13.1±0.3	84.1±1.7	13.4±0.6	$Z_1 \rightarrow E_4$
$^3D_3$(Q)	39.4±0.8	100.7±2.0	42.5±1.9	$Z_1 \rightarrow E_4$

* No rise time (and energy transfer time) as multiplet is pumped directly.

and the 13.2 μs obtained for Z → D excitation are vastly different from the fluorescence lifetime value of the J multiplet. The common factor of three between the magnitudes of the decay times obtained for Z → E and Z → D excitation and fluorescence lifetime measured for direct excitation might have some relevance to the mechanism involved. No satisfactory explanation of this result has been found at this stage.

The representative rise times are about 37.6 μs (as obtained from the F, M and Q multiplets) and 10.0 μs (as obtained from the E, F and J multiplets) for excitation of the E and D multiplets respectively (Table 8.3). These short rise times compare well with both the 25 - 28 μs values obtained for the $^4G_{9/2}$ and $^4G_{11/2}$ multiplets of Er^{3+} [85] for excitation of the $^4S_{3/2}$ multiplet and the 1.8 μs rise time obtained for the $^4F_{5/2}$ and $^4F_{3/2}$ multiplets of Nd^{3+} [11] for excitation of the $^4F_{7/2}$ multiplet.

The different rise times of 63.1 μs and 13.1 μs obtained for the J and P multiplets respectively, for Z → E excitation (Table 8.3), are likely to arise from there being different transfer rates associated with the $^5S_2$ and $^5F_4$ multiplets. In this case, the rise times observed would depend on which of the composite E multiplets, $^5S_2$ or $^5F_4$, the dimer centre ions were in just before the interaction. As the E_4 level at 18416.3 cm^{-1} which is being pumped belongs to the $^5F_4$ multiplet, it is possible for the ions to either interact at that energy or, through multiphonon ralaxation processes, they may interact at the lower energy of 18315.2 cm^{-1} which belongs to the $^5S_2$ multiplet. As these two multiplets are about 100 cm^{-1} apart, it is reasonable to expect different interaction rates for the ion pairs in either multiplet.

Observation of the two different rise times for Z → E excitation and monitoring D → Z fluorescence supports the upconversion scheme based on hetero-excited pair ions as proposed in Chapter 6 for the emission originating from the Q multiplet. The first rise time compares well with rise times for the F, M and Q multiplets, for Z → E excitation and therefore arises from interaction of the two ions in the E multiplet, which is responsible for the upconversion fluorescence observed from the F and D multiplets. The second rise time of 562 μs being similar to the fluorescence lifetime of the F multiplet is proposed to arise from the F → Z multiplet radiative decay which occurs faster than the D → Z multiplet radiative decay because of the shorter lifetime for the F multiplet. This is immediately followed by re-excitation of the same ion from the ground multiplet to the E multiplet by the laser pump frequency. At this stage the two ions from the same pair which were originally in the E multiplet are now in a hetero-excited pair with one ion in the E multiplet and the other in the D multiplet. This is exactly the sort of intermediate state which is required for the $[E\ ;\ D] \longrightarrow [Q\ ;\ Z]$ process leading to the observation of fluorescence from the Q multiplet.

8.2.3 Energy transfer rates for the Ho^{3+} ions in $CsCdBr_3$ crystals

For the principal Er^{3+} centre [29], a rise time of 226 μs was obtained for the $^2H_{9/2}$ multiplet with excitation of the $^4I_{9/2}$ multiplet while a similar rise time of 178 μs was obtained for the $^4F_{7/2}$ multiplet with excitation of the $^4I_{11/2}$ multiplet. The corresponding energy transfer rates for the $^4I_{9/2}$ and $^4I_{11/2}$ multiplets of Er^{3+} were calculated to be $1741\ s^{-1}$ and $128.3\ s^{-1}$ respectively. The fluorescence lifetime measured for direct excitation of the $^4S_{3/2}$ multiplet of Er^{3+} is 400 μs [31]. Therefore, using the rise time of 25 μs observed for the fluorescence from the $^4G_{11/2}$ multiplet [85] for example, the energy transfer rate for Er^{3+} ions excited to the $^4S_{3/2}$ multiplet is calculated to be $35000\ s^{-1}$. For the Er^{3+} principal dimer centre therefore, energy transfer is comparatively faster for excitation of the $^4S_{3/2}$ multiplet than for excitation of the $^4I_{9/2}$ and $^4I_{11/2}$ multiplets in the near infrared region of the spectrum.

Having measured the intrinsic lifetimes $(1/W_2)$ for both the E and D multiplets for Ho^{3+} here, upconversion energy transfer times $(1/W_t)$ for Z → E and Z → D excitation were calculated from equation 8.7(b). These are included in Table 8.3. The fluorescence decay times for both the E and D multiplets are two orders of magnitude longer than the energy transfer times. Corresponding energy transfer rates are much larger compared to the measured radiative decay rates for the E and D multiplets. Considering the F multiplet with $Z_1 \rightarrow E_4$ excitation for example, the radiative decay rate for the E multiplet (W_E) is 920.81 s^{-1} and so $2W_E + W_t$ is 27778 s^{-1}. The transfer rate W_t is therefore 25936 s^{-1} giving a transfer time of only 38.6 μs for ions in the E multiplet. Similarly, for $Z \rightarrow D$ excitation W_D is 896.06 s^{-1} and $2W_D + W_t$ is equal to 76923 s^{-1}. This gives a transfer rate of 75131 s^{-1} and a transfer time of 13.3 μs for pair ions excited to the D multiplet. Because the transfer rates here are much faster than the decay rates, the rise times measured almost solely comprise upconversion transfer times for the E and D multiplets. Energy transfer is faster for $Z \rightarrow D$ excitation than for $Z \rightarrow E$ excitation. The Ho^{3+} ions in this centre must be strongly coupled since the energy transfer times are so very short.

The energy transfer rate of 25936 s^{-1} for Ho^{3+} ions excited to the E multiplet is comparable to the 35000 s^{-1} derived for Er^{3+} ions excited to the similar energy E ($^4S_{3/2}$) multiplet of Er^{3+}. Fluorescence lifetime data for excitation of the $^4F_{9/2}$ (D) multiplet of Er^{3+}, which lies in the same spectral region as the $^5F_5$ (D) multiplet of Ho^{3+}, are not available and so comparison of transfer rates cannot be made for the D multiplets.

On the whole, the temporal results for the Ho^{3+} principal dimer centre substantiate the upconversion mechanisms proposed. The energy transfer rates for Nd^{3+}, Ho^{3+} and Er^{3+}, for excitation in the visible region, are all very fast and comparable while the transfer rates for infrared excitation appear to be relatively slow, as evidenced by the results of Cockcroft et al. [29] for Er^{3+}.

CHAPTER 9

HIGH RESOLUTION SPECTROSCOPY AND OPTICALLY DETECTED NUCLEAR MAGNETIC RESONANCE STUDIES OF Ho^{3+} IONS IN SrF_2 AND $CsCdBr_3$ CRYSTALS

The work reported in this Chapter was performed during a three week visit to the Australian National University, Canberra, as part of an ongoing collaboration between the two groups.

Introduction

Low temperature optical spectra of rare-earth ions in crystalline solids comprise groups of sharp transitions, most of which have small linewidths of 1 cm^{-1} or less. The linewidths are determined by both homogeneous and inhomogeneous broadening. Homogeneous broadening is caused by processes such as spontaneous phonon emission and spin (nuclear or electronic) fluctuations, which give rise to dynamical perturbations on the transition frequency. These dynamical perturbations are operative for all ions in the crystal and set a limiting linewidth to the transition. Inhomogeneous broadening arises from residual static lattice strains or from chemical impurities or other defects in the crystal, which give rise to different local environments for the different ions in the crystal.

For absorption transitions to a particular J multiplet at low temperatures, the transitions to the higher energy levels of the upper multiplet are homogeneously broadened by spontaneous phonon emission by relaxation to the lowest lying energy level of the excited multiplet and residual inhomogeneous broadening effects are negligible. Transitions to the lowest lying energy level are frequently wholly inhomogeneously broadened because the energy gap to the next lower energy multiplet levels is usually large, compared to the separations between levels of the same multiplet, and can only be bridged by the relatively slow multiphonon relaxation processes, hence the lowest energy level of the excited multiplet has a long fluorescence lifetime and a small homogeneous linewidth. The overall linewidth of transitions to such levels is therefore completely determined by inhomogeneous broadening, as shown in Figure 9.1.

Absorption transitions measured in low resolution (0.2 cm^{-1}) spectroscopy have additional broadening from unresolved hyperfine structure, arising from the coupling of the 4f electrons with the magnetic moment of the nucleus.

In high resolution spectroscopic studies, the hyperfine lines may be clearly resolved and these are commonly studied by the spectral holeburning technique, in which a narrow band single frequency laser is used to selectively excite a small portion of the inhomogeneously broadened transition. Bleaching of the absorption is observed as the ions resonant with the laser are removed from the ground state, creating a hole (a dip in intensity of the excited portion of the transition). The ion population driven from the ground state is stored in one of the other electronic or spin levels, known as reservoirs. These population reservoirs include the excited state itself, a metastable excited electronic state, hyperfine and superhyperfine levels. For rare-earth ions, the most important reservoirs are the hyperfine levels of the ground electronic state and the nuclear spin superhyperfine levels. An increase in the intensity of the hyperfine or superhyperfine reservoir level (antihole) is observed while a hole is being burnt in one of the hyperfine lines. The resolution in such holeburning experiments is limited by the frequency bandwidth of the laser.

A more powerful technique is that of optically detected nuclear magnetic resonance (ODNMR), as the resolution is that of the width of the rf resonance itself and is not limited by the bandwidth of the laser. In ODNMR experiments, an rf field is applied to the sample while burning a hole in one of the hyperfine lines and monitoring the resulting fluorescence. An increase in fluorescence is detected when the rf field resonates with any of the hyperfine or superhyperfine level splittings and the ion population in the reservoir level is driven back to the initial level, resonant with the laser. Superhyperfine resonances arise when an

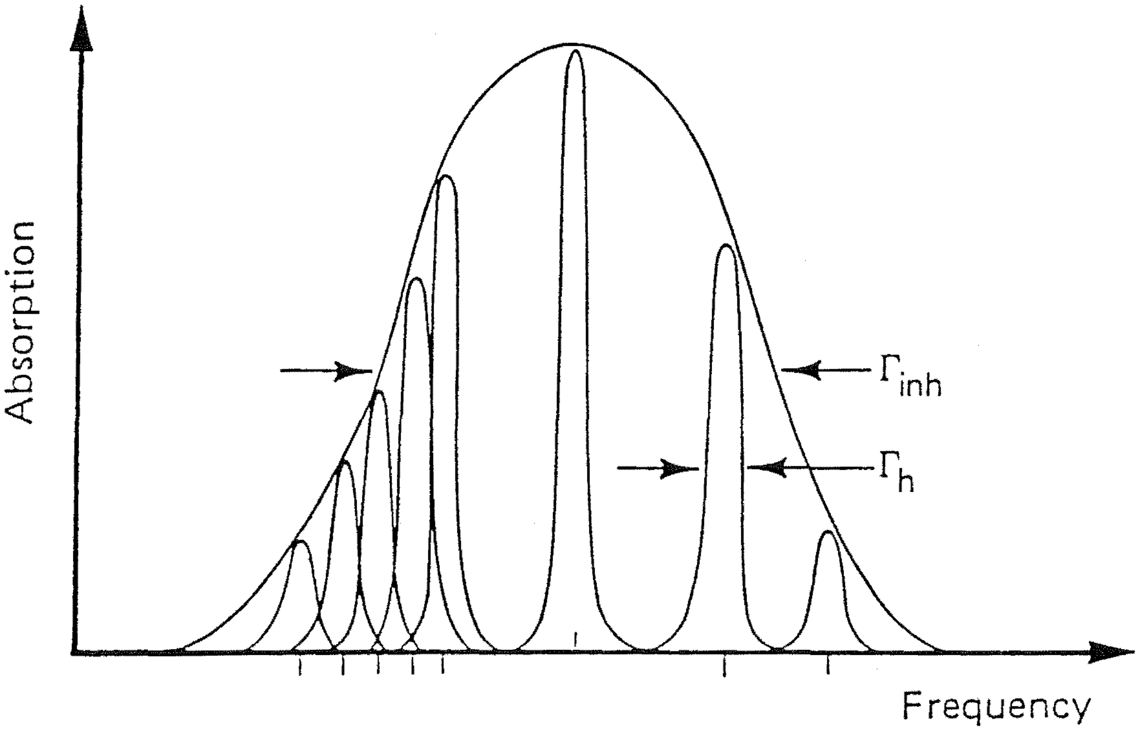

Figure 9.1: Profile of an optical transition showing inhomogeneous broadening (linewidth Γ_{ih}) in relation to homogeneous broadening (linewidth Γ_h).

anion nucleus in the neighbourhood of the rare-earth ion undergoes a spin flip in the magnetic field of the rare-earth ion. The process is shown schematically in Figure 9.2. By sweeping the rf field, all the ground state nuclear spin levels can be determined.

Holeburning and ODNMR experiments have been performed extensively for the Pr^{3+} C_{4v} symmetry centre in CaF_2 [21, 77, 78, 79] and SrF_2 [80, 105] crystals. The Pr^{3+} ion in the C_{4v} symmetry site has an orbitally degenerate γ_5 ground state and the characteristic six line fluorescence pattern for the ^{141}Pr nuclear spin I of $^5/_2$ was observed for excitation to the $^1D_2$ multiplet [21, 79]. The observed hyperfine lines had a common separation of 2.7 GHz and the hyperfine structure is attributed to the γ_5 doublet ground state of the lowest $^3H_4$ multiplet. Superhyperfine frequencies have been measured for the C_{4v} symmetry centres formed by the Pr^{3+} ion charge compensated by F^- ions [21] as well as H^-, D^- and T^- ions [80]. For the F^- compensated C_{4v} symmetry centre [21], superhyperfine resonancies were reported for the nearest neighbour (NN) lattice ^{19}F, the interstitial ^{19}F and the next nearest neighbour (NNN) ^{19}F nuclei. The relative positions of the NNN F^- ions with respect to the Pr^{3+} ion were determined from the local Pr^{3+} field measured at the F^- ion sites but exact positions for the NN and interstitial F^- ions could not be determined as the covalency effects, which are significant for both the NN F^- and the interstitial F^- ions, are not known. All the NNN F^- ions, except for the four furthest from the interstitial, were found to be shifted away from the Pr^{3+} ion and towards each other. The remaining four NNN F^- ions, furthest from the interstitial F^- ion, were found to retain the same positions as without the Pr^{3+} ion. Relative positions of the NN and interstitial F^- ions were estimated from those of the NNN F^- ions.

From the resonance frequencies found for the H^-, D^- and T^- compensated C_{4v} symmetry centres, the relative positions of the Pr^{3+} ion and the neighbouring ligands were proposed [80] as follows :-

The Pr^{3+} and H^- ions were displaced from the cube centre positions towards each other, while the four NN F^- ions between the Pr^{3+} and interstitial H^- ions were pushed outwards. The other set of four NN F^- ions further away from the interstitial H^- ion retained the same positions as with an F^- interstitial ion. Changes in the positions of the four NN F^- ions between the Pr^{3+} ion and the interstitial ion were found to be relatively small for the D^- and T^- charge compensated centres compared to those for the H^- compensated centre.

9.1 Previous High Resolution and ODNMR Studies of the C_{4v} Symmetry Centre in $CaF_2:Ho^{3+}$ Crystals

Hyperfine structures for ^{165}Ho have been reported for the C_4 symmetry centre in $LiYF_4:Ho^{3+}$ [2, 3, 4], the C_{3h} symmetry centre in $LaCl_3:Ho^{3+}$ [34], the C_{3v} symmetry centre in $CaF_2:Ho^{3+}$ [48, 49] and the C_{4v} symmetry centre in $CaF_2:Ho^{3+}$ [47, 81]. For the C_{3h} and C_{3v} symmetry centres, the characteristic eight line hyperfine structure arises from a degenerate ground state. For Ho^{3+} ions in sites of C_{4v} point group symmetry, the ground state Z_1 is an orbital singlet γ_1 level, but the D_2 level in CaF_2 at 15609.5 cm^{-1} is a doubly degenerate γ_5 level. If both levels were isolated, an eight line hyperfine structure in the $Z_1 \rightarrow D_2$ transition would arise from the hyperfine splittings of the degenerate γ_5 upper state as ^{165}Ho has nuclear spin I of $^7/_2$. Superhyperfine levels would not be observed as the isolated singlet Z_1 level does not have a magnetic moment.

From the laser selective excitation results presented in Chapter 4, it was observed that, for the C_{4v} symmetry centre in $CaF_2:Ho^{3+}$, the ground state Z_1 is not isolated as the first excited Z_2 level is only 1.9 cm^{-1} higher in energy. This small separation between the Z_1 and Z_2 levels results in the mixing of the wavefunctions for the Z_1 and Z_2 energy levels through the hyperfine interaction. In the resultant hyperfine structures for the $Z_1 \rightarrow D_2$ and $Z_2 \rightarrow D_2$ transitions, as measured by Hasan [47] and Martin et al. [81], this wavefunction mixing is

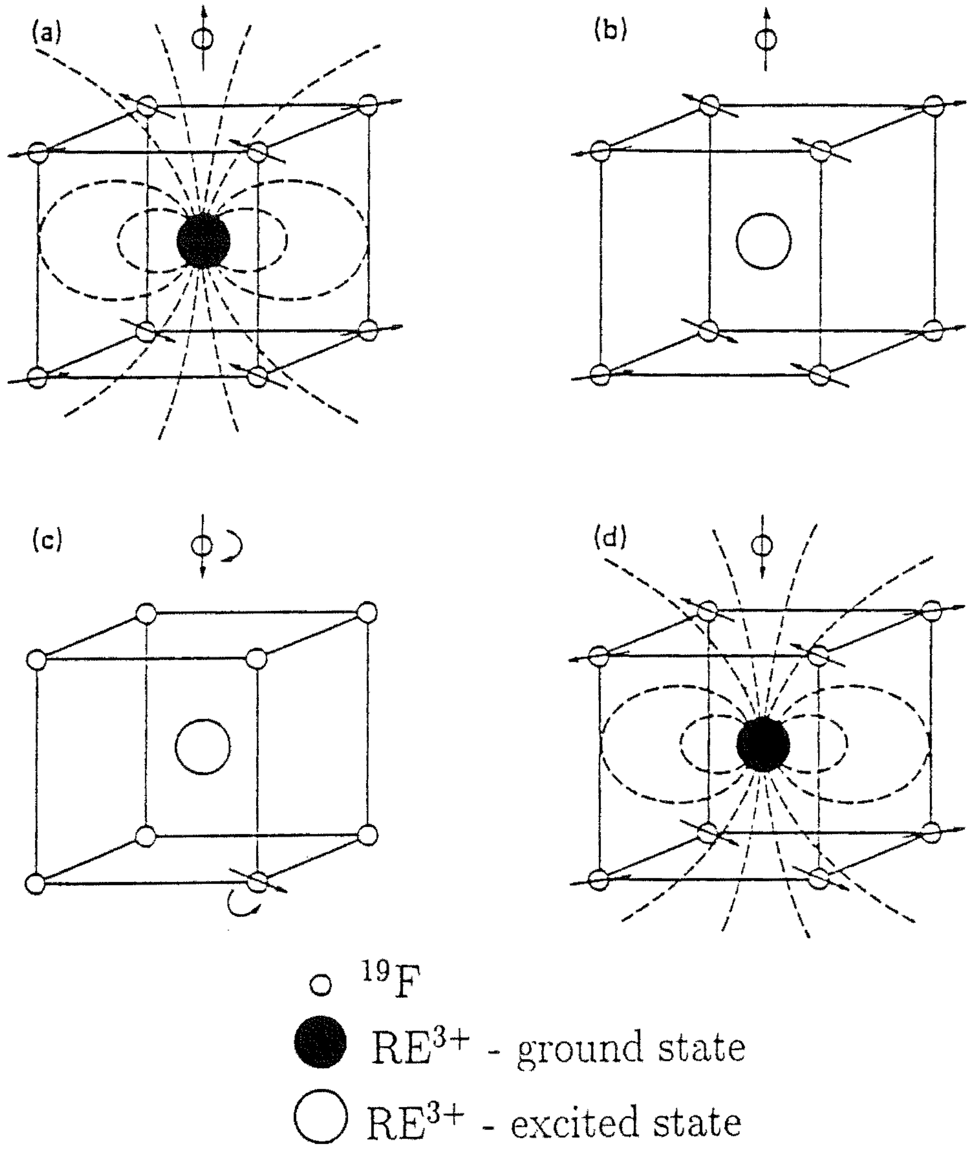

Figure 9.2: Pictorial representation of the hyperfine line holeburning process in a C_{4v} symmetry site :
(a) the RE^{3+} ion is in its ground state and spin flips of the surrounding ^{19}F nuclei are inhibited by the strong coupling with the RE^{3+} local magnetic field;
(b) & (c) the RE^{3+} ion is optically excited and its magnetic field greatly reduced, leaving the surrounding ^{19}F nuclei free to undergo spin flips;
(d) the RE^{3+} ion returns to its ground state, but is out of resonance with the laser because of the energy shift caused by the new configuration of neighbouring ^{19}F nuclear spins and a hole is burnt at the laser frequency.

evidenced by :-

(i) hyperfine structures with only five lines, instead of the eight expected for a $\gamma_1 \rightarrow \gamma_5$ type transition for nuclear spin I of $^7/_2$;

(ii) a significant departure from the Boltzmann intensity distribution expected for the hyperfine line structure. The three innermost lines were more than twice as strong as the two outer lines, in contrast to the expected gradual exponential increase in intensity. For the Pr^{3+} case, the intensities of the hyperfine lines were observed to vary by less than 20%;

(iii) a relatively large pseudo quadrupole splitting which results in the uneven separations between the hyperfine lines. The separation between the hyperfine lines varied from 0.7 GHz to 3.3 GHz whereas, for Pr^{3+}, the six hyperfine lines had a common splitting of 2.77 GHz.

(i) and (ii) result from the overlap between some of the hyperfine lines.

The wavefunction mixing also gives rise to an effective magnetic moment which results in the observation of ground state superhyperfine ODNMR lines. These superhyperfine resonances were observed by Martin et al. [81] in the 8 - 24 MHz range for the nearest neighbour and interstitial F^- ions and in the 0.5 - 3.5 MHz range for the next nearest and next next nearest neighbour F^- ions. The resonance frequencies measured could be assigned to one of the four $\pm\,^7/_2$, $\pm\,^5/_2$, $\pm\,^3/_2$ and $\pm\,^1/_2$ hyperfine (I_z) levels of the ground state (Figure 9.3).

The wavefunctions of the singlet Z_1 and Z_2 levels are of γ_1 and γ_2 symmetry respectively. Although these wavefunctions transform differently in C_{4v} symmetry and therefore do not interact through the crystal field, the presence of the hyperfine interaction couples the wavefunctions through the parallel hyperfine interaction $A_J I_z J_z$ of the Hamiltonian given below, giving the ground state a pseudo degenerate character. The Hamiltonian for the hyperfine coupling H_{hf} has the form

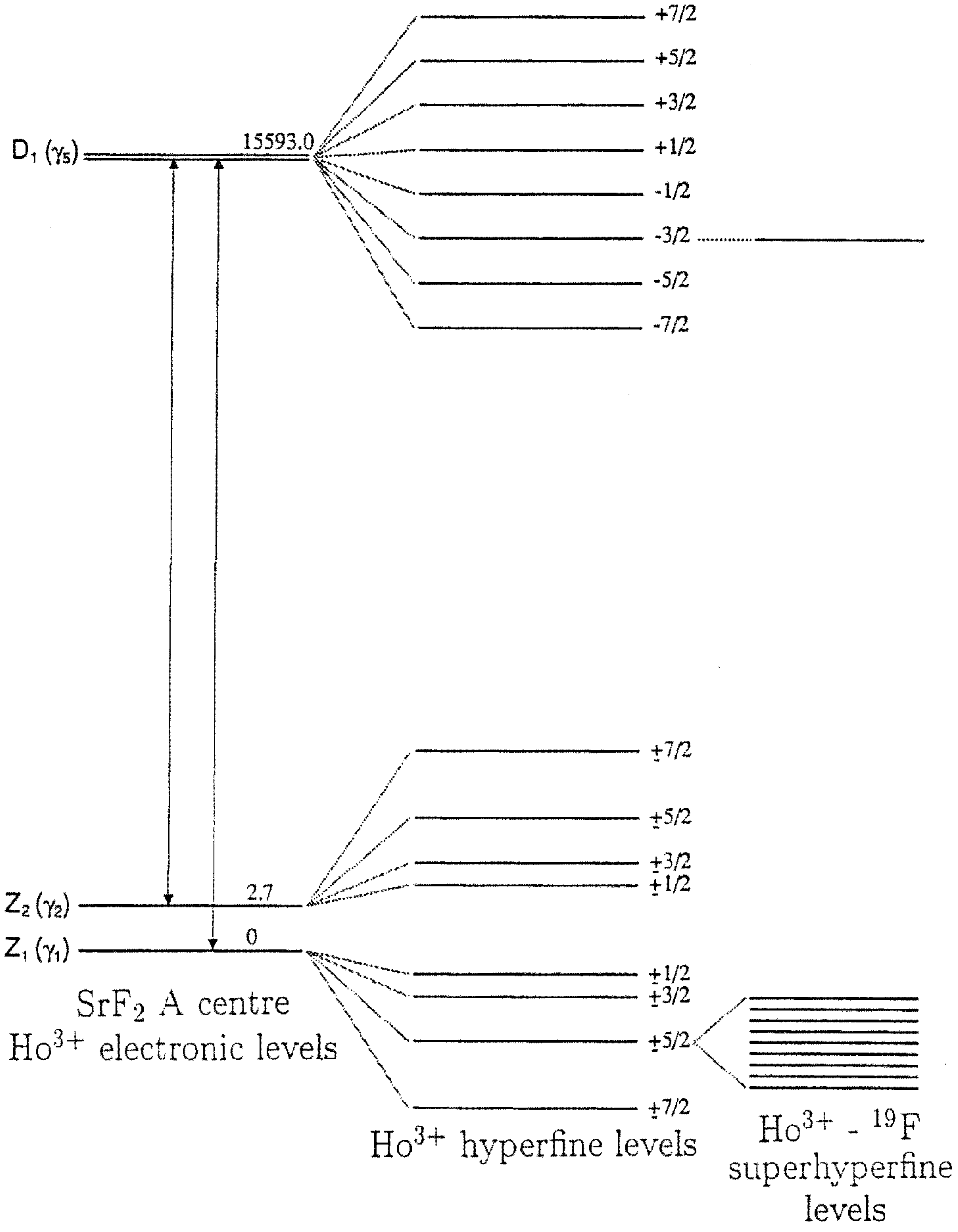

Figure 9.3: Energy level diagram of the Ho^{3+} ion in the C_{4v} symmetry site showing the hyperfine levels for nuclear spin $I = {}^7/_2$ and the superhyperfine levels. Superhyperfine levels are observed for the singlet Z_1 level because of the hyperfine coupling between the Z_1 and Z_2 levels, which results in an enhanced magnetic moment.

$$H_{hf} = A_j \left\{ I_z J_z + \frac{(I^+J^- + I^- J^+)}{2} \right\},$$

where A_j is the magnetic hyperfine constant.

From the analysis of the nearest neighbour and interstitial F^- resonance frequencies for the $Z_1 \rightarrow D_2$ transition of the Ho^{3+} C_{4v} symmetry centre in CaF_2 crystals [81], it was found that the ratios of the superhyperfine frequencies measured were close to the ratios of I_z for a particular pair of spin levels. This strong dependence on I_z shows that the first term of the Hamiltonian is the major contribution to the hyperfine interaction.

The hyperfine and superhyperfine spectra measured here for the SrF_2 A and SB1 centres in SrF_2:Ho^{3+}(0.001%) show two sets of four line structures in the high resolution (2 MHz) spectra for $Z_1,Z_2 \rightarrow D_1$ excitation (Figures 9.4 and 9.6). The two centres have Z_1 - Z_2 separations of 2.7 and 2.5 cm^{-1} respectively and a γ_5 degenerate D_1 energy level. The superhyperfine resonances are found to occur at lower frequencies (Tables 9.2 and 9.4) compared to those for the CaF_2 A centre.

For the dimer centre in $CsCdBr_3$:Ho^{3+}(0.01%), both the Z_1 and the D_1 energy levels are of the degenerate γ_3 symmetry and the eight line pattern expected for a nuclear spin I of $^7/_2$ is apparent (Figure 9.8), but complete analysis is hindered by the overlapping effects of the low symmetry crystal-field present and by ion pair splittings.

The results for the three centres, SrF_2 A, SB1 and the dimer centre, are discussed in turn in Sections 9.3, 9.4 and 9.5 respectively.

Similar measurements could not be made for the SC1 centre whose signal intensity was too weak to give any reliable results.

9.2 Experimental Aspects

The SrF_2:Ho^{3+}(0.001%) and $CsCdBr_3$:Ho^{3+}(0.01%) crystals used were cooled to either 4.2 K or 2 K.

The 514.5 nm argon ion laser line from a Spectra Physics model 2030 argon ion laser was used as the pump source for a CR 699 coherent ring dye laser. The DCM red dye used covered the $^5F_5$ multiplet region of the Ho^{3+} ion in both SrF_2 (15550 - 15800 cm^{-1}) and $CsCdBr_3$ (15300 - 15500 cm^{-1}) and the output from the dye laser had a linewidth of 1 - 2 MHz.

For the high resolution experiments, the dye laser was operated in scanning mode over a 20 GHz range.

For the ODNMR experiments, the crystal was mounted in the centre of a five turn copper coil. With the dye laser operated in fixed frequency mode, an rf frequency over the 1 - 21 MHz range as produced by a Hewlett Packard 8443A tracking generator and amplified by an ENI 10 W power supply was swept through the coil whilst the sample was irradiated with laser light.

The resulting fluorescence, for both high resolution and ODNMR experiments was detected by a Spex 1400 double monochromator equipped with a thermo-electrically cooled EMI GENCOM ZD-50 photomultiplier tube. A Princeton Applied Research 4202 signal averager was used to average a preset number of scans in each case.

9.3 High Resolution and ODNMR Studies of the A Centre in SrF_2:Ho^{3+}(0.001%) Crystals

The hyperfine and superhyperfine spectra are shown in Figures 9.4 and 9.5 respectively and the corresponding data is presented in Tables 9.1 and 9.2 respectively, for excitation of the $Z_1 \rightarrow D_1$ transition at 15593.0 cm^{-1} and the $Z_2 \rightarrow D_1$ transition at 15590.3 cm^{-1}, and monitoring the $D_1 \rightarrow Z_{10}$ transition at 15200.0 cm^{-1}. The hyperfine structure (Figure 9.4) has the same general shape as that observed for the CaF_2 A centre [47, 81]. The lines are broader for the SrF_2 case here because of the small amounts (of about 0.2%) of Ca^{2+} and Ba^{2+} ions present in the crystals, as discussed in Chapter 5. The superhyperfine lines observed arise from resonances of the eight nearest neighbour lattice F^- ions and of the one interstitial F^- ion. The eight nearest neighbour F^- ions give rise to two

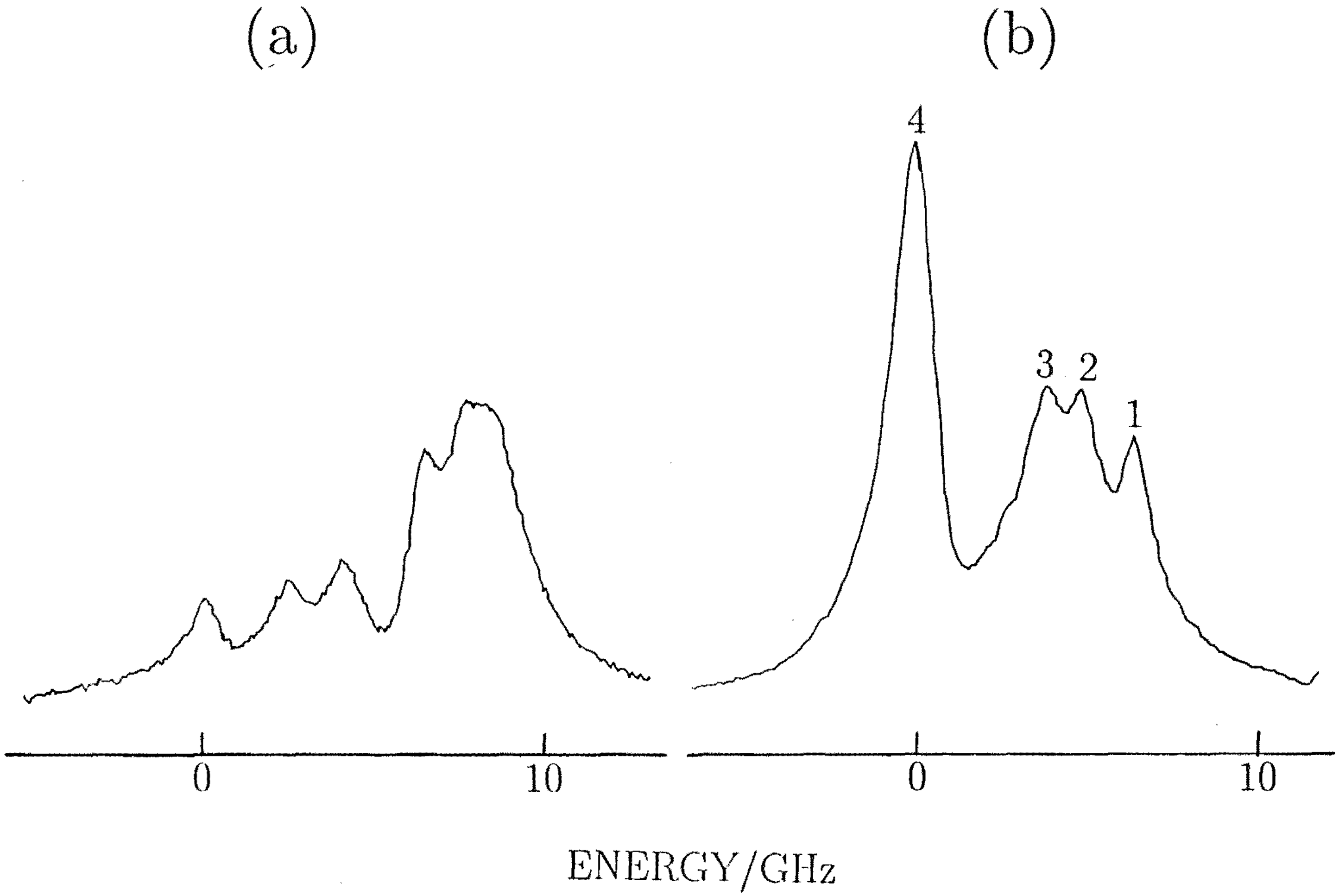

Figure 9.4: 2 K high resolution excitation spectra of the (a) $Z_2 \rightarrow D_1$ (15590.3 cm^{-1}) and (b) $Z_1 \rightarrow D_1$ (15593.0 cm^{-1}) transitions of the C_{4v} symmetry A centre in SrF_2:Ho^{3+}(0.001%) crystals.

Table 9.1: Relative energy positions for the hyperfine lines of the $Z_2 \rightarrow D_1$ and $Z_1 \rightarrow D_1$ transitions of the C_{4v} symmetry A centre in $SrF_2:Ho^{3+}$ crystals

Transition	Relative hyperfine line positions (GHz)
$Z_2 \rightarrow D_1$	0
	2.46
	4.01
	6.51
	7.96
$Z_1 \rightarrow D_1$	0
	3.89
	4.93
	6.43

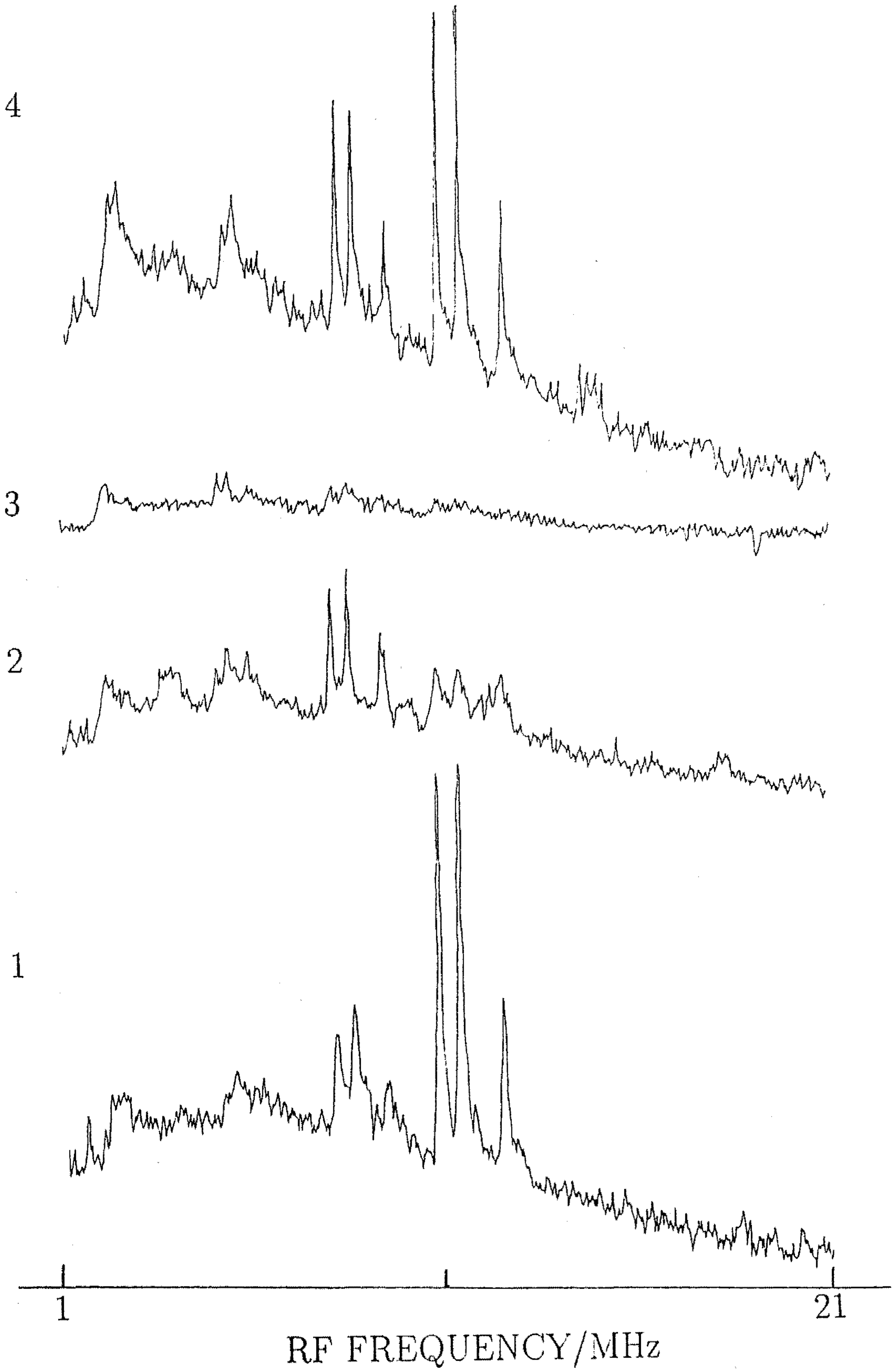

Figure 9.5: 2 K superhyperfine ODNMR spectra of the nearest neighbour and interstitial ^{19}F nuclei for the $Z_1 \rightarrow D_1$ transition of the C_{4v} symmetry A centre in $SrF_2:Ho^{3+}$(0.001%) crystals. The spectra are numbered 1 to 4 according to the hyperfine line of Figure 9.4(b) burnt.

Table 9.2: Superhyperfine ODNMR frequencies for the nearest neighbour and interstitial ^{19}F nuclei for the $Z_1 \rightarrow D_1$ transition of the C_{4v} symmetry A centre in $SrF_2:Ho^{3+}$ crystals, as measured at 2 K.

I_z level	**Measured ODNMR frequencies (MHz)**		**Ratio of frequencies**	**Ratio of I_z values**
	Nearest neighbour ^{19}F nuclei	Interestial ^{19}F nucleus		
$^{7}/_{2}$	10.7	11.94	1	1
	10.1			
$^{5}/_{2}$	7.89	8.81	0.737	0.714
	7.45			
$^{3}/_{2}$	4.79	5.35	0.447	0.429
	4.52			

distinct superhyperfine lines from the following sets of four F^- ions :-

(i) the four F^- ions between the Ho^{3+} ion and the interstitial F^- ion;

(ii) the remaining four F^- ions further away from the interstitial F^- ion.

The two sets of ions are inequivalent because of the presence of the interstitial ion. The ions in set (i) experience a different field of the Ho^{3+} ion resulting in a slight shift of the resultant superhyperfine resonance to lower frequency relative to that of the ions in (ii).

By burning a hole in each of the hyperfine lines of the $Z_1 \rightarrow D_1$ transition at 15593.0 cm^{-1} shown in Figure 9.4(b), the corresponding superhyperfine resonances were measured (Figure 9.5). Because of overlap between the hyperfine lines as a result of the broadness of the transitions, burning a hole in any single hyperfine line gave weaker resonances for the other lines as well. The resonances for the particular transition being burnt were much stronger than any from the other overlapping hyperfine lines, enabling characterisation of the lines according to their I_z (nuclear) spin levels.

For ^{165}Ho nuclei with spin I of $^7/_2$, the three sets of superhyperfine lines observed are assigned to correspond to I_z values of $^7/_2$, $^5/_2$ and $^3/_2$ (Figure 9.3). No resonances corresponding to the I_z value of $^1/_2$ were detected. As shown in Table 9.2, the resonances are mostly from the dominant first term of the hyperfine Hamiltonian, which gives a strong I_z dependence of the measured frequencies, as found for the CaF_2 case.

For the CaF_2 A centre, resonances due to the nearest neighbour and interstitial F^- ions were found to occur in the 8 - 24 MHz range while corresponding resonances for the SrF_2 case here are found to occur in the lower 5 - 11 MHz range (Figure 9.5). Overall, the resonance frequencies for the SrF_2 A centre are about half of those for the CaF_2 A centre, with the separations between the resonances of the two sets of four nearest neighbour F^- ions being three times larger for the SrF_2 case (Table 9.2).

The hyperfine field of the rare-earth ion, at the neighbouring ligand site comprises a dipolar field from the electrons of the rare-earth and a covalent bonding effect from the overlap between the valence orbitals of the rare-earth ion and those of the neighbouring ligand ions. Covalent bonding effects are strong for the nearest neighbour and interstitial F^- ions but are much less at the more distant sites. The hyperfine resonances from the nearest neighbour and interstitial F^- ions are dependent on both the dipolar field and the covalent bonding effects, while the hyperfine field experienced by the next nearest neighbour F^- ions is almost wholly from the dipolar effects.

These results from both high resolution and ODNMR studies of the SrF_2 A centre confirm the C_{4v} symmetry assignment made for this centre.

As the Z_1 - Z_2 energy level separation of 2.7 cm^{-1} for the SrF_2 A centre here is larger than the 1.9 cm^{-1} for the CaF_2 A centre, the hyperfine interaction mixing effects are weaker for the SrF_2 case and lower frequency resonances are obtained.

9.4 High Resolution and ODNMR Studies of the SB1 Centre in SrF_2:Ho^{3+}(0.001%) Crystals

The high resolution spectra for the C_{4v} symmetry SB1 centre, as shown in Figure 9.6, were obtained with excitation of the $Z_1 \rightarrow D_1$ and $Z_2 \rightarrow D_1$ transitions at 15588.0 and 15585.5 cm^{-1} respectively, while monitoring the $D_1 \rightarrow Z_{10}$ transition at 15205.5 cm^{-1}. Both transitions show the same four line structure as found for the SrF_2 A centre, but with different separations for some of the lines, as can be seen from comparison of Tables 9.1 and 9.3.

Just as for the SrF_2 A centre, the hyperfine lines could be assigned to particular I_z values of $^7/_2$, $^5/_2$ and $^3/_2$ (Figure 9.3) from their superhyperfine lines while no resonance was observed for I_z of $^1/_2$. The hyperfine line marked by * in Figure 9.6 does not give any superhyperfine resonances and is likely to be from a different centre. Again, as found for both the CaF_2 A centre [81] and the SrF_2 A centre, the I_z dependence of the resonance frequencies is pronounced (Table 9.4).

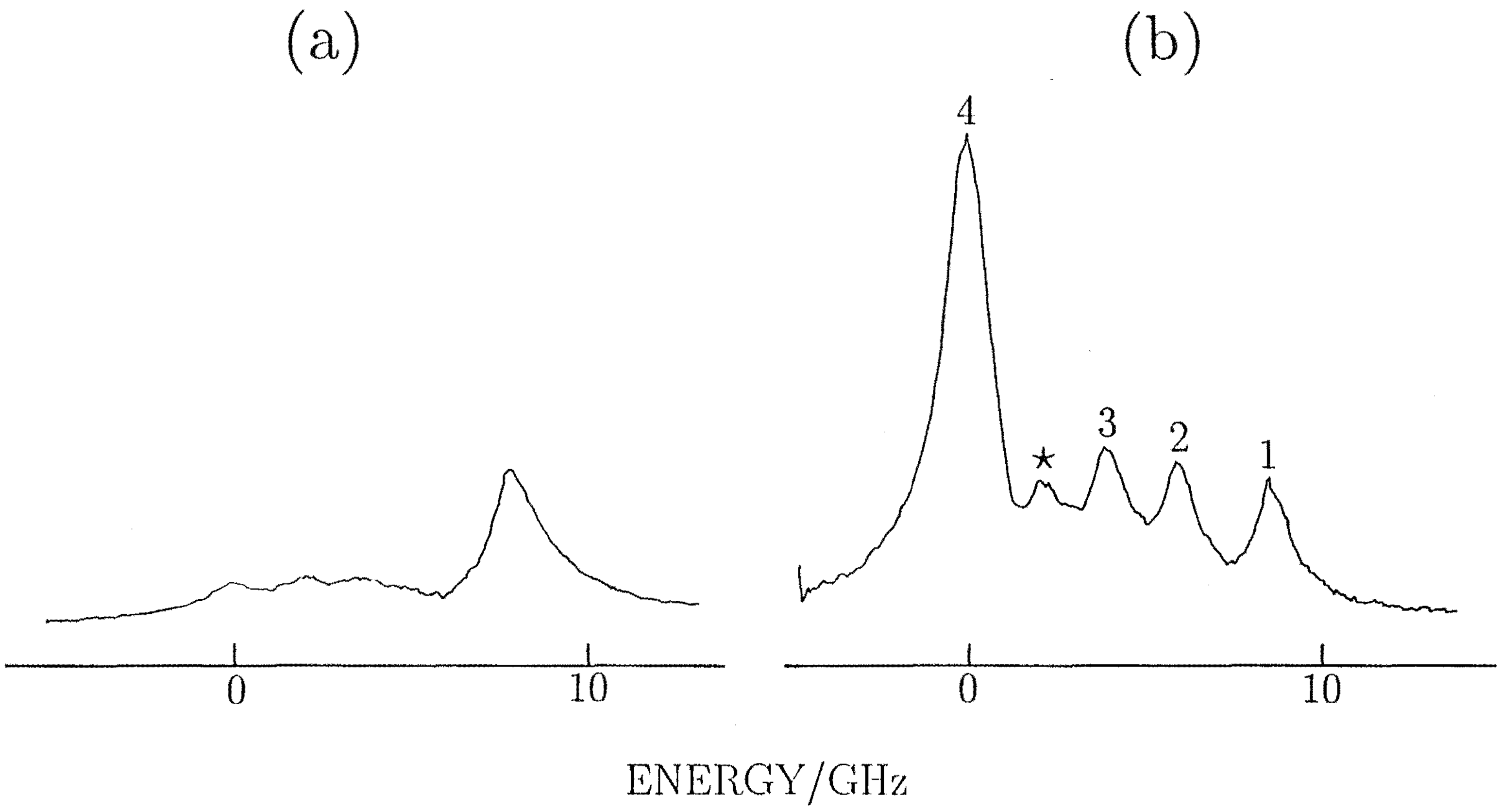

Figure 9.6: 2 K high resolution excitation spectra of the (a) $Z_2 \rightarrow D_1$(15585.5 cm^{-1}) and (b) $Z_1 \rightarrow D_1$(15588.0 cm^{-1}) transitions of the C_{4v} symmetry SB1 centre in SrF_2Ho^{3+}(0.001%) crystals.

Table 9.3: Relative energy positions for the hyperfine lines of the $Z_2 \rightarrow D_1$ and $Z_1 \rightarrow D_1$ transitions of the C_{4v} symmetry SB1 centre in $SrF_2:Ho^{3+}$ crystals

Transition	**Relative hyperfine line positions (GHz)**
$Z_2 \rightarrow D_1$	0
	1.99
	3.57
	7.75
$Z_1 \rightarrow D_1$	0
	2.07*
	3.87
	5.86
	8.46

*Holeburning this hyperfine line does not give any superhyperfine resonances.

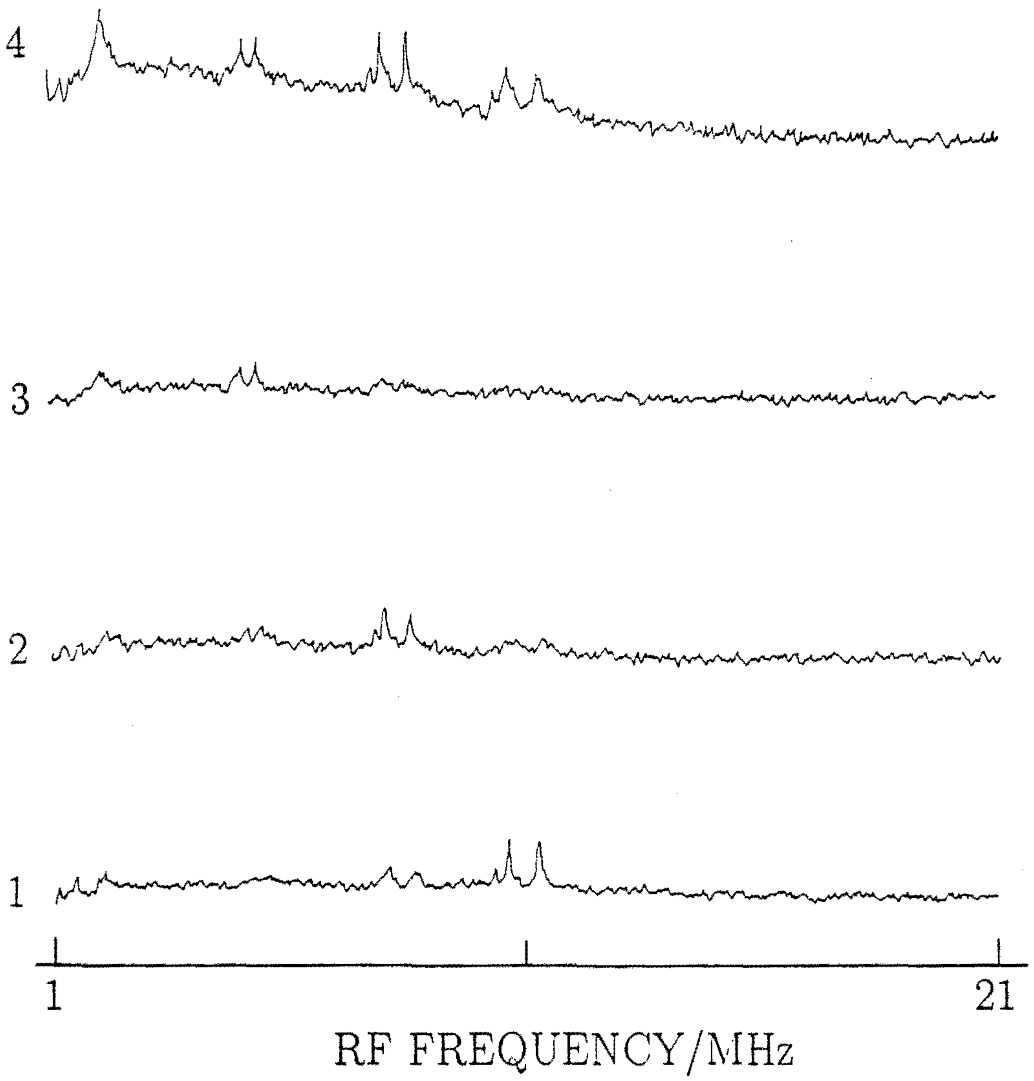

Figure 9.7: 2 K superhyperfine ODNMR spectra of the nearest neighbour and interstitial ^{19}F nuclei for the $Z_1 \rightarrow D_1$ transition of the C_{4v} symmetry SB1 centre in $SrF_2:Ho^{3+}$(0.001%) crystals. The spectra are numbered 1 to 4 according to the hyperfine line of Figure 9.6(b) burnt.

Table 9.4: Superhyperfine ODNMR frequencies for the nearest neighbour and interstitial ^{19}F nuclei for the $Z_1 \rightarrow D_1$ transition of the C_{4v} symmetry SB1 centre in $SrF_2:Ho^{3+}$ crystals, as measured at 2 K.

I_z level	Measured ODNMR frequencies (MHz)		Ratio of frequencies	Ratio of I_z values
	Nearest neighbour ^{19}F nuclei	Interestial ^{19}F nucleus		
$^7/_2$	10.7	9.84	1	1
	10.1			
$^5/_2$	7.89	7.26	0.737	0.714
	7.45			
$^3/_2$	4.83	4.40	0.447	0.429
	4.52			

From the superhyperfine results given in Figure 9.7 and Table 9.4, it can be seen that the nearest neighbour F^- ion resonances have identical frequencies to those for the SrF_2 A centre. The nearest neighbour F^- ions therefore retain the same positions in going from the parent C_{4v} symmetry centre to the modified C_{4v} symmetry centres. The cubic arrangement of the F^- ions around the Ho^{3+} ion is therefore not altered at all by the presence of the Ba^{2+} ion placed two lattice spacings away. Observation of the same resonance frequencies for the nearest neighbour F^- ions for both the SrF_2 A and SB1 centres supports the earlier crystal-field analyses which give almost the same cubic crystal-field parameters.

The resonance frequency for the interstitial F^- ion was found to be vastly shifted for the SB1 centre compared to those for the A centres, with the resonance frequency lower even than those for either set of nearest neighbour F^- ions. Introduction of the Ba^{2+} ion next to the interstitial F^- ion therefore has a marked effect on the position of the interstitial F^- ion. It is likely that the Ba^{2+} ion, being larger than the Sr^{2+} ion, causes repositioning of the interstitial F^- ion in the following way :-

> the lattice F^- ions between the Ba^{2+} and the interstitial F^- ions shift outwards to accommodate the Ba^{2+} ion. The interstitial F^- ion is then likely to shift towards the Ba^{2+} ion, away from the Ho^{3+} ion. Such repositioning would reduce the dipolar field experienced and hence lower the resonance frequency for the interstitial F^- ion.

An alternative and less likely mechanism is that since the region between the interstitial F^- ion and the rare-earth ion is already spatially extended, as determined by Burum et al. [21] for the Pr^{3+} case, the lattice F^- ions retain the same positions as in the parent SrF_2 A centre but the interstitial F^- ion shifts towards the Ho^{3+} ion to accommodate the Ba^{2+} ion. Since the interstitial F^- ion at this new site is nearer the Ho^{3+} ion, the dipolar field is increased, but if the covalency effects outweigh this dipolar field increase, the resultant resonance frequency could be lower than that for the parent SrF_2 A centre.

From the crystal-field calculations (Chapter 7), the second degree axial crystal-field parameter B^2_A, which is largely determined by the interstitial F^- ion, was found to be about half that for the SrF_2 A centre. This result together with the common resonance frequencies measured for the nearest neighbour ^{19}F nuclei resonancies, favour the repositioning of the interstitial F^- ion towards the Ba^{2+} ion as the more likely configuration of the SB1 centre.

Measurements for the SC1 centre could not be obtained as its signal intensity was too weak in the crystals available. It is however expected that Ca^{2+}, being smaller than Sr^{2+}, would give resonances for the interstitial F^- ion at slightly lower frequencies than those for the SrF_2 A centre. The change is not expected to be as large as observed here for the SB1 centre and a small shift, to lower frequency, in the resonances due to the interstitial F^- ion in the SC1 centre would follow the relatively small decrease in the value of the second degree axial crystal-field parameter B^2_A (Chapter 7) compared to that for the SrF_2 A centre.

Similar studies for the C_{4v} symmetry CS1 and CB1 centres found in the CaF_2 type crystals would be helpful for a complete understanding of the resonances from the interstitial F^- ion and the model configuration proposed for these centres. As both Sr^{2+} and Ba^{2+} are larger than the Ca^{2+} host alkaline-earth, both centres are expected to show the same behaviour as the SB1 centre above, with the CB1 centre showing the greater change. Because of the greater energy separation between the nearest neighbour and interstitial F^- ion resonances in the parent CaF_2 A centre, it is unlikely that the interstitial resonance frequencies would shift lower than those for the nearest neighbour F^- ions. A similar small shift in the resonance of the interstitial F^- ion to lower frequency was observed for the A2 centre in $Ca_{0.995}Sr_{0.005}F_2:Pr^{3+}$ crystals [64], for which the Sr^{2+} ion is located on the $Pr^{3+} - F^-$ axis with the C_{4v} symmetry configuration of Figure 1.4(a).

9.5 High Resolution Studies of the Dimer Centre in $CsCdBr_3:Ho^{3+}(0.01\%)$ Crystals

High resolution measurements have been reported for the Pr^{3+} Z_1 ($^3H_4$) → D_1 ($^1D_2$) transition (near 17010 cm^{-1}) in $CsCdBr_3:Pr^{3+}(0.1\%)$ crystals [27]. The line shape obtained was proposed to be from the combined effects of the hyperfine interaction and the low symmetry distortion from exact C_{3v} symmetry. From the spectral holeburning measurements made in the -80 to 80 MHz range for applied electric fields of up to 666 V/cm, the hole was found to split into two components whose separation was linearly dependent on the applied electric field. From these results, it was concluded that the effect of pair ion interaction was smaller than the inhomogeneous linewidth of the transition.

High resolution measurements were performed here on $CsCdBr_3:Ho^{3+}(0.01\%)$ crystals for excitation of the $Z_1 \rightarrow D_1$ and $Z_1 \rightarrow D_2$ transitions of the dimer centre at 15307.5 and 15314.5 cm^{-1} respectively, with monitoring of the $D_1 \rightarrow Z_{10}$ transition at 15090.5 cm^{-1}. The spectra are shown in Figure 9.8 (a) and (b) respectively, and the hyperfine line positions are presented in Table 9.5.

The spectrum for excitation of the $Z_1 \rightarrow D_1$ transition at 15307.5 cm^{-1} (Figure 9.8(a)), comprises two overlapping sets of eight line patterns. The first set of eight lines are compactly spaced with separations of 1.05 GHz while the second set of eight lines consists of two subsets of four lines each that are more widely spaced, with separations of 3.15 GHz in each subset and 7.75 GHz between the two innermost lines of the set. As both sets are centred in the same region, only six lines from the second set are apparent in Figure 9.8(a). Small splittings of up to 0.5 GHz are apparent on some of the lines. Using the π and σ polarisation convention defined as the E vector of the laser parallel and perpendicular respectively, to the c axis, these six lines were all found to be σ polarised. The closely spaced eight lines were all found to be π polarised. As this $Z_1 \rightarrow D_1$ transition is of $\gamma_3 \rightarrow \gamma_3$ (E → E) type in C_{3v} symmetry, the two sets

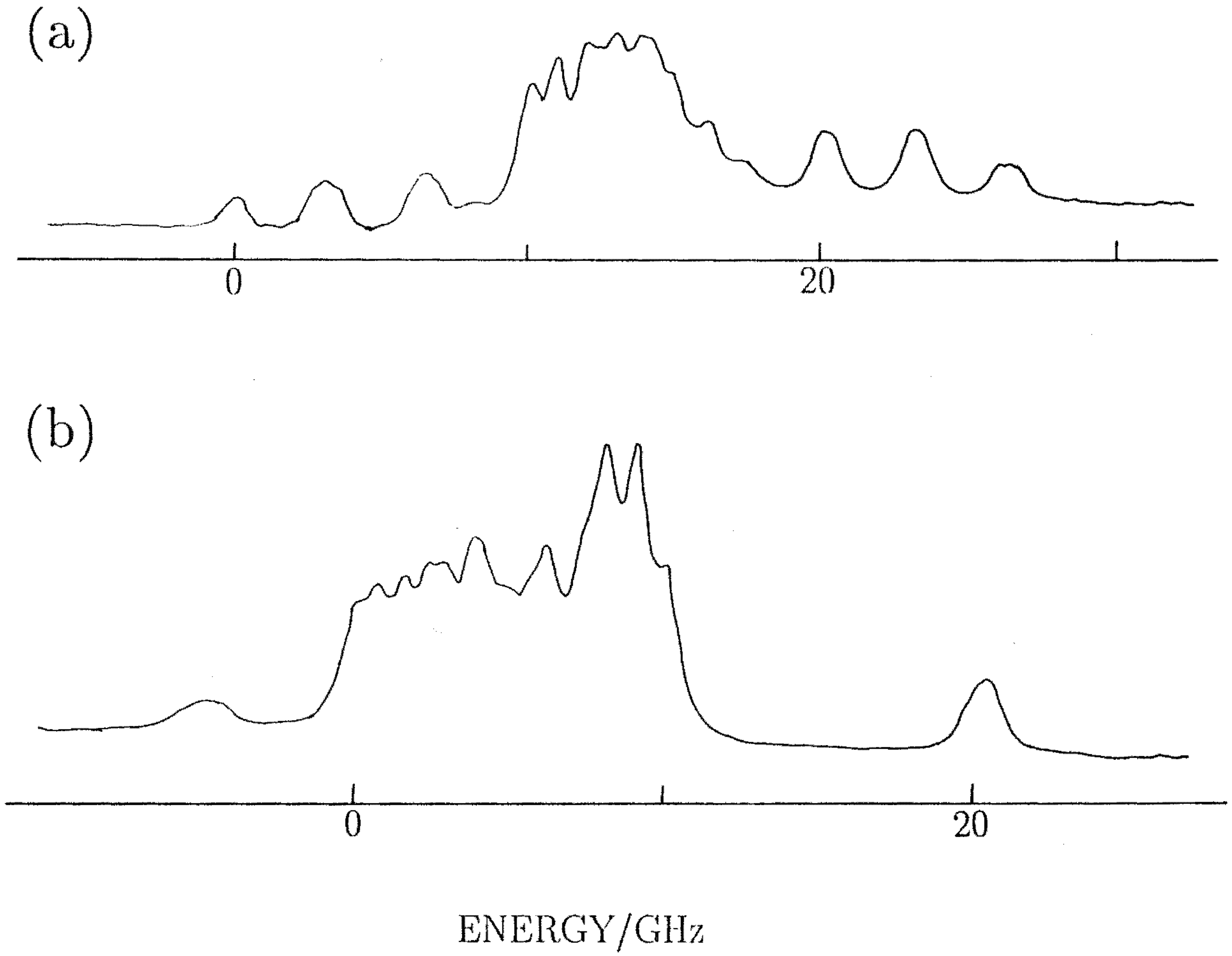

Figure 9.8: 2 K high resolution excitation spectra of the (a) $Z_1 \rightarrow D_1$(15307.5 cm^{-1}) and (b) $Z_1 \rightarrow D_2$(15314.5 cm^{-1}) transitions of the principal dimer centre in $CsCdBr_3:Ho^{3+}$(0.01%) crystals.

Table 9.5: Relative energy positions for the hyperfine lines of the $Z_1 \rightarrow D_1$ and $Z_1 \rightarrow D_2$ transitions of the dimer centre in $CsCdBr_3:Ho^{3+}$ crystals

Transition	**Relative hyperfine line positions (GHz)**	
$Z_1 \rightarrow D_1$	$E^+ \leftrightarrow E^-$	$E^{+(-)} \rightarrow E^{+(-)}$
	0	10.02
	3.15	10.94
	6.50	11.97
	20.05	12.96
	23.15	13.93
	26.35	14.98
		16.30
		17.26
$Z_1 \rightarrow D_2$	$E \rightarrow A$	
	0	
	0.54	
	1.36	
	2.22	
	2.69	
	3.74	
	5.97	
	7.85	
	8.86	
	9.84	
	-4.87	
	20.16	

of lines arise from superimposed hyperfine splittings from both the Z_1 and the D_1 levels. The more compact set of eight lines are therefore assigned as $E^+ \rightarrow E^+$ or $E^- \rightarrow E^-$ type transitions, while the second set are $E^+ \leftrightarrow E^-$ type transitions.

The high resolution spectrum for excitation of the $Z_1 \rightarrow D_2$ transitions at 15314.5 cm^{-1} (Figure 9.8(b)) was found to have a single set of eight lines, some of which also show small splittings of about 0.5 GHz. This set of lines were found to be σ polarised, which is consistent with the D_2 level being of γ_2 symmetry, as previously assigned in Chapter 6.

From the analysis of the dimer centre transitions in Chapter 6, low symmetry crystal-field splittings could not be determined for transitions from the D_1 level but were estimated to be at most 1 cm^{-1} from the broad profile of the $D_1 \rightarrow Z_1$ and $D_1 \rightarrow Z_3$ transitions. The high resolution spectra obtained here are therefore complicated by the presence of three comparable interactions, viz :-

(i) the hyperfine coupling;

(ii) the low symmetry crystal-field interaction;

(iii) the inter-ionic coupling between the Ho^{3+} ions of a pair.

Detailed analysis of the hyperfine line structures would require further knowledge of the low symmetry crystal-field and pair splittings before lines from the hyperfine coupling alone can be identified. As all the transitions are quite broad, lower Ho^{3+} concentration crystals might yield sharper and better defined lines.

Further high resolution measurements for excitation of the sharper transitions of the E and F multiplets are likely to be easier to analyse as the low symmetry crystal-field and pair splittings of these transitions are clearly resolved in the low resolution spectra (Chapter 6). A high resolution analysis of these well resolved transitions is expected to give a better measure of the low symmetry crystal-field effects and the ion pair interaction in the high resolution spectra, which would be helpful for interpreting the results found here for excitation of the $Z_1 \rightarrow D_1$ and $Z_1 \rightarrow D_2$ transitions.

CHAPTER 10

SUMMARY AND CONCLUSIONS

Results of a laser selective excitation study of Ho^{3+} ions in the three crystal hosts, CaF_2, SrF_2 and $CsCdBr_3$, have been described. Ho^{3+} centre symmetries and crystal-field energy level irrep labels have been determined and model configurations proposed for the various centres.

In CaF_2:Ho^{3+}(0.005%) crystals, polarisation ratio measurements have been used to confirm the C_{4v} and C_{3v} symmetry assignments proposed by [SW] for the A and B centres respectively. The major contribution of this study towards the interpretation of the spectra of these two Ho^{3+} centres has been in deriving the energy level schemes and assigning irrep labels to the crystal-field energy levels of both centres.

For the four new centres (CS1, CS2, CB1 and CB2) identified in the mixed $Ca_{0.99}Sr_{0.01}F_2$:Ho^{3+}(0.005%) and $Ca_{0.99}Ba_{0.01}F_2$:Ho^{3+}(0.005%) crystals, the Ho^{3+} site symmetries and crystal-field energy level irrep labels have been established from polarisation studies. The model configurations proposed show all four centres to be derived from the C_{4v} symmetry A centre by either an on-axis or an off-axis placement of the dopant Sr^{2+} or Ba^{2+} cation. The on-axis substitution of the host cation preserves the C_{4v} symmetry of the parent centre, as shown by the similarities of both the CS1 and CB1 centre spectra and polarisation behaviour to those of the C_{4v} symmetry parent A centre. The off-axis substitution, which creates a C_s symmetry centre, is shown by splittings on the C_{4v} symmetry γ_5 (doublet) type energy levels of the CS2 and CB2 centres. Polarisation studies show both the CS2 and CB2 centres to be (100) plane C_s symmetry centres with the C_s(b) configuration.

Of the five centres observed in SrF_2:Ho^{3+}(0.01%) crystals, two are the SrF_2 analogues of the A and B centres found in CaF_2. Unlike in CaF_2 where the A and B centres are of comparable intensities, the SrF_2 B centre is only 2% of the intensity of the SrF_2 A centre. With the principal centre in $SrF_2:Ho^{3+}$ being of C_{4v} symmetry while that in $SrF_2:Er^{3+}$ is trigonal [30, 68], the change over in the principal centre symmetry from C_{4v} to C_{3v}, for rare-earth ions in SrF_2 crystals occurs between the Ho^{3+} and Er^{3+} ions.

The three remaining centres, SC1, SC2 and SB1, also present in $SrF_2:Ho^{3+}$ crystals are from Ca^{2+} and Ba^{2+} impurities in the nominally pure SrF_2 starting material. The SC1 and SB1 centres have been assigned the same C_{4v} symmetry configuration as for the CS1 and CB1 centres, on the basis of the similarity between their spectra and polarisation behaviour and those of the SrF_2 A centre. The SC2 and SB2 centres are proposed to have the same C_s(b) configuration as the CS2 and CB2 centres.

The laser selective excitation study of deuterated $CaF_2:Ho^{3+}$ and $SrF_2:Ho^{3+}$ crystals was not as successful as had been hoped. Although the D^- analogue of the CaF_2 B centre was identified, neither of the two other centres found in $CaF_2:Ho^{3+}:D^-$ crystals could be assigned as the D^- C_{4v} symmetry centre analogous to the CaF_2 A centre. In $SrF_2:Ho^{3+}:D^-$ crystals, the four centres found have some resemblance to the SrF_2 A, SC1, SC2 and SB1 centres, but none of the four D^- centres could be assigned as a C_{4v} symmetry centre.

For $CsCdBr_3:Ho^{3+}$ crystals, the spectroscopy of the principal dimer centre has been documented, as done for Nd^{3+} [10, 11], Er^{3+} [29, 31] and Pr^{3+} [102]. The relatively strong upconversion fluorescence enabled energy levels up to 35522.5 cm^{-1} to be identified. Several energy transfer mechanisms have been proposed for the upconversion fluorescence observed. The small pair splittings of 0.20 to 0.44 cm^{-1} (from the coupling of the two Ho^{3+} ions of a dimer centre) and the low symmetry crystal-field splittings of up to 2.5 cm^{-1} apparent on some of the sharper transitions have been discussed. The low symmetry crystal-field splittings give direct evidence that the Ho^{3+} ions in $CsCdBr_3$ crystals are not in sites of exact C_{3v} symmetry.

Three minority centres L, M and N, present in $CsCdBr_3:Ho^{3+}$(0.3%),

$CsCdBr_3$:Ho^{3+}(0.01%) and $CsCdBr_3$:Ho^{3+}(0.3%):Na^+(1%) crystals respectively, have also been discussed and model configurations proposed.

The crystal-field fits show good agreement between the experimental and the calculated energies of the crystal-field levels. For both the C_{4v} and C_{3v} symmetry centres, the irrep label assignments based on polarisation measurements have been confirmed and the symmetries of the unassigned levels determined.

Fluorescence lifetimes have been measured for the major centres in CaF_2 and SrF_2 type crystals, except the weak SrF_2 B and SB2 centres. For the CS1, CS2, CB1 and CB2 centres, the fluorescence lifetimes are similar to those for the CaF_2 A centre while the SC1, SC2 and SB1 centres have lifetimes similar to those of the SrF_2 A centre. This is consistent with the modified centres being derived from the respective C_{4v} symmetry A centres.

For the dimer centre in $CsCdBr_3$:Ho^{3+}, fluorescence lifetime measurements confirm the energy transfer mechanism proposed for the population of the Q multiplet at ~32850 cm^{-1}. The energy transfer rates were found to be comparable to those for the Er^{3+} dimer centre, for excitation to multiplets in the same spectral region.

The high resolution and ODNMR measurements confirm the C_{4v} symmetry assignment proposed for the SrF_2 A and SB1 centres. Observation of the same superhyperfine ODNMR frequencies for the eight nearest neighbour F^- ions in both the SrF_2 A and the SB1 centres shows that the dopant cation does not have any appreciable effect on the positions of the nearest neighbour lattice F^- ions and only affects the positioning of the interstitial F^- ion, as evidenced by the decrease in its resonance frequency in going from the SrF_2 A centre to the SB1 centre.

From the preliminary high resolution study of the dimer centre in $CsCdBr_3$:Ho^{3+} crystals, the symmetry assignments for the Z_1, D_1 and D_2 energy levels have been confirmed. $CsCdBr_3$:Ho^{3+} is a promising candidate for high resolution studies of the pair splittings and low symmetry crystal-field effects, with the requirement that either the $^5S_2$ or the $^5F_3$ multiplet rather than the $^5F_5$

multiplet be excited, as both effects are well resolved for some transitions of the $^5S_2$ and $^5F_3$ multiplets in the 0.2 cm^{-1} resolution spectra.

A total of 23 Ho^{3+} centres, comprising six F^- and three D^- centres in CaF_2 type crystals, six F^- and four D^- centres in SrF_2 type crystals and two dimer and two single Ho^{3+} ion centres in $CsCdBr_3$ crystals, have been documented in this study. Laser selective excitation has been shown to be a useful technique for identifying and studying the various Ho^{3+} centres present in these CaF_2, SrF_2 and $CsCdBr_3$ type crystals and polarisation, a powerful tool for determining the centre symmetries and crystal-field energy level irrep labels.

Extensions of this study of Ho^{3+} ions in CaF_2, SrF_2 and $CsCdBr_3$ type crystals would include :

(i) EPR measurements in the 75 GHz range to confirm the principal centre symmetry assignment made here for SrF_2:Ho^{3+} and directly measure the Z_1 - Z_2 separation;

(ii) high resolution and ODNMR studies of the CS1, CB1 and SC1 centres in suitably doped crystals, to monitor the frequency changes for the resonance from the interstitial F^- ion and derive its position relative to that of the Ho^{3+} ion for all the modified C_{4v} symmetry centres in the mixed crystals;

(iii) high resolution studies of lowly doped (< 0.01%) $CsCdBr_3$:Ho^{3+} crystals, to characterise the pair splittings, low symmetry crystal-field effects and hyperfine interaction effects;

(iv) Zeeman spectroscopy of the principal dimer and M single ion centres in $CsCdBr_3$:Ho^{3+} crystals, for further study of the pair splittings and the low symmetry crystal-field effects;

(v) spectroscopic and temporal measurements of the visible upconversion fluorescence in $CsCdBr_3$:Ho^{3+} crystals for excitation in the infrared. The resulting upconversion mechanisms and energy transfer rates can then be compared with those for the Er^{3+} dimer centre.

REFERENCES

[1] Ackerman J.F., Cole G.M. and Holt S.L., *Inorg. Chem. Acta Rev.* **8**, 323 (1974)

[2] Agladze N.I. and Popova M.N., *Solid State Comm.* **55**, 1097 (1985)

[3] Agladze N.I., Vinogradov E.A. and Popova M.N., *Sov. Phys. JETP* **64**, 716 (1986)

[4] Agladze N.I., Vinogradov E.A. and Popova M.N., *Opt. Spectrosc. (USSR)* **61**, 1 (1986)

[5] Allain J.Y., Monerie M. and Poignant H., *Electron. Lett.* **26**, 261 (1990)

[6] Antipin A.A., Davydova M.P., Eremin M.V., Luks R.K., and Stolov A.L., *Opt. Spectrosc.* **33**, 372 (1972)

[7] Antipin A.A., Kurkin I.I., Livanova L.D., Potvorova L.Z. and Shekun L. Ya., *Sov. Phys. - Technical Physics* **11**, 821 (1966)

[8] Antipin A.A., Kurkin I.N., Livanova L.D., Potvorova L.Z. and Shekun L. Ya., *Sov. Phys. - Solid State* **8**, 2130 (1967)

[9] Antipin A.A., Livanova L.D. and Shekun L. Ya., *Sov. Phys. - Solid State* **10**, 1025 (1968)

[10] Barthem R.B., Buisson R. and Cone R.L., *J. Chem. Phys.* **91**, 627 (1989)

[11] Barthem R.B., Buisson R., Madéore F., Vial J.C. and Chaminade J.P., *J. Phys. (Paris)* **48**, 379 (1987)

[12] Barthou C. and Barthem R.B., *J. Lumin.* **46**, 9 (1990)

[13] Berdowski P.A.M., Lammers M.J.J. and Blasse G., *J. Chem. Phys.* **83**, 476 (1985)

[14] Blasse G., Wolfert A. and McPherson G.L., *J. Solid State Chem.* **57**, 396 (1985)

[15] Bleaney B., Llewellyn P.M. and Jones D.A., *Proc. Phys. Soc.* **B69**, 858 (1956)

[16] Boyn R., *Phys. Stat. Sol. (b)* **148**, 11 (1988)

[17] Brierley M.C., France P.W. and Millar C.A., *Electron. Lett.* **24**, 539 (1988)

[18] Brown M.R., Roots K.G., Williams J.M., Shand W.A., Groter C. and Kay H.F., *J. Chem. Phys.* **50**, 891 (1969)

[19] Brown M.R., Thomas H., Whiting J.S.S. and Shand W.A., *J. Chem. Phys.* **50**, 881 (1969)

[20] Buisson R. and Vial J.C., *J. Phys. (Paris) Lett.* **42**, L115 (1981)

[21] Burum D.P., Shelby R.M. and Macfarlane R.M., *Phys. Rev. B* **25**, 3009 (1982)

[22] Butler P.H., *Point Group Symmetry Applications* (Plenum Press : New York, 1981)

[23] CRC Handbook of Chemistry and Physics, ed. Weast R.C., (CRC Press : Cleveland, 1970)

[24] Campbell J.A., private communication

[25] Carnall W.T., Goodman G.L., Rajnak K. and Rana R.S., *J. Chem. Phys.* **90**, 3443 (1989)

[26] Caspers H.H., Rast H.E. and Fry J.L., *J. Chem. Phys.* **53**, 3208 (1970)

[27] Chaminade J.P., Macfarlane R.M., Ramaz F. and Vial J.C., *J. Lumin.* **48** & **49**, 531 (1991)

[28] Cockcroft N.J., *Ph.D. Thesis*, University of Canterbury (1987)

[29] Cockcroft N.J., Jones G.D. and Nguyen D.C., *Phys. Rev. B* **45**, 5187 (1992)

[30] Cockcroft N.J., Jones G.D. and Syme R.W.G., *J. Chem. Phys.* **92**, 2166 (1990)

[31] Cockcroft N.J., Jones G.D. and Syme R.W.G., *J. Lumin.* **43**, 275 (1989)

[32] Cockcroft N.J., Thompson D., Jones G.D. and Syme R.W.G., *J. Chem. Phys.* **86**, 521 (1987)

[33] Crosswhite H.M., Crosswhite H., Edelstein N. and Rajnak K., *J. Chem. Phys.* **67**, 3002 (1977)

[34] Dieke G.H., *Physica* **33**, 212 (1967)

[35] Dieke G.H., *Spectra and Energy Levels of Rare Earth Ions in Crystals* (Interscience : New York, 1968)

[36] Edgar A., Freeth C.A. and Jones G.D., *Phys. Rev. B* **15**, 5023 (1977)

[37] Edgar A., Jones G.D. and Presland M.R., *J. Phys. C: Solid State Phys.* **12**, 1569 (1979)

[38] Elcombe M.M. and Pryor A.W., *J. Phys. C: Solid State Phys.* **3**, 492 (1970)

[39] Eremin M.V., Luks R.K. and Stolov A.L., *Sov. Phys. - Solid State* **12**, 2820 (1971)

[40] Ershov B.V., Pimenov Yu.P., Prokhorov A.M. and Fedorov V.B., *Sov. Phys. - Solid State* **10**, 1300 (1968)

[41] Foo S.P., *Honours III Project Report*, University of Canterbury (1989)

[42] Freeth C.A. and Jones G.D., *J. Phys. C: Solid State Phys.* **15**, 6833 (1982)

[43] Freeth C.A., Jones G.D. and Syme R.W.G. *J. Phys. C: Solid State Phys.* **15**, 5667 (1982)

[44] Hall J.L. and Schumacher R.T., *Phys. Rev.* **127**, 1892 (1962)

[45] Han T.P.J., *Ph.D. Thesis*, University of Canterbury (1988)

[46] Hanna D.C., Percival R.M., Smart R.G., Townsend J.E. and Tropper A.C., *Electron. Lett.* **25**, 593 (1989)

[47] Hasan Z., *Solid State Comm.* **73**, 109 (1990)

[48] Hasan Z., Danby R. and Manson N.B., *J. Lumin.* **40** & **41**, 397 (1988)

[49] Hasan Z., Ghafoori Fard H. and Manson N.B., *J. Lumin.* **45**, 304 (1990)

[50] Hayes W., *Crystals with the Fluorite Structure* (Clarendon Press : Oxford, 1974)

[51] Hayes W., Jones G.D. and Twidell J.W., *Proc. Phys. Soc. (London)* **81**, 371 (1963)

[52] Henling L.M. and McPherson G.L., *Phys. Rev. B* **16**, 4756 (1977)

[53] Hüfner S., *Optical Spectra of Transparent Rare Earth Compounds* (Academic Press : New York, 1978)

[54] Hutchings M.T., *Point-Charge Calculations of Energy Levels of Magnetic Ions in Crystalline Electric Fields* in Solid State Physics Vol. **16**, ed. Seitz F. and Turnbull D. (Academic Press : New York, 1964)

[55] Jones G.D., Peled S., Rosenwaks S. and Yatsiv S., *Phys. Rev.* **183**, 353 (1969)

[56] Jones G.D. and Satten R.A., *Phys. Rev.* **147**, 566 (1966)

[57] Judd B.R., *Operator Techniques in Atomic Spectroscopy* (McGraw Hill : New York, 1963)

[58] Judd B.R., *Phys. Rev.* **141**, 4 (1966)

[59] Judd B.R., *Phys. Rev.* **127**, 750 (1962)

[60] Judd B.R., Crosswhite H.M. and Crosswhite H., *Phys. Rev.* **169**, 130 (1968)

[61] Kaminskii A.A., *Laser Crystals : their Physics and Properties* (Springer Series in Optical Sciences Vol. **14**), translation ed. Ivey H.F. (Springer-Verlag : Berlin, 1981)

[62] Kaplyanskii A.A. and Medvedev V.N., *Opt. Spectrosc.* **18**, 451 (1965)

[63] Khong Yoon Loong, *Ph. D. Thesis*, University of Canterbury (1991)

[64] Kong Yoon Loong, private communication

[65] Kintz G.J., Esterowitz L. and Allen R., *Electron. Lett.* **23**, 616 (1987)

[66] Kornienko L.S. and Rybaltovskii A.O., *Sov. Phys. - Solid State* **13**, 1785 (1972)

[67] Koster G.F., Dimmock J.O., Wheeler R.G. and Starz H., *Properties of the Thirty-two Point Groups* (M.I.T. Press : Cambridge, Massachusetts, 1963)

[68] Kurz M.D. and Wright J.C., *J. Lumin.* **15**, 169 (1977)

[69] Lai K.K., *Ph. D. Thesis*, University of Canterbury (1987)

[70] Lal B. and Ramachandra Rao D., *Indian J. Phys.* **54B**, 84 (1980)

[71] Lal B. and Ramachandra Rao D., *Chem. Phys. Lett.* **53**, 250 (1978)

[72] Lammers M.J.J. and Blasse G., *Chem. Phys. Lett.* **126**, 405 (1986)

[73] Lea K.R., Leask M.J.M. and Wolf W.P., *J. Phys. Chem. Solids* **23**, 1381 (1962)

[74] Lesniak K., *J. Phys. C: Solid State Phys.* **19**, 2721 (1986)

[75] Lesniak K. and Richardson F.S., *J. Phys. : Condens. Matter* **4**, 1743 (1992)

[76] Lupei V., *J. Phys. C: Solid State Phys.* **12**, L45 (1979)

[77] Macfarlane R.M., Burum D.P. and Shelby R.M., *Phys. Rev. B* **29**, 2390 (1984)

[78] Macfarlane R.M. and Shelby R.M., *Coherent Transient and Holeburning Spectroscopy of Rare Earth Ions in Solids,* Chapter 3 in Spectroscopy of Solids Containing Rare Earth Ions, ed. Kaplyanskii A.A. and Macfarlane R.M. (Elsevier Science : Amsterdam, 1987)

[79] Macfarlane R.M., Shelby R.M. and Burum D.P., *Opt. Lett.* **6**, 593 (1981)

[80] Manson N.B., Hasan Z., Fisk P.T.H., Reeves R.J., Jones G.D. and Macfarlane R.M., *J. Phys. C.*, to be published

[81] Martin J.P.D., Boonyarith T., Manson N.B., Mujaji M. and Jones G.D., to be published

[82] McPherson A.M. and McPherson G.L., *Solid State Comm.* **37**, 501 (1981)

[83] McPherson G.L. and Henling L.M., *Phys. Rev. B* **16**, 1889 (1977)

[84] McPherson G.L., McPherson A.M. and Atwood J.L., *J. Phys. Chem. Solids* **41**, 495 (1980)

[85] McPherson G.L. and Meyerson S.L., *Chem. Phys. Lett.* **167**, 471 (1990)

[86] McPherson G.L., Wai-ming Heung and Barraza J.J., *J. Am. Chem. Soc.* **100**, 469 (1978)

[87] Merz J.L. and Pershan P.S., *Phys. Rev.* **162**, 217 (1967)

[88] Merz J.L. and Pershan P.S., *Phys. Rev.* **162**, 235 (1967)

[89] Miller M.P. and Wright J.C., *J. Chem. Phys.* **71**, 324 (1979)

[90] Murdoch K., private communication

[91] Narayana Rao D., Prasad J. and Prasad P.N., *Phys. Rev. B* **28**, 20 (1983)

[92] Newman R.C., *Infra-red Studies of Crystal Defects*, ed. Coles B.R. and Mott N. (Taylor & Francis Ltd. : London, 1973)

[93] Nielson C.W. and Koster G.F., *Spectroscopic Coefficients for* p^n, d^n *and* f^n *Configurations* (M.I.T. Press : Cambridge, Massachusetts, 1964)

[94] Ofelt G.S., *J. Chem. Phys.* **37**, 511 (1962)

[95] Paris M.I., *Honours III Project Report*, University of Canterbury (1986)

[96] Pilla O., Cazzanelli E., Blanzat B., Andraud C., and Pelle F., *Phys. Stat. Sol. (b)* **144**, 845 (1987)

[97] Popov V.V. and Pissarenko V.F., *Phys. Stat. Sol.* **32**, K143 (1969)

[98] Pourat B., Pilawa B. and Kahle H.G., *J. Phys. : Condens. Matter* **3**, 6069 (1991)

[99] Rajnak K. and Krupke W.F., *J. Chem. Phys.* **46**, 3532 (1967)

[100] Rajnak K. and Wybourne B.G., *Phys. Rev.* **132**, 280 (1963)

[101] Ramaz F., Macfarlane R.M. and Vial J.C., to be published

[102] Ramaz F., Vial J.C., Macfarlane R.M., Chaminade J.P. and Madéore F., to be published

[103] Ranon U. and Lee K., *Phys. Rev.* **188**, 539 (1969)

[104] Ranon U. and Yaniv A., *Phys. Lett.* **9**, 17 (1964)

[105] Reeves R.J., *Ph. D. Thesis*, University of Canterbury (1987)

[106] Reeves R.J., Jones G.D. and Syme R.W.G., *Phys. Rev. B.*, to be published

[107] Reeves R.J., Jones G.D., Cockroft N.J., Han T.P.J. and Syme R.W.G., *J. Lumin.* **38**, 198 (1987)

[108] Reid M.F., *J. Chem. Phys.* **87**, 2875 (1987)

[109] Reid M.F. and Butler P.H., *J. Phys. C: Solid State Phys.* **15**, 4103 (1982)

[110] Reid M.F., private communication

[111] Reisfeld R. and Jorgensen C.K., *Lasers and Excited States of Rare Earths*, Chapter 2 in Inorgaic Chemistry Concepts Vol. **1** (Springer-Verlag : Berlin, 1977)

[112] Richman I., *Phys. Rev.* **133**, A1364 (1964)

[113] Riseberg L.A. and Moos H.W., *Phys. Rev.* **174**, 429 (1968)

[114] Riseberg L.A. and Weber M.J., *Relaxation Phenomena in Rare-Earth Luminescence*, Chapter III in Progress in Optics XIV, ed. Wolf E. (North-Holland : Amsterdam, 1976)

[115] Rotenberg M., Bivins R., Metropolis N. and Wooten J.K., *The 3-j and 6-j Symbols* (M.I.T. Press : Cambridge, Massachusetts, 1959)

[116] Seelbinder M.B., *Ph.D. Thesis*, University of Wisconsin (University Microfilms : Ann Arbor, Michigan, 1980)

[117] Seelbinder M.B. and Wright, J.C., *Phys. Rev. B* **20**, 4308 (1979) [SW]

[118] Sendova-Vassileva M., Iliev M. and Chadwick A.V., *J. Phys. : Condens. Matter* **3**, 5407 (1991)

[119] Sierro J., *Phys. Lett.* **4**, 178 (1963)

[120] Tallant D.R., Miller M.P. and Wright J.C., *J. Chem. Phys.* **65**, 510 (1976)

[121] Tallant D.R., Moore D.S. and Wright J.C., *J. Chem. Phys.* **67**, 2897 (1977)

[122] Tallant D.R. and Wright J.C., *J. Chem. Phys.* **63**, 2074 (1975)

[123] Tang S.H., Zhang H.Y., Kuok M.H. and Kee S.C., *Phys. Stat. Sol. (b)* **168**, 351 (1991)

[124] Timans J.W.J. and Den Hartog H.W., *Phys. Stat. Sol. (b)* **73**, 283 (1976)

[125] Voron'ko Yu.K., Kaminskii A.A., Osiko V.V. and Prokhorov A.M., *Soviet Phys. - JETP Lett.* **1**, 3 (1965)

[126] Watts R.K., *J. Chem. Phys.* **53**, 3552 (1970)

[127] Weber M.J. and Bierig R.W., *Phys. Rev.* **134,** A1492 (1964)

[128] Welsh H.K., *J. Phys. C: Solid State Phys.* **18**, 5637 (1985)

[129] Wolfert A. and Blasse G., *J. Solid State Chem.* **55**, 344 (1984)

[130] Wood D.L. and Kaiser W., *Phys. Rev.* **126**, 2079 (1962)

[131] Wright J.C., *Up-Conversion and Excited State Energy Transfer in Rare-Earth Doped Materials*, Chapter 4 in Topics in Applied Physics Vol. **15**, ed. Fong F.K. (Springer-Verlag : Berlin, 1976)

[132] Wybourne B.G., *Spectroscopic Properties of Rare Earths* (Interscience : New York, 1965)

[133] Yen W.M., *Experimental Studies of Energy Transfer in Rare Earth Ions in Crystals*, Chapter 4 in Spectroscopy of Solids Containing Rare Earth Ions, ed. Kaplyanskii A.A. and Macfarlane R.M. (Elsevier Science : Amsterdam, 1987)

APPENDIX

Publications co-authored

1. *Upconversion Fluorescence Spectroscopy of Ho^{3+} Dimer Pairs in $CsCdBr_3$*
M. Mujaji, G.D. Jones and R.W.G. Syme, J. Lumin., to be published in the proceedings of the 8th international conference on Dynamical Processes in Excited States of Solids, August 1991.

2. *A Polarisation Study and Crystal-Field Analysis of the Laser Selective Excitation Spectra of Ho^{3+} Ions in CaF_2 and SrF_2 crystals*
M. Mujaji, G.D. Jones and R.W.G. Syme, submitted to Phys. Rev. B (1992).

3. *Hyperfine Coupling between Crystal Field Levels in the Tetragonal Center of CaF_2:Ho^{3+} and its Measurement via Laser Spectroscopy*
J.P.D. Martin, T. Boonyarith, N.B. Manson, M. Mujaji and G.D. Jones, to be published.